THE RAMAN SPECTRA AND STRUCTURE OF GLASSES IN THE
ARSENIC-SULPHUR AND ARSENIC-SELENIUM SYSTEMS

BY

PETER J.S. EWEN

Thesis presented for the degree of
Doctor of Philosophy of the
University of Edinburgh

October 1978

ABSTRACT

The room-temperature Raman spectra of bulk As-S and As-Se glasses have been recorded. The compositions studied range throughout the glass-forming regions but are mainly close to the stoichiometric composition $As_{40}X_{60}$ (X = S or Se): eleven compositions in the range $As_{35}X_{65} - As_{45}X_{55}$ have been studied in each system. Polarisation measurements have been made on all the glasses and from them have been derived the depolarisation spectra.

The frequencies and polarisation states of the bands in the $a-As_{40}S_{60}$ and $a-As_{40}Se_{60}$ spectra can be accounted for using the Lucovsky-Martin molecular model. It is found that the spectra of these two glasses scale by the same two factors that relate the spectra of the corresponding crystals. The applicability of the interlayer scale factor to the glass spectra supports the presence of layer regions in the glasses.

The spectra on the chalcogen-rich side of the stoichiometric composition $As_{40}X_{60}$ have also been analysed in terms of the Lucovsky-Martin molecular model and indicate the replacement of the As–X–As links between the AsX_3 pyramid units by As–X–X–As links as the chalcogen content is increased. The presence of S_8 rings is increasingly apparent in the sulphide compositions more S-rich than $As_{37}S_{63}$.

In the case of the As-rich sulphides sharp spectral features characteristic of the crystal $\beta-As_4S_4$ appear near stoichiometry and increase smoothly as the As content is increased through the limit of the glass-forming region, $\sim As_{43}S_{57}$, and on into the phase-separated region. The results also indicate that As_4S_3 or As_4S_5 molecules are present and that As–As bonds are formed in the glass network. In the case of the As-rich selenides, for the compositions between $As_{40}Se_{60}$ and $As_{45}Se_{55}$ the additional As atoms go mainly into the formation of As–As

bonds in the network. For compositions containing more than 50 at.% As

the production of As_4Se_4 molecules predominates over the formation of

As—As bonds in the network, although these are still present.

DECLARATION OF ORIGINALITY

This thesis has been composed by myself and is the result of my own work except when otherwise indicated. Discussions with Dr. A.E.Owen and Dr. M.J.Sik have helped form some of the conclusions and where appropriate, reference to other investigators' work has been made and acknowledged.

Peter J.S. Ewen

ACKNOWLEDGEMENTS

TABLE OF CONTENTS /

INTRODUCTION

1.1   Non-crystalline solids

A solid is classified as either crystalline or non-crystalline according as its structure is periodic or aperiodic.   A crystal may be defined as a substance in which the atomic arrangement is 'periodic in three dimensions over intervals which are large compared with the unit of periodicity'[1].   A non-crystalline solid is one in which this periodicity is absent.

The ordered structure of a crystal can be described using the geometrical concept of a space lattice, a three-dimensional periodic array of points: for any crystal one can identify a basic unit of the structural pattern and a lattice such that the crystal structure can be obtained by placing one of these units at each lattice point.   The pattern unit — termed the 'basis' — may be a single atom or a group of atoms and its composition, arrangement and orientation is identical at each lattice point, so that any basis is in exactly the same environment as any other.   While the basis may be asymmetric the lattice always has some degree of symmetry — the defining property of a lattice is that it possesses translational symmetry.   The symmetry characteristics of both basis and lattice are taken into account when determining the crystal's 'space group', which expresses the symmetry of the crystal as a whole and is the set of all symmetry operations (rotations, inversions etc.) that map the crystal into itself; the space group specifies the long-range order (l.r.o.) of the crystal.

Because the group of atoms associated with each lattice point has the same composition, arrangement and orientation throughout the crystal, corresponding atoms in different unit cells of the lattice have identical

surroundings. Thus for a particular basis atom the local environment — that is, the number and positions of its neighbouring atoms — is the same anywhere in the crystal; this invariance of local environment is termed the short-range order (s.r.o.). The spatial configuration adopted by the atoms in a crystal is determined by the nature of the interatomic bonding, that is to say, the type of bonds formed, the number and strength of these bonds and their direction. (Since the bonds are affected by temperature and pressure the atomic arrangement in the crystal also depends on these thermodynamic factors). It is the electronic structure of the atoms in the crystal that determines the nature of the interatomic bonding.

The above discussion really refers only to ideal crystals: real crystals contain a variety of imperfections which interrupt the periodicity of the structure. The fact that real crystals are of finite size and hence bounded by surfaces is an inevitable imperfection; the atoms at the surface of a crystal are in a different environment to those in the interior. A more significant deviation from the ideal situation is that most crystalline solids are composed of an aggregate of minute crystals, termed 'crystallites' or 'grains'; as these crystallites are randomly oriented abrupt changes in the orientation of the lattice occur at the grain boundaries. The crystallites are typically $10^{-7} - 10^{-4}$ cm in diameter so that the structure of the crystal is periodic only over distances of the order of $10 - 10^4$ lattice parameters[1]. (This mosaic-like structure that real crystals possess was taken into account in the definition of the crystalline state given in the opening paragraph.) Within these crystallites defects such as impurities, broken bonds, dislocations and stacking faults may occur. Crystal alloys may exhibit compositional disorder, that is the various constituent atomic species may be distributed in an irregular way over the lattice sites. Phonons and other excitations also disturb the periodicity of the structure.

In the case of molecular crystals, the individual molecules may be identical but their orientations may vary irregularly throughout the sample.

The problem of surface atoms in real crystals is in general not important since the ratio of surface to interior atoms is small ($\sim 10^{-8}$ for a mole sample)[2]; the problem can be overcome by the use of periodic boundary conditions. Also, phonon and compositional disorder do not eliminate the l.r.o. of the structure: these imperfections are examples of 'cellular' disorder, that is disorder which is present only within the unit cell, and a lattice can still be defined for materials with this type of disorder[3] (the orientational disorder in molecular crystals is of this type). The other forms of imperfection can usually be regarded as perturbations of the periodicity. Hence although the atomic arrangement in real crystals deviates considerably from perfect periodicity the concept of a lattice is still useful in describing their structure. It should be noted, however, that the physical properties of crystals are significantly influenced by the imperfections they contain.

The distinguishing feature of non-crystalline solids is that their structure has no l.r.o.[4]: the atomic arrangement in a non-crystalline solid is not periodic and there is no way in which a lattice can be defined. This is not, however, equivalent to saying that the atomic arrangement is completely random as in a gas. The nature of the inter-atomic bonding in a solid is determined by the electronic structure of the constituent atoms, hence the bonding forces in a non-crystalline solid will be very similar to those of the corresponding crystal; since the local atomic environment is in turn determined by the bonding forces it will also be virtually the same in the non-crystalline solid as in the corresponding crystal. Thus non-crystalline solids, as well as crystals, possess s.r.o.; the s.r.o. in a non-crystalline solid extends

only for distances of three or four bond lengths, i.e. about 10 − 20 Å.

In the present study the terms 'amorphous', 'non-crystalline' and 'disordered' will be regarded as synonymous when applied to solids and will indicate the absence of l.r.o., though strictly speaking 'disordered' is a more general term and is sometimes applied to crystals. The terms 'vitreous' and 'glassy' will also be used to indicate the absence of l.r.o. in a solid but will be restricted to amorphous solids prepared by quenching from the liquid state. When it is necessary to indicate the structural nature of a particular solid under discussion it will some-times be convenient to use the standard convention of prefixing the solid's chemical formula by 'a' (for amorphous) or 'c' (for crystalline), thus for example amorphous arsenic trisulphide may be abbreviated $a-As_2S_3$.

One can establish whether or not l.r.o. exists in a solid by deter-mining its radial distribution function[5] (r.d.f.), D(r), given by

$$D(r) = 4 \pi r^2 \rho(r)dr \qquad (1.1)$$

where r is the radial distance from a reference atom and $\rho(r)$ is the number density of atom centres at this distance; the r.d.f. gives the number of atom centres in a spherical shell of radius r and thickness dr centred on the reference atom. When D(r) is plotted against r one obtains the radial distribution curve (r.d.c.) of the solid. If l.r.o. is absent in a material then its r.d.f. should tend to the limiting form $4 \pi r^2 \rho_0$ as r becomes large (ρ_0 being the average atomic density), i.e. at large values of r the r.d.c. tends to a parabola. If the r.d.f. does not tend to $4 \pi r^2 \rho_0$ for large r then l.r.o. is present in the solid; the r.d.c. of an ideal crystal would consist of a series of vertical lines separated by distances corresponding to the interatomic spacings of the crystal. R.d.f.'s are obtained by Fourier transformation of X-ray, electron or neutron diffraction data. These diffraction techniques can detect the presence of ordered regions greater than ~20 Å in extent. Since 20 Å is the upper limit of the s.r.o. in an amorphous

solid it can conveniently be taken as the dividing line between long- and short-range order, so that an amorphous solid may be defined as one in which there is no l.r.o., meaning order greater than 20 $\overset{\circ}{A}$ in extent.

Several types of disorder can occur in an amorphous solid, although absence of l.r.o., being the distinguishing characteristic of such solids, is the most important feature of the disorder. Many of the imperfections that are found in crystals can also occur in amorphous solids, for example phonons, impurities and, in particular, broken bonds. Compositional disorder may exist in compound amorphous materials, as in the case of crystals, possibly resulting in the formation of 'wrong' bonds, i.e. bond types not found in the corresponding perfect crystal. However, as remarked earlier, compositional disorder does not destroy l.r.o. It is the disordered arrangement of the atoms in an amorphous solid that is responsible for the lack of structural periodicity; this positional disorder arises from the distortion of bond lengths, bond angles and dihedral angles in the material. If disordering of the atomic arrangement results in the topology of the structure of an amorphous solid differing from that of the corresponding crystal then the structure is said to be topologically disordered. In topological disorder the atomic coordination remains the same as in the crystal but the connectivity of the network is disordered, so that the atomic arrangement in the amorphous solid cannot be transformed back to the crystalline arrangement without breaking bonds. Since topological disorder results in the occurrence of rings with different numbers of members it is easily identified. Some of the various types of disorder are illustrated in Figure 1.1, which shows a two-dimensional representation of the structure of a hypothetical compound of stoichiometry X_2Y_3 in its crystalline form (Figure 1.1(a)) and its amorphous form (Figure 1.1(b)). The periodic nature of the crystal structure is obvious in Figure 1.1(a) while Figure 1.1(b) shows clearly the disordered arrangement of the atoms in the non-crystalline form.
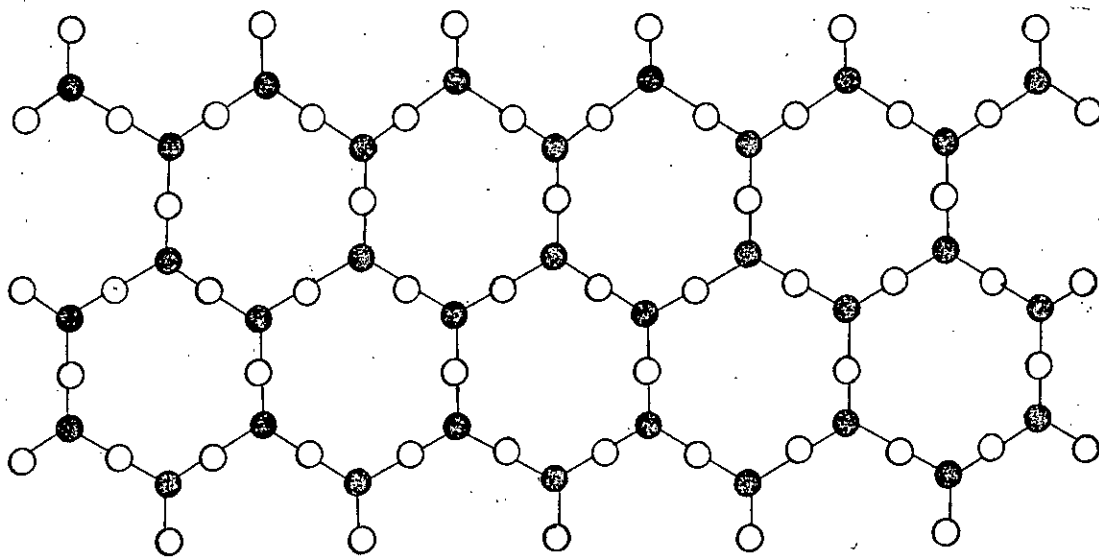
(a)
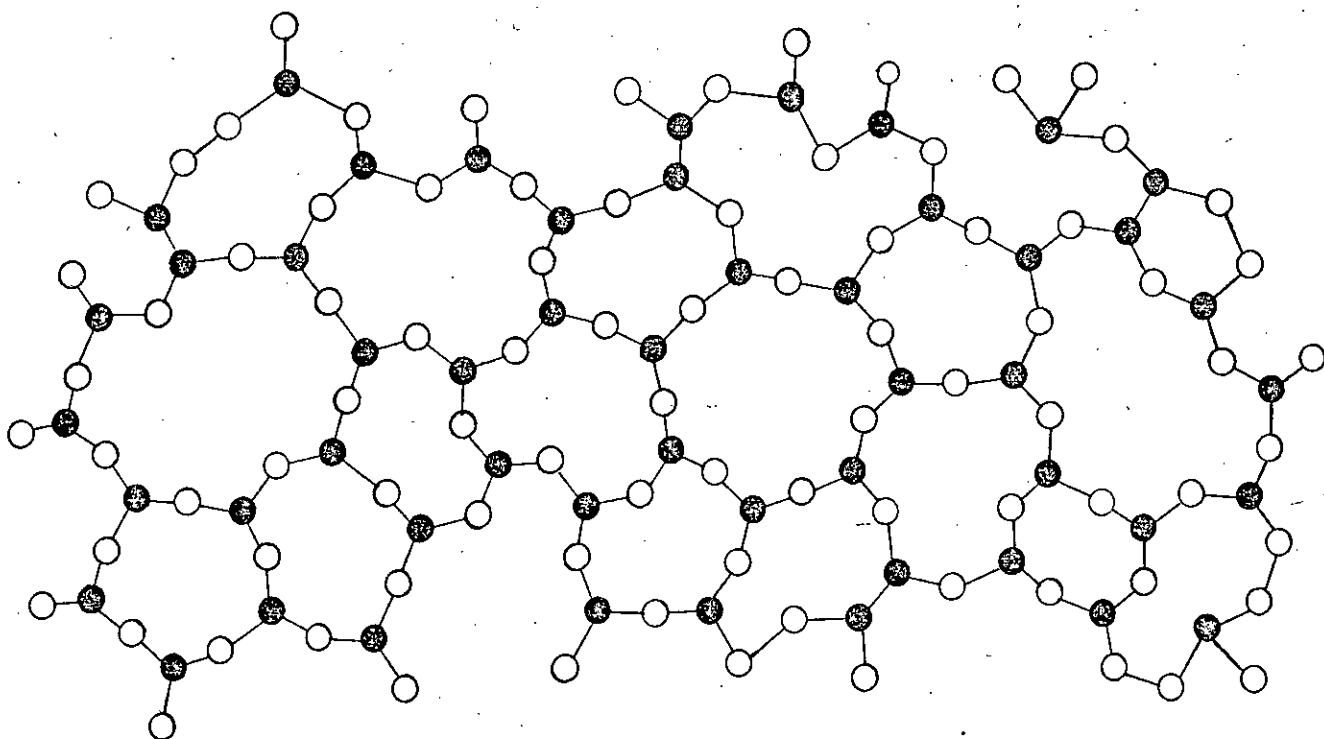
(b)

● X ○ Y

<u>Figure 1.1</u>

A two-dimensional representation of the structure of a hypothetical compound

of stoichiometry X_2Y_3 in (a) its crystalline form and (b) its amorphous form.

In addition to this positional disorder, compositional and topological disorder are present in the structure shown in Figure 1.1(b). The compositional disorder gives rise to the presence of X—X and Y—Y bonds (i.e. 'like-atom' bonds) in addition to the X—Y bonds which are the only type present in the perfect crystal. The existence of topological disorder is obvious since the number of atoms per ring varies from 6 to 16 whereas in the crystal the rings are all 12 membered.

There are several approaches to describing the structure of non-crystalline materials, the simplest being the perturbed crystal approach, in which the amorphous material is regarded as a crystal containing a high density of conventional structural defects[6]. This approach, however, is generally unsatisfactory since the entropy and degree of order it predicts are respectively too low and too high, and it cannot readily account for observed diffraction effects[7]. Other approaches fall into two categories: the microdomain approach, in which the solid is taken to be made up of small (typically $10 - 15$ Å in diameter), randomly oriented ordered regions, and the continuous random network (c.r.n.) approach, in which the solid is thought of as a continuously connected network having no regular structural unit apart from the nearest-neighbour configuration.

The ordered regions in microdomain models of amorphous solid structure are generally taken to be small crystallites; the micro-crystallite approach was suggested by early workers[8] to account for the type of diffraction pattern characteristic of amorphous materials, viz a series of broad, diffuse haloes. Whereas the diffraction pattern of a single crystal is composed of an array of isolated points, that of a polycrystalline specimen consists of a series of sharp, concentric rings; as the crystallite size decreases the rings broaden and become diffuse, and the diffraction pattern starts to resemble that for an amorphous solid. Hence it was proposed that an amorphous solid might

be composed of an assembly of randomly oriented crystallites 10 — 15 Å in size, each one being perfectly ordered internally in the simplest version of the model, though in other versions the crystallites may contain defects[9] or may have different crystal structures[7].

There are several objections to the microcrystallite model. Firstly, the boundaries between the crystallites are abrupt and the question arises of how the crystallites are connected to one another in order to minimise the number of broken bonds at the boundary atoms: if the majority of boundary atoms have broken bonds then this type of structure would be energetically unfavourable since about half the atoms in a crystallite of size 10 — 15 Å are at the surface. It has been suggested that the microcrystallites might be connected via positionally disordered regions but details of these regions and the way they connect with the crystallites have not been specified[10]. A second, more philosophical objection to the model is that since such a large proportion of the crystallite atoms reside at the surface can the domains really be regarded as crystalline? The most important objection, however, is the absence of the 3rd crystalline nearest-neighbour peak in the r.d.f.'s of all amorphous materials studied to date[11].

In some microdomain models the domains are not crystallites but polyhedral clusters of atoms; these units — termed 'amorphons' — are regular but not crystallographically symmetric[12]. The amorphons give rise to amorphous-like diffraction patterns with no 3rd crystalline nearest-neighbour peak. Because the amorphons have non-crystallographic symmetry they cannot fill all space and so it is necessary to regard the structure as a mixture of amorphons and crystallites continuously connected to each other. Even so, densities calculated from such models are much lower than observed values because of the unavoidable presence of large voids in the model structure[13].

Renewed interest in microdomain models has recently been stimulated

by the observation of 'fringes' in electron micrographs of some amorphous materials[14]. If the observed fringes are not artefactual they indicate the presence of ordered regions 10 — 15 Å in size. However, the interpretation of these fringes is still a matter of controversy[15] and even if they are genuine they can also be accounted for by a c.r.n. approach. The dark field electron microscopy of amorphous materials has been discussed by Stobbs[16].

In c.r.n. models of the structure of amorphous solids it is assumed that the atoms form a continuously connected random array. The c.r.n. approach was first proposed by Zachariasen[17] in 1932. Connectivity is the essential feature of the model and in an ideal c.r.n. there are no broken bonds. It is variations in bond lengths, bond angles and dihedral angles that enable all the bonds to be satisfied.

Since liquids (with the exception of liquid crystals) exhibit s.r.o. but no l.r.o. their structure is also amorphous. Liquids and amorphous solids have the same type of r.d.c., consisting of a few broad maxima at small values of the separation, r, and tending to a parabola as r becomes large. There is, however, a significant difference between the atomic arrangement in an amorphous solid and that in a liquid: in the former the atomic arrangement is essentially static whereas in the latter it is constantly changing due to the thermal motion of the atoms, so that for a liquid the r.d.c. is really a time average for a continuously changing configuration[5]. As a liquid is cooled its atoms move more and more slowly and if crystallisation can be prevented it can be cooled to the point where the atoms cease to move and the disordered atomic arrangement of the liquid becomes static or 'frozen in'. This is the principle behind glass formation.

If a molten material is cooled below its melting point, T_m, it becomes thermodynamically unstable with respect to a transformation into the solid state and will crystallise provided there is a crystal form and

sufficient time is available for nucleation and crystal growth[18].

In the growing process atoms diffuse from the liquid onto the surfaces

of the nuclei, the rate of diffusion being limited by the liquid's

viscosity, which generally increases as $e^{A/T}$, T being the absolute

temperature and A a constant. If the liquid is cooled quickly the

accompanying increase in its viscosity may be so rapid that crystal

growth is inhibited; for some cooling rates crystal growth may be

inhibited to such an extent that crystallisation does not take place,

so that the material remains a liquid below the melting point (in which

case it is said to be in a supercooled state). When the temperature

reaches a value at which the viscosity is so high that the material may

be regarded as a solid, it is called a 'glass', 'glassy solid' or

'vitreous solid'.

The atomic arrangement in the glass is identical with the 'frozen in'

configuration of the liquid at the temperature at which atomic motion

ceases. This temperature is called the glass transition temperature, T_g.

Strictly speaking, the glass transition occurs over a range of temperature,

so that T_g does not have a single, well-defined value. Also, T_g depends

on the cooling rate and the thermal history of the material. Over the

glass transition region first-order extensive thermodynamic variables

such as volume, enthalpy and entropy change continuously with temperature

but undergo a change of slope; however, second-order thermodynamic

quantities such as expansion coefficient, specific heat and compressibility

change discontinuously at T_g[5,19].

The crystalline state is the thermodynamically stable state of a

solid; amorphous solids are metastable with respect to their corresponding

crystals. A glass can always be made to revert to its crystal form by

holding it at a temperature just below the melting point for a sufficiently

long time[18]. There will always be some tendency for an amorphous solid

to crystallise; in some cases, particularly for certain amorphous materials

prepared in thin film form, crystallisation occurs rapidly. For some

glasses, however, the rate of crystallisation (devitrification) is

negligible, even at high temperatures, and from a practical viewpoint

they are perfectly stable.

1.2   The preparation of non-crystalline solids

There are numerous methods of preparing solids in amorphous form,

the principal ones being:

(a) Thermal evaporation[20]: In this method the source material is

heated until it evaporates and then part of the vapour is allowed to

condense on a substrate to form a thin amorphous film.   This is probably

the commonest method of producing such films.   Electron beam bombardment

or an electric filament is usually used to heat the source material and the

process is carried out in a vacuum of 1μ or better.   The technique has

several disadvantages.   Firstly, the vapour is generally contaminated

with atoms from parts of the evaporation system, e.g. the filament or

the evaporation crucible, and so the films produced may contain a high

level of impurities.   Secondly, in the case of amorphous compounds the

evaporated film may not have the same composition as the source material,

due to differences in the evaporation rates of the atomic species involved.

Also, the structure of the film is affected by the temperature of the

substrate, T_s.   If $T_s < T_g$ the effective 'cooling rate' is extremely high

and the atoms deposited in the film cannot rearrange themselves to any

significant extent; the structure of the film will differ from that of

the corresponding glass, being more disordered and containing more broken

bonds.   If T_s is slightly greater than T_g the film will be annealed and

its structure will be similar to that of the glass.   As well as reducing

the amount of disorder in a film, annealing can also alter the nature of

its structure, for example non-annealed films of a-As_2S_3 are made up partly

of As_4S_6 molecules but annealing causes this molecular component to poly-

merise, so that the annealed film has the network structure characteristic

of the glass.

Flash evaporation[21] is a variant technique designed to overcome the problem of differential evaporation encountered when producing films of compounds. In this method the source material is fed onto a 'hearth' electrically heated to a sufficiently high temperature that the material evaporates virtually instantaneously.

(b) Sputtering[20]: This is also a widely used technique for preparing thin amorphous films. In this method atoms or groups of atoms are 'knocked out' of the source material by the impact of ions and are deposited on a substrate. A d.c. or r.f. field is used to accelerate the ions onto the source material. Argon ions are commonly used but in 'reactive' sputtering a gas that combines with the source material is used in order to deposit a compound. Unlike evaporation rates, sputtering yields do not vary markedly from one atomic species to another, so that when depositing compounds, the film composition is closer to that of the source material than it is in the case of thermal evaporation. Also, the structure and properties of sputtered films are generally closer to the structure and properties of the corresponding glasses than are those of thermally evaporated films. However, films prepared by this method are always contaminated with the sputtering gas.

(c) Glass formation by cooling a liquid[5]: The physical principles of glass formation were outlined above. In practice the process involves melting the source material and then cooling the melt quickly enough to prevent nucleation and crystal growth. Most liquids can, in principle, be cooled to form a glass: it is simply a question of attaining a suff- iciently rapid cooling rate. The cooling rates that can be achieved at present cover twelve orders of magnitude, viz $10^{-5} - 10^{7}$ °C/s. The former rate is used in the production of the annealed glasses used in optical equipment while the latter is used to produce certain metallic alloys in glassy form. Quenching rates in the range $10^{5} - 10^{7}$ °C/s are achieved

using the 'splat cooling' technique[22], in which very small droplets of the molten source material are projected at high velocity onto a cold metal substrate. However, even quenching rates as high as 10^7 °C/s are not sufficient to vitrify certain materials, e.g. molten alkali halides. Te, Ge, Si, B, GeTe and a number of other materials cannot be prepared in amorphous form by cooling from the melt; for these materials the bonding in the liquid state is generally radically different from that in the solid. Nevertheless, a wide range of materials can be prepared in amorphous form using this method.

For any glass-forming melt there will be a minimum or critical cooling rate required for glass formation and all rates in excess of this will result in vitrification. Hence all materials which form glasses can also be prepared in amorphous form by deposition from the vapour phase.

(d) Glow-discharge decomposition[23]: This is another technique for producing thin amorphous films. In this method an r.f. field is used to decompose a gas containing the element to be deposited; atoms of the element that are liberated in the decomposition are collected on a substrate. For example, a-Si can be prepared from silane, SiH_4, by this method. Amorphous compounds can be prepared by using a mixture of gases, e.g. a mixture of SiH_4 and N_2O yields a-SiO_2. The decomposition takes place at a relatively low temperature, the energy required being supplied by the r.f. discharge.

Spear and co-workers[23] have used this technique with considerable success to produce a-Si from SiH_4. They maintain that films prepared by glow-discharge decomposition contain many fewer broken bonds than films obtained by thermal evaporation or sputtering[24], but there is some controversy over whether the low level of broken bonds is due to the nature of the deposition process or simply to the incorporation of hydrogen atoms (from the SiH_4) in the structure[25]. The number of defects in an amorphous film is of practical importance for it determines

whether or not the film is suitable for substitutional doping, which is the basic process involved in the fabrication of a p-n junction; if there are too many defects the extra states arising from the added impurities will have little influence on the conduction processes in the material. Spear et al.[24] claim that the glow-discharge technique is the most suitable method for producing films capable of being used in the fabrication of amorphous p-n junctions.

There are various other methods of preparing amorphous materials, including vapour-phase pyrolysis or hydrolysis, electrolytic deposition from solution, chemical reaction and precipitation from solution, dessication, oxidation and loss of a volatile constituent. Certain crystals can be transformed to the amorphous state by shock waves or by irradiation with fast neutrons, gamma rays or ions, and in some cases the surface of a crystal can be amorphised by grinding or comminution. Some of the above methods, however, are applicable only to a very limited range of materials.

1.3 The classification of amorphous semiconductors

Amorphous materials do not belong exclusively to any one class of solid: there exist amorphous metals (e.g. alloys in the Cu-Zr and Au-La systems), amorphous semiconductors (e.g. a-Si and a-As_2Se_3) and amorphous insulators (e.g. a-SiO_2 and a-As_2O_3). The amorphous semiconductors can be divided into several chemically different groups, the principal three being:

   (i)   the tetrahedrally coordinated amorphous semiconductors such as a-Si, a-Ge and the amorphous III — V compounds;

   (ii) the transition-metal oxide glasses — in these the major constituent is a transition metal oxide such as V_2O_5;

   (iii) the chalcogenide amorphous semiconductors — these contain one or more of the chalcogen elements S, Se and Te.

It is the last group that is of most interest in the present case since

the glasses investigated in this study are all in the As-S or As-Se systems.

In the chalcogenides the elements S, Se and Te are usually combined with one or more of the elements from groups IV and V, e.g. Ge or As. a-As_2S_3 and a-As_2Se_3 are regarded as typical members of this group, though a-Se is probably the most studied chalcogenide material. Unlike the tetrahedrally coordinated amorphous semiconductors, which cannot be produced by cooling from the melt, most chalcogenides are readily prepared in glassy form; As_2Se_3 and As_2S_3 are particularly easy to vitrify, the latter forming a very stable glass. Also, the properties of amorphous chalcogenides are generally not as sensitive to the method and conditions of preparation as are those of the tetrahedrally coordinated materials; in particular, they are not significantly affected by the presence of impurities, though there are some exceptions to this.

A wide range of compositions in the As-S and As-Se systems can be prepared in vitreous form: the glass-forming region extends from 5 to 43 at.% As in the As-S system and from 0 to 55 at.% As in the As-Se system[26]. In this study compositions will generally be written in terms of atomic percentage, e.g. $As_{25}S_{75}$ rather than AsS_3. However, except when they are being discussed in relation to the non-stoichiometric glasses, those materials — particularly the crystals — which are better known by their molecular or empirical formulae will be referred to by those formulae, e.g. c-As_2S_3 rather than c-$As_{40}S_{60}$. Also, the terms 'As-rich', 'S-rich' and 'chalcogen-rich' that are used throughout this account will, unless otherwise stated, mean rich relative to the stoichiometric composition $As_{40}X_{60}$, X = S or Se.

1.4 Experimental methods for determining the structure of amorphous solids

X-ray, electron and neutron diffraction are the traditional techniques for determining the structure of condensed matter. These techniques provide information in the form of an r.d.f., from which can be deduced the

number of first nearest neighbours, the average separation between them, and the density of the material; bond angle distributions and rotations can also be derived[27]. The r.d.f. is of most use in the case of elemental amorphous solids since for amorphous compounds and alloys it is a convolution of the diffractions produced by the different types of atoms present and can thus be difficult to interpret. In particular, the mixing of diffractions in the case of amorphous compounds and alloys makes it difficult to identify r.d.f. features arising from 'wrong' or 'like-atom' bonds in such materials[28]. In principle the contribution to the r.d.f. from each type of atom in a multi-component system could be determined by making use of the fact that the dependence of the atomic scattering factor on incident wavelength is not the same for each atomic species, but this has not yet been done.

One general shortcoming of diffraction experiments is that the r.d.f. does not provide a sufficiently sensitive test for structural models: radically different models of the same material can yield a satisfactory fit to its r.d.f. For example the r.d.f.'s of the elemental amorphous solids a-Si and a-Ge can be fitted by a random network model containing numerous 5- and 7-fold rings[29] and also by one in which such rings are absent[30].

Hence although diffraction experiments provide much useful information they do not give a complete picture of the structure; in fact, there is no one experimental technique that can be used to uniquely specify the structure of an amorphous solid and a complete picture can only be obtained by using a variety of techniques in conjunction. Other methods of structural determination include nuclear magnetic resonance, nuclear quadrupole resonance, electron spin resonance, optical and electron microscopy, density measurement, calorimetry, and vibrational spectroscopy, which is discussed in more detail in the following section. Of particular importance is the new technique of extended X-ray absorption fine structure

which seems a promising method for deconvolving the structural features
of multi-component amorphous solids[31].

1.5   The vibrational spectroscopy of amorphous solids

Vibrational spectroscopy is an indirect method of structural deter-
mination in which information on the structure is derived from the
infra red (i.r.) or Raman spectrum of the material.   The frequencies at
which the atoms in a substance vibrate against one another are determined
mainly by the atomic masses — which are well known —, the interatomic
forces and the structure, and hence structural information can be deduced
from a knowledge of the vibrational frequencies and the interatomic
potential[28].   In some instances information, such as the identity of
discrete molecular species, can be obtained by comparison with known
spectra;   for example the presence of S_8 rings in an As-S glass can be
established by comparing its vibrational spectrum with that of the S_8 ring
(see Section 5.5.2).

Raman and i.r. spectroscopy may generally be regarded as complementary
techniques and usually both must be employed in order to obtain a complete
determination of the vibrational spectrum of a material.   This is because
vibrations which give rise to intense Raman(i.r.) lines sometimes contribute
only weakly — or even not at all — to the i.r.(Raman) spectrum.   In the
case of amorphous materials, however, such complementarity of i.r. and Raman
spectra is less common since the structural disorder leads to a relaxation
of the selection rules governing i.r. and Raman activity.   Thus in general
more information is contained in the individual spectra of non-crystalline
solids than in those of crystals.

In the case of crystals i.r. and Raman spectroscopy provide information
on not only the frequencies of the vibrations but also their symmetry
properties.   For amorphous materials, however, only Raman scattering can
yield any information on the symmetry properties, because only the Raman

process involves a tensor quantity (the polarisability). This gives Raman scattering an advantage over i.r. spectroscopy in the study of amorphous materials.

The structural information that can be obtained from the vibrational spectra of non-crystalline solids largely relates to the local bonding: the types of covalent bond present in the material can be identified (hence the technique is suitable for detecting like-atom bonds[28]) and the basic structural units of the material can be deduced. Also, if molecular species or phase-separated materials are present they can be identified by comparison with known spectra.

In certain cases vibrational spectroscopy not only reveals the nearest-neighbour atomic arrangements but also yields information on the atomic arrangements over larger regions. In the case of Ge-Se glasses, for example, vibrational spectroscopy has identified the basic structural unit as a $GeSe_4$ tetrahedron and has shown that these tetrahedra are generally positioned in such a way that they form larger structural elements, viz 10- to 16-membered rings[32]. Similarly, DeFonzo and Tauc[33] have shown that it is possible to deduce from the vibrational spectrum of a-As_2S_3 'not only that a well-defined unit exists but also that certain correlations between these units are preferred' (the units in this instance are AsS_3 pyramids). Also, in the case of molecular amorphous solids vibrational spectroscopy can yield information on the packing of the molecules[34].

Further information on the structure of an amorphous solid beyond the first coordination sphere can be obtained from the low-frequency region of the light-scattering spectrum, for it is possible to determine the structural correlation range (s.c.r.) from this region[35 — 39]. The s.c.r. is one of the key parameters specifying the structure of a disordered material and is the characteristic length over which the positions of atoms in the solid are correlated. Raman scattering has

been used to determine the s.c.r. of a-Se[36], a-As$_2$O$_3$[37], a-GeS$_2$[38,39], a-GeSe$_2$, a-As$_2$S$_3$, a-As$_2$Se$_3$ and amorphous alloys in the $(As_2S_3)_{1-x}(GeS_2)_x$ system[39].

As well as yielding information on the structure of amorphous materials, vibrational spectroscopy, of course, provides information on their vibrational excitations.   For many amorphous materials one can derive from the i.r. or Raman spectrum a reasonable approximation to the vibrational density of states[40,41], which can then be used to calculate other thermodynamic quantities such as specific heat.   This is not possible in the case of the chalcogenide glasses but even for them, much information on the phonons can be obtained from the vibrational spectra: for example, from a Raman study of the light-induced crystallisation of a-As$_2$Se$_3$ Finkman et al.[42] were able to deduce the approximate shape of the phonon dispersion curves in c-As$_2$Se$_3$.   Also, it is possible to obtain through light-scattering and i.r. experiments information on the anomalous low-temperature thermal effects which are exhibited by non-crystalline solids and which are currently of great interest: i.r. spec-troscopy[43] and Raman and Brillouin scattering[44,45] have been used to investigate the nature of the very low frequency vibrational states thought to be responsible for these effects.

As well as having certain general advantages over other techniques used in the analysis of amorphous solid structure, Raman spectroscopy is an ideal tool for investigating the photo-induced structural changes that take place in some of these materials[28,46 — 48].   The photo-induced processes that occur (e.g. crystallisation, dissociation, phase separation and polymerisation) usually involve molecular species or crystal products and Raman spectroscopy is a sensitive method of detecting these; also, the molecules or crystals concerned can often be identified simply by comparison with known spectra.   For example, X-ray diffraction studies of as-deposited evaporated a-As$_2$S$_3$ films show that they are composed

of densely packed As_4S_6 molecules which polymerise on illumination or annealing to form the network structure characteristic of the bulk or sputtered material[49]; Raman experiments, however, indicate firstly that not only are As_4S_6 molecules present in the as-deposited films but also other species such as As_4S_4, and secondly that the films contain a considerable amount of polymeric As_2S_3 to begin with[46].

Raman scattering also has certain practical advantages over other methods of analysis. For example, both Raman scattering and X-ray diffraction can be used to test nominally amorphous samples for traces of crystallinity but the former method is considerably quicker: Brodsky[48] reports that the Raman examination of an a-Si film can be completed 'in about 5 minutes compared with the several hours required for diffraction'.

Possibly one of the most important advantages of Raman spectroscopy as a structural probe of amorphous solids is that it can also be used to relate the electronic properties of these materials to their structure. The electronic properties of non-crystalline solids differ in many respects from those of crystalline materials and one of the fundamental questions in the study of the amorphous state is how these differences result from the difference in the structural nature of these two classes of solid. Light scattering can be used to investigate electronic states because the coupling of the incident light to the vibrations in a material involves these states. Information on the electronic states is obtained by monitoring the Raman spectrum as a function of the frequency of the light used to excite the spectrum: as this frequency approaches the frequency of an electronic transition of the material the scattering efficiency of those Raman bands associated with the vibration involving this transition is enhanced, so that one observes resonances in the spectra (hence the technique is known as resonance Raman spectroscopy). So far the technique has mainly been applied to $a-As_2S_3$ [50 — 52], where it has been used to

investigate the nature of the states in the region of the absorption edge and to determine the structural origin of defect states. Resonance Raman scattering has also been studied in a-Se[53] and a-Si[54].

1.6 Aims of the present work

The present study is part of a more general investigation being carried out in these laboratories into the properties and applications of amorphous semiconductors. Other projects in this programme include photomobility measurements in As_2Te_3, As-Se, As_2Se_3-As_2Te_3 and in multi-component glasses, photoconductivity in As_2Te_3, As-Se and multicomponent glasses, transit-time drift mobility measurements in a-Se and As-Se glasses, optical absorption in As-Se and Cu-As-Se glasses and conductivity, thermopower and optical absorption measurements in V_2O_5-TeO_2 glasses. The use of amorphous chalcogenides as solid-state switches and ion-selective electrodes is also being studied.

The aim of the present study is to obtain information on the structure of glasses in the As-S and As-Se systems using Raman spectroscopy as the structural probe. The reason for investigating a range of glasses in these systems is two-fold: firstly, while the properties of the prototype chalcogenide glasses As_2S_3 and As_2Se_3 have been extensively studied, research into the non-stoichiometric glasses has been limited, and secondly, determining how properties change as a function of composition is often of value in understanding the physics of amorphous materials. In the present case, measuring the spectra of the non-stoichiometric glasses will not only yield structural information on them, but will also help in interpreting the spectra of the compound compositions As_2S_3 and As_2Se_3.

As well as being of general use, the information obtained in this study will form the basis of a future project in which it is hoped to relate the electrical properties of these glasses to their structure.

This project will use the technique of resonance Raman scattering, described in the previous section.   Also, the structural information obtained in this study will provide a starting point for investigating the potentially useful photostructural changes that occur in these materials.

1.7   References

1.   Lonsdale, K., 'Crystals and X-rays', Bell, London, 1948.

2.   Sachs, M., 'Solid State Theory', McGraw-Hill, New York, 1963.

3.   Ziman, J., J. Phys. C 2, 1704 (1969).

4.   Mott, N.F. and Davis, E.A., 'Electronic Processes in Non-Crystalline Materials', Clarendon Press, Oxford, 1971.

5.   Owen, A.E., Contemp. Phys. 11, 227 (1970).

6.   Eckstein, B., Mat. Res. Bull. 3, 199 (1968).

7.   Finney, J.L., in 'The Structure of Non-Crystalline Materials' (Gaskell, P.H., editor), Taylor and Francis, London, 1977, p. 35.

8.   Randall, J.T., Rooksby, H.P. and Cooper, B.S., J. Soc. Glass Tech. 14, 219 (1930).

9.   Ninomiya, T., in 'The Structure of Non-Crystalline Materials' (Gaskell, P.H., editor), Taylor and Francis, London, 1977, p. 45.

10.   Richter, H. and Breitling, G., Mat. Res. Bull. 4, 19 (1969).

11.   Moss, S.C. and Graczyk, Proc. 10th Int. Conf. on the Physics of Semiconductors, Cambridge, Mass., U.S.A.E.C., 1970.

12.   Grigorovici, R. and Manaila, R., Thin Solid Films 1, 343 (1967).

13.   Turnbull, D. and Polk, D.E., J. Non-Cryst. Solids 8 — 10, 19 (1972).

14.   Rudee, M.L. and Howie, A., Phil. Mag. 25, 1001 (1972).

15.   McFarlane, S.C. and Cochran, W., J. Phys. C 8, 1311 (1975).

16.   Stobbs, W.M., in 'The Structure of Non-Crystalline Materials' (Gaskell, P.H., editor), Taylor and Francis, London, 1977, p. 253.

17.   Zachariasen, W.H., J. Am. Chem. Soc. 54, 3841 (1932).

18.   Koerber, G.G., 'Properties of Solids', Prentice-Hall International, London, 1962.

19.   Jones, G.O., 'Glass', Methuen, London, 1956.

20. 'Handbook of Thin Film Technology' (Maissel, L.I. and Glang, R., editors), McGraw-Hill, New York, 1970.

21. Beam, W.R. and Takahashi, T., Rev. Sci. Instr. $\underline{35}$, 1623 (1964).

22. Chen, H.S., in 'The Structure of Non-Crystalline Materials' (Gaskell, P.H., editor), Taylor and Francis, London, 1977, p.79.

23. Spear, W.E. and Le Comber, P.G., 7th Int. Conf. on Amorphous and Liquid Semiconductors, Edinburgh (Spear, W.E., editor), C.I.C.L., Edinburgh, 1977, p.309.

24. Spear, W.E. and Le Comber, P.G., Solid State Commun. $\underline{17}$, 1193 (1975).

25. Fritzsche, H., Proc. 7th Int. Conf. on Amorphous and Liquid Semiconductors, Edinburgh (Spear, W.E., editor), C.I.C.L., Edinburgh, 1977, p.3.

26. Flaschen, S.S., Pearson, A.D. and Northover, W.R., J. Am. Ceram. Soc. $\underline{42}$, 450 (1959).

27. Grigorovici, R., in 'Electronic and Structural Properties of Amorphous Semiconductors' (Proc. Scottish Univ. Summer School in Physics, Aberdeen, Aug. 1972) (Le Comber, P.G. and Mort, J., editors), Academic Press, London, 1973, p.191.

28. Solin, S.A., A.I.P. Conf. Proc. $\underline{31}$, 205 (1976).

29. Polk, D.E., J. Non-Cryst. Solids $\underline{5}$, 365 (1971).

30. Connell, G.A.N. and Temkin, R.J., Phys. Rev. B $\underline{9}$. 5323 (1974).

31. Sayers, D.E., Proc. 7th Int. Conf. on Amorphous and Liquid Semiconductors, Edinburgh (Spear, W.E., editor), C.I.C.L., Edinburgh, 1977, p.61.

32. Nemanich, R.J., Solin, S.A. and Lucovsky, G., Solid State Commun. $\underline{21}$, 273 (1977).

33. DeFonzo, A.P. and Tauc, J., Solid State Commun. $\underline{18}$, 937 (1976).

34. Martin, R.M. and Lucovsky, G., Proc. 12th Int. Conf. on the Physics of Semiconductors, Stuttgart (Pilkuhn, M.H., editor), Teubner, Stuttgart, 1974, p.184.

35. Martin, A.J. and Brenig, W., Phys. Stat. Sol. (b) $\underline{64}$, 163 (1974).

36. Gorman, M. and Solin, S.A., Solid State Commun. $\underline{18}$, 1401 (1976).

37. Solin, S.A., Phys. Rev. B $\underline{13}$, 1741 (1976).

38. Nemanich, R.J., Gorman, M. and Solin, S.A., Solid State Commun. $\underline{21}$, 277 (1977).

39. Nemanich, R.J., Phys. Rev. B $\underline{16}$, 1655 (1977).

40. Shuker, R. and Gammon, R.W., Phys. Rev. Lett. $\underline{25}$, 222 (1970).

41. Shuker, R. and Gammon, R.W., Proc. 2nd Int. Conf. on Light Scattering in Solids, Paris (Balkanski, M., editor), Flammarion, Paris, 1971, p.334.

42. Finkman, E., DeFonzo, A.P. and Tauc, J., Proc. 12th Int. Conf. on the Physics of Semiconductors, Stuttgart (Pilkuhn, M.H., editor), Teubner, Stuttgart, 1974, p.1022.

43. Bosch, M.A., Phys. Rev. Lett. 40, 879 (1978).

44. Winterling, G., Phys. Rev. B 12, 2432 (1975).

45 Winterling, G., Proc. 3rd Int. Conf. on Light Scattering in Solids, Campinas, Brazil, Flammarion, Paris, 1975, p.663.

46. Solin, S.A. and Papatheodorou, G.N., Phys. Rev. B 15, 2084 (1977).

47. deNeufville, J.P., in 'Optical Properties of Solids — Recent Developments' (Seraphin, B.O., editor), North-Holland, Amsterdam, 1975.

48. Brodsky, M.H., in 'Light Scattering in Solids' (Cardona, M., editor), Springer-Verlag, Berlin, 1975, p.208.

49. deNeufville, J.P., Moss, S.C. and Ovshinsky, S.R., J. Non-Cryst. Solids 13, 191 (1974).

50. Kobliska, R.J. and Solin, S.A., Solid State Commun. 10, 231 (1972).

51. Razzetti, C. and Fontana, M.P., Phys. Stat. Sol. (b) 70, 173 (1975).

52. Howard, R.E., Macedo, P.B. and Moynihan, C.T., Solid State Commun. 17, 1475 (1975).

53. Zakharova, N.B. and Chekasov, Yu.A., Sov. Phys. Solid State 12, 1572 (1971).

54. Bermejo, D., Cardona, M. and Brodsky, M.H., Proc. 7th Int. Conf. on Amorphous and Liquid Semiconductors, Edinburgh (Spear, W.E., editor), C.I.C.L., Edinburgh, 1977, p.343.

CHAPTER 2

THE STRUCTURE OF MATERIALS IN THE As-S AND As-Se SYSTEMS

2.1   Introduction

When determining the structure of an amorphous solid it is useful to know the structure of the related crystals; also, since no single technique can give a complete picture of the structure of a disordered material it is necessary to utilise information from all types of measurements.   Consequently, this chapter surveys the existing information on the structure of crystalline and amorphous solids in the As-S and As-Se systems.   Only information obtained by techniques other than vibrational spectroscopy is included in this survey; information derived from i.r. and Raman experiments is presented elsewhere.

2.2   Structure of the crystals

2.2.1 $c\text{-}As_2S_3$

Morimoto[1] and Mullen and Nowacki[2] have shown that arsenic trisulphide crystallises in a monoclinic structure, the space group being $P2_1/n$ (C_{2h}^5).   The unit cell dimensions are a = 11.475, b = 9.577 and c = 4.256 Å.   The angle between the a and c crystallographic axes is $90° 41'$ [2]; because this is almost a right angle the structure can be considered as orthorhombic for many purposes[3,4].

The atomic arrangement in $c\text{-}As_2S_3$, which is a layer crystal, is shown in Figure 2.1; Figure 2.1(a) shows part of a single layer as viewed along the normal to the layer plane while Figure 2.1(b) shows the layers edge on. The layer planes are parallel to the ac plane and perpendicular to the b axis so that   Figure 2.1(a) is a projection along the [010] direction and Figure 2.1(b) is a projection along the [001] direction.   Figure 2.1(b) shows that the alignment of adjacent layers is determined mainly by packing considerations.

Figure 2.1

The atomic arrangement in c-As$_2$S$_3$. (a) A view along the b axis, looking down on a single layer. (b) A view along the c axis, looking at the layers edge on. The five inequivalent atoms in the unit cell are labelled in (b).

(a)

(b)

○ As   ● S
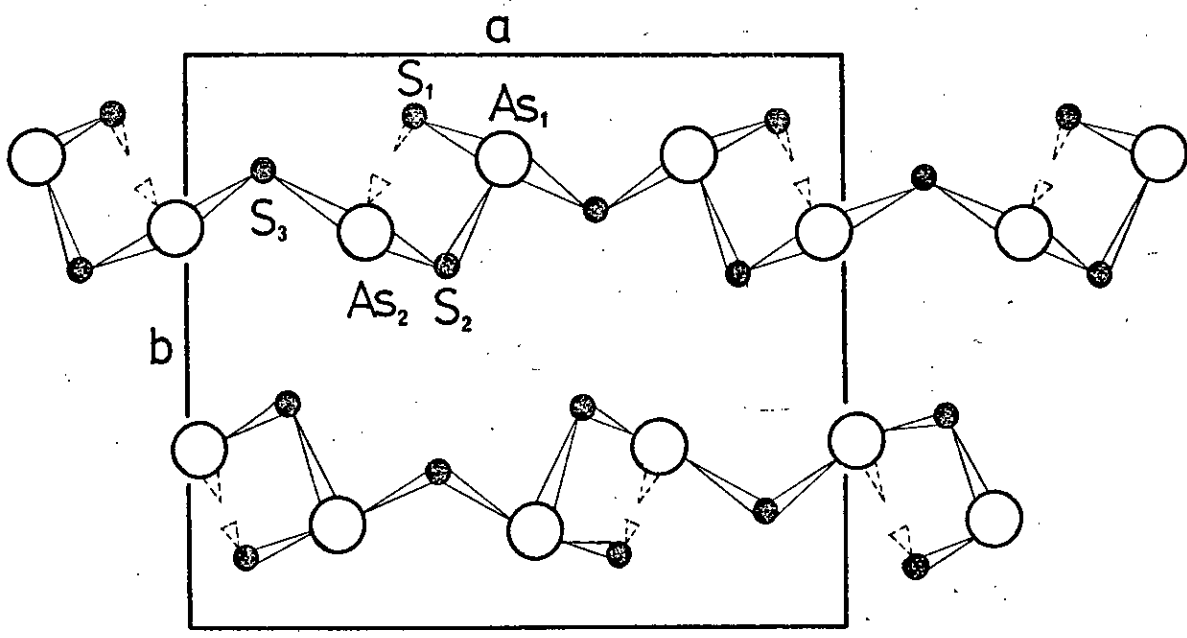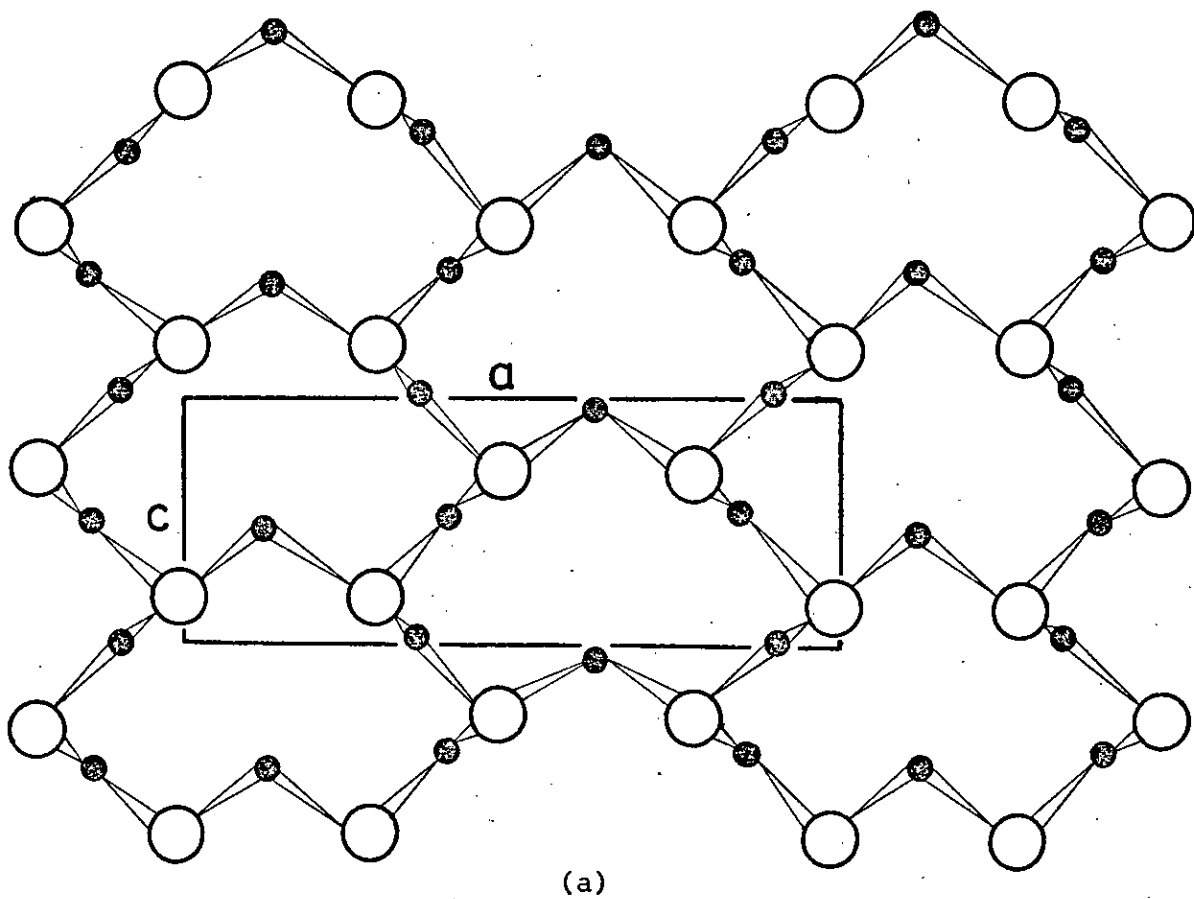
c-As_2S_3 can be regarded as a molecular crystal in which the molecular unit is a layer infinitely extended in two dimensions. In directions parallel to the layers, this crystal is a network solid while in the direction perpendicular to the layers it is a molecular solid.

In accordance with the 8-n rule each As atom is covalently bonded to three S atoms while each S atom is covalently bonded to two As atoms. These covalent bonds are only formed between atoms in the same layer, so that there is no cross-linking of the layers. The bonding between layers is primarily of the weak, van der Waals type. As a result of this very weak interlayer bonding c-As_2S_3 exhibits perfect micaceous cleavage parallel to the layer plane[2,4].

The relation of the unit cell axes a, b and c to the atomic arrangement is also indicated in the diagrams of Figure 2.1. There are twenty atoms in the unit cell — eight arsenics and twelve sulphurs. However, only two of the As atoms are inequivalent and only three of the S atoms are so; these inequivalent atoms are labelled As_1, As_2, S_1, S_2 and S_3 in the figure. Figure 2.1(b) shows that the unit cell contains segments from two layers.

It is clear from Figure 2.1 that the basic structural unit of the layers is an AsS_3 pyramid. Each pyramid is linked to three neighbouring AsS_3 units via the three shared S atoms at its base. In fact the AsS_3 units that make up c-As_2S_3 are not identical: two types of pyramid can be identified in the structure. The pyramids adjacent to any particular pyramid of one type are always of the other type, so that the basic structural unit of the crystal is really a linked pair of these two different AsS_3 pyramids[5]; such a pair is shown in Figure 2.2(a). Allowing for the S atoms that are shared with other pyramids there are five atoms per pair-unit; all five inequivalent atoms in the crystal unit cell are represented in the pair-unit.
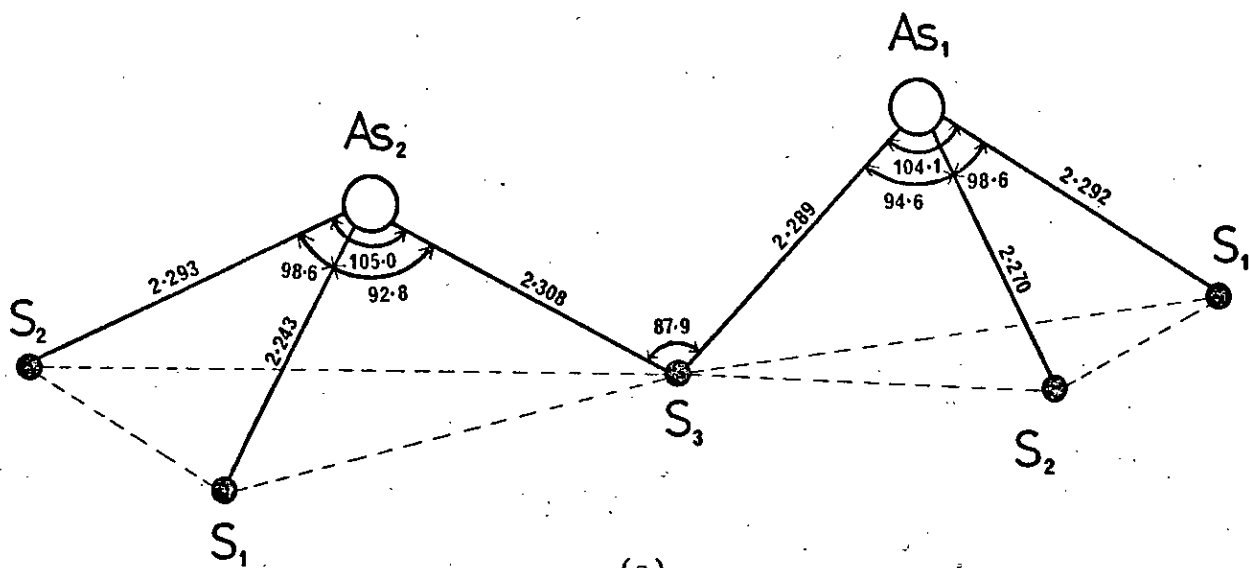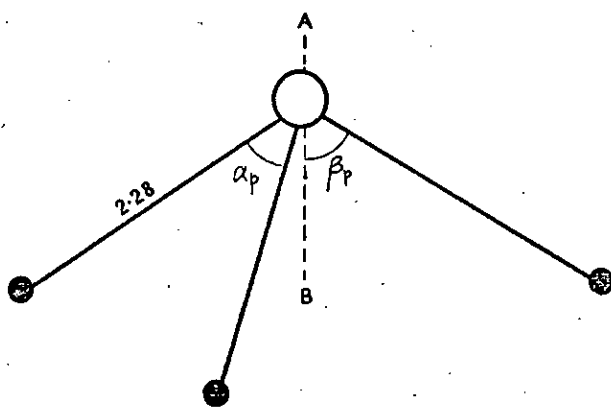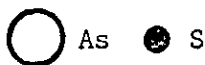
Figure 2.2

(a) The basic structural unit of c-As_2S_3.

(b) The 'average' pyramid based on the structure of the c-As_2S_3 units: the pyramid is regular and its bond length and apex angle are the average values for the crystal units. AB is the three-fold axis.

Data on the geometry of the two types of AsS_3 pyramid — which are both irregular — is given in the figure. The average As–S bond length for the AsS_3 units is 2.28 Å and the average of their S–As–S angles 98.95° (since the crystal is made up of a number of pair-units identical with the one shown, these average values also apply to the crystal as a whole). Both types of pyramid are fairly shallow. It is noteworthy that the smallest interatomic separation between the layers is 3.24 Å [2], which is ~42% greater than the average As–S bond length. This reflects the fact that the bonding between the layers is much weaker than the intralayer bonding.

It is clear from Figure 2.2(a) that although the two types of pyramid are not identical they are similar, and in practice it is often sufficient to consider a single pyramid based on the structures of the two types. If this average pyramid is taken, for simplicity, to be regular then it is specified by a single bond length and apex angle, and these parameters can be set equal to the average values given above. Such an average pyramid is shown in Figure 2.2(b). The pyramidal angle, β_p, of a regular pyramid is defined as the angle between the axis of symmetry (AB in the figure) and any of the three edges that intersect it (in the present case the As–S bonds form these edges); β_p is related to the apex angle, α_p, by the relation

$$\sin \beta_p = \frac{2}{\sqrt{3}} \sin (\alpha_p/2) \qquad (2.1)$$

The value of β_p for the approximate pyramid (for which $\alpha_p = 98.95°$) is 61.4°. This average pyramid will be of use later in determining the vibrational frequencies of vitreous As_2S_3.

Ito et al.[6] consider the layers of c-As_2S_3 to be composed of —As–S–As–S— spiral chains running parallel to one another in the c direction. The chains are linked to each other by sulphur bridges between neighbouring As atoms in adjacent chains. The bridging S atoms and the spiral chains (viewed end on) are obvious in Figure 2.1(b). Figure 2.3(c) (after p.28) shows one of the chains viewed along a direction normal to the c axis.

The repetition length of the chain is simply the length of the unit cell side c, i.e. 4.256 Å. It is noteworthy that the As—S—As angles in the chain differ considerably from the As—S—As angle at the S atoms bridging the chains: the angle As_1—S_3—As_2 is 87.9° but the angles As_1—S_1—As_2 and As_1—S_2—As_2 are 103.7° and 101.0° respectively[2].

As well as chains, rings can also be identified in the structure of c-As_2S_3. These rings are obvious in Figure 2.1(a) which shows them viewed along the normal to the planes in which they lie. The rings are puckered and have twelve members. The ring diameter is ~8.3 Å in the a direction and is equal to the unit cell side c (4.256 Å) in the c direction.

c-As_2S_3 occurs in nature as the yellow mineral orpiment. No polymorphs have been reported at room temperature and pressure; a red modification is known to exist but it has not been determined whether this material has a different crystal structure to orpiment or whether it simply contains impurities[7]. It is well established that when orpiment is heated above ~170° C it transforms to a red modification β-As_2S_3[8 — 11] which is structurally different to orpiment. At high temperatures and high pressures two other polymorphs occur, ζ- and ϵ-As_2S_3[12].

2.2.2   c-As_4S_4

The structure of c-As_4S_4 has been determined by several workers[2,6,13,14]. Porter and Sheldrick[13] have shown that this material occurs in two polymorphic forms, α- and β-As_4S_4, α-As_4S_4 being identical with the mineral realgar; the crystal structure of both polymorphs is monoclinic. In the case of α-As_4S_4 the space group is $P2_1/n$ and the unit cell parameters have the following values: a = 9.325, b = 13.571, c = 6.587 Å and β = 106° 23'[2]. For β-As_4S_4 the space group is C2/c and the unit cell dimensions are a = 9.957, b = 9.335, c = 8.889 Å and β = 102.48°[13]. The unit cell volumes for the two

polymorphs are similar, being 797.4 and 806.7 $\mathring{A}^3$ for the α and β forms respectively[13].

Both polymorphs consist of discrete, covalently bonded As_4S_4 molecules bound to one another by van der Waals forces. The As_4S_4 molecules of the α modification are identical with those of the β form but the packing of the molecules is different in the two polymorphs. The As_4S_4 molecule, which is of D_{2d} symmetry, has the cradle-like structure shown in Figure 2.3(a) (see also Figure 2.4(a) after p.32); the four S atoms and the four As atoms form a square and a tetrahedron respectively, with the square cutting through the tetrahedron in the middle.

The average values of the As—S and As—As covalent-bond lengths are 2.237 and 2.569 $\mathring{A}$ respectively. The As_4S_4 molecule of the crystals is almost identical with the gaseous As_4S_4 molecule[15,16]. The α and β polymorphs both have four As_4S_4 molecules in the unit cell. The shortest intermolecular As···As distance in α-As_4S_4 is considerably longer than that in β-As_4S_4, being ~3.51 $\mathring{A}$ in the former and ~3.97 $\mathring{A}$ in the latter.

Although the bond lengths and bond angles of c-As_4S_4 are similar to those of c-As_2S_3, there appears, at first sight, to be little similarity between the structures of the two crystals: c-As_4S_4 is made up of small discrete molecules while c-As_2S_3 is formed from layers effectively infinite in extent. Ito et al.[6], however, have shown that on closer inspection the structures of the two crystals are remarkably similar; both structures are in fact made up of the same basic unit.

The As_4S_4 molecule is in the form of a closed loop, as Figure 2.3(b) shows, and can be divided into two virtually identical halves; by rotating the molecule about an axis passing through the mid-points of the two As—As bonds (these are omitted in Figure 2.3(b)) it can be brought into approx-imate coincidence with itself. The four atoms labelled A — D make up one of the halves of the As_4S_4 molecule; these atoms are arranged in the order

(a)

(b)

○ As

● S

(c)
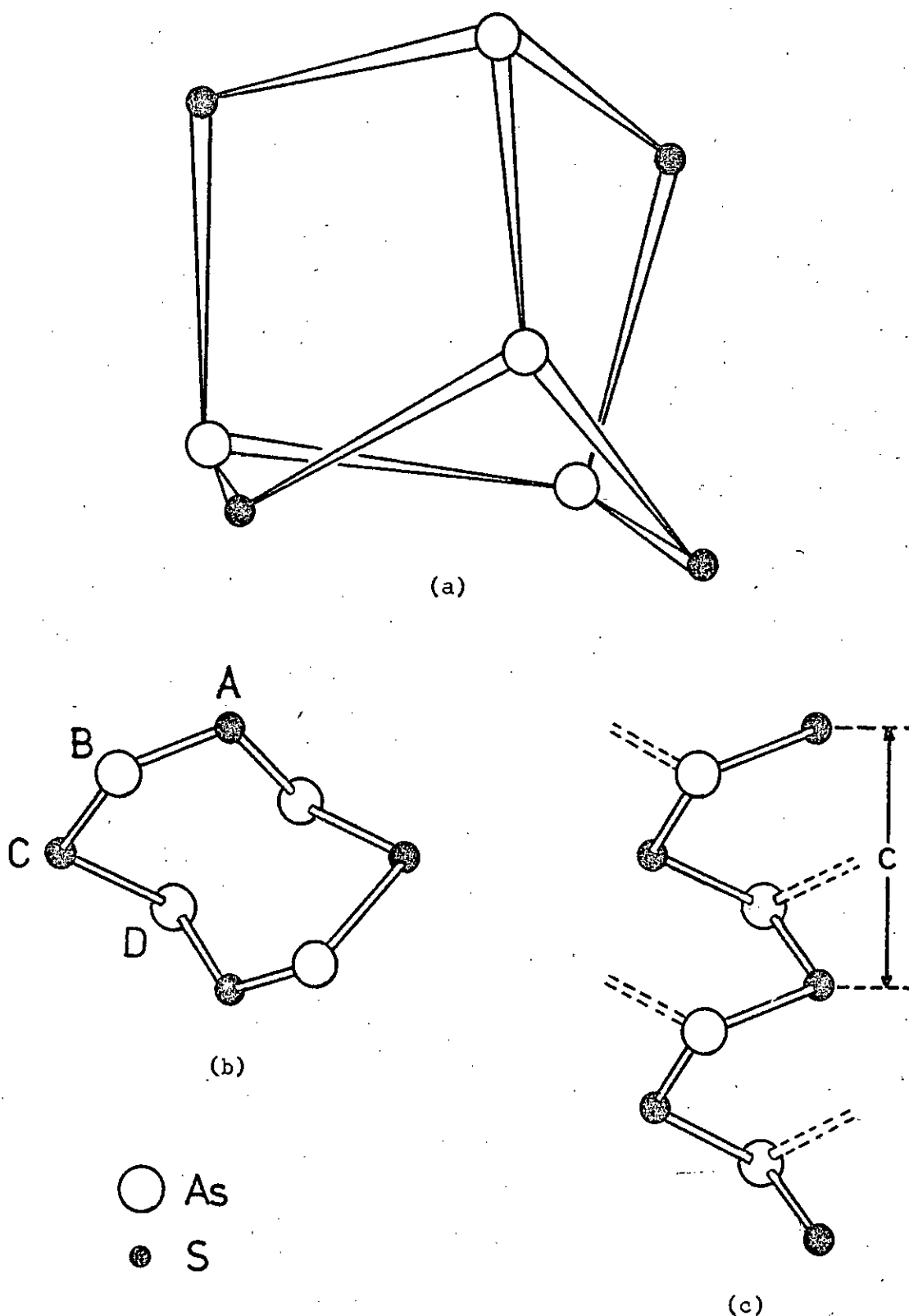
Figure 2.3

(a) The realgar molecule, As_4S_4.

(b) The As_4S_4 molecule oriented to emphasise its closed loop form (the As—As bonds are omitted).   (After Reference 6.)

(c) The spiral chains that can be generated from the molecule; c is the repeat length.   (After Reference 6.)

S—As—S—As and form a spiral. If a number of these As_2S_2 spiral units are identically oriented and placed end to end one obtains a chain running in the direction of the spiral axis (see Figure 2.3(c)). These chains are almost identical with those observable in the $c-As_2S_3$ structure (see p.26). To account for stoichiometry in the case of $c-As_2S_3$ there must be an additional S atom with every As_2S_2 unit; these extra S atoms form the bridges between neighbouring chains.

According to some workers[6,17,18] $c-As_4S_4$ changes readily to $c-As_2S_3$ on exposure to light. Ito et al.[6] suggest that the ease with which the transformation occurs is a result of the similarity of the basic structural units of these two crystals. Porter and Sheldrick[13], however, find no evidence for the formation of $c-As_2S_3$ when α- and $\beta-As_4S_4$ are illuminated although they do find that the two polymorphs undergo some light-induced structural change. These authors suggest that the discrete As_4S_4 molecules polymerise on irradiation, presumably forming a network containing As—As bonds.

2.2.3 $c-As_4S_3$

$c-As_4S_3$ exists in two polymorphic forms, α- and $\beta-As_4S_3$; both polymorphs occur in nature, the corresponding minerals being α- and β-dimorphite. The structure of the two modifications has been determined by Whitfield[19,20]. The crystal structure of both polymorphs is ortho-rhombic, the unit cell dimensions being a = 9.12, b = 7.99 and c = 10.10 Å in the case of $\alpha-As_4S_4$, and a = 11.21, b = 9.90 and c = 6.58 Å in the case of $\beta-As_4S_4$. For both crystals the space group is Pnma. The unit cell volumes are similar, being 736.0 and 730.2 $Å^3$ for the α and β forms respectively.

The two polymorphs consist of discrete, covalently bonded As_4S_3 molecules bound to each other by van der Waals forces. The As_4S_3 molecules of the α form are identical with those of the β form and have the structure

shown in Figure 2.4(b); the four As atoms are at the corners of a tetra-hedron and the three S atoms form bridges along the three adjacent apical edges. The molecule is of C_{3v} symmetry. The average values of the As—S and As—As covalent-bond lengths are 2.21 and 2.45 Å respectively. The α and β polymorphs both have four molecules in the unit cell. The shortest intermolecular As···As and As···S distances in α-As_4S_3 are 3.60 and 3.47 Å respectively, compared with 3.83 and 3.47 Å respectively in the case of β-As_4S_3. β-As_4S_3 is stable at room temperature but transforms to α-As_4S_3 on heating above 130° C.

2.2.4   c-As_4S_5

c-As_4S_5 is less well known than the other crystalline phases in the As–S system. The structure of this material, which is not naturally occurring, has been determined by Whitfield[21]. The crystal is mono-clinic, with space group $P2_1/m$, and the unit cell dimensions are a = 7.98, b = 8.10, c = 7.14 Å and β = 101.0°. The unit cell volume is 453 Å^3.

c-As_4S_5 is made up of discrete, covalently bonded As_4S_5 molecules having the structure shown in Figure 2.4(c). The As_4S_5 molecules, of which there are two in the unit cell, are linked to one another by van der Waals forces and form strings parallel to the b axis of the crystal. The As_4S_5 molecule is of C_{2v} symmetry. The average value of the As—S covalent-bond length is 2.24 Å and the single As—As bond has a length of ~2.55 Å. The shortest intermolecular As···S distance is 3.37 Å.

2.2.5   c-As_2Se_3 and c-As_4Se_4

Since c-As_2Se_3 and c-As_4Se_4 have been shown to be isomorphic with the corresponding sulphide crystals much of the discussion in Sections 2.2.1 and 2.2.2 is applicable to these two materials also; the structures of c-As_2Se_3[22,23] and c-As_4Se_4[23,24] differ only in detail from those of orpiment and realgar. The mean As—Se bond length is 2.40 Å in c-As_2Se_3 and 2.38 Å in c-As_4Se_4[23].

2.2.6   Other As-S and As-Se crystals

There are a number of crystals in the As-S system whose existence is in dispute or has not been confirmed.   In order of increasing S content they are:

As_3S: In the first quarter of this century two reports[25,26] appeared describing methods of preparing a solid compound having the formula As_3S. Its existence was not generally accepted[8] and a more recent investigation[27] asserts that it definitely does not exist. As_3S molecules, however, have been observed in the vapour of some As-Se-S compounds[28].

As_4S_4: A new isomeric form of As_4S_4 has recently been reported[29]. Like realgar, this new crystal is a molecular solid made up of discrete As_4S_4 units bound to one another by van der Waals forces.   However, the structure of the molecule in the new form is significantly different from that of the realgar molecule: the four As and four S atoms in the new molecule are arranged as shown in Figure 2.4(d).   The crystal structure is monoclinic and the unit cell parameters are a = 11.193, b = 9.994, c = 7.153 Å and β = 92.8°.   The space group of the crystal is $P2_1/n$.

$As_2S_{2.15}$: Crystals with the non-stoichiometric composition $As_2S_{2.15}$ have recently been reported[30,31].   The crystals are made up of As_4S_4 realgar molecules with a small number of S atoms randomly distributed in the lattice. The crystal structure is monoclinic and the unit cell parameters are a = 9.89, b = 9.46, c = 9.05 Å and β = 103°.   The unit cell contains four $(As_4S_4 + S_{0.3})$ units.   The space group of the crystal is Cc.

As_2S_5: The existence of a solid compound As_2S_5 is well established.   The majority of chemistry texts list As_2S_5 as one of the principal sulphides of As along with As_2S_3 and As_4S_4, and describe the method for producing it chemically[32 — 34].   Generally, though, the structure of this solid is not specified.   It has been asserted that As_2S_5 exists only in amorphous form[34], in which case it is perhaps misleading to put it in the same

category as As_2S_3, As_4S_4 and the other arsenic sulphide compounds since a wide range of As-S compositions can be prepared in amorphous form and As_2S_5 is not exceptional in any way (any As-S mixture containing between 5 and 43 at.% As can be made into a glass). A crystalline form of As_2S_5 does, however, exist at high temperatures and pressures: above 250° C and at pressures between 50 — 70 kilobars a-As_2S_5 crystallises in an orthorhombic structure having unit cell parameters a = 10.37, b = 9.9 and c = 8.66 Å [35].

c-As_4Se_3 has recently been synthesised[36] (it occurs in two polymorphic forms) and As_3S_4, As_3Se and As_3Se_4 molecules have been observed in the vapour of certain As-S-Se and As-Se compounds[28] but no solids having these formulae have been reported. As_4S_6 molecules have been observed in the vapour from orpiment[15] and are also believed to be present in non-annealed evaporated films of a-As_2S_3[37 — 39] but there is no crystalline compound corresponding to arsenolite, a stable polymorph of As_2O_3 consisting of As_4O_6 molecules.

2.2.7 Arsenic

There are two crystalline forms of arsenic, rhombohedral and orthorhombic As (arsenolamprite). Rhombohedral As consists of double layers in which each atom is bonded to three neighbours, the layers being held together by weak mesomeric bonds[40]. The unit cell parameters are a = 4.132 Å and α = 54.126°. There are 6 atoms in the unit cell and the space group of the crystal is D_{3d}^5 [41].

Orthorhombic As also consists of layers; it is isostructural with black phosphorous. The unit cell contains 8 atoms and has the dimensions a = 3.63, b = 4.45 and c = 10.96 Å [42]. The space group of the crystal is V_h^{18}.

2.2.8 Sulphur

There are numerous solid allotropes of sulphur but the only modification thermodynamically stable at room temperature and pressure is
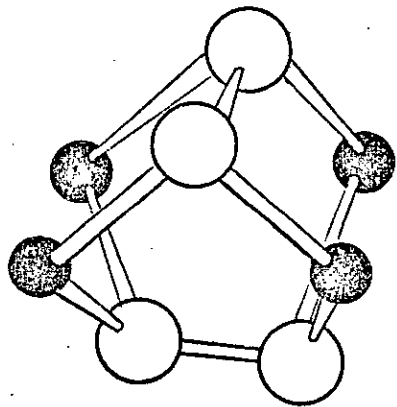
(a) As_4S_4 (in realgar)
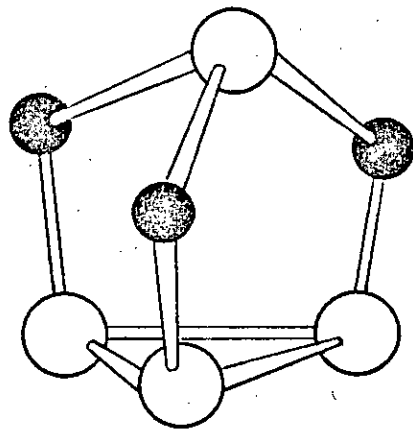
(b) As_4S_3
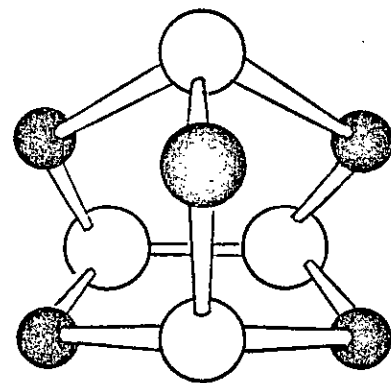
(c) As_4S_5
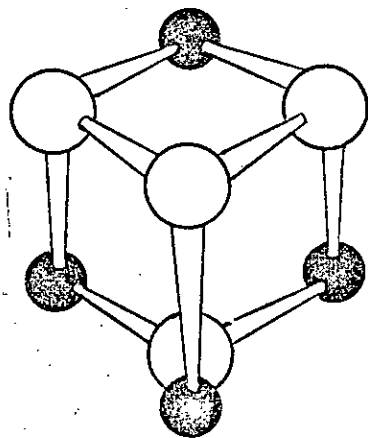
(d) As_4S_4
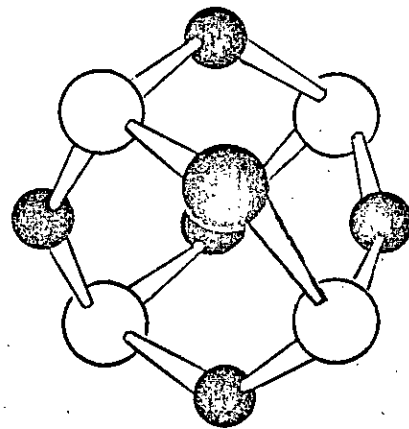
(e) As_4S_6

Figure 2.4

The molecular species in the As-S system.

orthorhombic S (α-S_8), a molecular crystal composed of S_8 rings in the form of a puckered octagon[43]. The unit cell contains 16 S_8 molecules and has the dimensions a = 10.437, b = 12.845, c = 24.369 Å. The space group of the crystal is D_{2h}^{24}. The structures of the allotropes are described in Section 5.5.1.5.2.

2.2.9   Selenium

Selenium also exhibits extensive allotropy but again only one form, trigonal Se, is thermodynamically stable at room temperature and pressure. Trigonal Se is composed of infinite unbranched helical chains packed closely together and running parallel to one another[44]. The hexagonal unit cell parameters are a = 4.366 and c = 4.954 Å and the space group of the crystal is either D_3^4 or D_3^6. There are 3 atoms in the unit cell. The structures of the allotropes are described in Section 6.5.1.5.2.

2.3   Structure of the non-crystalline solids

2.3.1   a-As_2S_3

X-ray diffraction studies of vitreous As_2S_3 have been carried out by a number of workers[45 – 51]. The structural information obtained in these studies can be summarised as follows:

(a)   The nearest-neighbour configuration in the glass closely resembles that in the crystal, so that both forms are made up from similar structural units, namely shallow AsS_3 pyramids. In fact, the s.r.o. in the glass resembles that in the crystal out to next-nearest neighbours.

(b)   The distribution of As–S bond lengths in the glass is Gaussian, the average bond length being that for c-As_2S_3, viz 2.28 Å, and the r.m.s. deviation being 0.1 Å [51], so that there is approximately a ±4% spread in bond lengths.

(c)   Vitreous As_2S_3 is a network glass in which the simple covalent bonding requirements given by the 8-n rule are satisfied, so that the As and S atoms are three-fold and two-fold coordinated respectively.

(d)   Because the s.r.o. of the glass is similar to that of the crystal one might expect the layer structure of $c-As_2S_3$ to be present in the glass to some extent[45]. Direct evidence for the presence of a sheet-like structure in vitreous As_2S_3 is provided by the fact that the first diffraction maximum of the glass is extremely sharp and corresponds in position to the (020) orpiment reflection, which arises from the stacking of the parallel layers along the b axis[50,51].

The first peak in the diffraction pattern of the glass does not, however, occur exactly at the position of the (020) $c-As_2S_3$ peak, but the density of the glass (3.14 g/cm^3) is less than that of the crystal (3.46 g/cm^3) and it can be shown that if the separation of the layers in $c-As_2S_3$ were increased so that the crystal density was reduced to the glass value then the difference between the peak positions would be very small. This suggests that the layer separation in the glass is larger than that in the crystal: the calculated layer separation for vitreous As_2S_3 is about 5 $\mathring{A}$, compared with 4.79 $\mathring{A}$ in $c-As_2S_3$. It seems that the lower density of the glass is predominantly due to the wider separation between its layers; the atomic density within the layers must be very similar to what it is in the crystal.

In the glass the correlation length perpendicular to the layers is found to be ~15 $\mathring{A}$, which means that on average the interlayer correlation extends over about four layers since the layer separation is ~5 $\mathring{A}$. The correlation length within the layers is ~11 $\mathring{A}$, so correlation between layers extends further than correlation within layers[51].

(e)   There is no feature in the r.d.f. of vitreous As_2S_3 corresponding to the cross-ring distance c (4.256 $\mathring{A}$), i.e. the repetition length of

the ring pattern in the c direction[50,51]. This indicates that the ring structure of the c-As_2S_3 layers is not preserved in the glass. The layers in the glass will be disordered, possibly being wavy and cross-linked[45]. The absence of a peak at ~4.3 Å in the r.d.f. of the glass means that microcrystallite models based on the orpiment structure are not appropriate.

(f)   The number of like-atom bonds formed is very small.

Neutron[50,51] and electron[52] diffraction studies of vitreous As_2S_3 yield much the same information as the X-ray studies.

Small angle X-ray scattering (s.a.x.s.) measurements on As_2S_3 glass[53] show no evidence for the presence of voids in the structure and suggest that it is a homogeneous material; the results indicate that the maximum volume which could be occupied by voids is less than 1% of the sample volume. Hence the 8% density deficiency of the glass compared with the crystal cannot be attributed to the presence of voids. These measurements are inconsistent with a microcrystallite model of the glass since such a model would lead to a void volume in excess of 1%.

The s.a.x.s. data also supports the presence of layer-like regions in vitreous As_2S_3, and the 1% limit on void volume implies that the lateral extent of the layers is greater than the 15 Å correlation length perpendicular to the layers.

Nuclear quadrupole resonance (n.q.r.) measurements[5,54] on vitreous As_2S_3 also support the presence of layer-like regions. In addition they show that the distribution of pyramidal apex angles (i.e. the S—As—S angles) in the glass has a halfwidth of ~1°.

The structure of sputtered and annealed evaporated films of a-As_2S_3 has been shown by X-ray diffraction to be identical with that of the bulk glass[38]. S.a.x.s. measurements[53] indicate that evaporated films are as homogeneous and void-free as the bulk glass. However, non-annealed

evaporated films of a-As_2S_3 have been shown by X-ray[38,55] and neutron[56] diffraction to be composed partly of network regions and partly of molecular species such as As_4S_6 and As_4S_4. When the as-deposited evaporated films are illuminated with band-gap radiation or annealed the molecular component polymerises, so that the film eventually acquires the network structure characteristic of the bulk glass[38].

2.3.2   Other amorphous arsenic sulphides

The structure of a number of As-S glasses with compositions ranging from $As_2S_{2.7}$ ($As_{42.6}S_{57.4}$) to As_2S_{12} ($As_{14.3}S_{85.7}$) has been investigated by Tsuchihashi and Kawamoto[48] using a variety of techniques, including X-ray diffraction and density measurements. These authors deduce from their results that all the glasses studied have a layer structure. In the case of the S-rich glasses they conclude that as the S content increases above 60 at.% the additional S atoms go at first into the formation of chains between As atoms in the network, so that the As—S—As linkages are gradually replaced by As—$S_{\overline{n}}$As units; however, in the compositions more S-rich than As_2S_8 — $As_2S_{9.5}$ ($As_{20}S_{80}$ — $As_{17.4}S_{82.6}$) S_8 rings are also formed. In the case of the As-rich glasses, the As—S—As linkages disappear as the As content increases above 40 at.% and As—As bonds are formed in the network. As a result of As—As bond formation the layers become deformed and their thickness increases relative to that of the layers in vitreous $As_{40}S_{60}$. The interlayer separation is found to increase from 5 Å to 5.19 Å as the composition changes from $As_{40}S_{60}$ to $As_{41.2}S_{58.8}$ ($As_2S_{2.85}$).

The structure of a number of As-rich compositions between $As_{40}S_{60}$ and $As_{44.4}S_{55.6}$ ($As_2S_{2.5}$) has been investigated by Maruno and Noda[49] also using a variety of techniques, including X-ray diffraction, density measurement, differential thermal analysis and electron microscopy. These authors conclude that only those As-rich glasses with more than ~57 at.% S have a layer structure containing As—As bonds: those compositions having less than

~57 at.% S have a phase-separated structure and consist of regions of As_4S_4 molecules in a matrix of $a-As_2S_3$.

2.3.3 $a-As_2Se_3$

There have been a number of X-ray diffraction studies of vitreous As_2Se_3[38,45,50,51,57]; the information they yield on the structure of As_2Se_3 glass is essentially the same as that obtained in the X-ray studies of the related glass As_2S_3, the only differences being in the details. The findings of these studies can be summarised as follows:

(a)   The nearest-neighbour configuration in the glass closely resembles that in the crystal, so that both forms are made up from similar structural units, namely shallow $AsSe_3$ pyramids.   In fact, the s.r.o. in the glass resembles that in the crystal out to next-nearest neighbours.

(b)   The distribution of As—Se bond lengths in the glass is Gaussian, the average bond length being that for $c-As_2Se_3$, viz ~2.4 Å, and the r.m.s. deviation being 0.08 Å [51], so that there is approximately a ±3% spread in bond lengths.

(c)   . Vitreous As_2Se_3 is a network glass in which the simple covalent bonding requirements given by the 8-n rule are satisfied, so that the As and Se atoms are three-fold and two-fold coordinated respectively. Perfect coordination throughout the structure is not expected but the number of vacancies, interstitials and atoms with dangling bonds cannot exceed 2 or 3%[51].

(d)   Because the s.r.o. of the glass is similar to that of the crystal one might expect the layer structure of $c-As_2Se_3$ to be present in the glass to some extent[45].   Direct evidence for the presence of a sheet-like structure in vitreous As_2Se_3 is provided by the fact that the first diffraction maximum of the glass is extremely sharp and corresponds in position to the (020) $c-As_2Se_3$ reflection, which arises from the

stacking of the parallel layers along the b axis[50,51].

The first peak in the diffraction pattern of the glass does not, however, occur exactly at the position of the (020) c-As_2Se_3 peak, but the density of the glass (4.58 g/cm^3) is less than that of the crystal (4.85 g/cm^3) and it can be shown that if the separation of the layers in c-As_2Se_3 were increased so that the crystal density was reduced to the glass value then the difference between the peak positions would be very small. This suggests that the layer separation in the glass is larger than that in the crystal, as was the case for the sulphide. It seems that the lower density of the glass is predominantly due to the wider separation between its layers; the atomic density within the layers must be very similar to what it is in the crystal.

In the glass the correlation length perpendicular to the layers is found to be 20 Å, which corresponds to four to five layers occurring together on average. The correlation length within the layers is ~11 Å, so correlation between layers extends further than correlation within layers[51].

It should be noted that Renninger and Averbach[57] maintain that their X-ray diffraction data does not support the presence of layers in vitreous As_2Se_3 but rather chains. However, there is much evidence from other experiments that layer-like regions exist in this glass.

(e)   There is no feature in the r.d.f. of vitreous As_2Se_3 corresponding to the cross-ring distance c (4.30 Å), i.e. the repetition length of the ring pattern in the c direction[50,51]. This indicates that the ring structure of the c-As_2Se_3 layers is not preserved in the glass. The layers in the glass will be disordered, possibly being wavy and cross-linked[45]. The absence of a peak at ~4.3 Å in the r.d.f. of the glass means that microcrystallite models based on the orpiment structure are not appropriate[50,51,57].

(f)   The number of like-atom bonds formed is very small.

Neutron[50,51] and electron[52] diffraction studies of vitreous As_2Se_3 yield similar information to the X-ray studies.

S.a.x.s. measurements on vitreous As_2Se_3[53] indicate that it, also, is a homogeneous material with a void volume of less than 1%.   As in the case of As_2S_3, these measurements are inconsistent with a microcrystallite model of the glass but support the presence of layer-like regions.

N.q.r. measurements[5,54] on As_2Se_3 glass also support the presence of layer-like regions and show that the distribution of pyramidal apex angles (i.e. the Se—As—Se angles) in the glass has a halfwidth of $\sim 3^{\circ}$. This distribution is broader than that for As_2S_3 glass (for which the half-width is ~ 1%) because the average apex angles of the two inequivalent pyramids in c-As_2Se_3 differ more than those for c-As_2S_3.   Leadbetter and Apling[51] calculate from their X-ray and neutron diffraction results that the average Se—As—Se angle in vitreous As_2Se_3 is 96.8° (the value for c-As_2Se_3 is 99.7°).

X-ray diffraction experiments have shown that sputtered and annealed evaporated films of a-As_2Se_3 have the same structure as the bulk glass[38] but that non-annealed evaporated films of a-As_2Se_3 contain molecular species such as As_4Se_6.   As in the case of As_2S_3, when these as-deposited evaporated films are illuminated with band-gap radiation or annealed the molecular component polymerises to form the network structure characteristic of the bulk glass.

2.3.4   Other amorphous arsenic selenides

The structure of a number of amorphous arsenic selenides with compositions ranging from elemental Se to $As_{50}Se_{50}$ has been investigated by X-ray[38,50,51,57] and neutron[50,51] diffraction.   The results of these studies suggest that the As and Se atoms in these materials are three-fold and two-fold coordinated respectively.   The results for compostions near

$As_{40}Se_{60}$ are consistent with the excess atoms being incorporated into the $As_{40}Se_{60}$ network structure through the formation of As—As and Se—Se bonds, the number of like-atom bonds formed being the minimum number needed to satisfy compositional requirements[50,51]. Layer-like regions occur in all the glasses with compositions between about $As_{50}Se_{50}$ and $As_{30}Se_{70}$[50,51], the layer structure becoming more pronounced with increasing As concentration as a result of steric factors[51]. The layers are disordered and the interlayer separation increases from 5.1 Å to 5.6 Å as the As content increases[50,51]. The nearest-neighbour correlation peak shifts linearly from 2.35 Å in a-Se to 2.41 Å in $As_{36}Se_{54}$ glass but remains constant at this value at higher As concentrations[57].

Monte Carlo models of the atomic arrangements in sputtered films and glasses with compositions ranging from elemental Se to $As_{50}Se_{50}$ have been developed by Renninger et al.[58]. The models yield information on the bond-length and bond-angle distributions in these materials and indicate that the films and glasses have very similar structure, though the films are more disordered, their bond-length and bond-angle distributions being broader than those of the corresponding glasses.

2.3.5 Amorphous arsenic

The structure of a-As is more similar to that of orthorhombic As than to that of the rhombohedral modification[59] and is well represented by a three-fold coordinated c.r.n. model[60 — 62]. In this model the nearest-neighbour separations are within 1% of the bond length in rhombohedral As (2.49 Å), and the bond-angle distribution peaks at 98.2° (the average bond angle in rhombohedral As is 97°) and has an r.m.s. deviation of 7.4°. Although the model is based on the structure of the crystalline forms it is not layer-like in appearance but is three dimensional. The network is fully connected but still contains voids, these being interconnected to form a cavern-like structure. The presence of these 'caverns' enables the model

to reproduce the 10 — 20% density deficit of a-As compared with the crystalline forms.

2.3.6 Amorphous sulphur

Although sulphur can be prepared in an amorphous state[63,64] this form of the element is not stable at room temperature and pressure; it consists of twisted helical chains $10^4 - 10^5$ atoms in length. The bond lengths, bond angles and dihedral angles in the chains have the values 2.04 Å, 106° and 95° respectively.

2.3.7 Amorphous selenium

a-Se is not thermodynamically stable under room conditions but may be regarded as stable in the practical sense[65]. It is believed to be composed of twisted helical chains and Se_8 rings[58,65 — 68], though some workers dispute the presence of the latter[69]. The Se_8 rings in a-Se have the same structure as those in monoclinic Se and the bond lengths and bond angles in the chains are essentially those of the chains in trigonal Se, viz 2.373 Å and 103.1° respectively; there is some controversy over whether the dihedral angles along the chains have random magnitude or a fixed value equal to that in trigonal Se[69 — 72].

2.4 References

1.   Morimoto, N., Miner. J. (Japan) 1, 160 (1954).

2.   Mullen, D.J.E. and Nowacki, W., Z. Krist. 136, 48 (1972).

3.   Treacy, D. and Taylor, P.C., Phys. Rev. B 11, 2941 (1975).

4.   Zallen, R., Slade, M.L. and Ward, A.T., Phys. Rev. B 3, 12 (1971).

5.   Rubinstein, M. and Taylor, P.C., Phys. Rev. B 9, 4258 (1974).

6.   Ito, T., Morimoto, N. and Sadanga, R., Acta Cryst. 5, 775 (1952).

7.   'Kirk-Othmer Encyclopedia of Chemical Technology', Vol.2, Wiley, New York, 1969.

8.   Mellor, J.W., 'A Comprehensive Treatise on Inorganic and Theoretical Chemistry', Vol.9, Longmans, London, 1929.

9.   'A Text-Book of Inorganic Chemistry' (Friend, J.N., editor), Vol.6, Charles Griffin, London, 1938, p.246.

10.   Blank, E.W., J. Chem. Education 20, 171 (1943).

11.   Kirkinskii,V.A., Eksp. Issled. Mineral., 9 (1969).

12.   Kirkinskii, V.A., Ryaposov A.P. and Korolyuk, V.N., Eksp. Issled. Mineral. 1972 — 1973, 24 (1974).

13.   Porter, E.J. and Sheldrick, G.M., J.C.S. Dalton, 1347 (1972).

14.   Bastow, T.J. and Whitfield, H.J., Solid State Commun. 11, 1015 (1972).

15.   Lu, C.S. and Donohue, J., J. Amer. Chem. Soc. 66, 818 (1944).

16.   Allen, P.W. and Sutton, L.E., Acta Cryst. 3, 67 (1950).

17.   Forneris, R., Am. Miner. 54, 1062 (1969).

18.   Ursu, I., Lupei, A. and Lupei, V., Rev. Roum. Phys. 15, 569 (1970).

19.   Whitfield, H.J., J. Chem. Soc. (A), 1800 (1970).

20.   Whitfield, H.J., J.C.S. Dalton, 1737 (1973).

21   Whitfield, H.J., J.C.S. Dalton, 1740 (1973).

22.   Vaipolin, A.A., Sov. Phys. Crystallogr. 10, 509 (1966).

23.   Renninger, A.L. and Averbach, B.L., Acta Cryst. B29, 1583 (1973).

24.   Bastow, T.J. and Whitfield, H.J., J.C.S. Dalton, 1739 (1973).

25.   Scott, A., J. Chem. Soc., 651 (1900).

26.   Farmer, W. and Firth, J.B., J. Chem. Soc., 2019 (1927).

27.   Harris, F.R., J. Chem. Soc., 698 (1951).

28.   Knox, B.E. and Ban, V.S., Mat. Res. Bull 3, 885 (1968).

29.   Kutoglu, A., Z. Anorg. Allg. Chem. 419, 176 (1976).

30.   Ghosh, B., Kothiyal, G.P. and Amirthalingam, V., India, A.E.C., Bhaba At. Res. Cent. (Rep.), 776 (1974).

31.   Kothiyal, G.P. and Ghosh, B., J. Cryst. Growth 32, 29 (1976).

32.   Partington, J.R., 'General and Inorganic Chemistry', Macmillan, London, 1947, p.629.

33.   Lagowski, J.J., 'Modern Inorganic Chemistry', Marcel Dekker, New York, 1973, p.425.

34. Ephraim, F., 'Inorganic Chemistry' (5th English edition by Thorne, P.C.L. and Roberts, E.R.), Gurney and Jackson, London, 1948, p.753.

35. Timofeeva, N.V., Vinogradova, G.Z., Feklichev, E.M., Dembovskii, S.A. and Kalashnikov, Ya. A., Dokl. Akad. Nauk S.S.S.R. 190, 902 (1970).

36. Bastow, T.J. and Whitfield, H.J., J.C.S. Dalton, 959 (1977).

37. Tanaka, K., to be published in Thin Solid Films (1978).

38. deNeufville, J.P., Moss, S.C. and Ovshinsky, S.R., J. Non-Cryst. Solids 13, 191 (1974).

39. Solin, S.A. and Papatheodorou, G.N., Phys. Rev. B 15, 2084 (1977).

40. Krebs, H., J. Non-Cryst. Solids 1, 455 (1969).

41. Barrett, C.S., J. Appl. Cryst. 2, 30 (1969).

42. Johan, Z., Chem. der Erde 20, 71 (1959).

43 Pawley, G.S. and Rinaldi, R.P., Acta Cryst. B28, 3605 (1972).

44. Cherin, P. and Unger, P., Inorg. Chem. 6, 1589 (1967).

45. Vaipolin, A.A. and Porai-Koshits, E.A., Sov. Phys. Solid State 5, 178 (1963).

46. Petz, J.I., Kruh, R.F. and Amstutz, G.C., J. Chem. Phys. 34, 526 (1961).

47. Hopkins, T.E., Pasternak, R.A., Gould, E.I. and Herndon, J.R., J. Phys. Chem. 66, 733 (1962).

48. Tsuchihashi, S. and Kawamoto, Y., J. Non-Cryst. Solids 5, 286 (1971).

49. Maruno, S. and Noda, M., J Non-Cryst. Solids 7, 1 (1972).

50. Apling, A.J., in 'Electronic and Structural Properties of Amorphous Semiconductors' (Proc. Scottish Univ. Summer School in Physics, Aberdeen, Aug. 1972) (Le Comber, P. and Mort, J., editors), Academic Press, London, 1973, p.243.

51. Leadbetter, A.J. and Apling, A.J., J. Non-Cryst. Solids 15, 250 (1974).

52. Nabitovich, I.D., Stetsiv, Ya. I. and Andreiko, A.M., Sov. Phys. Crystallogr. 21, 348 (1976).

53. Bishop, S.G. and Shevchik, N.J., Solid State Commun. 15, 629 (1974).

54. Rubinstein, M. and Taylor, P.C., Phys. Rev. Lett. 29, 119 (1972).

55. Apling, A.J., Leadbetter, A.J. and Wright, A.C., J. Non-Cryst. Solids 23, 369 (1977).

56. Leadbetter, A.J., Apling, A.J., Daniel, M.F., Wright, A.C. and Sinclair, R.N., in 'The Structure of Non-Crystalline Solids' (Gaskell, P.H., editor), Taylor and Francis, London, 1977, p.23.

57. Renninger, A.L. and Averbach, B.L., Phys. Rev. B $\underline{8}$, 1507 (1973).

58. Renninger, A.L., Rechtin, M.D. and Averbach, B.L., J. Non-Cryst. Solids $\underline{16}$, 1 (1974).

59. Smith, P.M., Leadbetter, A.J. and Apling, A.J., Phil. Mag. $\underline{31}$, 57 (1975).

60. Greaves, G.N. and Davis, E.A., Phil. Mag. $\underline{29}$, 1201 (1974).

61. Greaves, G.N. and Davis, E.A., Proc. 12th Int. Conf. on the Physics of Semiconductors, Stuttgart (Pilkuhn, M.H., editor), Teubner, Stuttgart, 1974, p.1047.

62. Davis, E.A., Elliott, S.R., Greaves, G.N. and Jones, D.P., in 'The Structure of Non-Crystalline Solids' (Gaskell, P.H., editor), Taylor and Francis, London, 1977, p.205.

63. Dultz, W., Hochheimer, H.D. and Müller-Lierheim, W., Proc. 5th Int. Conf. on Amorphous and Liquid Semiconductors, Garmisch-Partenkirchen, Germany (Stuke, J. and Brenig, W., editors), Taylor and Francis, London, 1974, p.1281.

64. Prins, J.A., in 'Non-Crystalline Solids' (Fréchette, V.D., editor), Wiley, New York, 1960, p.322.

65. Chizhikov, D.M. and Shchastlivyi, V.P., 'Selenium and Selenides', Collet's, London, 1968, p.3.

66. Bagnall, K.W., 'The Chemistry of Selenium, Tellurium and Polonium', Elsevier, Amsterdam, 1966.

67. Kaplow, R., Rowe, T.A. and Averbach, B.L., Phys. Rev. $\underline{168}$, 1068 (1968).

68. Moscinski, J., Renninger, A. and Averbach, B.L., Phys. Lett. $\underline{42}$ A, 453 (1973).

69. Malaurent, J.C. and Dixmier, J., in 'The Structure of Non-Crystalline Materials' (Gaskell, P.H., editor), Taylor and Francis, London, 1977, p.49.

70. Meek, P.E., Phil. Mag. $\underline{34}$, 767 (1976).

71. Robertson, J., Phil. Mag. $\underline{34}$, 13 (1976).

72. Meek, P.E., in 'The Structure of Non-Crystalline Materials' (Gaskell, P.H., editor), Taylor and Francis, London, 1977, p.235.

CHAPTER 3

THE RAMAN EFFECT

3.1   Introduction

This chapter is concerned with some of the theoretical aspects of Raman scattering.   The basic concepts are first outlined and then discussed in relation to crystalline and amorphous solids.   Numerous texts and reviews on Raman scattering, particularly in crystals, have been written; Anderson's book[1] contains much information on the historical, theoretical and experimental aspects of the Raman effect and includes references to many other works on the subject.

The section dealing with amorphous solids (Section 3.4) describes how the vibrational spectra of such materials can be interpreted and outlines the methods for extracting structural and other information from the data.   Chapters 5 and 6 contain detailed discussions of these methods in relation to a-As_2S_3 and a-As_2Se_3.   Section 3.4 also contains a brief summary of the results of the many vibrational studies that have been carried out on amorphous materials.   More comprehensive and detailed reviews of the vibrational spectroscopy of amorphous semi-conductors have been given by Lucovsky[2] and Brodsky[3], while Böttger[4], and Bell[5] and Dean[6] have reviewed the vibrational studies of general non-crystalline solids and oxide glasses respectively. Solin[7] has discussed the use of optical probes for investigating the structure of disorded solids.

3.2   Principles of Raman scattering

Light may be either elastically or inelastically scattered by matter. Elastic scattering by particles that are small compared with the wave-length of the incident light is termed 'Rayleigh scattering', while 'Brillouin scattering' and 'Raman scattering' both refer to the inelastic

scattering of photons by such particles, Brillouin scattering being the historical name for inelastic scattering by sound waves in the illuminated material.

In the case of Raman scattering from rarefied gases an incident photon undergoes a change in energy through interaction with one of the constituent molecules and an equal and opposite change is produced in the vibrational and/or rotational energy of the molecule. The magnitudes of these changes correspond to differences between the molecule's vibrational and/or rotational energy levels, which are determined by the structure and components of the molecule. It is often possible to account for an observed Raman spectrum by setting up a simplified model of the molecule in question and calculating the spectrum the model would exhibit. The parameters of molecular geometry, bond strengths, internal interactions etc. needed to specify the model may be obtained from other types of experiment and then varied within experimental limits to give the best fit to the Raman spectrum.

The simple classical theory of Raman and Rayleigh scattering considers the oscillating dipole moment, M, induced in a polarisable molecule by the electric field of the incident radiation :

$$M = \alpha E \cos 2\pi\nu_i t \qquad (3.1)$$

where α is the molecular polarisability, E the amplitude of the oscillating electric field and ν_i the frequency of the incident radiation. The polarisability depends on the motion of the nuclei in the molecule so that if these are already oscillating with frequency ν_m, α can be written as the sum of a constant part, α_o, and an oscillating part with amplitude α_1:

$$\alpha = \alpha_o + \alpha_1 \cos 2\pi\nu_m t \qquad (3.2)$$

Substituting this in Equation 3.1,

$$M = \alpha_o E \cos 2\pi\nu_i t + \alpha_1 E \cos 2\pi\nu_i t \cos 2\pi\nu_m t$$

$$= \alpha_o E \cos 2\pi\nu_i t + \tfrac{1}{2}\alpha_1 E\left\{\cos\left[2\pi(\nu_i + \nu_m)t\right] + \cos\left[2\pi(\nu_i - \nu_m)t\right]\right\} \qquad (3.3)$$

Two beat frequencies, $\nu_i \pm \nu_m$, have now appeared in the expression for M.

From classical electromagnetic theory the rate at which power is radiated by the oscillating dipole is given by

$$I = \frac{16\pi^4 \nu^4}{3c^3} \mathcal{M}^2 \tag{3.4}$$

Inserting Equation 3.3 in the above and omitting the cross terms, which usually make a negligible contribution to the radiated power, one obtains

$$I = \frac{16\pi^4 \nu^4}{3c^3} \left\{ \alpha_o^2 E^2 \cos^2 2\pi \nu_i t + \alpha_1^2 E^2 \cos^2 \left[2\pi(\nu_i + \nu_m)t \right] + \alpha_1^2 E^2 \cos^2 \left[2\pi(\nu_i - \nu_m)t \right] \right\} \tag{3.5}$$

The first term in the bracket accounts for the Rayleigh scattering, i.e. scattering without change of frequency, while the other two account for the frequency-shifted radiation at $\nu_i \pm \nu_m$, i.e. the Raman scattering. Hence the spectrum of the scattered light consists of lines symmetrically placed on either side of the incident frequency. The low-frequency lines ($\nu_i - \nu_{m_1}$, $\nu_i - \nu_{m_2}$,....) are referred to as 'Stokes lines', and the high-frequency lines ($\nu_i + \nu_{m_1}$, $\nu_i + \nu_{m_2}$,..) are called 'anti-Stokes lines'. (Since it is the vibrational frequencies, ν_{m_j}, that are of interest the abscissa of the Raman spectrum is taken to be not the absolute frequency of the scattered radiation but its <u>frequency shift</u>, i.e. the difference in frequencies between the incident and scattered light. These differences are identical with the ν_{m_j} .)

The classical theory, however, is unable to account for the relative intensities of corresponding Stokes and anti-Stokes lines, for although the bands are symmetrically situated about ν_i they are not symmetric with respect to intensity. The quantum explanation is that the molecules of a sample in thermal equilibrium at temperature T are distributed over the possible energy levels according to the relation

$$N_w = N_o e^{-\hbar w/kT} \tag{3.6}$$

where k is Boltzmann's constant, w is the angular frequency of a normal mode, N_w is the number of molecules in the state with energy $\hbar w$ and N_o the number in the ground state, so that more molecules are available for Stokes scattering, in which energy is transferred from the incident

photons to the molecules, than for anti-Stokes scattering, where
energy passes from excited molecules to the photons.

Observation of the temperature dependence of band intensities is
one method of differentiating fundamentals or first-order bands
($\mathcal{V}_i \pm \mathcal{V}_{m_1}$, $\mathcal{V}_i \pm \mathcal{V}_{m_2}$, . . .), overtones ($\mathcal{V}_i \pm 2\mathcal{V}_{m_1}$, $\mathcal{V}_i \pm 2\mathcal{V}_{m_2}$, . . .)
and combination bands ($\mathcal{V}_i \pm \mathcal{V}_{m_1} \pm \mathcal{V}_{m_2}$, . . .), for the last two types
may also appear in the spectrum of the scattered light. First-order
Stokes and anti-Stokes lines are proportional to $1 + n(w,T)$ and $n(w,T)$
respectively where $n(w,T)$ is the Bose-Einstein occupation factor:

$$n(w,T) = \left[\exp(\hbar w/kT) - 1 \right]^{-1} \qquad (3.7)$$

An important feature of Raman scattering is the fact that the
bands may be polarised to some extent, but not necessarily identically
for each band. Measurement of the degree of depolarisation of the
Raman lines is necessary in order to assign them to particular normal
modes and can help in deciding the actual geometrical arrangement of
the atoms in the molecule. The quantity used to specify the degree of
polarisation is the depolarisation ratio, ρ, which is the ratio of $I_\perp$,
the intensity of the scattered light polarised perpendicular to the
direction of polarisation of the incident light, to $I_\parallel$, the intensity
of the scattered light polarised parallel to this direction:

$$\rho = I_\perp/I_\parallel \qquad (3.8)$$

Not all the fundamental frequencies of the irradiated molecule
appear in the spectrum of the scattered light for while Rayleigh scatter-
ing arises from the polarisability of the molecule, and so is expected to
occur in all substances, Raman scattering is due to changes in the
polarisability during molecular motions, and not all motions produce such
changes. A fundamental frequency will appear in the Raman spectrum if
the amplitude of the dipole moment induced by the incident radiation
changes during the molecular motion concerned. Such motions and fre-
quencies are termed 'Raman active', while the missing ones are said to
be 'Raman inactive'.

3.3   Raman scattering in crystals

In the case of a rarefied gas the molecular motions responsible
for Raman scattering may be rotational or vibrational or both and the
resulting spectra arise from changes of polarisability during the
rotations or vibrations of the individual constituent molecules.   As
the molecular density is increased collisions between molecules become
more frequent and these, together with other intermolecular interactions
that begin to occur, lead to spectral changes, the most obvious being
the broadening of the rotation lines.   In general, by the time the
gas has condensed into the liquid phase quantised rotation is not possible
and rotational fine structure is no longer observed in the Raman spectrum.
In solids rotational motion is hindered to an even larger extent than
in liquids, due to intermolecular coupling, so that rotational features
are generally absent from solid-phase spectra.

The Raman spectrum of molecules in a molecular crystal differs in
several other respects from that of the free molecules.   The vibrations
of the atomic nuclei in crystals can generally be divided into two types:
lattice or external vibrations and molecular or internal vibrations.
The former are between the molecules considered as rigid entities and
arise from the hindered rotations and translations of the molecules in
the solid phase.   They give rise to new, low-frequency bands in the
Raman spectrum of the solid.   The molecular vibrations occur <u>within</u>
the individual molecules and are modifications of the vibrations of the
free molecules.   These modifications are caused by the intermolecular
forces that hold the solid together, the degree of modification depend-
ing on the strength of these forces — the stronger they are the more the
crystal spectrum will differ from the gas-phase spectrum.   These mod-
ifications take the form of frequency shifts, changes of relative band
intensities, and the splitting of bands into multiplets.   The last
may be due to the coupling of identical vibrations of adjacent molecules

in the crystal unit cell or to the removal of degeneracies by a lowering of the effective symmetry of the molecule on account of its environment. A further feature of the Raman spectra of solids is that, in the case of a single crystal, the observed Raman spectrum depends on the overall orientation of the sample, since the molecules in the crystal have certain fixed orientations whereas gas molecules can assume all orientations.

In crystals the vibrations of the component molecules or atoms are coupled, producing lattice waves, or phonons, which propagate through the crystal. Depending on the circumstances and the particular material, waves other than these vibrational ones may be obtained in the crystal. Plasmons and magnons are examples of such waves and, like phonons, can scatter light. In the present study only phonons are the scattering excitation, and, in particular, optic phonons, since Brillouin scattering is not being investigated.

Whereas for gases and liquids only energy conservation need be considered, in crystalline solids, because of the wave nature of the vibrations, conservation of wavevector must also be taken into account. In the case of one-phonon scattering, in which a single phonon is created or destroyed, the two laws may be written :

$$\underline{K} \equiv \underline{k}_i - \underline{k}_s = \underline{K}_h \pm \underline{q} \quad \text{— wavevector conservation} \qquad (3.9)$$

$$\hbar W \equiv \hbar(w_i - w_s) = \pm \hbar w_j(\underline{q}) \quad \text{— energy conservation} \qquad (3.10)$$

where w_i and $\underline{k}_i$ are respectively the angular frequency and wavevector of the incident photon and w_s and $\underline{k}_s$ are those of the scattered photon; $\underline{K}$ is the wavevector transfer, $\underline{q}$ is the phonon wavevector, $\underline{K}_h$ is a reciprocal lattice vector, W is the frequency transfer and $w_j(\underline{q})$ the phonon frequency, j being the branch index of the dispersion curve. $\underline{k}_i$ and $\underline{k}_s$ are the photon wavevectors inside the crystal, so that $|\underline{k}_i| = 2\pi n / \lambda_i$, $|\underline{k}_s| = 2\pi n / \lambda_s$ where n is the refractive index of the crystal and λ_i and λ_s are the respective free-space wavelengths.

Diagram A of Figure 3.1(a) shows a schematic phonon dispersion relation for a particular symmetry direction in a crystal. The Brillouin zone boundary occurs at $\underline{q} = \underline{q}_{max} = \frac{\pi}{a}\frac{\underline{q}}{|\underline{q}|}$, where a is the crystal lattice constant corresponding to the symmetry direction. Since practical and theoretical considerations usually require the light source to be in the visible, the wavelength, λ_i, of the incident light is generally very much greater than the unit cell dimensions, λ_i being in the range 4000 — 7000 Å while a is typically $\sim$5 Å. Accordingly $|\underline{k}_i|$ and $|\underline{k}_s|$ are of the order 10^5 cm^{-1} while $|\underline{q}_{max}| \sim 10^8$ cm^{-1}, so that if crystal momentum is to be conserved a solution to Equation 3.9 exists only for $\underline{K}_h$ = 0 and values of $\underline{q}$ very small compared with the Brillouin zone dimensions, i.e. the scattering can create or destroy only phonons with $\underline{q} \approx 0$.

Because the optical branches of the phonon dispersion relation vary slowly with $\underline{q}$ near $\underline{q}$ = 0, the frequencies in the Raman spectrum are practically independent of the angle of scattering and correspond to intersections of the dispersion curves with the $\underline{q}$ = 0 axis (see B in Figure 3.1(a)), though not all optic modes of zero wavevector are Raman active. The general requirement for one-phonon scattering to occur is that the polarisability of the atoms should vary with the same frequency as the optic mode in question. The $\underline{q} \approx 0$ selection rule does not apply in the case of two-phonon scattering since here all that is needed to conserve crystal momentum is that the wavevectors of the two phonons involved should cancel, and thus phonons throughout the Brillouin zone can participate in the scattering. Consequently two-phonon spectra are generally broad and continuous, unlike one-phonon crystal spectra, exemplified by B in Figure 3.1(a), which consist mainly of sharp discrete lines.
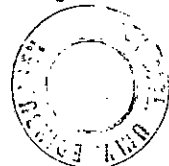
Figure 3.1

(a) Diagram A is a schematic phonon dispersion relation for a particular symmetry direction in a crystal, a being the crystal lattice constant corresponding to that direction.   Diagram B shows how the Raman bands of the crystal correspond to inter-sections of the dispersion curves with the $q = 0$ axis.

(b) Typical form of the Raman spectrum of an amorphous material.

(c) The reduced Raman spectrum of the same amorphous material.

(d) The form of $1 + n(w,T)$ over the range $0 - 400$ cm^{-1} for $T = 300^{\circ}$ K.

A

B

Frequency

o   π/a

q →

Intensity

Frequency

Intensity

(b)

Frequency

Reduced
Intensity

(c)

Freq.(cm⁻¹)

400

200

0

T=300°K

0   2   4   6

1+n(ω,T)

(d)

(a)
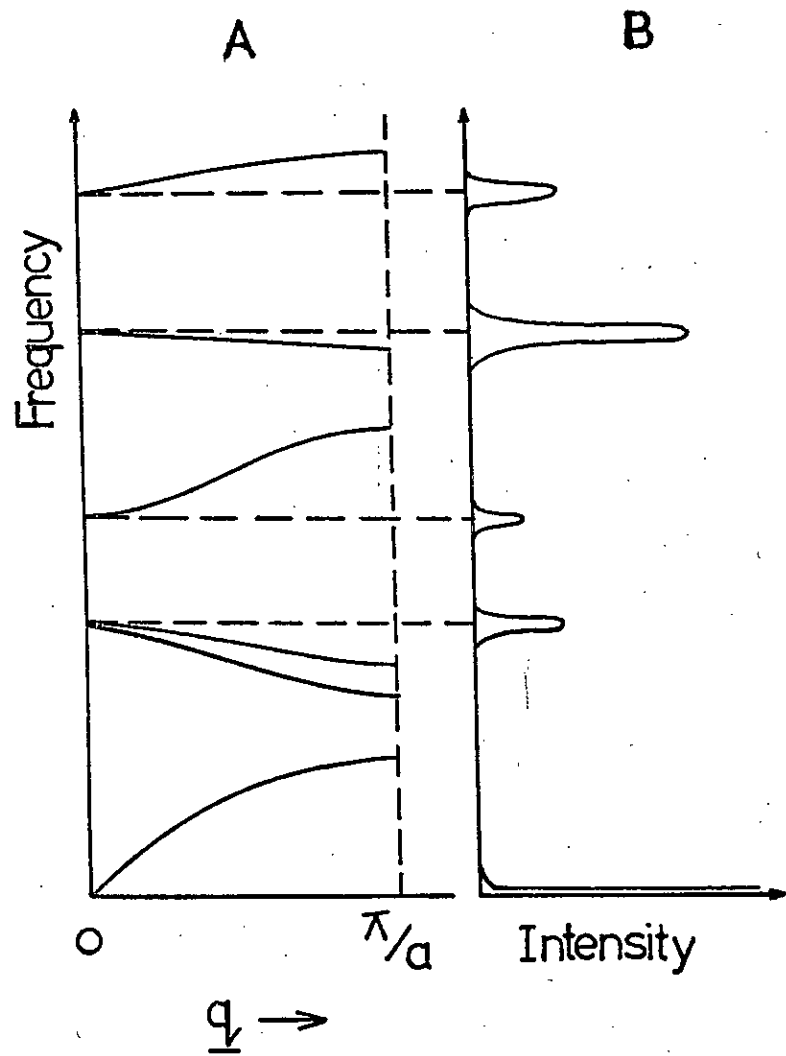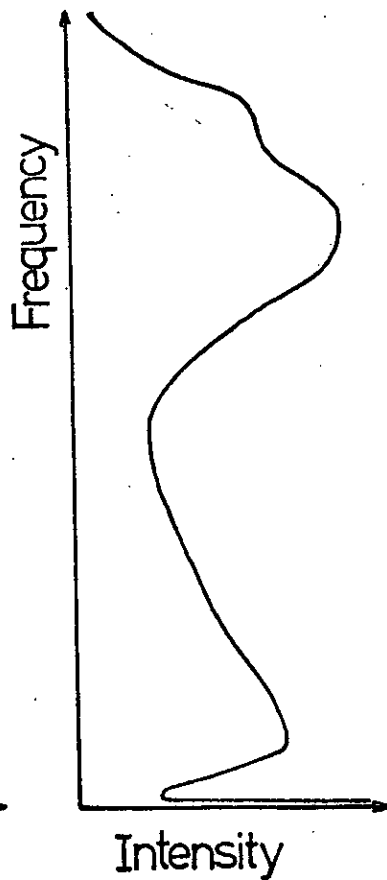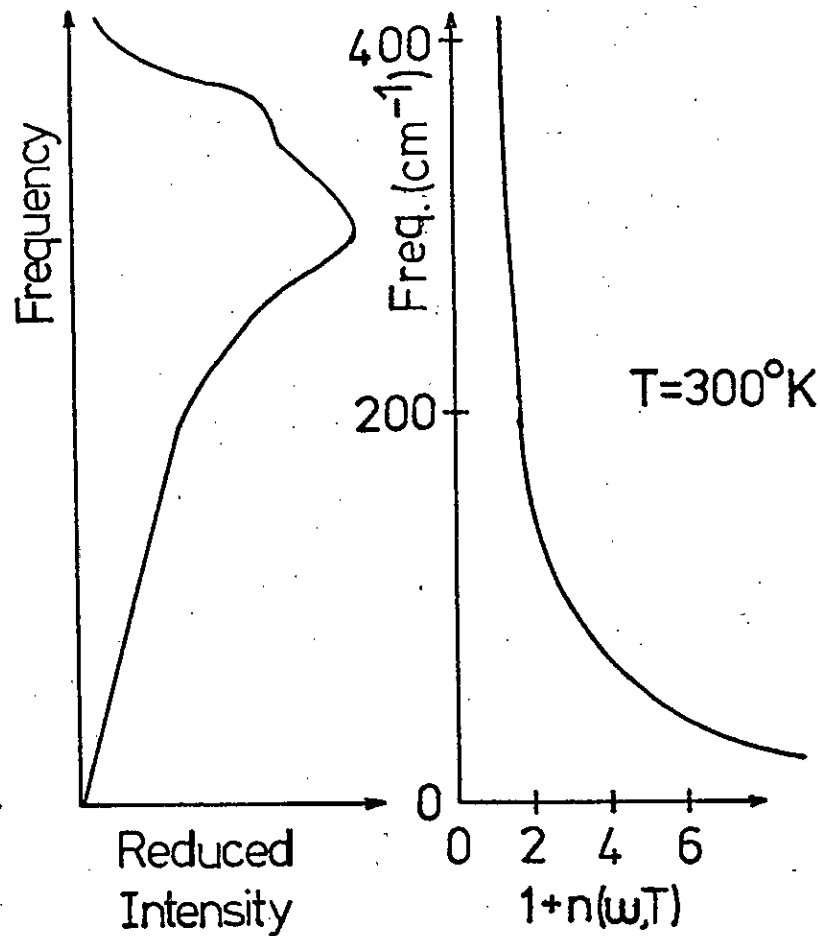
3.4   Raman scattering in non-crystalline materials

The absence of long-range order in amorphous materials leads to the relaxation of the $q \approx 0$ selection rule, so that, as for two-phonon scattering, all modes can participate in the scattering process. Consequently Raman scattering yields much more information on vibrational spectra in the case of amorphous materials and the Raman spectra of these solids consist of very broad bands instead of the narrow lines observed in crystal spectra (see Figure 3.1(b)).

3.4.1   The density-of-states interpretation

The Stokes and anti-Stokes intensities for first-order processes are temperature dependent since they are proportional to $1 + n(w,T)$ and $n(w,T)$ respectively. Because this temperature dependence is negligible for high frequency shifts but is marked at low frequency shifts, where $n(w,T)$ is greatest (see Figure 3.1(d)), the shape of the spectrum of an amorphous solid changes considerably between $0°$ K and room temperature. As the temperature increases from absolute zero there appears in the low-frequency region a peak that is due not to a vibrational mode but to the thermal population of the lower states[8 – 11]. This spurious peak, which is characteristic of first-order Raman scattering from an amorphous solid[12], can be removed by dividing the Stokes or anti-Stokes intensity at each frequency shift w by $1 + n(w,T)$ or $n(w,T)$ respectively. In some studies this boson peak has been incorrectly interpreted as a genuine vibrational band.

As the scattering is due to vibrations the data must also be corrected for the harmonic oscillator amplitude, w^{-1}, and as the scatterers are induced dipoles the data must be corrected for its fourth-power dependence on the scattered frequency, w_s: $w_s = w_i - w$. The spectra obtained by dividing the measured intensity at each frequency shift w by w_s^4/w and the appropriate temperature factor are termed 'reduced spectra' (see Figure 3.1(c)).

For some amorphous materials the reduced spectrum is not just a means for presenting data unambiguously but is of theoretical importance also. Shuker and Gammon[9,13] have shown that under certain conditions the reduced spectrum of an amorphous material is closely related to its phonon density-of-states, from which it is possible to calculate other thermodynamic properties, e.g. specific heat. This result is a consequence of the fact that all modes can participate in the scattering process because of the disorder-induced breakdown of crystal and momentum selection rules.

In an ideal harmonic crystal the correlation lengths, Λ_j, which characterise the spatial extent of the normal modes of vibration, are infinite and the normal modes are plane waves of the type $e^{iq_j \cdot r}$. These waves, or phonons, have well defined wavevector, q_j, and the plane-wave nature of the vibrations leads to the $q \approx 0$ selection rule. In a real crystal, defect and coupled-phonon damping mechanisms reduce the correlation lengths to values of the order 1000 Å but the crystal momentum selection rule is still a useful approximation. Shuker and Gammon assumed that in a disordered material the Λ_j are short ($\sim 10 - 100$ Å), which implies that the vibrational modes are nearly localised and so can no longer be represented by plane waves. Under these circumstances the vibrations are better approximated by plane waves with spatial decay. If this decay is exponential then the jth normal mode can be represented by the product

$$e^{iq_j \cdot r} e^{- r /\Lambda_j} \tag{3.11}$$

where $e^{- r /\Lambda_j}$ is the damping factor. The q_j are no longer good quantum numbers and there is no longer any $q \approx 0$ selection rule. The exponential spatial damping mixes the formerly distinct q states so that modes are no longer characterised by a single wavevector.

The scattered Raman intensity of the jth mode is proportional to the Fourier transform of its space-time correlation function, which is in turn

proportional to expression 3.11. Summing over the modes, all of which are now allowed to contribute to the scattering, Shuker and Gammon find that the non-resonant Stokes intensity at frequency shift w is given by

$$I_{\alpha\beta,\gamma\delta}(w,T) = \sum_b C_b^{\alpha\beta,\gamma\delta}(1/w)\left[1 + n(w,T)\right]g_b(w) \qquad (3.12)$$

where $g_b(w)$ is the density of vibrational states in band b, and $C_b^{\alpha\beta,\gamma\delta}$ is a polarisation-dependent coupling coefficient that describes the coupling of band b to the incident radiation — the tensor components $\alpha\beta(\gamma\delta)$ index the polarisation of the incident(scattered) light. These authors assume that the vibrations fall into bands and that the vibrations in each band have similar microscopic motions, similar optical coupling factors and similar correlation volumes, Λ_j^3, so that the $C_b^{\alpha\beta,\gamma\delta}$ are constants. Thus it is assumed that all vibrations within a band couple equally to the incident radiation and the coupling coefficients are frequency independent over the whole band. Kobliska and Solin[14,15] point out that the well-known fourth-power frequency dependence of an induced dipole scatterer is contained in the coupling coefficients so they are not, in fact, frequency independent. Shuker and Gammon apparently assume that the variation in w_s^4 is negligible for scattered frequencies in the range 0 — 550 cm^{-1} but Kobliska and Solin[14] show that for incident radiation of wavelength 6328 Å the w_s^4 term for a 5 cm^{-1} Stokes shift is 9% larger than it is for a 380 cm^{-1} Stokes shift. Accordingly, in the present study the expression obtained by Shuker and Gammon has been modified to show this w_s^4 dependence explicitly: Equation 3.12 becomes

$$I_{\alpha\beta,\gamma\delta}(w,T) = \sum_b A_b^{\alpha\beta,\gamma\delta}(w_s^4/w)\left[1 + n(w,T)\right]g_b(w) \qquad (3.13)$$

where the $A_b^{\alpha\beta,\gamma\delta}$ are now the true coupling constants. The anti-Stokes intensity is obtained simply by replacing $1 + n(w,T)$ by $n(w,T)$ in Equation 3.13. Equation 3.13 predicts a continuous first-order Raman spectrum for a disordered material, in contrast to the line spectrum exhibited by crystalline solids.

The reduced Stokes Raman intensity at frequency shift w, $I_{\alpha\beta,\gamma\delta}^{red}(w,T)$,

is derived from the measured intensity, $I_{\alpha\beta,\gamma\delta}(w,T)$, by dividing the latter by the temperature factor, $1 + n(w,T)$, the dipole scattering term, w_s^4, and the harmonic oscillator amplitude, $1/w$:

$$I^{red}_{\alpha\beta,\gamma\delta}(w,T) = \frac{wI_{\alpha\beta,\gamma\delta}(w,T)}{w_s^4[1 + n(w,T)]} \qquad (3.14)$$

Re-writing Equation 3.13 in terms of the reduced Raman intensity defined by Equation 3.14 one obtains

$$I^{red}_{\alpha\beta,\gamma\delta}(w,T) = \underset{b}{\leqq} A_b^{\alpha\beta,\gamma\delta} g_b(w) \qquad (3.15)$$

The vibrational density of states, $G(w)$, is simply given by

$$G(w) = \underset{b}{\leqq} g_b(w) \qquad (3.16)$$

so the right hand side of Equation 3.15 may be regarded as an approximate density of states — the less the coupling coefficients $A_b^{\alpha\beta,\gamma\delta}$ vary from band to band the better the approximation, and if they are completely band independent then they can be taken outwith the summation in Equation 3.15 and the reduced Raman spectrum will be exactly proportional to the actual density of states, $G(w)$.

For essentially the same reasons the i.r. spectrum of an amorphous solid is also reducible to an approximate density of states which is exactly proportional to $G(w)$ if the coupling coefficients involved are again band independent. If the i.r. and Raman spectra of a particular amorphous solid are closely related to its vibrational density of states then the reduced spectra should be similar to one another. Thus by comparing the reduced i.r. and Raman spectra of the material in question it is possible to determine whether this density-of-states interpretation is applicable — the less similar the spectra, the less likely it is that the reduced Raman spectrum is a good approximation to $G(w)$. If the vibrational density of states of the material has been measured or calculated then the extent to which the reduced Raman spectrum can be regarded as a measure of $G(w)$ can be ascertained directly. For a dis-ordered material with a corresponding crystalline phase, a reasonable

approximation to G(w) can be obtained by broadening the one-phonon density of states of the crystal (or sometimes even its Raman spectrum) using a Gaussian convolution function.

One of the advantages of Raman scattering over i.r. spectroscopy in the study of amorphous materials is that the former provides inform- ation on not only the frequencies of the vibrations but also their symmetry properties. This extra information is contained in the polar- isation states of the Raman bands. As the Raman spectrum of an amorphous material is continuous the depolarisation ratio will also be a continuous function of frequency shift and this function may be termed the 'depolarisation spectrum' of the material[14]. If the coupling constants, $A_b^{\alpha\beta,\delta\delta}$, are really band independent for a given amorphous solid then its polarised Raman spectra should have the same shape and so the corresponding depolarisation spectrum should have a constant amplitude[14]. Thus the applicability of the Shuker-Gammon theory to the Raman spectrum of a particular amorphous material can be determined from the depolarisation spectrum of the scattered radiation and no knowledge of the material's i.r. spectrum or actual density of vibrational states is required. The more irregular the depolarisation spectrum is, the less valid is the density-of-states interpretation of the reduced Raman spectrum.

In the case of the tetrahedrally coordinated amorphous semiconductors it is found that the Shuker-Gammon theory is indeed applicable. The reduced Raman spectra of the elements (e.g. Si and Ge), compounds (e.g. GaAs and InP) and alloys (e.g. $Si_{1-x}Ge_x$ and $Ge_{1-x}Sn_x$, $0 < x < 1$) in this relatively simple class of amorphous material are broadly similar to the corresponding reduced i.r. spectra and, in the case of the elements and compounds, approximately resemble a broadened crystalline density of vibrational states. Differences in relative intensity between corresponding features in the reduced Raman and i.r. spectra can be attributed to frequency-dependent coupling coefficients or the incomplete breakdown of

selection rules in the disordered material. Lannin[16 – 18] has investigated the frequency dependence of the coupling coefficients $C_b^{\alpha\beta,\gamma\delta}$ of Equation 3.12 for a-Si and a-Ge and finds that in both cases $C_b^{\alpha\beta,\gamma\delta}(w) \propto w^2$ in the low-frequency range where $G(w)$ is expected to be Debye-like. Taking the $C_b^{\alpha\beta,\gamma\delta}(w)$ as constant for materials where they vary as w^2 will tend to depress the low-frequency region of the reduced Raman spectrum relative to the high-frequency region and will also depress it relative to the low-frequency region of the reduced i.r. spectrum[19]. Intensity differences may also arise from the fact that the selection rules operative in the crystal may not break down completely in the disordered material so that for the latter, bands that correspond to Raman(i.r.)-active vibrations in the crystal will be stronger in the Raman(i.r.) spectrum than bands whose activity is solely disorder induced[2].

In the case of the compounds the vibrational spectra may exhibit structure that has no counterpart in the broadened crystalline density of states. This extra structure arises from the presence of 'wrong' bonds in the disordered material, e.g. P–P bonds in InP[20] or C–C bonds in SiC[21]. In the crystalline compounds these bonds between like atoms are not present. Spectral features due to bonds between like atoms are also observed in the case of the alloys, e.g. $Ge_{0.5}Si_{0.5}$[22].

Several other theoretical approaches to the vibrational spectra of the tetrahedrally coordinated amorphous semiconductors have been proposed. Using a random network model employing a two-parameter elastic potential energy and local-bond optical coupling mechanisms for the i.r. and Raman activities, Alben et al.[23 – 25] have calculated i.r. and Raman spectra for a-Si and a-Ge which are in excellent agreement with experiment. Alben et al. considered isolated-cluster models as well as periodic models of these materials and found that both types of model gave similar results provided boundary effects were taken into account. Thorpe[26] has put

forward a method for establishing physically reasonable boundary

conditions for the dangling bonds of surface atoms of clusters and

employs this method in his own small-cluster approach[27] to calculating

the vibrational spectra of a-Si and a-Ge. Although only the density

of states has been calculated, Thorpe's model can be extended to

calculating the Raman spectrum.

Mitra et al.[28] and von Heimendahl[29] calculate the vibrational

spectra by methods which basically broaden crystalline effects in accord

with the broadening of the pair correlation function. These methods

reproduce the basic shape of the reduced Raman spectrum and in the case

of von Heimendahl's approach the w^2 dependence of its low-frequency

region is reproduced analytically.

Weaire and Alben[30] have propounded a theorem which accounts for

the general features of the vibrational density of states of tetra-

hedrally bonded solids. Their theorem states that the phonon density

of states of a tetrahedrally coordinated system subject to the Keating

form of the short range potential energy[31] — the form used by Alben

et al.[23 − 25] and von Heimendahl[29] — should have the form of a

'one-band' Hamiltonian density of states bracketed by two bands which

tend to delta functions as the ratio of the bond-bending to bond-stretching

force constants tends to zero.

3.4.2   The molecular model

It has recently been shown[32] that the density-of-states interp-

retation is applicable not only to the tetrahedrally coordinated amorphous

semiconductors but also to the more complicated materials a-GaSe, a-MoS$_2$

and amorphous graphite. However, there is a large class of amorphous

materials whose vibrational spectra are not well described by a density-

of-states approach — these are the amorphous chalcogenides. The reduced

i.r. and Raman spectra of these materials are often complementary rather

than similar, which suggests that selection rules are still operative
in these solids. This complementarity of i.r. and Raman activity is
clearly evident in the case of a--As_2S_3[33]. Also, the reduced spectra
of some amorphous chalcogenide materials, e.g. a-Te[34], do not resemble
broadened versions of their corresponding crystalline densities of states.
The depolarisation spectra of the chalcogenides, furthermore, are rich
in structure and do not exhibit the unvarying amplitude that would be
expected if the corresponding reduced Raman spectra were density-of-
states-like. The irregularity of $\rho(w)$ in the case of a-As_2S_3 is clearly
seen in Figure 5.14, after p.119.

The sharpness of the features in the chalcogenide spectra compared
with those of the density-of-states-like spectra, together with the fre-
quent complementarity of i.r. and Raman activity in the chalcogenides,
has lead some workers[2,33,35,36] to suggest a molecular approach to these
materials. Such an approach will be appropriate for those amorphous
solids composed of small, weakly coupled, molecule-like units. The
approach consists of identifying a basic structural unit for the material
concerned and using the well-established techniques of molecular vibrational
analysis to determine the frequencies of its normal modes. Some amorphous
materials are truly molecular and consist of discrete units (a-S and a-Se
fall in this category), but in other materials the basic units are joined.
The effects of inter-unit coupling in the non-molecular materials can be
accounted for by considering the links between the units: the frequencies
of the coupled modes are determined by applying the above techniques to
the link 'molecule' connecting the units. The continuous nature of the
vibrational spectra of the amorphous solid can be thought of as arising
from a spread in the bond lengths, bond angles and force constants of the
link and unit 'molecules', and the structure in the depolarisation spectrum
reflects the prevailing i.r. and Raman 'molecular' selection rules.

The molecular model is also applicable to materials other than the

chalcogenides, e.g. a-SiO$_2$[37] is a suitable candidate for this type of analysis because the strongly bonded SiO$_4$ tetrahedral units of which it is composed are only weakly coupled, as a result of the softness of the bond-bending force constant associated with the oxygen atoms bridging the tetrahedra. A molecular approach is clearly inappropriate for materials in which all chemical bonds are equivalent: in a-Si, for example, the bonding at the bridging Si atoms is as strong as the bonding within the basic SiSi$_4$ tetrahedral units, which cannot, therefore, be regarded as weakly coupled.

Although it seems naive to suppose that a non-molecular material might be regarded as being composed of decoupled, molecule-like units, it is possible to justify this approach theoretically. DeFonzo and Tauc[38,39] have studied the conditions for the potential and kinetic decoupling of vibrations of local units in a network and have found that decoupling is possible provided the structure satisfies certain geometrical conditions. (It follows that if the vibrations in a material are found to be decoupled, further information on its structure can be deduced using these conditions). Thus a weak bond-bending force constant at the bridging atoms shared by neighbouring units may be a necessary condition for a molecular analysis to be appropriate but it is not a sufficient one. Their theory, which they term the 'decoupled network' approach, was first applied by them to the case of a-As$_2$S$_3$.

Lucovsky and co-workers have demonstrated that the molecular approach is applicable in the case of the three amorphous chalcogen elements, which are truly molecular. They have shown that using the molecular model it is possible to interpret the vibrational spectra of a-S[35], a-Se[35,40 — 42] and a-Te[35,43,44], although account must be taken of intermolecular forces in the last two cases. In the case of the amorphous arsenic chalcogenides the molecular model has been successfully applied to a-As$_2$S$_3$[2,33,35,45,46], a-As$_2$Se$_3$[2,33,35,45,46] and a-As$_2$Te$_3$[2,47]; the molecular analysis of the

a-As_2S_3 and a-As_2Se_3 spectra is discussed in detail in Sections 5.4.4.4, 5.4.5, 6.4.4.4 and 6.4.6 where it is shown that the model yields very good agreement with experiment. Solin and Papatheodorou[48,49] have recently shown that the vibrational spectra of the related amorphous material a-As_2O_3 can also be accounted for by the molecular model. In Sections 5.5.1.5.4 and 6.5.1.5.4 the model is applied for the first time to binary arsenic-chalcogen alloys; it will be shown there that the spectral changes occuring in the As-S and As-Se systems as the chalcogen content increases above 60 at.% can be accounted for by the molecular model. The vibrational spectra of the ternary alloys in the a-$(As_2S_3)_{1-x}$ — $(As_2Se_3)_x$ [2,45,46,50] and a-$(As_2Te_3)_{1-x}(As_2Se_3)_x$ [2,51] systems have also been shown to be consistent with the molecular model.

A molecular approach is appropriate in the case of the amorphous germanium chalcogenides too: it has been successfully applied to the vibrational spectra of the compounds a-GeS_2 [2,45,46,52], a-$GeSe_2$ [2,45,46] and a-$GeTe_2$ [2,53], the alloy a-GeSSe [2], and the alloy systems a-$Ge_{1-x}S_x$ [2,52,54,55], a-$Ge_{1-x}Se_x$ [2,55] and a-$Ge_{1-x}Te_x$ [53]. It is also applicable in the case of the alloy systems a-$(As_2S_3)_x(GeS_2)_{1-x}$ [2,45,46] and a-$(As_2Se_3)_x(GeSe_2)_{1-x}$ [45,46] which contain both As and Ge.

Between the limiting situations of purely molecular spectra and purely density-of-states-like spectra there is a continuum of behaviour. For example, since in the periodic table As lies between Ge, whose spectra are predominantly density-of-states-like, and Se, whose spectra are molecular, one expects the spectra of a-As to exhibit a combination of these two types of behaviour[2] and it will be shown in Section 5.3.2 that this expectation is confirmed.

Brodsky[3] and Lucovsky[56] have pointed out that conceptually the molecular and density-of-states approaches are not very different, for the dispersion in the optic modes of a truly molecular system is inherently small and dispersion curves confined in narrow energy bands give rise to

sharp structure in G(w). (Finkman et al.[57] have used this fact to deduce the form of the dispersion curves of c-As$_2$Se$_3$ from observations of the Raman spectrum of a sample of a-As$_2$Se$_3$ undergoing photo-induced crystallisation between T$_g$ and T$_m$). Thus the sharpness of the spectral features of the chalcogenides compared with those of the tetrahedrally bonded semiconductors, whose dispersion curves are broad in energy space and therefore lead to broad features in G(w), is still compatible with a density-of-states description. The Raman spectra of a-As$_2$S$_3$ and a-As$_2$Se$_3$ are to a certain extent amenable to the density-of-states approach[14]: both spectra, for example, are similar to broadened versions of the respective crystalline Raman spectra. This is because even in the crystals the main contribution to the density of states comes from modes with a molecular nature. The application of the density-of-states approach to a-As$_2$S$_3$ and a-As$_2$Se$_3$ is discussed in detail in Sections 5.4.4.1 and 6.4.4.1 respectively. Other models for the vibrational spectra of a-As$_2$S$_3$ and a-As$_2$Se$_3$ are discussed in Sections 5.4.4 and 6.4.4.

3.4.3 Low-frequency Raman scattering

The low-frequency region of the Raman spectrum of an amorphous material is of considerable importance: it can be used to investigate the frequency dependence of the coupling coefficients, $C_b^{\alpha\beta,\gamma\delta}$, of Equation 3.12, it can be used to derive an upper bound to the structural correlation range in the material, and it can contain, at very low frequencies, information on the states responsible for the specific heat anomaly that non-crystalline solids display.

The reduced Raman intensity, as defined by Shuker and Gammon, at frequency shift w is proportional to $\leq_b C_b^{\alpha\beta,\gamma\delta} g_b(w)$ where $\leq_b g_b(w) = G(w)$, the vibrational density of states (see p.54). If the form of G(w) is known the frequency dependence of the $C_b^{\alpha\beta,\gamma\delta}$ can be found. At low frequencies G(w) is expected to be Debye-like, i.e. to vary as w^2, and

hence the coupling coefficients in this region can be determined from the reduced Raman spectrum. Theory[19,58 − 60] predicts that the $c_b^{\alpha\beta,\gamma\delta}$ are also proportional to w^2 for vibrations whose average wavelength, λ, is much greater than the correlation length, L, of the fluctuations, i.e. for vibrations which satisfy the inequality

$$L/\lambda \ll 1 \qquad\qquad (3.17)$$

Equation 3.17 defines the 'long-wavelength limit'. Lannin has shown that the low-frequency coupling coefficients do, indeed, vary as w^2 in the case of a-Si[17] and a-Ge[18]. G(w) is expected to be Debye-like below $\sim$65 cm^{-1} in a-Si and $\sim$35 cm^{-1} in a-Ge, and in these spectral ranges Lannin found that $c_b^{\alpha\beta,\gamma\delta} \propto w^2$. The low-frequency coupling coefficients of a-As$_2$S$_3$, a-As$_2$Se$_3$, a-GeS$_2$ and a-GeSe$_2$ have also been shown to vary as w^2 [61].

For an amorphous solid the correlation length, L, of the fluctuations is expected to be comparable with the structural correlation length obtained from diffraction experiments[17]. Martin and Brenig[59] have derived expressions for the scattered-light intensity in the region where the $c_b^{\alpha\beta,\gamma\delta}$ are expected to vary as w^2. Their theory is valid in the frequency range for which

$$\hbar c w L / v_t \ll 1 \qquad\qquad (3.18)$$

where c is the velocity of light and v_t the transverse sound velocity in the material (w being the frequency in wavenumbers). On the basis of this inequality, which is similar to Equation 3.17, Martin and Brenig have deduced from the data of Reference 17 an upper limit to L in a-Si of 4 Å. Using the Martin-Brenig model, Nemanich[61] has determined the structural correlation ranges of a-As$_2$S$_3$, a-As$_2$Se$_3$, a-GeS$_2$ and a-GeSe$_2$: the values obtained are 6.5 $\pm$ 1 Å and 8.5 $\pm$ 1 Å for the As and Ge chalcogenides respectively.

It was stated above that for an amorphous solid, as in a crystal, the vibrational modes at low frequencies are expected to be Debye-like.

This is not strictly true for it has been suggested that at very low frequencies there occur, in addition to the Debye phonons, special modes which account for the anomalous specific heat in these materials. If these special modes couple to the incident light with sufficient strength they will produce a detectable contribution to the Raman spectrum and it will be possible to obtain some information on the nature of these states from light-scattering experiments.

The low-frequency Raman spectrum of an amorphous material is believed to be predominantly due to disorder-induced scattering from high-frequency sound waves. Current theories[9,13,58,59] of disorder-induced scattering are based on the Debye model and so predict that the scattered intensity should vanish as $w \to 0$. According to the Martin-Brenig model, for example, the spectrum in the frequency range satisfying Equation 3.18 should consist of the Brillouin peaks and an 'amorphous' background that is expected to vary as w^2 at not too small temperatures (i.e. at temperatures for which $(1/w)[n(w,T) + 1]$ varies as w^{-2} and so cancels the w^2 dependence of the $C_b^{\alpha\beta,\gamma\delta}$). Winterling[62,63], however, has measured the low-frequency Raman spectra of $a\text{-}SiO_2$, $a\text{-}B_2O_3$, $a\text{-}As_2S_3$ and the borosilicate glass BK7 and finds that the scattered intensity does not tend to zero as $w \to 0$ but reaches a finite minimum and then increases slightly. In $a\text{-}SiO_2$ the minimum occurs at 10 cm^{-1}. Winterling has established that this excess intensity arises from true inelastic scattering and points out that it is peculiar to the amorphous state since the scattered intensity at low frequencies is much weaker in the corresponding crystals: in $c\text{-}SiO_2$, for example, the scattering in the range $4 < w < 20$ cm^{-1} is about one order of magnitude weaker than in $a\text{-}SiO_2$.

Brillouin lines have been observed in $a\text{-}SiO_2$[12,63 − 65] thus confirming the presence of Debye phonons of very low frequency (<1 cm^{-1}). Winterling has deduced from intensity and polarisation measurements on the excess scattering that it cannot be attributed to the high-frequency tails that appear on the Brillouin lines as a result of disorder-induced damping of

these very low frequency phonons.   He has also examined the temperature
dependence of the excess scattering and found it to be inconsistent with
second-order processes — in the case of crystals such processes, particularly
difference processes, can contribute to the scattering at low frequencies.

The models proposed to explain the specific heat anomaly in amorphous
materials fall into two classes: those based on atomic tunnelling between
two near-equivalent equilibrium positions[66,67] and those assuming the
presence of special low-frequency vibrational states[68,69], e.g. strongly
damped high-frequency sound waves.   Winterling has shown that his observ-
ations on the excess scattering are consistent with disorder-induced
scattering from damped high-frequency sound waves but not with a Raman
process involving a two-level system.   However, he points out that his
measurements extend only to 40° K and any contribution arising from atomic
tunnelling might be detectable at lower temperatures.   In principle
atomic tunnelling could give rise to excess scattering at low frequencies
and Winterling proposes a mechanism for the direct coupling of the incident
light to the defects.   Investigations of Brillouin and excess Raman
scattering below 40° K are necessary to determine whether atomic tunnelling
also occurs in these materials.

As the present study is primarily concerned with a structural invest-
igation of As-S and As-Se glasses no detailed examination of the low-
frequency (<10 cm^{-1}) regions of their spectra has been carried out.   No
one has yet experimentally determined the vibrational density of states of
any of the As-S or As-Se glasses so no firm conclusions can be reached on
the form of the frequency dependence of the $C_b^{\alpha\beta,\gamma\delta}$ or on the correlation
lengths of the fluctuations in these materials.

3.5 References

1. 'The Raman Effect' (Anderson, A., editor), Marcel Dekker, New York, 1973.

2. Lucovsky, G., Proc. 5th Int. Conf. on Amorphous and Liquid Semiconductors, Garmisch-Partenkirchen, Germany (Stuke, J. and Brenig, W., editors), Taylor and Francis, London, 1974, p.1099.

3. Brodsky, M.H., in 'Light Scattering in Solids' (Cardona, M., editor), Springer-Verlag, Berlin, 1975, p.205.

4. Böttger, H., Phys. Stat. Sol. (b), 62, 9 (1974).

5. Bell, R.J., Rep. Progr. Phys. 35, 1315 (1972).

6. Dean, P., Rev. Mod. Phys. 44, 127 (1972).

7. Solin, S.A., A.I.P. Conf. Proc. 31, 205 (1976).

8. Haas, M., Solid State Commun. 7, 1069 (1969).

9. Shuker, R. and Gammon, R.W., Phys. Rev. Lett. 25, 222 (1970).

10. Haas, M., J. Phys. Chem. Solids 31, 415 (1970).

11. Stolen, R.H., Phys. Chem. Glasses 11, 83 (1970).

12. Flubacher, P., Leadbetter, A.J., Morrison, J.A. and Stoicheff, B.P., J. Phys. Chem. Solids 12, 53 (1969).

13. Shuker, R. and Gammon, R.W., Proc. 2nd Int. Conf. on Light Scattering in Solids, Paris (Balkanski, M., editor), Flammarion, Paris, 1971, p.334.

14. Kobliska, R.J. and Solin, S.A., Phys. Rev. B 8, 756 (1973).

15. Kobliska, R.J. and Solin, S.A., J. Non-Cryst. Solids 8 – 10, 191 (1972).

16. Lannin, J.S., Solid State Commun. 11, 1523 (1972).

17. Lannin, J.S., Solid State Commun. 12, 947 (1973).

18. Lannin, J.S., Proc. 5th Int. Conf. on Amorphous and Liquid Semiconductors, Garmisch-Partenkirchen, Germany (Stuke, J. and Brenig, W., editors), Taylor and Francis, London, 1974, p.1245.

19. Prettl, W., Shevchik, N.J. and Cardona, M., Phys. Stat. Sol. (b) 59, 241 (1973).

20. Wihl, M., Cardona, M. and Tauc, J., J. Non-Cryst. Solids 8 – 10, 172 (1972).

21. Gorman, M. and Solin, S.A., Solid State Commun. 15, 761 (1974).

22. Shevchik, N.J., Lannin, J.S. and Tejeda, J., Phys. Rev. B 7, 3987 (1973).

23. Alben, R., Smith, J.E., Jr., Brodsky, M.H. and Weaire, D., Phys. Rev. Lett. 30, 1141 (1973).

24. Alben, R., Weaire, D., Smith, J.E., Jr. and Brodsky, M.H., Proc. 5th Int. Conf. on Amorphous and Liquid Semiconductors, Garmisch-Partenkirchen, Germany (Stuke, J. and Brenig, W., editors), Taylor and Francis, London, 1974, p.1231.

25. Alben, R., Weaire, D., Smith, J.E., Jr. Brodsky, M.H., Phys. Rev. B 11, 2271 (1975).

26. Thorpe, M.F., Phys. Rev. B 8, 5352 (1973).

27. Thorpe, M.F., Proc. Int. Conf. on Tetrahedrally Bonded Amorphous Semiconductors, Yorktown, American Institute of Physics, New York, 1974, p.267.

28. Mitra, S.S., Bendow, B. and Tsay, Y.F., Proc. 3rd Int. Conf. on Light Scattering in Solids, Campinas, Brazil, Flammarion, Paris, 1975, p.646.

29. von Heimendahl, L., Proc. 5th Int. Conf. on Amorphous and Liquid Semiconductors, Garmisch-Partenkirchen, Germany (Stuke, J. and Brenig, W., editors), Taylor and Francis, London, 1974, p.853.

30. Weaire, D. and Alben, R., Phys. Rev. Lett. 29, 1505 (1972).

31. Keating, P.N., Phys. Rev. 145, 637 (1966).

32. Lannin, J.S., Proc. 7th Int. Conf. on Amorphous and Liquid Semiconductors, Edinburgh (Spear, W.E., editor), C.I.C.L., Edinburgh, 1977, p.110.

33. Lucovsky, G., Phys. Rev. B 6, 1480 (1972).

34. Brodsky, M.H., Gambino, R.J., Smith, J.E., Jr. and Yacoby, Y., Phys. Stat. Sol. (b) 52, 609 (1972).

35. Lucovsky, G. and Martin, R.M., J. Non-Cryst. Solids 8 – 10, 185 (1972).

36. Austin, I.G. and Garbett, E.S., Phil. Mag. 23, 17 (1971).

37. Bell, R.J., Bird, N.F. and Dean, P., J. Phys. C 1, 299 (1968).

38. Tauc, J., Proc. 3rd Int. Conf. on Light Scattering in Solids, Campinas, Brazil, Flammarion, Paris, 1976, p. 621.

39. DeFonzo, A.P. and Tauc, J., Solid State Commun. 18, 937 (1976).

40. Lucovsky, G., Mooradian, A., Taylor, W., Wright, G.B. and Keezer, R.C., Solid State Commun. 5, 113 (1967).

41. Mooradian, A., in 'Laser Handbook' (Arecchi, F.T. and Shulz-Dubois, E.O., editors), Vol.2, North-Holland, Amsterdam, 1972, p.1409.

42. Martin, R.M., Lucovsky, G. and Helliwell, K., Phys. Rev. B 13, 1383 (1976).

43. Lucovsky, G., Phys. Stat. Sol. (b) 49, 633 (1972).

44. Martin, R.M. and Lucovsky, G., Proc. 12th Int. Conf. on the Physics of Semiconductors, Stuttgart (Pilkuhn, M.H., editor), Teubner, Stuttgart, 1974, p.184.

45. Lucovsky, G., Nemanich, R.J., Solin, S.A. and Keezer, R.C., Solid State Commun. 17, 1567 (1975).

46. Nemanich, R.J., Solin, S.A. and Lucovsky, G., Proc. 3rd Int. Conf. on Light Scattering in Solids, Campinas, Brazil, Flammarion, Paris, 1976, p.631.

47. Taylor, P.C., Bishop, S.G. and Mitchell, D.L., Solid State Commun. 16, 167 (1975).

48. Papatheodorou, G.N. and Solin, S.A., Solid State Commun. 16, 5 (1975).

49. Papatheodorou, G.N. and Solin, S.A., Phys. Rev. B 13, 1741 (1976).

50. Felty, E.J., Myers, M.B. and Lucovsky, G., Solid State Commun. 6, 765 (1968).

51. Lucovsky, G., Thornburg, D.D., Six, H.A. and Johnson, R.I., cited in Reference 2.

52. Lucovsky, G., Galeener, F.L., Keezer, R.C., Geils, R.H. and Six, H.A., Phys. Rev. B 10, 5134 (1974).

53. Fisher, G.B., Tauc, J. and Verhelle, Y., Proc. 5th Int. Conf. on Amorphous and Liquid Semiconductors, Garmisch-Partenkirchen, Germany (Stuke, J. and Brenig, W., editors), Taylor and Francis, London, 1974, p.1259.

54. Lucovsky, G., deNeufville, J.P. and Galeener, F.L., Phys. Rev. B 9, 1591 (1974).

55. Lucovsky, G., Galeener, F.L., Geils, R.H. and Keezer, R.C., in 'The Structure of Non-Crystalline Materials' (Gaskell, P.H., editor), Taylor and Francis, London, 1977, p.127.

56. Lucovsky, G. and Knights, J.C., Phys. Rev. B 10, 4324 (1974).

57. Finkman, E., DeFonzo, A.P. and Tauc, J., Proc. 12th Int. Conf. on the Physics of Semiconductors, Stuttgart (Pilkuhn, M.H., editor), Teubner, Stuttgart, 1974, p.1022.

58. Whalley, E. and Bertie, J.E., J. Chem. Phys. 46, 1264 (1967).

59. Martin, A. and Brenig, W., Phys. Stat. Sol.(b) 64, 163 (1974).

60. Connell, G.A.N., Phys. Stat. Sol. (b) 69, 9 (1975).

61. Nemanich, R.J., Phys. Rev. B 16, 1655 (1977).

62. Winterling, G., Proc. 3rd Int. Conf. on Light Scattering in Solids, Campinas, Brazil, Flammarion, Paris, 1976, p.663.

63. Winterling, G., Phys. Rev. B 12, 2432 (1975).

64. Love, W.F., Phys. Rev. Lett. 31, 822 (1973).

65.   Pohl, R.O., Love, W.F. and Stephens, R.B., Proc. 5th Int.
       Conf. on Amorphous and Liquid Semiconductors, Garmisch-
       Partenkirchen, Germany (Stuke, J. and Brenig, W., editors),
       Taylor and Francis, London, 1974, p.1121.

66.   Anderson, P.W., Halperin, B.I. and Varma, C.M., Phil. Mag.
       $\underline{25}$, 1 (1972).

67.   Phillips, W.A., J. Low Temp. Phys. $\underline{7}$, 351 (1972).

68.   Rosenstock, H.B., J. Non-Cryst. Solids $\underline{7}$, 123 (1972).

69.   Zeller, R.C. and Pohl, R.O., Phys. Rev. B $\underline{4}$, 2029 (1971).

CHAPTER 4

EXPERIMENTAL TECHNIQUES

4.1   Introduction

This chapter outlines the methods and equipment used in the production of the samples, in the Raman experiments themselves, and in the processing of the Raman data.   Only a brief description is needed since the apparatus is fairly standard, most of it being of commercial origin, while comprehensive accounts of many of the techniques, which are also fairly standard, already exist.

The basic requirements for a Raman scattering experiment are a monochromatic light source, a target, a dispersing element and a light-detector.   The laser is an eminently suitable source for Raman experiments and has almost completely replaced the arc-lamp.   Modern lasers provide a selection of excitation frequencies in the visible, near i.r. and near u.v. and their intense, polarised radiation is stable and of narrow linewidth (typically 0.005 cm^{-1}).   Solids in their various forms, gases and liquids may all be examined by light scattering and sampling techniques have been developed for all types of specimen. Grating spectrometers have replaced prism instruments as the dispersing element and the photographic plate has given way to the photomultiplier as detector.

The historical development and present features of experimental Raman spectroscopy are described in many texts, e.g. Reference 1.   Future developments include the use of automation techniques[2] and tunable lasers for excitation[3].

4.2   The samples

The information given in this section is summarised in Table 4.1, after p.80.

4.2.1   Material production and sources

4.2.1.1 Glasses: $As_{35}S_{65} - As_{45}S_{55}$

The amorphous samples used in the Raman experiments were all in the form of bulk ingots and were prepared by the staff of the Department's chemistry laboratory, in the usual way, by melting the constituents under vacuum in a quartz tube, as outlined below.

Appropriate amounts of the pure constituents were weighed out and placed in a quartz tube of approximately 1 cm bore.   As pure arsenic oxidises quickly it was more convenient to use an arsenic-sulphur compound rather than arsenic as one of the initial constituents, for example $As_{40}S_{60}$ and S could be used to produce all glasses more S-rich than $As_{40}S_{60}$.   Pure As was only used when no suitable compound was available, and in the making of the base compound itself.   In the case of the eleven glasses centred on the stoichiometric composition $As_{40}S_{60}$ (see Figure 5.1, after p.107) ~70 gm of each of the two end compositions, $As_{45}S_{55}$ and $As_{35}S_{65}$, were made up first and the remaining nine compositions were made up, in ~10 gm quantities, from mixtures of these.

The tube was then evacuated, sealed and placed in a rocking furnace at 850° C for 24 hours.   Next, the material was annealed for several hours just below its glass transition temperature, Tg — which is around 200° C for these materials[4] — and then cooled slowly to ambient temperature.   It was found that the annealing stage was necessary for three reasons.   First, the samples tended to break up during cutting and polishing unless annealed[5].   Secondly, it was found that laser-induced changes (see Section 4.3.5) were more pronounced in a non-annealed glass, as would be expected[5].   Finally, annealing is necessary to reduce the

amount of strain-induced birefringence in the glass since this effect

hampers the recording of accurate polarisation data[6].

The annealing routine was as follows. The tube containing the

molten sample was removed from the furnace and allowed to cool in air

until the contents had solidified. The top of the melt was warmed in

a bunsen flame during this process; this increased the vapour pressure

above the melt and so prevented it from boiling. It was then inserted

in a brass block at 240° C and the temperature of the block allowed to

fall freely to 205° C. The block was then maintained at 195 - 205° C

for between 4 and 16 hours, the exact annealing period not being critical

provided it was longer than about 2 hours. After this the block was

cooled to 170° C at the rate of approximately 0.25° C/min and then from

170° C to 120° C at the rate of 1° C/min. Finally, the temperature of

the block was allowed to fall freely from 120° C to ambient.

The stoichiometries of three of the melts, $As_{36}S_{64}$ and the two end

compositions $As_{45}S_{55}$ and $As_{35}S_{65}$, were checked by chemical analysis,

particularly with respect to possible variations through the bulk.

Several specimens from each of the three melts were analysed by the method

of gravimetric titration and the results showed no significant variation

through the bulk and no significant difference from the nominal comp-

ositions. The glasses are within $\pm\frac{1}{2}$ at.% of the stated stoichiometries.

The Raman spectra of all the materials studied in this project were

compared with the reported spectra of the various arsenic oxides and

as the characteristic spectral features of these contaminants were not

observed in the glass spectra, significant quantities of these oxides

cannot be present in the samples or produced in them during laser illumin-

ation.

The Raman spectra obtained from the glasses were typical of vitreous materials, that is they were continuous and consisted of broad features. As a further check on the composition and nature of the samples, two sets of spectra for the stoichiometric glass $As_{40}S_{60}$ were compared, one being run on a commercial sample and the other on the sample produced in the Department. The commercial sample was obtained from the American Optical Company and chemical analysis showed it to have a slightly As-rich composition, viz $As_{40.3}S_{59.7}$. The two sets of spectra — 1, 5 and 6 (commercial) and 2, 3 and 4 (Department) — of Figure 4.14 (see also Figure 4.15) do not differ significantly and are in good agreement with the published spectra of this glass[6,7,8,9]. Spectra of some of the other compositions were compared with Ward's[10] spectra for bulk As-S glasses and found to be in agreement with them. The homogeneity of the samples was evident in the experiments since no significant differences were observed between spectra run in different places in the same sample.

4.2.1.2 Other As-S glasses

The four other glasses examined, $As_{28.6}S_{71.4}$ (i.e. As_2S_5), $As_{25}S_{75}$, $As_{15}S_{85}$, and As_5S_{95}, were also made up by melting the constituents under vacuum in a quartz tube but did not all undergo the standard annealing procedure. In the case of As_2S_5 the glass resulted from an attempt to make the crystal form of this composition. The components were fused together in the usual way and the furnace was switched off after 24 hours, but the melt, instead of being removed for annealing, was left inside where it cooled slowly at the cooling rate of the furnace. The resulting material, however, was perfectly glassy, as evinced by its Raman spectrum, which was broad and continuous and in agreement with Ward's data[10].

The glass transition temperature, Tg, of the As-S glasses peaks at $As_{40}S_{60}$, where Tg $\approx 200^{\circ}$ C, and falls linearly as the sulphur content is increased[4]. Tg for the As_5S_{95} composition is approximately 0° C and

this glass was not annealed. This composition did not vitrify when cooled in air but turned opaque and pale yellow, presumably due to the formation of sulphur crystallites. The material had to be re-melted and quenched in water. A transparent, dark yellow, elastic glass was produced which turned opaque within 24 hours and which eventually lost its elasticity. Raman spectra recorded in the transmission mode while the sample was still transparent and in the back reflection mode once it had turned opaque were identical to Ward's spectrum of this material[10]. The region irradiated by the laser turned opaque more quickly than the non-irradiated regions.

The $As_{15}S_{85}$ melt was mistakenly annealed at 160° C, $\sim 100^{\circ}$ C above Tg for this glass, but yielded a satisfactory sample. The standard annealing procedure was carried out on the $As_{25}S_{75}$ melt, (Tg$\approx 120^{\circ}$ C).

There was no significant difference between the behaviour of the standard-anneal glasses and that of the three S-rich glasses which underwent different cooling procedures. The latter were no more difficult to polish than the others and exhibited the same level of photo- and strain-induced effects. The spectra recorded from them were typically vitreous and in agreement with Ward's work.

4.2.1.3 The selenides

The amorphous arsenic selenides used by Dr. Sik were also in the form of bulk ingots and were all prepared and checked by the same methods that were used for the sulphide glasses, Tg in the annealing regime being taken from Reference 4 again. The samples were all black and opaque.

4.2.1.4 The crystals

The crystal compositions that exist in the As-S system are discussed fully in Section 2.2. c-As_2S_3, which is the most widely known and

studied of the crystalline arsenic-sulphides, occurs naturally as the mineral orpiment and can also be made synthetically by chemical[11] or physical[12] means, though with some difficulty in the latter case. It is extremely difficult to devitrify glassy As_2S_3[13]. Two forms of c-As_2S_3 exist[14,15] : α-As_2S_3, the ordinary yellow mineral orpiment, and a red modification, though it is not known whether this represents another crystal structure or is due to impurities.

In our investigation we used samples of orpiment obtained from two sources: the Department of Geology of the Royal Scottish Museum and the Department of Geology, University of Edinburgh. The specimens provided by the Museum were in the form of small ($\sim$2 mm diameter) irregularly shaped yellow platelets of poor optical quality. Those obtained from the latter source were opaque, pink lumps ($\sim$2 cm diameter) speckled with yellow. The Raman spectra obtained from these specimens were in excellent agreement with one another and also with the published spectra of orpiment[16-20,6].

c-As_4S_4 is the other well-known crystalline form of arsenic sulphide and occurs naturally as the mineral realgar. It exists in two polymorphic forms[21,22,14]: α-As_4S_4, the red mineral realgar, and β-As_4S_4. In addition to obtaining a sample of the mineral from the Department of Geology of the Royal Scottish Museum an attempt was made to produce a specimen in the Department. The procedure used was the same as that mentioned in Section 4.2.1.2 for the As_2S_5 crystal and consisted simply of fusing the constituents together and cooling the melt slowly in the furnace. The Raman spectrum of this material (see Figure 5.4) was very similar to the spectra of β-As_4S_4 shown in Reference 22. The material is more fully discussed in Section 2.2.2.

The Raman spectrum of the Museum specimen, which was a deep red, transparent lump ($\sim$8mm diameter) of poor optical quality, showed it to

be a completely crystalline sample of α-As$_4$S$_4$ and agreed with the published spectra[7,16,17,22].

The compound As$_4$S$_3$ is less well known. It occurs naturally as the mineral dimorphite[23] and, as the name suggests, exists in two polymorphs, α-As$_4$S$_3$ and β-As$_4$S$_3$[24,25] with distinct crystal structures. As a specimen of this rare mineral could not be obtained, the compound was synthesised in the Department. The material produced, using the above method of slow cooling of the melt, was opaque and dark pink in colour, and its Raman spectrum was typically crystalline. Only the i.r. spectrum of this substance has so far been published[26] so that a complete comparison of our spectrum with published data is not possible. However, the Raman frequencies are in agreement with the i.r. data for β-As$_4$S$_3$.

Little is known of the compounds As$_2$S$_5$ and As$_3$S, neither of which occur in nature, though vitreous As$_2$S$_5$ has been much studied. Specimens of these two compositions were made up by slow cooling of the corresponding melts. The As$_3$S turned out to be a brittle, dark brown material while the As$_2$S$_5$, as mentioned before, was perfectly glassy.

The recently reported compound As$_4$S$_5$[27] is also not naturally occuring. The c-As$_4$S$_5$ specimen used in these experiments was made by allowing a solution of As$_4$S$_3$ in CS$_2$ to evaporate slowly to dryness, as outlined by Whitfield[27]. The process was carried out in a dark cupboard to prevent the light-induced formation of realgar. This method provided a yellow powder in which were dispersed fine, needle-like, orange crystals.

The sample of crystalline As$_2$Se$_3$, a black wafer $\sim$3 mm x 5 mm, was synthetically produced and supplied by Philips Research Laboratories (Eindhoven).

4.2.1.5 Other materials

The sample of sulphur used was a 6N pure powder obtained from Koch-Light Laboratories Ltd. Its Raman spectrum was in good agreement with the published spectra of orthorhombic sulphur[7,28,29,30]. The a-As specimens were also provided by Koch-Light and were in the form of 6N pure lumps of ∼15 mm diameter.

4.2.2 Specimen preparation

4.2.2.1 The transparent glasses

The glass-forming region in the As-S system extends approximately from As_5S_{95} to $As_{43}S_{57}$[4,31]. In bulk form the glasses, which are transparent, range in colour from deep red at the composition $As_{43}S_{57}$, through orange, to dark yellow at As_5S_{95}. The specimens of $As_{43}S_{57}$ and $As_{45}S_{55}$, the two compositions studied which are outwith the glass-forming region, are pink, opaque and granular in appearance.

The standard scattering configuration for specimens that are transparent to the laser line — red in this case — is the transmission mode (see Figure 4.5(a)). Accordingly, the specimens of the transparent compositions were prepared as follows. For each composition the ∼1 cm i.d. quartz tube containing the solidified melt was sawn through with a diamond saw at approximately 1 cm intervals to produce cylinders of material ∼1 cm high by ∼1 cm diameter. As the glasses did not adhere to the quartz the cylinders slipped easily from the surrounding quartz annuli. A cylinder was then selected and its two faces ground and polished flat on a Logitech PM2 polishing machine. Since these materials are fairly soft, having Vickers hardnesses of ∼140 kg/mm^2 [32], the grinding, which was done on a brass plate using 600 mesh carborundum powder, did not take long. The polishing was done using filtered 'Syton' solution on a porous pad.

These materials tended to crack when heated, because of their low thermal conductivity, so great care had to be taken in the mounting of the sample for grinding and polishing since it involved placing the cylinder in a well of hot wax (Cottrell's Sticky Wax) on an aluminium holder, which was screwed into the polishing jig once the wax had solidified and was holding the sample in place. The procedure used was as follows. After being melted initially with a hot-air blower, the wax in the well was left to cool while the cylinder was warmed carefully with the blower; the cylinder was only placed in the well once the wax had started to whiten and become tacky. It was found that an effective method of avoiding heat damage to the sample when removing it from the wax after polishing was to leave the aluminium mount, with the sample still attached, in a beaker of trichloro-ethylene, which soon dissolved the wax.

Once polished on both faces the samples were ready for experiment-ation. Although striations, produced in the formation process, were present in the glasses they had no effect on the unanalysed Raman spectra — spectra recorded on the a-As_2S_3 made in the Department were effectively identical with spectra from the commercial a-As_2S_3, which was of good optical quality (see Figures 4.14 and 4.15). The striations, however, did prevent the acquisition of accurate polaris-ation data since they tended to depolarise the incident beam. The output polarisation of the He-Ne laser is vertical in the lab frame and the linear cross component is given by the manufacturer as $<.03\%$. With the polarised 6328 Å He-Ne laser light an extinction ratio of $\sim$27 db was measured on the American Optical a-As_2S_3 while this ratio for the samples made in the Department was typically $\sim$10 db. The consequences of this are more fully discussed in Section 5.5.1.3.

4.2.2.2 The opaque glasses

Because of the positions of their respective absorption edges, the selenides were not transparent to the laser radiation available, while the sulphides $As_{44}S_{56}$ and $As_{45}S_{55}$ were opaque because of their granularity. The standard scattering configuration for opaque samples is the back-reflection mode (see Figure 4.5(b)), for which only one area of sample surface need be polished. In this mode the scattering is from a surface layer of the material so that thick specimens are unnecessary. Accordingly, the quartz tubes containing the opaque melts were sawn through at ~2 mm intervals to produce discs of material ~2 mm thick and ~1 cm in diameter. The sulphide discs were mounted and ground and polished on one face by exactly the same methods that were used for the transparent sulphides. The mounting and polishing of the selenide discs was slightly different. They were mounted with 'sticky' wax on a 3 cm diameter aluminium disc during grinding and polishing and as this served as the mount for the spinner (see Section 4.3.1) there was no need to de-mount the samples after polishing, which was done with 1μ and $\frac{1}{4}\mu$ solder laps rather than 'Syton'. The selenides were fairly straightforward to polish, with the exception of the most As-rich composition studied, $As_{55}Se_{45}$, which was extremely brittle. Several of the discs broke up during the sawing and grinding stages. A specimen was eventually polished, though the finish was of poor quality.

4.2.2.3 The crystals

None of the crystalline samples was of sufficient optical quality or size for transmission-mode experiments and, either because of their size or fragility, few were in a form suitable for polishing. The specimens obtained from outside the Department were in the form of platelets, wafers or lumps of ~2 — 20 mm diameter, and for the Raman

experiments they were used as they were or powdered. The Department-made As_4S_3 and As_4S_4, both of which basically consisted of micro-crystals, were either cut, mounted and polished on one face in the same way as the opaque sulphides, or crushed to a powder. An attempt was made to polish a sample of As_3S but because of the brittleness of this material a good polish was not obtained. Unpolished lumps of As_3S were also examined. The As_4S_5 was used in powder form, as this was the form in which it was produced.

All the spectra were recorded by back reflection and, despite the nature of the samples, very intense spectra were obtained with all the compositions except As_3S, crystals of which probably do not exist (see Section 2.2.6).

4.2.2.4 Other materials

As a-As is a very weak scatterer of visible radiation a well-polished surface was essential for the a-As samples in order to maximise the weak signal. However, it is not an easy material to polish because it is fairly brittle. The first sample used was ground and then polished carefully by hand using diamond polishing paste. An acceptable finish was obtained in this way but in the first experiment the sample was damaged by the laser radiation. It was realised that a spinning sample (see Section 4.3.2) would be necessary and for this a <u>flat</u> polished surface is required, so in the end the polishing machine had to be used. An a-As lump with an already approximately flat face was selected and ground and polished using the 1μ and $\frac{1}{4}\mu$ solder laps. Although parts of the edge broke off during the process, an acceptable sample was eventually produced with an approximately rectangular polished face $\sim$10 mm x 15 mm.

The crystalline sulphur used was supplied in powder form and the

State	Material	Source	Form(s)	Appearance of bulk specimen	Remarks
c	S_8	K	pd	y	Orthorhombic sulphur.
a	As_5S_{95}	D	sc,sd	y,t*	Initially elastic.
a	$As_{15}S_{85}$	D	sc	o,t	
a	$As_{25}S_{75}$	D	sc	o,t	
a	$As_{28.6}S_{71.4}$	D	sc	o,t	As_2S_5
a	$As_{35}S_{65}$	D	sc,sp	r,t	sa
a	$As_{36}S_{64}$ (1)	D	sc	r,t	sa
	(2)	D	sc	r,t	Not annealed.
a	$As_{37}S_{63}$	D	sc	r,t	sa
a	$As_{38}S_{62}$	D	sc	r,t	sa
a	$As_{39}S_{61}$	D	sc	r,t	sa
a	$As_{40}S_{60}$ (1)	D	sc,f	r,t	sa
	(2)	AO	cu	r,t	
c	$As_{40}S_{60}$ (1)	M	pd,pl	y	Orpiment.
	(2)	G	l	p	Orpiment; speckled with yellow.
a	$As_{41}S_{59}$	D	sc	dr,t	sa
a	$As_{42}S_{58}$	D	sc	dr,t	sa
a	$As_{43}S_{57}$	D	sc	dr,t	sa
m	$As_{44}S_{56}$	D	sd	p	sa; granular in appearance.
c	$As_{44.4}S_{55.6}$	D	pd	y	As_4S_5
m	$As_{45}S_{55}$	D	sp,l,sd,f	p	sa; granular in appearance.
m	$As_{50}S_{50}$	D	s	dp	
c	$As_{50}S_{50}$	M	l	dr,t	Realgar (α-As_4S_4).
c	$As_{57.1}S_{42.9}$	D	s	dp	α-Dimorphite (As_4S_3).
m	$As_{75}S_{25}$	D	l,lp	brown	As_3S; brittle.
a	As	K	lp	metallic	Brittle.
a	Selenides	D	sd	black	sa; $As_{55}Se_{45}$ was extremely brittle.
c	$As_{40}Se_{60}$	Ph	w	black	

*The material had turned opaque after ~24 hours.

a – amorphous	K – Koch-Light Labs Ltd.	r – red
AO – American Optical Company		sa – standard anneal (see text)
c – crystalline	l(p) – lump (polished)	sc – standard cylinder, viz ~1 cm long and ~1 cm in diameter
cu – cuboid	m – phase-separated mixture	
D – Department of Electrical Engineering	o – orange	
dp – deep pink	p – pink	sd – standard disc, viz ~0.2—1 cm long and ~1 cm in diameter
dr – deep red	pd – powder	
f – sputtered film	Ph – Philips	
G – Department of Geology	pl – platelet	s(p) – slab (polished)
M – Royal Scottish Museum		t – transparent
		y – yellow

Table 4.1 Summary of the information relating to sample production and

preparation.

α-S_8 spectrum was recorded from the powder by back reflection.

4.2.2.5 Films

A few compositions were also prepared as thin films so that the spectra of this form could be compared with the bulk glass spectra. The films were r.f. sputtered by the usual techniques onto glass slides. To ensure that the Raman spectrum of the glass substrate should not contribute to the observed spectrum, a layer of aluminium or gold was first evaporated onto the slide and the chalcogenide material was sputtered onto this layer. The metal layer prevents the beam from reaching the glass substrate and as the metals have very weak spectra they do not affect the chalcogenide spectra.

4.3   Experimental aspects of the Raman scattering

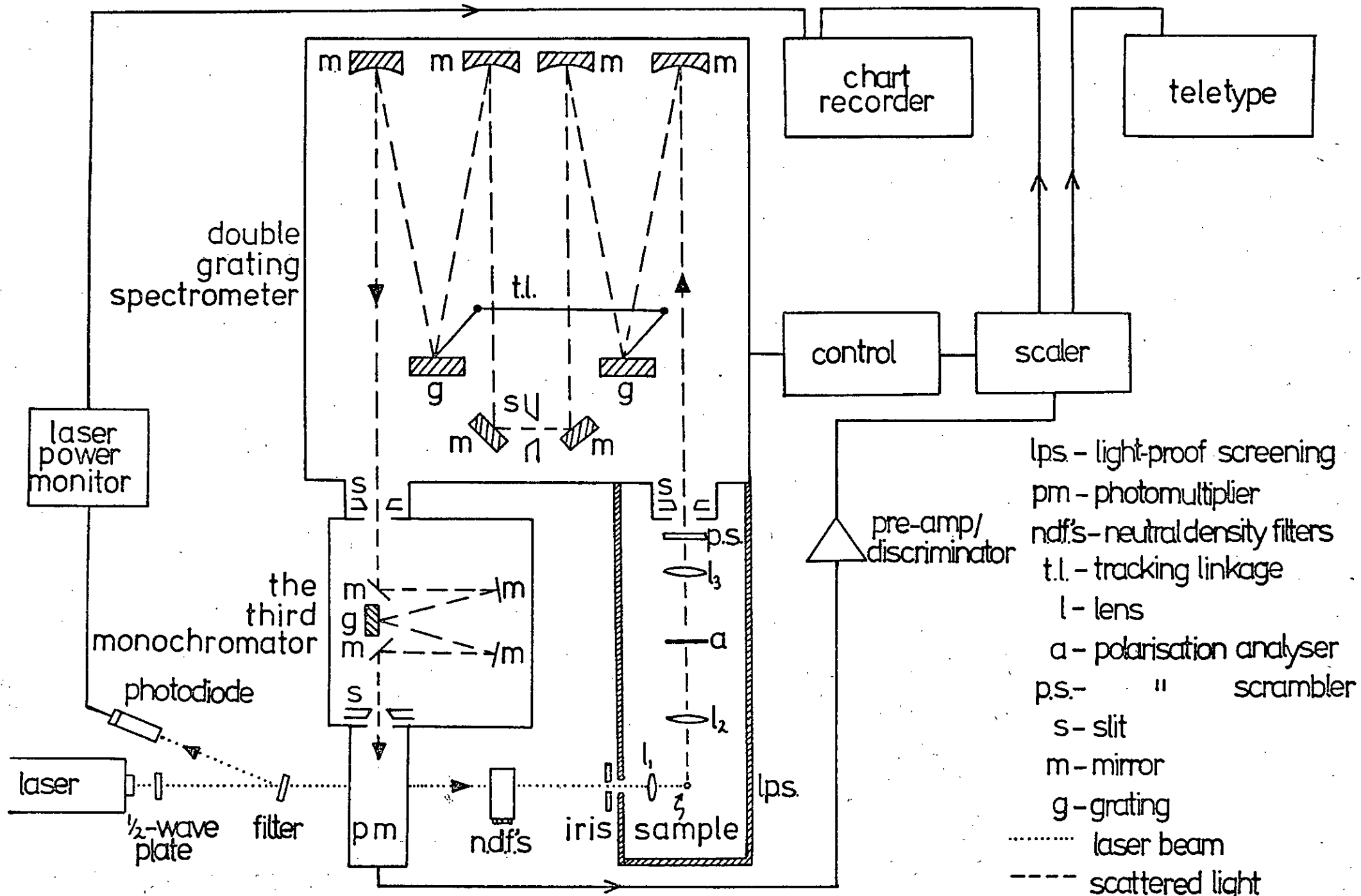### 4.3.1   The apparatus and method

The methods and equipment used to record the spectra in this study are standard in experimental Raman spectroscopy.   The system that was employed is shown schematically in Figure 4.1 and a photo-graph of the optical stage is presented in Figure 4.2.   Figure 4.3 gives the key to the photograph.   The components, not all of which are needed for each experiment, are listed and described below; numbers in square brackets refer to Figure 4.3.

Laser

The red 6328 Å line of a He-Ne laser (Spectra Physics model 125) [1] was initially used to excite the sulphide spectra.   This is the line most often used in Raman studies of these materials[6,7,8,9,10], which are strong scatterers at red wavelengths.   The maximum output power of the laser at 6328 Å was ~80 mW and the short term amplitude stability was better than 1% peak to peak.   The long-term stability

Figure 4.1

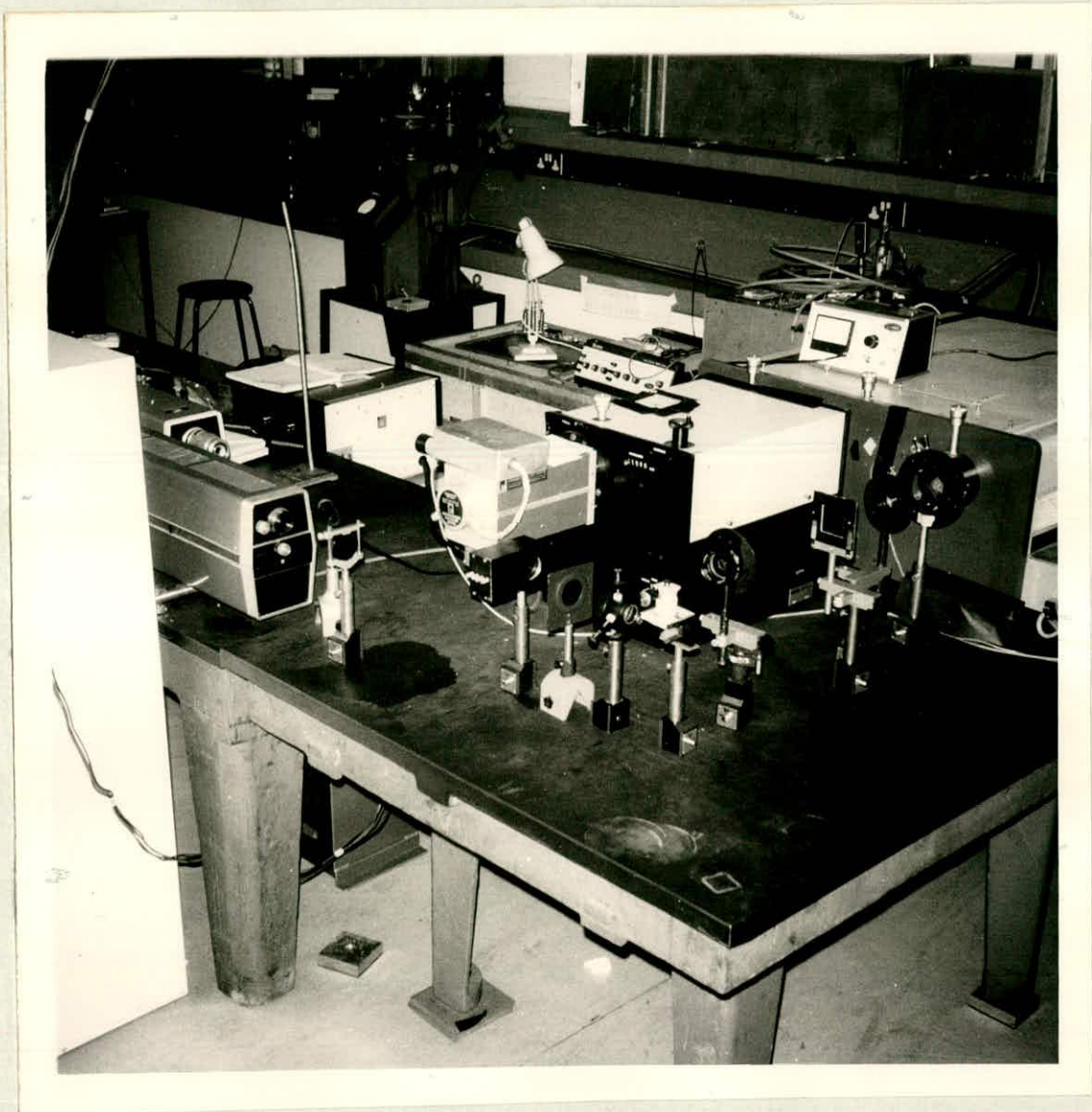A schematic diagram of the experimental system.

m · · · · · m · · · · · m · · · · · m
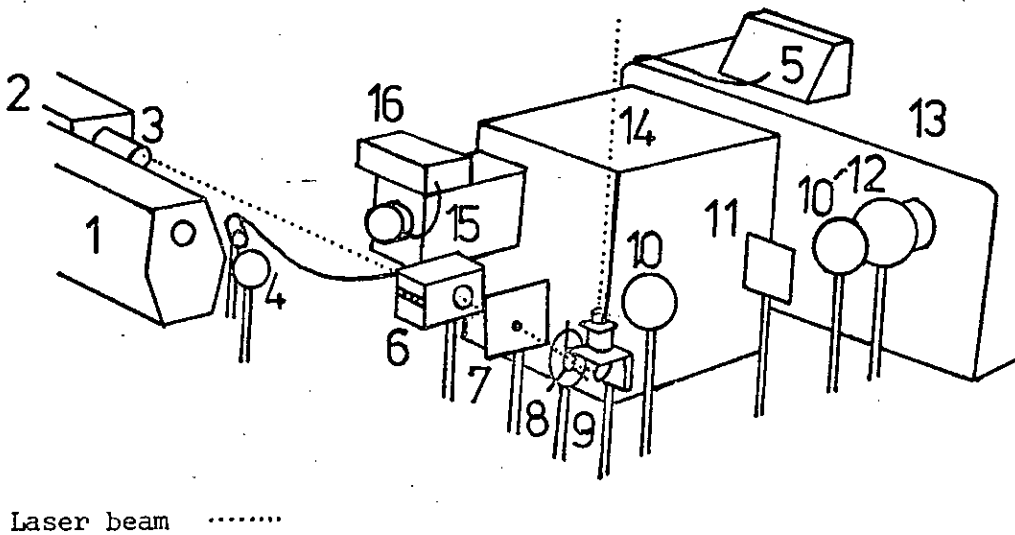
double grating spectrometer

t.l.

g · · · g

s

m · · · m

laser power monitor

the third monochromator

photodiode

m · · · m

g

m · · · m

s

laser

½-wave plate · · · filter

p m

n.d.f's

iris

l₁

sample

l.p.s.

p.s.

l₃

a

l₂

chart recorder

teletype

control · · · scaler

pre-amp/ discriminator

lps. — light-proof screening

pm — photomultiplier

ndf's — neutral density filters

t.l. — tracking linkage

l — lens

a — polarisation analyser

p.s. — " scrambler

s — slit

m — mirror

g — grating

· · · · · · · · · · laser beam

— — — — scattered light

Figure 4.2

The optical elements.

Laser beam ....

Figure 4.3

Key to Figure 4.2.

1. He-Ne laser
2. Kr-ion laser
3. Polarisation rotator
4. Plasma line rejection filter
5. Laser power monitor
6. Neutral density filters
7. Iris
8. Floating lens
9. Specimen stand
10 & 10'. Collection lenses
11. Polaroid analyser
12. Polarisation scrambler
13. Spectrometer
14. The third monochromator
15. Photomultiplier housing
16. Pre-amp

over a three hour period was better than 3%. In the course of the study a Kr-ion laser (Spectra Physics model 165-01) [2] became available and later experiments were performed with this. As it provided a more powerful and stable source of red light than the He-Ne laser, better quality spectra were obtainable with it. Many of the earlier experiments were repeated using this laser as the light source but the spectra, apart from their reduced noise level, were identical with those excited by the He-Ne laser. The 6471 Å line, which was used to excite the sulphide spectra, had an output power in excess of 500 mW (though to avoid sample damage the power used never exceeded 250 mW) and the long term power stability was $\pm 0.5\%$ over 10 hours. The r.m.s. noise in the beam intensity was typically 0.2%.

Because the arsenic selenide glasses are highly absorbing at red wavelengths ($\alpha(6328 \text{ Å}) > 10^4 \text{ cm}^{-1}$ [33]) the spectra excited with the 6328 Å line were of very poor quality, having peak counts ~ 50 counts/sec. However, good spectra were obtained using the 7993 Å i.r. line of the Kr laser, since radiation of this wavelength is not so strongly absorbed. The output power of this line is ~ 60 mW. The positions of several of the available exciting lines with respect to the absorption edges of a-As_2S_3, a-As_2Se_3 and a-As are shown in Figure 4.4.

Polarisation rotator

The output polarisation of the lasers is vertical, the linear cross component being less than .03%. This polarisation was suitable for the transmission-mode experiments but in the case of back reflection from polished surfaces a better signal was obtained using horizontally polarised light. The polarisation was rotated through 90° by a $\frac{1}{2}$-wave plate or a polarisation rotator (Spectra Physics model 310-21) [3].
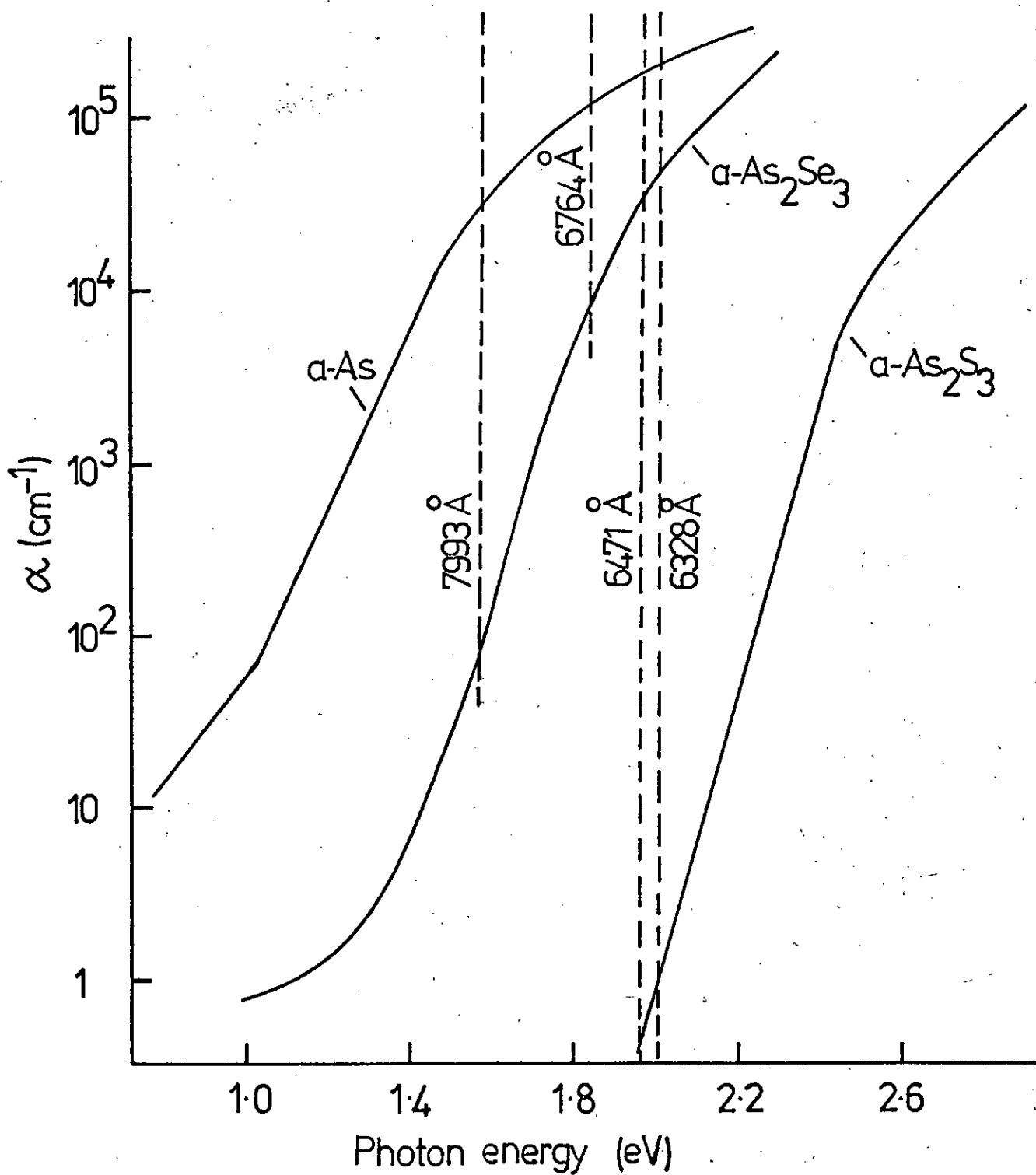
Figure 4.4

The positions of the exciting lines used relative to the absorption edges of a-As (Reference 38), a-As$_2$Se$_3$ (Reference 33) and a-As$_2$S$_3$ (Reference 37).

Plasma line rejection filter

This element [4] is a narrow-band filter and is used to isolate the laser frequency from the accompanying plasma emission (see Section 4.3.3). A filter was available only for the 6328 Å line. The effect of this filter (Grubb Parsons narrow band type 2) on the emission spectrum is shown in Figure 4.9. The filter had a transmission of ∼50%.

Laser-power monitor

The output power of the He-Ne laser, which had no power-stabiliser, was monitored continuously during experiments. The photo-diode of a laser-power monitor (Scientifica and Cook) [5] was placed in the beam reflected by the rejection filter. The detector was connected to the chart recorder, which registered the beam power and Raman signal simultaneously.

Neutral density filters

These [6] could be used to attenuate the laser beam by a factor of $\sim 10^{-n}$, where $n = 1, 2, \ldots, 7$.

Iris

This [7] blocks the cone of non-lasing emission which surrounds the beam.

Floating lens

The power density of the laser beam, which is initially ∼3 mm in diameter, can be considerably increased at the sample by using a lens [8] to focus the beam into it. In the case of the glasses, however, high incident power densities damaged the samples[6] (see Section 4.3.5) so the unfocussed 3 mm beam was used. The lens was used with the selenides, which were spun in the beam to overcome this damaging effect, and with the crystals, which were not affected by the focussed radiation.

Specimen stand

For the transparent samples this [9] consisted of a mirror set beneath a platform containing an aperture ~3 mm in diameter. The sample is placed on the platform so that it covers the aperture and is held in place with tape. The mirror reflects the beam upwards through $90°$ so that it passes through the aperture and the volume of sample vertically above it (see Figure 4.5(a)).

In the case of the opaque samples, the back reflection technique is used. The platform is removed and the sample is mounted on a plate which is held in the vertical beam by a stand (see Figure 4.5(b)). The surface of the sample faces the spectrometer and is set so that the angle of incidence of the beam is equal to the Brewster angle[34]. The Brewster angle for a-As_2S_3 is $71.5°$[9].

As focussed radiation was necessary in the case of the selenides a special rotating mount to spin the sample in the beam had to be made in order to avoid laser damage. The mount, built by Dr. Sik, consisted of a circular brass plate attached by a collar to the shaft of an electric motor. The whole was held steady in a sturdy frame which had provision for orienting the motor and attatched plate. The aluminium mounts to which the selenide samples were fixed could be bolted onto the plate.

By focussing the beam near the rim of the disc sample the heating effect of the beam was spread over a large area. The mount proved very effective, for no laser damage occurred to the rotating samples.
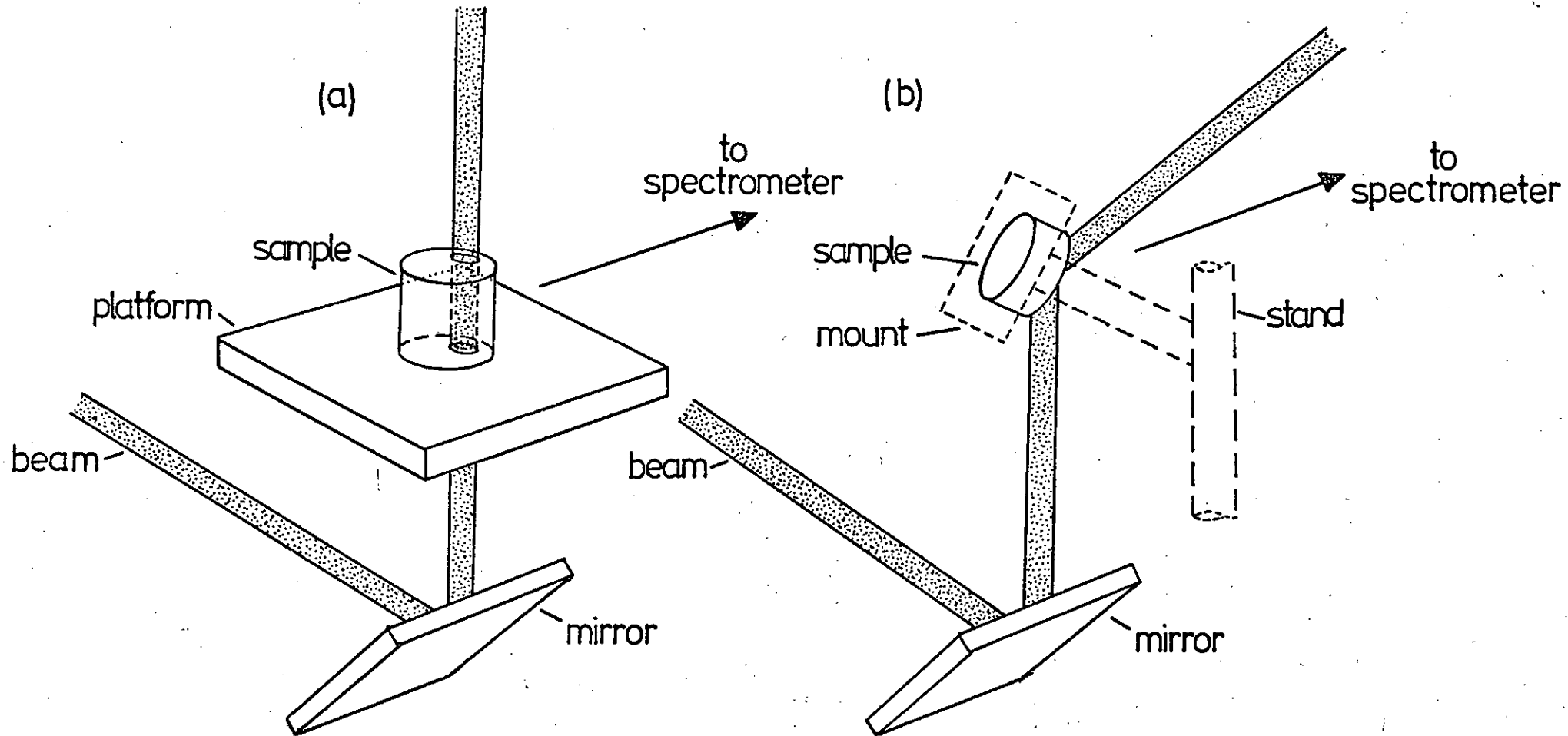
Light-proof screening

In order to prevent background light from entering the spectrometer, either black card or a light-proof wooden box was used to screen the region in front of the entrance slit.

Figure 4.5

The sampling arrangements:

    (a)   transmission mode

    (b)   back reflection

(a)

sample

platform

beam

to spectrometer

mirror

(b)

sample

mount

beam

to spectrometer

stand

mirror

Collection lenses

Two lenses [10,10'] collect the light scattered at 90° to the
vertical plane containing the laser beam and focus it onto the
entrance slit of the spectrometer.

Polarisation analyser

By inserting a sheet of polaroid [11] in the collected light the
polarisation of the scattered radiation can be analysed.   Polarisation
spectra as well as unanalysed spectra have been recorded for all the
glass samples studied.

Since the pairs of polarised spectra for each of the compositions
were to be used to obtain depolarisation data it was essential that
they be recorded under identical conditions.   Accordingly the two
spectra were always recorded successively, in the usual way, with the
only change in experimental conditions being the rotation of the
analyser by 90° between scans.   The program which generated the
depolarisation spectrum from the polarised spectra applied a correction
to each one to compensate for any change in incident laser power or any
photo-induced effects occurring over the period taken to scan the two
spectra.

Discrepancies in the value of the depolarisation ratio, which
should lie in the range 0 to $\frac{3}{4}$, between the published data and that
obtained in the present study can be attributed to the depolarising
effect of striations and imperfections in the specimens (see Section
4.2.2.1).   However, these do not affect the structure in the spectra.

Polarisation scrambler

As the transmission factor of a grating varies with the polaris-
ation of the incident light a polarisation scrambler [12] must be
placed in front of the entrance slit of the spectrometer, or else a

correction for the transmission factor must be applied to the raw data. The polarisation scrambler simply changes the polarisation of the light incident on it to a mixture of polarisations.

Spectrometer

The element used to disperse the scattered radiation was a double grating spectrometer (Spex 1400) [13]. The scanning in this instrument was linear in wavelength and driven by a 'stepper' motor. The spectrometer control is described in Reference 35.

Unless otherwise stated, the mechanical slit widths used were 200 μ (l.), 200 μ (m.), 200 μ (r.) for the glasses and 100 μ (l.), 100 μ (m.), 100 μ (r.) for the crystal samples, which correspond to a spectral slit width of $\sim$3 cm^{-1} and $\sim$1.5 cm^{-1} respectively.

The third monochromator

Stray light in the spectrometer can mask weak Raman features — especially near the exciting line, where it is most intense — and can also give rise to spurious features (grating ghosts). One way of overcoming this problem is to attach another grating monochromator at the spectrometer's exit slit. This extra stage acts as a variable bandpass, variable frequency filter. The width of the spectral region passed is determined by the width of the exit slit of the added monochromator, and the central frequency of this region is set by the angular orientation of its grating. Stray light rejection is achieved by tuning the extra monochromator so that the exciting line is occulted by one of its exit slit blades.

In the course of this study a third monochromator (Spex TTM) [14] was added to the system for the reason outlined above. Improved stray light rejection was not necessary for most of the glasses, partly because they produced a strong Raman signal well above the background and partly

because the low-frequency region near the exciting line was of minor

interest in the present study. When this facility was not required

the third monochromator was turned into an optical relay by replacing

the grating with a high-reflectance mirror. However, this facility

was useful for the optically poor samples, which reflected much of

the incident radiation into the spectrometer. The bandpass profile

for the third monochromator is shown in Figure 4.6(a) (the slope in

the plateau is due to the white light source used for this test).

The cut-offs are fairly sharp, occuring over a $\sim$5 cm^{-1} interval, as

is seen in Figure 4.6(b) and (c), which show the two edges of the

bandpass profile in greater detail. As the maximum width of the

bandpass was $\sim$260 cm^{-1} for the excitation used it was necessary to

shift the 'window' along when recording Raman spectra extending more

than $\sim$260 cm^{-1}. This was done by interrupting the recording of the

spectrum at a suitable point and rotating the grating to shift the

centre of the bandpass to the appropriate frequency. As the plateau

in Figure 4.6(a) is horizontal, after allowance is made for the source,

no discontinuities in intensity were produced at the points in the

spectra where the shifting operation was performed. This is seen in

spectra 3 and 4 of Figure 4.14 which were run using this facility.

From Figure 4.14 comparison of 3 and 4 with the others, which were

recorded before the third monochromator was introduced, show that the

addition of this instrument to the system has not altered the performance

of the spectrometer, apart from improving its stray light rejection

capability. Spectra recorded using the mirror mode of the third mono-

chromator are identical with those recorded before its addition to the

system.

The efficiency of the third monochromator in rejecting stray light

near the exciting line is illustrated in Figure 4.7, which shows two

Figure 4.6

(a) The bandpass profile for the third monochromator.

(b) Magnification of the low-frequency edge of the bandpass profile.

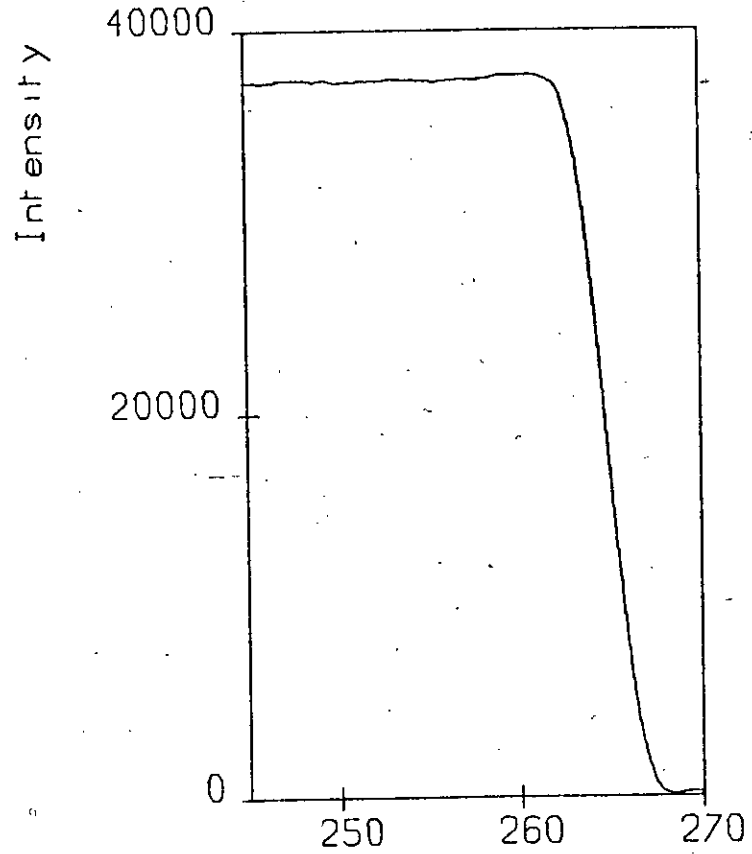(c) Magnification of the high-frequency edge of the bandpass profile.

(a)

(b)

(c)

Wavenumber [cm⁻¹] -->

Wavenumber [cm⁻¹] -->

Wavenumber [cm⁻¹] -->

Intensity
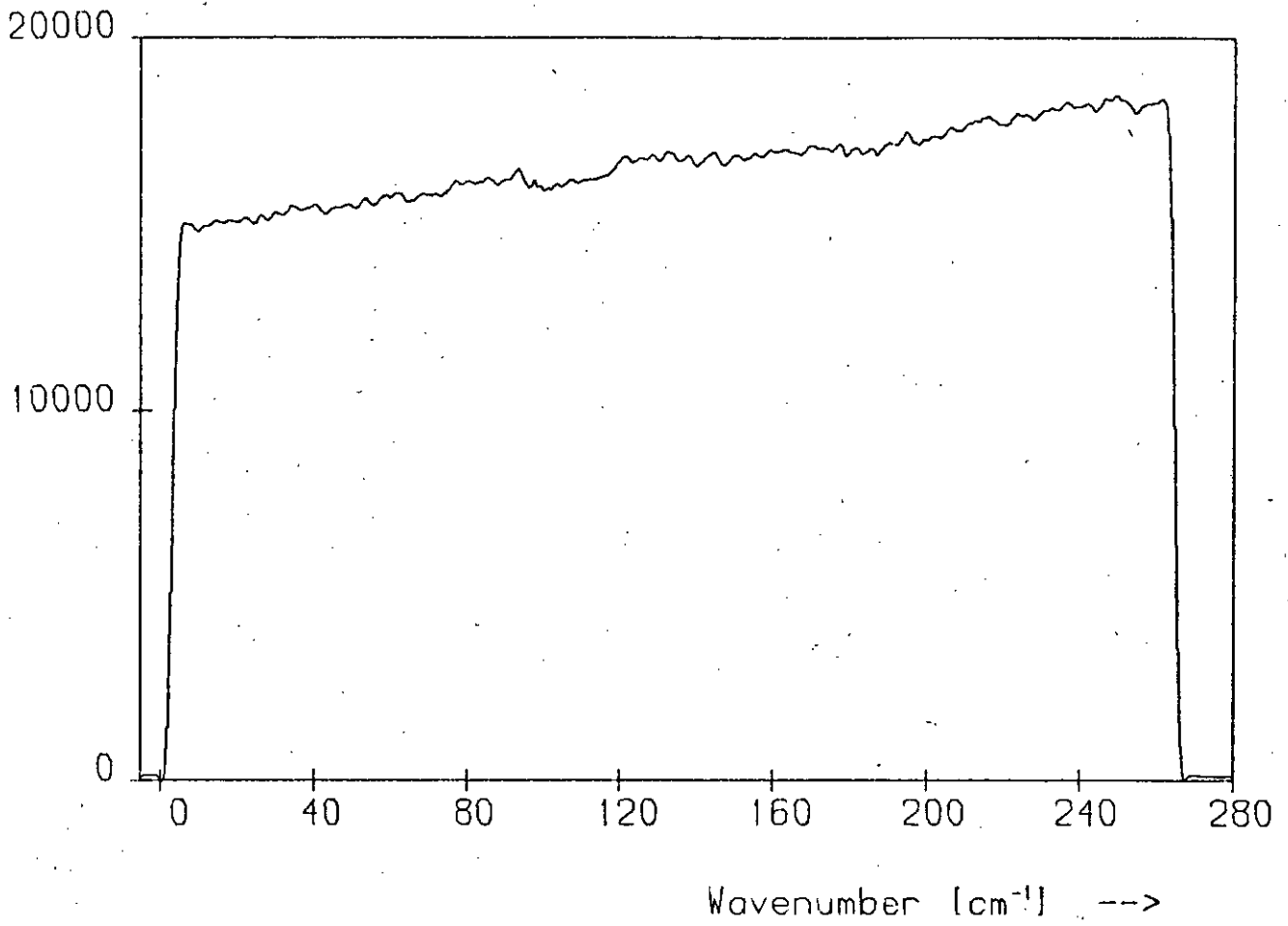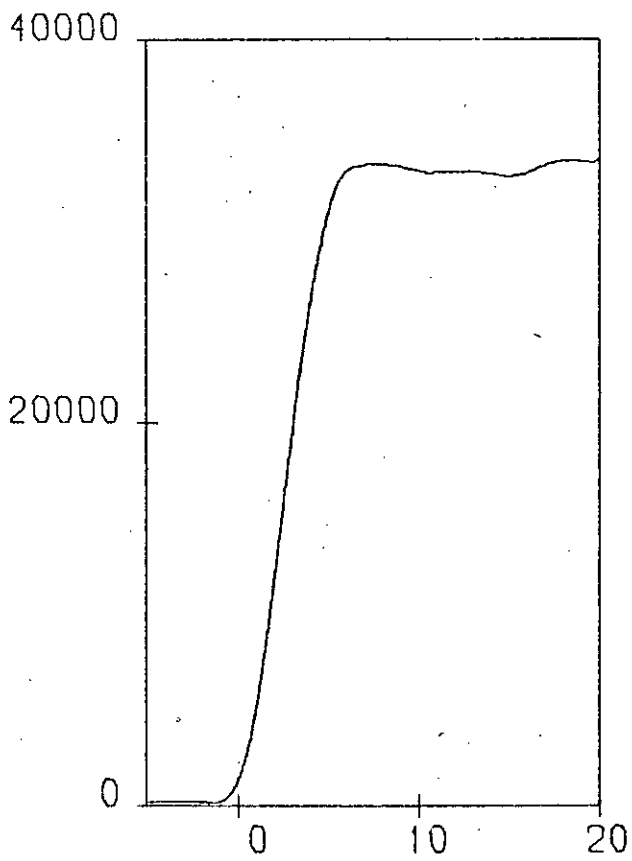
spectra obtained from a powdered sample of c-As$_2$S$_3$. Spectrum (a) was obtained before its addition while (b) was recorded using it in the grating mode. In spectrum (b) much of the background has been removed, along with a number of spurious features.

Photomultiplier

Photoelectric detection was used in this system, the detector being a cooled RCA C31034A photomultiplier. The sensitivity of this tube throughout its spectral range, which includes the laser frequencies used, is extremely high, rising from 100 mA/W at 265 nm to 155 mA/W at 830 nm. The total dark count obtained was ~10 cps.

The detection system

The method of detection used was photon counting, whereby the current pulses from the photomultiplier are amplified, shaped, passed through an analyser which discriminates against noise pulses and then fed to a counting scaler. The scaler displays the number of counts and outputs to a chart recorder and a teletype. The recorder plots the spectrum, together with the beam power in some cases, while the teletype records the individual counts and punches them on paper tape for the computer.

The repetitive 'step, stop-and-count' process used to measure the spectra is controlled by a unit which links the scaler and the 'stepper' motor rotating the tandem gratings in the spectrometer. Prior to running a spectrum the desired number of steps, step-size and count-time are set on this control, which is also used for slewing the motor in either direction and stopping and starting the scan. It is also possible to interrupt the recording of the spectrum from this control without spoiling data or calibration. The design and operation of the scanning system is discussed in detail in Reference 35.
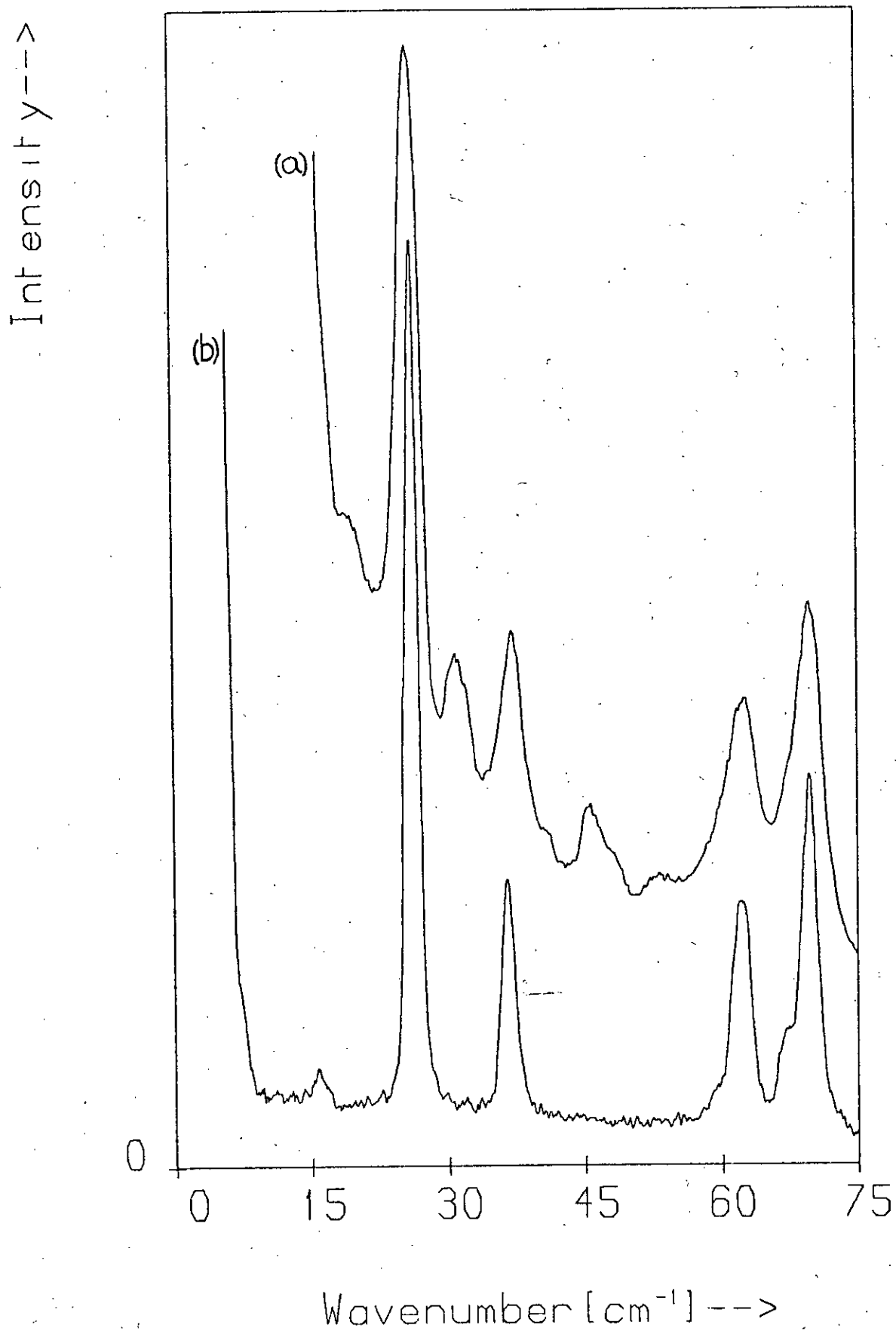
Figure 4.7

The stray-light rejection capability of the third monochromator

demonstrated on a sample of c-As$_2$S$_3$.   (Courtesy of Dr. M.J.Sik,

Reference 36.)

                (a)   Recorded without TTM.

                (b)   Recorded with TTM in grating mode.

RAMAN SPECTRA As$_2$S$_3$

In these experiments count-times of 3 and 4 seconds were used for the sulphide and selenide glasses respectively. The crystalline materials generally yielded very intense spectra, so the minimum count-time of 1 second was sufficient for most of these. The step-size used in all the sulphide experiments corresponded to a channel-width of ~0.5 cm^{-1}, and that used for the selenides corresponded to a channel-width of ~0.4 cm^{-1}.

The maximum signal obtained for the glasses was ~5000 cps and ~20000 cps for the sulphides excited with the He-Ne and Kr lasers respectively, and ~3000 cps for the selenides excited with the i.r. line.

4.3.2   The amorphous arsenic experiment

It was mentioned earlier (see Section 4.3.1) that very poor spectra were obtained for the selenides when red excitation was used, because of their high absorption at these frequencies. The Raman signal from the a-As was also very weak, even when the 7993 Å i.r. line was used, presumably for the same reason since the optical gaps for a-As$_2$S$_3$, a-As$_2$Se$_3$ and a-As are 2.32[37], 1.76[33] and 1.1 ev[38] respectively (see Figure 4.4). As the a-As was opaque to the radiation available the back-reflection technique had to be employed and the weak signal necessitated the use of a long count-time. In these circumstances several problems arise. The Raman lines become comparable in intensity to spurious features such as plasma lines and air lines, and the distortion of the spectrum, due to time-dependent signal loss arising from laser-induced damage to the sample, is exacerbated. Preliminary spectra obtained for the a-As were dominated by plasma lines, for the peak Raman signal was ~50 cps, of which ~10 cps was dark count. This peak signal fell to ~35 cps in the course of a scan lasting 10 hours

because over this period the laser beam had gradually cut a groove in the polished surface of the specimen.

To overcome these problems the following experimental scheme, suggested by Mr. H. Vass and shown in Figure 4.8, was used. The 6764 Å red line of the Kr laser was chosen for excitation — a compromise between the needs for a powerful line and one of long wavelength. As no plasma line rejection filter was available for this wavelength the system of prisms, irises and mirrors shown in the figure was used to reduce the amount of non-lasing emission entering the spectrometer. This system proved very effective since no plasma lines were apparent in the final spectrum (Figure 5.9, after p.115).

For maximum transmission through the optics and maximum coupling to the sample the laser radiation had to be polarised horizontally. A polarisation purifier was placed just before the sample to correct any depolarisation of the beam on passing through the optics. Of the 210 mW of power output by the laser ~80 mW reached the sample, the remainder being lost at the irises and optical elements.

To avoid laser-induced sample damage the spinning mount made by Dr. Sik for the selenides (see Section 4.3.1) was used to rotate the specimen rapidly in the beam. Because the sample was being spun, its irradiated face had to be flat, in addition to being well polished, to minimise the stray light background in the spectrum.

In order that the Raman lines of air should not appear in the spectrum the sample was kept in an argon atmosphere. Rather than lose signal by enclosing the sample in an argon-filled container, argon gas was simply blown over the sample as shown in the inset in Figure 4.8. A tube from the Ar cylinder fed the gas to a short length of copper pipe positioned so that the reflected beam passed axially up it.

Figure 4.8

The configuration used in the recording of the a-As spectrum.   The

inset shows the arrangement for blowing argon gas across the face of

the sample.

argon flow

spinner

a-As

M

laser

I

M

I

I

M

P P

I

P.P. S
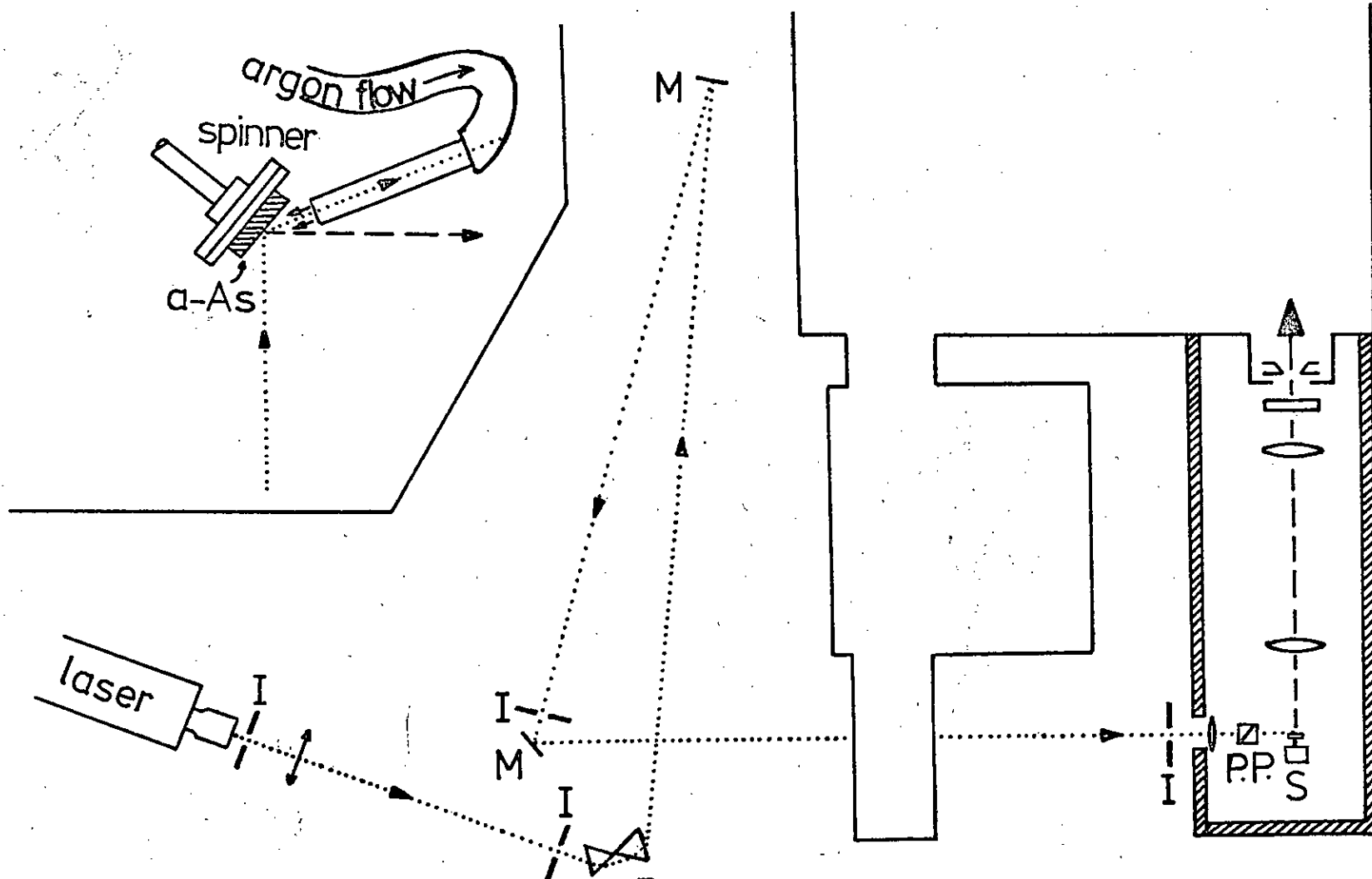
I—Iris
P—Prism
M—Mirror
P.P.-Polarisation Purifier
S—Spinner
.............Laser light
-----Scattered light

The mechanical slit widths were 300 μ(l.), 300 μ(m.), 300 μ(r.), and the count-time was 60 seconds. The third monochromator was used for additional stray-light rejection. There was no detectable signal loss or sample damage over the 10 hours it took to scan the spectrum.

4.3.3   Plasma lines

In addition to the intense coherent radiation of the lasing frequency, relatively weak incoherent light of other frequencies emerges from the laser. This light arises from non-lasing transitions in the energising discharge from the plasma and can give rise to spurious lines — termed 'emission' or 'plasma' lines — in the Raman spectra. As certain features in Ward's Raman spectrum of a-As_2S_3[10] have been attributed by Kobliska and Solin[39] to these plasma lines, particular care has been taken in the present study to exclude such lines from the spectra.

The non-lasing emission passes through the output window of the laser along with the coherent radiation and diverges to form a cone around the beam. Some of this light is scattered or reflected by the sample into the spectrometer and appears in the Raman spectra as a set of very sharp lines. Because the intensity of the emission reaching the sample is very much less than the beam intensity the emission lines are typically $\sim 10^{-7}$ of the intensity of the Rayleigh line in the spectrum and observable Raman spectra corresponding to each of the emission lines are not produced.

There are certain standard methods of reducing the amount of emission entering the spectrometer, the simplest being the insertion of an iris (7 in Figure 4.3) to block off the cone of emission surrounding the beam. Since the emission accompanying the beam diverges, the amount passing through a certain area at a fixed distance, L, from the output window falls off as L^{-2} so that the iris should be

placed as near the sample as possible and the path length of the beam
from the laser to the sample should be made large, perhaps by the use
of mirrors and prisms (see Figure 4.8). Inevitably some emission
passes through the iris and reaches the sample but the amount diffusely
reflected into the spectrometer by the sample can be reduced by using
well polished samples in the case of back reflection and samples free
from internal cracks, bubbles etc. when the transmission mode is being
used. A narrow-band filter (4 in Figure 4.3) inserted in the beam
can also be used to isolate the laser frequency. As the emission may
escape from other apertures in the laser, such as cooling vents, and
be reflected into the spectrometer from, for example, the laboratory
walls, it is necessary to screen off the region round about the entrance
slit (see Figure 4.1).

If the Raman signal is intense the plasma lines may be swamped
and unnoticeable, even when filters, irises etc. are not used.
However, in the recording of weak spectra where high sensitivity and
long count-times are required, plasma lines may be observed in the
spectra despite the use of the above experimental precautions. Thus
it is necessary to know the positions and relative intensities of the
emission lines in the frequency range of interest so that they can be
identified.

Two laser lines have been used in the present investigation of
the arsenic-sulphur glasses : the 6328 $\overset{o}{A}$ line of a He-Ne laser and
the 6471 $\overset{o}{A}$ line of a Kr-ion laser. A Grubb-Parsons plasma line
rejection filter was available for the 6328 $\overset{o}{A}$ line only. A in
Figure 4.9 shows the emission lines of the He-Ne laser in the region
$0 - 475$ cm^{-1} on the Stokes side of the exciting line (15,802 cm^{-1}).
B in Figure 4.9 shows the effect of the plasma line rejection filter
on the emission spectrum. The effect of plasma lines on the spectra
is seen in Figures 4.11, 4.12 and 4.13 in which the spectra were

Figure 4.9

The plasma lines of the He-Ne laser in the range 0 — 475 cm^{-1} on the
Stokes side of the 6328 Å line.   Spectrum A is the emission spectrum
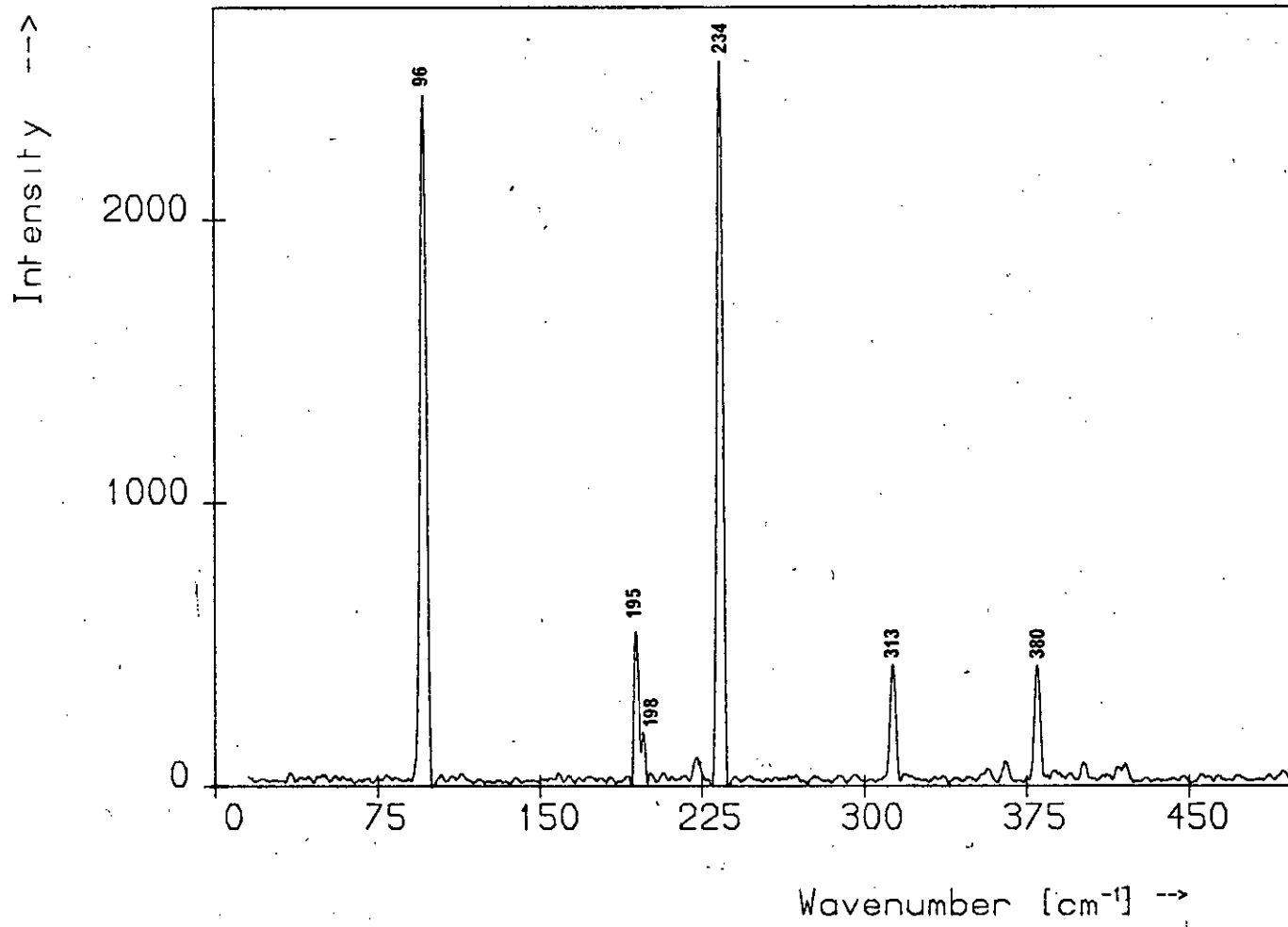and B shows the effect on it of inserting a plasma line rejection
filter in the laser beam.

Figure 4.10

The plasma lines of the Kr laser in the range 0 — 475 cm^{-1} on the
Stokes side of the 6471 Å line.

Plasma lines of the He – Ne laser.
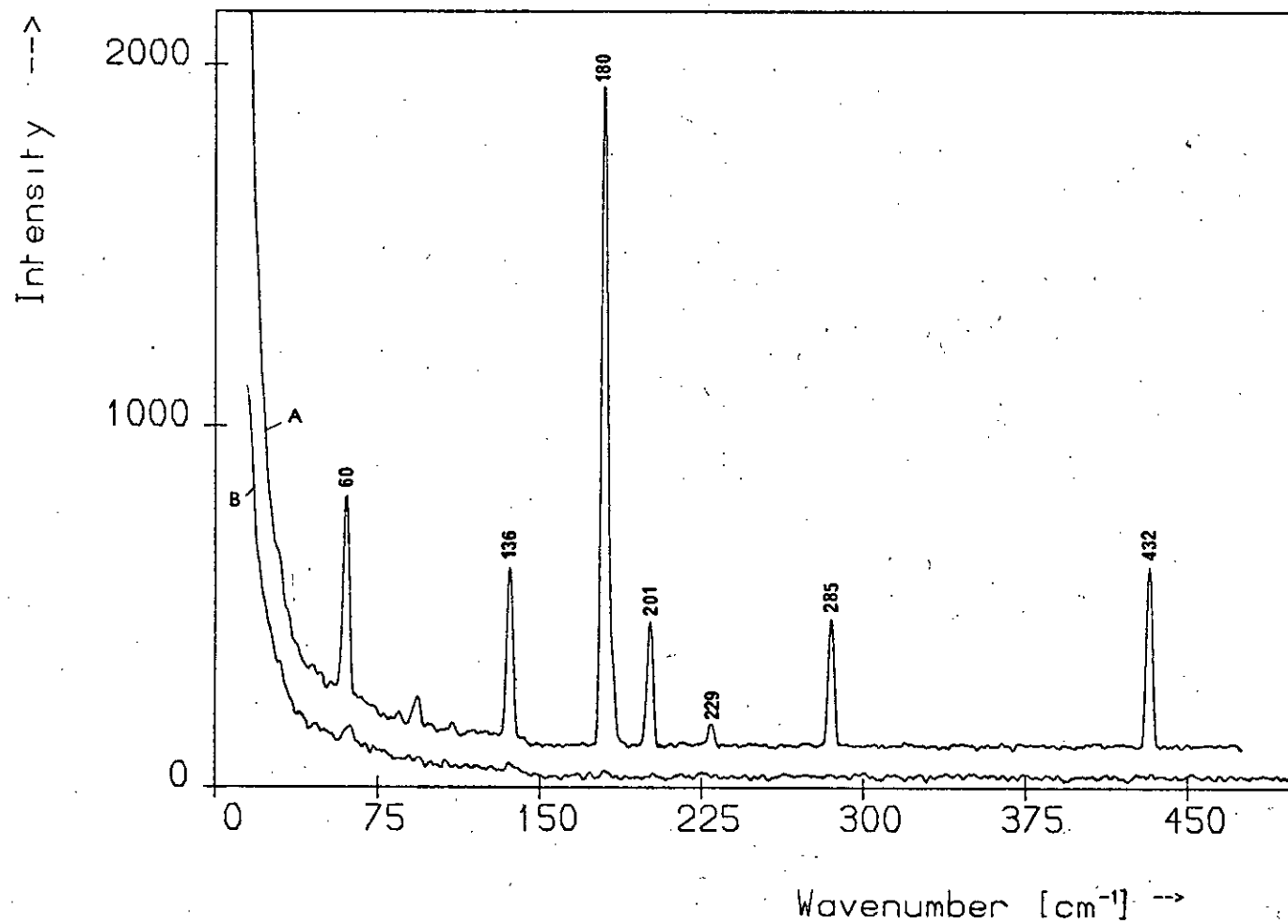
Plasma lines of the krypton laser.

Absolute frequency (cm^{-1})	Frequency shift (cm^{-1})
-12510.9	0
12408.5	102.4
12362.5	148.4
12339.6	171.3
12327.4	183.5
12324.4	186.5
12300.1	210.8
12277.8	233.1
12230.9	280.0
12211.5	299.4
12200.0	310.9
12192.4	318.5
12169.2	341.7

Table 4.2   The frequencies of the principal plasma lines of the Kr-ion laser on the Stokes side of the 7993 Å $(12510.9 \text{ cm}^{-1})$ laser line in the range 0 — 350 cm^{-1}.

unavoidably weak due to the conditions necessary for these three experiments. The sharp peaks marked 'P' at $\sim$180 cm^{-1} and $\sim$432 cm^{-1} in these spectra are due to the intense plasma lines at these frequencies.

No filter was available for the 6471 Å line of the Kr-ion laser and an iris alone was used to reduce the amount of emission reaching the sample. However, the Raman signal generated by this laser was intense — peak counts of approximately 20,000 counts/sec were typical — and the plasma lines were not noticeable. Figure 4.10 shows the emission spectrum of the Kr-ion laser in the region 0 — 500 cm^{-1} on the Stokes side of the 6471 Å (15,454 cm^{-1}) line.

The special precautions taken in the recording of the a-As spectrum are detailed in Section 4.3.2. The Stokes plasma line frequencies of the 7993 Å line of the Kr-ion laser, which was used in the experiments on the As-Se glasses, are given in Table 4.2. No filter was available for this line but the plasma lines were effectively excluded from the spectra by the use of irises. All the spectra presented in this investigation were recorded with screening in place around the entrance slit of the spectrometer so that no emission could be reflected into it from surfaces in the laboratory.

Comparison of the emission spectra in Figures 4.9 and 4.10 with the spectra of Figure 4.14 shows that the contribution of non-lasing emission to the spectra recorded in this study is negligible. There is, for example, no trace in spectra 1,2,3,5 or 6 of Figure 4.14 (which were excited with 6328 Å radiation) of the 432 cm^{-1} plasma line although it occurs in a region where the Raman signal is weakest. Finally, comparison of spectrum 4 (which was excited by the Kr-ion laser) with the other spectra of Figure 4.14 shows no significant differences between them (see also Figure 4.15). It can therefore be

concluded that none of the features in the spectra is attributable to plasma lines. The implications of this result in the light of Ward's and Kobliska and Solin's work are discussed in Section 5.6.1.

4.3.4   Effect of absorption on the spectra

In Figure 4.15 an increasing divergence in intensities as one approaches the origin is obvious but this difference is not important. As the spectra are normalised near 338 cm^{-1} they are in good agreement here and the small spread in intensities at lower wavenumbers is a manifestation of small changes in absorption due to positioning of the sample in the laser beam, different exciting frequencies and to heat- and light-induced effects. These changes in absorption lead to changes in relative intensities because the absorption coefficient increases as the photon frequency increases. As these are Stokes spectra the 338 cm^{-1} peak corresponds to scattered light of a lower frequency than that of the scattered light corresponding to the 30 cm^{-1} peak so that the latter radiation is absorbed more strongly than the former.

The divergence in the spectra at low energies is, of course, hardly observable when one compares the reduced spectra normalised to the peak at 338 cm^{-1} because the low energy band disappears as a result of the reduction process.

Figure 4.11 shows the effect of increased absorption due to an increase in the path length of the scattered light through the sample. Spectrum A was obtained from a cuboidal sample, $\sim$1.5 x 1.5 x 0.8 cm, with the laser beam positioned as close as possible to the face nearest the spectrometer — this was the standard position used in the experiments and in this position the centre of the beam was $\sim$0.2 cm from the side facing the spectrometer. Spectrum B was deliberately recorded with the beam near the opposite face of the sample, so that the distance

Figure 4.11

The effect on the Raman spectra of changes in absorption due to
increasing the path length of the scattered light through a sample
of a-As_2S_3 from ~0.2 cm (A) to ~1.3 cm (B).   The spectra are
normalised to the height of the 338 cm^{-1} band.

The Effect of Absorbtion on the Spectra.
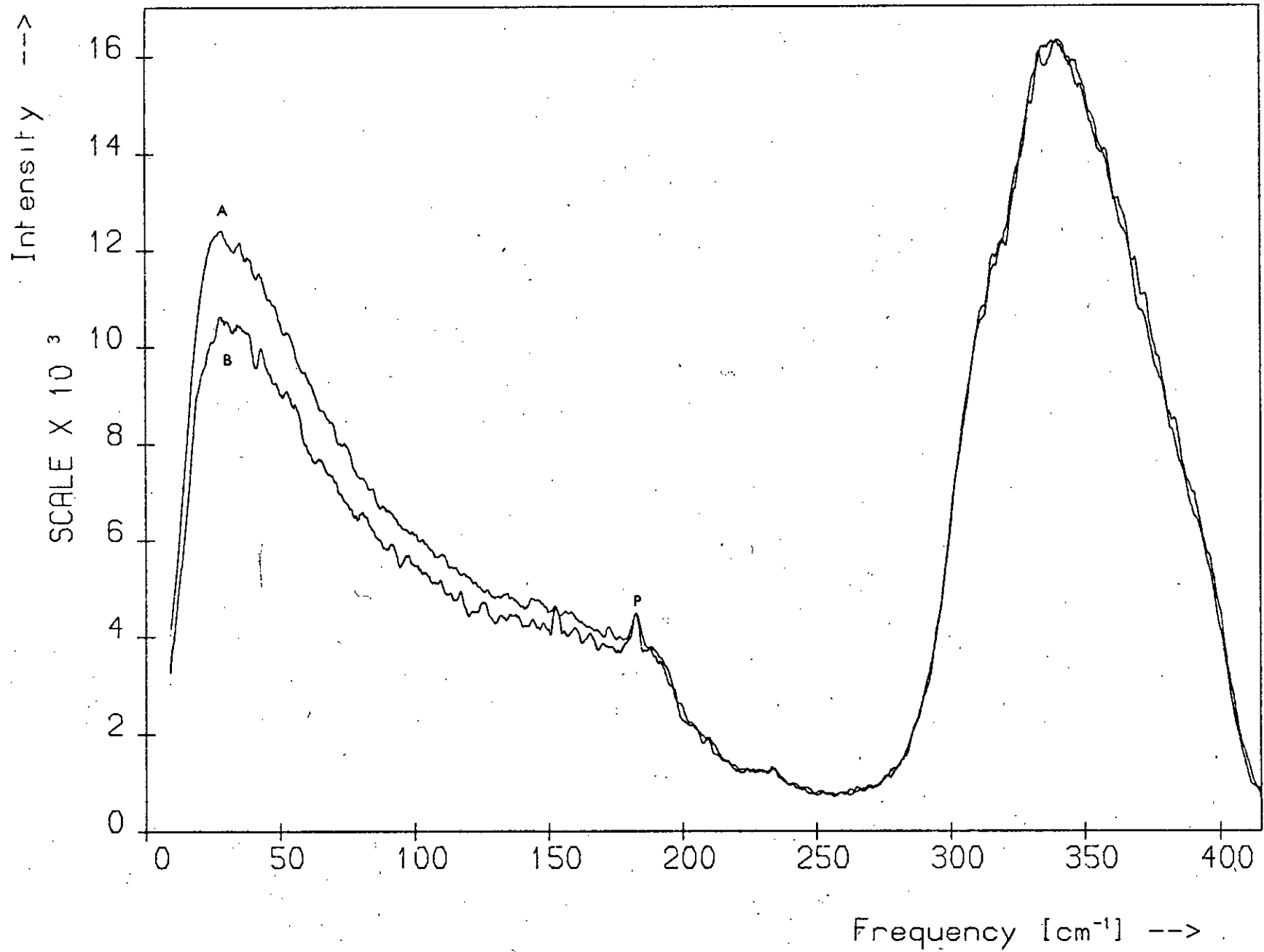
of the beam centre to the side nearest the spectrometer was ~1.3 cm.

The intensity ratio $I(\nu_1)/I(\nu_2)$ for any two spectral frequencies

ν_1, ν_2 is related to the absorption coefficient $\alpha(\nu)$ in the following

way :

$$\frac{I(\nu_1)}{I(\nu_2)} = \frac{K(\nu_1,\ldots)}{K(\nu_2,\ldots)} \times \frac{e^{-\alpha(\nu_1)d}}{e^{-\alpha(\nu_2)d}} \tag{4.1}$$

where d is the path length of the scattered light through the sample

and the $K(\nu,\ldots)$ account for the other factors governing the observed

Raman intensity.   On comparing this ratio for two spectra recorded

under identical conditions, but corresponding to different values of d,

one obtains

$$\frac{I_A(\nu_1)/I_A(\nu_2)}{I_B(\nu_1)/I_B(\nu_2)} = e^{-\left\{\alpha(\nu_1) - \alpha(\nu_2)\right\}(d_A - d_B)} \tag{4.2}$$

where the subscripts A and B index the spectra.   If the spectra are

normalised at ν_2 the L.H.S. = $I_A(\nu_1)/I_{B_{norm}}(\nu_1)$.

Taking d as the distance from the centre of the beam to the front

face, $d_A - d_B \approx 1$ cm in this experiment. For the 29 cm^{-1} and 338 cm^{-1}

peaks $\nu = 15,773$ cm^{-1} and 15,464 cm^{-1} respectively since the exciting

frequency was 15,802 cm^{-1} in this case.   The difference in absorption

coefficients at the two frequencies is 0.15 cm^{-1} so that I_A/I_B = 1.16

for the 29 cm^{-1} peak.   Experimentally from Figure 4.11 the ratio is 1.17.

In this project changes in absorption have been minimised by making

a simple correction, discussed in Section 4.3.5, for the small

temperature- and light-induced changes that occur during runs and also

by standardising the experimental procedures,e.g. performing all runs at

a fixed distance d from the front of the sample.   However, the change in

absorption due to the use of different compositions in the experiments is

unavoidable.   For the sulphur-rich glasses near stoichiometry it is known

that in the region of the exciting frequency, 15,802 cm^{-1}, the absorption

coefficient varies exponentially with ν [37] so that for a composition $As_{100-x}S_x$

$$\alpha_x(\nu) = C_x e^{b_x \nu} \tag{4.3}$$

where x indexes the sulphur content and C_x, b_x are constants. It is also found[37] that an approximately parallel shift to higher frequencies occurs in the plots of $\log(\alpha_x(\nu))$ versus ν as the sulphur content is increased from the stoichiometric value of 60 at.%, which implies that the change in $\alpha_x(\nu)$ with x occurs in the pre-exponential constant C_x and so is frequency independent. Hence $\alpha_x d \longrightarrow$ const. x $\alpha_x d$ as x changes and the effect is equivalent to changing d. In going from $As_{40}S_{60}$ to $As_{35}S_{65}$, $\alpha_x(\nu)$ decreases by approximately a factor of 1/2 which is 1/3 of the fractional change in d in the measurement on which Figure 4.11 is based. It is not necessary to make a correction for this compositional change in the absorption since, as Figure 4.11 shows, the consequent change in αd does not affect the spectral features significantly. A comprehensive correction for the absorption of both incident and scattered radiation would, however, be essential in a study of the resonance Raman effect in these materials[40,41].

4.3.5 Laser damage and photo-induced effects

It is customary in laser Raman spectroscopy to focus the beam onto the sample so as to maximise the incident power density. However, when 50 mW of focussed 6328 Å radiation (corresponding to a power density of 2×10^6 mW/cm^2) was incident on samples of a-As_2S_3 a rapid decrease occurred in the initially intense Raman signal. Over the first 10 minutes of exposure the initial Raman intensity, I_0, fell to about $I_0/3$, but the rate of count loss tapered off so that after 20 minutes the intensity had reached $I_0/5$ and was decreasing linearly with time at a rate of 20 — 25% of this value per hour.

Examination of the irradiated sample under a microscope revealed a

small pit (~200μ diameter) on the surface at the point of incidence
and showed a black region ~2 mm long extending from this point into the
sample. Similar damage with a focussed beam has been observed by other
workers[6,42]. Vitreous As_2S_3 has a very low thermal conductivity
(4 x 10^{-4} cal/sec cm $^{\circ}$C) and it seems that the focussed radiation is
sufficiently intense to vaporise a small region on the surface of the
glass around the point of incidence and also to cause subsurface physical
or chemical changes near this point. The pit formed in the initially
polished surface effectively defocusses the beam and the consequent
reduction in incident power density decreases the rate at which the
surface and subsurface damage is occuring. This defocussing effect
accounts for the rapid initial count loss but a stage is probably reached
where further melting does not occur, or does not increase the defocussing
of the beam, and subsurface damage becomes the principal mechanism for
decreasing the Raman signal. The incident power density must still be
sufficient to cause the physical or chemical changes that are producing
the blackening and as the blackened regions grow they will attenuate the
beam. Since the scattered light entering the spectrometer originates
from a volume in the centre of the sample and well above the damaged
region, these phenomena affect the Raman intensity only indirectly, that
is by reducing the power density in the scattering volume.

An attempt was made to reduce the heating effect of the laser beam
at the point of incidence by using the technique of refractive index match-
ing, whereby the sample is immersed in a liquid of similar refractive
index so that reflection at the point of incidence is reduced. However,
the count loss was markedly present even when the sample was immersed in
a cell of silicone oil, which is a good thermal conductor.

It was then decided simply to use the focussing lens to defocus the
beam until no optical damage occurred. For incident beam widths of
~3 — 5 mm in diameter (corresponding to power densities of ~700 — 250 mW/cm^2)

the rate of count loss was found to be considerably decreased, though it was not entirely removed, and no pitting or blackening of the sample was observed. As the initial signal, I_O, obtained with the 5 mm beam, which was the widest one investigated, was not acceptable, a 3 mm beam was preferable. The lens was made redundant by the fact that the normal diameter of the laser beam was ~3 mm so that reproducible spectra of reasonable intensity could be obtained simply by using the direct, unfocussed beam. The count loss rate under these conditions was linear and ~3% of I_O per hour — the time taken for a scan.

When a sample that had been exposed to the laser radiation (either focussed or unfocussed) was viewed under a polarising microscope a change in optical density throughout the region traversed by the beam was clearly evident, indicating that laser-induced changes are also occurring within the sample. The path of the beam through the sample appears in the polarising microscope as a sharply defined volume differing in colour from the unirradiated region. As no surface or subsurface damage occurs when the samples are exposed to unfocussed radiation, the small count loss rate observed in this case can be attributed to these internal changes. For the focussed beam case the rapid intensity loss is primarily due to the laser damage and the internal changes make only a small contribution.

To investigate the nature of the count loss due to these physical or chemical changes taking place inside the samples several experiments were performed to observe the scattered intensity as a function of time. An unfocussed 50 mW beam was incident on the samples and the laser power was monitored continuously throughout each experiment so that changes in scattered intensity could not be attributed to fluctuations in beam power. The following points emerged :

    a) the effect occurs in all the As-S glasses $As_{35}S_{65} - As_{45}S_{55}$;

    b) the scattered intensity decreases linearly with time over the

first 1 — 2 hours of exposure but tails off at long times;

c) for the standard-anneal samples the count loss rate is approximately the same for all compositions viz ~3% of I_o per hour;

d) the only non-annealed sample examined yielded a count loss rate of ~10% of I_o per hour.

A number of experiments were carried out to ascertain whether the signal loss was accompanied by any changes in the shape of the spectra. These experiments consisted of exposing a sample to 50 — 80 mW of unfocussed radiation for several hours and recording Raman spectra at intervals using an attenuated beam. The spectra were then compared and examined for new features, peak shifts etc. The results of Figure 4.12 are taken from a typical experiment of this type on a-As_2S_3. Each of the five spectra shown was excited with ~5 mW of unfocussed 6328 Å radiation, the first spectrum, A, being recorded before the sample was exposed to the full beam. One hour's exposure to the unattenuated 50 mW beam occurred between each of the first four recordings. To see whether or not the sample recovered after exposure, the fifth spectrum, B, was recorded eleven hours after the fourth with no irradiation at all during that interval. The only difference in the five spectra, which have been normalised to the height of the 338 cm^{-1} band, is the increasing reduction in intensity of the last four spectra relative to the first as one approaches the origin. This discrepancy in intensities would be expected if the count loss mentioned earlier was frequency dependent, being larger for higher absolute scattered frequencies. There are no signs of any new features appearing in the spectra nor of any change in the features already present but there is some indication of recovery in the final spectrum, B.

Apart from the changes in relative intensity of certain features in the spectra of the As-rich glasses as a function of exposure (see Section 5.7),
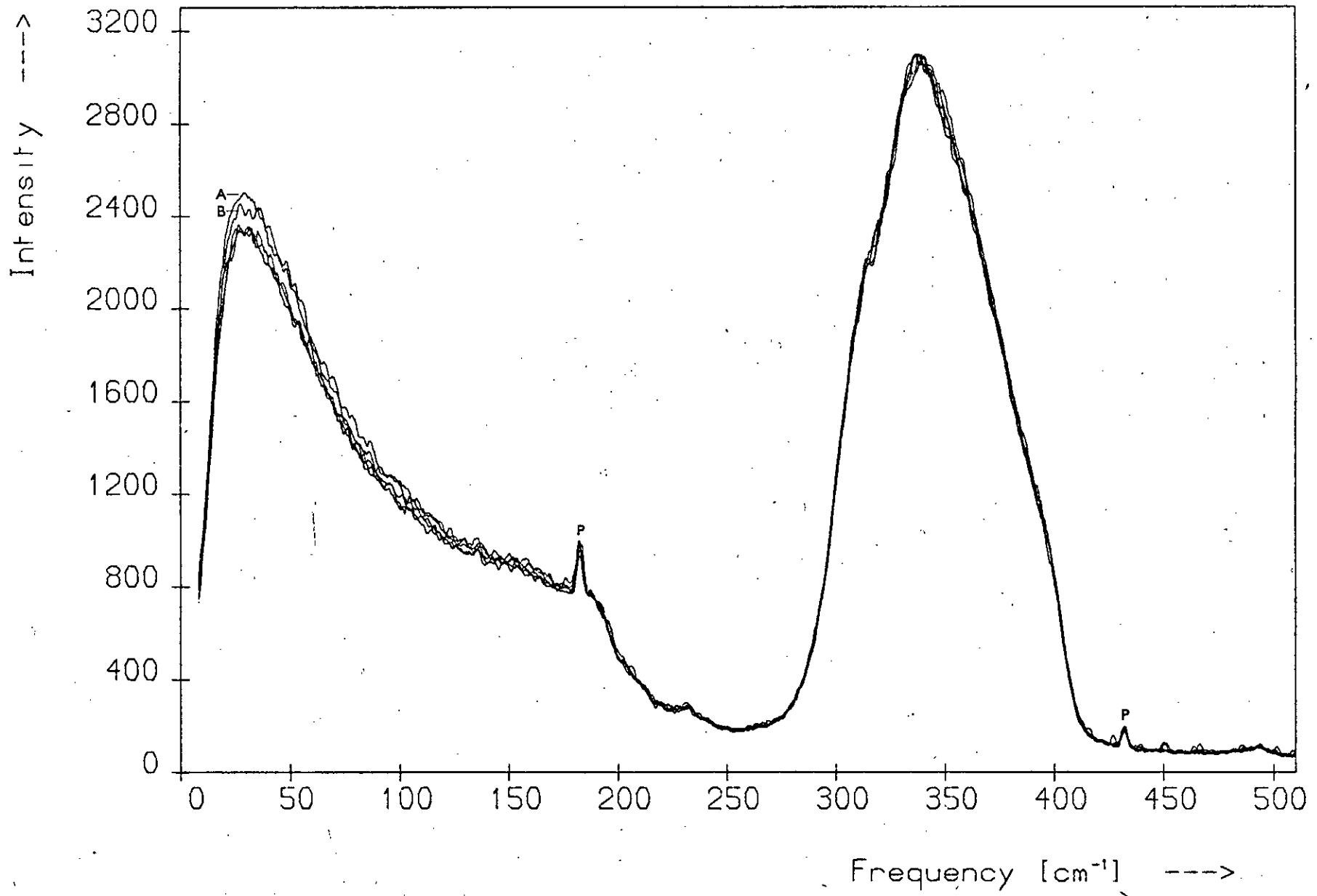
Figure 4.12

The effect on the Raman spectrum of a-$As_{40}S_{60}$ of prolonged exposure to laser radiation. Five spectra, normalised to the height of the 338 cm^{-1} band, are shown, A being recorded first and B last, after an eleven-hour period of recovery.
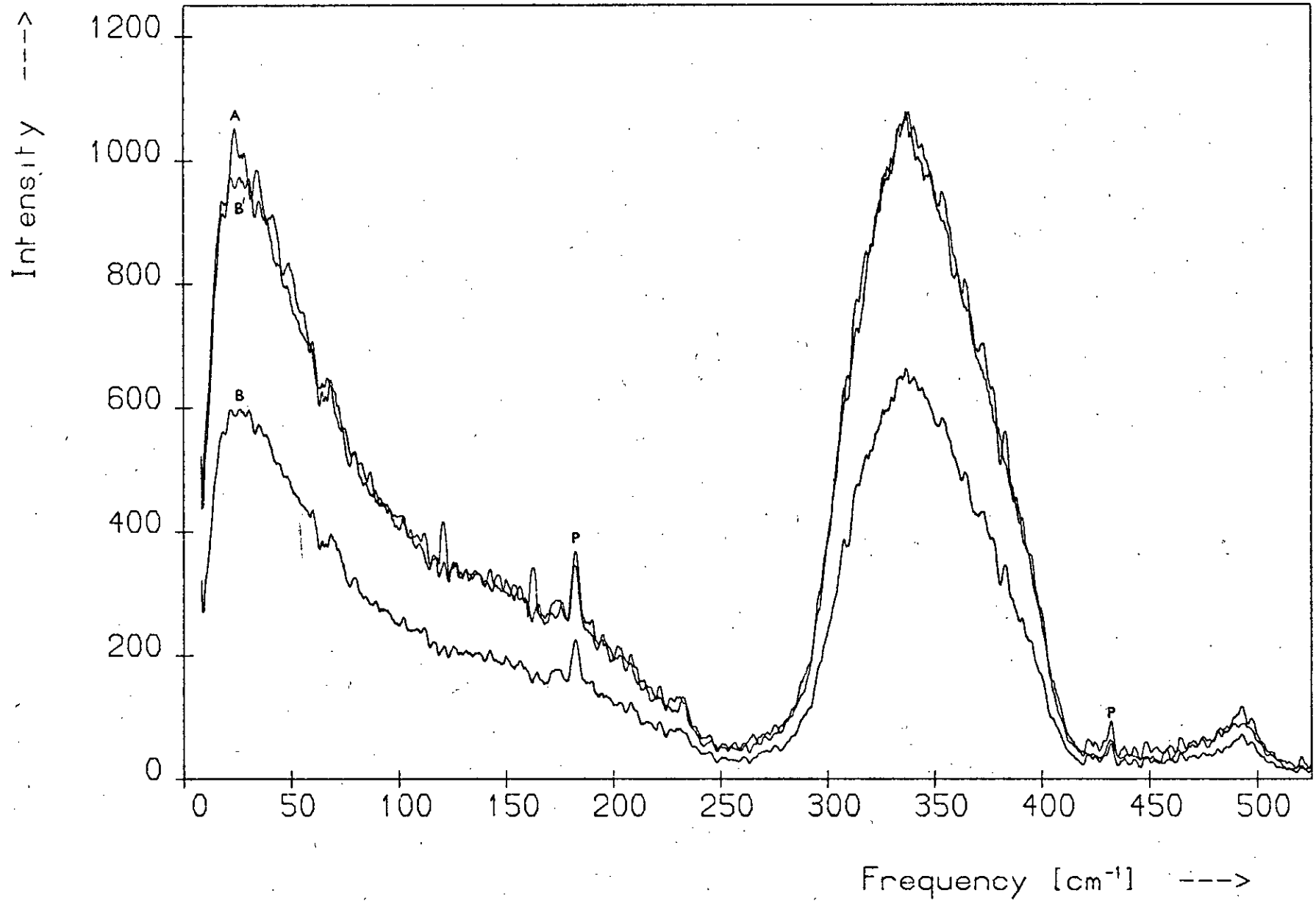
Figure 4.13

The effect on the Raman spectrum of a non-annealed sample of $As_{36}S_{64}$ of prolonged exposure to laser radiation. Spectrum A was recorded before exposure and spectrum B after exposure to 50 mW of 6328 $\overset{o}{A}$ radiation for $3\frac{1}{2}$ hours. B' is B normalised to the height of the 338 cm^{-1} band of spectrum A.

Raman Spectra: $As_{40}S_{60}$

Raman Spectra: $As_{40}S_{60}$ plot of Intensity (0 to 3200) versus Frequency [cm^{-1}] (0 to 500), showing curves labeled A and B with peaks marked P.

Raman Spectra: $As_{36}S_{64}$

no changes in spectrum profile were observed in these experiments, in which the maximum continuous exposure and the maximum total exposure of one region to the 50 mW beam was 6 hours and 10 hours respectively. Figure 4.13 shows spectra obtained from the non-annealed sample of $As_{36}S_{64}$, which exhibited a much larger count loss than the annealed samples. Before exposing the sample to the full beam, spectrum A was recorded using a 5 mW beam. Then the full 50 mW beam was passed through the sample for $3\frac{1}{2}$ hours, after which spectrum B was recorded using the attenuated beam. Comparison of A and B shows that the Raman signal has fallen by almost 50% after the $3\frac{1}{2}$ hour exposure but there is no sign of any change in profile. Comparison of A and B'(which is spectrum B scaled so that A and B' are normalised to the height of the 338 cm^{-1} band) shows that the increasing intensity discrepancy as one approaches the origin is again present (cf. Figure 4.12). The increased noise level in the spectra of Figure 4.13 is due to the use of an attenuated beam and no compensating long count-time.

The only laser-induced spectral changes observed in these experiments were due to the wavelength-dependent signal loss. This loss is consistent with a shift in the absorption edge to lower energies as a result of irradiation. Several workers[5,43] have observed heat- and light-induced shifts of the absorption edge in these materials. There is no indication that the samples recover completely when left after exposure, since the blackened regions and the regions of changed optical density were still visible under the microscope three years later.

In the selenides also, gross physical damage occurred when focussed radiation was incident on the samples. However, as a focussed beam was necessary to obtain an acceptable Raman signal the problem was overcome by rapidly rotating the sample in the beam rather than by simply defocussing it. This method proved extremely effective, for under these conditions absolutely no count loss was observed. No experiments were

performed to see whether a photodarkening effect similar to that in the

sulphides occurs in the As-Se glasses but a signal loss may well set in

as the rate of rotation is decreased. Heat- and light-induced absorp-

tion edge shifts have also been observed in the selenides[5,44,45].

The only other material damaged by focussed radiation was the

a-As, which had to remain in the beam for 10 hours for its spectrum to

be scanned. This problem was again overcome by using a rapidly rotat-

ing sample and no signal loss occurred when this method was used. The

crystal samples, which were all excited with focussed radiation, showed

no sign of damage and their spectra exhibited no change in profile or

intensity over the period required for a scan, viz 20 — 60 minutes.

Heat- and light-induced changes have been observed, however, in

c-As$_2$S$_3$[14,46] and particularly in c-As$_4$S$_4$ which can photodecompose in

several ways[14,22,47,48].

All Raman spectra of the As-S glasses recorded subsequent to the

experiments outlined in this section were excited with unfocussed beams,

the incident beam powers used being ~50 mW, ~240 mW and ~60 mW for the

6328 Å, 6471 Å and 7993 Å lines respectively. As no spectral changes

occurred during six hours continuous exposure to the full beam it is

unlikely that any such changes would occur in a spectrum during the

hour taken to scan it. Moreover, the total exposure of any region in

a sample never exceeded the 10 hour maximum total exposure during which

no spectral changes occurred (apart from the one region used which set

this maximum) and spectra were generally recorded from unexposed samples

or unexposed regions of samples. To compensate approximately for the

small intensity loss occurring in the course of a scan, a simple linear

correction was applied to the data. At the end of each scan the inten-

sity of the low energy peak was re-measured and comparison of this with

the initial intensity gave a value for the combined intensity loss due

to laser-induced effects and drift in beam power occurring over the

recording period. A computer routine was written to correct each intensity value in the spectrum by the appropriate fraction of the total loss.

4.3.6   Data handling

In this study extensive use was made of the computer to process, analyse and present the spectral data, the work being carried out on the multi-access system provided by the Edinburgh Regional Computing Centre. A comprehensive library of routines, written by Dr. J.W. Arthur[35], was already available for handling Raman data and all that was required was to add to this the programs arising from the special requirements of this particular study. These extra programs were either written by Dr. M.J. Sik or by the present author. Listed below are the operations that could be carried out on the data.

Basic preparation

The following preliminary operations were performed on all the spectra :

* Removal of substitute characters.

  Subtraction of dark count.

  Removal of noise spikes.

  Linear correction for fall-off in laser power or for the photo-darkening (see Section 4.3.5).

* Conversion from wavelength to wavenumber.

Processing

* Smoothing.

  Normalisation to area, peak height etc. (see Section 5.5.1.1).

+ Shuker-Gammon reduction (see Section 3.4.1).

Analysis

* Peak finding.

* Integration and differentiation.

* Curve fitting.

* Graphing/multiple graphing on line-printer or teletype.

Presentation

* Graphing/multiple graphing on the Calcomp computer graph-plotter
  attached to the system.

Miscellaneous operations

* Determination of location and value of maximum count on any interval.
  Subtraction of one spectrum from another to obtain the difference
  spectrum.

  Generation of the depolarisation spectrum from two polarised spectra.

+ Convolution with a Gaussian.

+ Changing intensity scale from linear to logarithmic.

A number of housekeeping routines were also available for storing
the spectra and for listing and altering their parameters and contents.
The spectra could be translated, expanded or contracted along either the
intensity or the frequency axis.   The routines marked + were written in
Fortran IV by Dr. Sik while those marked * were written by Dr. Arthur in
Imp[49], which was the language used by the present author.

All the spectra presented in this study have been automatically
plotted by the computer graph-plotter.

4.3.7   Reproducibility

The reproducibility of the results is illustrated in Figures 4.14
and 4.15 which show typical spectra for the stoichiometric glass As_2S_3.
The same set of six spectra, normalised to the peak intensity of the
338 cm^{-1} band, are shown displaced above each other in Figure 4.14 and
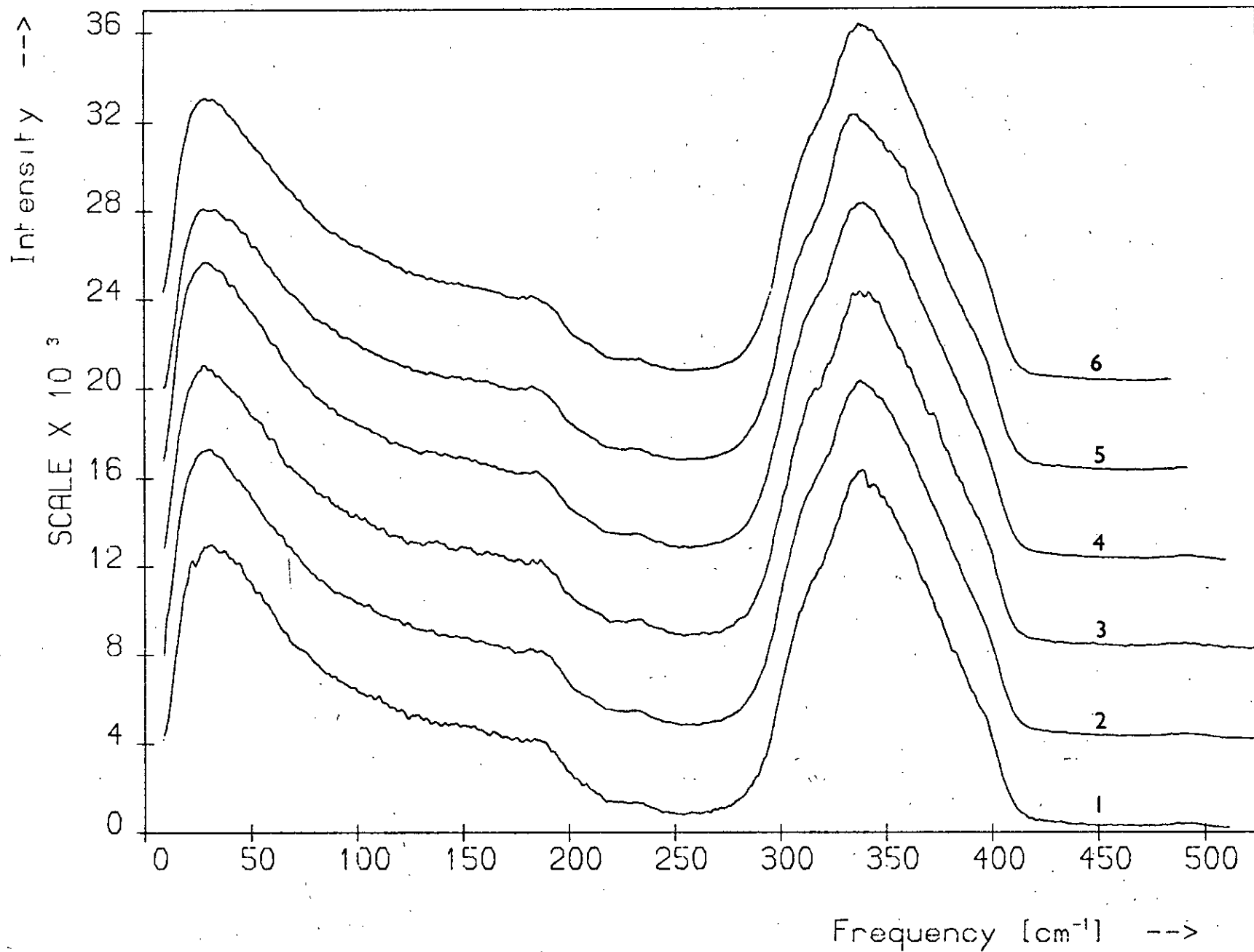
Figure 4.14

Six spectra of the As_2S_3 glass obtained under different experimental

conditions (see Table 4.3).   The spectra are all normalised to the

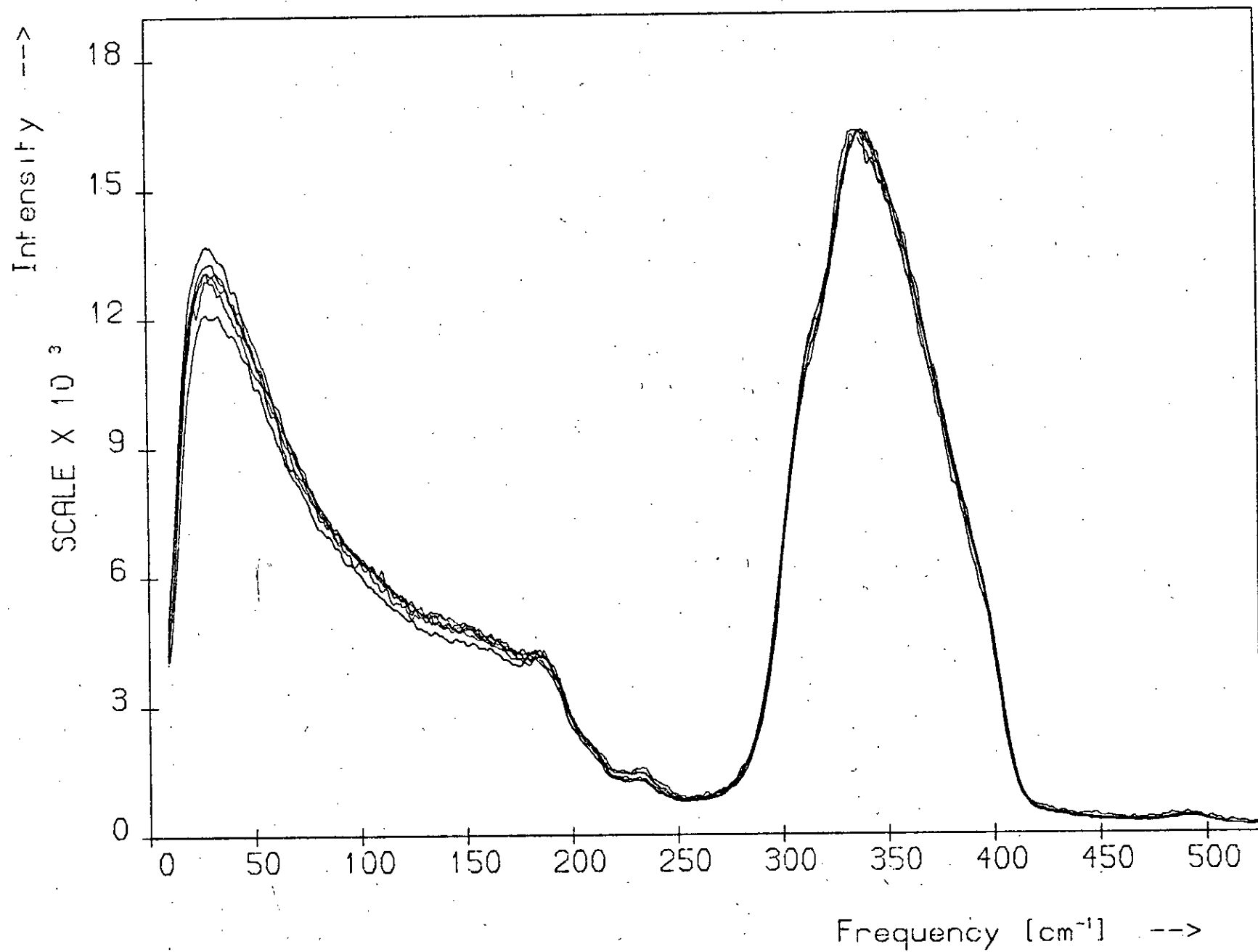height of the 338 cm^{-1} band and are shown displaced above one another.

Figure 4.15

The same six spectra of Figure 4.14 superimposed.

Spectra of the Stoichiometric Glass, As_2S_3.

Spectra of the Stoichiometric Glass, As_2S_3.

Spectrum	Source of sample	TTM grating in	Exciting line ($\overset{\circ}{A}$)	Slits (μ) l:m:r	Incident power (mW)	Count time (s)	Step size*
1	A.O.C.	No	6328	80:100:80	75	6	6
2	Department	No	6328	200:200:200	50	3	8
3	Department	Yes	6328	200:200:200	50	3	8
4	Department	Yes	6471	200:200:200	140	3	8
5	A.O.C.	No	6328	150:150:150	50	7	7
6	A.O.C.	No	6328	150:150:150	50	7	7

A.O.C. - American Optical Company

* Step size is in multiples of $\sim$0.03 $\overset{\circ}{A}$.

Table 4.3 The main experimental factors varying between the six recordings of the a-As_2S_3 spectrum shown in Figures 4.14 and 4.15.

superimposed in Figure 4.15.   The six spectra were recorded at various stages in the project and under different conditions, some being recorded specifically to test the effects of experimental factors on the spectra while others are taken from the various Raman experiments performed.   Table 4.3 gives the main experimental factors that vary among the six runs.   No significant differences between the spectra are apparent and all the features mentioned in Section 5.4.1 are present in the spectra, apart from the weak hump around 160 cm^{-1}, which appears only in the most intense spectra, and the 490 cm^{-1} peak in spectra 5 and 6.

Since some runs on the same sample are separated by more than 16 months it is clear from the agreement of the spectra that no sample deterioration occurs over this period, even though the samples were stored in ordinary room conditions and not in an evacuated or dessicated atmosphere.   There is no evidence of oxidation, decomposition or crystallisation.   Because As_2S_3 glass has a very low hygroscopicity[50], it would be expected that the samples are unaffected by humidity.

Using the peak finding routine[35] it was found that the frequencies of corresponding peaks in the six spectra agreed to within ±1.5 cm^{-1} and this value is taken as the reproducibility of the frequencies for the glass spectra in this project.

4.4   References

1.   'The Raman Effect' (Anderson, A., editor), Marcel Dekker, New York, 1973.

2.   Arthur, J.W. and Lockwood, D.J., J. Raman Spectrosc. 2, 53 (1974).

3.   Cardona, M., in 'Light Scattering in Solids', Springer-Verlag, Berlin, 1975, p.1.

4.   Myers, M.B. and Felty, E.J., Mat. Res. Bull. 2, 535 (1967).

5.   deNeufville, J.P., Moss, S.C. and Ovshinsky, S.R., J. Non-Cryst. Solids 13, 191 (1973).

6. Kobliska, R.J. and Solin, S.A., Phys. Rev. B $\underline{8}$, 756 (1973).

7. Ward, A.T., J. Phys. Chem. $\underline{72}$, 4133 (1968).

8. Markov, Yu. F. and Reshetnyak, N.B., Sov. Phys. Solid State $\underline{14}$, 1063 (1972).

9. Howard, R.E., Macedo, P.B. and Moynihan, C.T., Solid State Commun. $\underline{17}$, 1475 (1975).

10. Ward, A.T., Adv. in Chemistry $\underline{110}$, 163 (1972).

11. De Barry Barnett, E. and Wilson, C.L., 'Inorganic Chemistry', Longmans, London, 1953, p.389.

12. Bowlt, C. and Ghosh, B.N., Brit. J. Appl. Phys. $\underline{16}$, 1762 (1965).

13. Dembovskii, S.A., Polyakov, Yu.A. and Vaipolin, A.A., Izv. Akad. Nauk S.S.S.R., Neorg. Mater. $\underline{4}$, 767 (1968).

14. Mellor, J.W., 'A Comprehensive Treatise on Inorganic and Theoretical Chemistry', Vol.9, Longmans, London, 1929.

15. 'Kirk-Othmer Encyclopedia of Chemical Technology', Vol.2, Wiley, New York, 1969.

16. Scheuermann, W. and Ritter, G.J., Z. Naturforsch. $\underline{24}$A, 408 (1969).

17. Forneris, R., Amer. Mineral. $\underline{54}$, 1062 (1969).

18. Zallen, R., Slade, M.L. and Ward, A.T., Phys. Rev. B $\underline{3}$, 4257 (1971).

19. Zallen, R. and Slade, M.L., Phys. Rev. B $\underline{9}$, 1627 (1974).

20. Mathieu, J.P. and Poulet, H., Bull. Soc. Fr. Mineral Cristallogr. $\underline{93}$, 532 (1970).

21. Bastow, T.J. and Whitfield, H.J., J.C.S. Dalton, 1739 (1973).

22. Porter, E.J. and Sheldrick, G.M., J.C.S. Dalton, 1347 (1972).

23. 'Dana's System of Mineralogy', Vol.1, 7th edition, Wiley, New York, 1944, p.197.

24. Whitfield, H.J., J. Chem. Soc. (A), 1800 (1970).

25. Whitfield, H.J., J.C.S. Dalton, 1737 (1973).

26. Whitfield, H.J., Aust. J. Chem. $\underline{24}$, 697 (1971).

27. Whitfield, H.J., J.C.S. Dalton, 1740 (1973).

28. Ward, A.T., J. Phys. Chem. $\underline{72}$, 744 (1968).

29. Ozin, G.A., J. Chem. Soc. (A), 116 (1969).

30. Arthur, J.W. and Mackenzie, G.A., J. Raman Spectrosc. $\underline{2}$, 199 (1974).

31. Flaschen, S., Pearson, A. and Northover, W., J. Amer. Ceram. Soc. $\underline{42}$, 450 (1959).

32. Tsuchihashi, S. and Kawamoto, Y., J. Non-Cryst. Solids 5, 286 (1971).

33. Felty, E.J. and Myers, M.B., cited in Mott, N.F. and Davis, E.A., 'Electronic Processes in Non-Crystalline Materials', Clarendon Press, Oxford, 1971, p.251.

34. Dawson, P., J. Raman Spectrosc. 1, 359 (1973).

35. Arthur, J.W., Ph.D. Thesis, University of Edinburgh, 1974.

36. Owen, A.E., Sik, M.J. and Ewen, P.J.S., Report on S.R.C. Grant B/SR/7873, January 1975 (Unpublished).

37. Kosek, F. and Tauc, J., Czech. J. Phys. B 20, 94 (1970).

38. Greaves, G.N. and Davis, E.A., Phil. Mag. 34, 265 (1976).

39. Kobliska, R.J. and Solin, S.A., J. Non-Cryst. Solids 8 — 10, 191 (1972).

40. Kobliska, R.J. and Solin, S.A., Solid State Commun. 10, 231 (1972).

41. Loudon, R., J. Phys. 26, 677 (1965).

42. Razzetti, C. and Fontana, M.P., Phys. Stat. Sol. (b) 70, 173 (1975).

43. Tauc, J., Menthe, A. and Wood, D.L., Phys. Rev. Lett. 25, 749 (1970).

44. Asahara, Y. and Izumitani, T., Phys. Chem. Glasses 16, 29 (1975).

45. Berkes, J.S., Ing, S.W. and Hillegas, W.J., J. Appl. Phys. 42, 4908 (1971).

46. Kirkinskii, V.A., Eksp. Issled. Mineral., 9 (1969).

47. Lagowski, J.J., 'Modern Inorganic Chemistry', Marcel Dekker, New York, 1973, p.424.

48. Ursu, I., Lupei, A. and Lupei, V., Rev. Roum. Phys. 15, 569 (1970).

49. Burns, J.G., McKendrick, A. and Stephens, P.D., IMP Language Manual, Edinburgh Regional Computing Centre (1970).

50. Glaze, F.W., Blackburn, D.H., Osmolov, J.S., Hubbard, D. and Black, M.H., Bur. Stand. J. Res. 59, 83 (1957).

CHAPTER 5

RESULTS AND DISCUSSION: THE As-S SYSTEM

5.1   Introduction

This chapter presents and discusses the results obtained for the

arsenic sulphides: amorphous and crystalline materials throughout the

As-S system, including the elements, have been investigated in the

present study, with particular emphasis on the composition range around

the stoichiometric glass As_2S_3. Figure 5.1 shows the compositions

investigated in this study and also those examined in Raman and i.r.

studies carried out by other researchers, including Ward[1,2], whose

work on the As-S glasses has been augmented by the present study, which

includes polarisation measurements on all the glasses and examines in

greater detail the composition range within ± 5 at.% of a-As_2S_3. Eleven

near-stoichiometric compositions extending from $As_{35}S_{65}$ to $As_{45}S_{55}$ in

1 at.% steps have been investigated.

Raman spectra presented here are substantially in agreement with

the corresponding spectra obtained in the other studies, though some new

features in the glass spectra have been observed and there is no sign of

the spurious structure apparent in Ward's results[3,4]. All the spectra

presented in this study were recorded at room temperature.

5.2   Spectra of the crystalline As-S compounds

A knowledge of the vibrational spectra of the crystals in the system

is essential in the study of the glasses, firstly because it may help in

the identification of individual features in the glass spectra and secondly

because a comparison of crystal and glass spectra for the same composition

will show to what extent the structure of the glass is related to that of

the crystal. Consequently, the Raman spectra of as many as possible of

the numerous crystal compounds which occur in the As-S system (see Section 2.2)

This Study   Other Studies

at.% As	at.% S	Amorphous	Crystal	Amorphous	Crystal
100	0				
95	5				
90	10				
85	15				
80	20		As_3S (?)		
75	25				
70	30				
65	35				
60	40		As_4S_3		
55	45				
50	50		As_4S_4		
45	55		As_4S_5		
40	60		As_2S_3		
35	65				
30	70				
25	75				
20	80				
15	85				
10	90				
5	95				
0	100				

glass-forming region
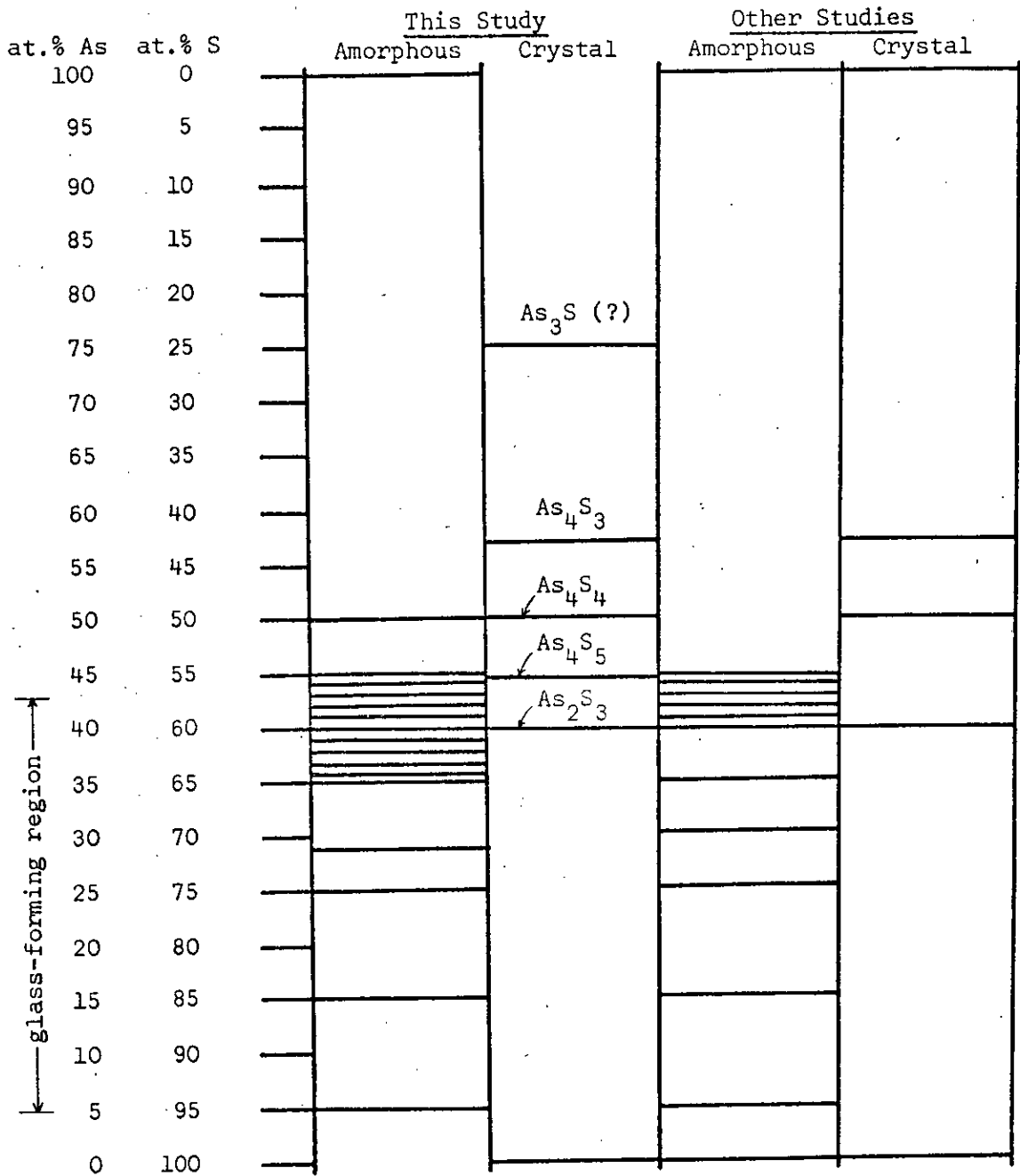
Figure 5.1

The compositions investigated in vibrational studies of materials in the As-S system.

have been recorded in this study. It is evident from Figures 5.2 – 5.6, which show the crystalline Raman spectra obtained in this study, that the vibrational spectra of these materials are complex. Apart from As_3S, all the compounds were very strong scatterers at red wavelengths.

5.2.1   c-As₂S₃

The Raman spectrum of the mineral orpiment is presented in Figure 5.2. The spectrum is representative of the present results, which were obtained on mineral samples from two independent sources. Several investigations of the Raman[2,3,5 – 10] and i.r.[3,5,7,9 – 12] spectra of this material have been carried out by other workers and the effects of pressure[13] and low temperature[3,6,11] on the spectra have also been examined. Zallen et al.[5,6] discovered that the optical properties of c-As₂S₃ are determined not by the C_{2h}^5 space group symmetry of the crystal but by the C_{2v} symmetry of the individual layers in the crystal. For one of the c-As₂S₃ layers in isolation there are 3 zone-centre acoustic modes and 27 non-degenerate (i.e. with no symmetry-induced degeneracies) zone-centre optical vibrations, all of which are Raman active. The symmetries of the 27 optical modes are given by $\Gamma - P = 7A_1 + 7A_2 + 7B_1 + 6B_2$. As the crystal unit cell contains two layer units there are twice as many normal modes for the crystal as for the layer, that is 60. If the interaction between layers were to tend to zero, the 60 crystal vibrations would collapse to 30 degenerate doublets, each pair corresponding to a single layer vibration with adjacent layers vibrating with equal or opposite phase. The weak interlayer interaction lifts these degeneracies, however, resulting in a set of closely spaced doublets one member of which is Raman active and the other i.r. active.

The crystal also gives rise to three low-frequency zone-centre rigid-layer modes, all Raman active. These are the layer-crystal counterparts of the rigid-molecule, or external, vibrations which occur in

Figure 5.2

The Raman spectrum of $c\text{-As}_2\text{S}_3$.

Raman Spectrum of Crystalline As₂S₃.
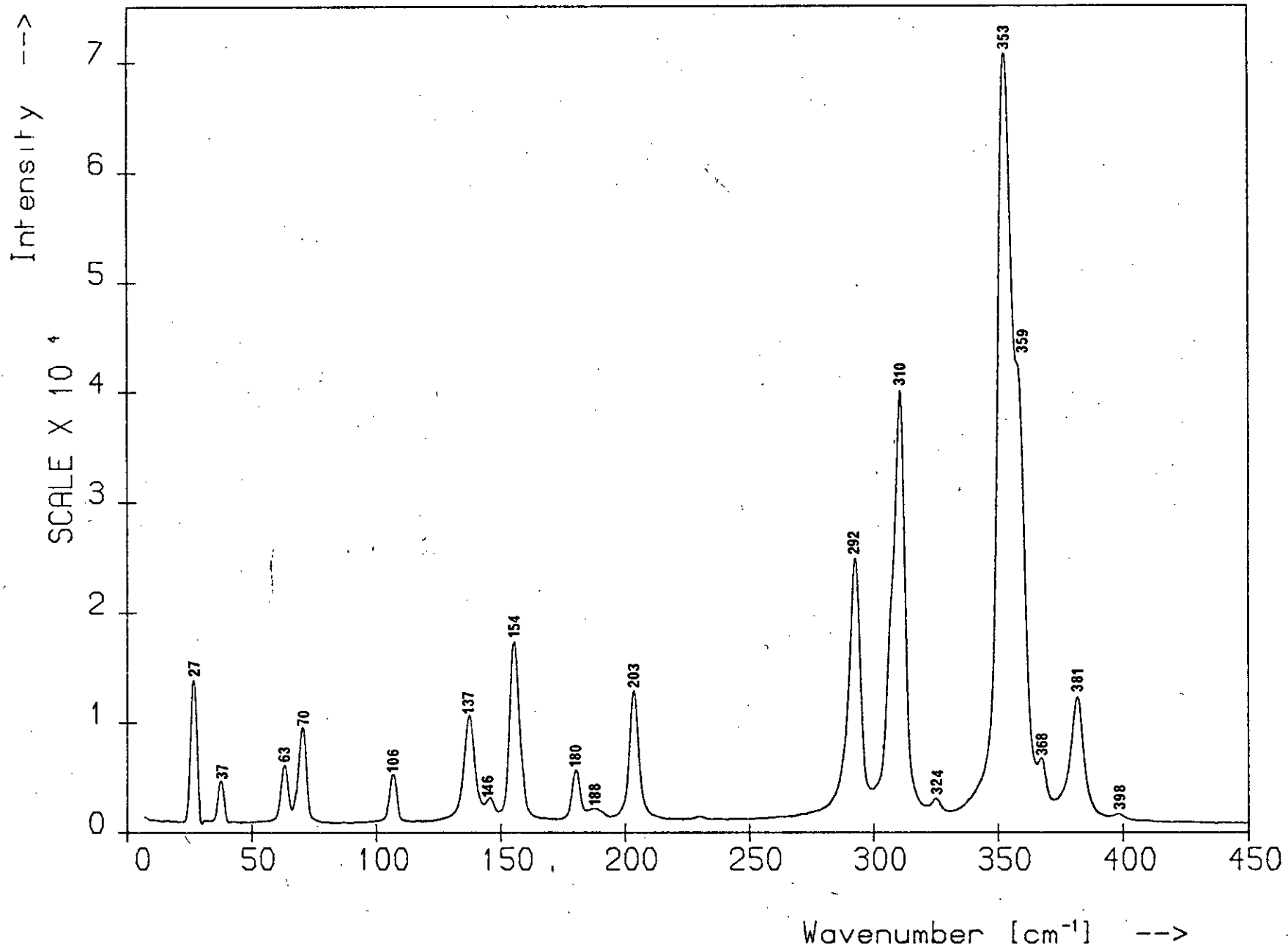
crystals composed of small molecules. Because the crystal unit cell is two layers thick and the crystal space group contains centres of symmetry which interchange adjacent layers, these rigid-layer modes are of even symmetry and thus i.r. inactive. Two of these modes are shear vibrations in which adjacent layers slide over each other in opposite directions parallel to the layer planes, while the third is a compressional vibration in which adjacent layers beat against each other along the normal to the layer planes. Hence there are 30 lines possible in the first-order Raman spectrum of c-As_2S_3: 19 have been observed.

The symmetry assignments for the observed frequencies of orpiment have been determined by Zallen et al.[5], from Raman polarisation measurements, and Mathieu and Poulet[7], mainly from i.r. measurements, but the two sets of results are not in complete agreement. No polarisation data could be obtained in the present study because of the poor optical quality of the specimens.

From Figure 5.2 it is seen that the bands occur in three distinct spectral regions: below 80 cm^{-1}, between 100 and 210 cm^{-1} and from 290 to 400 cm^{-1}. Those in the high-frequency region are the As-S bond-stretching modes and those in the $100 - 210$ cm^{-1} range are the bond-bending modes[9]. The four low-frequency bands are the rigid-layer modes. In the scaling relation (see Section 6.4.5) that has been shown to exist[5,6] between c-As_2S_3 and c-As_2Se_3 these four bands scale differently to the others. Those at 27 and 37 cm^{-1} are the two non-degenerate shear modes. The compressional rigid-layer mode is also Raman active in c-As_2S_3 and it appears that this mode has become heavily intermixed with one of the low-frequency bond-bending intralayer modes to produce the doublet at 63 and 70 cm^{-1} [6]. Some of the very weak features in the spectrum may be due to overtones or combinations[9].

5.2.2   c-As$_4$S$_4$

The Raman spectrum of the mineral realgar (α-As$_4$S$_4$) and the synthetic sample (β-As$_4$S$_4$) are displayed in Figures 5.3 and 5.4 respectively.   In the case of α-As$_4$S$_4$ both the Raman[1,2,9,10,14] and i.r.[9 − 11,15] spectra have been investigated by other workers. Since the Raman spectrum of this molecular crystal cannot result from the van der Waals forces between the As$_4$S$_4$ molecules the spectrum has to be explained in terms of the D$_{2d}$ molecular symmetry rather than the C$_{2h}^5$ crystal symmetry.   This leads to the following distribution of vibrational fundamentals: 3A$_1$ + 2A$_2$ + 2B$_1$ + 3B$_2$ + 4E[9].   All modes are Raman active except those of A$_2$ symmetry, which may, however, become active in the crystal due to the lower site symmetry.

Examination of Figure 5.3 reveals that the principal Raman bands of α-As$_4$S$_4$ fall into three distinct spectral regions, as did those of c-As$_2$S$_3$: below 70 cm^{-1}, between 120 and 225 cm^{-1} and from 320 to 380 cm^{-1}. On the basis of the assignment determined for the spectrum of the As$_4$S^{2-} ion[16] the high-frequency bands are associated with the As—S bond-stretching modes and the bands in the range 120 − 225 cm^{-1} are mainly attributable to bond-bending modes[9].   The frequencies below 70 cm^{-1} can be ascribed to the external vibrations of the molecules and deform-ations of the cradle involving movement of the neighbouring As atoms.

Tentative symmetry assignments for the observed frequencies have been made by Forneris[9].   Once again, no polarisation data could be obtained in the present study because of the poor optical quality of the sample used.   The symmetries of the As—S stretching modes are distributed as A$_1$ + A$_2$ + B$_1$ + B$_2$ + 2E and thus five As—S stretching bands are expected in the high-frequency region of the Raman spectrum: five are observed, viz 328, 343, 354, 368 and 374 cm^{-1}.   The symmetries of the cradle deformations are distributed as 2A$_1$ + A$_2$ + B$_1$ + 2B$_2$ + 2E so seven bending bands are expected: according to Forneris's interpretation these would

Figure 5.3

The Raman spectrum of α-As_4S_4.

Figure 5.4

The Raman spectrum of β-As_4S_4.

Raman Spectrum of Crystalline As$_4$S$_4$.

Raman Spectrum of As₄S₄.

Raman Spectrum of As_4S_4.

X-axis: Wavenumber [cm^{-1}] —>
Y-axis: Intensity —> SCALE X 10^4

Labeled peaks: 24, 33, 40, 61, 119, 135, 144, 153, 165, 175, 186, 200, 211, 218, 233, 271, 313, 332, 343, 351, 360, 382
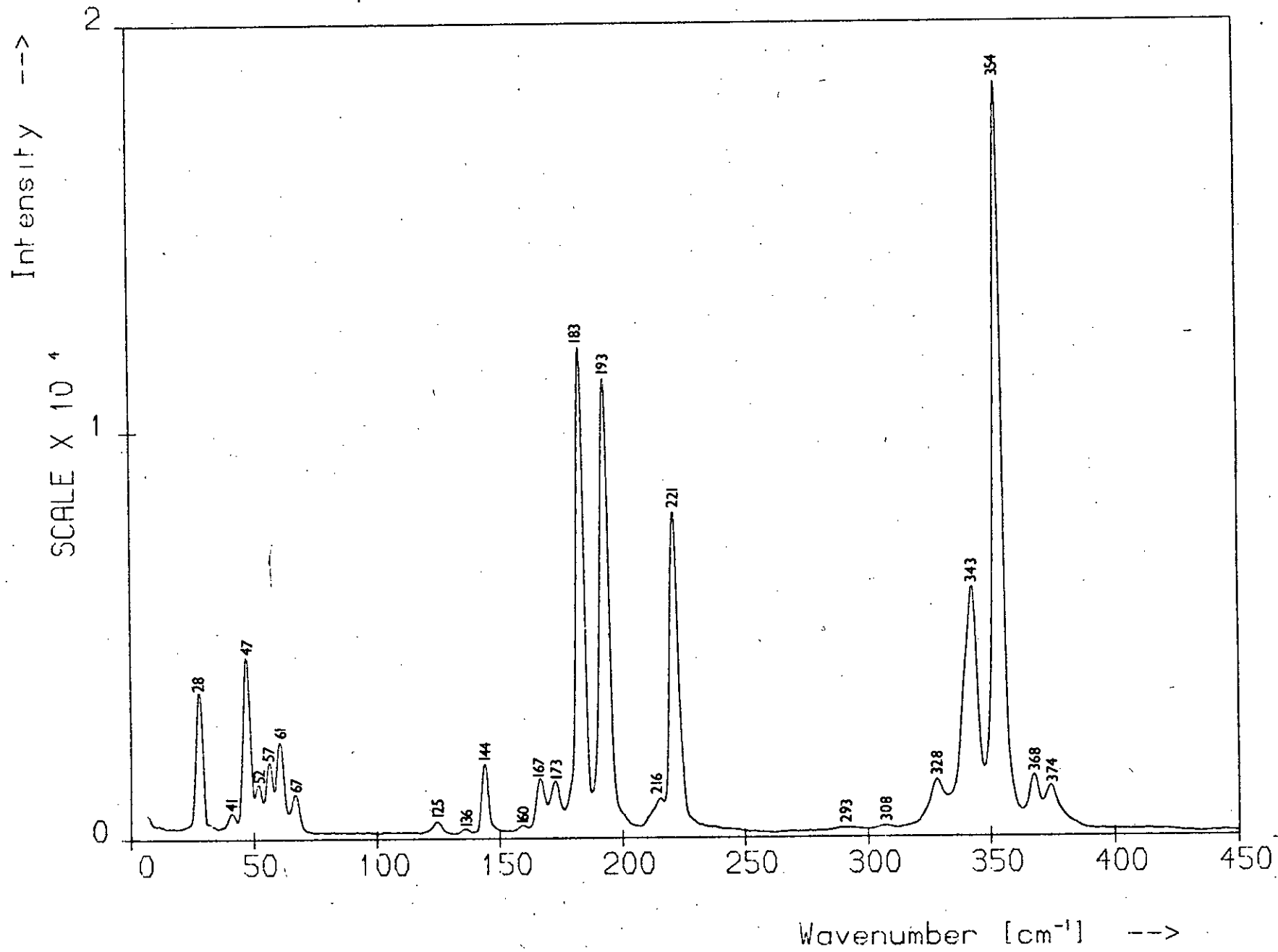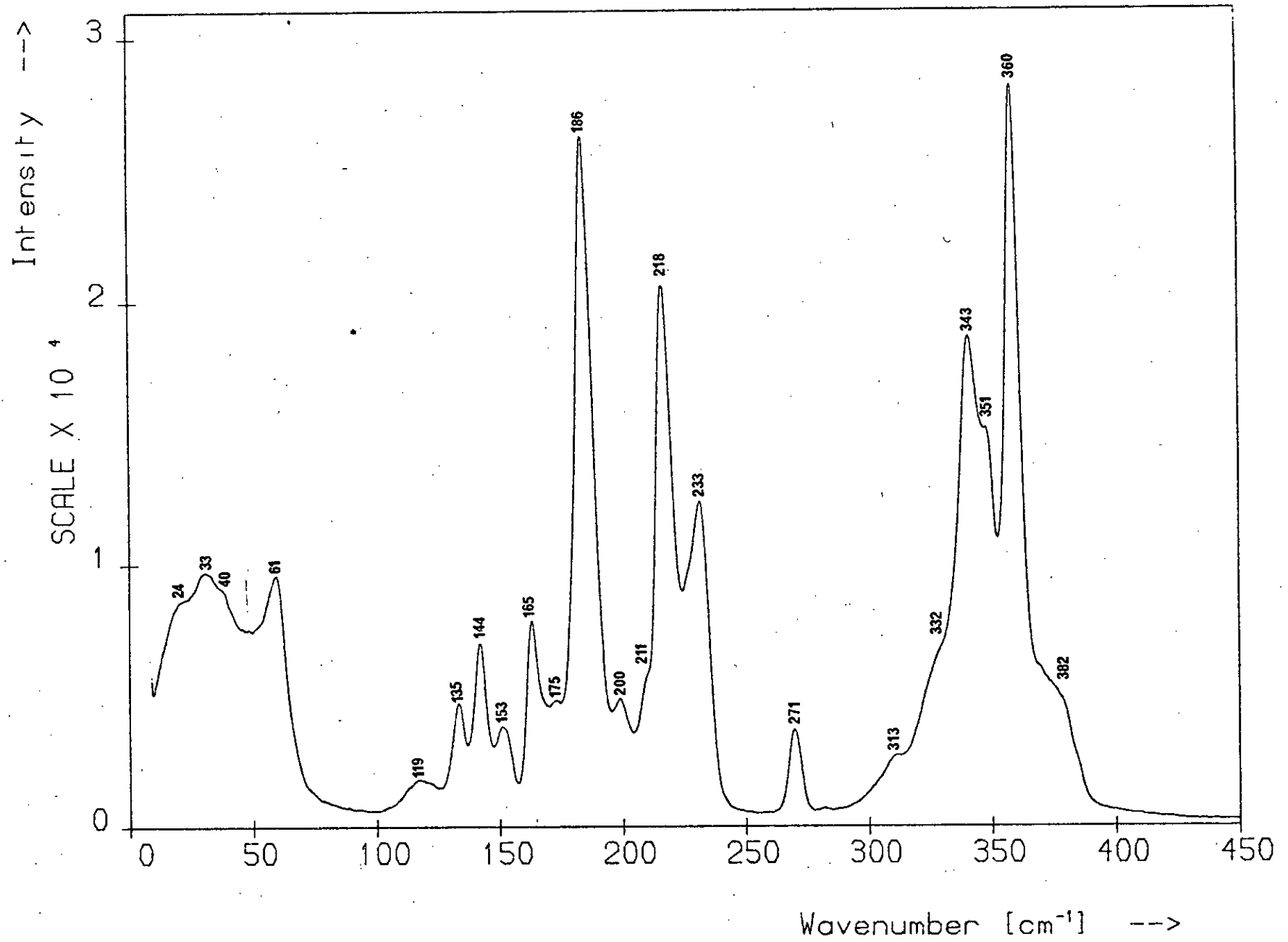
be the bands at 47, 61, 144, 173, 183, 193 and 221 cm^{-1}. The lowest two of the seven frequencies correspond to deformations in which the pairs of As atoms on the same side of the plane formed by the four S atoms move toward and away from each other.

Whitfield[11] suggests that the band at 235 cm^{-1} in Forneris's Raman spectrum may arise from an As–As stretching mode. This may well be correct but the feature at 235 cm^{-1} is absent from the spectrum observed in this study (and also from Ward's data[1,2]) and is possibly due to light-induced structural changes in the material[14]. This is discussed fully in Section 5.7.

The very weak bands appearing in the spectrum may be due to overtones or combinations, or may arise from already present or photo-induced regions of c-As_2S_3 in the sample. For example, the features at 293 and 308 cm^{-1} occur near strong orpiment bands.

In the case of β-As_4S_4 only the Raman spectrum has been previously recorded[14] and no vibrational analysis exists. The As_4S_4 molecules in β-As_4S_4 are identical to those in α-As_4S_4 but the space group for the crystal is C2/c. The molecules are arranged in an approximately cubic close-packed array and the shortest intermolecular As...As distances are considerably longer than in α-As_4S_4. The Raman spectrum of β-As_4S_4 is shown in Figure 5.4 (see also Figure 5.76 after p.193) and is fairly similar to that of α-As_4S_4, the bands falling in the same three spectral regions. There are, however, a number of peak shifts and the intense doublet centred at 188 cm^{-1} in the spectrum of α-As_4S_4 is replaced by a single band in the spectrum of β-As_4S_4.

Porter and Sheldrick[14] also observe light-induced structural changes in both forms and comparison of the spectrum of β-As_4S_4 obtained in this study with the spectra of irradiated c-As_4S_4 obtained by them suggests that these extrinsic structural features are already present in our sample

since their characteristic bands are apparent in Figure 5.4. This is discussed fully in Sections 5.6.3 and 5.7. Ignoring these extraneous bands the spectrum presented here is in reasonable agreement with the published data.

5.2.3 c-As$_4$S$_3$

Figure 5.5 shows the Raman spectrum of the synthetic β-As$_4$S$_3$ produced in the Department. Only the i.r. spectrum of this material has been published[11]. The As$_4$S$_3$ molecule has point-group symmetry C$_{3v}$ and of its ten fundamental frequencies nine should appear in the Raman spectrum, four belonging to the symmetrical class A$_1$ and five to the degenerate class E.

Once again the principal Raman bands fall into three spectral regions: below 60 cm^{-1}, between 160 and 280 cm^{-1} and from 330 to 380 cm^{-1}. The high-frequency bands are due to the stretching of As—S bonds, those in the intermediate range arise mainly from bond-bending modes and the low-frequency lines arise from external vibrations. From Whitfield's[11] interpretation of the i.r. spectrum of β-As$_4$S$_3$, the feature at 373 cm^{-1} can be attributed to the symmetric stretch of the apical As atom with respect to the three attached S atoms, the band at 336 cm^{-1} can be attributed to the symmetric stretch of the As—S bonds of the triangle of As atoms with respect to the attached S atoms, and the doublet at 171 and 178 cm^{-1} can be ascribed to the S—As—S bending mode of degenerate class E. On the basis of a valence force field calculation Rogstad[17] attributes the band at 271 cm^{-1} to a cage 'breathing' mode with emphasis on the As$_3$ basal triangle. The features at 230 and 236 cm^{-1} may arise from an As—As stretching mode. Whitfield calculates the As—As single bond stretching frequency to be 264 cm^{-1}, assuming a bond length of 2.45 Å, and attributes the 235 cm^{-1} band in Forneris's[9] Raman spectrum of α-As$_4$S$_4$ to an As—As stretching mode.

Figure 5.5

The Raman spectrum of β-As$_4$S$_3$.

Raman Spectrum of Hs$_4$S$_3$.
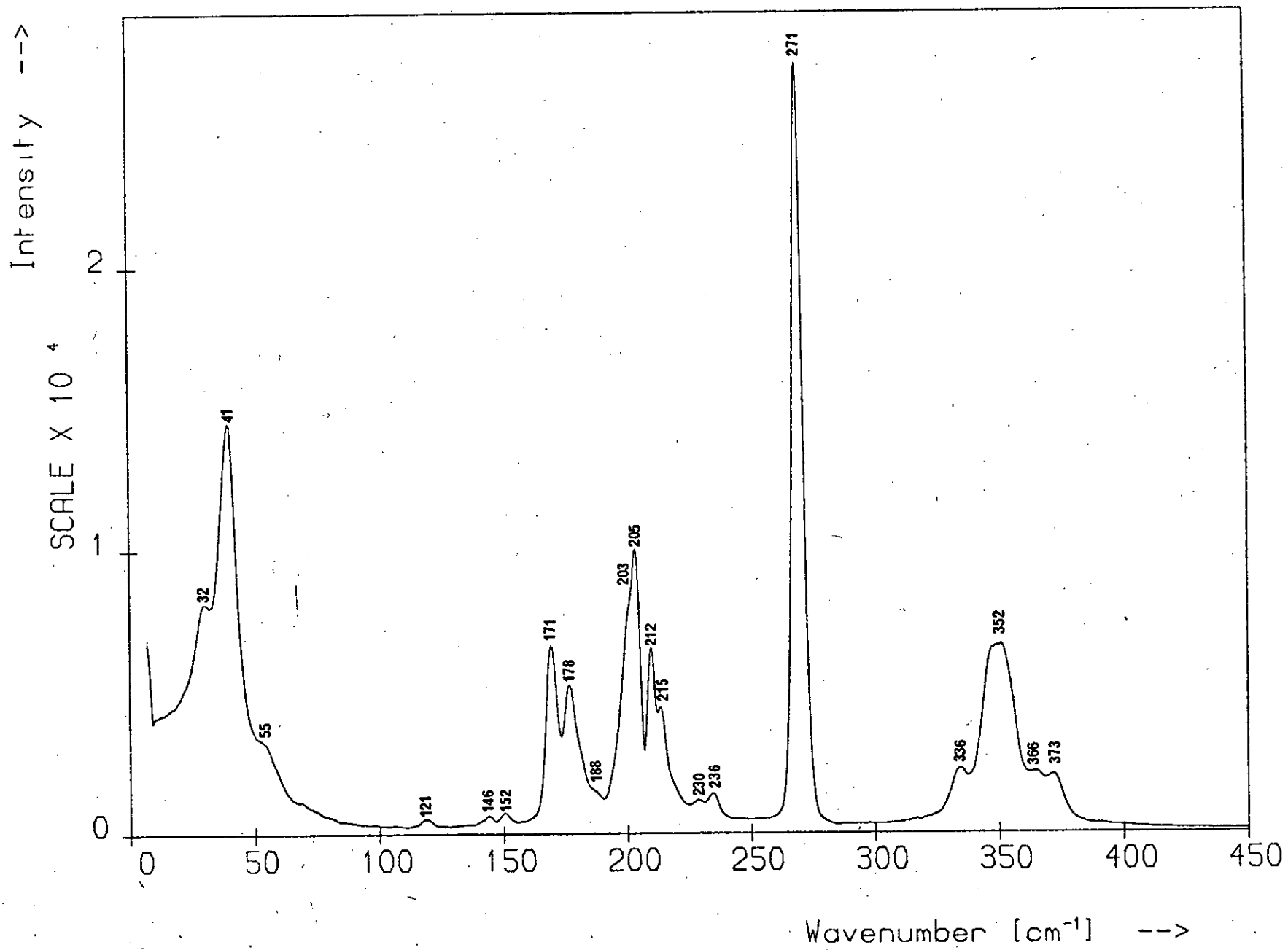
5.2.4   c-As$_4$S$_5$

Figure 5.6 shows the Raman spectrum of the yellow powder obtained by Whitfield's[18] method for producing c-As$_4$S$_5$. As the vibrational spectrum of this crystal has not been previously recorded it cannot be asserted that the substance investigated here is pure c-As$_4$S$_5$. The sample is certainly a crystalline arsenic sulphide since the main bands are sharp and occur in the frequency regions characteristic of the As-S crystals. The presence of certain impurities can be ruled out immediately: there is no feature near 473 cm^{-1}, the highest vibrational frequency of orthorhombic sulphur (see Figure 5.7 after p.114), and there are no CS$_2$ features present. Any impurities in the sample will probably be other arsenic sulphides but comparison of Figure 5.6 with the other crystalline spectra recorded in this study suggests that these better-known forms are not present, since many of their strong lines are absent from the spectrum. As the vibrational spectra of the less well-known arsenic sulphides have not been measured one cannot determine whether they are contributing to the spectrum in Figure 5.6, but since the vibrational spectrum of α-As$_4$S$_3$ is very similar to that of β-As$_4$S$_3$[19] the former material is possibly responsible for some of the spectral features, e.g. the strong band at 271 cm^{-1}. However, even if the specimen studied is a mixture of these less well-known crystals its spectrum is still of use in identifying crystalline features in the glass spectra. Nevertheless, it will be assumed here that the material is predominantly c-As$_4$S$_5$.

Like the other As-S crystal spectra, the principal bands in the c-As$_4$S$_5$ spectrum fall into three regions: a low-frequency region below 60 cm^{-1}, an intermediate region centred around 200 cm^{-1} and a high-frequency region centred around 350 cm^{-1}. The three belts of frequencies can be attributed to external vibrations, predominantly bond-bending modes, and As-S bond-stretching modes respectively. The 233 cm^{-1} feature may arise from stretching of the As-As bond.

Figure 5.6

The Raman spectrum of c-As$_4$S$_5$.

Raman Spectrum of c-As₄S₅
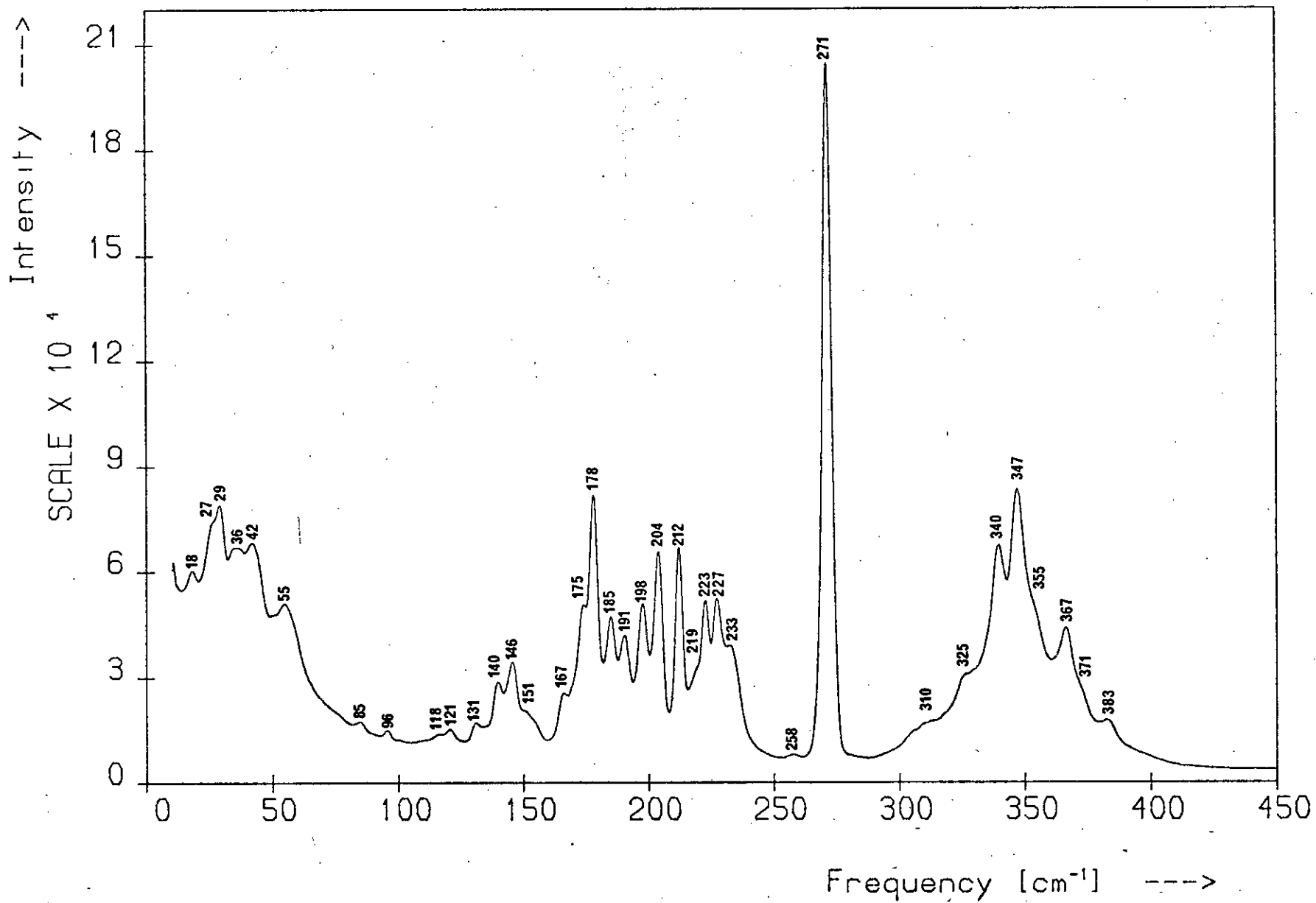
5.2.5   Other crystalline compounds

The As_3S examined yielded a very weak spectrum which was a combination of the spectra of α- and β-As_4S_4.   It is unlikely that this compound exists and the material is probably mainly a mixture of arsenic and c-As_4S_4.

The vibrational spectra of the other crystalline compounds and polymorphs in the As-S system have not, as far as is known to the present author, been reported.

5.3   Spectra of the elements

5.3.1   Orthorhombic sulphur

The crystalline form of sulphur thermodynamically stable at room temperature and pressure is orthorhombic sulphur (α-S_8), a molecular crystal composed of S_8 rings.   Its vibrational spectrum has been extensively studied in i.r.[20 – 22] and Raman[1,2,23 – 25] experiments and the effect of temperature[2,26,27] and pressure[13] on the spectrum have been investigated.   The external vibrations have been investigated by Arthur and Mackenzie[28].   The spectrum obtained in the present study from a powdered sample is shown in Figure 5.7 and is in agreement with the published data.   As α-S_8 is a strong scatterer at red wavelengths intense spectra were easily obtained.

The isolated S_8 molecule, which is a puckered octagon of D_{4d} symmetry, has eleven fundamental vibrations distributed as follows: $2A_1 + 3E_2 + 2E_3$ (Raman active), $B_2 + 2E_1$ (i.r. active) and B_1 (inactive).   The presence of four S_8 molecules in the crystal unit cell leads to splitting of the fundamentals and a group theoretical analysis shows that the Raman spectrum of the crystal should contain 48 bands, twelve of which arise from external modes[27].   However, since the van der Waals intermolecular forces in α-S_8 are weak compared with the covalent intramolecular forces, not all

<u>Figure 5.7</u>

The Raman spectrum of orthorhombic sulphur.

<u>Figure 5.8</u>

The normal modes and frequencies of the S_8 ring (after Reference 29).

Raman Spectrum of Orthorhombic Sulphur
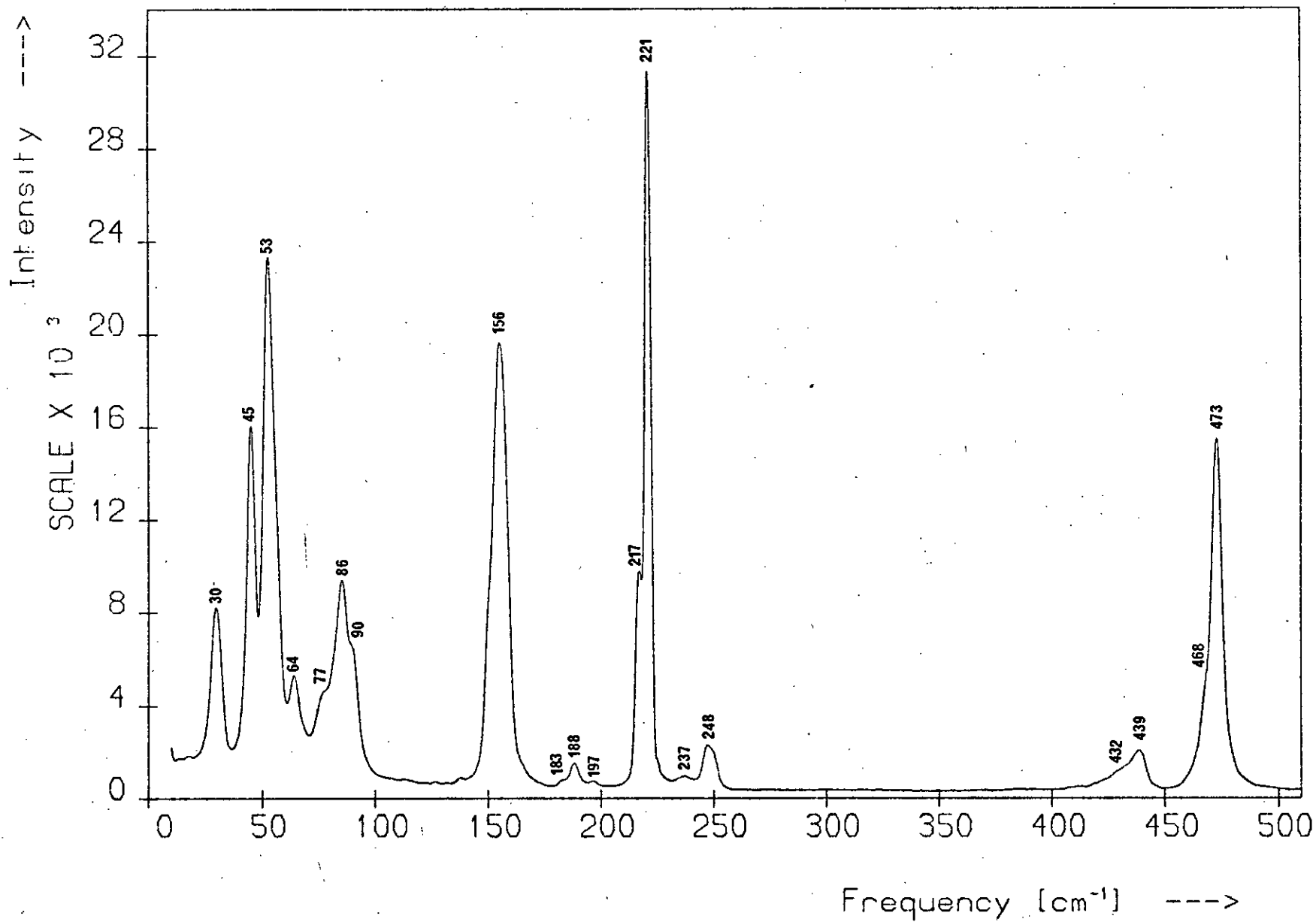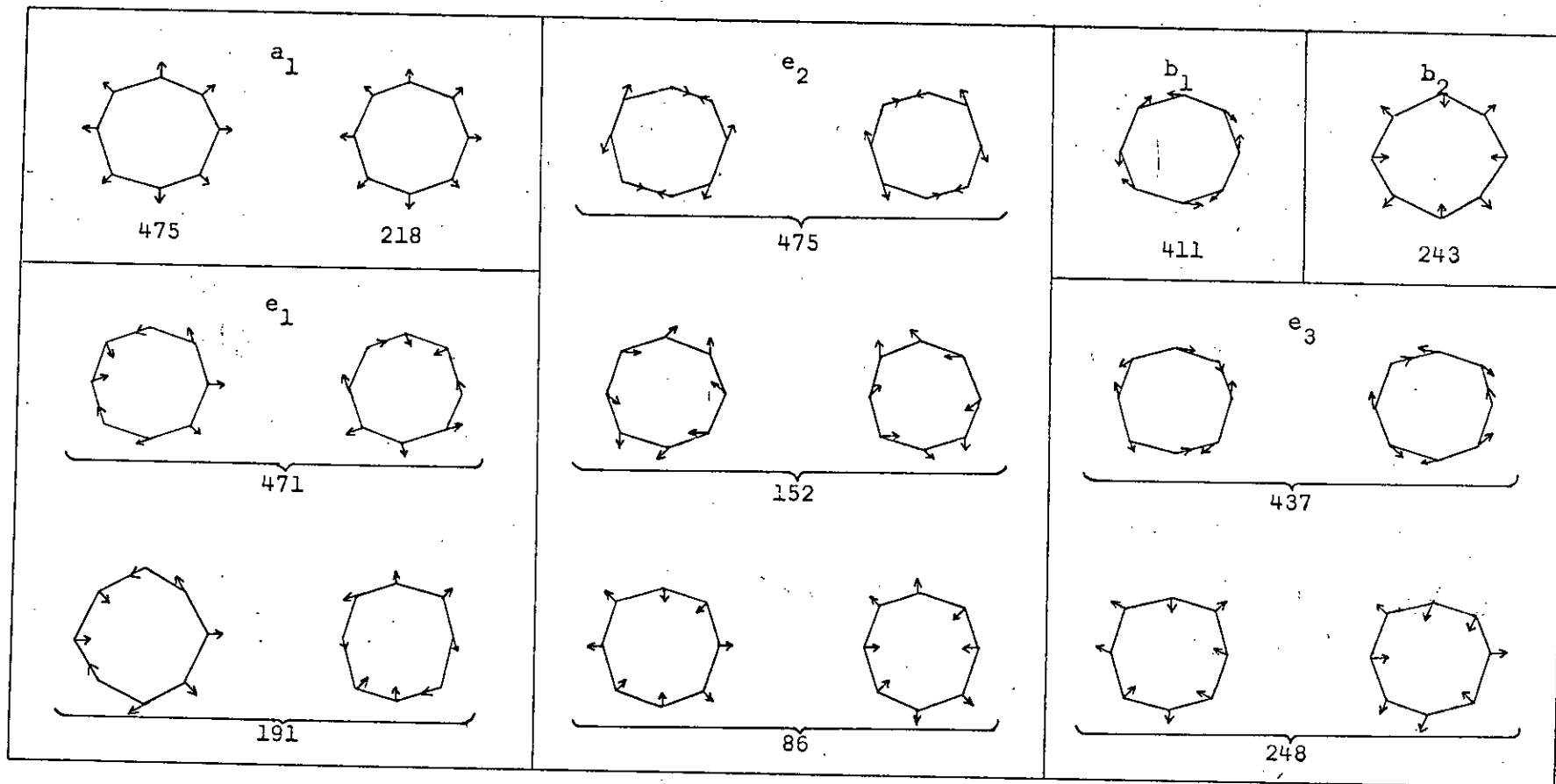
All frequencies in cm^{-1}.

48 bands may be observable in the Raman spectrum. Symmetry assignments for the observed frequencies are proposed in several of the studies referred to[23 − 25,27,28].

Although the spectrum presented in Figure 5.7 is in general agreement with the published data, a number of the splittings have not been resolved. To observe the splittings fully one must use good single crystals or make measurements at low temperatures. However, their observation is not essential in the present study.

Using the normal coordinate analysis of the isolated S_8 molecule carried out by Scott et al.[29], Anderson and Loh[27] have related the crystal frequencies to the specific vibrations of the S_8 ring. This is shown in Figure 5.8, where the frequencies obtained are shown beside the corresponding normal modes of the S_8 molecule. The bands below 80 cm^{-1} arise from external vibrations.

5.3.2 Amorphous arsenic

The Raman spectrum of bulk a-As obtained in the present study is shown in Figure 5.9 and is in good agreement with the results of Lannin[30,31]. The i.r. spectrum of the bulk material has been recorded by Lucovsky and Knights[32], and the first-[33,34] and second-order[34] Raman spectra of rhombohedral arsenic have also been reported. Renucci et al.[33] have also studied resonance Raman scattering in the rhombohedral crystal.

The spectrum of Figure 5.9 consists of a broad, asymmetric band centred at ~225 cm^{-1} together with two much weaker bands at ~145 and 280 cm^{-1}. The main band peaks at 200 cm^{-1} and has a shoulder at ~237 cm^{-1}. These frequencies are in agreement with those obtained in the other vibrational studies of a-As[30 − 32], though the two sharp, weak features at ~115 and 165 cm^{-1} in the i.r. spectrum are not observed in the spectrum of Figure 5.9, possibly due to its poor signal/noise ratio.

Figure 5.9

The Raman spectrum of amorphous arsenic.

Raman Spectrum of a-As
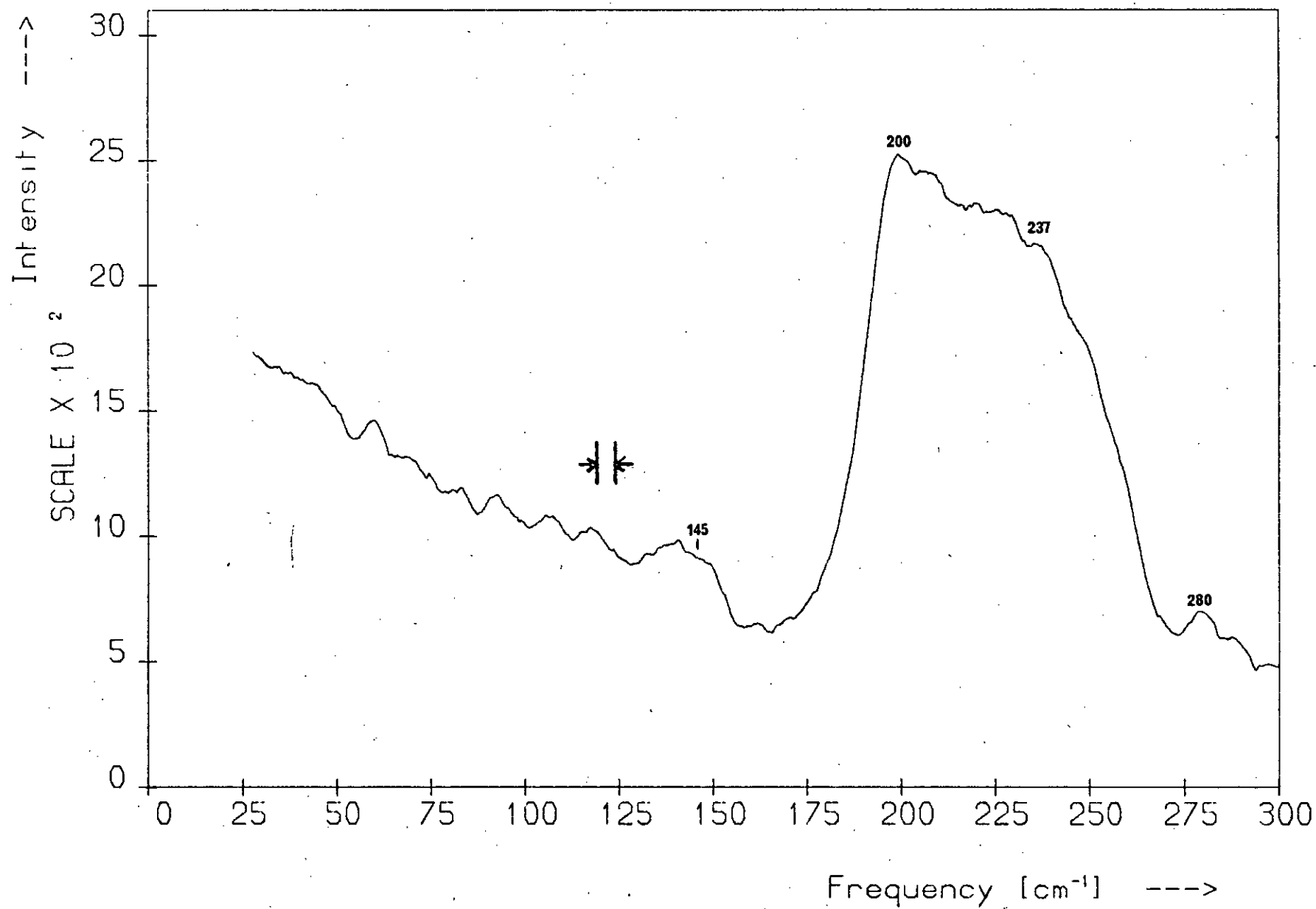
The Raman spectrum of rhombohedral arsenic has two bands in the 150 — 300 cm^{-1} region, one at 195 cm^{-1} and the other at 257 cm^{-1} [33,34].

The depolarisation ratios (corrected for the background) measured for the 237, 200 and 145 cm^{-1} bands were 0.46, 0.28 and 0.54 respectively. These values are in agreement with the polarisation measurements made by Lannin[31] and indicate that the 200 cm^{-1} band is polarised while the 237 and 145 cm^{-1} bands are predominantly depolarised.

The vibrational spectra of a-As are expected to be partly 'molecular' and partly density-of-states-like[35]. Comparison of the i.r. and Raman spectra suggests that they are similar rather than complementary, which is consistent with a density-of-states description. Also, the reduced Raman spectrum of a-As is similar to the density of states determined for this material by inelastic neutron scattering[31]. In contrast, the large rise in the depolarisation ratio between 200 and 237 cm^{-1} is typical of 'molecular' spectra, for a perfectly 'non-molecular' amorphous solid is expected to have a depolarisation spectrum of constant amplitude[3]. Hence the expectation of dual behaviour is borne out.

As this is an elemental material a totally molecular approach is precluded since the equivalence of all chemical bonds in such materials implies that the intermolecular coupling would be as strong as the intramolecular forces. However, Lucovsky and Knights[32] have shown that the general form of the vibrational spectrum of a-As can be derived by considering a small structural unit, viz an As_4 pyramid. The two crystalline forms of arsenic, orthorhombic and rhombohedral As, are made up from layers composed of As_4 pyramids and these pyramids have been taken as the basic structural units of a-As[36]. Lucovsky and Knights calculate the vibrational frequencies of the As_4 pyramid and show that these account for the number of gross features in the a-As spectra; they do not attempt to explain the finer structure in the spectra.

5.4   The stoichiometric glass: $As_{40}S_{60}$

5.4.1   The polarisation-unanalysed spectrum

Room-temperature, polarisation-unanalysed Raman spectra represent-
ative of the results obtained in this study for vitreous As_2S_3 are dis-
played in Figures 5.10 and 5.11.   An anti-Stokes spectrum is included in
Figure 5.11 for comparison with the Stokes data but for all other com-
positions examined in the present investigation only the Stokes spectrum
has been recorded, since no further information of interest can be obtained
from the anti-Stokes data.   The spectra in Figure 5.11 have been normal-
ised to the height of the 29 cm^{-1} band.

The Raman[1 - 4,8,37 - 46] and i.r.[11,46 - 51] spectra of this
extensively studied glass have been recorded by several workers.   The
spectra of Figures 5.10 and 5.11 are in good agreement with the published
Raman spectra, with the exception of some features of Ward's results.
Pronounced features at 140, 189, 230 and 490 cm^{-1} in Ward's[1,2] spectrum
of a-As_2S_3 have been attributed to plasma lines by Kobliska and Solin[3,4],
who maintain that these features are absent from their spectra.   However,
since Kobliska and Solin's investigation, the spectrum has been re-recorded
under various experimental conditions by a number of workers[8,39,44] who
confirm the presence of structure at these frequencies.   These features
were also observed in the a-As_2S_3 spectra obtained in the present study
which are free of plasma lines (see Section 4.3.3).   The structure is
apparent in both Stokes and anti-Stokes spectra, as Figure 5.11 shows, and
is present in spectra excited by different light sources, viz the He-Ne
and Kr-ion lasers.   In fact, the structure is evident in many of Kobliska
and Solin's spectra[3,4,38] also.

The difference between Ward's spectra and those of other workers is
one of degree, as this structure is far more pronounced in his results
than elsewhere.   Since features grow rapidly at 135, 146, 187 and 233 cm^{-1}

Figure 5.10

The polarisation-unanalysed Stokes Raman spectrum of vitreous As_2S_3.

Figure 5.11

The Stokes and anti-Stokes Raman spectra of vitreous As_2S_3.

Raman Spectrum of a-$As_{40}S_{60}$.
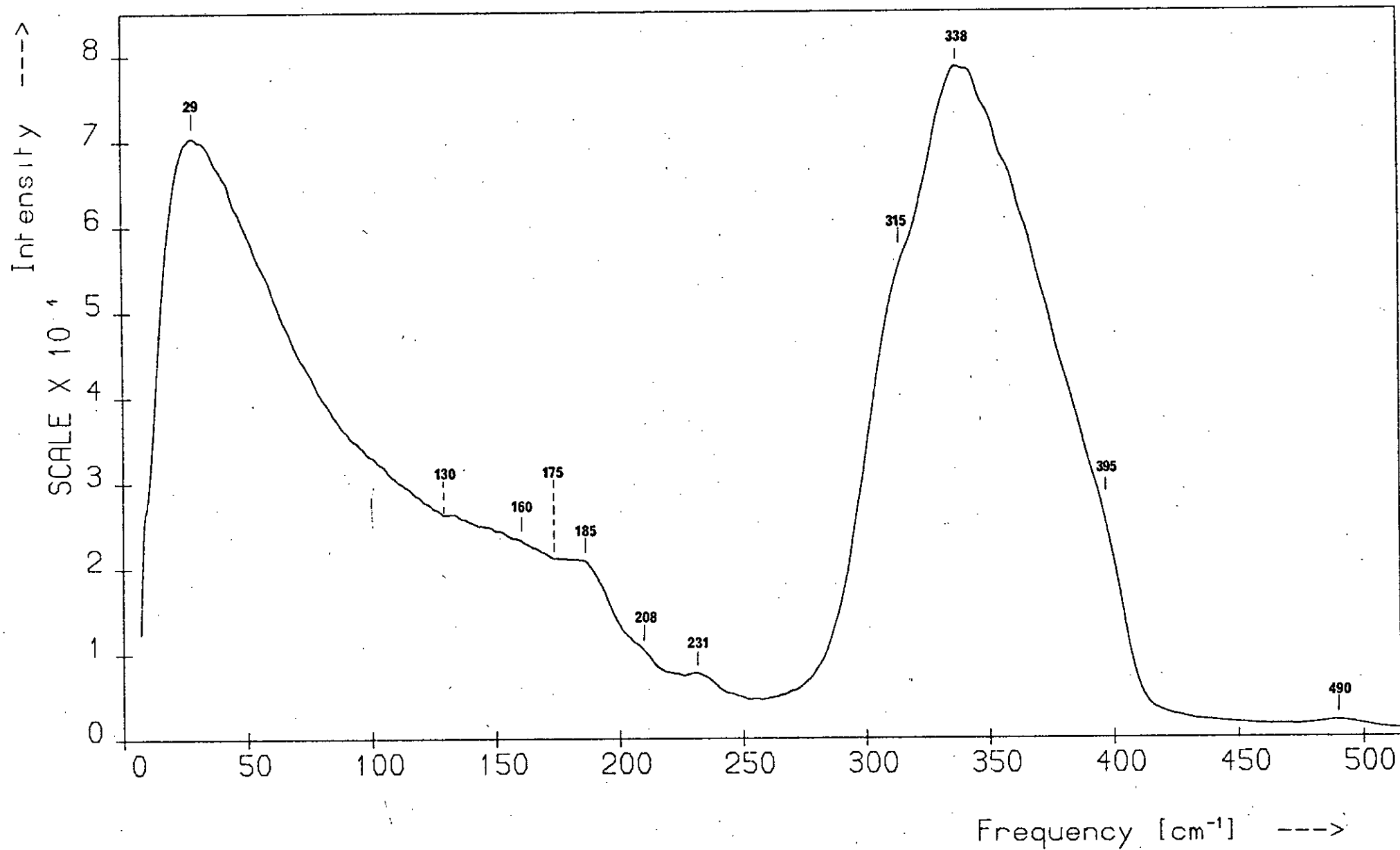
Stokes and Anti-Stokes Spectra: $As_{40}S_{60}$
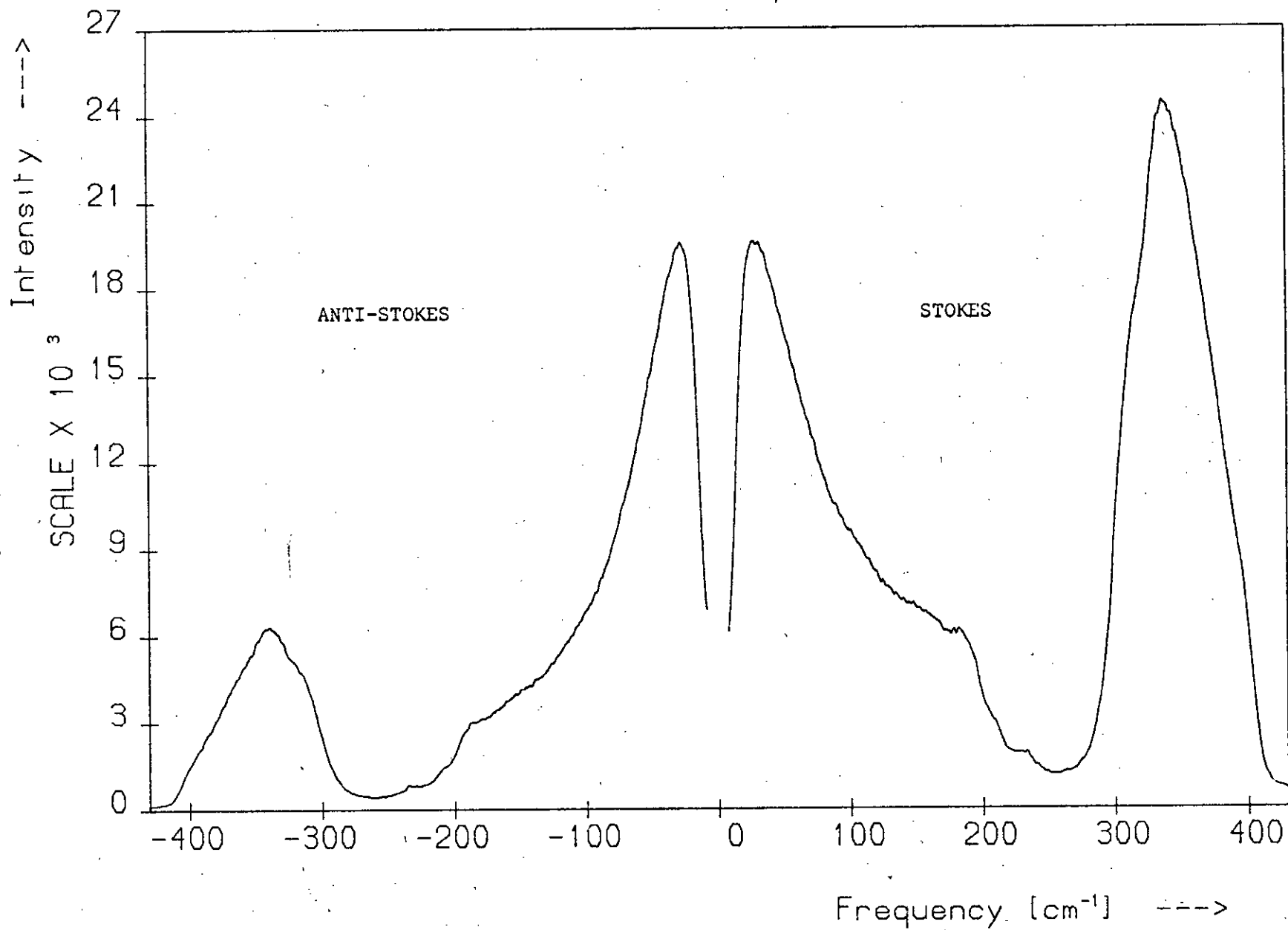
as the As content of the glass is increased (see Section 5.6.1) it is probable that this prominent structure in his spectra arises from a slightly As-rich specimen.

Kobliska and Solin[3,4] have studied the temperature dependence of the Raman spectrum of a-As_2S_3 in the range $0 - 500$ cm^{-1} and have shown it to be that characteristic of first-order Raman scattering. Most of the features observed in the present study have been observed by other workers and Table 5.1 (after p.122) compares the published frequencies with those obtained here. The weak 490 cm^{-1} band is shown at greater magnification in Figure 5.36 (after p.147).

5.4.2   Polarisation measurements

Kobliska and Solin[3] have also pointed out the importance of polarisation measurements in Raman scattering investigations of amorphous solid structure and have defined a new type of spectrum, called the 'depolarisation spectrum', which they measure for a-As_2S_3. The depolarisation ratio, $\rho(w)$, of a Raman band is defined as the ratio of the intensity of scattered light polarised in the scattering plane to that polarised perpendicular to the plane. Whereas the Raman spectrum of a crystalline material consists of a set of discrete lines with a corresponding set of discrete depolarisation ratios, the Raman spectrum of an amorphous solid is continuous and so the associated depolarisation ratio is a continuous function of frequency shift. It is this continuous function that is termed by Kobliska and Solin the 'depolarisation spectrum' of the material. This spectrum provides a test for the applicability of structural models and determines the extent to which the reduced spectrum of the glass can be regarded as a measure of the phonon density of states. The more 'molecular' an amorphous solid is, the more irregular is its depolarisation spectrum.

The polarisation data obtained in this study for a-As_2S_3 is shown in

Figure 5.12. In the abbreviations such as VV and VH used in various places throughout this account the first letter indexes the polarisation of the incident beam with respect to the scattering plane and the second indexes that of the scattered beam with respect to the scattering plane; H and V correspond to radiation which is polarised in and perpendicular to the scattering plane respectively. Figure 5.13 compares the unanalysed spectrum with the VV and VH spectra, Figure 5.14 shows the depolarisation spectrum and Figure 5.15 compares it with the unanalysed and polarised spectra. As a check on the polarisation data, spectrum A in Figure 5.13 has been generated by adding the VV and VH spectra, whose intensities are as originally measured, and is compared with the unanalysed spectrum, B, which was run consecutively with the polarised spectra. The two spectra are virtually indistinguishable.

The depolarisation spectrum of Figure 5.15 agrees with the published data[3,40 − 42] both in terms of absolute value for $\rho(w)$ and shape, although some of the structure is absent from Kobliska and Solin's[3] original spectrum because of the large channel width between their data points. Finkman et al.[39] also report a number of these new features in the depolarisation spectrum and Kobliska and Solin[3] have shown that the depolarisation spectrum is temperature independent.

In addition to being of use in the interpretation of the Raman results, the polarisation data yield a more accurate value for certain frequencies in the vibrational spectrum and emphasise the presence of others. For example, the shoulder on the low-frequency side of the 338 cm^{-1} band in the unanalysed spectrum is transformed into a well-defined peak at 315 cm^{-1} in the VH spectrum and the previously unreported knee on the high-frequency side appears as a well-defined dip at 400 cm^{-1} in the depolarisation spectrum. The depolarisation data also reveals structure in the vibrational spectrum at 106 and 160 cm^{-1}.

Figure 5.12

The VV- and VH-polarised spectra of a-As_2S_3. As the VH spectrum is considerably weaker than the VV spectrum (see Figure 5.13) they have been normalised by equalising the intensities of the 315 and 339 cm^{-1} bands of the VH and VV spectra respectively. 11,500 counts have been subtracted from the ~20 — 60 cm^{-1} region of the VH spectrum.

Figure 5.13

A comparison of the VV, VH and polarisation-unanalysed spectra. The spectra have not been normalised in any way. Spectrum A is the sum of the two polarised spectra; spectrum B was recorded consecutively with the polarised data.

Figure 5.14

The depolarisation spectrum of a-As_2S_3.

Figure 5.15

The VV, VH, depolarisation (D) and polarisation-unanalysed (PU) spectra of a-As_2S_3.

Polarised Spectra: a-As$_{40}$S$_{60}$

Raman Spectra: $a\text{-}As_{40}S_{60}$

Intensity --->

SCALE X 10^4

A

B

Polarisation-unanalysed

VV

VH

Frequency $[cm^{-1}]$ --->
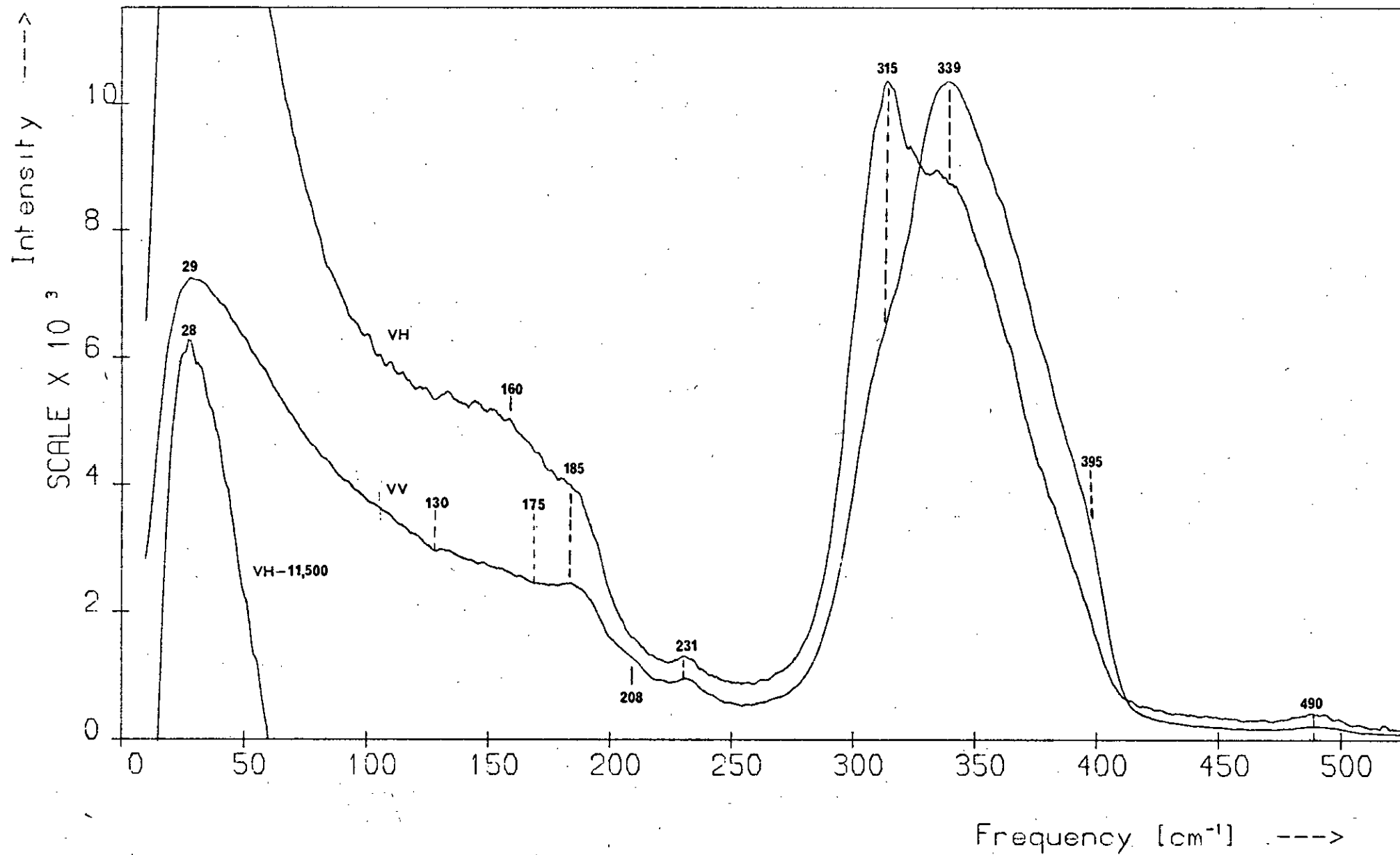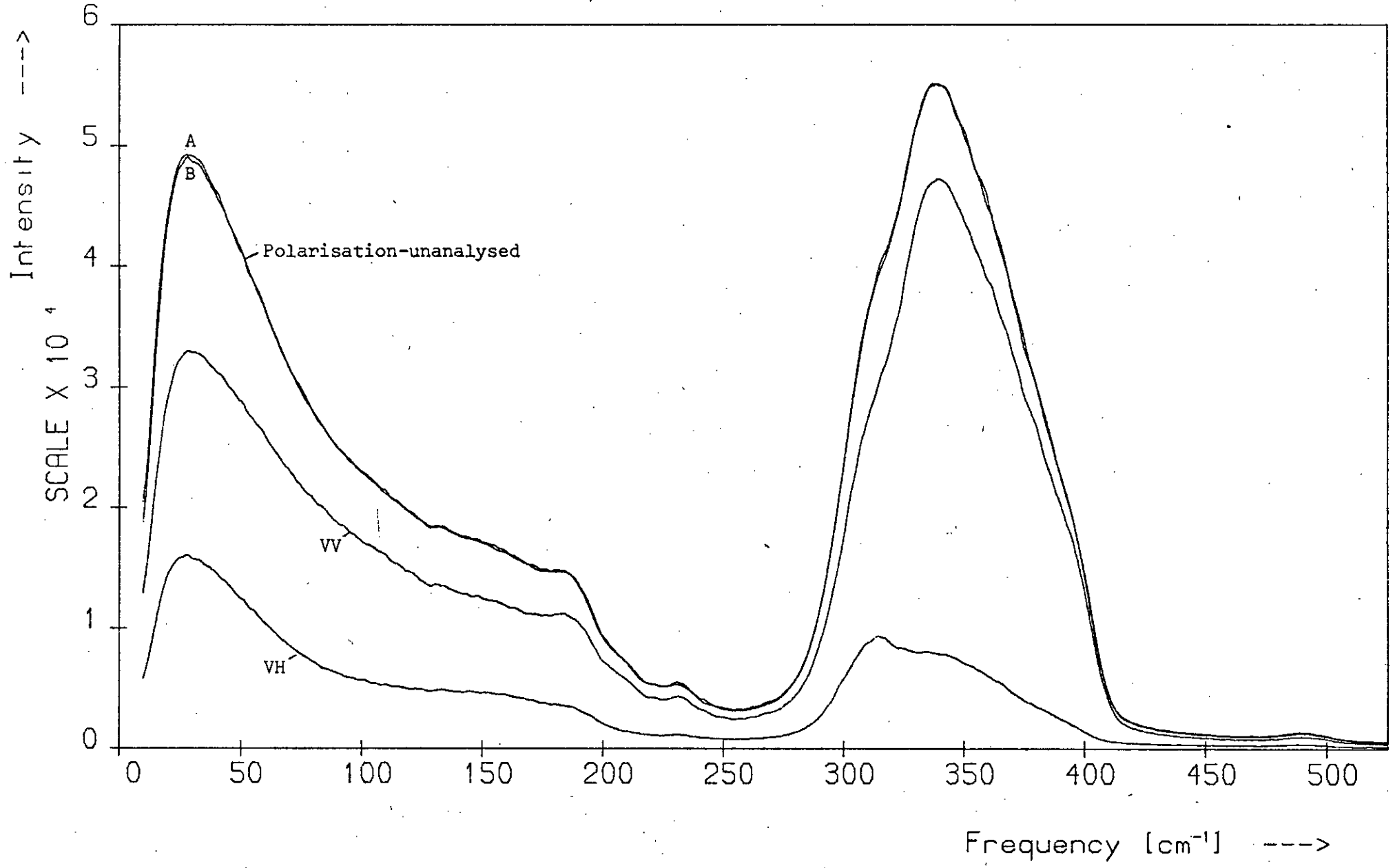
Depolarisation Spectrum of a-As$_{40}$S$_{60}$
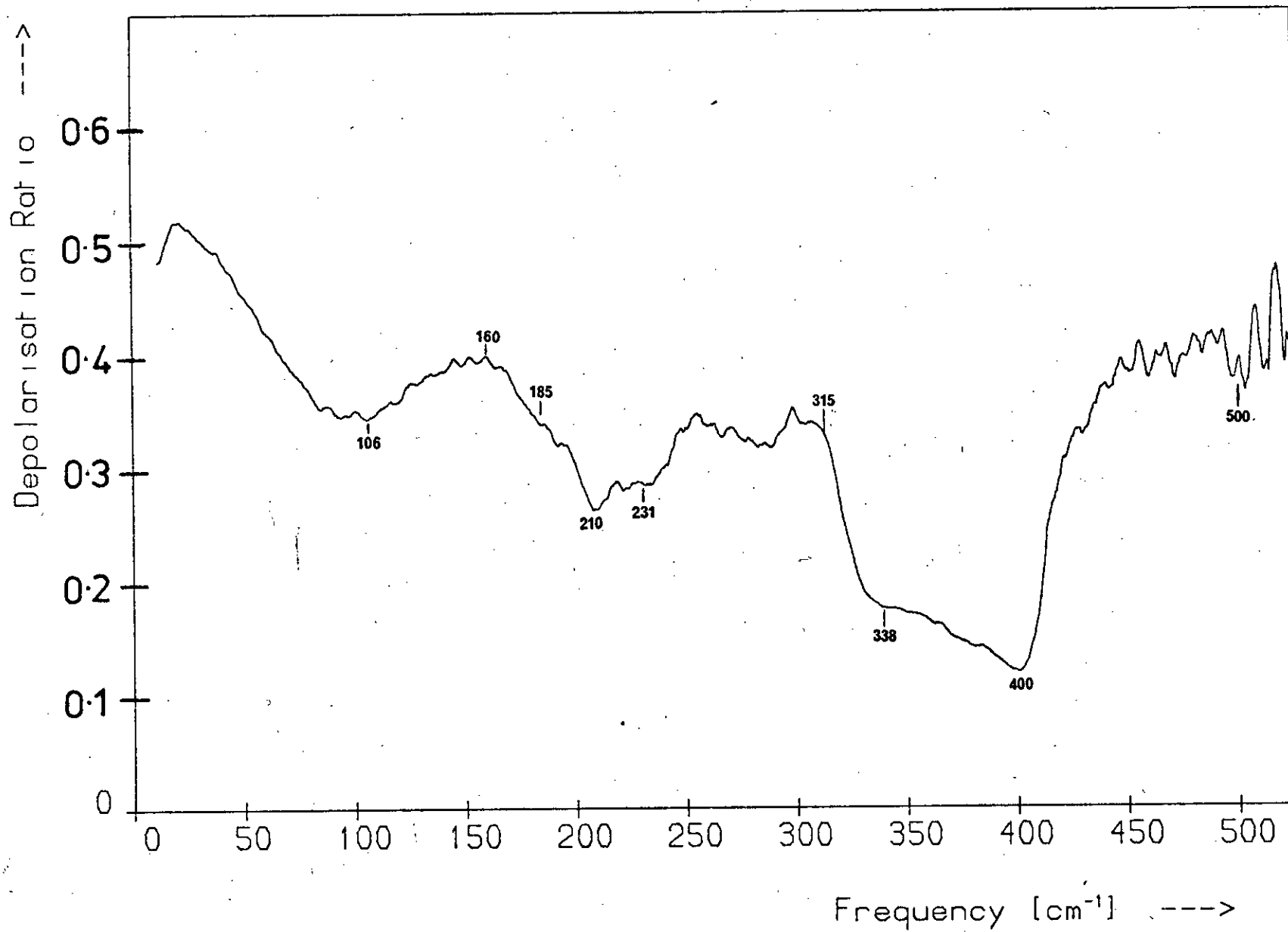
VV, VH, Depolarisation and Unanalysed Spectra
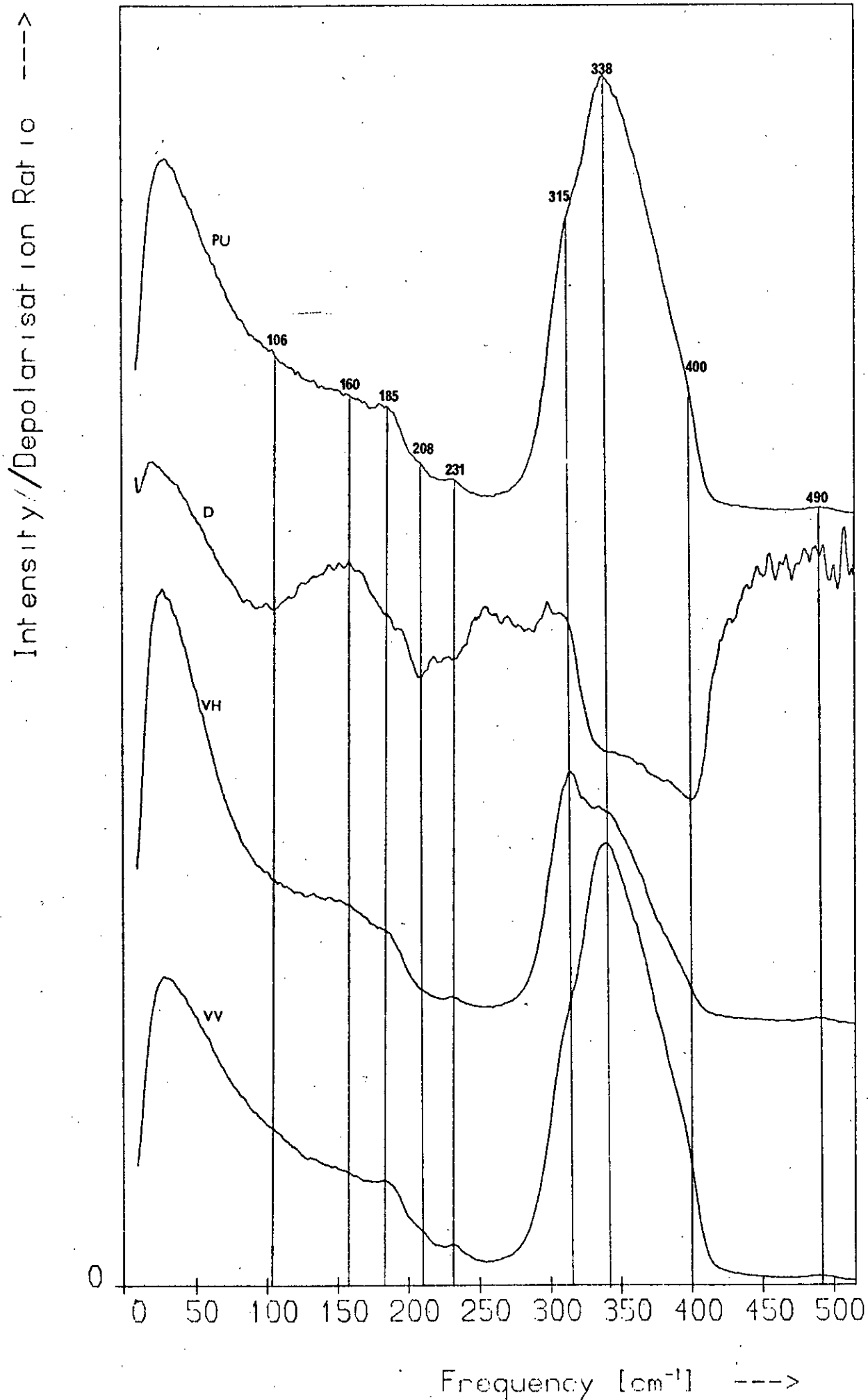
5.4.3   Deconvolution of the main band

In the molecular model the continuous nature of the a-As$_2$S$_3$ Raman spectrum arises from the distribution in both pyramid apex angles and force constants.   If these distributions are Gaussian then it should be possible to construct the Raman spectrum by summing the amplitudes of a set of overlapping Gaussian lines, each line being centred on a vibrational frequency.   This procedure was carried out by Ward[2] and is also described in Section 5.4.4.3 (see Figure 5.24 after p126) but in both cases the vibrational frequencies used were those of orpiment. In this section it is seen whether the main band of the a-As$_2$S$_3$ spectrum can be generated by a set of Gaussian lines centred on the observed frequencies for a-As$_2$S$_3$.   The shape of the main i.r. absorption band of a-As$_2$Se$_3$ has been shown to be Gaussian[50], though there is some controversy over this[49], and Lucovsky and Martin[62] have pointed out that this would also arise naturally in their model as inhomogeneous line broadening due to molecular interactions.

In the case of the main band the results of this study show that at least three vibrational frequencies occur in the region 250 — 420 cm^{-1}, namely those at 315, 339 and 395 cm^{-1}.   Inspection of Figure 5.16 shows that the main band (dotted curve) is highly asymmetric, having a shoulder on the low-frequency side of the peak and an almost linear fall-off on the high-frequency side ending in a knee at ~395 cm^{-1}.   Comparison of the two sides of the main band suggests that at least one other frequency is present between 339 and 395 cm^{-1}.   If it is assumed that these two or more bands at frequencies >339 cm^{-1} make a negligible contribution to the intensity occurring on the low-frequency side of the peak (section AB in Figure 5.16) then it is possible to fit to section AB two uniquely determined Gaussian lines centred at 315 and 339 cm^{-1}.   Provided that the disorder-induced broadening gives rise to the same standard deviation, σ, for each Gaussian, only three points in section AB are needed to

determine the Gaussians.

The dotted curve in Figure 5.16 is the measured $250 - 450$ cm^{-1} region of the a-As$_2$S$_3$ spectrum after the weak background has been subtracted. The full curve was fitted to section AB of the observed spectrum using the method outlined above and is the sum of two Gaussians centred at 312 and 340 cm^{-1} and with $\sigma = 13$ cm^{-1}. The fit on the low-frequency side is fairly exact but clearly these bands cannot account for the high-frequency side. Even ignoring the inflections at 315 and 395 cm^{-1} the main band is highly asymmetric. Gaussians with standard deviations greater than 13 cm^{-1} could not be made to fit the low-frequency side of the main band. Figure 5.17 compares the measured a-As$_2$S$_3$ VH spectrum, in which the 315 cm^{-1} peak is prominent, with the 312 cm^{-1} Gaussian band used in generating the fitted curve of Figure 5.16. It is clear that this Gaussian is of approximately the correct width. The standard deviation of 13 cm^{-1} is comparable with the ± 15 cm^{-1} spread in the 339 cm^{-1} frequency calculated by Kobliska and Solin[3] and arises mainly from a $\pm 9\%$ spread in the stretching force constant — the distribution of S—As—S angles in a-As$_2$S$_3$ has been shown by Taylor and Rubinstein[66] to have an upper limit of $\pm 2°$ which leads to an approximately $\pm 1\%$ spread in the vibrational frequencies.

Figure 5.18 shows the difference curve (dotted line) obtained by subtracting the fitted curve of Figure 5.16 from the measured spectrum. The difference curve has a peak at 367 cm^{-1} and exhibits a knee at 395 cm^{-1}. The breadth and asymmetry of this curve show that it cannot arise from a single Gaussian band of standard deviation equal to 13 cm^{-1}. It was found, however, that two such bands could account for the curve. The full curve shown in the figure was fitted to the difference curve using the same procedure that was used above; both Gaussians had a standard deviation of 13 cm^{-1} and were centred near the inferred frequencies. The overall fit is reasonable but agreement at the base is poor and the

Figure 5.16

The main band (dotted curve) of the a-As_2S_3 spectrum after subtraction of the background.   The full curve has been fitted to section AB of the main band and is the sum of two Gaussians.

Figure 5.17

The main band of the a-As_2S_3 VH spectrum (dotted curve) and a Gaussian of standard deviation equal to 13 centred at 312 cm^{-1} (full curve). The Gaussian has been scaled so that its maximum intensity equals the intensity of the VH spectrum at 312 cm^{-1}.


Figure 5.18

The difference curve (dotted line) obtained by subtracting the fitted curve of Figure 5.16 from the main band of the polarisation-unanalysed spectrum.   The full line has been fitted to the difference curve and is the sum of two Gaussians.

Figure 5.19

The four Gaussians used in the analysis and the curve generated by summing them (A).   Curve B is the observed main band of the polarisation-unanalysed spectrum after subtraction of the background.

The Main Band of the αAs₂S₃ Spectrum
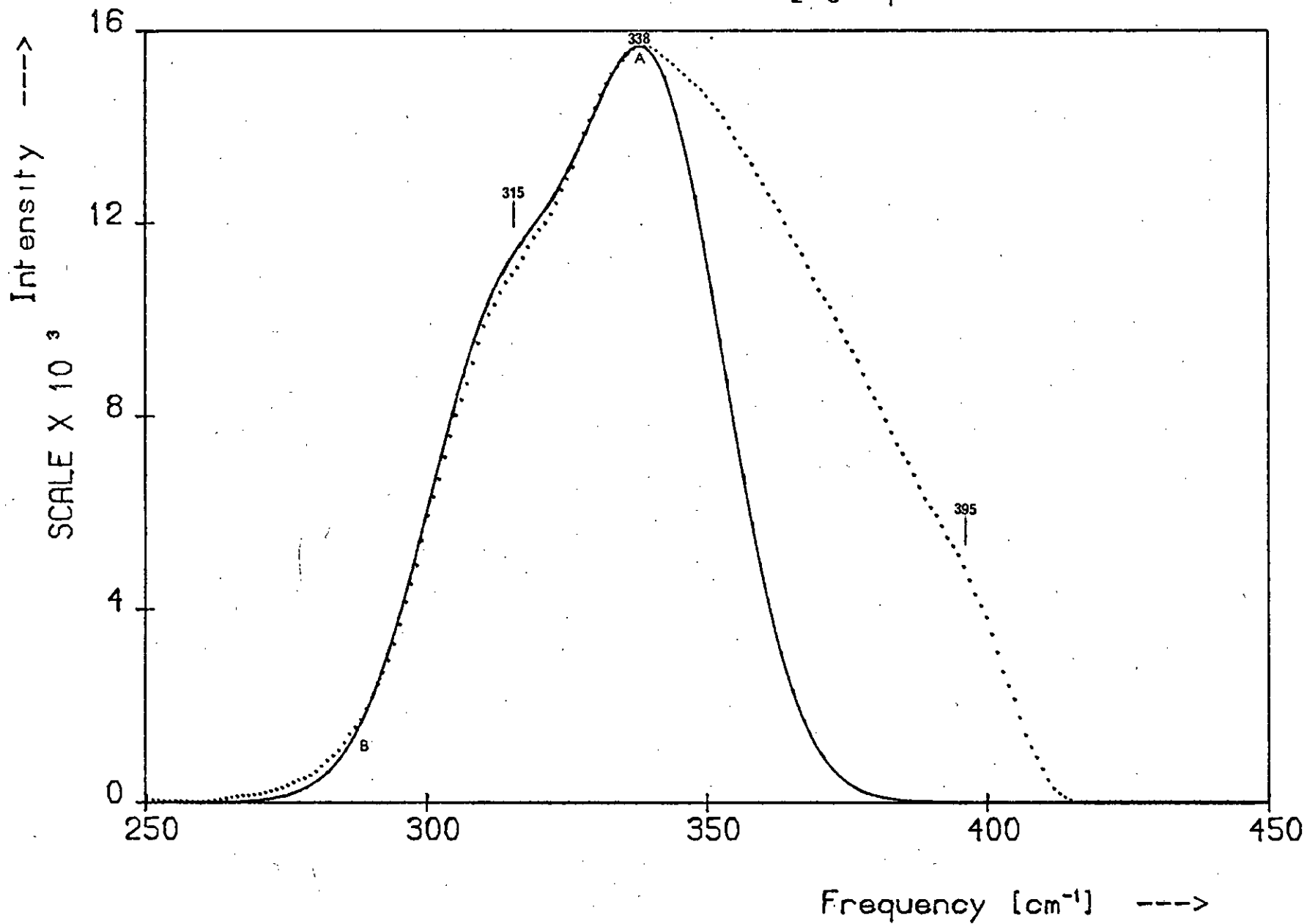
The Main Band of theaAs₂S₃ VH Spectrum
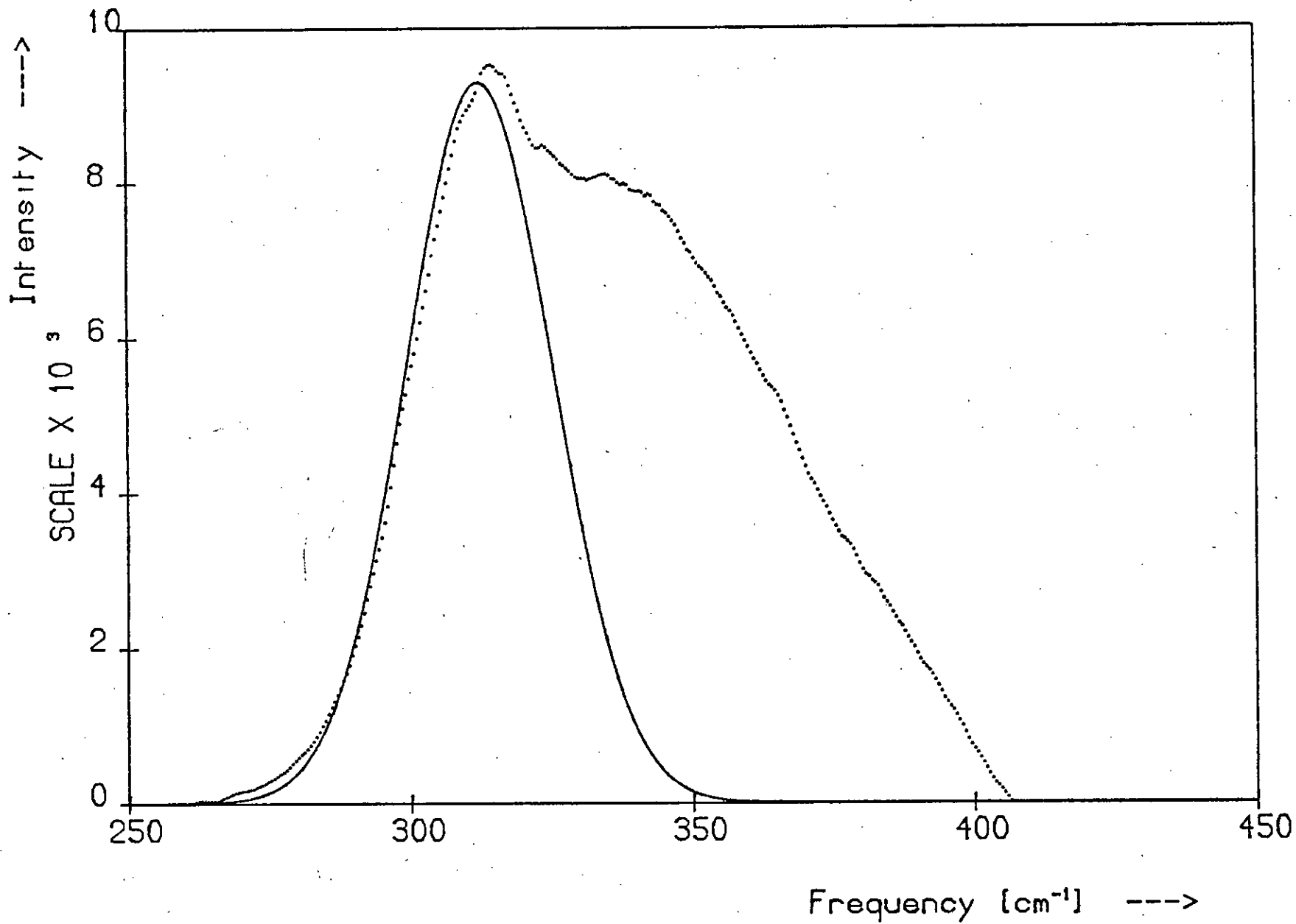
Difference Curve
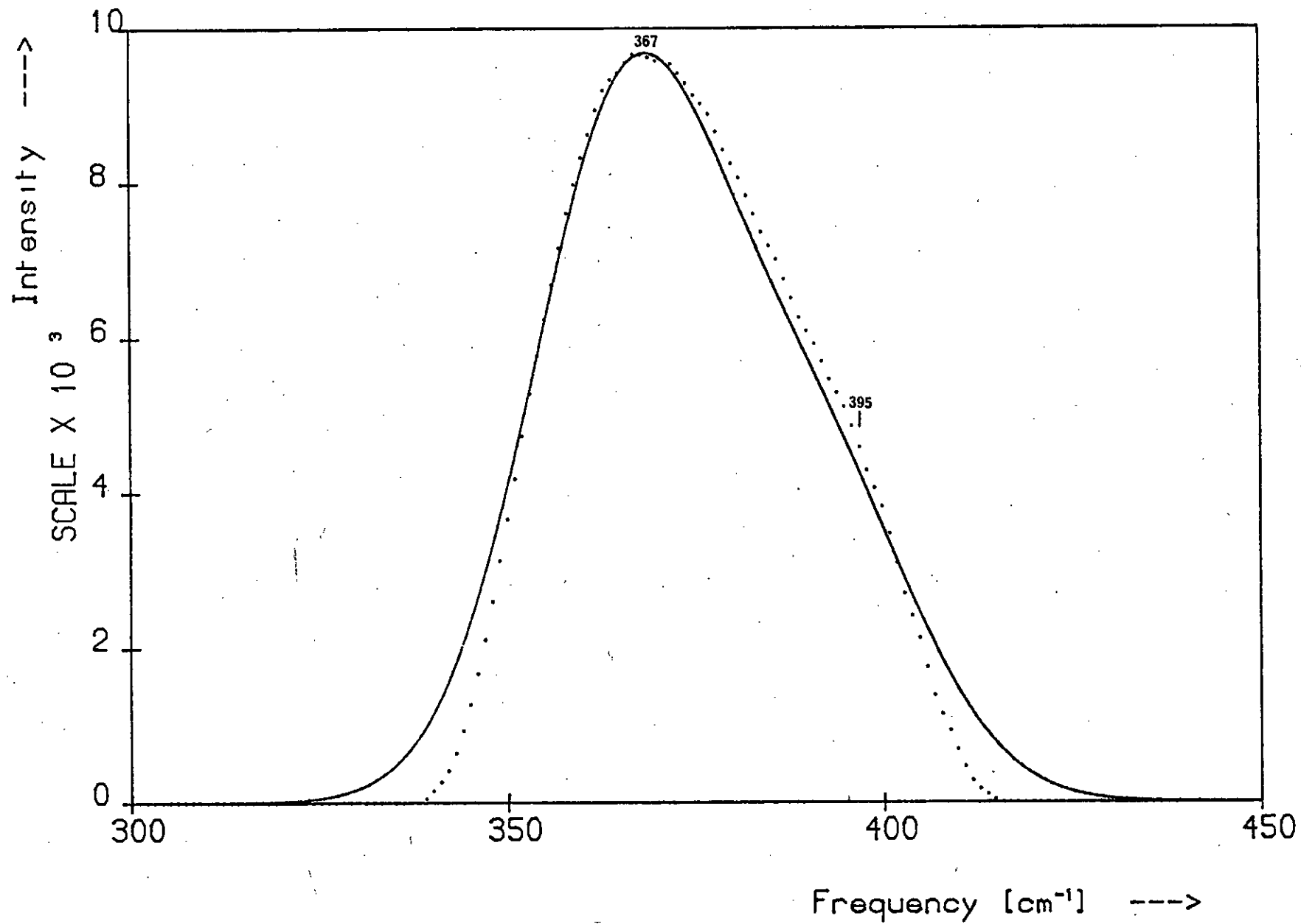
Deconvolution of the Main Band
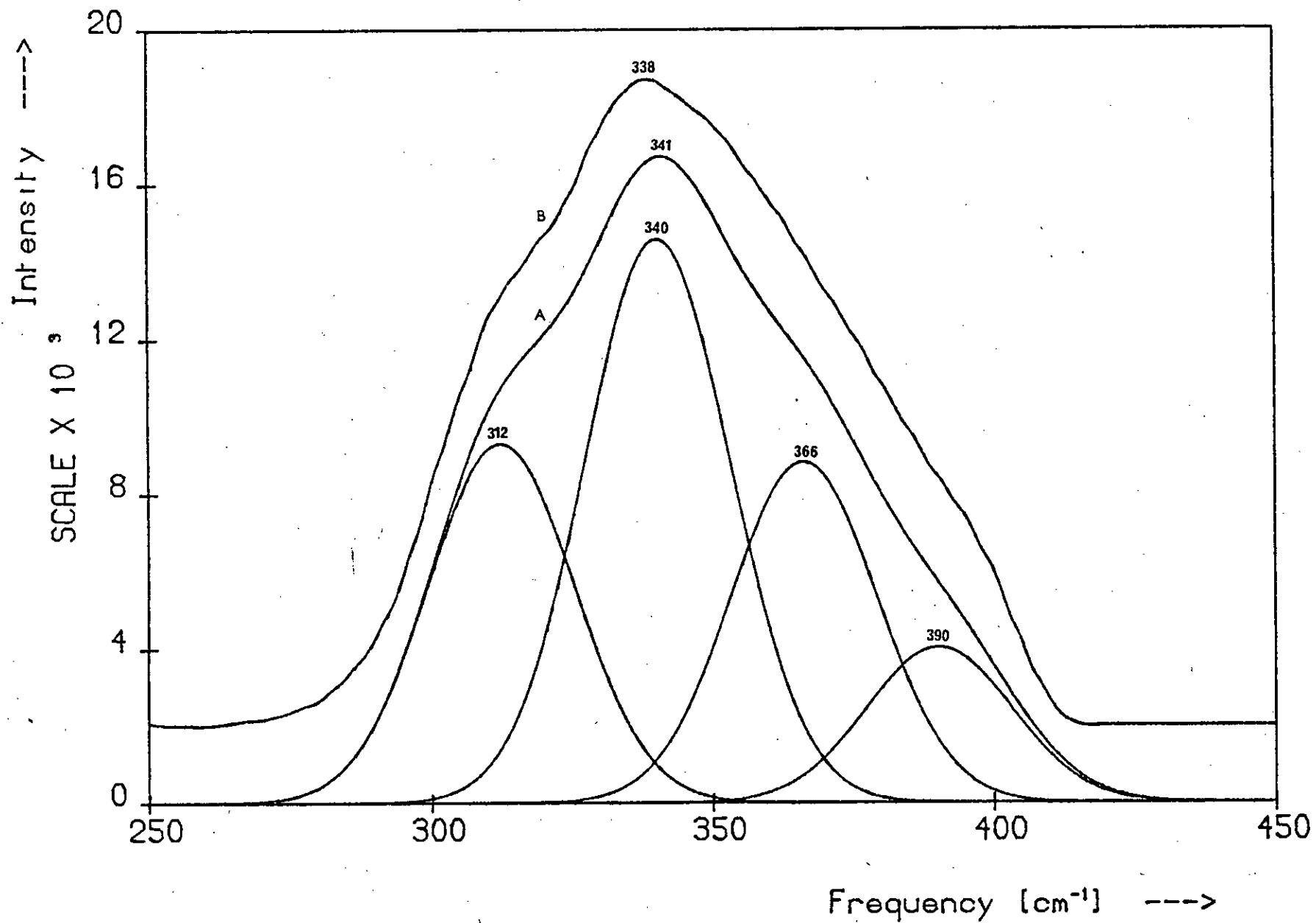
knee at 395 cm^{-1} is not reproduced exactly in the fitted curve. This is possibly because the assumption that each Gaussian in the main band has the same standard deviation is only approximately correct; two slightly narrower Gaussians would fit the data better. Both of these bands are thought to arise from vibrations of the As—S—As inter-pyramidal link (see Section 5.4.4.4) whereas the 315 and 338 cm^{-1} bands are attributable to vibrations of the pyramid itself, so the slight difference in line width for the two pairs of bands might be due to slight differences in the bond-angle and force-constant distributions for the two 'molecules'. The hidden 367 cm^{-1} line in the main band can be attributed to the ν_3 vibration of the As_2S 'molecule'. Although there is no sign of any feature at 367 cm^{-1} in the Raman spectrum, Lucovsky[49] reports an inflection at 375 cm^{-1} in the i.r. spectrum.

Figure 5.19 shows the four Gaussians derived in the analysis and the curve generated by adding them together (curve A). Displaced above is the observed main band (curve B). The four Gaussians clearly produce a reasonable facsimilie of the observed main band.

5.4.4 Structural interpretations of the vibrational spectrum

5.4.4.1 The density-of-states description

In Section 3.4.1 it was shown that Shuker and Gammon's theory[52,53] leads to the following approximation for the one-phonon density of states of an amorphous solid:

$$I^{red}_{\alpha\beta,\gamma\delta}(w,T) = \frac{wI_{\alpha\beta,\gamma\delta}(w,T)}{w_s^4[1 + n(w,T)]} \tag{5.1}$$

$I^{red}_{\alpha\beta,\gamma\delta}$ is referred to as the approximate density of states or the reduced Raman spectrum and if the coupling coefficients it contains are band independent then it is simply proportional to the actual density of states, $G(w)$. Figure 5.20 shows the reduced Raman spectrum of a-As_2S_3 obtained by multiplying the observed Stokes Raman intensity, $I_{\alpha\beta,\gamma\delta}(w,T)$, at each frequency

Figure 5.20

The reduced Raman spectrum of a-As_2S_3.

Figure 5.21

The reduced (full line) and unreduced (dotted line) spectra of a-As_2S_3.

Figure 5.22

The reduced spectra of a- and c-As_2S_3.   The crystal spectrum was obtained by applying Equation 5.1 to the Raman spectrum of a powdered sample of orpiment.
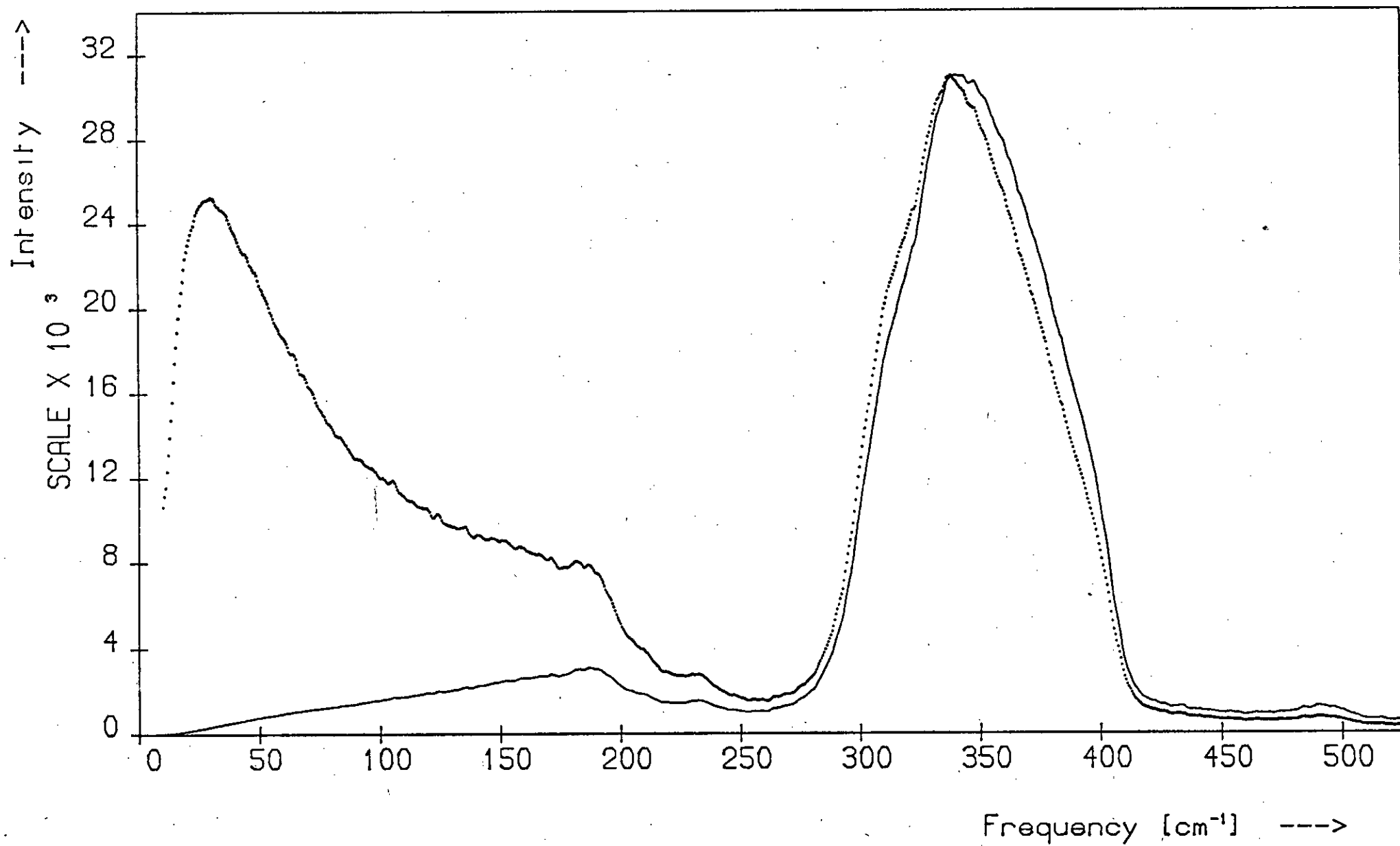

Figure 5.23

The reduced VH (dotted line) and VV (full line) spectra of a-As_2S_3.   The VH spectrum has been scaled to make its peak intensity at 316 cm^{-1} equal to that of the 342 cm^{-1} band of the VV spectrum.

The Reduced Raman Spectrum of a-$As_{40}S_{60}$
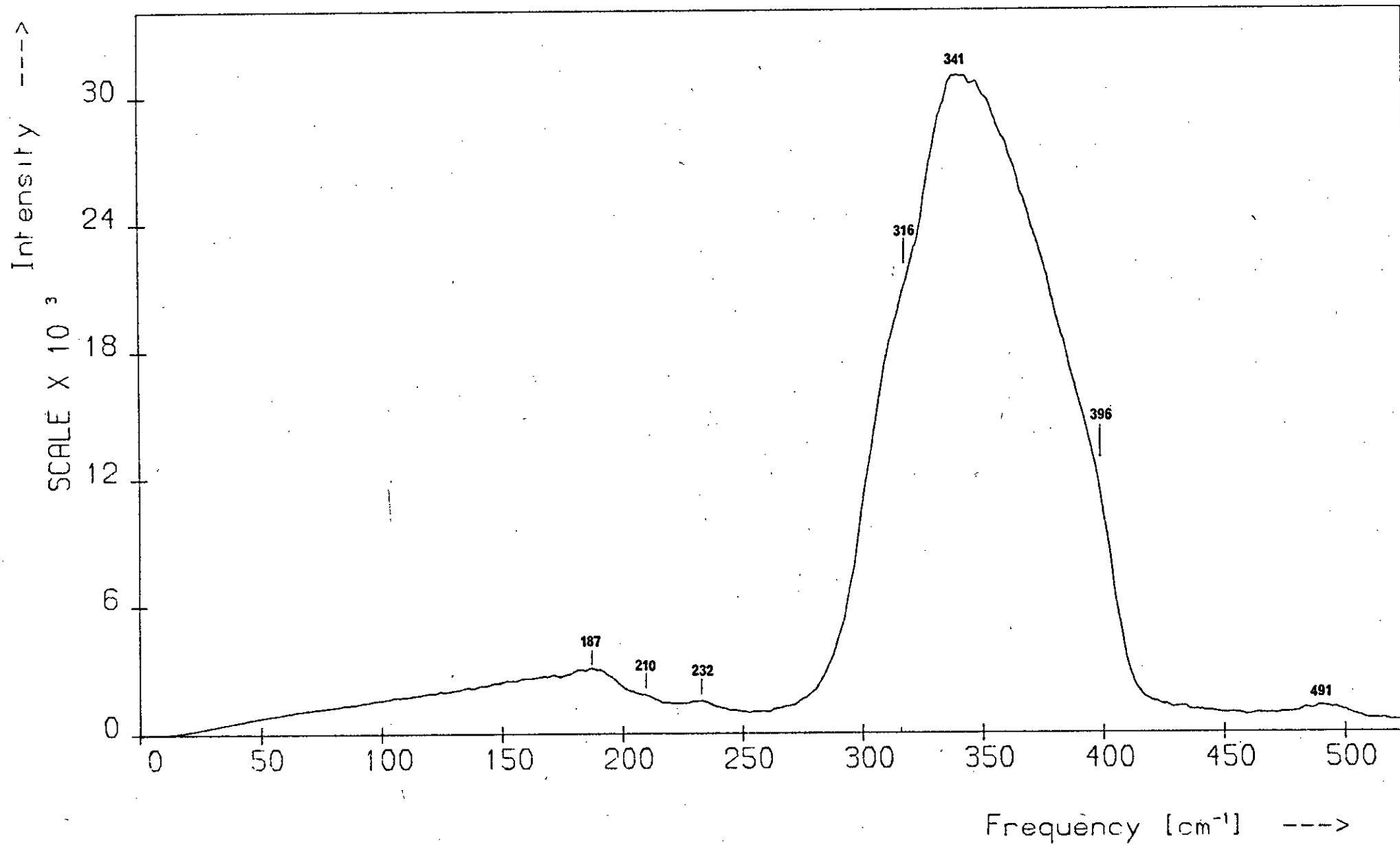
Raman and Reduced Spectra of a-As$_{40}$S$_{60}$

The Reduced Raman Spectra of c- and a-As$_{40}$S$_{60}$

Intensity --->

SCALE X 10^3

Frequency [cm^{-1}] --->
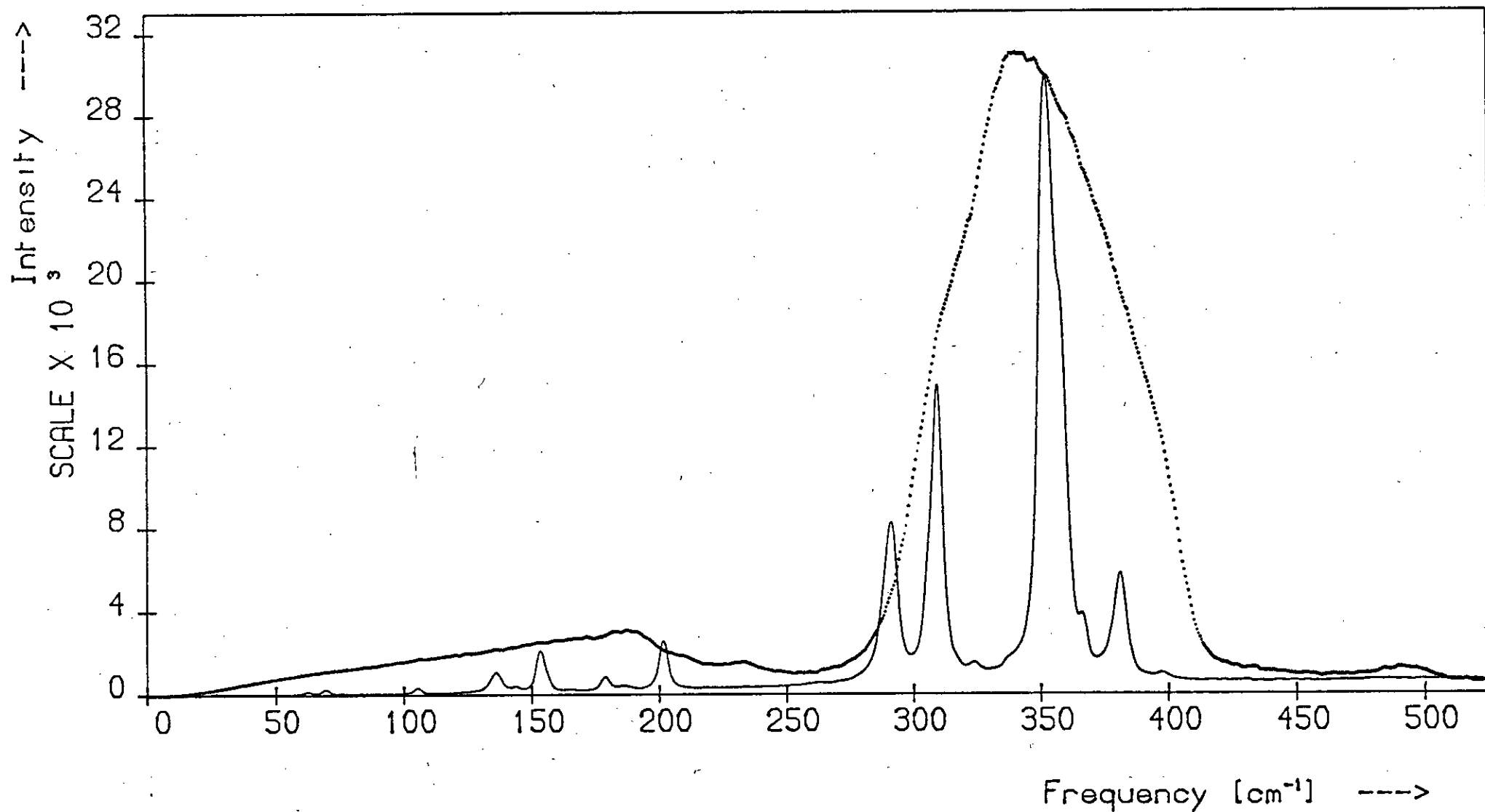
Reduced Polarised Spectra of a-As$_{40}$S$_{60}$
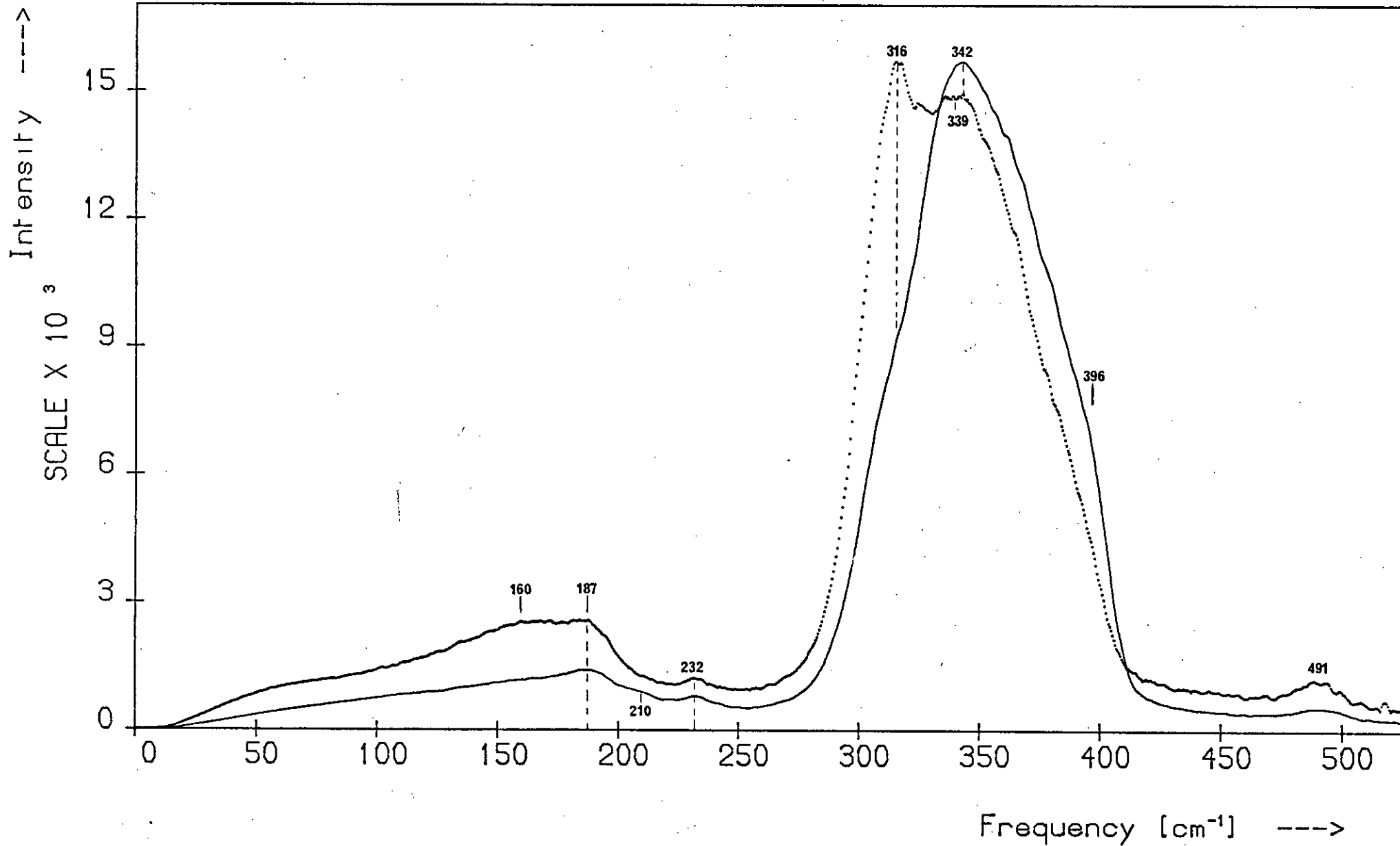
| OTHER STUDIES | | | | | | | | THIS STUDY | | | | | | | | | |
| RAMAN | | | | | I.R. | | | UNREDUCED | | | REDUCED | | | | | | |
Ref. 1/2	Ref. 3/4	Ref. 8	Ref. 39	Ref. 44	Ref. 47	Ref. 48	Ref. 49	VV	VH	PU	VV	VH	PU	DS	ALL	PS	ASSIGNMENT
	30	27						29	28	29					29	dp	boson peak
														106	106	p	ν_2 As_2S
140					164		163	130–175	160	130–175		160		160	160	dp	ν_4 AsS_3
189		180	185	170–190				185	185	185	187	187	187		185	p	ν_2 AsS_3
								208		208	210		210	210	208	p	ν_3 As_2S_2
230		232	230	235				231	231	231	232	232	232	231	231	p	As—As bond
	310/325		310		310	310	309	315	315	315	316	316	316	315	315	dp	ν_3 AsS_3
340	340/344	340	344	340			340	339	339	338	342	339	341	338	339	p	ν_1 AsS_3
							375								367*	?	ν_3 As_2S
							400	395		395	396		396	400	395	p	ν_1 As_2S
490			490	485		490		490	490	490	491	491	491	500	490	p	ν_1 As_2S_2

PU – polarisation unanalysed; PS – polarisation state; p – polarised; dp – depolarised; DS – depolarisation spectrum; VV and VH refer to the polarised spectra.
All frequencies in cm^{-1}.

* This value is deduced from the deconvolution analysis.

Notes: 1. Many of the other vibrational studies show structure near some of the frequencies observed in the present study but do not quote frequency values.
2. In the present study the uncertainty in the frequencies is not the same for each value shown in the table.

Table 5.1   The observed vibrational frequencies of a-As_2S_3.

shift w by the factor $w/w_s^4 \left[1 + n(w,T)\right]$. With the exception of the low-frequency band, all the features present in the Raman spectrum are present in the reduced spectrum, though at slightly increased frequencies. The two spectra are compared in Figure 5.21.

Kobliska and Solin have pointed out that the coupling coefficients $c_b^{\alpha\beta,\gamma\delta}$ of Equation 3.12 are not band independent for a-As$_2$S$_3$ because in the VV and VH spectra (Figure 5.12) the ratio of the intensities of the low- and high-frequency bands is quite different. Thus the reduced spectrum is not proportional to $G(w)$. Moreover, it is not a good approximation to $G(w)$ because the density of states derived from the Raman spectrum should be identical with that deduced from the i.r. spectrum but for a-As$_2$S$_3$ the two reduced spectra are complementary[3,35,49]. Although the Shuker-Gammon theory was developed to account for the Raman spectra of molecular glasses such as a-As$_2$S$_3$ it is least successful for these materials.

It is nevertheless useful to reduce the data using Equation 5.1 since this corrects the observed Raman spectrum for its dependence on temperature and exciting frequency. The low-frequency peak at 29 cm^{-1} is not due to a vibrational mode but to the thermal population of the lower states and is highly temperature dependent[52,53]. The reduced spectrum resembles the low-temperature Raman spectrum of the glass[3,4], in which the 29 cm^{-1} peak is absent. It has been shown[3] that the reduced spectrum of a-As$_2$S$_3$ is temperature independent over the range $20 - 450^\circ$ K, which is consistent with its being interpreted as a phonon density of states, since $G(w)$ is expected to change very little with temperature over the above range. It was observed[4,39] that the half-width of the 338 cm^{-1} band in the reduced spectrum was temperature independent and a constant half-width is a characteristic of $G(w)$. The inclusion of the w_s^4 term in Equation 5.1 accounts for the well-known fourth-power-law dependence of scattered intensity for an induced-dipole scatterer. For 6328 Å excitation the w_s^4 term for a 5 cm^{-1} Stokes shift is 9% larger than that for a 380 cm^{-1} Stokes shift[3].

Although the evidence is mainly not compatible with interpreting the reduced spectrum as a good approximation to G(w) the reduced spectrum is, however, very similar to the phonon density of states derived from the crystal spectrum. Figure 5.22 compares the reduced spectrum obtained for a powdered sample of orpiment with that for the glass; the two spectra are normalised to the peak intensity of the 353 cm^{-1} orpiment band. The glass spectrum is approximately the envelope of the crystal lines, which implies that the phonon dispersion curves of c-As_2S_3 are relatively flat[4]. If the force-constant and bond-angle distributions in a-As_2S_3 are Gaussian then the spectrum obtained by replacing each peak in the reduced spectrum of the crystal with a Gaussian-broadened line and summing the overlapping amplitudes should be similar to G(w)[3]. Figure 5.24 compares a spectrum generated by the above process with the reduced spectrum of the glass; the two spectra are very similar in shape and resemble the density of states calculated by Bermudez[54].

The reduced VH and VV spectra exhibit the same properties as the reduced unanalysed spectrum[3]; they are shown in Figure 5.23.

As the reduction process tends to obscure spectral features below ~150 cm^{-1}, the corresponding unreduced spectra are also presented in this study. In addition, since the process introduces a small blue shift in the spectrum, frequencies quoted will refer to the unreduced spectrum unless otherwise stated.

5.4.4.2 The random network model

It is believed by many workers[55 — 58] that the layer structure of crystalline As_2S_3 and As_2Se_3 is retained to some extent in the corresponding glasses, so a reasonable structural model for vitreous As_2S_3 and As_2Se_3 might be based on a single disordered layer. With the object of estimating force constants and assigning the observed vibrational frequencies for the two glasses, Bermudez[54] has considered such a model, consisting of a

computer-generated 390-atom c.r.n. Although the layers in c-As$_2$S$_3$ and c-As$_2$Se$_3$ are really three-dimensional, the network studied by Bermudez is strictly two-dimensional.

The force constants obtained from the model are reasonable and the calculated spectra are generally in agreement with the experimental data, though in the case of a-As$_2$S$_3$ Bermudez ignores the structure at 140, 189, 230 and 490 cm^{-1} on the strength of Kobliska and Solin's attribution of these features to plasma lines. The model breaks down, however, when the polarisation properties of the Raman spectrum are considered, for it predicts a rise in the depolarisation spectrum of a-As$_2$S$_3$ between 310 and 340 cm^{-1} whereas the measured spectrum decreases over this range[3,40 — 42] (see Figure 5.14). Thus the planar-random-network model is of limited use in explaining the vibrational properties of these glasses.

5.4.4.3 The layer model

Taylor et al.[51] have proposed a model for the vibrational spectra of a-As$_2$S$_3$ and a-As$_2$Se$_3$ which is based on the layer structure of the corresponding crystals. They generate approximate i.r. absorption spectra for these materials by broadening an average of the three principal-axis contributions to the corresponding crystalline absorption spectra using a single Gaussian convolution function. The resulting spectra have the same general features as the observed absorption spectra and these authors take this as evidence that a layer model is appropriate.

Zallen et al.[5,6] have shown that the Raman spectra of c-As$_2$S$_3$ and c-As$_2$Se$_3$ are related via an exact scaling relation: the internal bands for these crystals scale by a factor of 0.71 while the external bands (which correspond to interlayer vibrations in layer crystals — see Section 5.2.1) scale by a factor of 0.81. It will be shown in Section 6.4.5 that the Raman spectra of the glasses are also related by the same scale factors. The two lowest-frequency features in the spectra — the intense

peak < 30 cm^{-1} in the Raman spectra and the first dip in the depolar-
isation spectra — scale by a factor of ~ 0.81 which suggests that the
layers are possibly retained in the glasses.   As the layer modes in
c-As$_2$S$_3$ and c-As$_2$Se$_3$ lie below 100 and 70 cm^{-1} respectively, the presence
of the dips at 106 and 86 cm^{-1} in the corresponding glass spectra
indicates that the compressional rigid-layer mode in the glasses may be
more heavily intermixed with the low-lying bond-bending modes than in
the crystal case, possibly as a result of cross-linking of the layers.
This intermixing means that associating these dips in $\rho(w)$ with the
layers does not affect the assignment of these frequencies to the bond-
bending mode of the As$_2$X (X = S, Se) link in the molecular model (see
Sections 5.4.5 and 6.4.6).

Such a model is limited in that it is only applicable to amorphous
materials which have a corresponding crystal with a layer structure.
For example, it is inapplicable to the glass of composition As$_{39}$S$_{61}$,
which may contain layers but has no corresponding crystal, and also to
a-Se, which has a corresponding crystal but one which is not layered.
Although the general features of the observed absorption spectrum of
a-As$_2$S$_3$ are reproduced in the generated spectrum, quantitative agree-
ment is poor.   The Raman equivalent of the approximate spectrum of
Taylor et al. is shown in Figure 5.24.   This spectrum (A) was obtained
by broadening the reduced polarisation-unanalysed Raman spectrum of
polycrystalline orpiment using a Gaussian convolution function.   The
spectrum was computer-generated by Dr. M.J.Sik and is shown above the
reduced Raman spectrum of vitreous As$_2$S$_3$ (spectrum B).   As in the i.r.
case, most of the features of the measured Raman spectrum are present in
the model spectrum;   the broad low-frequency peak, the shoulder on the
main band and the high-frequency peak are all reproduced in the generated
spectrum.   In the model spectrum, however, the peak occurs at ~ 355 cm^{-1}
and the shoulder on the main band is far more pronounced and is shifted

Figure 5.24

Reduced Raman spectra of As_2S_3: spectrum A has been generated by broadening the reduced Raman spectrum of polycrystalline orpiment using a Gaussian convolution function, while spectrum B is the measured reduced spectrum of a-As_2S_3. (Courtesy of Dr. M.J.Sik).
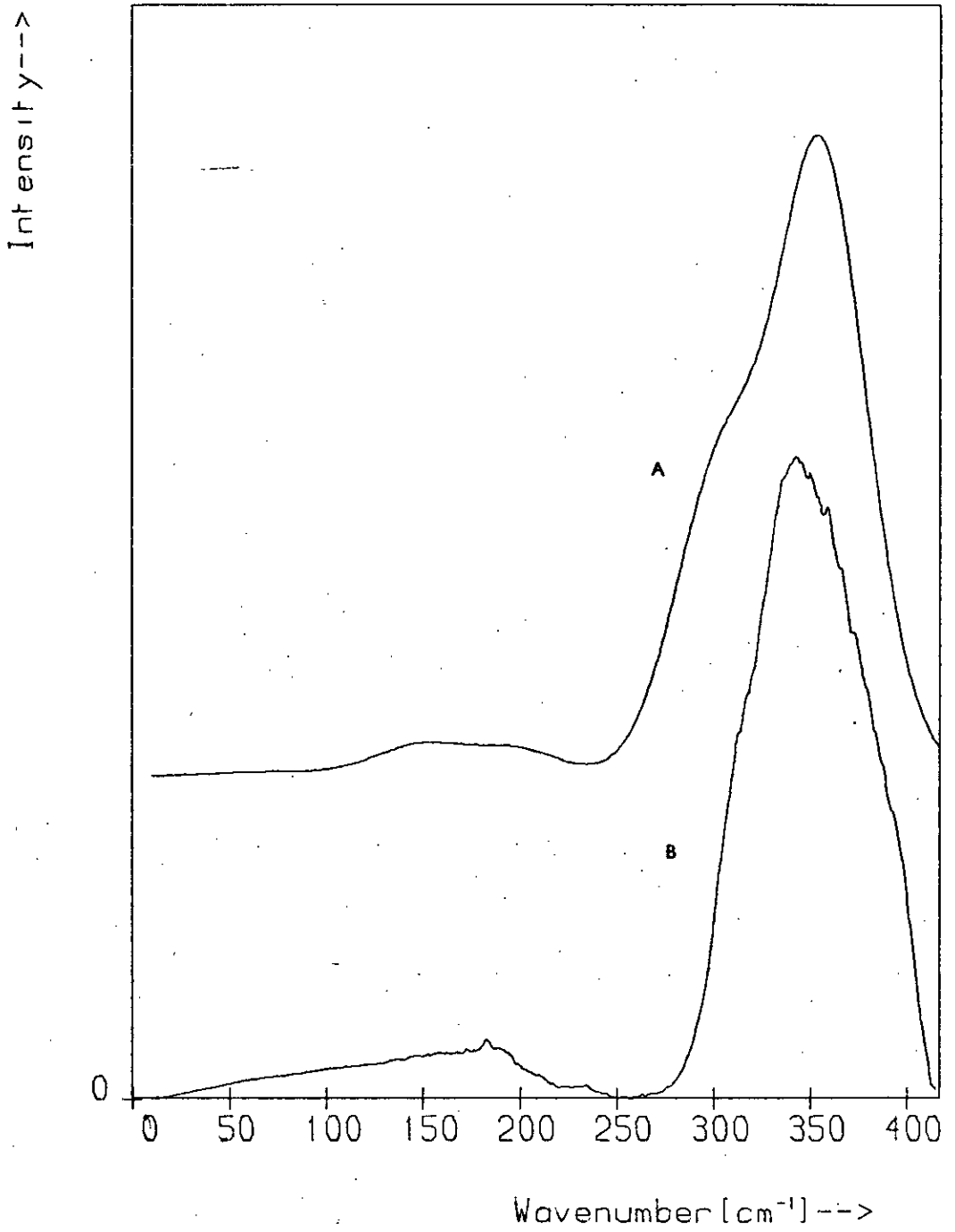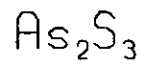
As_2S_3

to ~300 cm^{-1}. The shoulder in the model spectrum arises from the strong orpiment bands at 292 cm^{-1} (which lies outside the main band of a-As$_2$S$_3$ — see Figure 5.22) and 310 cm^{-1}. In addition, the broadening process does not give rise to a knee at ~395 cm^{-1} on the main Raman band, though the corresponding feature in the i.r. spectrum is reproduced by the model. However, the small feature at 231 cm^{-1} in both observed spectra does not appear in either of the model spectra. It will be seen in Section 5.4.5 that this feature can be attributed to As—As bonds in the As—S network. Such bonds are believed to be a genuine feature of the a-As$_2$S$_3$ structure and are not due to deviations in the stoichiometry of the samples used. c-As$_2$S$_3$ contains no As—As bonds and as there is no line near 231 cm^{-1} in its spectra the broadening process fails to reproduce this feature. This illustrates one of the deficiencies of such a quasi-crystalline model, that is its inability to account for compositional disorder in the amorphous counterpart of the crystal. Although the region beyond 450 cm^{-1} is not shown in Figure 5.24 or in the data of Taylor et al., the same considerations apply to the 490 cm^{-1} peak present in the measured i.r. and Raman spectra of the glass. This peak is attributable to S—S bonds in the As—S network. Such bonds are not part of the intrinsic c-As$_2$S$_3$ structure but are thought to be a genuine feature of the a-As$_2$S$_3$ structure (see Section 5.4.5). The orpiment spectra have no lines near 490 cm^{-1} and so the model cannot account for this band in the glass.

The depolarisation spectrum of a-As$_2$S$_3$ obtained by Kobliska and Solin[3] has a constant amplitude of ~$\frac{1}{2}$ between 100 and 300 cm^{-1}. The basic structural unit of c- and a-As$_2$S$_3$ is an AsS$_3$ pyramid and Taylor et al. state that this feature of the depolarisation spectrum would be expected if the inter- and intra-pyramidal coupling could not be separated, whereas a depolarisation ratio of ~$\frac{3}{4}$ should be observed if the molecular model were valid. However, the failure of the depolarisation

spectrum to achieve the theoretical maximum amplitude of $\frac{3}{4}$ can be accounted for in the molecular model by intermolecular coupling[3].

Also, since Kobliska and Solin's investigation the a-As_2S_3 depolarisation spectrum has been recorded by other workers[40 − 42], including the present author (see Figure 5.14), and has been shown to exhibit considerable structure below 300 cm^{-1}; this is more readily accounted for by the molecular model.

Taylor et al.[59] also suggest that the layers in As_2X_3 type glasses disintegrate at a characteristic temperature, T_s, which is approximately the temperature at which $10^3 \leqslant \eta \leqslant 10^4$ P where η is the viscosity. Solin and Papatheodorou[60] show that in the case of a-As_2O_3, which is believed to be structurally similar to a-As_2S_3, neither the Raman nor the depolarisation spectrum changes significantly in shape with temperature, and the spectra of the liquid at 920° K are essentially the same as those of the glass at 300° K. Yet T_s for As_2O_3 lies in the range $625 < T_s < 725$ °K [60]. These authors point out that similar behaviour has been reported for amorphous and liquid As_2S_3 — all the prominent Raman bands of a-As_2S_3 persist up to 1040° K. T_s for a-As_2S_3 is in the range $600 < T_s < 700$ °K [61]. There seems to be no evidence, therefore, of layer-breakdown in disordered As_2S_3.

The vibrational evidence for the existence of layer regions in these glasses is thus not conclusive, and even if they are present the model is of limited use.

5.4.4.4   The molecular model

The vibrational spectra of a-As_2S_3 and a-As_2Se_3 have been analysed in terms of a molecular model by Lucovsky and Martin[62], who advocate this approach for the chalcogenide glasses in general, and Austin and Garbett[63], who use it in their discussion of the i.r. spectra of c- and a-As_2Se_3. The sharpness of the spectral features and the complementary nature of the i.r.

and Raman spectra for a-As_2S_3 suggest that the selection rules governing i.r. and Raman activity still operate in the glass and the disorder-induced breakdown of these rules is incomplete. This behaviour would arise if the glass were composed of weakly coupled identical structural units. Lucovsky and Martin have chosen as the molecular unit for a-As_2S_3 an AsS_3 pyramid, which is the basic structural unit of the crystal, and using this have obtained a vibrational spectrum in good agreement with experiment. It is found that the dominant bands in the i.r. and Raman spectra at ∼310 and 340 cm^{-1} respectively do not arise from the same vibration but correspond to different vibrational modes of the As_3S pyramid.

The Lucovsky-Martin model is based on the local atomic arrangement shown in Figure 5.25. The glass is regarded as a network of randomly positioned AsS_3 pyramids joined to one another via shared S atoms; three of these pyramids are shown in Figure 5.25. When calculating the normal modes of a cluster of AsS_3 pyramids, which is a closer approximation to the real structure than a single pyramid, it is necessary to consider the interaction between the pyramids since they are coupled. This interaction is accounted for by considering the bent As—S—As chains which connect the pyramid molecules. Provided the coupling at the bridging S atoms is sufficiently weak the intramolecular (AsS_3) and intermolecular (As_2S) modes can be treated independently.

For the symmetric pyramidal XY_3 molecule, which belongs to the point group C_{3v}, there are two totally symmetric vibrations (species A_1) and two doubly degenerate vibrations (species E)[64]. These are shown in Figure 5.26. The molecule remains a symmetric pyramid throughout the former oscillations but it does not in the latter. General valence force field formulae for the four vibrational frequencies, all of which are both i.r. and Raman active, have been determined by Herzberg[64] and are given in Appendix I. Using force constants scaled from the existing molecule $AsCl_3$, which has a similar structure and mass ratio to the AsS_3 'molecule',
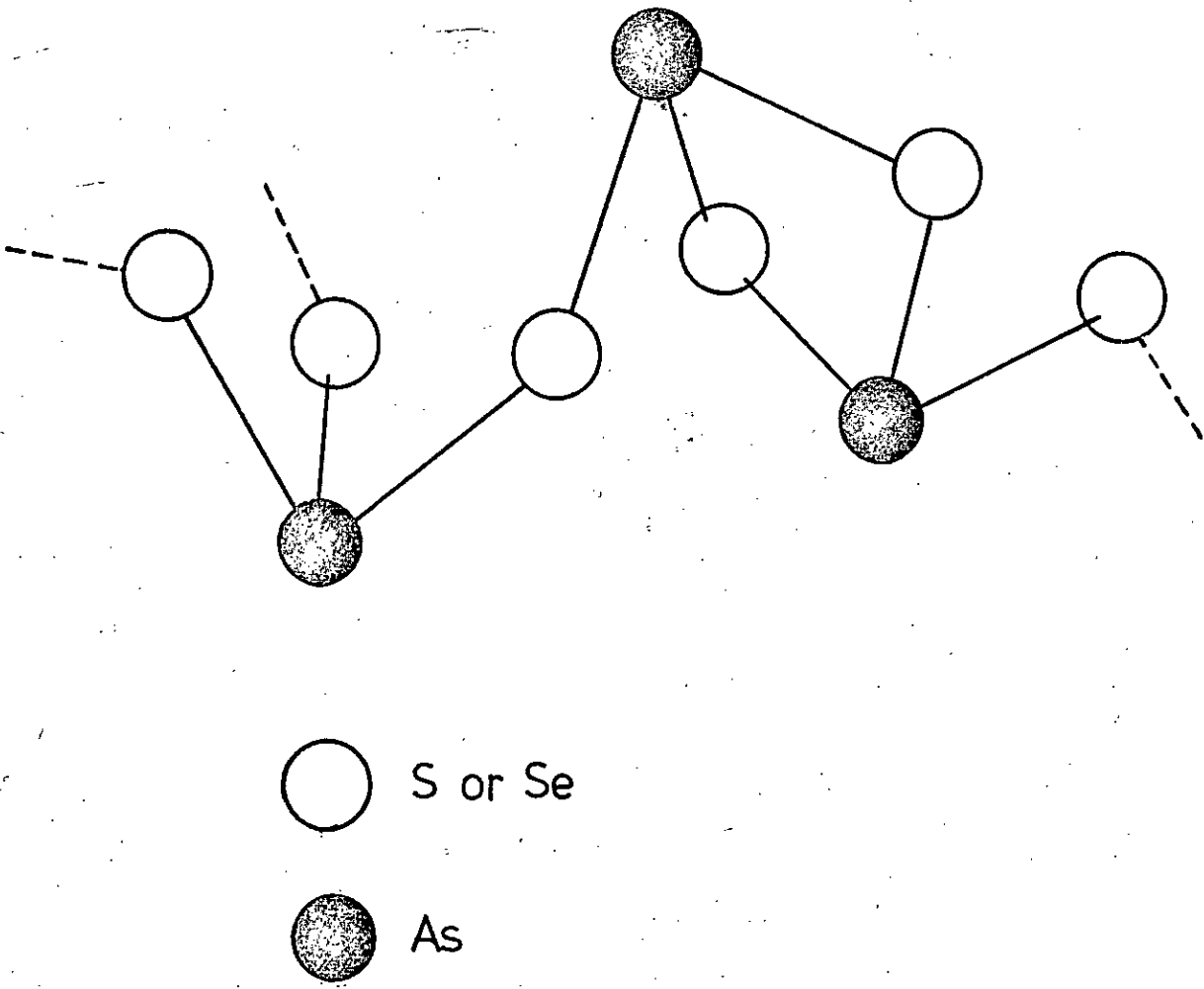
Figure 5.25

A schematic representation of the molecular structure of a-As_2S/Se_3; three pyramid 'molecules' are depicted. (After Reference 62.)

and geometrical parameters based on the two shallow, asymmetric pyramids of the orpiment structure, Lucovsky and Martin have obtained for the frequencies of the symmetric AsS_3 molecule the values 133, 162, 310 and 344 cm^{-1} for the ν_4, ν_2, ν_3 and ν_1 modes respectively. These are in reasonable agreement with the observed values.

As the dominant i.r. and Raman modes for the XY_3 molecule are the ν_3 and ν_1 vibrations respectively, the model accounts for the complementary nature of the two types of spectra. Also, since the ν_1 mode should generate a polarised Raman band and dominate the VV spectrum while the ν_3 mode should generate a depolarised line and dominate the VH spectrum (neglecting the low-frequency thermal peak), the model explains the polarised spectra and the dip in the depolarisation spectrum between ~310 and 344 cm^{-1} [3]. The failure of the depolarisation spectrum to attain the theoretical maximum amplitude of $\frac{3}{4}$ for the antisymmetric vibrations is attributed to intermolecular coupling. The coupled modes have admixtures of symmetric and antisymmetric eigenvectors of the AsS_3 unit.

For the non-linear, symmetric X_2Y molecule, which belongs to the point group C_{2v}, there are two symmetric vibrations (species A_1) and one antisymmetric vibration (species B_1). These are shown in Figure 5.27. General valence force field formulae for the three vibrational frequencies, all of which are both i.r. and Raman active, have been determined by Herzberg and are given in Appendix I. When applying these formulae to calculate the frequencies of the bent As—S—As chain molecule, Lucovsky and Martin use the As—S bond-stretching force constant obtained for the AsS_3 molecule and, as the coupling at the bridging sulphur is assumed to be weak, they take the bond-bending force constant to be 1/100th of this (as is the case in SiO_2 [65]). The As—S—As angle is taken to be 150° [3]. The frequencies they obtain for the As_2S 'molecule' are 55, 218 and 438 cm^{-1} for the ν_2, ν_1, and ν_3 modes respectively. No features have been observed at these frequencies in the vibrational spectra but a similar

Figure 5.26

The non-planar symmetric XY_3 molecule and its normal modes of vibration.

Figure 5.27

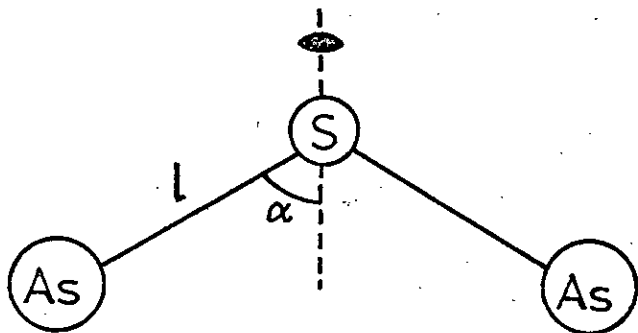The non-linear symmetric X_2Y molecule and its normal modes of vibration.

Point group : C_{3v}

$X = As = $ ●
$Y = S = $ ○
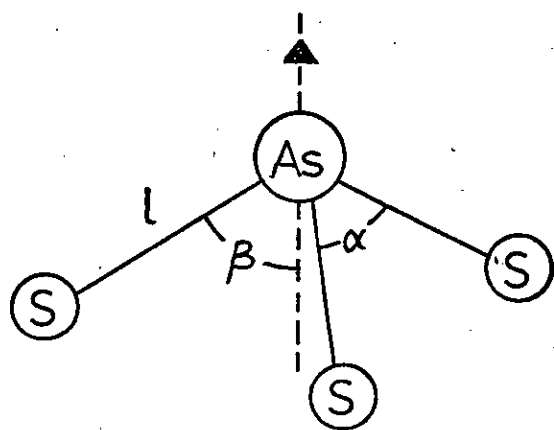
	v_1	v_2	v_3	v_4
Raman active	yes	yes	yes	yes
i.r. active	yes	yes	yes	yes
Species	A_1	A_1	E	E
Description	Symmetric stretch	Symmetric bend	Antisymmetric stretch	Antisymmetric bend

The Non-Linear Symmetric X_2Y Molecule

Point group : C_{2v}

$X = As = $ ⊛

$Y = S = $ ○

	v_1	v_2	v_3
Raman active	yes	yes	yes
i.r. active	yes	yes	yes
Species	A_1	A_1	B_1
Description	Symmetric stretch	Symmetric bend	Antisymmetric stretch

calculation for the As_2Se 'molecule' of a-As_2Se_3 gives good agreement with experiment.

In the molecular model the continuous nature of the Raman spectrum of a-As_2S_3 arises from the spread in the values of the bond angles, lengths and force constants. Rubinstein and Taylor[66] have set an upper limit of $\pm2°$ on the distribution in pyramidal apex angles in vitreous As_2S_3. Transferring this limit to the symmetric AsS_3 'molecule', Kobliska and Solin[3] have shown that a $\pm2°$ variation in the S—As—S angle about a nominal value of $97.2°$ produces a $\pm2 - 4$ cm^{-1} spread in the individual frequencies of the AsS_3 'molecule' and so cannot account for the continuous spectrum.* However, they find that a $\pm9\%$ spread in the bond-stretching force constant produces a considerable broadening and conclude that the continuous nature arises from the cumulative effects of distributions in both apex angles and force constants. They argue that in view of the force constant distribution that would arise from the varying bond lengths in orpiment a 9% spread in force constants in the glass is quite feasible.

The molecular nature of the glass spectra is consistent with the well-established fact[55 − 58] that the local atomic arrangement in a-As_2S_3 is similar to that in orpiment. Since crystalline nearest-neighbour distances are mainly preserved in the glass, the principal bond-stretching frequencies of the group will also be retained, so the model also accounts for the similarity between the reduced spectra of crystalline and vitreous As_2S_3 (see Figure 5.22). Since both crystal and glass are built up from similar pyramidal 'molecules' it is not surprising that the main bands of orpiment fall near the frequencies determined from the molecular model. In principle, the molecular model could be used to calculate the vibrational spectrum of c-As_2S_3 by considering a larger structural unit consisting of

---

* A more recent study by Taylor and Rubinstein[66] sets an even smaller upper limit to the S—As—S bond-angle distribution in a-As_2S_3, viz $\pm1°$.

several pyramids arranged as they are in the crystal.

In conclusion, the model gives better agreement with experiment than the planar-random-network model and is not as limited as the layer model since it can be extended to the non-stoichiometric glasses[46]. However, with the simple AsS_3 pyramid as the molecular unit the model cannot discriminate between the proposed alternative structures for a-As_2S_3 since these are all composed of AsS_3 pyramids. There are also a number of minor failings in the model as it stands at present and these are discussed in Section 5.4.5.

5.4.4.5 The composite model

Finkman et al.[39] have proposed a composite model for the structure of vitreous and liquid As_2S_3 incorporating features of both the molecular model and the layer model. They suggest that the disordered phases contain layer-like regions in which the AsS_3 pyramid units of the molecular model are each joined to three neighbours, as they are in the crystal, and regions where the pyramids are joined via double As—S—As bridges, i.e. regions containing this structural feature: $-As\!\!\begin{smallmatrix}S\\<\\S\end{smallmatrix}\!\!>As-$. This model is more fully described in Section 5.7 where it is shown how Finkman et al. use it to account for the temperature dependence of the reduced Raman spectra of these materials. The doubly bridged pyramids are not present in the crystal layer and when the $-As\!\!\begin{smallmatrix}S\\<\\S\end{smallmatrix}\!\!>As-$ units link to one another they form chain-like structures.

Claudetite, one of the forms of c-As_2O_3, is a layer crystal and is in fact isomorphic with c-As_2S_3. Solin and Papatheodorou[60,67] have studied the Raman spectrum of a-As_2O_3, which may be structurally similar to a-As_2S_3, and show that only the composite model satisfactorily accounts for all the spectral features. However, these authors point out that the molecular and layer models are more similar than dissimilar, and the differences between them are differences of degree rather than kind, for

the layers are made up from the pyramid 'molecules'[60]. Both the layer and composite models can be regarded as special cases of the molecular model.

5.4.5 Discussion

When Lucovsky and Martin proposed their model only one unequivocal vibrational feature, the peak at ~ 340 cm^{-1}, had been found in the Raman spectrum of a-As$_2$S$_3$ and their analysis was based on the vibrational frequencies obtained from i.r. experiments. Since then, this and other Raman studies have authenticated the additional frequencies observed by Ward and have reported new features. It will be shown in this section that all the observed vibrational frequencies can be accounted for by the molecular model.

In the model the frequencies of the AsS$_3$ pyramid are calculated from Equations A.1 − A.4 (see Appendix I) using the average values of ℓ and β for c-As$_2$S$_3$ and force constants scaled from those of the known molecule AsCl$_3$. The scaling relation for the force constants can be derived from either Equation A.2 or Equation A.4. In the case of Equation A.2 it is seen that for two pyramidal molecules $X^I Y^I_3$ and $X^{II} Y^{II}_3$, with the same geometry, the frequencies ν^I_1 and ν^I_2 will scale with ν^{II}_1 and ν^{II}_2 if the force constants scale, i.e.

$$k^{II}_j = ck^I_j \ (j = 1, 1', \delta, \delta') \Rightarrow \nu^{II}_i = n \nu^I_i \ (i = 1, 2)$$

where n and c are the frequency and force constant scale factors respectively. The latter is given by

$$c = \frac{m^{II}_y (1 + 3m^I_y/m^I_x)^{\frac{1}{2}}}{m^I_y (1 + 3m^{II}_y/m^{II}_x)^{\frac{1}{2}}} \, n^2 \tag{5.2}$$

If, as well as being isostructural, the two molecules have the same mass ratio m_y/m_x then Equation 5.2 reduces to

$$c = \frac{m^{II}_y}{m^I_y} \, n^2 \tag{5.3}$$

and from Equation A.4 it will be seen that in this case we also have $\nu_i^{II} = n \nu_i^{I}$ (i = 3, 4). For the AsS_3 'molecule' Lucovsky and Martin take ν_1, the symmetric-stretch frequency, to be the frequency of the principal Raman band in $a-As_2S_3$ and obtain n by comparing this measured frequency with the observed value of ν_1 for $AsCl_3$. Taking $AsCl_3$ and AsS_3 as molecules I and II respectively, the actual values used are $\nu_1^{I} = 410$ cm^{-1} [64], $\nu_1^{II} = 344$ cm^{-1} [2,4] and n = 344/410 = 0.839. Inserting n and the masses in Equation 5.3 one obtains a value for c of 0.655, which can now be used in the relations $k_j^{II} = ck_j^{I}$ to generate a set of force constants k_j^{II} for the AsS_3 'molecule' from the known force constants k_j^{I} of the $AsCl_3$ molecule[64]. The values obtained for k_1^{II}, k_δ^{II}, $k_{1'}^{II}$ and $k_{\delta'}^{II}$ are, in units of md/Å, 1.33, 0.15, 0.125 and 0.013 respectively and using these, Equations A.1 — A.4 can be solved for the frequencies of the AsS_3 'molecule'. The resulting frequencies are given by Lucovsky and Martin and are in fair agreement with the observed frequencies.

In the present study the calculation for deriving the set of force constants k_j^{II} and that for determining the frequencies of the XY_3 molecule were set up in programs and carried out by computer. This made it possible not only to repeat Lucovsky and Martin's calculations but also to examine with ease the dependence of the k_j^{II} and ν_i^{II} on the various parameters. The program for computing the frequencies ν_i of the XY_3 molecule was checked with data from Herzberg[64] on existing XY_3 molecules.

Using the frequencies and force constants of the known molecule $AsBr_3$[68], Lucovsky and Martin perform an identical calculation for the $AsSe_3$ pyramid and again obtain frequencies in good agreement with those observed in the corresponding glass. However, when the results of the model for both $a-As_2S_3$ and $a-As_2Se_3$ are compared they are not entirely satisfactory in view of the work of Zallen et al.[5,6] on the crystal forms. Zallen and co-workers have shown that the Raman frequencies, ν_R, of $c-As_2S_3$ and $c-As_2Se_3$

accurately obey the scaling relation $\nu_R(c-As_2Se_3) = K_c\,\nu_R(c-As_2S_3)$ where $K_c = 0.81 \pm 0.05$ for the rigid-layer modes (which occur below 80 cm^{-1}) and $K_c = 0.71 \pm 0.01$ for the intralayer modes. In the case of the molecular model the ratios, K_a^i, of corresponding selenide and sulphide frequencies lie in the range $0.59 < K_a^i < 0.71$ and average to 0.65. The difference between K_c for the intralayer modes and the K_a^i is not important in itself and could arise if the structure of the AsS_3 pyramid differed from that of the $AsSe_3$ pyramid to a larger extent in the glasses than in the crystals. However, Zallen et al. show that the scaling relation for the intralayer frequencies implies that the intra-layer bonds in As_2Se_3 are about 10% softer than those in As_2S_3. The values of the bond-stretching force constants for a-As_2S_3 and a-As_2Se_3 derived from the Lucovsky-Martin model[42] imply that the As—Se bonds are 20% softer than the As—S bonds. It is unlikely that such a difference in relative bond strengths should exist between the crystals and the glasses, and it would seem, therefore, that there is a failure in the model. However, the results and calculations of the present study suggest that this discrepancy is not due to a flaw in the model but to a mistake in fitting the observed frequencies to the model. In Section 6.4.5, the scaling relation between the crystals and the glasses is dis-cussed more fully and evidence is put forward which indicates that the most intense Raman peak in each of the unanalysed glass spectra does not correspond to the same vibration and ν_1 for the $AsSe_3$ 'molecule' is 246 cm^{-1} rather than 227 cm^{-1}, the value used by Lucovsky and Martin. It will be shown in Section 6.4.6 that when this value for ν_1 is used the model yields a set of frequencies in good agreement with experiment and a bond-stretching force constant which is ~10% softer than that for the As—S bond.

A minor point concerning the bond-stretching force constants for As_2S_3 and As_2Se_3 is the difference between the values obtained from the molecular model and those computed from Gordy's rule[69]. For the As—S

bond Gordy's rule yields a value of 1.98 md/$\mathring{A}$, compared with 1.33 md/$\mathring{A}$ from the model calculation. This large discrepancy is not significant because in the case of XY_3 molecules the rule is a good approximation only if the atomic-radius ratio $r_X/r_Y > \sim 1.5$, i.e. if X is sufficiently larger than Y to ensure no interaction between non-bonded atoms. $r_{As}/r_S \approx 1.14$ and for this value a 33% deviation from the force constant derived from Gordy's rule is not unreasonable.

In the case of a-As_2S_3, using the value of ν_1 determined in this study (339 cm^{-1}) and taking geometrical parameters from the most recent investigation of the crystal structure of orpiment[70], the following values for the frequencies and force constants of the AsS_3 'molecule' were obtained:

k_j = 1.35, 0.14, 0.14, 0.016 md/$\mathring{A}$ for j = 1, 1', δ, δ' respectively

ν_i = 340, 159, 312, 130 cm^{-1} for i = 1, 2, 3, 4 respectively

The calculation for the set of force constants k_j took into account differences in β and ℓ between the $AsCl_3$ and AsS_3 pyramids as well as differences in the mass ratios and used force constants for $AsCl_3$ obtained from the frequencies reported by Davis and Long[71]. The values of β used were 61° [72] and 61.4° for the $AsCl_3$ and AsS_3 pyramids respectively, the sulphide angle being an average of the crystal values[70]. The calculated frequencies, ν_i, are in agreement with the observed values (see Table 5.2). The two low frequencies are not in such close agreement as the two high frequencies due to the greater solid state interactions they experience[35] (the polarisation data indicates that the calculated frequencies 130 and 159 cm^{-1} can be taken to correspond to the 160 and 185 cm^{-1} features in the observed spectrum).

Inspection of Figure 5.15 reveals that the model not only yields the correct frequencies but also gives the correct symmetry properties, for the ν_1 and ν_2 bands should be polarised and the ν_3 and ν_4 bands should be depolarised.

As was mentioned earlier, the coupled modes are dealt with in terms of an As—S/Se—As bent chain 'molecule' and it is assumed that the coupling is sufficiently weak that the pyramid and chain modes can be treated independently.   The three frequencies of the X_2Y molecule are calculated in the model from Equations A.5 — A.7 (see Appendix I).   The bond-stretching force constant, k_1, is known from the pyramid calculation and Lucovsky and Martin assume that the ratio of k_1 to k_δ, the bond-bending force constant, is 100 : 1 (k_1 and k_δ now refer to Equations A.5 — A.7). This high ratio accounts for the weak intermolecular coupling.   The frequencies reported by Lucovsky and Martin for the chain 'molecules' As_2S and As_2Se agree with experiment in the case of the selenide but in the case of the sulphide they have not been observed in the vibrational spectra.

Again, the calculation for determining the frequencies, ν_i (i = 1, 2, 3), of the X_2Y molecule was set up in a program and carried out by computer so that the ν_i could be generated easily for any combination of the various parameters.   The program was checked with data on X_2Y molecules taken from Herzberg.   Lucovsky and Martin's calculation was repeated but it was found that for both the As_2S and As_2Se 'molecules' the values of ν_i reported by these authors could not be obtained without using values for α that were considerably different from those derived from c-As_2S_3 and c-As_2Se_3, and values for k_1 that differed from those derived from the pyramid 'molecules'.   For the sulphide the reported frequencies could be obtained using the values 1.58, 0, 0.0158 md/$\overset{o}{A}$ and 75.2° ($\equiv$ 104.8° — see below) for k_1, k_{12}, k_δ and α respectively.   From the structure of orpiment α, which is half the As—S—As angle, is expected to be ~49°.   In their discussion of the Lucovsky-Martin model, Kobliska and Solin[3] state that the As—S—As angle in the model is 150° but do not comment on this value.   Coincidentally, taking 2α = 150° is almost equivalent in Equations A.5— A.7 to taking the full value of the As—S—As

angle as α instead of as 2α, i.e. if α were 105° then 2α would be the reflex angle 210° which is equivalent to the obtuse angle 150°. Similarly in the case of the selenide the reported frequencies could be obtained exactly using the values 1.26, 0, 0.0126 md/Å and 104° for k_1, k_{12}, k_δ and α respectively. In c-As_2Se_3 the average As—Se—As angle is $\sim 94^\circ$ [73].

If a non-zero value is taken for the interaction constant k_{12} in Equations A.5 − A.7, the simple valence force field is extended to a more general force field and a more accurate description of the vibrational frequencies should result. By examining the variation in the calculated frequencies as k_{12} is changed it should be possible to find the value for k_{12} which best improves the agreement between the observed and calculated frequencies. In the present case, for both the selenide and the sulphide, an abnormal value for α still had to be used in addition to k_{12} and even then the frequencies generated agreed only approximately with those reported by Lucovsky and Martin.

Although the ratio of bond-stretching to bond-bending force constants is typically 10 : 1 [74] (provided the latter have the dimensions of energy per unit length), Lucovsky and Martin assume this ratio is 100 : 1 in the As_2S and As_2Se 'molecules', which is equivalent to assuming very weak coupling between the AsX_3 pyramids. Kobliska and Solin have suggested that the failure of the depolarisation spectrum to attain its maximum theoretical amplitude of $\frac{3}{4}$ is due to intermolecular coupling, which may therefore not be as weak as expected by Lucovsky and Martin and may yield a smaller value for the ratio of k_1 to k_δ. Variation in k_δ mainly affects ν_2, the bending frequency, and produces only small percentage changes in ν_1. As k_δ appears only in the equations for ν_1 and ν_2' (Equations A.5 & A.6), ν_3 is unaffected by this parameter. If k_1 for a-As_2S_3 is taken as 1.35 md/Å then k_δ is $\sim$0.135 md/Å, assuming the above ratio is 10 : 1, and when these values are inserted in Equations A.5 − A.7 together with the correct value

for α, viz 49°, the following frequencies are obtained for the simple valence force field case $(k_{12} = 0)$: $\nu_1 = 323$, $\nu_2 = 101$, $\nu_3 = 334$ cm^{-1}.

Whereas the Lucovsky-Martin calculation predicts a very low frequency line (55 cm^{-1}), a line at high frequency (438 cm^{-1}) and one intermediate between these (218 cm^{-1}), the above calculation suggests a different arrangement of bands, namely one medium-frequency line (101 cm^{-1}) and two high-frequency lines (323 and 334 cm^{-1}) falling on the main band of the a-As_2S_3 spectrum.   This picture is more compatible with the experimental results since there are two observed frequencies in the high-frequency region which have not been accounted for, viz 367 and 395 cm^{-1} (the former is discussed in Section 5.4.3).   The calculated value for ν_2 is also close to a feature in the vibrational spectrum, i.e. the dip at 106 cm^{-1} in the depolarisation spectrum.

Both calculations fail, however, to account for the polarisation properties of the spectrum since in each case ν_3, the frequency of the antisymmetric vibration, is larger than ν_1, the symmetric-stretch frequency, and so the depolarised line is predicted to occur at a higher frequency than the polarised line.   Excluding the 490 cm^{-1} band, which is associated with S—S bonds, the highest frequency band in the a-As_2S_3 spectrum occurs at 395 cm^{-1} and as this line corresponds to the minimum in the depolarisation spectrum it is clearly polarised and must therefore arise from a symmetric vibration.   The 367 cm^{-1} band is not polarised to the same extent as the 395 cm^{-1} band and its depolarisation ratio is possibly reduced from the expected value of $\frac{3}{4}$ by intermolecular coupling.

In the case of the Lucovsky-Martin calculation the reversal of ν_1 and ν_3 is a serious failing since ν_1 (218 cm^{-1}) occurs so far below ν_3 (438 cm^{-1}) that agreement with experiment cannot be obtained even by varying the interaction constant k_{12} within realistic limits.   In the present case, however, this problem can be overcome by taking a non-zero value for k_{12}.   As k_{12} is increased ν_1 increases while ν_3 decreases.

Using the corrected values for k_1, k_δ and α given above it was found that ν_1 and ν_3 coincided at 328 cm^{-1} for k_{12} = 0.05 md/Å and that for values of k_{12} greater than this $\nu_1 > \nu_3$. However, with these values for k_1, k_δ and α quantitative agreement with experiment could not be obtained by varying k_{12} since the cross-over frequency, 328 cm^{-1}, is already well below the lower experimental frequency. Quantitative agreement could be achieved only by using unrealistic values for the other parameters.

Just as the van der Waals interaction between the non-bonded sulphurs in the AsS$_3$ pyramid 'molecule' led to a discrepancy between the calculated value for k_1 and that predicted from Gordy's rule, so it may be that the valence force field potential function for the As$_2$S 'molecule' is an inadequate representation of the real intramolecular potential because of the van der Waals interaction between the non-bonded arsenic atoms. By extending the simple valence force field (i.e. that with k_{12} = 0) for the X$_2$Y molecule to include a central force between the two non-bonded X atoms it is possible to derive, using the expected values for the various parameters, a set of frequencies which is in agreement with the polarisation properties and which is in better quantitative agreement with the experimental values. For k_1 = 1.35, k_δ = 0.135 md/Å and α = 49° and taking the central force constant, a_{33}, as 0.3 md/Å the following frequencies were calculated: ν_1 = 342 cm^{-1}, ν_2 = 106 cm^{-1}, ν_3 = 334 cm^{-1}.

A summary of the preceding results is presented in Tables 5.2 and 5.3. The corresponding analysis for a-As$_2$Se$_3$ is given in Section 6.4.6.

Including the hidden 367 cm^{-1} band there are eleven features in the first-order Raman and depolarisation spectra of a-As$_2$S$_3$ (see Table 5.1). One of these is the Bose peak, four arise from vibrations of the AsS$_3$ pyramid units and three are due to the As$_2$S links between these pyramids. The three weak features at 208, 231 and 490 cm^{-1} are unaccounted for. None of these features scale with structure in the a-As$_2$Se$_3$ spectrum

Observed values	Parameter	Model value	% Diff. in freqs.
	k_1	1.35	
	$k_{1'}$	0.14	
	k_δ	0.14	
	$k_{\delta'}$	0.016	
61.4	β	61.4	
339	ν_1	340	0.3
185	ν_2	159	14
315	ν_3	312	1
160	ν_4	130	19

All frequencies and force constants are in units of cm^{-1} and md/Å respectively; β is in degrees.

Table 5.2   The molecular model parameters and frequencies for the AsS_3 'molecule'. · The last column gives the difference between the observed and calculated frequencies expressed as a percentage of the former.

Observed values	Parameter	Model value	% Diff. in freqs.	Model value	% Diff. in freqs.	Model value	% Diff. in freqs.	Model value	% Diff. in freqs.
	k_1	1.58		1.35		1.35		1.35	
	k_δ	0.0158		0.135		0.135		0.135	
	k_{12}	0		0		0.05		0	
	a_{33}	0		0		0		0.3	
49	α	75(105)		49		49		49	
395	ν_1	218	—	323	18	328	17	342	13
106	ν_2	55	—	101	5	101	5	106	0
367	ν_3	438	—	334	9	328	11	334	9

All frequencies and force constants are in units of cm^{-1} and $md/\text{Å}$ respectively; α is in degrees.

Table 5.3   The molecular model parameters and frequencies for the As_2S

'molecule'.   The differences between the observed and calculated

frequencies expressed as a percentage of the former are also given.

(see Section 6.4.5) which suggests that the structural elements giving rise to them are not present in c-As_2S_3. In Section 5.5.1 it will be shown that the 208 and 490 cm^{-1} features grow as the sulphur content of the glasses is increased and can be attributed to —S—S— links between the As atoms in the network (because the 492 cm^{-1} —S—S— band is very weak in the a-As_2S_3 spectrum and is superimposed on a sloping background it is shifted slightly to 490 cm^{-1}).

Applying the 0.71 scale factor derived by Zallen et al.[5,6], one would expect the a-As_2Se_3 counterpart of the 231 cm^{-1} band to occur at ~164 cm^{-1}. As will be shown in Section 6.4 there is no feature in the Raman or depolarisation spectra of a-As_2Se_3 near this frequency, though a weak band at 156 cm^{-1} appears in some of the published i.r. spectra. Figure 6.33 (after p.242) shows, however, that as the arsenic content of the selenide glasses is increased beyond 40 at.% two bands grow in the Raman spectrum at ~155 and 220 cm^{-1} so it is possible that the 156 cm^{-1} feature observed in some of the i.r. studies is due to a slight excess of As in the samples used or As—As bonds in the As-Se network, for, as will be shown below, the 231 cm^{-1} feature in the a-As_2S_3 spectrum can be attributed to As—As bonds in the As-S network.

The 231 cm^{-1} a-As_2S_3 band differs from the rest of the vibrational features in certain respects. Finkman et al.[39] have shown its temperature dependence to differ from that of the main band and resonance Raman studies[43,44] show that this is the only feature to resonate about the optical gap energy (2.32 eV at $300°$ K). The Raman scattering efficiency over the whole a-As_2S_3 spectrum increases monotonically as the incident photon energy, $h\nu_{in}$, increases[43] and shows no resonance in the range $1.8 < h\nu_{in} < 2.7$ eV, apart from the 231 cm^{-1} band, which resonates smoothly about the optical gap energy. Figure 5.28 compares two spectra obtained for a-As_2S_3 under identical experimental conditions with the exception that one was excited with 6328 $\mathring{A}$ (1.96 eV) radiation

Figure 5.28

Raman spectra of a-As_2S_3: one spectrum was excited with near band-gap radiation (λ_{exc}= 5145 Å) and the other with 6328 Å radiation which is weakly absorbed. The change in spectral density around 231 cm^{-1} is a manifestation of the resonance Raman effect.

THE RAMAN SPECTRUM OF a-As$_{40}$S$_{60}$

λ_{exc}= 6328Å

λ_{exc}= 5145Å

231
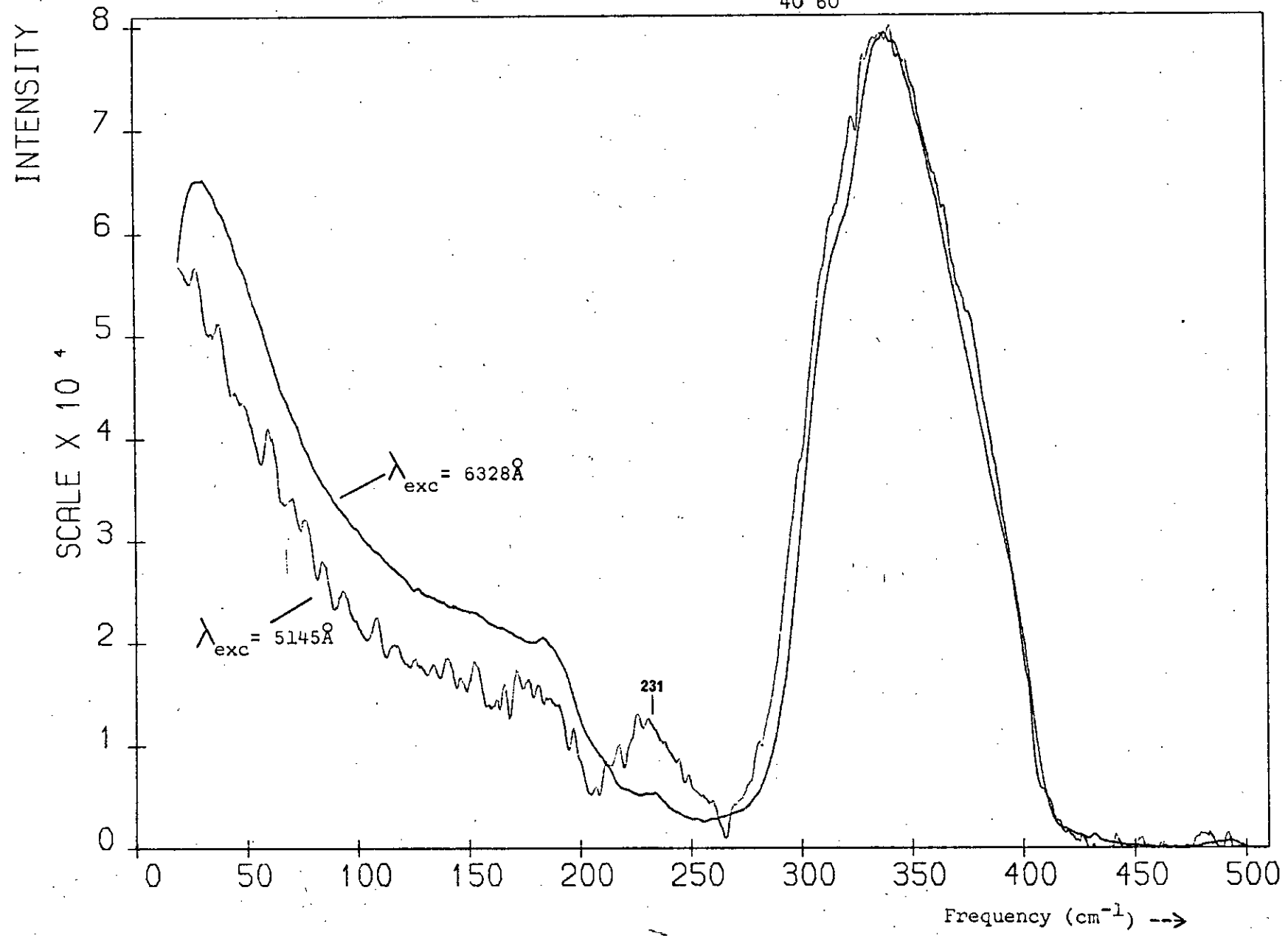
and the other with 5145 Å (2.41 eV) radiation which is close to the band-gap energy. The poor signal/noise ratio in the near-resonance spectrum is due to the fact that the band-gap radiation is being strongly absorbed. The difference in absorption coefficients at 5145 and 6328 Å also accounts for the increasing divergence in intensities at frequencies below 338 cm^{-1}, which is the frequency at which the spectra are normalised. The shapes of the two spectra are identical, ignoring the intensity divergence, except for the 231 cm^{-1} feature, which is very pronounced in the near-resonance spectrum. In molecules the fundamental displaying the resonance Raman effect is principally bond stretching in form, which suggests that the vibration responsible for the 231 cm^{-1} frequency is associated with As—As bonds since the bond-stretching frequencies of As—S and S—S bonds are much higher than 231 cm^{-1}.

The 231 cm^{-1} feature grows as the As content of the glasses is increased beyond 40 at.% (see Section 5.6), which is consistent with it being associated with As—As bonds. In addition, the vibrational spectra of elemental As[30 — 34] contain features near 231 cm^{-1}. In the As-Se glasses a feature also grows at 220 cm^{-1} as the As content is increased beyond 40 at.% (see Section 6.6) and cannot be attributed to monomeric species.

Porter and Sheldrick[14] show that the Raman spectrum of c-As$_4$S$_4$ changes after prolonged irradiation and deduce that the changes are due to photo-induced polymerisation of the As$_4$S$_4$ molecules. One of the changes is the growth of a strong band near 230 cm^{-1} which may well arise from the presence of As—As bonds in the polymeric product. Whitfield[11] attributes the 235 cm^{-1} band of Forneris's[9] α-As$_4$S$_4$ Raman spectrum to As—As bonds, though he does not suggest that these bonds are part of any network structure.

It has been suggested[37] that the 185 and 231 cm^{-1} bands are due to the presence of As$_4$S$_4$ monomers in the As$_2$S$_3$ glass. This seems unlikely

since these bands grow very rapidly as the As content is increased beyond 40 at.% but no such rapid change occurs as the As content is decreased below this value. Attempts to normalise the S-rich spectra to obtain a regular decrease near 185 cm^{-1} as a function of increasing S content led to inexplicable changes in other regions of the spectra. Also, there is no sign in the a-As_2S_3 spectrum of other characteristic As_4S_4 bands. Numerous As_4S_4 bands are observed in the Raman spectra of the As-rich sulphide glasses excited with red light but as Figure 5.75 (after p.193) shows, these bands virtually disappear when near band-gap radiation (5145 Å) is used to excite the spectra. Figure 5.28 shows, however, that the 185 cm^{-1} feature of the a-As_2S_3 spectrum is still present in the spectrum excited with 5145 Å radiation.

As most of the published Raman studies report bands at 231 and 490 cm^{-1}, these are probably genuine features of the a-As_2S_3 spectrum and do not arise from deviations in the stoichiometries of the samples used. If the samples are stoichiometric then the presence of S—S bonds in the network implies the presence of As—As bonds and vice versa.

5.5 The sulphur-rich glasses

5.5.1 The compositions $As_{40}S_{60} - As_{35}S_{65}$

5.5.1.1 Normalisation

The observed polarisation-unanalysed Raman spectra of the five near-stoichiometric S-rich glasses, together with the a-$As_{40}S_{60}$ spectrum for comparison, are presented in Figure 5.29. The spectra, which are normalised to the height of the 338 cm^{-1} band, are shown displaced above one another. The corresponding reduced spectra are displayed in Figure 5.30 and exhibit the same structure, apart from the thermal peaks, as the ordinary spectra, though it is shifted slightly to higher frequencies.

These results show that several spectral changes occur with increasing

Figure 5.29

The polarisation-unanalysed Raman spectra of the compositions
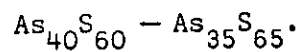
$As_{40}S_{60} - As_{35}S_{65}$.

Spectrum		Composition
A	—	$As_{35}S_{65}$
B	—	$As_{36}S_{64}$
C	—	$As_{37}S_{63}$
D	—	$As_{38}S_{62}$
E	—	$As_{39}S_{61}$
F	—	$As_{40}S_{60}$

Figure 5.30

The reduced spectra corresponding to those in Figure 5.29.

Raman Spectra: $As_{40}S_{60} - As_{35}S_{65}$.
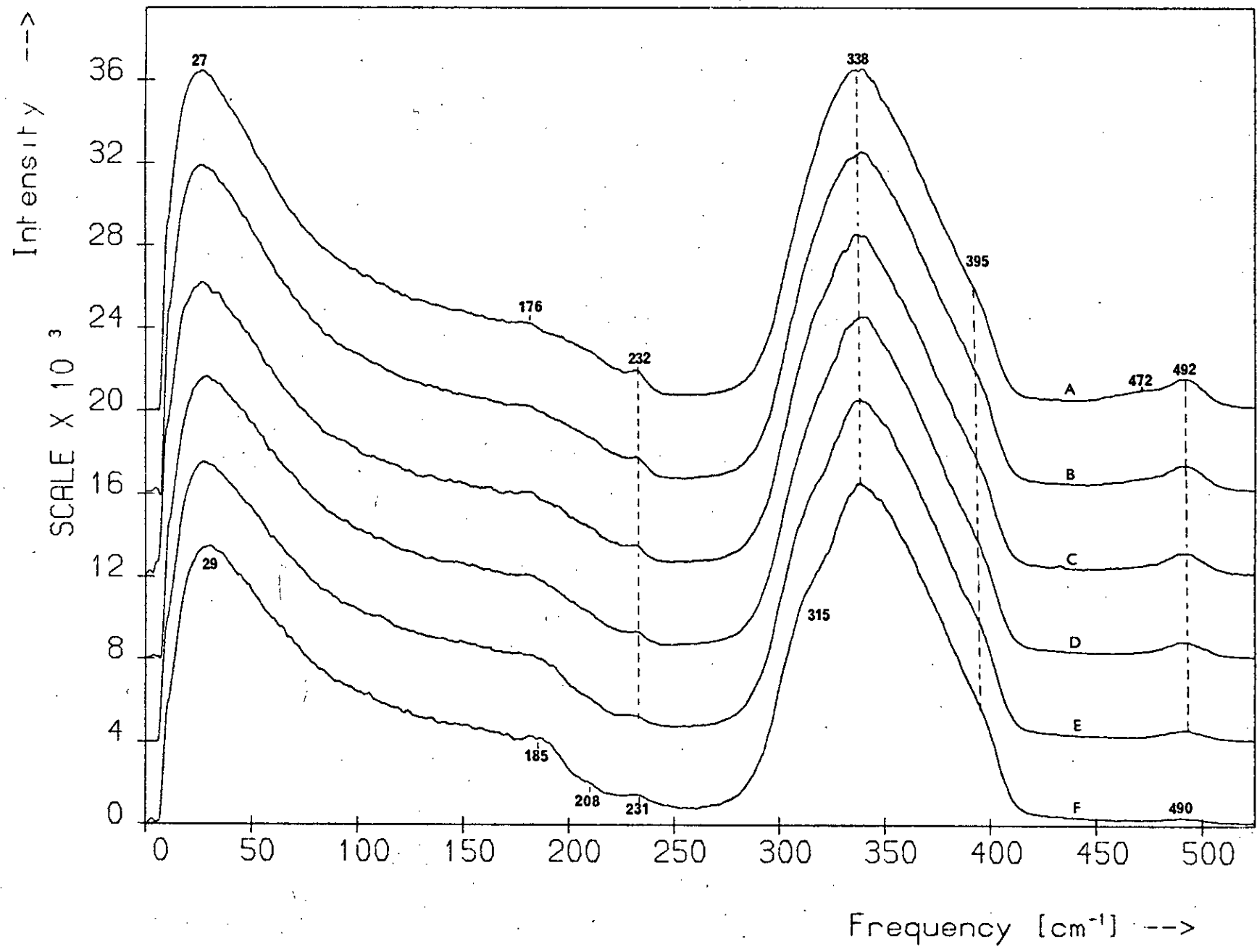
Reduced Spectra: As$_{40}$S$_{60}$ – As$_{35}$S$_{65}$
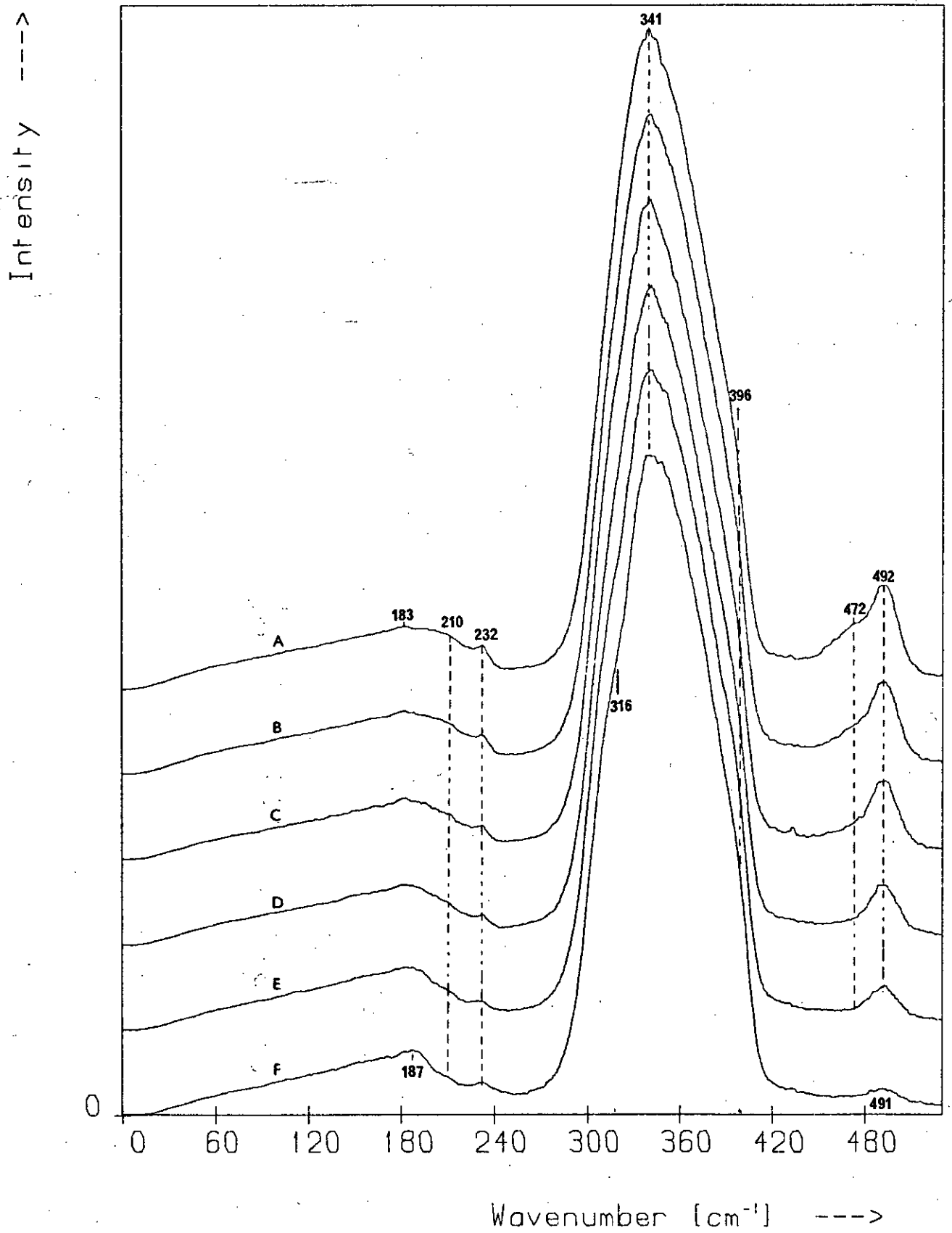
S content, the most obvious being the growth of a peak at 492 cm^{-1}. A shoulder emerges on this peak at ~472 cm^{-1} while the shoulder at 315 cm^{-1} in the a-As$_{40}$S$_{60}$ spectrum gradually disappears. There is also a change of profile in the region 160 — 240 cm^{-1}, with a small peak appearing at 232 cm^{-1}. Also, the thermal peak grows relative to the 338 cm^{-1} band and shifts slightly.

Some of these changes in shape are more obvious if the spectra are superimposed and a more exact set of values for the frequencies of the changing features can be obtained by generating difference spectra. However, in both of these procedures it is necessary to consider the normalisation of the spectra, for although the frequencies of the changing features can be determined unambiguously the interpretation of these changes depends on the normalisation.

Several methods of normalisation were investigated, including normalisation by:

(a) maximum intensity of the 300 — 400 cm^{-1} band;

(b) intensity at 338 cm^{-1};

(c) intensity at 395 cm^{-1};

(d) intensity at 185 cm^{-1};

(e) integrated intensity over the range 0 — 510 cm^{-1};

(f) integrated intensity of the 300 — 400 cm^{-1} band;

(g) basewidth of the 300 — 400 cm^{-1} band.

Because the low-frequency region of the spectra is more affected by temperature than the high-frequency region, method (e) was applied only to the reduced spectra; the Bose peak itself is strongly temperature dependent and so is not suitable for normalisation purposes. Also, since the peak frequency of the main band does not shift appreciably over this composition range, methods (a) and (b) are virtually equivalent.

Of the various methods, (g) was the most satisfactory; the other normalisation procedures turned out to be biased by the spectral changes

and yielded sets of spectra which either did not change in an ordered way as a function of composition or which indicated structural changes that were not consistent with other data. For example, Figure 5.31 shows the $260 - 340 \text{ cm}^{-1}$ region of a set of difference spectra obtained from the unreduced spectra — normalised to the height of the main peak — by subtracting each one in turn from the $a\text{-As}_{40}\text{S}_{60}$ spectrum. (This region corresponds to the low-frequency side of the main band and similar results are obtained for sets of spectra normalised by methods (b) and (f); noise is responsible for the fine structure in the curves.) Although these difference spectra change in an ordered way with increasing S content they indicate either that a band is growing at $\sim 325 \text{ cm}^{-1}$ while one is disappearing at $\sim 300 \text{ cm}^{-1}$, or, more probably, that the 315 and 338 cm^{-1} bands are shifting towards one another; other results obtained in this study show, however, that there is no band at 300 cm^{-1} in the $a\text{-As}_{40}\text{S}_{60}$ spectrum and that the 315 and 338 cm^{-1} bands do not shift over this composition range.

Method (g), hereafter referred to as 'normalisation by basewidth', was applied to both polarisation-unanalysed and polarised spectra and unless otherwise stated the results presented in this chapter have all been standardised in this way or are derived from spectra so normalised. An example of the difference spectra obtained from data normalised by basewidth is provided by Figure 5.33 (after p.146). These difference spectra, which were generated by subtracting the spectrum of the $\text{As}_{40}\text{S}_{60}$ glass from each normalised spectrum, are positive over most of the range $0 - 525 \text{ cm}^{-1}$ and increase in an ordered way with increasing S content. These spectra do not, however, change uniformly as a function of composition, due possibly to deviations from the nominal stoichiometries of the samples, or inaccuracy in the normalisation procedure. The latter would account for the fact that as the S content is increased the individual features in the difference spectra do not all grow at the same rate although most of

Figure 5.31

Difference spectra obtained from the polarisation-unanalysed Raman spectra of the compositions $As_{39}S_{61} - As_{35}S_{65}$ by subtracting each spectrum from that of $a\text{-}As_{40}S_{60}$. The Raman spectra were normalised to intensity at ~ 338 cm^{-1}.

Spectrum		Compositions
A	—	$As_{40}S_{60}$ - $As_{35}S_{65}$
B	—	$As_{40}S_{60}$ - $As_{36}S_{64}$
C	—	$As_{40}S_{60}$ - $As_{37}S_{63}$
D	—	$As_{40}S_{60}$ - $As_{38}S_{62}$
E	—	$As_{40}S_{60}$ - $As_{39}S_{61}$

Difference Spectra: S-Rich Compositions
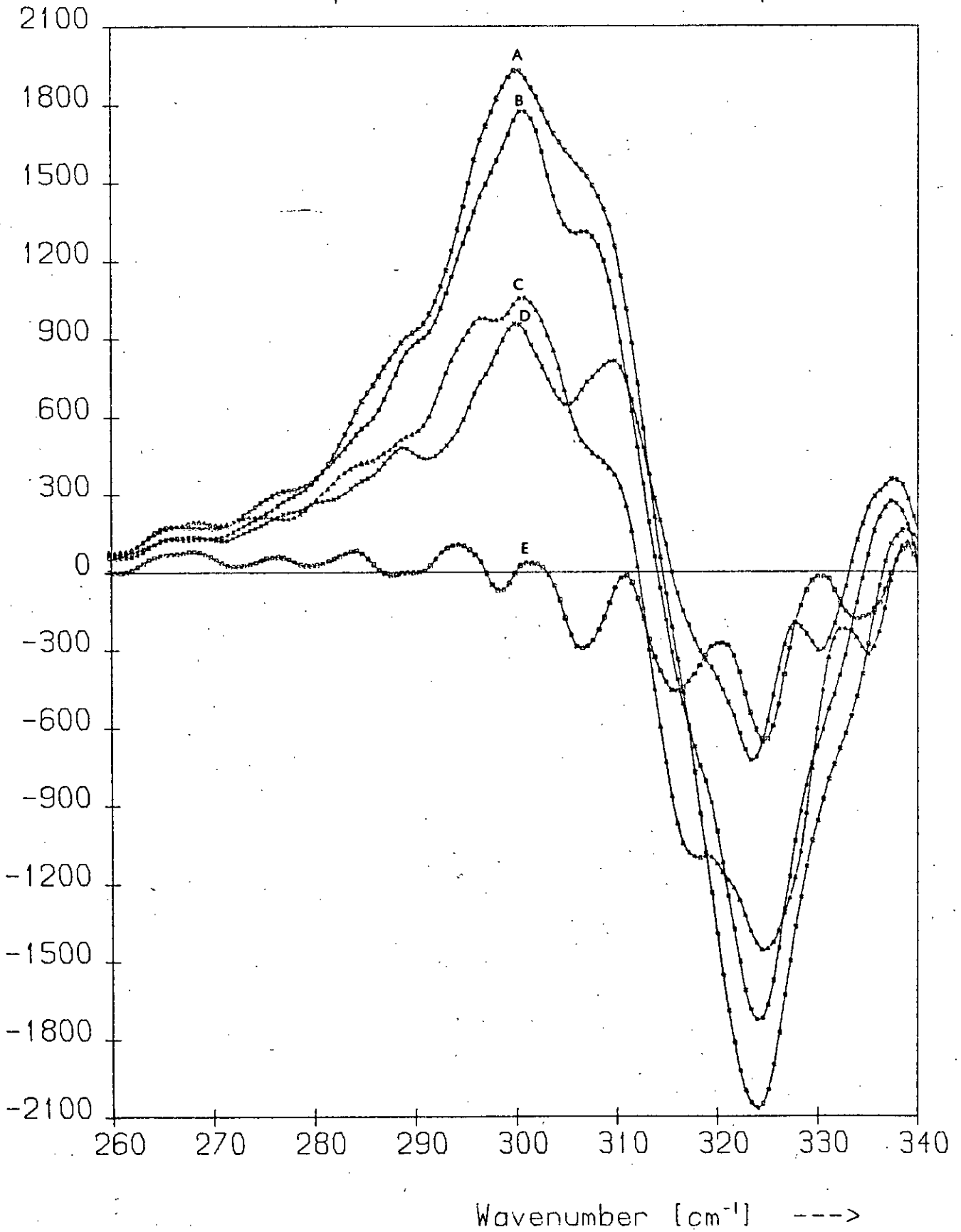
them arise, as will be seen in Section 5.5.1.5.4, from the same structural

element. In Figure 5.33 the frequency ranges where the difference spectra

all coincide at zero intensity difference correspond to regions over which

the Raman spectra are normalised.

In a similar vibrational study of Ge-S glasses Lucovsky et al.[75]

base the normalisation procedure for their Raman spectra on the linear

dependence on S content of certain features in their i.r. reflectance

spectra and show that this method of normalisation can be deduced from

theoretical considerations of the structure of the glasses. In the

present case no corresponding i.r. study exists and structural consider-

ations do not lead to a normalisation procedure.

5.5.1.2   The polarisation-unanalysed spectra

Figure 5.32 shows the polarisation-unanalysed Raman spectra of the

glasses $As_{40}S_{60}$ — $As_{35}S_{65}$;   they are normalised by basewidth and are shown

superimposed (cf. Figure 5.29).   The spectral changes noted in Section

5.5.1.1 are more obvious when the data is presented in this way;   these

changes occurring as the S concentration increases are: the growth of

a band at 492 cm^{-1}, the emergence on this band of a shoulder at ~472 cm^{-1},

the gradual disappearance of the shoulder at 315 cm^{-1} on the main band,

and a change of profile in the region 160 — 240 cm^{-1}, with a small peak

appearing at 232 cm^{-1}.   The growth of the thermal peak relative to the

338 cm^{-1} band is also evident.   The intensities of the spectra increase

in an ordered, but not uniform, manner as the compositions become richer

in sulphur.

An even clearer picture of the spectral changes is provided by the

difference spectra derived from the normalised spectra of Figure 5.32 by

subtracting the a-$As_{40}S_{60}$ spectrum from each of the others.   The difference

spectra, shown in Figure 5.33, also provide a more exact set of values for

the frequencies of the changing regions: they exhibit a series of features

Figure 5.32

The polarisation-unanalysed Raman spectra of the compositions
$As_{40}S_{60} - As_{35}S_{65}$ normalised by basewidth.

Spectrum		Composition
A	—	$As_{35}S_{65}$
B	—	$As_{36}S_{64}$
C	—	$As_{37}S_{63}$
D	—	$As_{38}S_{62}$
E	—	$As_{39}S_{61}$
F	—	$As_{40}S_{60}$

Figure 5.33

Difference spectra obtained from the basewidth-normalised spectra of
Figure 5.32 by subtracting the $a-As_{40}S_{60}$ spectrum from each.

Spectrum		Compositions
A	—	$As_{35}S_{65} - As_{40}S_{60}$
B	—	$As_{36}S_{64} - As_{40}S_{60}$
C	—	$As_{37}S_{63} - As_{40}S_{60}$
D	—	$As_{38}S_{62} - As_{40}S_{60}$
E	—	$As_{39}S_{61} - As_{40}S_{60}$

Figure 5.34

The reduced spectra corresponding to those in Figure 5.32.

Figure 5.35

Difference spectra obtained from the reduced spectra of Figure 5.34.
The spectra are labelled as those in Figure 5.33.

Raman Spectra: $As_{40}S_{60} - As_{35}S_{65}$
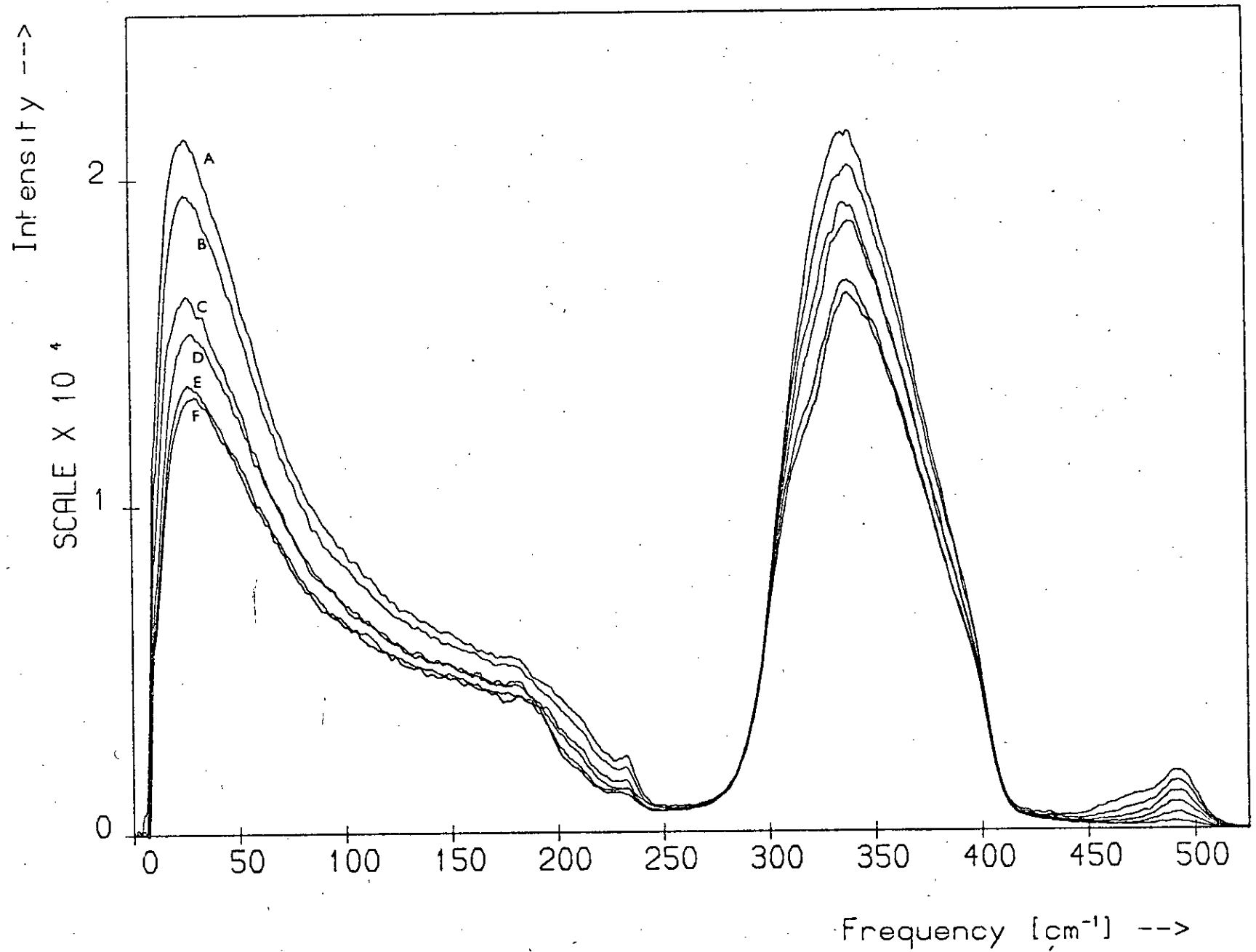
Difference Spectra for the S-Rich Compositions.
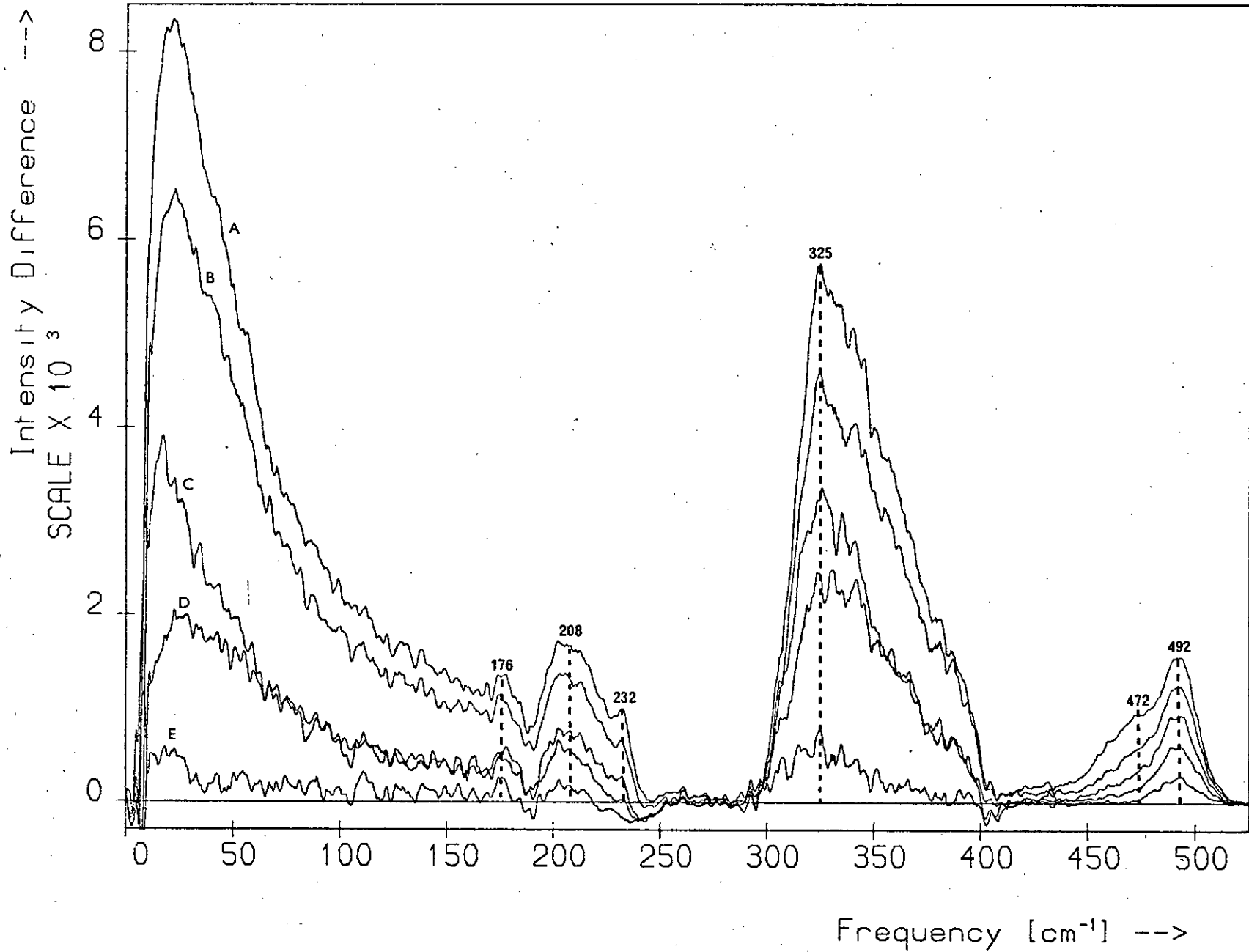
Reduced Raman Spectra: $As_{40}S_{60} - As_{35}S_{65}$
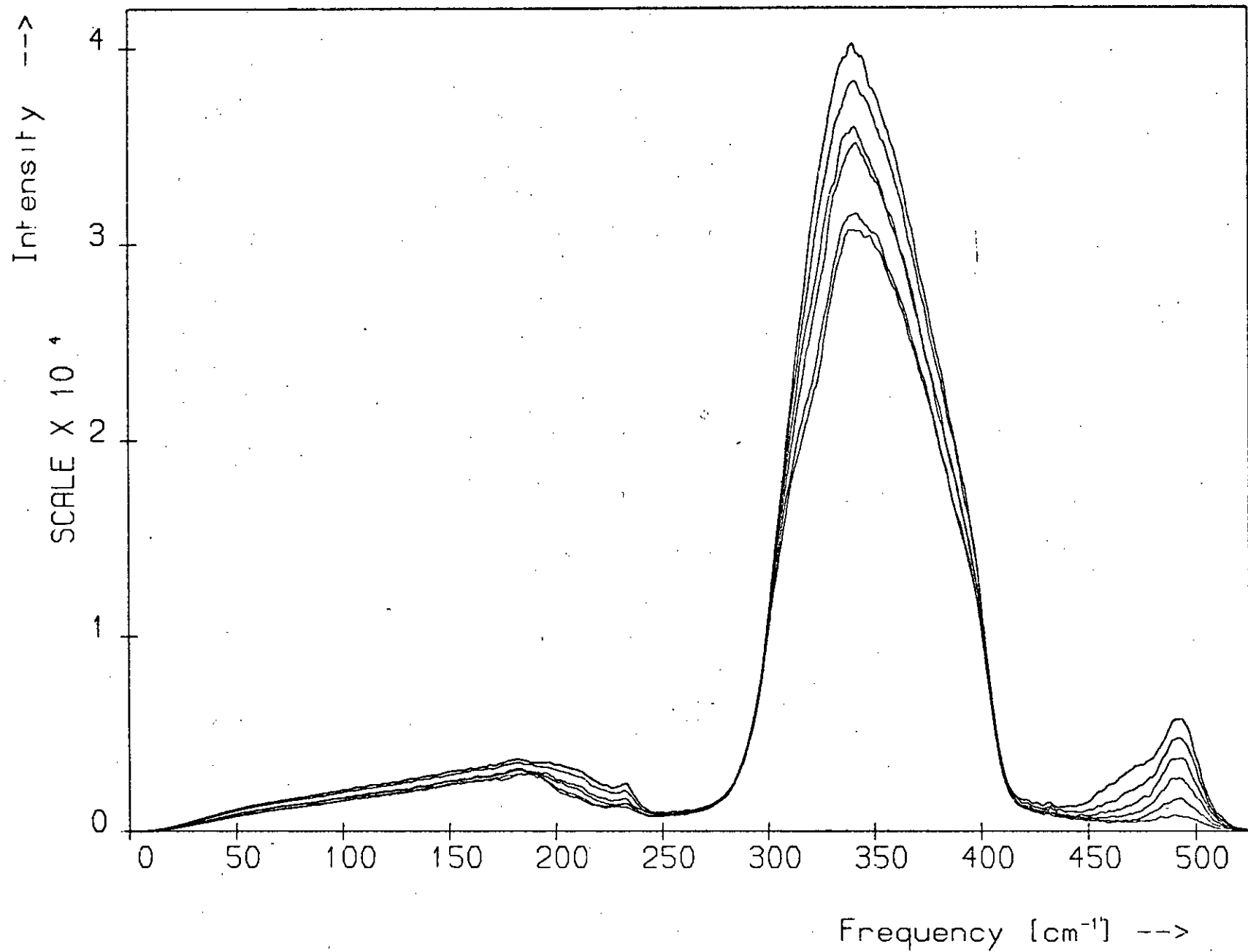
Difference Spectra for the S-Rich Compositions
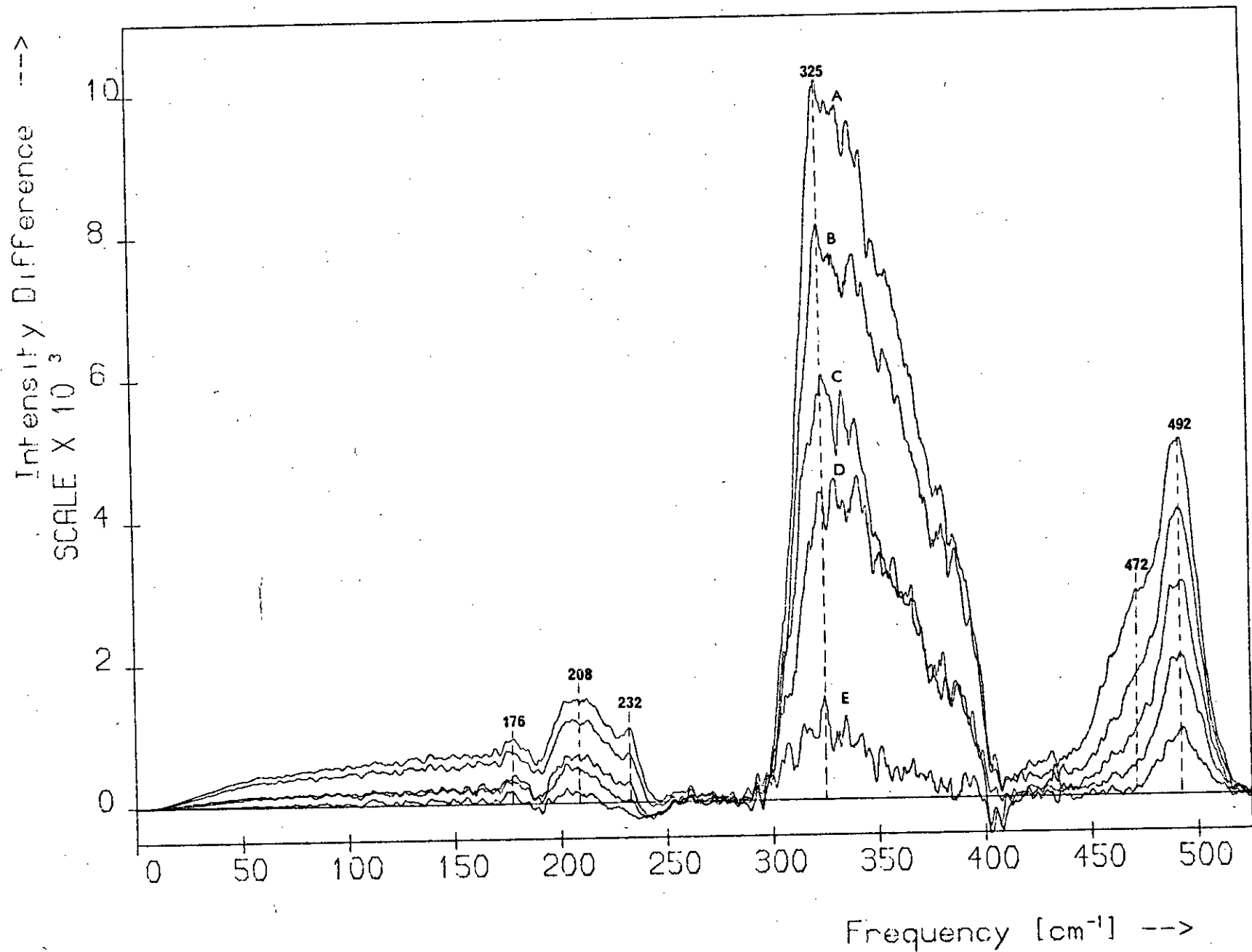
growing at 176, 208, 232, 325 and 492 cm^{-1} as the S content increases. In addition, it is possible that the highly asymmetric 300 — 400 cm^{-1} peak contains a band on its high-frequency side. Also, a feature develops at 472 cm^{-1} on the high-frequency peak and is apparent as a shoulder in the uppermost spectrum.

The reduced spectra of the compositions $As_{40}S_{60}$ — $As_{35}S_{65}$ are shown normalised by basewidth in Figure 5.34. Comparison with Figure 5.32 shows that the same features, with the exception of the thermal peaks, appear in each pair of corresponding reduced and unreduced spectra, although in the former the features have different relative intensity and are shifted slightly to higher frequencies.

Difference spectra were derived from the basewidth-normalised reduced spectra by subtracting from each spectrum that of the $As_{40}S_{60}$ glass. They are shown in Figure 5.35 and apart from the intensity difference and the absence of the low-frequency peak they match the difference spectra of Figure 5.33.

The growth of the 492 cm^{-1} peak with increasing S content is shown in Figure 5.36, which is an enlargement of the 440 — 530 cm^{-1} region of the spectra in Figure 5.29. The presence at 472 cm^{-1} on this band of a wing in the $As_{36}S_{64}$ spectrum and a shoulder in the $As_{35}S_{65}$ spectrum is obvious in this enlargement. In the VV spectra (see Figure 5.43 after p.149) this shoulder is resolved into a peak. Also obvious is the presence of the high-frequency band in the a-$As_{40}S_{60}$ spectrum, though because the feature is weak for this composition and is superimposed on a sloping background the peak frequency is shifted slightly to 490 cm^{-1}. Every spectrum of vitreous $As_{40}S_{60}$ obtained in this study, whether it was recorded from a commercial sample or one produced in the Department, contained this feature and it is also present in the a-$As_{40}S_{60}$ spectra reported in the literature[2,39,44]. Thus it is unlikely that deviations in the S content of these samples above its nominal value of 60 at.% are

Figure 5.36

The 472 and 492 cm^{-1} bands. This figure is an enlargement of the 440 — 530 cm^{-1} region of the polarisation-unanalysed spectra normalised to the height of the 338 cm^{-1} peak. The spectra are labelled as those in Figure 5.32.
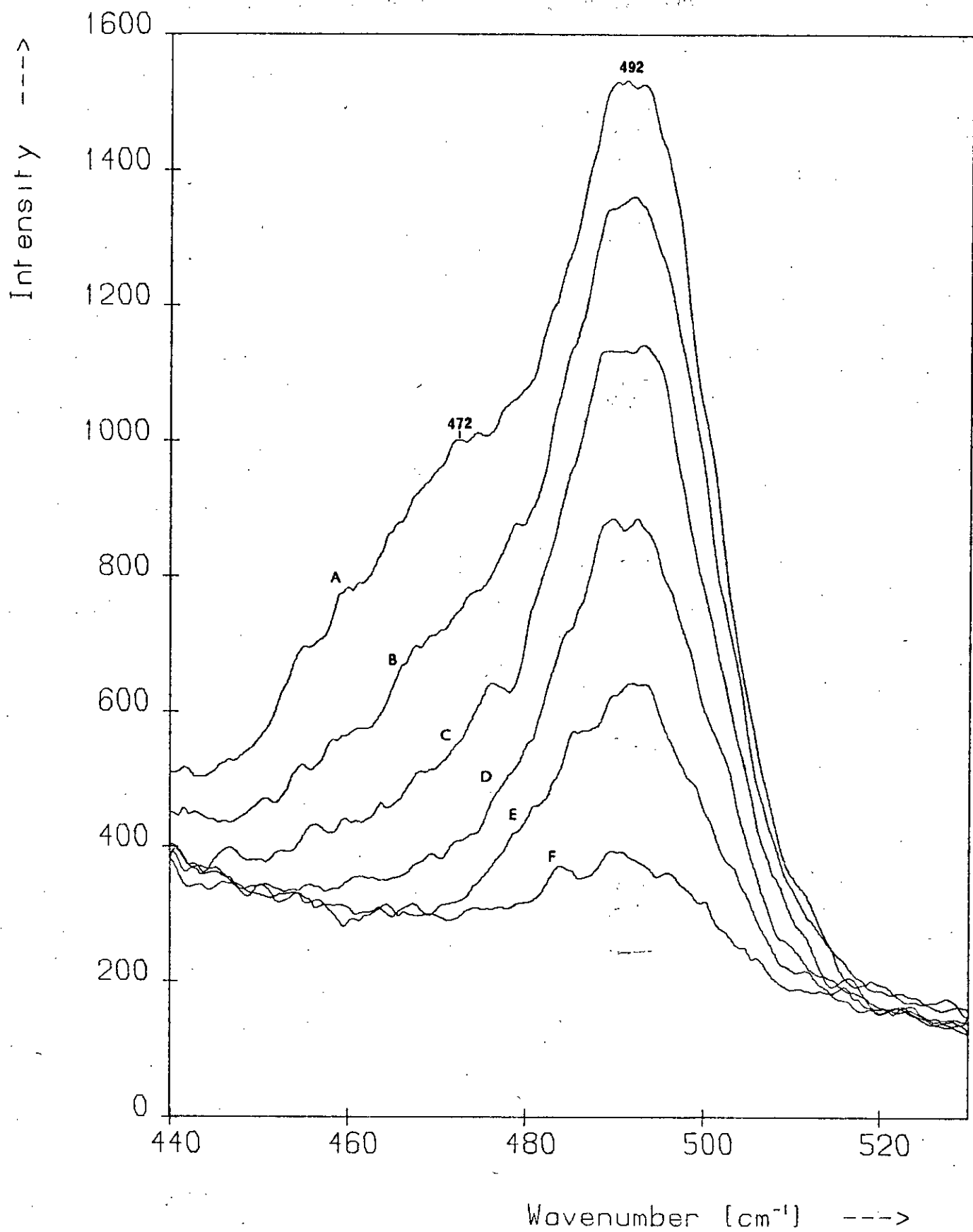
responsible for this feature, particularly since chemical analysis of the commercial sample showed it to be slightly As rich. In Section 5.5.1.5.4 it is shown that the growth of the 492 cm^{-1} peak with increasing S concentration is due to the replacement of the bridging S atoms between the AsS_3 pyramids by —S—S— linkages. If it is correct that the a-$As_{40}S_{60}$ samples studied contain no significant excess of sulphur then the presence of this peak in their spectra indicates that S—S bonds are a genuine characteristic of the a-$As_{40}S_{60}$ network. The fact that S—S bonds are not present in c-$As_{40}S_{60}$ accounts for the absence in its spectrum of any feature near 492 cm^{-1}. If As—As bonds are present in a-$As_{40}S_{60}$ (see Section 5.4.5) then S—S bonds would also be expected.

In addition to being the most obvious change in the spectra, the growing 492 cm^{-1} peak was found to be the only feature that changed in an ordered way with S content irrespective of the method of normalisation. The intensity over the region 450 — 520 cm^{-1} increased monotonically with increasing S content for every normalising procedure mentioned in Section 5.5.1.1.

5.5.1.3 Polarisation measurements

The observed VV-polarised Raman spectra of the compositions $As_{40}S_{60}$ — $As_{35}S_{65}$ are shown in Figure 5.37. The spectra, which are normalised to the intensity of the 339 cm^{-1} peak, are shown displaced above one another. Since the VV spectra are very similar to their polarisation-unanalysed counterparts the results they yield are essentially identical with those of Section 5.5.1.2 and require no further comment. Figures 5.38 and 5.39 show, respectively, the VV spectra normalised by basewidth and superimposed, and the difference spectra derived from these by subtracting the a-$As_{40}S_{60}$ VV spectrum from each of the others. Figures 5.40 and 5.41 show the corresponding results for the reduced spectra.

Figure 5.37

The VV-polarised Raman spectra of the compositions $As_{40}S_{60} - As_{35}S_{65}$.

Spectrum   Composition

A — $As_{35}S_{65}$

B — $As_{36}S_{64}$

C — $As_{37}S_{63}$

D — $As_{38}S_{62}$

E — $As_{39}S_{61}$

F — $As_{40}S_{60}$

Figure 5.38

The spectra of Figure 5.37 normalised by basewidth (A — F as above).

Figure 5.39

The difference spectra obtained from the spectra of Figure 5.38.

Spectrum   Composition

A $As_{35}S_{65} - As_{40}S_{60}$

B $As_{36}S_{64} - As_{40}S_{60}$

C $As_{37}S_{63} - As_{40}S_{60}$

D $As_{38}S_{62} - As_{40}S_{60}$

E $As_{39}S_{61} - As_{40}S_{60}$

Figure 5.40

The reduced spectra corresponding to those in Figure 5.38.

Figure 5.41

The difference spectra obtained from the spectra of Figure 5.40.   The spectra are labelled as in Figure 5.39.

VV Polarisation Spectra : $As_{40}S_{60} - As_{35}S_{65}$.
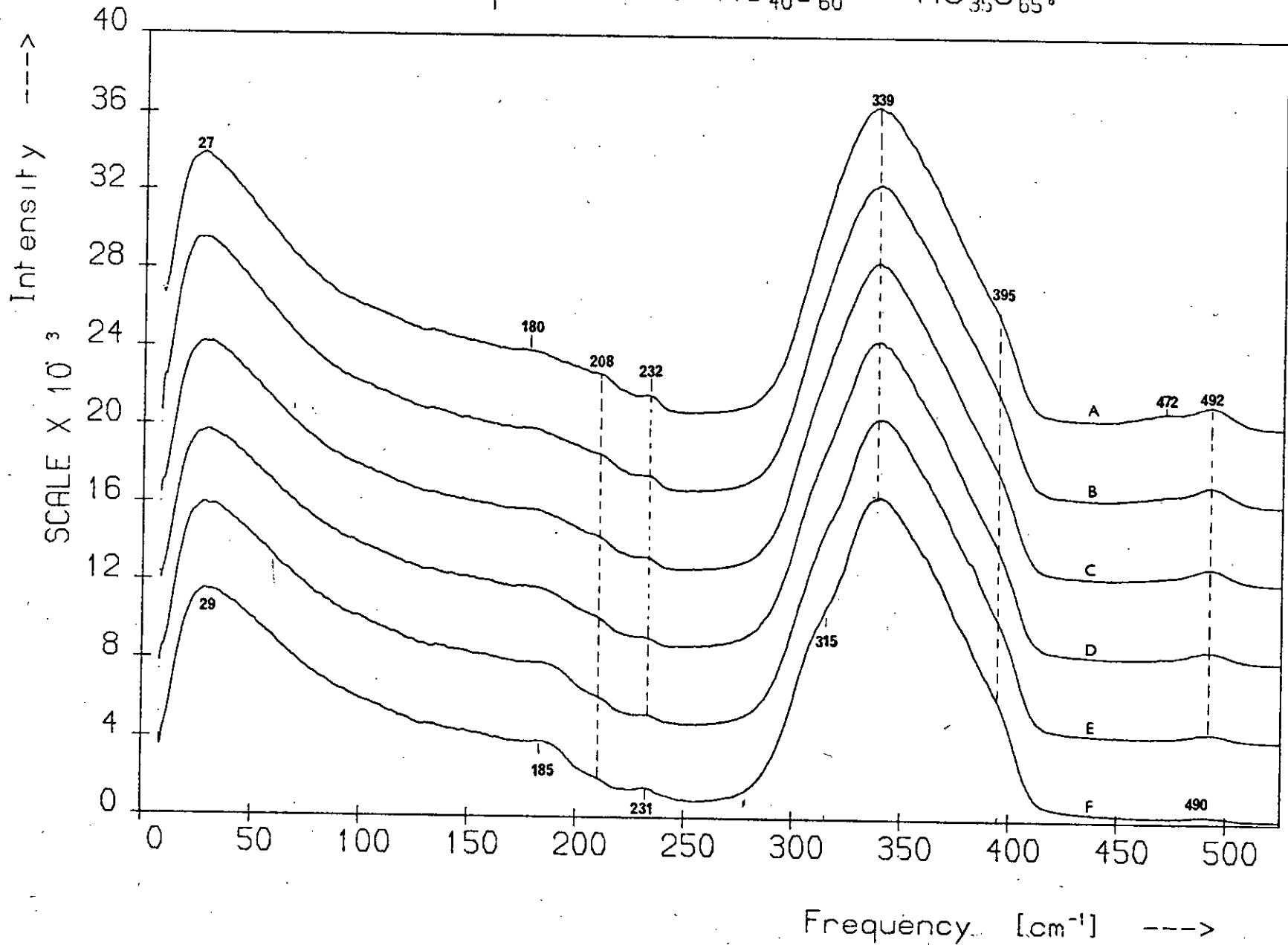
VV Polarisation Spectra : $As_{40}S_{60}$ – $As_{35}S_{65}$.
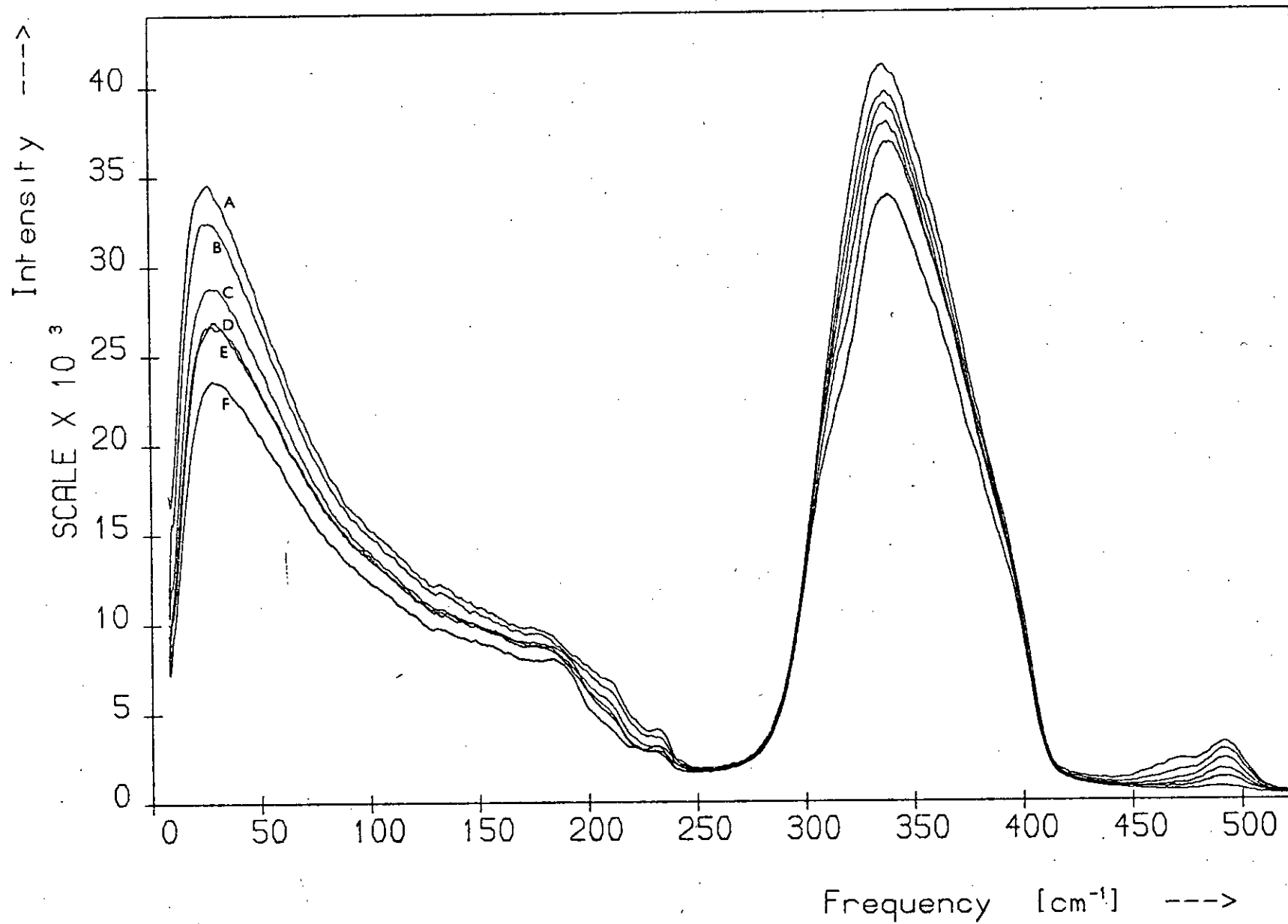
Difference Spectra for the S-Rich Compositions
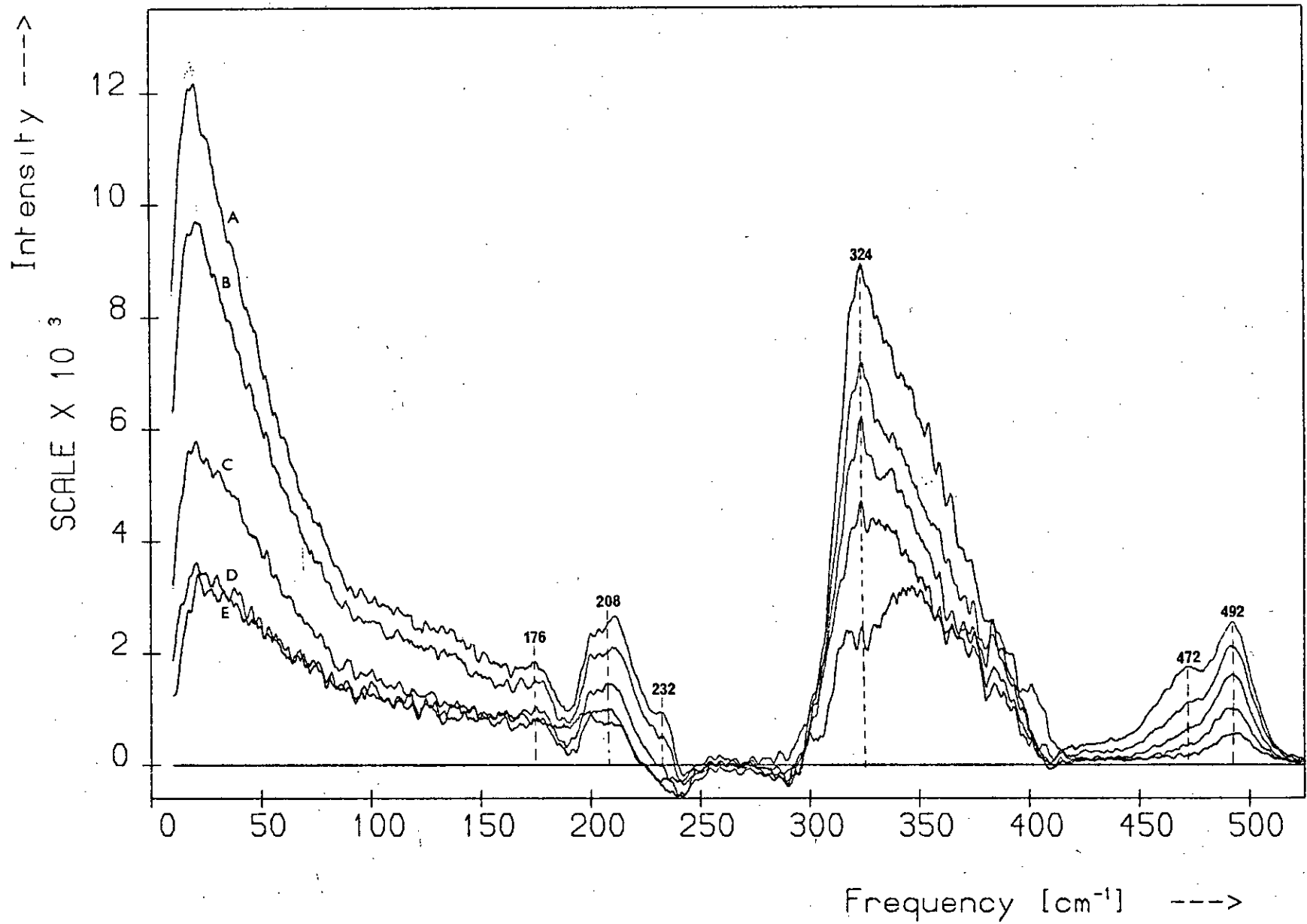
Reduced VV Spectra : $As_{40}S_{60} - As_{35}S_{65}$.
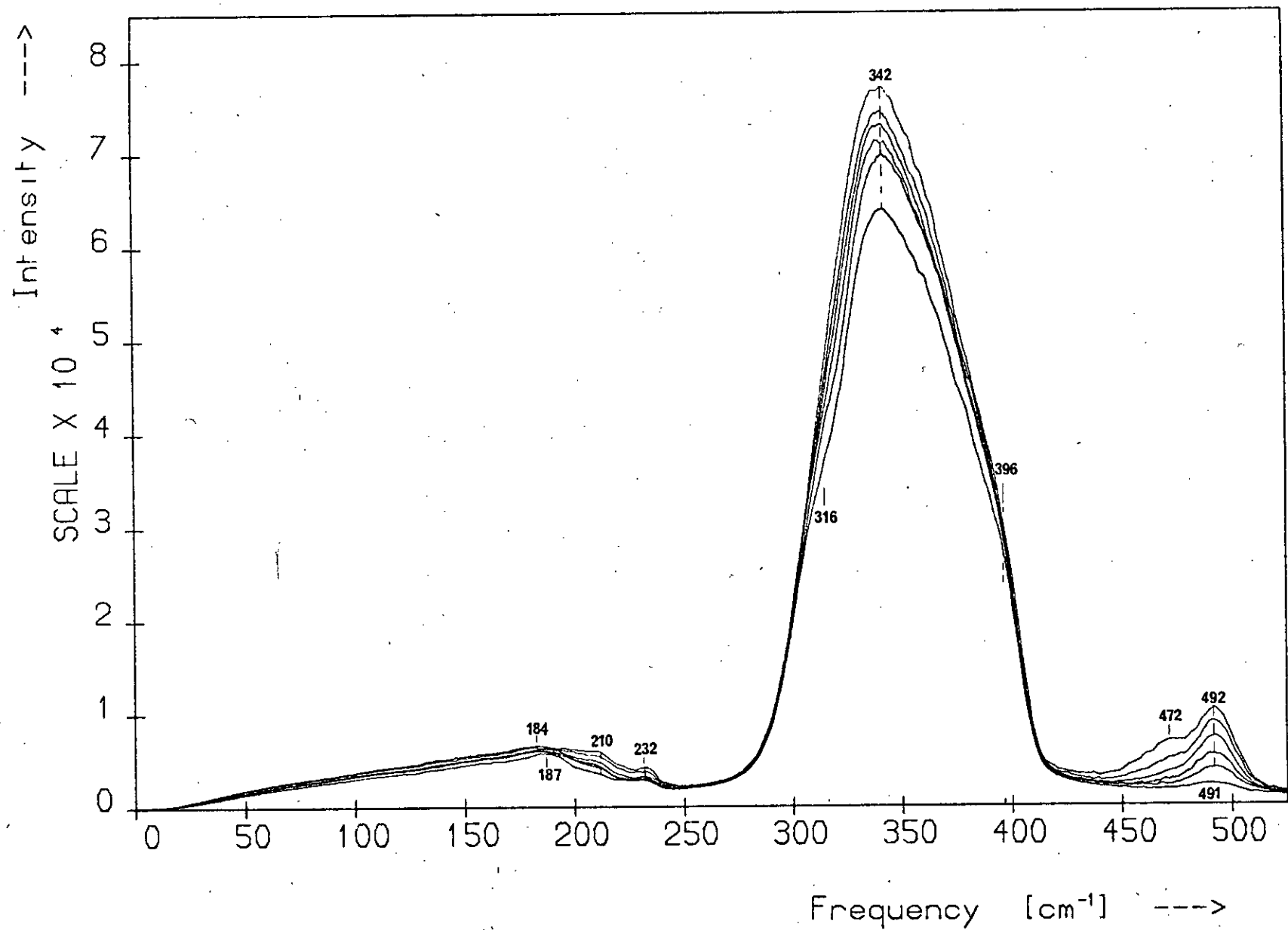
Difference Spectra for the S-Rich Compositions
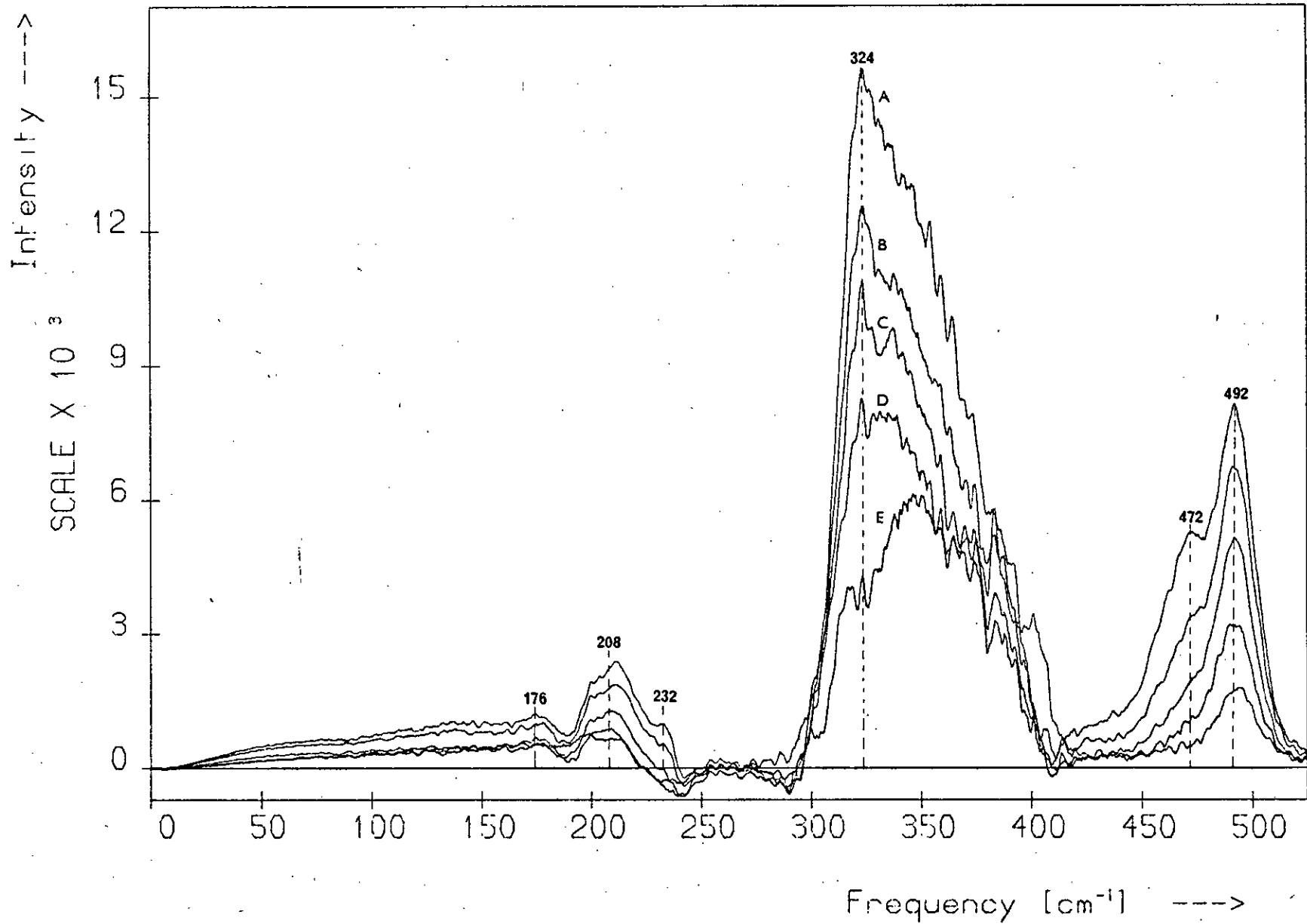
One feature which is significantly different in the VV spectra, however, is the shoulder at ~472 cm^{-1} in the spectra of the two most S-rich glasses. Figure 5.42 is an enlargement of the 440 — 520 cm^{-1} region of the spectra in Figure 5.38 and when compared with Figure 5.36 shows clearly that this feature is more pronounced in the VV spectra than in the polarisation-unanalysed spectra. In fact, when the experimental conditions are improved slightly this feature in the VV spectrum of $As_{35}S_{65}$ is just resolved into a peak at 472 cm^{-1}, as shown in Figure 5.43 where the spectra were recorded using a narrower than normal channel width between data points.

The observed VH-polarised Raman spectra of the compositions $As_{40}S_{60}$ — $As_{35}S_{65}$ are shown in Figure 5.44 and clearly differ considerably from the VV and polarisation-unanalysed spectra. The VH spectra, which are normalised to the intensity of the 315 cm^{-1} peak in the a-$As_{40}S_{60}$ spectrum, are shown here displaced above one another. The VH spectra differ most obviously from the other two types in the shape of the 300 — 400 cm^{-1} band and in the intensity of the thermal peak relative to this band: in the VH spectra the low-frequency peak is much more intense than the 300 — 400 cm^{-1} band, which for the compositions $As_{40}S_{60}$ — $As_{38}S_{62}$ has a peak at 315 cm^{-1} rather than a shoulder. Although the changes produced in the VH spectra by the increasing S content occur over the same frequency regions as they do in the other two sets of spectra, some of the changes are of a slightly different nature. As before, a peak grows at 492 cm^{-1} and a change in profile occurs over the range 160 — 240 cm^{-1}, with a small peak appearing at 232 cm^{-1}. However, in the VH spectra no wing or shoulder develops at 472 cm^{-1} on the high-frequency peak and instead of a disappearing shoulder at 315 cm^{-1} on the main band there is a disappearing peak. As in the case of the polarisation-unanalysed and VV spectra, the low-frequency peak grows relative to the 300 — 400 cm^{-1} band shifts towards the origin. Similar results are obtained with the reduced spectra, shown in Figure 5.47, although
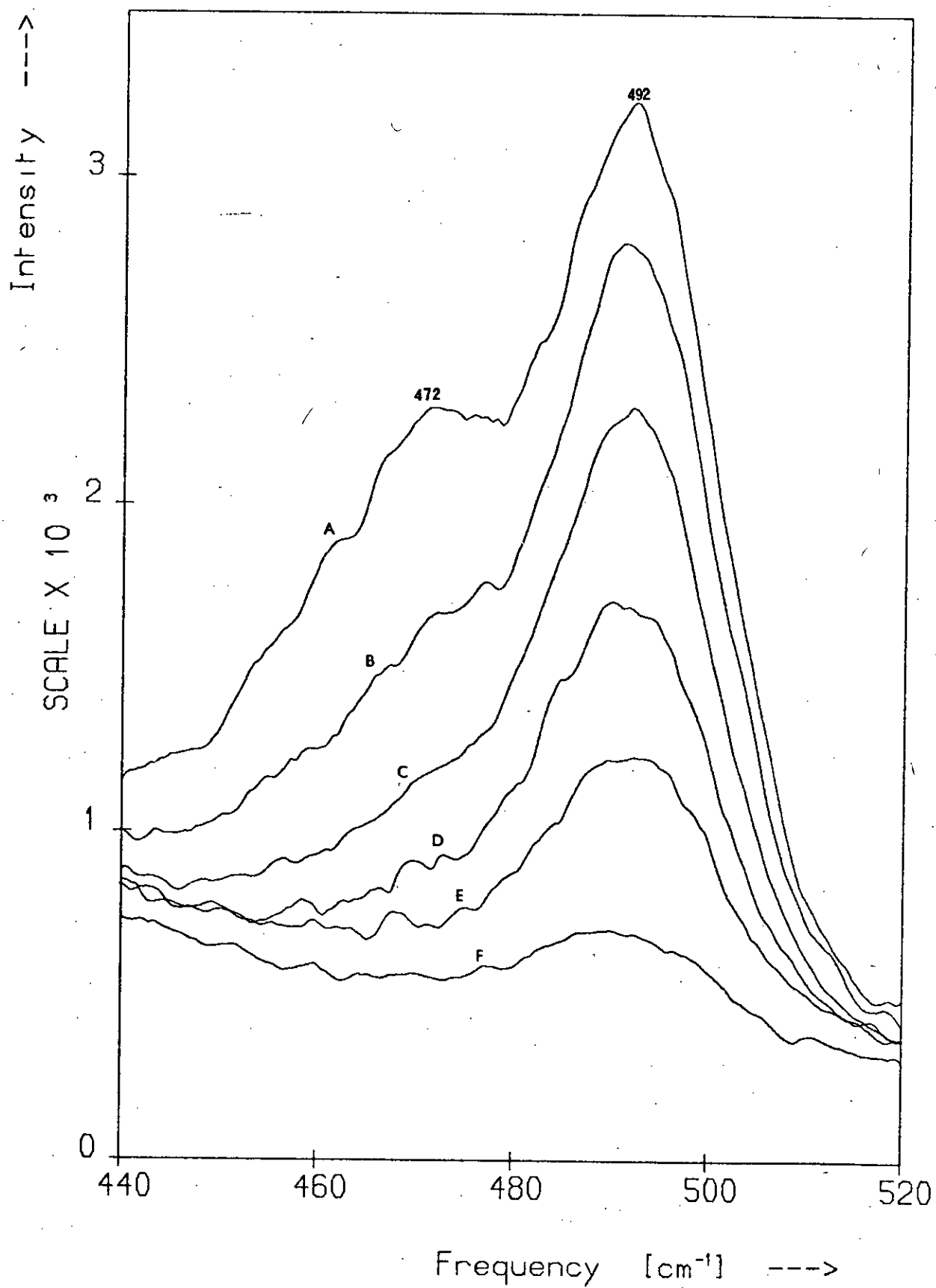
Figure 5.42

The $440 - 520$ cm^{-1} region of the VV-polarised spectra of the compositions $As_{40}S_{60} - As_{35}S_{65}$. The spectra are labelled as in Figure 5.37.

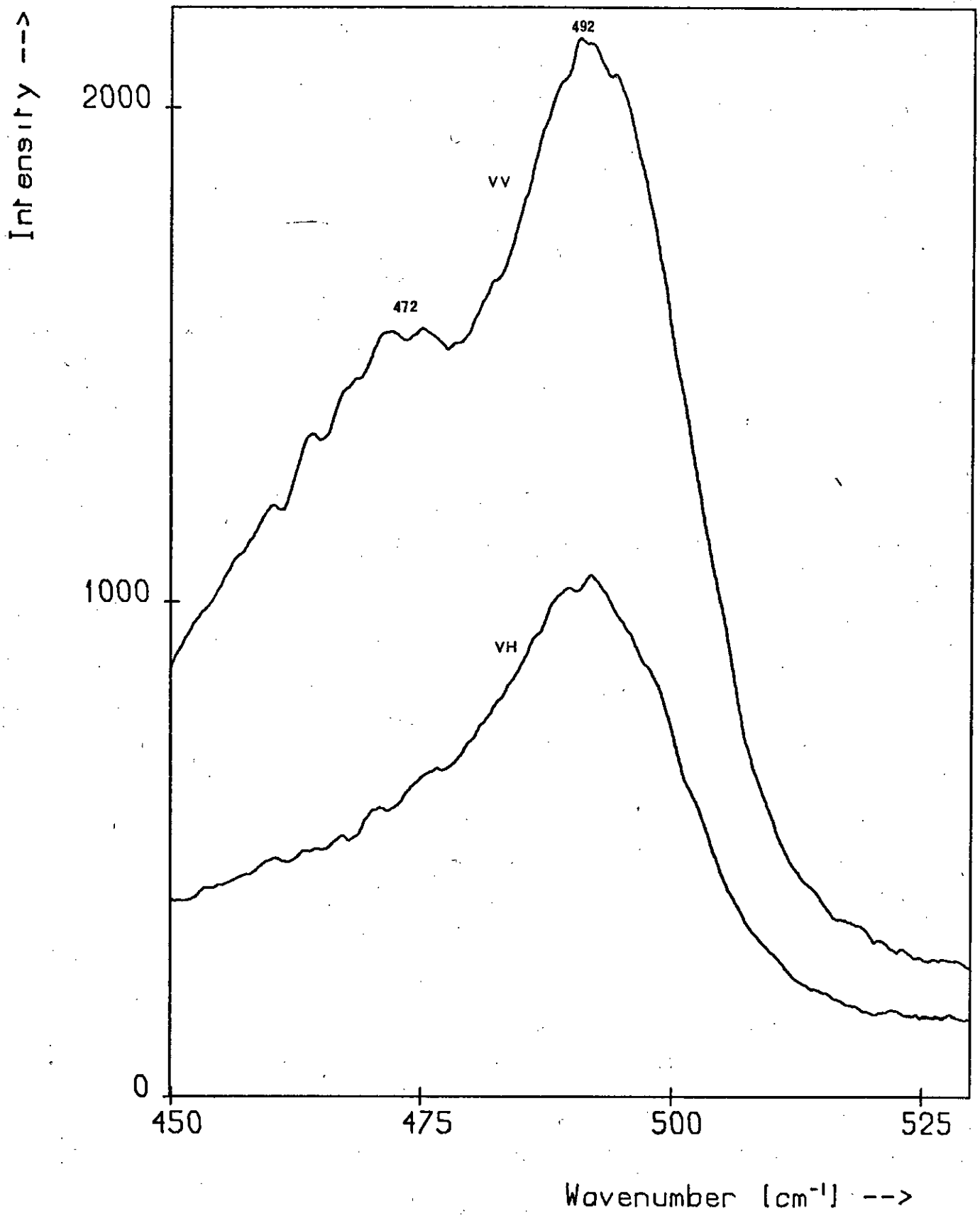## Figure 5.43

The VV and VH spectra of $As_{35}S_{65}$ glass over the range $450 - 530$ cm^{-1} recorded using a channel-width of 0.25 cm^{-1}. The 472 cm^{-1} band is resolved in the VV spectrum.

VV Polarisation Spectra : $As_{40}S_{60}$ – $As_{35}S_{65}$.

Polarisation of the 472 cm^{-1} Band

the thermal peaks are absent in these and the features are shifted slightly to higher frequencies. The reduction process has also transformed the shoulder at 339 cm^{-1} in the unreduced VH spectra into a peak.

The spectral changes are more obvious in Figure 5.45 which shows the unreduced VH spectra normalised by basewidth and superimposed. The intensities of these spectra increase in order of increasing S content. Difference spectra, derived from the spectra of Figure 5.45 by subtracting the a-As$_{40}$S$_{60}$ VH spectrum from each of the others, are displayed in Figure 5.46 and show a series of features growing at 176, 204, 222, 232, 332 and 491 cm^{-1} as the S content increases. Another feature may also be present on the high-frequency side of the highly asymmetric 300 — 400 cm^{-1} band. There is clearly no shoulder at 472 cm^{-1} in these spectra.

The reduced VH spectra are shown normalised by basewidth in Figure 5.47. Comparison with Figure 5.45 shows that corresponding pairs of unreduced and reduced VH spectra exhibit essentially the same set of features, with the exception of the thermal peaks. The transformation of the 339 cm^{-1} shoulder into a peak as a result of the reduction process is obvious in Figure 5.47. Difference spectra, derived from the reduced VH spectra in the standard way, are displayed in Figure 5.48 and, apart from the absence of the low-frequency peak, they are similar to those of Figure 5.46, although their features have different relative intensities.

The results shown in Figure 5.43, which compares the 450 — 530 cm^{-1} regions of the VV and VH spectra of the most S-rich composition, As$_{35}$S$_{65}$, are not enlargements taken from other spectra but were recorded in a separate experiment using a channel width equal to half of that normally used. The 472 cm^{-1} feature is just resolved into a peak in the VV spectrum but is completely absent in the VH spectrum, indicating that this vibration is strongly polarised. The depolarisation ratio at 472 cm^{-1} is ~0.4.

The depolarisation spectra for the compositions As$_{40}$S$_{60}$ — As$_{35}$S$_{65}$ are

Figure 5.44

The VH-polarised Raman spectra of the compositions $As_{40}S_{60} - As_{35}S_{65}$.

Spectrum	Composition
A	$As_{35}S_{65}$
B	$As_{36}S_{64}$
C	$As_{37}S_{63}$
D	$As_{38}S_{62}$
E	$As_{39}S_{61}$
F	$As_{40}S_{60}$

Figure 5.45

The spectra of Figure 5.44 normalised by basewidth (A — F as above).

Figure 5.46

The difference spectra obtained from the spectra of Figure 5.45.

Spectrum	Composition
A	$As_{35}S_{65} - As_{40}S_{60}$
B	$As_{36}S_{64} - As_{40}S_{60}$
C	$As_{37}S_{63} - As_{40}S_{60}$
D	$As_{38}S_{62} - As_{40}S_{60}$
E	$As_{39}S_{61} - As_{40}S_{60}$

Figure 5.47

The reduced spectra corresponding to those in Figure 5.45.

Figure 5.48

The difference spectra obtained from the spectra of Figure 5.47. The spectra are labelled as in Figure 5.46.

VH Polarisation Spectra : $As_{40}S_{60} - As_{35}S_{65}$.
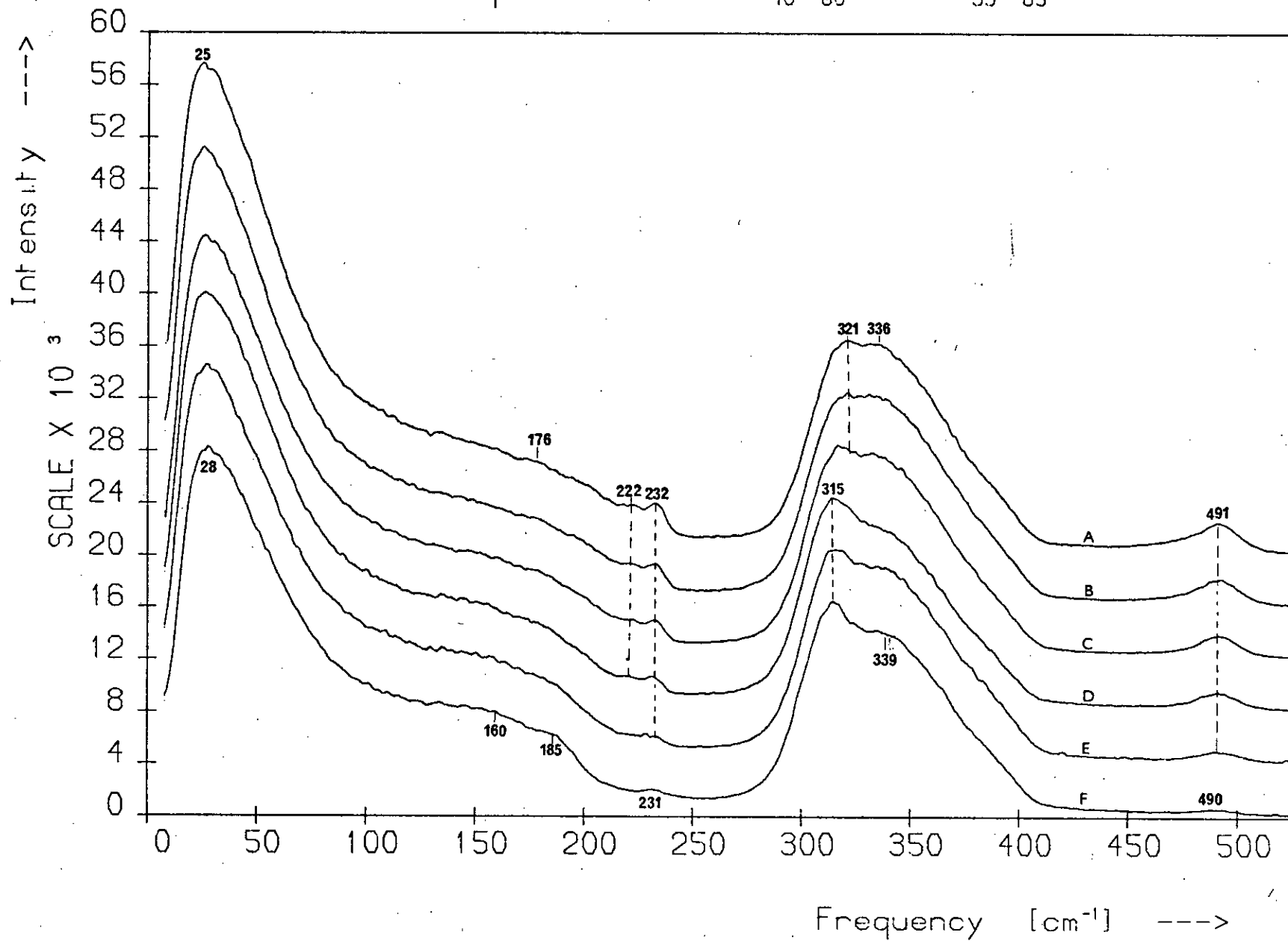
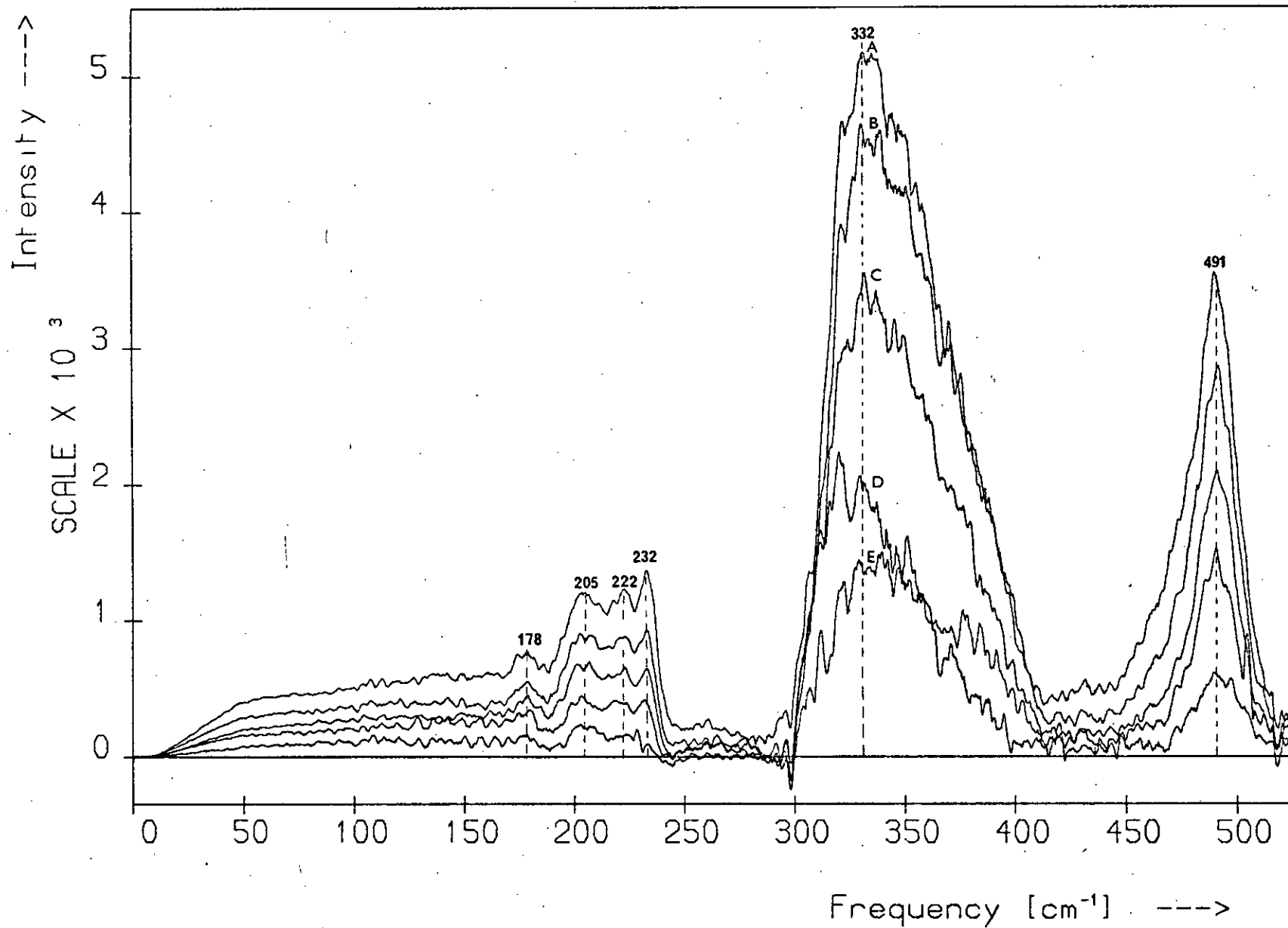VH Polarisation Spectra : $As_{40}S_{60} - As_{35}S_{65}$.
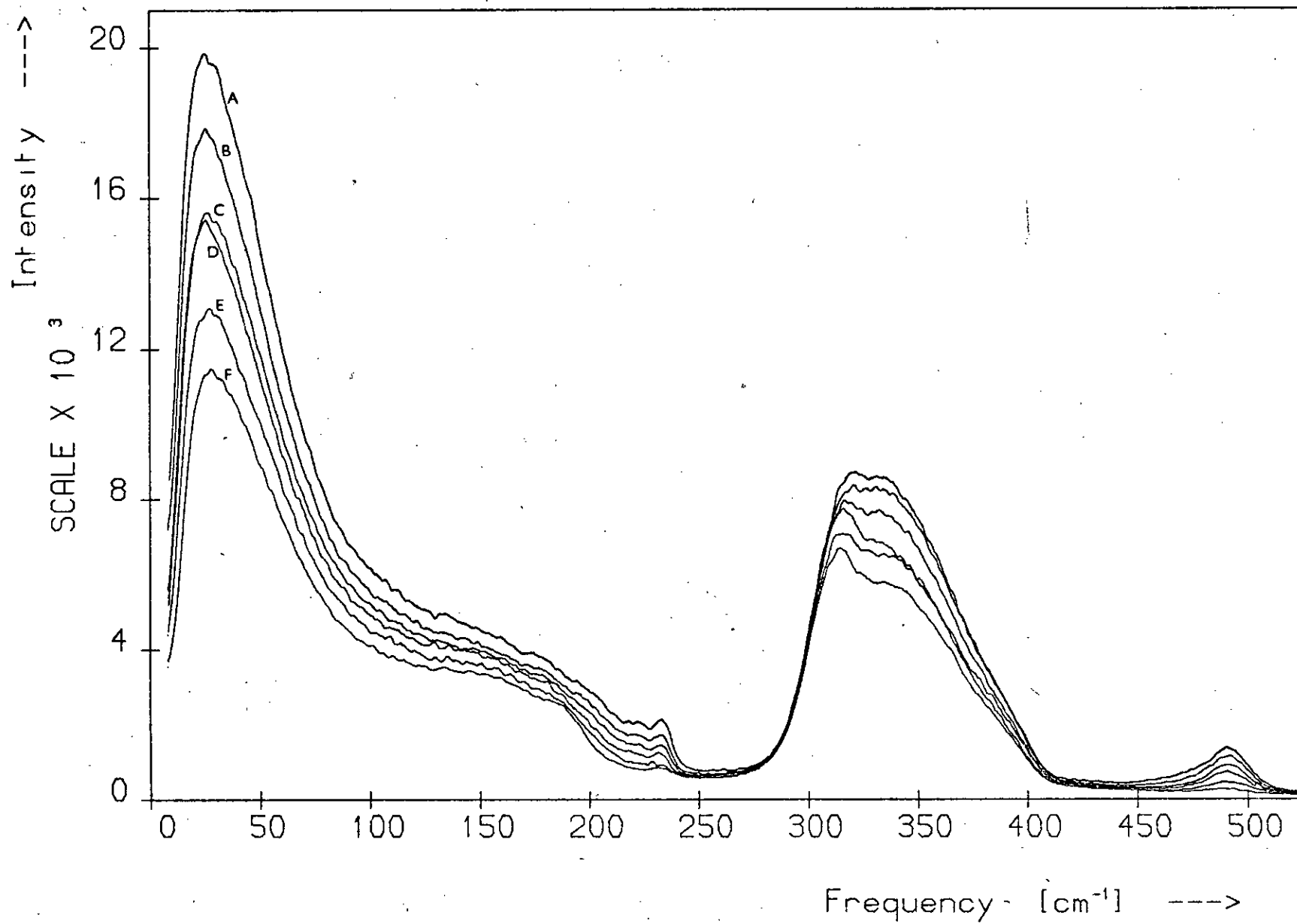
Difference Spectra for the S-Rich Compositions
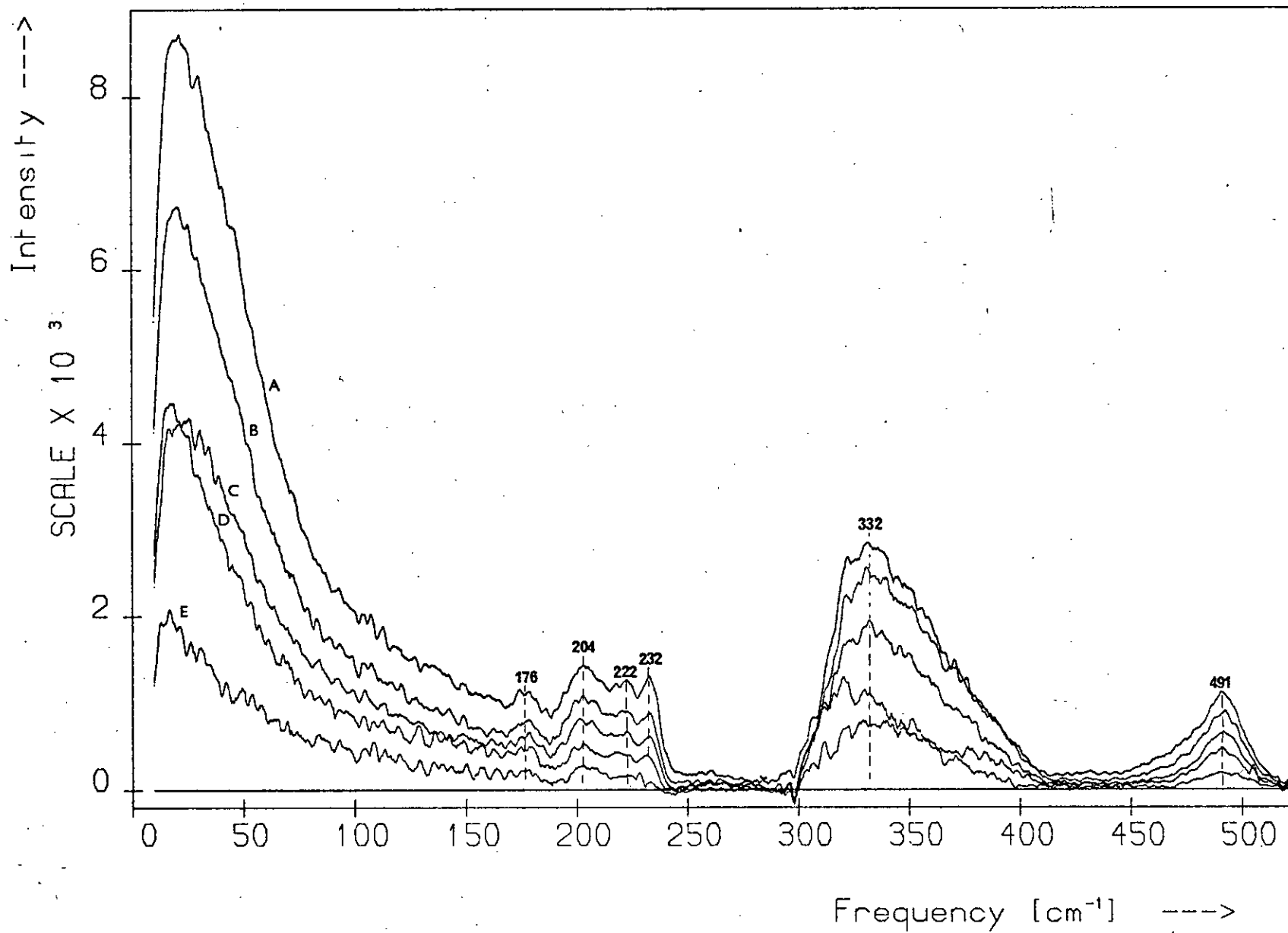
Reduced VH Spectra : $As_{40}S_{60} - As_{35}S_{65}$.
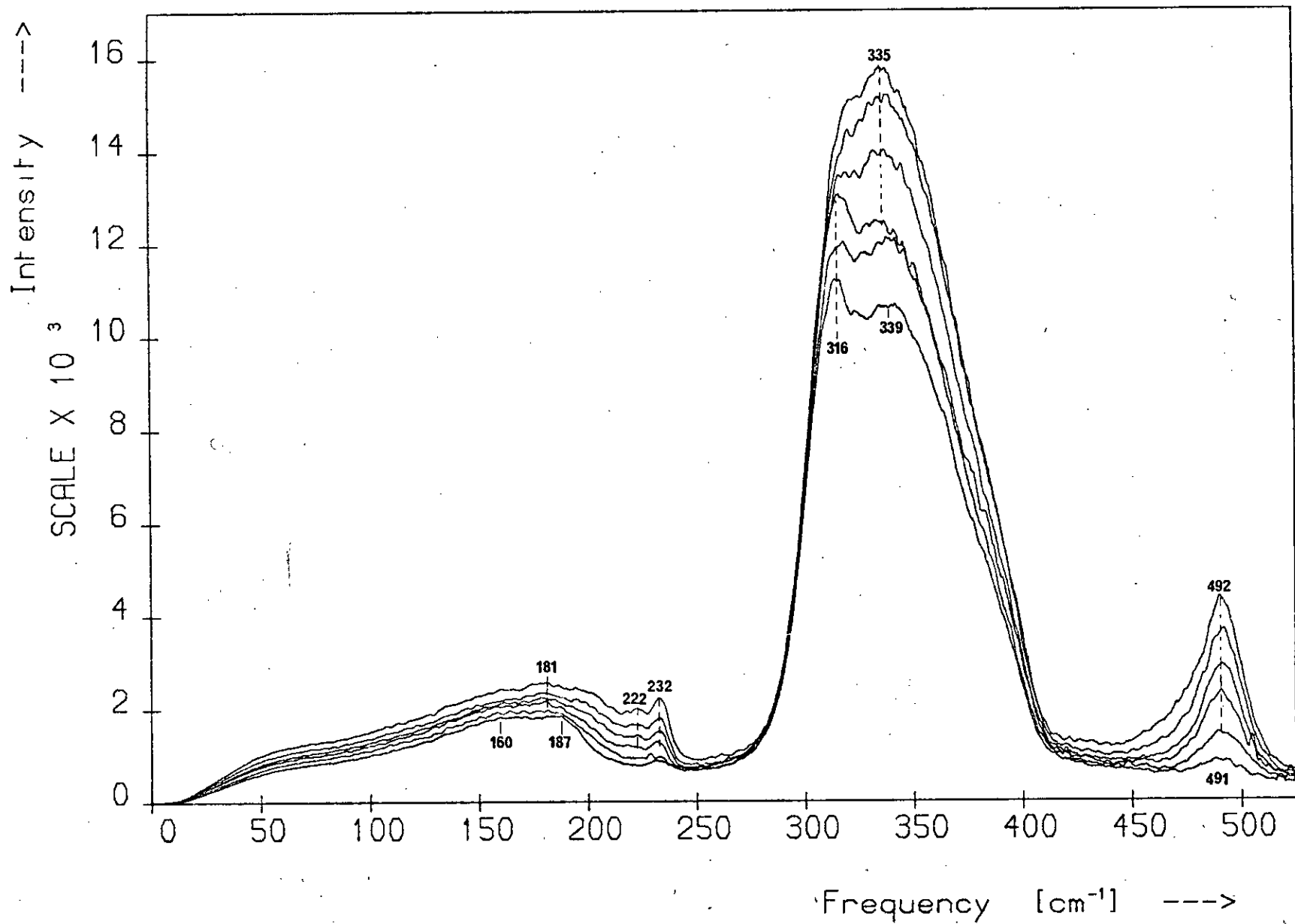
Difference Spectra for the S-Rich Compositions

shown in Figure 5.49. For clarity they have been displaced vertically in order of increasing S content. The spectra are similar in many respects: they all decrease initially to a minimum around ~106 cm^{-1} and they all have a broad peak at ~160 cm^{-1} and a well-defined trough with a sloping bottom at ~300 − 425 cm^{-1}. Dips at 211, 400 and 500 cm^{-1} are present in each spectrum. As the S content increases, however, several changes occur in the spectra relative to the a-As$_{40}$S$_{60}$ spectrum, the most obvious being the growth of a peak and other structure in the region 210 − 240 cm^{-1}. The broad peak at ~160 cm^{-1} becomes flatter, a peak grows at 233 cm^{-1} and dips appear at 226 and 467 cm^{-1}.

The incident laser beam is partly depolarised on traversing the samples because of their imperfect optical quality and thus the polarisation measurements are only qualitatively correct[75]. It was found that when the depolarisation spectra were superimposed they did not change in a completely ordered way with increasing S content and since the spectra do not require normalising these discrepancies must arise from experimental effects. The frequencies of some of the features in the depolarisation spectra do not coincide exactly with features in the Raman spectra; in some cases, such as that of the 492 cm^{-1} band, this is due to weak signal but in others, e.g. the 395 cm^{-1} knee, it probably arises from overlapping of bands.

Although the depolarisation spectra have the advantage that when recorded from samples of good optical quality they do not require normalisation, they are of limited use in showing up spectral changes, for while the intensity of a Raman band may change as the population of the associated structural element changes, its depolarisation ratio remains constant. For example, though the population of AsS$_3$ pyramids decreases relative to the S atom population as the S content of the glasses increases, the depolarisation ratios of the four pyramidal vibrations will not change. The only circumstances that will give rise to changes in the depolarisation
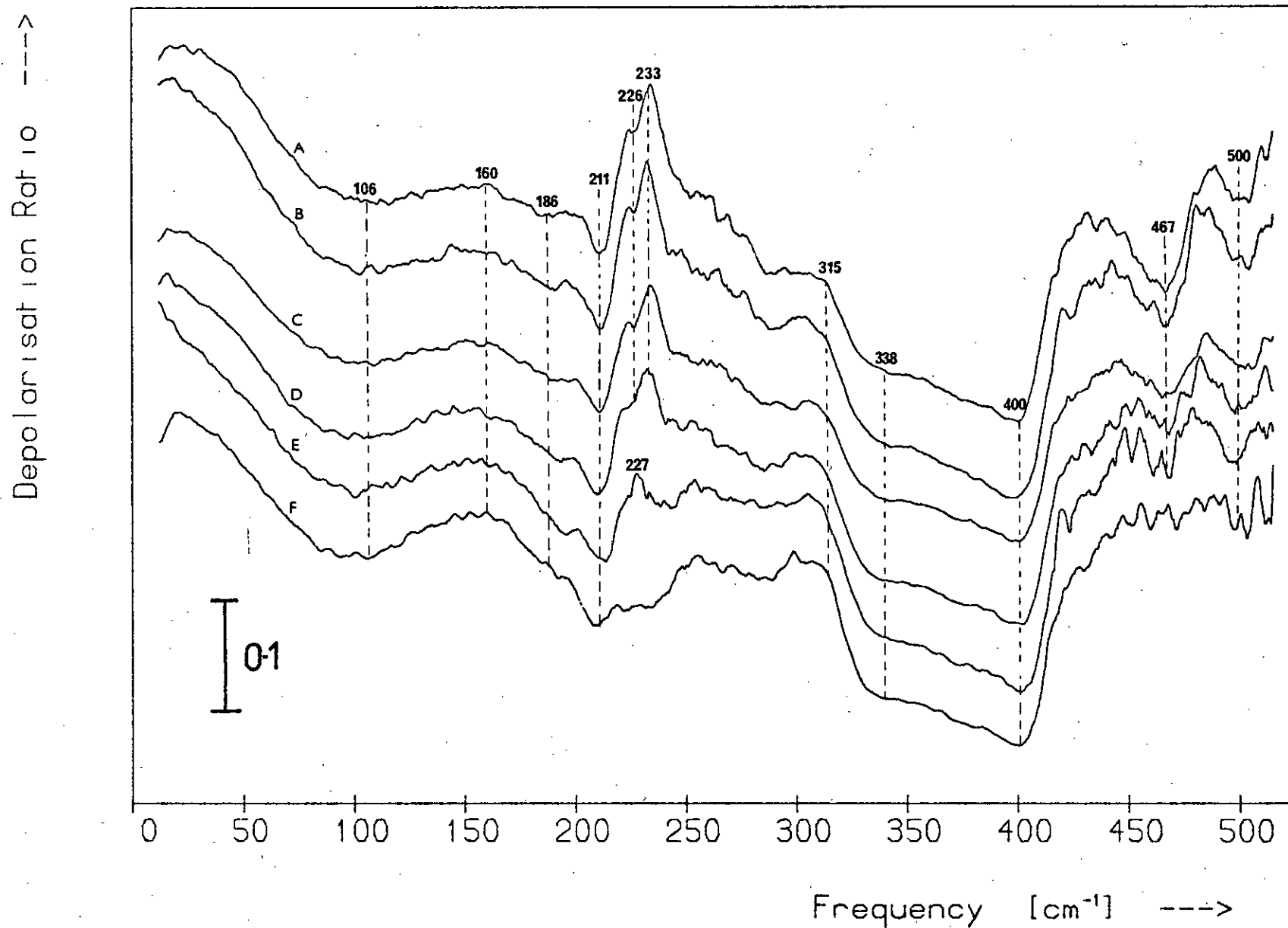
Figure 5.49

Depolarisation spectra of the compositions $As_{40}S_{60} - As_{35}S_{65}$.

Spectrum		Composition
A	—	$As_{35}S_{65}$
B	—	$As_{36}S_{64}$
C	—	$As_{37}S_{63}$
D	—	$As_{38}S_{62}$
E	—	$As_{39}S_{61}$
F	—	$As_{40}S_{60}$

Depolarisation Spectra : $As_{40}S_{60} - As_{35}S_{65}$.

spectra are the occurrence in the Raman spectra of shifting bands or of overlapping bands whose intensities are changing at different rates, though in the latter case no changes will be observed if the bands have the same depolarisation ratio. Should the changes in the environment of a species of 'molecule' affect the depolarisation ratios of its vibrations then corresponding changes will, of course, be observed in the depolarisation spectra. Discontinuous changes will occur when a fading band is on the point of disappearing completely or when a new band, e.g. that at 492 cm^{-1}, is just appearing — once it is established no change should occur unless any of the above circumstances are prevailing. The main use of the depolarisation spectra is in revealing hidden vibrations in the Raman spectra and helping in relating the bands to structural features in the glasses.
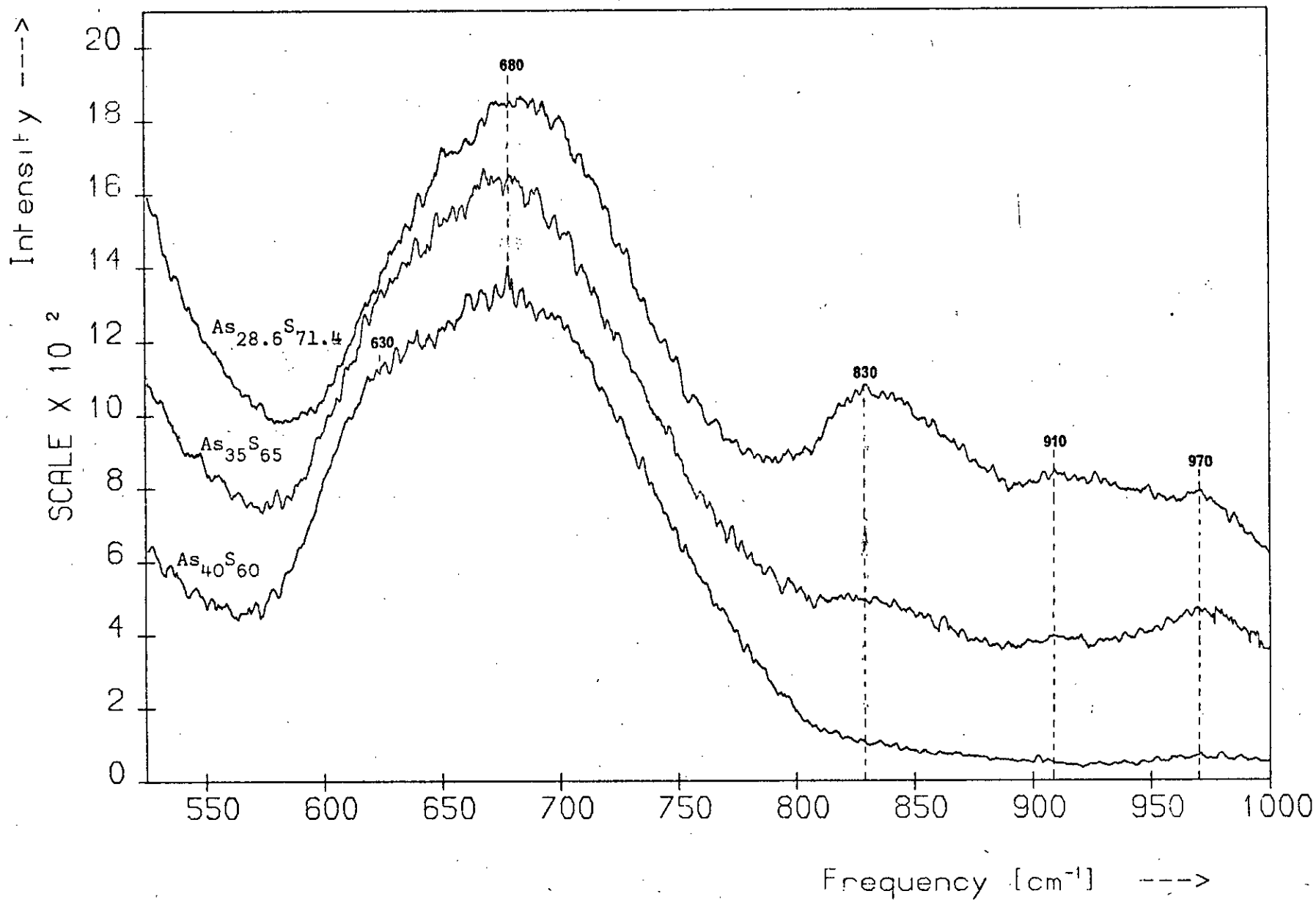
5.5.1.4 Second-order spectra

In order to confirm that the first-order spectra of these glasses lie entirely below 500 cm^{-1} the spectral regions beyond this frequency were, in a number of cases, examined for any additional features. Although structure was, in fact, observed above 500 cm^{-1} in these experiments it could be satisfactorily accounted for as overtones or combinations of first-order bands and there was no sign of any features that could be definitely attributed to first-order processes.

Figure 5.50 shows the 500 — 1000 cm^{-1} region of the a-$As_{40}S_{60}$, $As_{35}S_{65}$ and $As_{28.6}S_{71.4}$ (As_2S_5) spectra. The results have not been normalised in any way and are shown superimposed. The bands are relatively weak, having peak intensities ~0.1 of those of the corresponding main first-order bands, and are situated between the frequencies 600 and 1000 cm^{-1}, which are double the frequencies that bound the strongest first-order bands, i.e. 300 and 500 cm^{-1}. All the features in these spectra can be attributed to overtones or combinations of bands contained in the 300 — 500 cm^{-1} region of the corresponding first-order spectra, e.g. 630 = 2 x 315, 680 ≈ 2 x 339[76].

Figure 5.50

Second-order Raman spectra of the compositions $As_{40}S_{60}$, $As_{35}S_{65}$ and $As_{71.4}S_{28.6}$ (As_2S_5).

Second-Order Spectra

Plot showing Intensity (SCALE X 10², Intensity ---->) versus Frequency [cm⁻¹] for three curves labeled As$_{28.6}$S$_{71.4}$, As$_{35}$S$_{65}$, and As$_{40}$S$_{60}$. Peaks marked at 630, 680, 830, 910, and 970.

The results for a-As$_{40}$S$_{60}$ are in general agreement with those obtained by Howard et al.[44,77] who, on the basis of both i.r. and Raman studies of this spectral region, also attribute these bands to multiphonon effects. It can thus be concluded that the spectra of Figure 5.50 are simply the second-order spectra of the glasses.

Although there is no band at ~710 cm^{-1} in the a-As$_{40}$S$_{60}$ spectrum of Figure 5.50 whereas there is in the Raman data of Howard et al., this may be due to the fact that these authors excite their spectra with 5145 Å (2.41 eV) radiation. This was the wavelength used to excite the resonance spectrum in Figure 5.28 and it is significant that in the Raman experiments of Howard et al., as the sample temperature decreases (and therefore as the a-As$_{40}$S$_{60}$ band gap approaches 2.41 eV), the 710 cm^{-1} peak grows along with the 235 cm^{-1} band and a broad weak feature at 485 cm^{-1}. This effect is possibly similar to the multiple excitation effect observed in crystalline semiconductors at resonance[78] and the 485 and 710 cm^{-1} lines may simply be overtones of the resonating 235 cm^{-1} band (2 x 235 = 470, 3 x 235 = 705). If the 710 cm^{-1} shoulder in the a-As$_{40}$S$_{60}$ spectrum of Howard et al. cannot be attributed to a resonance effect it may be further evidence for the presence of the hidden vibrational mode on the high-frequency side of the main band since the frequency is double 355 cm^{-1}; the frequency deduced in Section 5.4.3 for the hidden band was 367 cm^{-1}.

Markov and Reshetnyak[8] also report a band at 680 cm^{-1} in the a-As$_{40}$S$_{60}$ spectrum and attribute it to an overtone of the main first-order band.

5.5.1.5 Discussion

There are four possible explanations of the results presented in Sections 5.5.1.2 and 5.5.1.3. The spectral changes described in these sections can be attributed to one or more of the following processes which

might occur as the S content of the glasses is increased:

(i) the appearance of some form(s) of elemental sulphur in the glasses;

(ii) the disappearance of features of the a-$As_{40}S_{60}$ structure, such as AsS_3 pyramids, As—As bonds or As—S—As bridges;

(iii) the formation of new features in the network e.g. the incorporation of sulphur chains between As atoms to give As_2S_n 'molecules', n = 2,3,...;

(iv) the distortion of the a-$As_{40}S_{60}$ structure as a result of the other three processes.

These processes are discussed separately below, starting with the last case.

5.5.1.5.1 Geometrical changes

Shifts in the bond-length or bond-angle distributions of a-$As_{40}S_{60}$ caused by the addition of S atoms are more likely to give rise to frequency shifts in the Raman spectra, rather than growing bands such as the one at 492 cm^{-1}, and hence can only account for some of the spectral changes. It was mentioned in Section 5.5.1.1 that when the Raman data was normalised by the maximum intensity of the 300 — 400 cm^{-1} peak it yielded difference spectra that could best be interpreted as evidence that the 315 and 338 cm^{-1} bands shifted towards one another as the S content increased. (It is unlikely that geometrical changes alone are responsible for the spectral changes in this region since the calculations of Section 5.5.1.5.4, which are necessary to account for the 492 cm^{-1} peak, suggest that new bands are growing here.) When the appropriate values for the AsS_3 pyramids are inserted, it can be shown from Equations A.1 — A.4 that while a change in the length (and hence in the stretching force constant) of the As—S bond will not lead to this behaviour, the frequencies ν_3 and ν_1, which correspond to the 315 and 338 cm^{-1} bands respectively, do converge if the pyramid angle, β, increases. This is illustrated in Figure 5.51 which shows the frequency variation of

Figure 5.51

The effect of changes in the pyramid angle β on the frequencies ν_1 and ν_3 of the AsS$_3$ pyramid.   (Courtesy of Dr. M.J.Sik.)
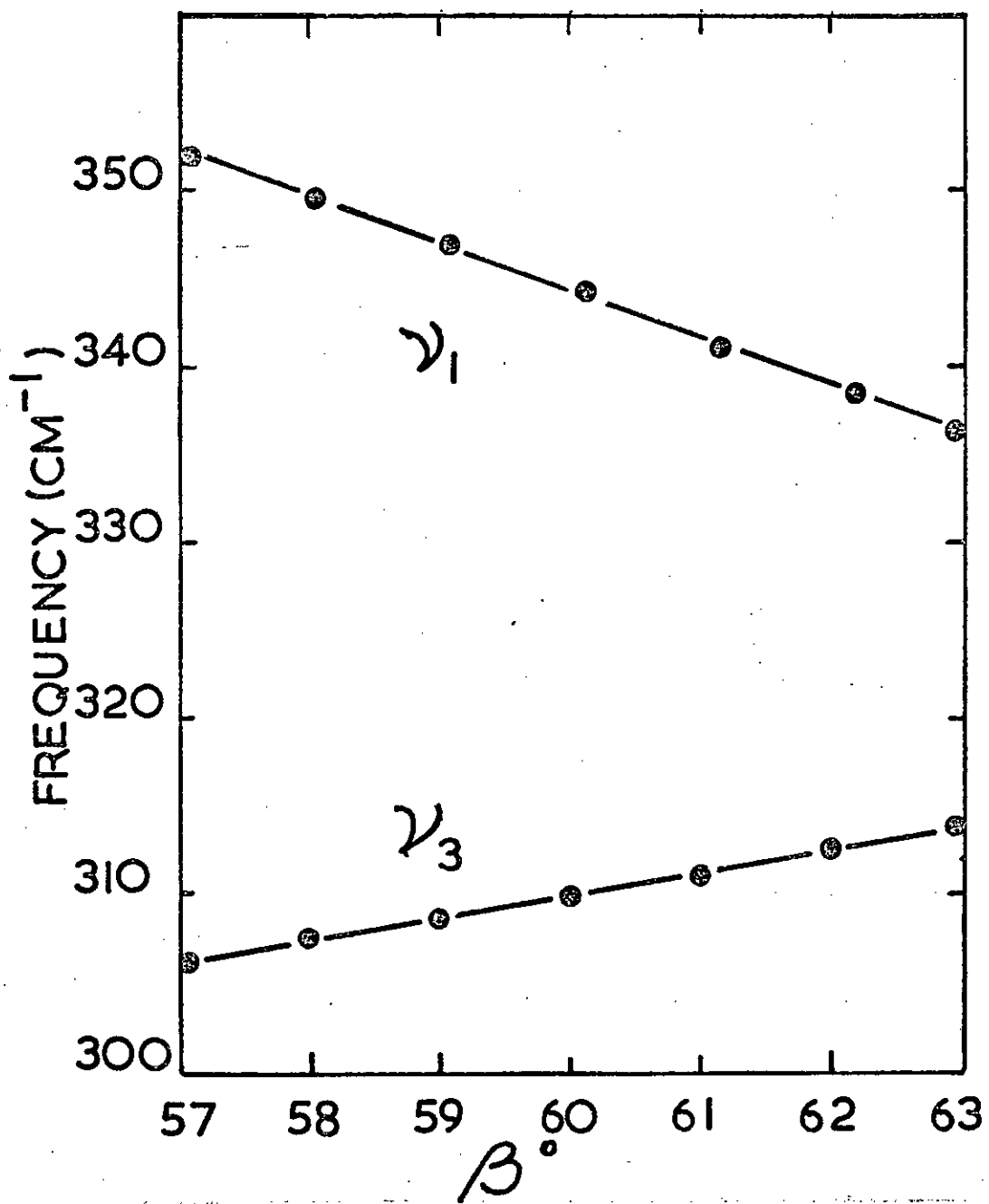
the ν_1 and ν_3 modes as a function of β for the values of k_1 and k_δ shown; for a-$As_{40}S_{60}$ $\beta \approx 61^{\circ}$. However, analysis of the VH-polarised spectra of the compositions $As_{40}S_{60} - As_{37}S_{63}$ shows that as the S content increases there is no shift in the frequency of the ν_3 mode, which is present in these spectra as a well-defined peak (see Figures 5.45 and 5.47). Indeed, none of the features in any of the a-$As_{40}S_{60}$ spectra shifts with the increase in S content, apart from the boson peak. Thus significant general distortions of the geometry of the a-$As_{40}S_{60}$ network do not occur.

5.5.1.5.2 The presence of sulphur allotropes

The most obvious explanation of the spectral changes is that as the S content of the glasses is increased the additional sulphur does not combine in any way with the a-$As_{40}S_{60}$ structure but exists alongside. it in the form of pure sulphur allotropes. There is no evidence of phase separation in these glasses, unlike the case of the As-rich compositions, and their optical properties are those of a homogeneous system[79] so the size of individual pure-sulphur regions, if they occur, is not large.

Over 30 solid allotropes of sulphur have been reported[80] though only one form, orthorhombic sulphur (α-S_8), is thermodynamically stable at room temperature and pressure. The other allotropes exist only under non-standard conditions and eventually revert to α-S_8 as the temperature and pressure of their environment approach room conditions. The allotropes are all made up of either rings or unbranched chains that are weakly bound to each other by van der Waals forces.

In their dissolution experiments Tsuchihashi and Kawamoto[81] established the presence of S_8 rings in As-S glasses more S-rich than $As_2S_{8-9.5}$ ($As_{20}S_{80} - As_{17.4}S_{82.6}$) but did not detect any in compositions with less sulphur than this. In the present study similar experiments carried out on the compositions $As_{40}S_{60}$ and $As_{35}S_{65}$ also failed to detect S_8 rings. However, Ward's work[1,2] and the results of Section 5.5.2

show that S_8 rings are certainly present in those glasses more S-rich than $As_{29}S_{71}$ and suggest that they are present at even smaller S concentrations. Figures 5.55 — 5.60 (after p.168) show that as the S content is increased beyond 65 at.% the features at 472, 232 and 222 cm^{-1} in the $As_{35}S_{65}$ spectrum grow rapidly and overtake the other emerging bands. The figures also show that the Raman spectrum of $\alpha-S_8$ contains bands very near these frequencies. Ozin[24] has shown that the 248 cm^{-1} band in $\alpha-S_8$ is depolarised while the 221 and 473 cm^{-1} bands, which arise from totally symmetric modes, are polarised, the 473 cm^{-1} band more strongly than the other. It is seen in Figure 5.49 that the corresponding bands in the $As_{35}S_{65}$ spectrum have the $\alpha-S_8$ polarisation properties, the 233 cm^{-1} feature having almost the largest depolarisation ratio in the spectrum while the 222 and 472 cm^{-1} bands both give rise to dips. It is due to its strongly polarised nature that the 472 cm^{-1} feature is resolved into a peak in the VV spectrum (see Figure 5.42). As geometrical changes or the disappearance or appearance of network features cannot account for these particular spectral changes and as it is shown below that the glasses do not contain significant amounts of the other allotropes, these three growing features can be attributed to the increasing presence of S_8 rings. It can thus be concluded that S_8 rings occur in all the glasses more S-rich than $As_{37}S_{63}$, since these features are first detectable in the Raman spectrum of this composition, and judging by the depolarisation spectra, S_8 rings may even be present, though in very small amounts, for glasses less S-rich than this — the structure characteristic of S_8 rings is also observable in the depolarisation spectra of the compositions $As_{39}S_{61}$ — $As_{37}S_{63}$.

The failure of the dissolution experiments to detect the S_8 rings in glasses less S-rich than approximately As_2S_8 is probably due to the fact that $a-As_{40}S_{60}$ is insoluble in CS_2, which was the solvent used in these experiments, so that the S_8 rings in the bulk are trapped.

The presence or absence of any other S allotrope in the glasses can similarly be determined by comparing its vibrational spectrum with the glass spectra[82 – 84]. The Raman spectra of the following cyclic forms were compared with the glass spectra: β-monoclinic S[85] (this is also made up of S_8 rings), hexasulphur (S_6)[86], cycloheptasulphur (S_7)[87] and cyclododecasulphur (S_{12})[88]. It was concluded from this comparison that β-monoclinic S and S_6, S_7 and S_{12} rings are not present in appreciable quantities in these glasses. The vibrational spectra of other cyclic forms have not yet been recorded but Steudel[89] has carried out a theoretical analysis of the vibrational spectra of the cyclic S_n molecules. Comparison of the As-S spectra with his results suggests that other ring species are also absent from these glasses.

In addition to rings, S atoms can form unbranched chains of up to 10^5 atoms in length[80]. The glass spectra were compared with the Raman spectra of the following polymeric S allotropes: purple sulphur[90,91], fibrous sulphur[92], sublimed sulphur[2] and 'crystex'[2], in which the chains are stabilised by organic substituents. They were also compared with the Raman spectrum of the S_2 diradical[93] and the calculated vibrational frequencies of the linear S_4 molecule[94]. The comparisons indicated that there are no appreciable quantities of either long or short S_n chains in these glasses.

It can thus be concluded that the only form of sulphur present in the glasses is the S_8 ring, which is as expected since this is the basic unit of the only allotrope thermodynamically stable at room temperature and pressure.

5.5.1.5.3 Disappearing features

As was seen in Section 5.4.5, the features of the a-$As_{40}S_{60}$ structure are AsS_3 pyramids, As_2S bridges, As—As bonds and S—S bonds. Spectral changes due to the disappearance of these features will only be observed

in the normalised results if the <u>ratio</u> of the populations changes, i.e.
if some of these structural elements are disappearing faster than others.
This explanation of the spectral changes is limited because it cannot
account for bands which are definitely growing in the spectra, such as
the 492 cm^{-1} band.   It is also unable to account for different changes
occurring in spectral features associated with the same structural element
since such features would be expected to decrease in intensity at the same
rate; thus the change occurring on the low-frequency side of the main
band cannot be attributed to this process, for the 315 and 338 cm^{-1} bands
are both associated with the AsS$_3$ 'molecule'.

It will be shown in the following section that the number of S—S
bonds in the network does in fact increase as the S content is increased
so they need not be considered in this section.   The increase in the
number of S—S bonds in the network should lead to a change in the ratio
of AsS$_3$ pyramids to As$_2$S bridges, for the latter are being replaced by
As—S—S—As links; however, the spectral changes arising from the change
in this ratio are difficult to assess because the AsS$_3$ and As$_2$S bands
occur in regions where spectral changes due to other processes are
occurring.

As—As bonds give rise to only one feature in the a-As$_{40}$S$_{60}$ spectrum,
namely the weak band at ~231 cm^{-1}.   Figure 5.32 shows that little change
seems to occur in this region with increasing S content apart from the
appearance of a peak at 232 cm^{-1} in the more S-rich compositions.   It
was seen in the previous section that this peak can be attributed to the
appearance of S$_8$ rings in the glasses.   However, the region of the
depolarisation spectra (Figure 5.49) around 230 cm^{-1} changes markedly
and rapidly as a function of S content.   A considerable change in profile
around 230 cm^{-1} occurs even on increasing the S content from 60 to 61 at.%.
The depolarisation spectrum of a-As$_{40}$S$_{60}$ contains a dip at ~231 cm^{-1} but
this is absent for the other compositions.   As the S content increases

a peak grows rapidly at 233 cm^{-1} in the depolarisation spectra. In Section 5.5.1.3 it was remarked that structural features that are disappearing or newly appearing will only give rise to changes in the depolarisation spectrum when they are on the verge of disappearing or have just appeared. In the previous section the peak at 233 cm^{-1} in the depolarisation spectra was associated with the depolarised 248 cm^{-1} band of the S_8 ring which is starting to appear in the glasses. It is possible that the marked change around 230 cm^{-1} in the depolarisation spectra of these first few S-rich compositions may be partly due to the rapid disappearance of the As—As bonds and the predominantly VV-polarised scatter they give rise to at this frequency. The polarisation-unanalysed spectra show no noticeable change in intensity over the region 225 — 240 cm^{-1}, with increasing S content, since the reduced contribution from As—As bonds is compensated by the growth of the S_8 band but as the S_8 and As—As bands have different polarisation properties this substitution is revealed in the depolarisation spectra.

Further evidence for the disappearance of As—As bonds from the matrix is furnished by Figure 5.52 which compares two spectra recorded by back reflection from a sample of $As_{35}S_{65}$ glass, one being excited by 5145 Å radiation and the other by 6328 Å radiation. Comparing this with Figure 5.28, which was obtained in a similar experiment, it is clear that there is no resonance of the 231 cm^{-1} feature in the $As_{35}S_{65}$ spectrum excited with band-gap radiation. This absence of resonance cannot be attributed to the compositional shift in the absorption edge[79] since the optical gap of $As_{35}S_{65}$ glass is closer to the incident photon energy than is the optical gap of a-$As_{40}S_{60}$. The non-resonance of this feature in the $As_{35}S_{65}$ spectrum can be accounted for if there are no longer any As—As bonds in the matrix so that the feature is due solely to S_8 rings.

The absence of significant quantities of As—As bonds in the S-rich glasses is consistent with the chemically ordered network model for the

Figure 5.52

Raman spectra of the glass $As_{35}S_{65}$: one was excited with near band-gap radiation (λ_{exc}= 5145 Å) and the other with 6328 Å radiation, which is weakly absorbed.

THE RAMAN SPECTRUM OF As$_{35}$S$_{65}$ GLASS

INTENSITY

SCALE X 10^4

λ_{exc}= 6328Å

λ_{exc}= 5145Å

Frequency (cm^{-1}) -->
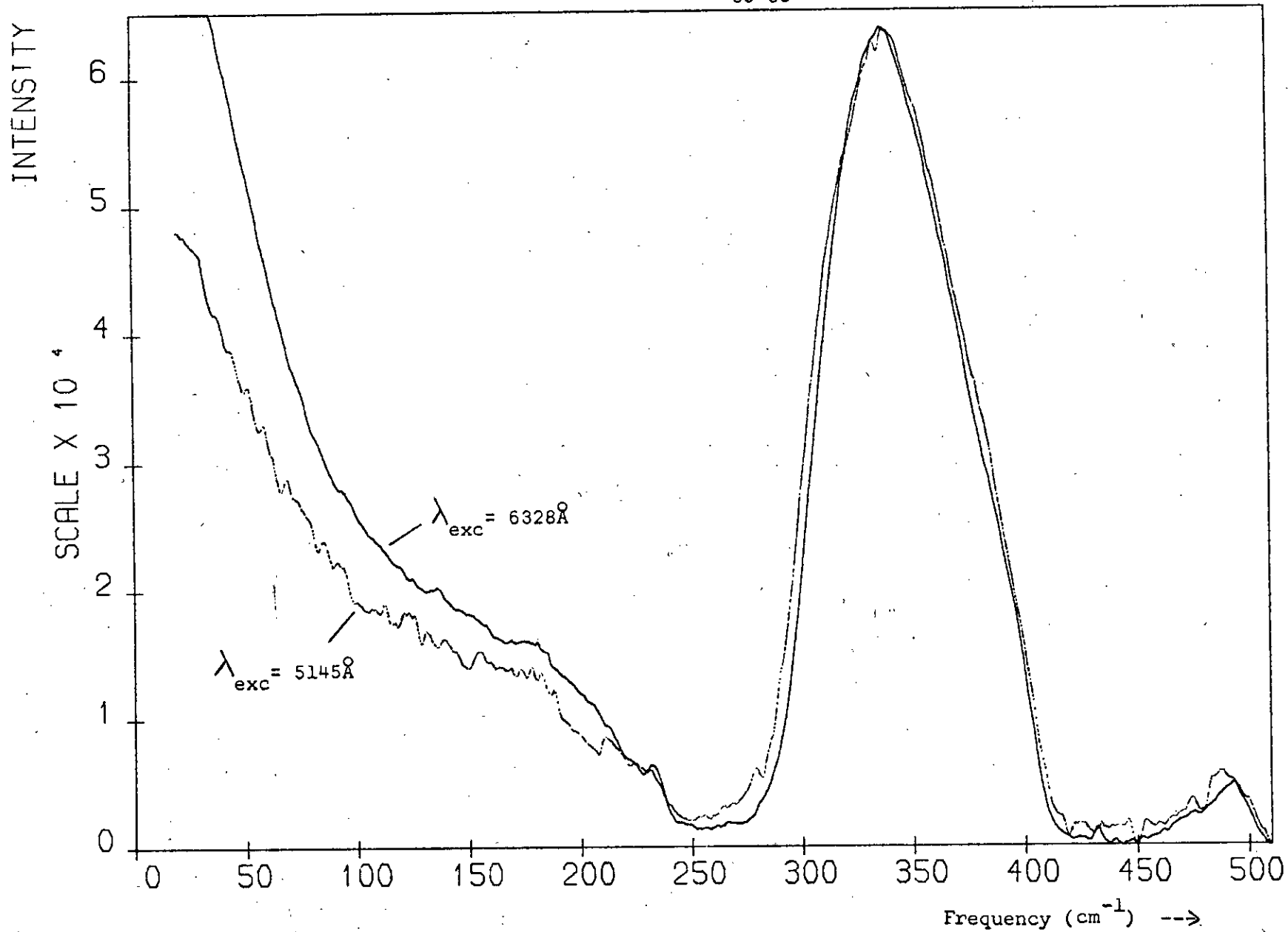
composition dependence of bond types[46]. According to this model, which has been shown to be applicable to many amorphous chalcogenides, bonds between like atoms do not occur in compositions which are deficient in that species of atom relative to the stoichiometric composition.

5.5.1.5.4 The appearance of new features — the As—S—S—As bridge

The fourth process possibly occurring in the glasses as the S content increases, and hence leading to spectral changes, is the formation of new structural features other than S_8 rings. There is no indication in the S-rich spectra that the various monomer species or regions of elemental As are present, which is not surprising since increasing the S concentration is not expected to lead to a break up of the a-$As_{40}S_{60}$ network[95,96]. Any new structural elements appearing must therefore be part of the network. It was shown in the previous section that the number of As—As bonds decreases and therefore these new elements can only be due to the incorporation of extra S atoms between the As atoms. Because sulphur is divalent, forming only rings and unbranched chains, the S atoms between the As atoms must form a chain and the new features are simply As—S_n—As (n > 1) bridges. The spectral changes resulting from this process will consist of the appearance of new bands specific to the As—S_n—As bridges; the growing 492 cm^{-1} peak may be such a band.

Because these As_2S_n 'molecules' contain S—S bonds it is expected that each type will give rise to at least one band in the characteristic range of stretching frequencies for the S—S bond viz ~450 — 550 cm^{-1}. Two bands do, in fact, appear in this region but as they grow at different rates with increasing S content they cannot both be associated with the same structural feature. The one at 472 cm^{-1} was attributed in Section 5.5.1.5.2 to S_8 rings, so only the 492 cm^{-1} band can be associated with a stretching vibration of the S—S bonds in these 'molecules'. The presence of only one band attributable to S—S stretching suggests that

one type of As_2S_n 'molecule' may preponderate, assuming that the scattered intensity does not vary significantly with n, since the S—S stretching frequencies for the various 'species' are not necessarily the same.   If no particular value of n is favoured in the formation of these 'molecules' and their populations are determined on a stochastic basis, then As_2S_2 links will occur more frequently than any other type.   The predominance of As_2S_2 'molecules' is further suggested by the absence in the spectra of features characteristic of the polymeric sulphur species, for as n increases, the vibrations of these 'molecules' will be less influenced by the terminal As atoms and will increasingly approximate to those of S_n chains.   There is no evidence in the spectra for the presence of polymeric S species in the glasses so it seems unlikely that As_2S_n bridges with $n > 2$ occur in significant quantities.   Other workers[97,98] have also proposed that some of the additional S atoms in the S-rich glasses go into the formation of these As—S—S—As links in the network.

The molecular model can be extended to account for the spectral changes resulting from the appearance of such links by considering now a second type of intermolecular coupling between the AsS_3 pyramids. In the S-rich glasses a pyramid can be joined to a neighbouring pyramid by either an As—S—As or an As—S—S—As bridge and the coupled modes arising from the latter can be treated in the same way as those due to the single bridging S atom (see Section 5.4.4.4).   Assuming that the bridge and pyramid modes can be dealt with independently the new frequencies appearing in the spectra will simply be those of an As_2S_2 'molecule'.

The simplest case is a linear bridge.   Frequency formulae for a linear X_2Y_2 molecule of $D_{\infty h}$ symmetry have been derived by Herzberg[64] on the basis of a general valence force field and are given in Equations A.8 — A.12.   Figure 5.53 shows the form of this molecule and its five normal modes of vibration, only three of which are Raman active.   As at
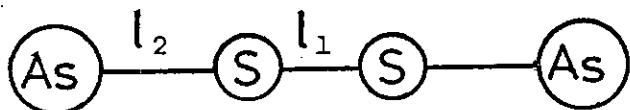
Figure 5.53

The linear symmetric X_2Y_2 molecule and its normal modes of vibration.

Figure 5.54

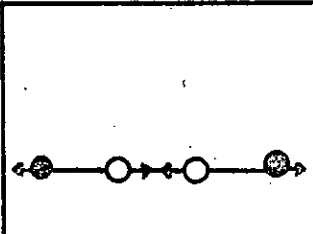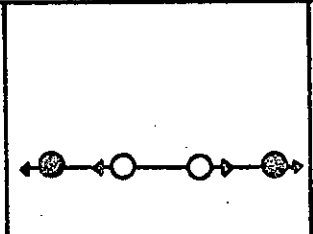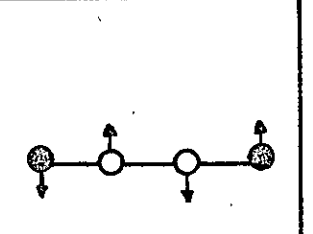The non-planar X_2Y_2 molecule of C_2 symmetry and its normal modes of vibration.

Point group : $D_{\infty h}$

$X = As = $ ⊕

$Y = S = $ ○
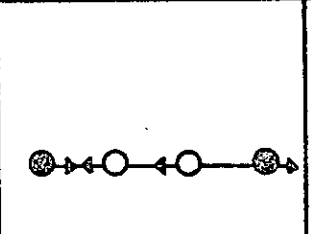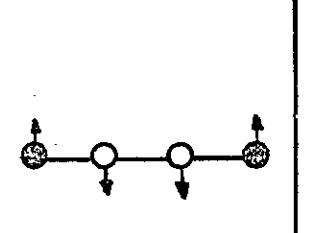
	v_1	v_2	v_3	v_4	v_5
Raman active	yes	yes	no	yes	no
i.r. active	no	no	yes	no	yes
Species	Σ_g^+	Σ_g^+	Σ_u^+	Λ_g	Λ_u
Description	Symmetric stretch	Symmetric stretch	Antisymmetric stretch	Antisymmetric bend	Symmetric bend
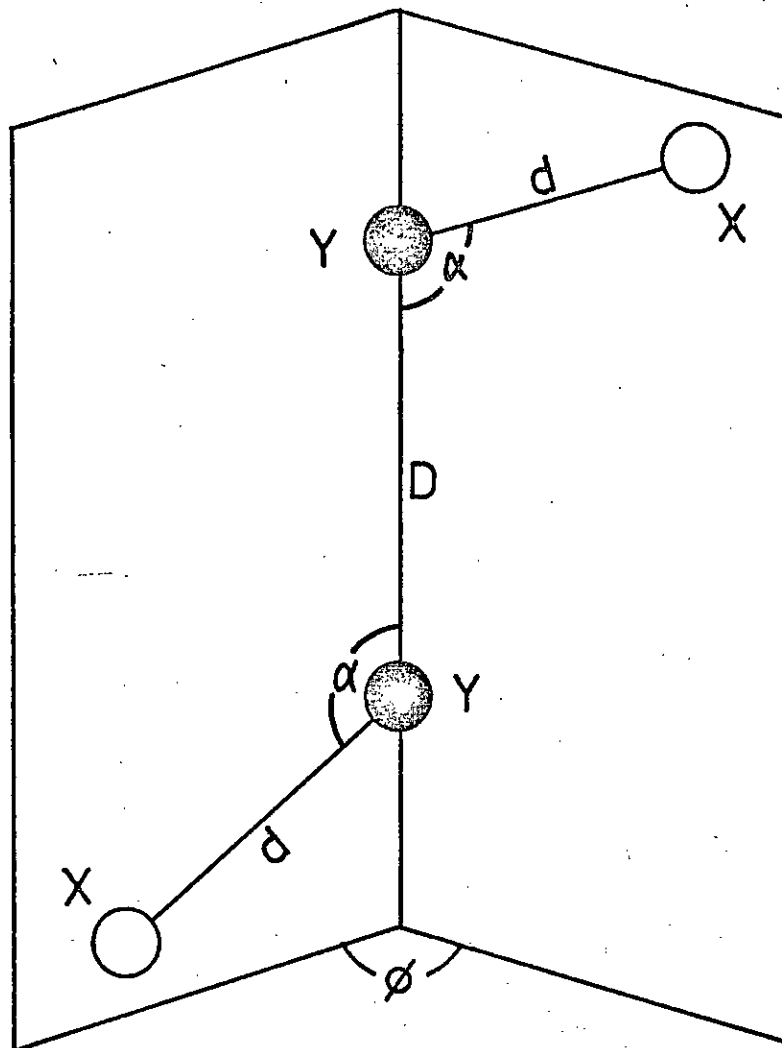
X = As
Y = S
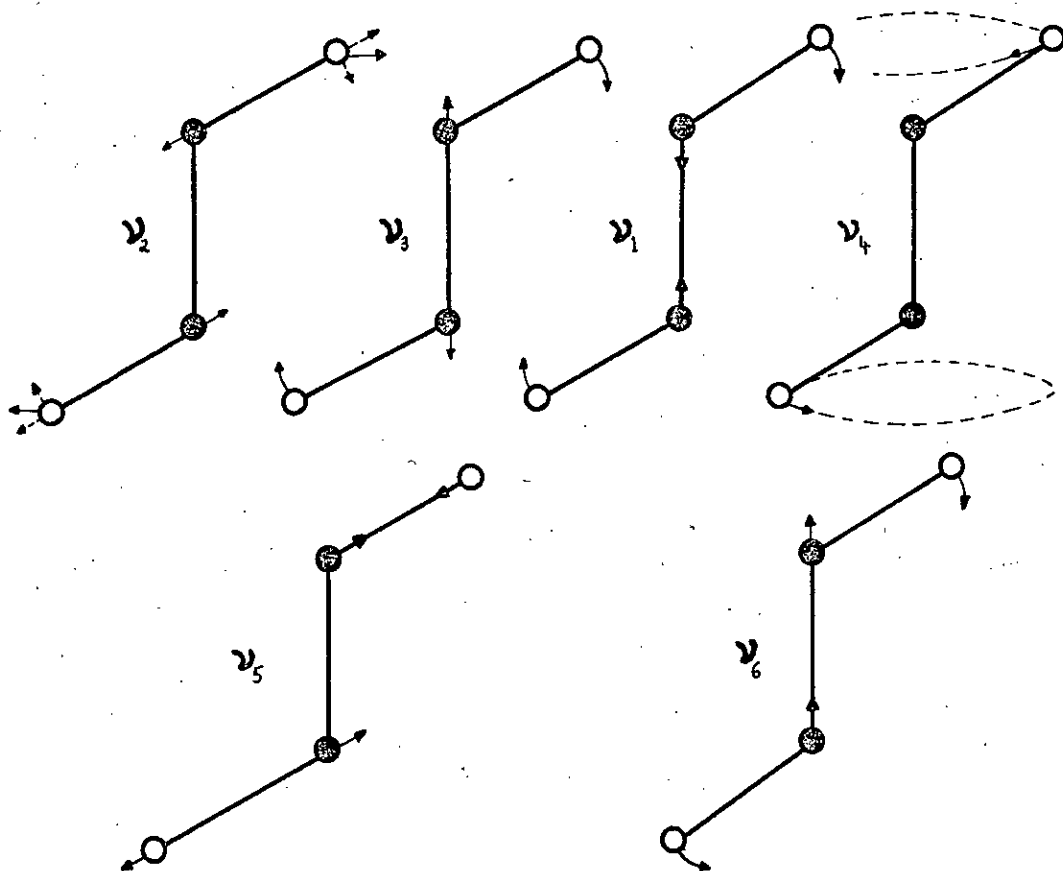
least four, and possibly five, new bands appear in the S-rich Raman spectra a linear As_2S_2 'molecule' cannot account for all the spectral changes unless the molecular selection rules break down and allow the two Raman-forbidden bands to appear.

The calculation for the frequencies of the linear As_2S_2 'molecule' using Equations A.8 — A.12 was set up in a computer program so that a set of frequencies could readily be generated for any combination of values of M_X, M_Y, k_{Y-Y}, k_{X-Y} and k_{int}. The effect of changes in these parameters on the frequencies was thus easy to investigate. The program was tested with data on linear X_2Y_2 molecules taken from Herzberg[64]. The bond lengths and bond-stretching force constants for the As_2S_2 'molecule' are expected to be similar to those in other compounds containing As—S and S—S bonds and the atomic masses are, of course, well known.

Equation A.8 shows that the frequency, ν_2, of the symmetric Y—Y bond-stretching mode, which is Raman active, depends only on the atomic masses, the bond-stretching force constants and the interaction constant for the adjacent bonds. When ν_2 was calculated for various sets of potential constants, keeping the accurately known atomic masses fixed, it was found that the value of 492 cm^{-1} could only be achieved using an exceptionally small value of the S—S bond-stretching force constant, k_{S-S}, or an exceptionally large interaction constant. k_{S-S} is usually in the range 2.35 — 2.60 md/Å and interaction constants rarely exceed one tenth of the average of the bond-stretching force constants of a molecule. Table 5.4, which gives ν_2 for various sets of potential constants, shows that, for a simple valence force field ($k_{int} = 0$), using $k_{As-S} = 1.35$ md/Å — the value derived from the molecular model analysis of a-$As_{40}S_{60}$ (see Section 5.4.5) — and $k_{S-S} = 2.5$ md/Å yields a value of ~590 cm^{-1} for ν_2, which is much too large. Frequencies obtained from a simple valence force field treatment should be within

k_{S-S}	k_{As-S}	k_{int}	ν_2
2.50	1.35	0	585
2.50	1.35	0.45	492
1.50	1.35	0	490
2.10	1.35	0.25	495
2.50	0	0	514

All frequencies and force constants are in units of cm^{-1} and $md/\overset{\circ}{A}$ respectively.

Table 5.4   The symmetric S—S bond-stretching frequency, ν_2, of the linear As_2S_2 'molecule' for various values of the force constants affecting it.

10% of the observed frequencies[74]. In view of this it seems unlikely that the As_2S_2 link is linear.

The more general and complicated case is that of the non-linear, non-planar X_2Y_2 molecule shown in Figure 5.54. This molecule is of C_2 symmetry and has six normal modes of vibration, which are also shown in the figure. The fact that all six of these modes are Raman active is not inconsistent with the observation of only five new bands since the frequency of the torsional mode is expected to be < 100 cm^{-1} and would thus be difficult to detect in the glass spectra. The five new bands occur beyond 170 cm^{-1}.

The six vibrational frequencies of the As_2S_2 molecule of C_2 symmetry can be calculated using the FG matrix method[74,101], in which the frequencies, ν_i, are found by solving the secular equation

$$\left| FG - I\lambda \right| = 0$$

where F is the matrix of potential constants, G is the inverse kinetic energy matrix, I is the identity matrix and $\lambda_i = 4\pi^2\nu_i$, the λ_i being the roots of the equation. The general valence force field and G matrix elements for this molecule, expressed with respect to its valence coordinates, are given in References 99 and 100 respectively (the G matrix elements are listed in Appendix II). Generally it is more convenient to express F and G in terms of symmetry coordinates: normalised and orthogonal symmetry coordinates for this molecule are also given in Reference 99.

Once again, the calculation was set up in a computer program so that the frequencies could be readily generated for any set of values of the input parameters. The program was tested with eighteen sets of data on various X_2Y_2 molecules of C_2 symmetry and gave satisfactory results in each case. The test molecules were H_2O_2[99,102,103], D_2O_2[102,103], S_2Br_2[102,104,105], S_2Cl_2[102,104,105,106], Se_2Br_2[105], Se_2Cl_2[105],

Observed freqs. & polns.	Parameter	Value 1	% Diff. in freqs.	Value 2	% Diff. in freqs.	Value 3	% Diff. in freqs.	Value 4	% Diff. in freqs.
	k_D	2.5	----	2.5		2.5		2.37	
	k_d	1.35		1.35		1.35		1.33	
	k_α	0.2		0.18		0.18		0.18	
	k_ϕ	0.05		0.16		0.16		0.16	
	$k_{D\alpha}$	0		0		0.15		0.15	
	α	90		108		108		108	
	ϕ	90		102		102		102	
492 p	ν_1	526	7	530	8	509	3	496	1
~350 p?	ν_2	336	—	353	—	339	—	337	—
208 p	ν_3	152	27	211	1	213	2	212	2
—	ν_4	60	—	90	—	92	—	92	—
325 dp?	ν_5	340	5	330	2	330	2	328	1
176 dp?	ν_6	171	3	177	1	177	1	177	1

p - polarised; dp - depolarised.
All frequencies and force constants are in units of cm^{-1} and md/Å respectively; α and ϕ are in degrees.

Table 5.5   Parameter values and frequencies of the As_2S_2 'molecule' of C_2 symmetry.   The differences between the observed and calculated frequencies expressed as a percentage of the former are also given.

Molecule	S—S bond length ($\overset{\circ}{A}$)	Bond angle (degrees)	Dihedral angle (degrees)
S_2F_2 (105)	1.888	108.3	87.9
S_2Cl_2 (105)	1.931	108.2	84.8
S_2Br_2 (105)	1.98	106	83
S_8 (80)	2.048	107.9	98.9
S_n (80,92)	2.04	106	95

Table 5.6   Geometrical parameters of S_8, S_n and some X_2Y_2 molecules

containing S—S bonds.

S_2F_2 [105], S_2H_2 [102,105] and D_2S_2 [107]. The program was also successful in the special case of linear X_2Y_2 molecules ($\alpha = 180°$) e.g. C_2H_2 [64].

The parameters involved in the calculation are the atomic masses (M_{As} and M_S), the bond lengths and bond angles (D, d, α and ϕ), the principal force constants (k_D, k_d, k_α and k_ϕ) and the interaction constants (k_{Dd}, $k_{D\alpha}$ etc.), of which there are nine. M_{As} and M_S are accurately known and the bond lengths are expected to be close to their usual values. The bond-stretching force constants are also expected to be close to their values in other compounds and many of the interaction constants will have little effect on the frequencies, so the only unknowns are α, ϕ, k_α, k_ϕ and the few significant interaction constants. However, the possible range of values for α and ϕ can be estimated from the other X_2Y_2 molecules and setting all the interaction constants equal to zero (simple valence force field case) should still yield frequencies within 10% of those observed. Bond-bending force constants are generally about a factor of 0.1 smaller than the corresponding stretching force constants[74] and hence a rough estimate of k_α and k_ϕ can be obtained.

The first step in finding the As_2S_2 frequencies was to calculate them approximately using a set of trial values for the parameters and to observe how they were affected by changes in these parameters. The trial values and corresponding frequencies are given in column 1 of Table 5.5. Each parameter in turn was varied while the others were kept fixed at their initial values and the new frequencies generated were compared with the original set. It will be seen from column 1 of Table 5.5 that these first approximate frequencies follow the same pattern as the observed bands, that is one occurs at ~500 cm^{-1}, two occur in the region ~300 – 400 cm^{-1} and two occur in the region ~100 – 200 cm^{-1}. The torsional mode, ν_4, as expected, occurs below 100 cm^{-1}. It was found that this pattern was preserved even for large deviations in the parameters from their trial

values. k_α and k_ϕ were varied between 0.05 and 0.4 md/Å and the inter-action constants between -0.2 and 0.2 md/Å but the same distribution of frequencies was always produced.

The symmetric-stretch frequency, ν_1, was found to be significantly influenced only by k_D, $k_{D\alpha}$ and α .   Since k_D is expected to be ~ 2.5 md/Å and $k_{D\alpha} = 0$ in the simple valence force field case only α can be varied to bring ν_1 within 10% of 492 cm^{-1}.   As α was increased from $0°$ ν_1 decreased but reached a minimum at $\alpha \approx 92°$ and then started to increase with increasing α .   The six frequencies changed very little as α was varied throughout the range $92 \pm 18°$.   The minimum value of ν_1 for $k_D = 2.5$ md/Å was 526 cm^{-1}, which is within 10% of 492 cm^{-1}. ν_1 remained within 10% of 492 cm^{-1} for all values of α between $66°$ and $119°$, which covers the range of values for α observed in other compounds with S–S bonds (see Table 5.6).   Hence this bent As_2S_2 bridge can certainly account for the 492 cm^{-1} frequency. α can be taken as $108°$, the average of the values given in Table 5.6.

The six frequencies were found to be relatively insensitive to the dihedral angle ϕ .   Varying ϕ throughout the range $90 \pm 25°$ had almost no effect on ν_1, ν_3 and ν_6 and did not alter any other frequency by more than 8% of its original value.   The values of ϕ shown in Table 5.6 lie in the range $90 \pm 10°$.   Assuming the dihedral angle of the As_2S_2 'molecule' is in the range $90 \pm 15°$, any error in the value chosen for it will not affect ν_1, ν_3 and ν_6 and will lead to an error in the other frequencies of at most $\sim 4\%$.   Accordingly, ϕ can be taken as $102°$.   This value is consistent with the fact that there is no change in the geometry of the AsS_3 pyramids and As_2S bridges with increasing S content, for $102°$ is the value ϕ must have in order that the As–As spacing in the As_2S_2 bridge is the same as that for the As_2S bridge.

The only principal force constants that affected ν_6, the antisymmetric bending frequency, were k_α and k_d. ν_6 was influenced by certain

interaction constants but for the simple valence case these are taken to be zero. ν_6 varies slowly with α over the range 115 to 100° and, as was mentioned above, is almost completely independent of ϕ. Since k_d and ϕ have been fixed, a more exact value for k_α can be found by fitting ν_6 to the experimental value of 176 cm^{-1}. It was found that ν_6 was within 10% of 176 cm^{-1} for all values of k_α between 0.14 and 0.22 md/Å so that as k_α is expected to lie in the range ~ 0.135 to 0.25 md/Å an exact value of k_α is not required in order to account for this frequency on the simple valence force field picture. However, ν_6 took the value 176 cm^{-1} for $k_\alpha = 0.18$ md/Å.

The final parameter needed for the simple valence force field calculation is k_ϕ. Only ν_3 and, of course, the torsional frequency ν_4 were affected by k_ϕ; the other frequencies were completely independent of it. A more exact value for k_ϕ can thus be obtained by fitting ν_3 to its observed value of 208 cm^{-1}. The 208 cm^{-1} band can be assigned to the ν_3 mode on the basis of its polarisation properties since it corresponds to a sharp dip in the depolarisation spectra and thus arises from a symmetric vibration. If the torsional frequency had been detected it would have provided a check on this process. It was found on inserting the revised values of the other parameters that ν_3 was within 10% of 208 cm^{-1} for all values of k_ϕ between 0.11 and 0.2 md/Å. The expected value for k_ϕ is ~ 0.14 md/Å and the value which makes $\nu_3 = 208$ cm^{-1} is 0.16 md/Å.

The revised values of the parameters for the simple valence force field case, together with the new calculated frequencies, are given in column 2 of Table 5.5. The agreement with experiment is reasonable. The largest percentage deviation from the measured values is in ν_1 and is $\sim 8\%$. k_D is known and any change in α will increase ν_1 so only $k_{D\alpha}$ can be altered to bring ν_1 closer to 492 cm^{-1} since none of the other parameters significantly affect this frequency. A value of 0.15 md/Å

for $k_{D\alpha}$ yields a value of 509 cm^{-1} for ν_1. This value for $k_{D\alpha}$ is comparable with values for $k_{D\alpha}$ observed in other X_2Y_2 molecules. It was found that $k_{D\alpha}$ had no effect on the two antisymmetric frequencies and only slightly influenced ν_2, ν_3 and ν_4. The final set of parameter values used and the corresponding frequencies are given in column 3 of Table 5.5. The parameter values given in column 4 of this table were obtained by adjusting those in column 3 to give the best fit to the observed frequencies.

The spectrum of the As_2S_2 'molecule' must not only match the observed bands in frequency but must also have the correct polarisation properties. The three observable symmetric modes, ν_1, ν_2 and ν_3, are expected to give rise to dips in the depolarisation spectra while the two antisymmetric modes, ν_5 and ν_6, should correspond to raised regions. Figure 5.49 shows that dips do occur in the depolarisation spectra at 211 cm^{-1} (ν_3) and ~492 cm^{-1} (ν_1) but that no new structure occurs at the other frequencies. In Section 5.5.1.3 it was pointed out that new Raman bands which overlap existing ones and have similar depolarisation ratios to these will not give rise to changes in the depolarisation spectra. It is therefore possible that the absence of new structure at 176, 325 and ~350 cm^{-1} in the S-rich depolarisation spectra is due to the fact that these three As_2S_2 bands have similar depolarisation ratios to the three pyramid and As_2S bands to which they are in proximity, viz those at 185, 315 and 367 cm^{-1}. If this is the case then the observed bands at 176, 325 and ~350 cm^{-1} do have the required polarisation properties since the a-$As_{40}S_{60}$ bands at 315 and 367 cm^{-1} arise from antisymmetric vibrations while that at 185 cm^{-1} is due to a symmetric mode.

Alternatively, the weakness of these three As_2S_2 bands compared with the pyramid and As_2S bands they overlap may mean their contribution to the depolarisation ratio is swamped by that of the latter. It is

perhaps significant that the pronounced changes that do occur in the depolarisation spectra are in regions of low Raman signal. If the polarisation states of the growing bands at 176, 325 and 350 cm^{-1} are being masked then no definite conclusions on the presence of the As_2S_2 bridge can be drawn from the depolarisation spectra.

5.5.2 The compositions $As_{35}S_{65} - As_5S_{95}$

5.5.2.1 The polarisation-unanalysed spectra

Figure 5.55 shows the polarisation-unanalysed Raman spectra of the four compositions studied in the range $As_{28.6}S_{71.4} - As_5S_{95}$; for the purpose of comparison the corresponding spectra of a-$As_{40}S_{60}$, $As_{35}S_{65}$ and powdered α-S_8 are also shown. The spectra have been vertically displaced for clarity and have been scaled in such a way that the peak intensity of the low-frequency band in each of the glass spectra is equal to the intensity of the 156 cm^{-1} band in the α-S_8 spectrum. Figure 5.56 shows the same set of glass spectra superimposed with the α-S_8 spectrum below. The results are in good agreement with those obtained by Ward[1,2]. Figure 5.57 shows the reduced spectra for these six glasses. For clarity the $As_{28.6}S_{71.4}$ spectrum has been arbitrarily scaled to separate it more from the $As_{25}S_{75}$ spectrum.

The spectral changes that occur as the S content is increased beyond 65 at.% consist of the steady growth of sharp peaks at frequencies characteristic of S_8 rings and the transformation and disappearance of the 300 - 400 cm^{-1} band.

5.5.2.2 Polarisation measurements

The VV- and VH-polarised Raman spectra for the compositions $As_{28.6}S_{71.4} - As_5S_{95}$ are shown, together with the corresponding spectra of a-$As_{40}S_{60}$ and $As_{35}S_{65}$, in Figures 5.58 and 5.59 respectively. The spectra have been vertically displaced for clarity and have been normalised

Figure 5.55

The polarisation-unanalysed Raman spectra of α-S_8 and compositions in the range $As_{40}S_{60}$ — As_5S_{95}.

Spectrum	Composition
A —	As_5S_{95}
B —	$As_{15}S_{85}$
C —	$As_{25}S_{75}$
D —	$As_{28.6}S_{71.4}$ (As_2S_5)
E —	$As_{35}S_{65}$
F —	$As_{40}S_{60}$

Figure 5.56

The glass spectra of Figure 5.55 superimposed and the α-S_8 spectrum.

A ⸺

B ✳

C ☐

D ⸺

E •

F Δ ⸺

Figure 5.57

The reduced spectra corresponding to the glass spectra of Figure 5.56.

A ⸺

B ✳

C •

D ☐

E ⸺

F Δ

S-Rich Spectra
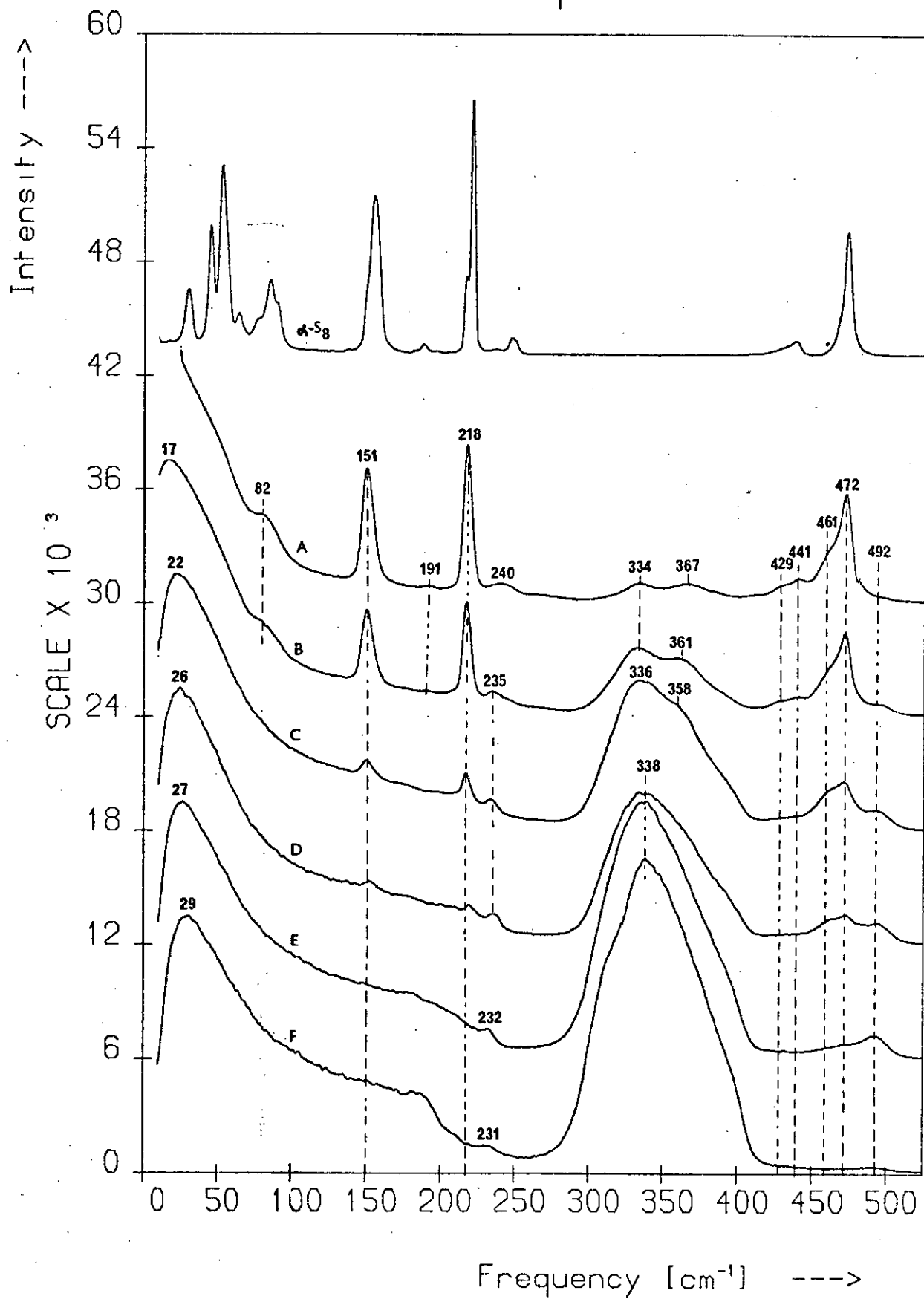
S-Rich Spectra

Intensity ---->
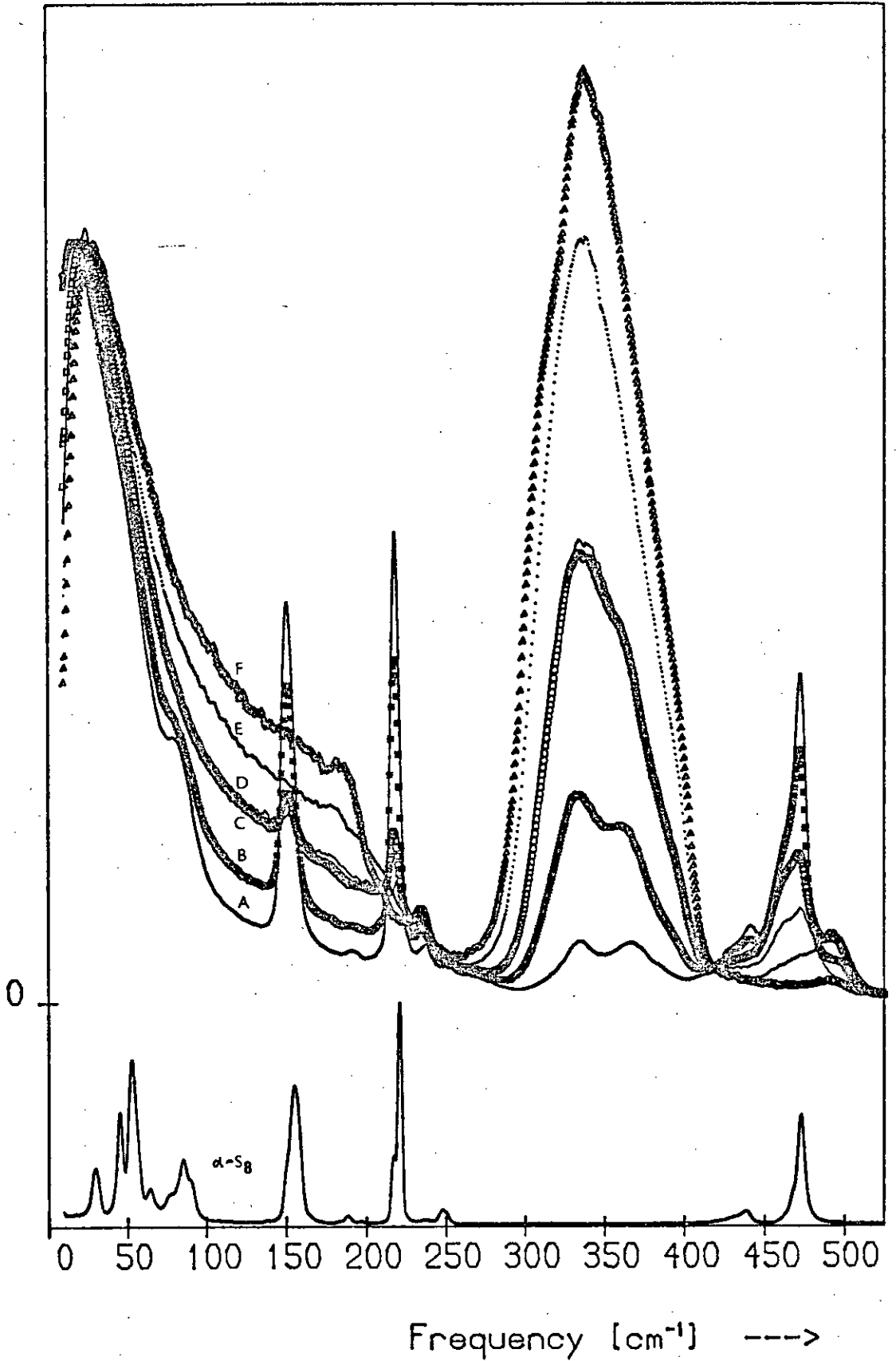
Frequency [cm⁻¹] ---->

Reduced S-Rich Spectra
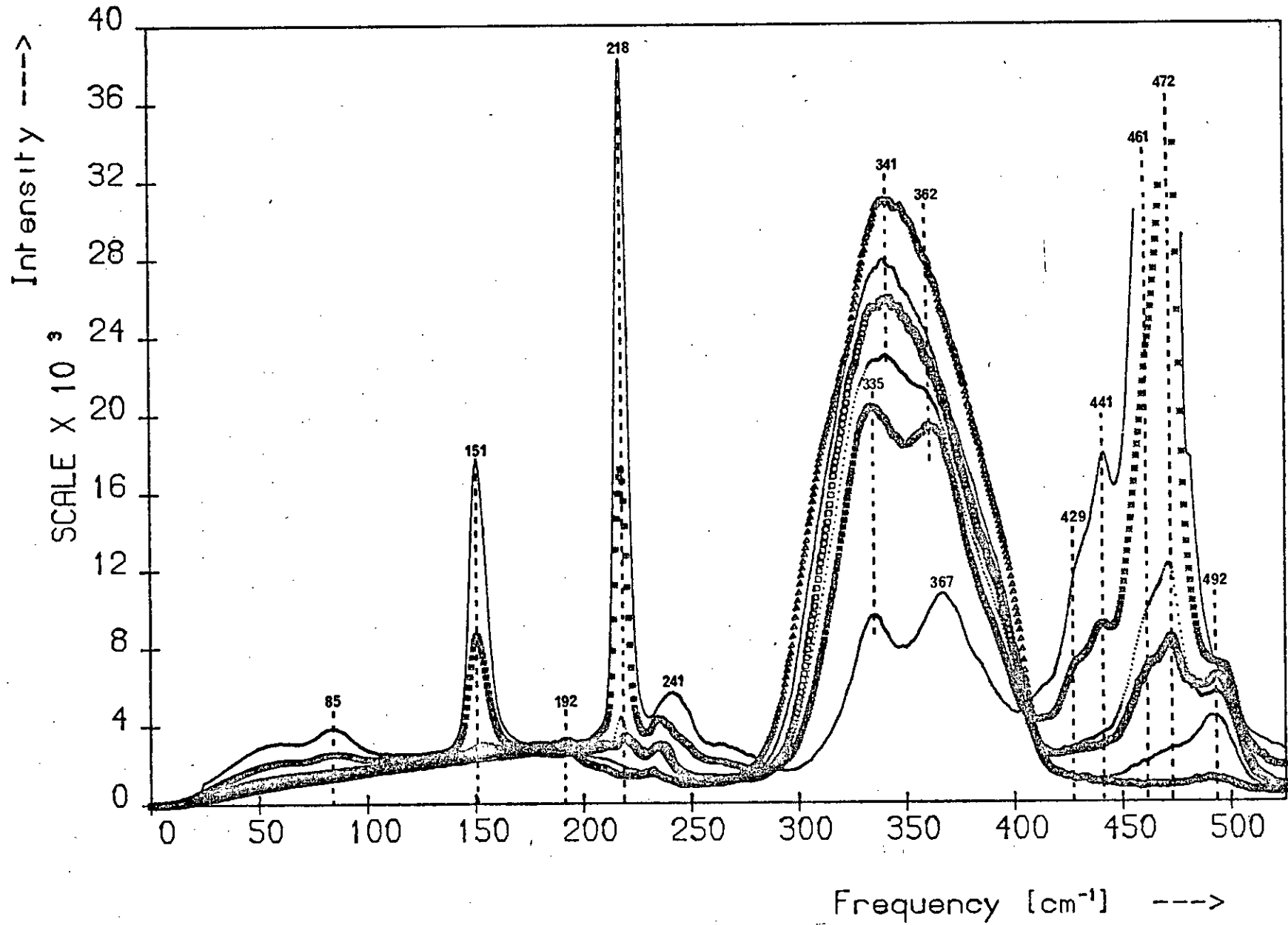
by the peak intensities of the low-frequency bands. Figure 5.60 shows the depolarisation spectra for these six compositions. No polarisation data on these S-rich glasses has previously been reported, with the exception of Ward's measurements on As_5S_{95} at elevated temperatures[2].

The spectral changes that occur in the VV and VH spectra with increasing S content are essentially the same as those outlined above for the polarisation-unanalysed data — S_8 bands grow steadily while the 300 — 400 cm^{-1} band changes shape and gradually disappears. Corresponding VV and VH spectra are not, of course, identical since the various spectral features are polarised to different extents and this is reflected in the depolarisation spectra.

In addition to the appearance of sharp structure due to S_8 rings, the following changes occur in the depolarisation spectra of Figure 5.60 as the S content increases: the dip at ~106 cm^{-1} in the a-$As_{40}S_{60}$ spectrum moves to higher frequencies, there is an increase in the depolarisation ratio over the ranges ~170 — 210 cm^{-1} and 220 — 300 cm^{-1}, and a change in the shape of the 340 — 400 cm^{-1} trough.

5.5.2.3 Discussion

It is clear from Figure 5.55 that the S_8 component of the glass spectra does not exactly match the α-S_8 spectrum. Of the α-S_8 lattice modes only the 86 cm^{-1} band stands out from the low-frequency background and even this band is not resolved and is evident only in the $As_{15}S_{85}$ and As_5S_{95} spectra. Also, in the glass spectra most of the S_8 bands are broader than their counterparts in the α-S_8 spectrum; the 472 cm^{-1} band has a pronounced shoulder at 461 cm^{-1} while the α-S_8 feature at 217 cm^{-1} is not resolved. The ratio of the peak intensities of the S_8 bands in the glass spectra is different from that of the α-S_8 lines as well. In fact, the S_8 component of the glass spectra resembles more the Raman spectrum of liquid sulphur than the α-S_8 spectrum. Ward[2] has recorded

Figure 5.58

The VV-polarised Raman spectra of compositions in the range $As_{40}S_{60} - As_5S_{95}$. The frequencies of the bands are identical with those of Figure 5.55.

Spectrum		Composition
A	—	As_5S_{95}
B	—	$As_{15}S_{85}$
C	—	$As_{25}S_{75}$
D	—	$As_{28.6}S_{71.4}$ (As_2S_5)
E	—	$As_{35}S_{65}$
F	—	$As_{40}S_{60}$

Figure 5.59

The VH-polarised Raman spectra corresponding to the compositions of Figure 5.58. The frequencies of the bands are identical with those of Figure 5.55. The spectra are labelled as in Figure 5.58.

Figure 5.60

The depolarisation spectra corresponding to the compositions of Figure 5.58 (A — F as in Figure 5.58).

VV Polarised Spectra: $As_{40}S_{60}$ – As_5S_{95}
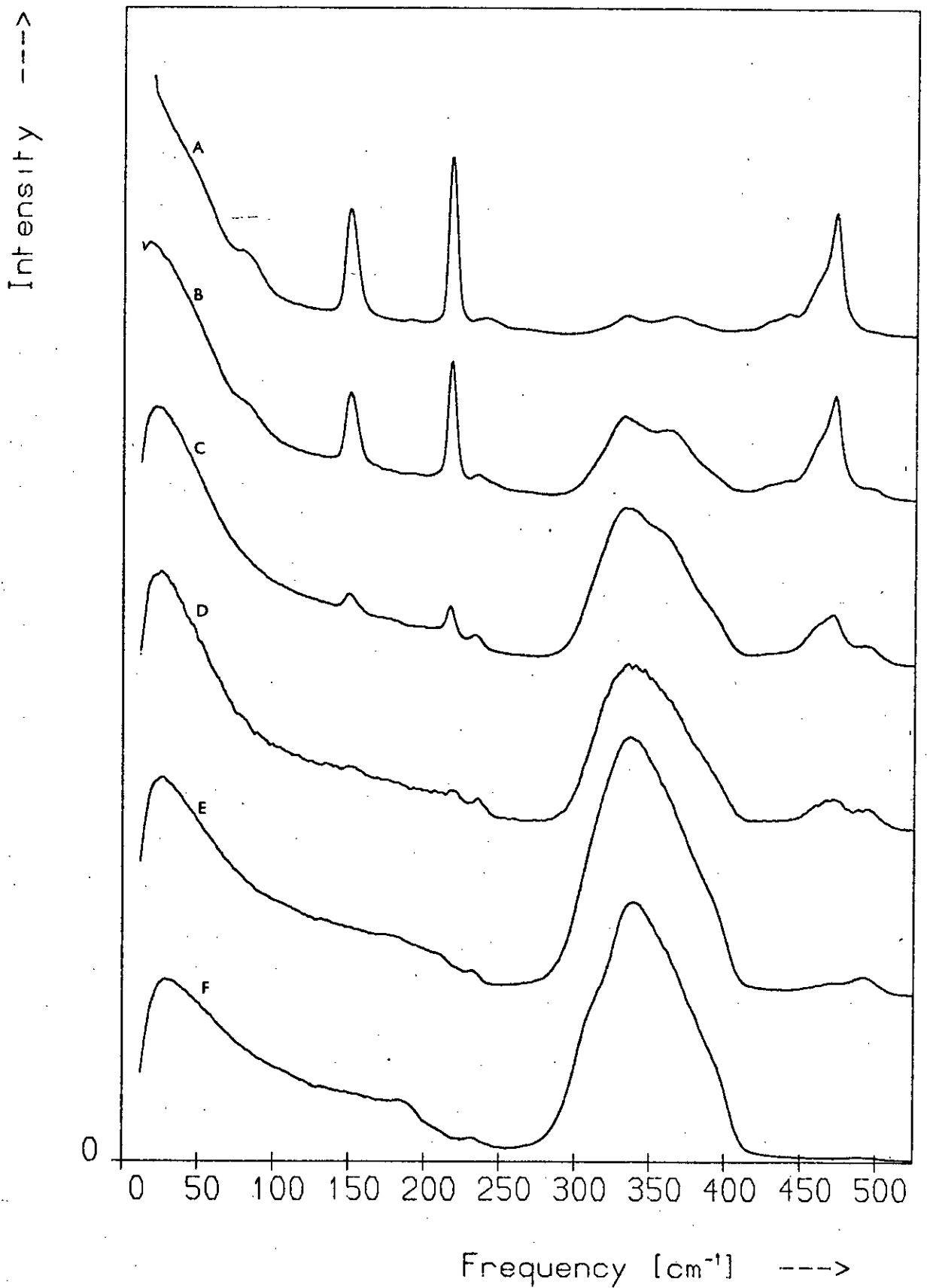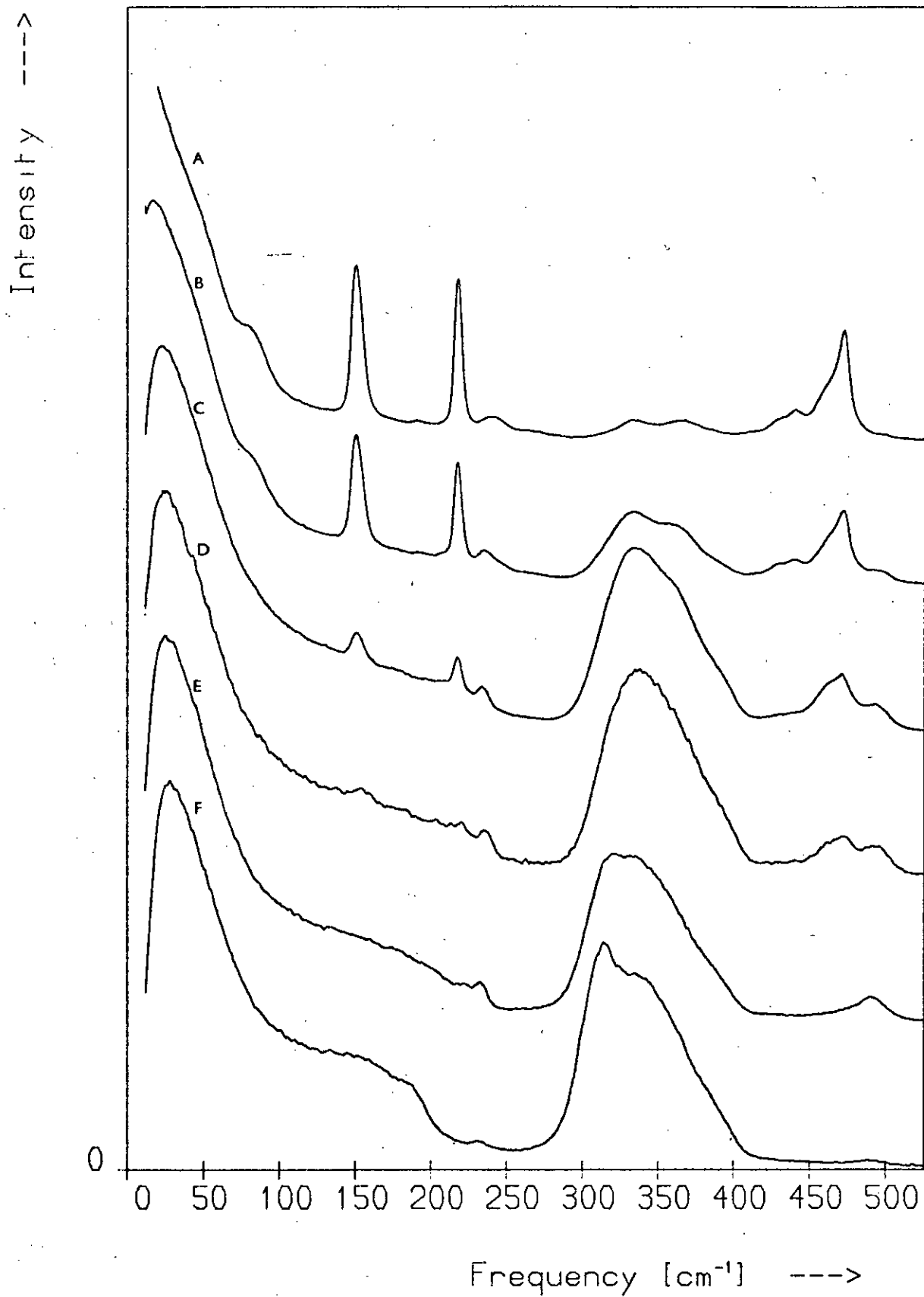
Intensity ——>

Frequency [cm^{-1}] ———>

VH Polarised Spectra: $As_{40}S_{60} - As_5S_{95}$

Intensity --->

Frequency [cm^{-1}] --->

Depolarisation Spectra : $As_{40}S_{60}$ - As_5S_{95}
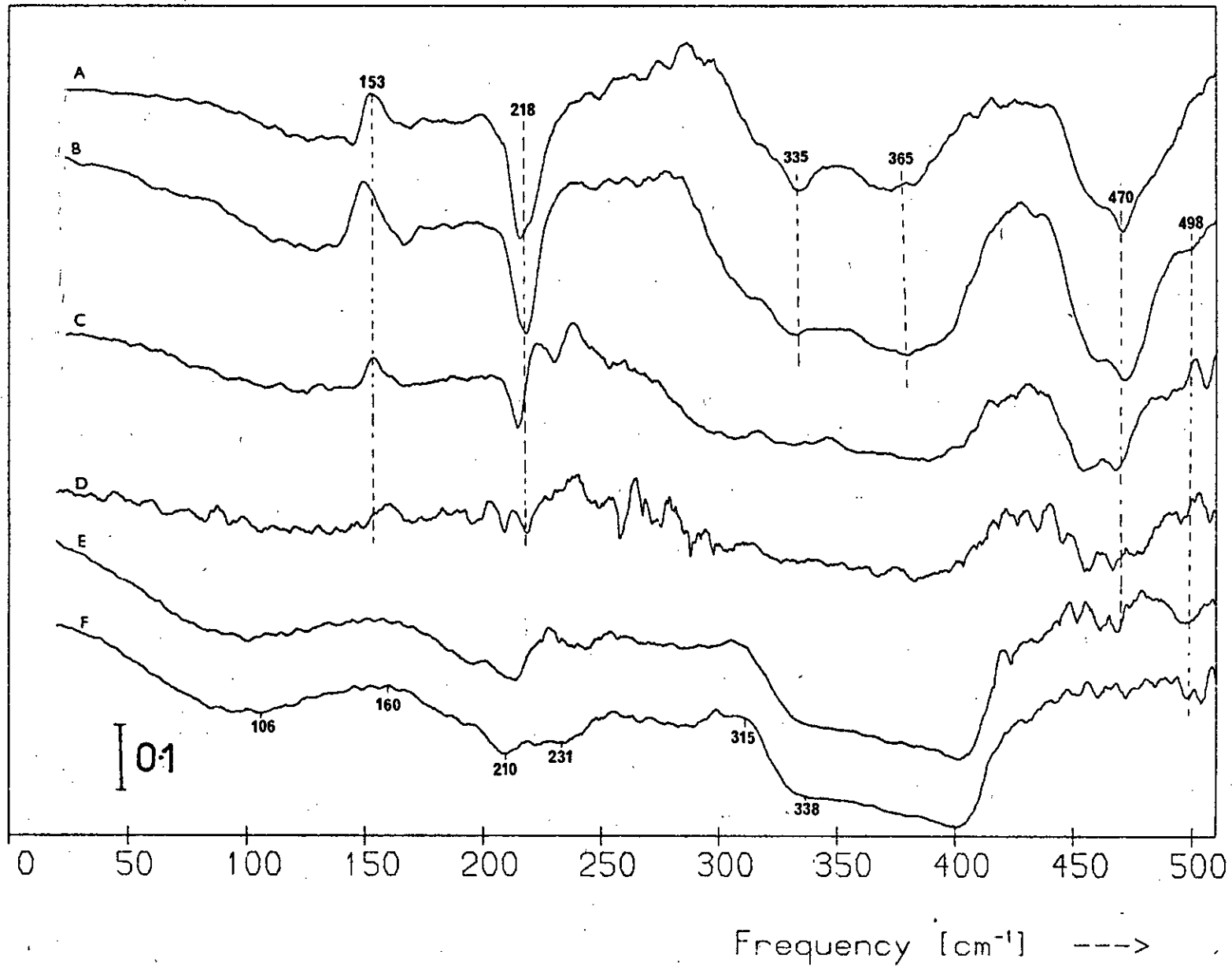
the Raman spectrum of liquid sulphur at various temperatures and his results show that the bands in the crystal and liquid spectra differ in the same way as the S_8 bands in the crystal and the As-S glasses: in the spectrum of liquid S_8 the bands are broader than their α-S_8 counterparts and the external bands are absent or barely resolved. The intensity ratio for the lines in the liquid spectrum also differs from that for the α-S_8 bands. A particularly noteworthy similarity between the liquid sulphur and the glass spectra is the behaviour of the weak S_8 band at ~232 cm^{-1}. In Ward's data[2] this band occurs at 247 cm^{-1} in α-S_8 at 25° C and shifts steadily to lower frequencies as the temperature increases. Just above the melting point it is at 243 cm^{-1} while in the liquid at 213° C it is at 237 cm^{-1}. In the case of the As-S glasses the band occurs at 240 cm^{-1} in As_5S_{95} and shifts steadily to lower frequencies as the As content increases until at the composition $As_{35}S_{65}$ it is at 232 cm^{-1}. As this band occurs in a region where the Raman signal from the As-S network is weak its shift cannot be attributed to changes in the background on which it is superimposed.

As Ward points out, these temperature-dependent changes are particularly marked in the 473 cm^{-1} band, which grows relative to the 221 and 156 cm^{-1} bands and broadens considerably as the temperature increases, developing a wing on its low-frequency side. The ~472 cm^{-1} bands of the liquid and As-S glass spectra are very similar. Ward suggests that this temperature-induced broadening and growth of the 473 cm^{-1} band is due to either the formation of polymeric species, S_n, or the appearance of Raman-forbidden S_8 fundamentals near this frequency. From theoretical considerations[2], Raman-active fundamentals of S_n are expected at ~450 and ~420 cm^{-1} and so could account for the very broad wing on the 473 cm^{-1} band in the liquid sulphur spectra but there is nothing significant in the glass spectra at these frequencies. The 472 cm^{-1} S_8 band of the As-S spectra barely extends to 450 cm^{-1} and there

is no feature at all at 420 cm^{-1}. The Raman spectra of the various polymeric forms of sulphur all have a band of strong to medium intensity in the region 456 – 466 cm^{-1}, which does span the frequency range over which the pronounced shoulder on the 472 cm^{-1} band in the glass spectra occurs. If, however, the 461 cm^{-1} shoulder is due to S_n chains one would expect to see bands in the glass spectra at ~420 and ~275 cm^{-1} since these are also present in the polymeric S spectra and are characteristic of S_n chains. Bands at 420 and 275 cm^{-1} would be easily detected since the Raman signal due to other bands is very weak in these regions but no features are observed at these frequencies.

The alternative explanation of the temperature-dependent broadening and growth of the 473 cm^{-1} band is that the Raman-forbidden S_8 ring fundamental that occurs in the region ~465 – 471 cm^{-1} [2,29] becomes Raman active as a result of the thermally induced distortion of the S_8 ring symmetry. If the S_8 rings in the As-S glasses are also distorted, in keeping with the disordered nature of these materials, then this explanation may also account for the wing on the 472 cm^{-1} band in the glass spectra.

Thus the resemblance of the S_8 component of the glass spectra to the spectrum of liquid sulphur suggests that the S_8 rings in the sulphur regions inside the glasses do not form regular arrays but are randomly arranged as in liquid sulphur. Further, the shoulder at 461 cm^{-1} in the glass spectra suggests that the S_8 rings themselves may be distorted in the glasses.

It is seen in Figure 5.55 that the spectral signature of S_8 is certainly present in all spectra more S-rich than $As_{28.6}S_{71.4}$ (As_2S_5). This conflicts with the results of the dissolution experiments of Tsuchihashi and Kawamoto. [81] which suggest that S_8 rings are present only in the glasses more S-rich than $As_{20}S_{80}$. As was mentioned in Section 5.5.1.5.2, the inability of their experiments to detect S_8 rings

in the glasses with less than 80 at.% S is probably due to the rings

being trapped in the insoluble As-S matrix.   It was shown in Section

5.5.1.5.2 that the rings are present in glasses of 63 at.% S and possibly

even in glasses of 61 at.% S.

It is also clear from Figure 5.55 that the S_8 bands rapidly over-

take and dwarf the As-S-S-As bridge features as the S content is increased.

The As_2S_2 features are the first to appear and in the $As_{35}S_{65}$ spectrum

they are larger than the S_8 bands.   However, in the $As_{28.6}S_{71.4}$ spectrum

the S_8 bands are well established and exceed the chain features.

Figure 5.61 compares the As_2S_5 difference spectrum (obtained by subtracting

the reduced a-$As_{40}S_{60}$ spectrum from the basewidth-normalised, reduced As_2S_5

spectrum) with corresponding spectra for the compositions $As_{40}S_{60}$ - $As_{35}S_{65}$.

The features marked S are the S_8 bands.   It seems that the additional

sulphur in the glasses more S-rich than ~$As_{30}S_{70}$ goes mainly into producing

S_8 rings, though the presence of a feature at 492 cm^{-1} in each of the glass

spectra indicates that As-S-S-As bridges are still being formed in these

glasses, as would be expected.   The 492 cm^{-1} feature is very weak in the

As_5S_{95} spectrum but is just visible in Figure 5.55 and in Ward's spectrum

of this composition.

As the 260 - 420 cm^{-1} region of the S_8 spectrum is completely devoid

of structure the changes in the band that occurs in this region of the glass

spectra cannot be attributed to the appearance of S_8 rings.   Other sulphur

forms or As-S monomers are not present so the changes in this band must be

due to changes in the As-S network i.e. changes in the structure or relative

populations of the various 'molecules'.

In Section 5.5.1.5.4 it was shown that the As_2S_2 'molecule' is expected

to give rise to two bands in the 300 - 400 cm^{-1} region.   The asymmetric

300 - 400 cm^{-1} peak in the difference spectra (see Figure 5.33) was

attributed to these bands and yielded a frequency of 325 cm^{-1} for one of

them.   As the S content of the glasses increases it might reasonably be

Figure 5.61

The difference spectrum of vitreous As_2S_5 ($As_{28.6}S_{71.4}$) obtained
by subtracting the reduced a-$As_{40}S_{60}$ spectrum from the reduced
As_2S_5 spectrum. The five lower spectra are the difference spectra
of Figure 5.35. The features marked S are characteristic of the S_8
ring.

Difference Spectra for the S-Rich Glasses
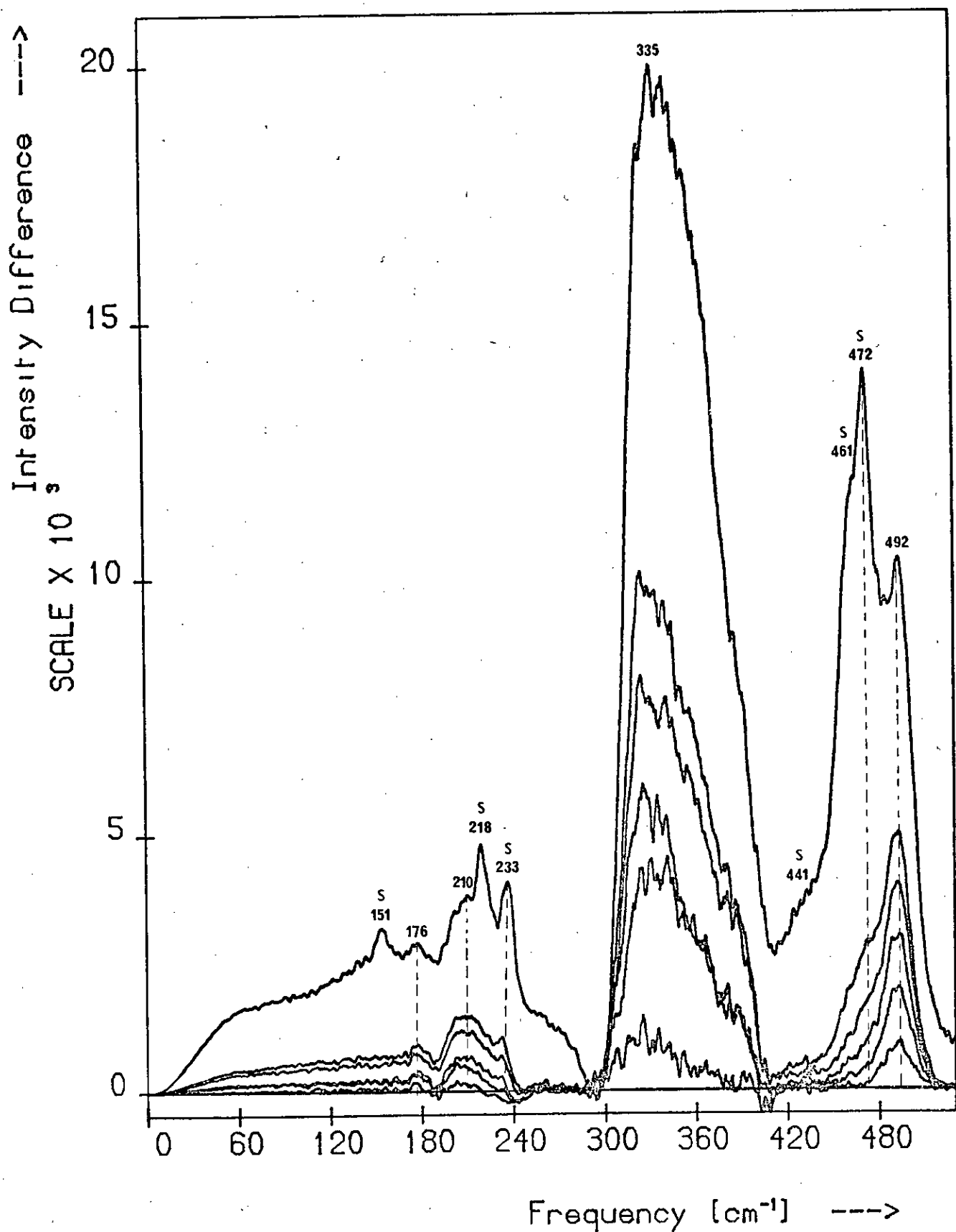
expected that more and more of the As_2S links would be replaced by the As_2S_2 chains so that the number of the latter would increase relative to the number of pyramids. If this were the case, the Raman intensity due to the As_2S_2 'molecules' would also increase relative to that due to the pyramids and one might expect any As_2S_2 bands initially swamped by other features to appear for large S concentrations. The fact that the ratio of the intensities at ~338 cm^{-1} and 492 cm^{-1} (the highest As_2S_2 frequency) increases as the S content is increased supports this supposition and it is possible that the new structure appearing on the main band at 334 and ~360 cm^{-1} is due to the emergence of the two chain bands. In the limiting situation every AsS_3 pyramid will be coupled via As—S—S—As links so that the ratio of pyramids to As_2S_2 'molecules' will be 2 : 3 and the As_2S component of the spectrum will have been completely replaced.

Only the 221 and 473 cm^{-1} bands of α-S_8 arise from totally symmetric vibrations and are polarised. Figure 5.60 shows that the glass-spectra bands attributed to S_8 have the correct polarisation properties, for of the sharp features only those at 218 and 472 cm^{-1} correspond to pronounced dips in the depolarisation spectra. Liquid sulphur exhibits similar polarisation properties to α-S_8. The 400 — 500 cm^{-1} region of the liquid sulphur spectrum is strongly polarised and its polarisation is virtually independent of temperature which suggests that any new features growing in this range with increasing temperature must also arise from totally symmetric vibrations[2]. According to Ward this supports the presence of S_n chains in the liquid since the ~450 cm^{-1} vibration of such species is totally symmetric. In the case of the S_8 component of the glass spectra the 461 cm^{-1} shoulder is apparent only in the spectra of the compositions $As_{28.6}S_{71.4}$ — As_5S_{95} and Figure 5.60 shows that in the large dip that occurs over the 450 — 500 cm^{-1} region of the depolarisation spectra of these four glasses there is a small upward kink at ~465 cm^{-1}. This small kink would arise if the broad, strongly polarised band at

472 cm^{-1} overlapped a weaker depolarised band at ~ 465 cm^{-1} so the

shoulder at 461 cm^{-1} is not necessarily due to a totally symmetric vib-

ration. In their Raman study of polymerisation in the glasses $As_{15}S_{85}$

and As_5S_{95} Ward and Myers[26] showed that 'free' S_n chains — i.e. chains

not incorporated in the As-S network — did not occur below $\sim 120^o$ C. If,

as was suggested in Section 5.5.1.5.4, the Raman spectrum of S_n ($n > 2$)

chains between As atoms in the network is similar to that of the 'free'

chains then the results of Ward and Myers indicate that at room temp-

erature S_n chains are not present in the network either. Thus it seems

more likely that the 461 cm^{-1} shoulder is due to the activation of a

Raman-forbidden S_8 fundamental as a result of disorder-induced distortion

of the S_8 ring symmetry.

The rise in the depolarisation ratio over the region $220 - 300$ cm^{-1}

is initially greatest near 233 cm^{-1} and is due to the disappearance of

As—As bonds and to the growth of a depolarised S_8 band. However, for

large S concentrations the rise occurs mainly at the high-frequency end

of this range and is due to the weakness of the Raman signal in this region

relative to the background. The depolarisation ratio rises towards that

of the depolarised stray-light background, just as it does in the region

above ~ 500 cm^{-1} where there is also little Raman signal. The increase

in the depolarisation ratio over the range $170 - 210$ cm^{-1} may be attribut-

able to the appearance of the depolarised 176 cm^{-1} band of the As_2S_2

'molecule' (see Section 5.5.1.5.4).

The 300 to 400 cm^{-1} trough changes shape considerably with increasing

S concentration: the minimum at 400 cm^{-1} in the a-$As_{40}S_{60}$ spectrum shifts

to lower frequencies and becomes well resolved from the ~ 338 cm^{-1} dip.

The shifts in the 338 cm^{-1} and 400 cm^{-1} dips suggest at first that

geometrical changes may be taking place in the 'molecules'. As the

~ 338 cm^{-1} dip does not shift significantly no pronounced geometrical

changes can be occurring in the AsS_3 pyramid and the shifting 400 cm^{-1}

dip must arise from some other structural feature. In Section 5.4.5 it was suggested that both the 395 and 106 cm^{-1} vibrations were associated with the As$_2$S 'molecule'. As the ratio of As$_2$S links to AsS$_3$ pyramids cannot increase beyond its value in a-As$_{40}$S$_{60}$, that is approximately 3 : 2, the ~360 cm^{-1} feature that appears in these very S-rich Raman spectra cannot be attributed to these links since it grows relative to the pyramid bands. It seems, therefore, that these shifts cannot be attributed to geometrical changes.

The shift of the ~106 cm^{-1} dip in the a-As$_{40}$S$_{60}$ depolarisation spectrum to higher frequencies with increasing S content may be due to a decrease in the layer separation[81] or simply to the increase in the relative intensity of the depolarised boson peak.

5.6   The arsenic-rich glasses: As$_{40}$S$_{60}$ — As$_{45}$S$_{55}$

5.6.1   The polarisation-unanalysed spectra

Figure 5.62 shows the polarisation-unanalysed Raman spectra of the compositions As$_{40}$S$_{60}$ — As$_{45}$S$_{55}$. They have been normalised to the intensity of the ~338 cm^{-1} band and are shown displaced above one another. The spectral changes that occur with increasing As content are obvious and consist of the rapid growth of numerous sharp features. Figure 5.63 shows a similar set of spectra extended vertically to emphasise these features, which are visible even in the As$_{41}$S$_{59}$ spectrum. (Irregularities in the relative intensities of the sharp bands will be discussed in Section 5.7.) The corresponding reduced spectra are shown in Figure 5.64 and illustrate one of the disadvantages of such spectra, namely the possibility of losing information at low frequencies. In this case the structure at 135, 146 and 167 cm^{-1} is barely visible for the compositions As$_{41}$S$_{59}$ — As$_{43}$S$_{57}$.

The sharp features grow very rapidly as the As content is increased, the first to appear being the bands at 187, 222 and 233 cm^{-1}. Comparison

The polarisation-unanalysed Raman spectra of the compositions
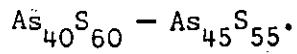
$As_{40}S_{60} - As_{45}S_{55}$.

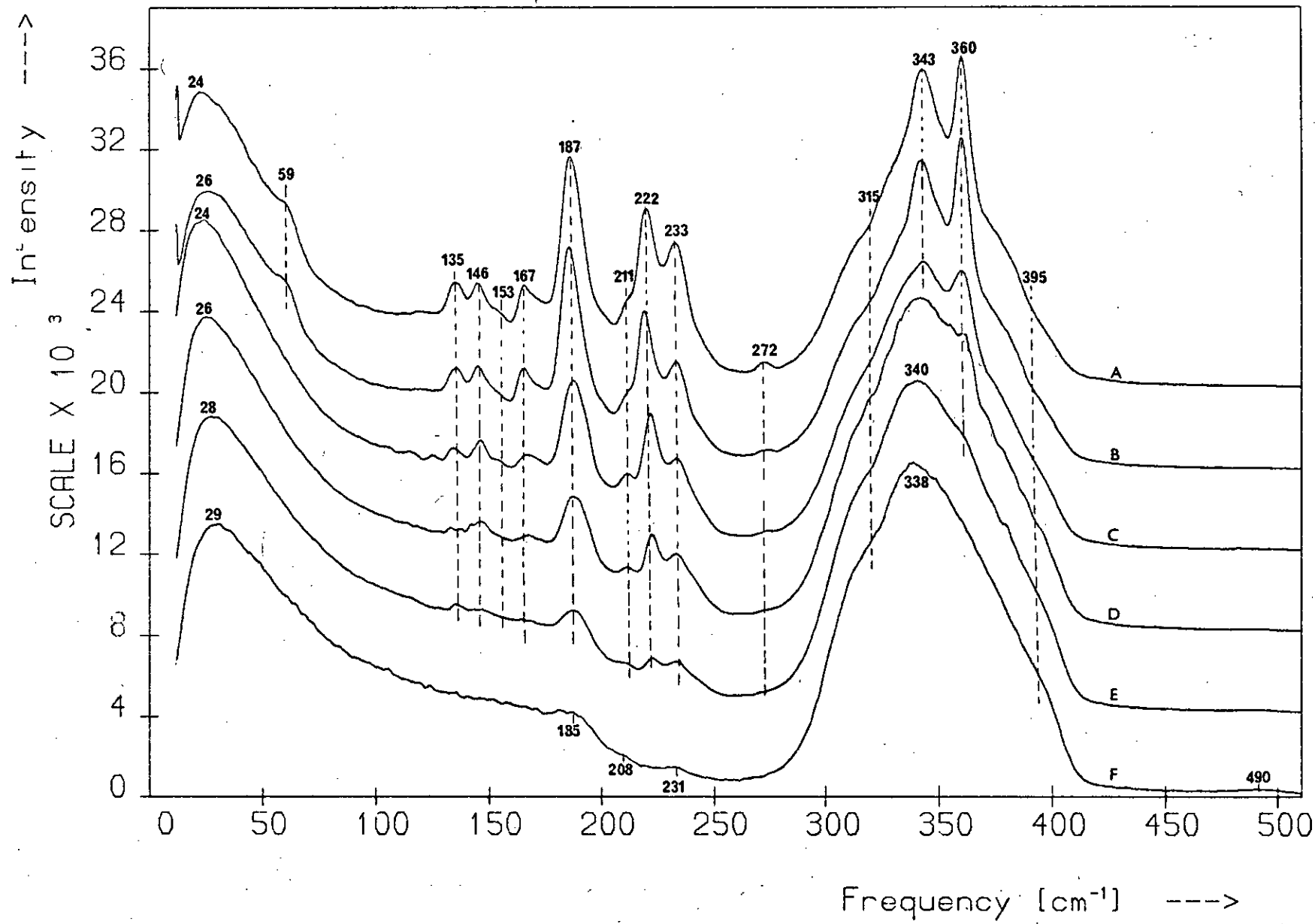| Spectrum	Composition
A	— $As_{45}S_{55}$
B	— $As_{44}S_{56}$
C	— $As_{43}S_{57}$
D	— $As_{42}S_{58}$
E	— $As_{41}S_{59}$
F	— $As_{40}S_{60}$

The reduced spectra corresponding to those of Figure 5.63 (A — F as above).

Raman spectra of $As_{43}S_{57}$, the most As-rich transparent glass studied.

Spectrum A was recorded in the transmission mode and B by back reflection.

Raman Spectra of the As-Rich Glasses

Raman Spectra: $As_{40}S_{60}$ - $As_{45}S_{55}$

Intensity --->

Wavenumber [cm⁻¹] --->

Reduced Spectra: As$_{40}$S$_{60}$ - As$_{45}$S$_{55}$

Intensity --->

Wavenumber [cm^{-1}] --->
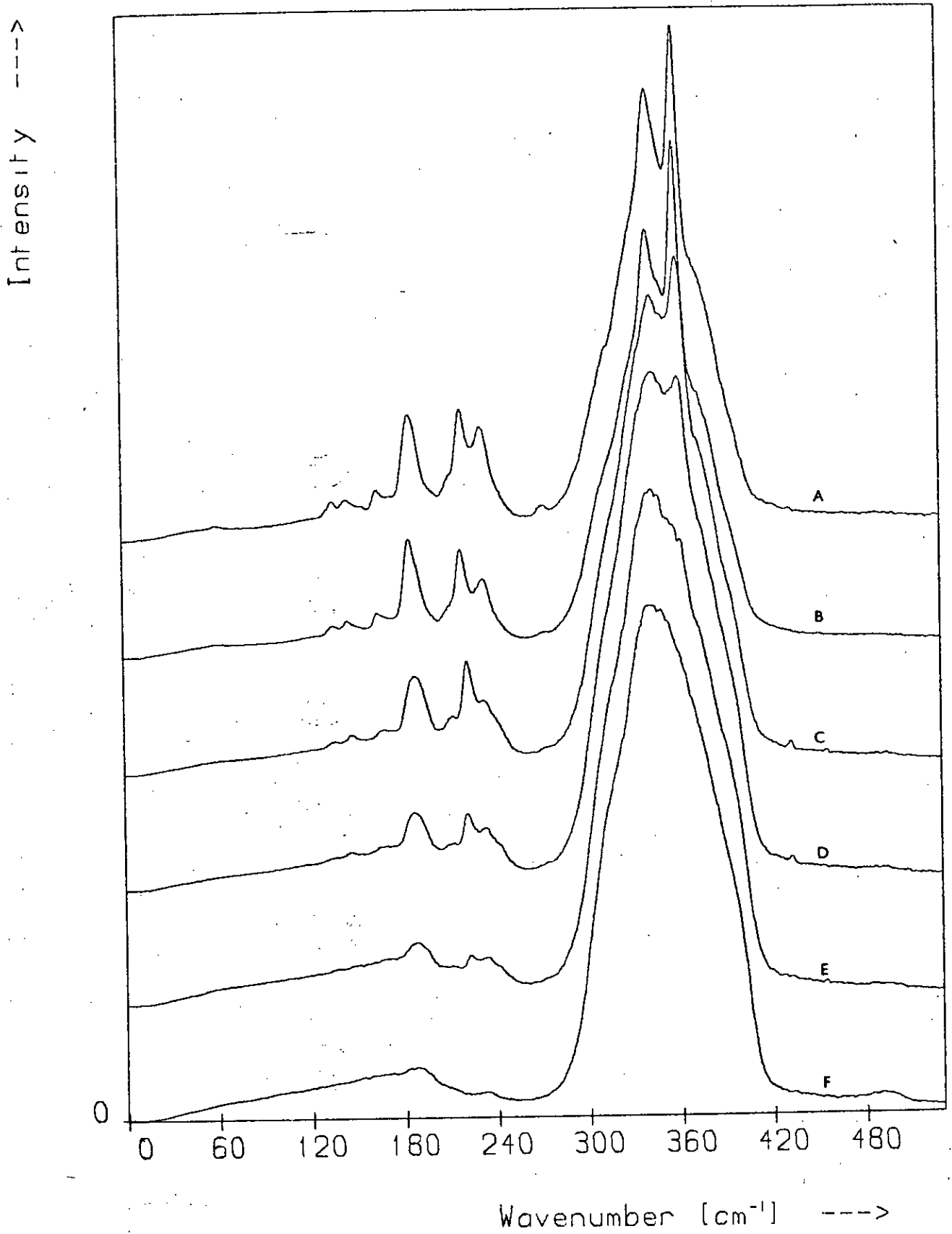
Raman Spectra: $As_{43}S_{57}$
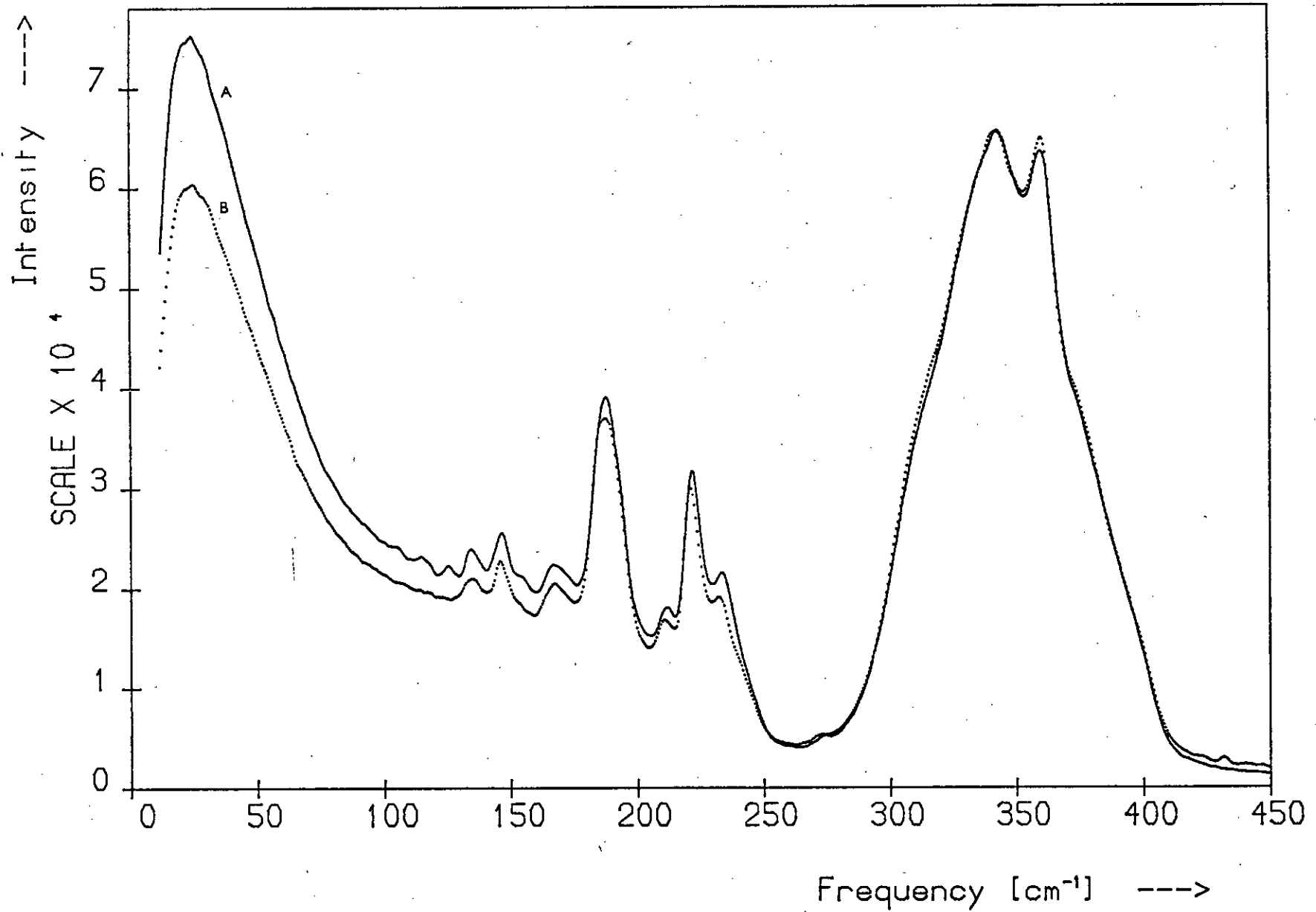
of Figure 5.62 with Ward's data[1] suggests that the pronounced features at these frequencies in his a-$As_{40}S_{60}$ spectrum are due to an excess of arsenic in his sample rather than to plasma lines.

The use of the back-reflection scattering geometry in the case of the two opaque compositions, $As_{44}S_{56}$ and $As_{45}S_{55}$, has no significant effect on their spectra. Figure 5.65 shows two spectra obtained for the most As-rich transparent composition studied, $As_{43}S_{57}$, spectrum A being recorded in the back-reflection mode and spectrum B in the transmission mode. The spectra are normalised to the intensity of the 343 cm^{-1} peak and are virtually identical, apart from the divergence in intensities on either side of the normalisation frequency. This divergence was discussed in Section 4.3.4 and arises from the increased absorption of the scattered light in the transmission mode.

As the spectra of the As-rich glasses and the As-S crystals have no first-order bands beyond 450 cm^{-1} the region above this frequency is omitted in most of the remaining figures in this section.

5.6.2 Polarisation measurements

The observed VV-polarised Raman spectra of the transparent As-rich glasses are shown in Figure 5.66, along with the corresponding spectrum of a-$As_{40}S_{60}$ for comparison. The spectra, which are normalised to peak intensity at $\sim$339 cm^{-1}, are displaced vertically for clarity. As in the case of the S-rich glasses, the VV spectra are very similar to their polarisation-unanalysed counterparts and yield no further information.

The VH spectra obtained for these four compositions are shown in Figure 5.67 and differ considerably from the VV and polarisation-unanalysed spectra. They have been normalised to peak intensity at $\sim$315 cm^{-1} and are shown displaced above one another. The VH spectra differ significantly from the other two types in three respects: the shape of the 300 – 400 cm^{-1} band, the intensity of this band relative to the low-frequency peak and the

The VV-polarised Raman spectra of the compositions $As_{40}S_{60} - As_{43}S_{57}$.

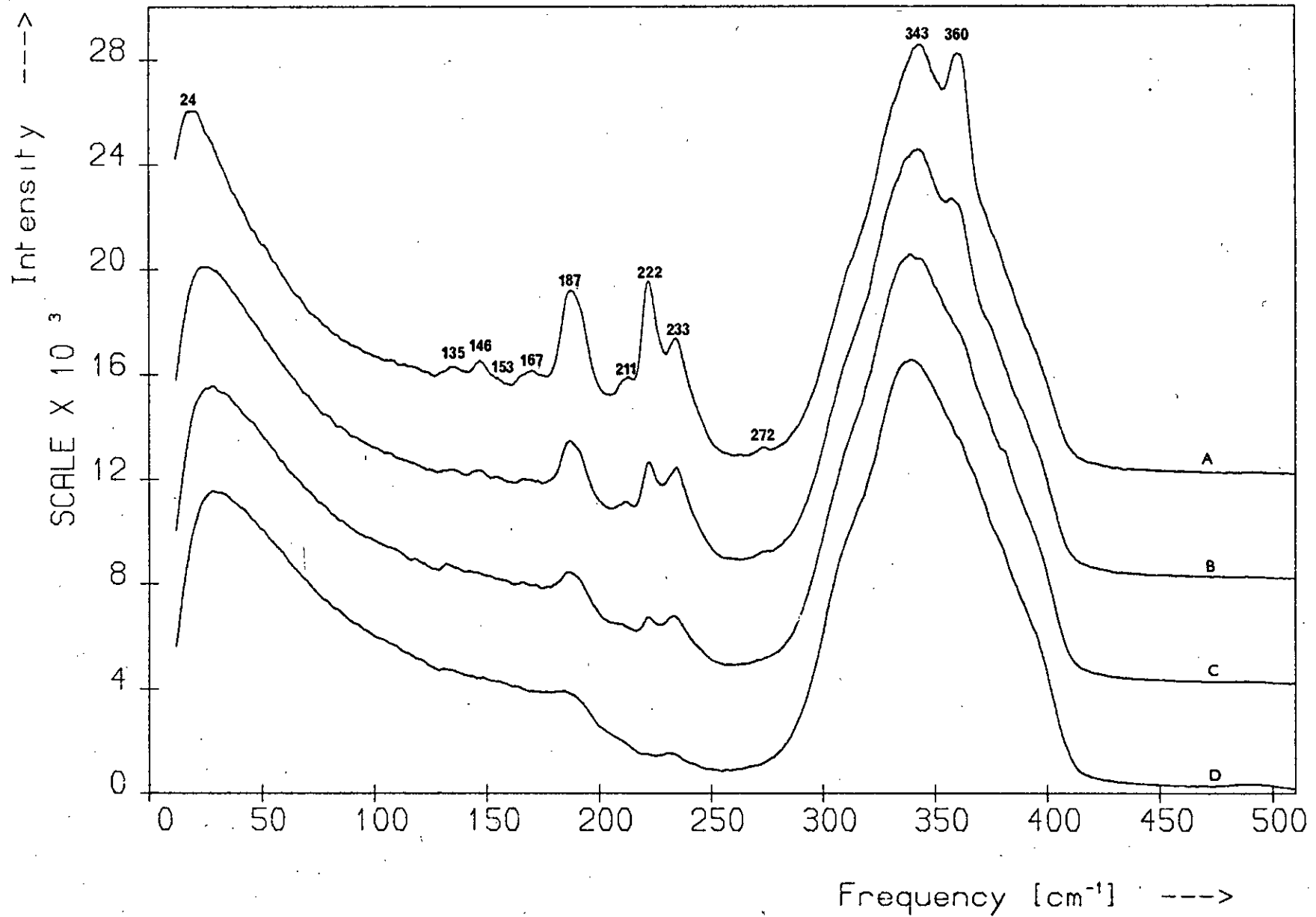| Spectrum		Composition
A	—	$As_{43}S_{57}$
B	—	$As_{42}S_{58}$
C	—	$As_{41}S_{59}$
D	—	$As_{40}S_{60}$

The VH-polarised Raman spectra corresponding to the compositions in

Figure 5.66 (A — D as above).

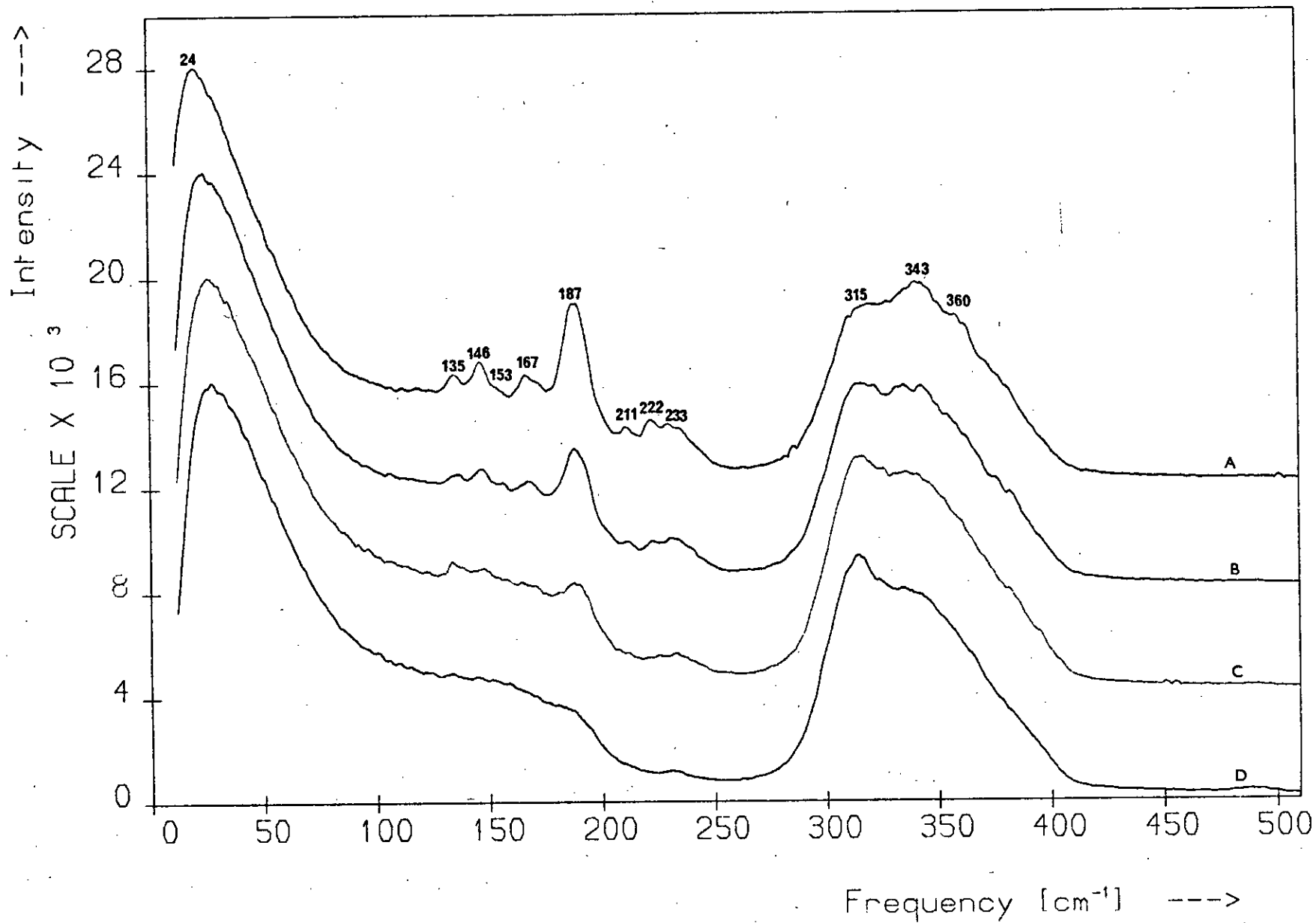The depolarisation spectra corresponding to the compositions in
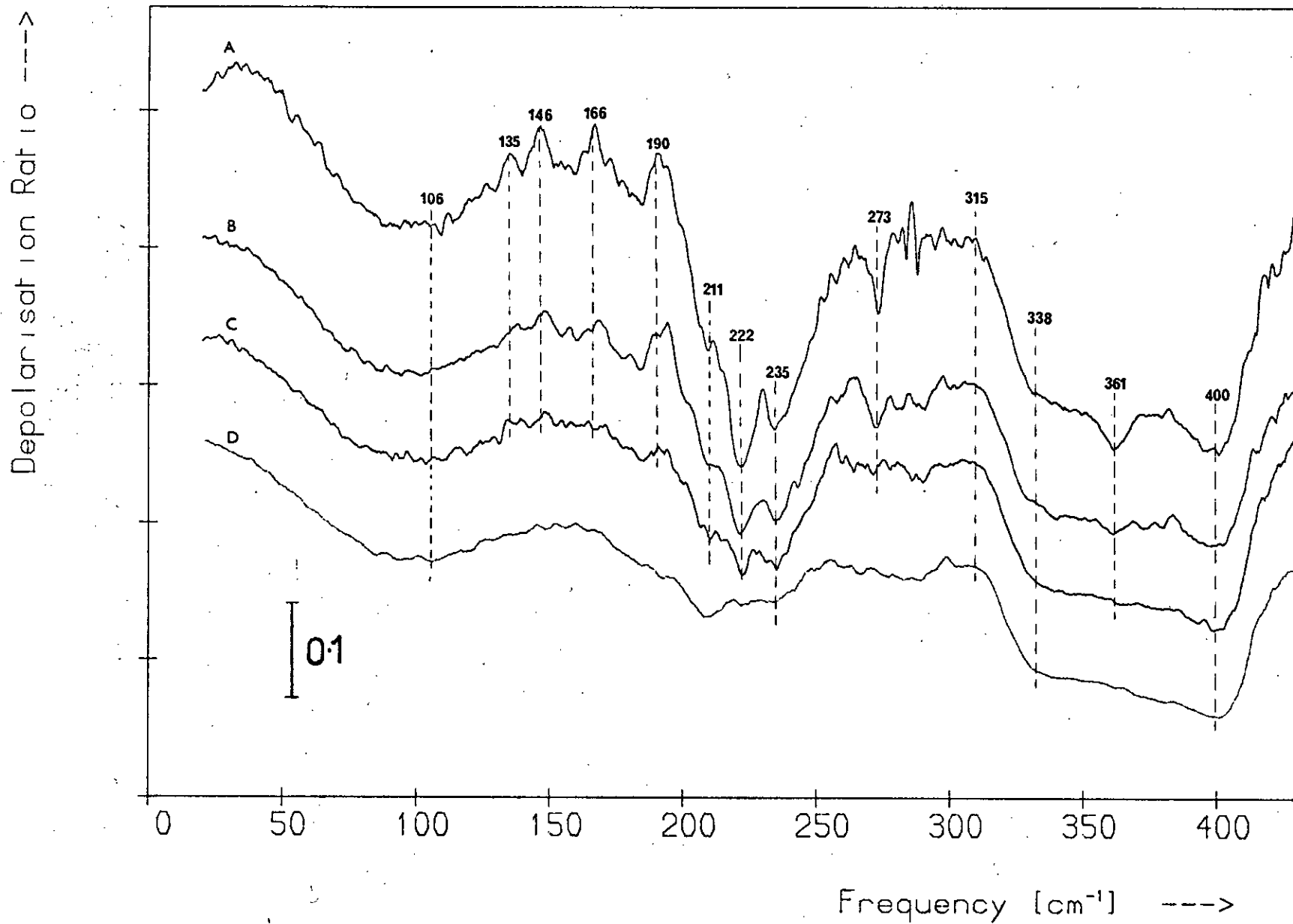
Figure 5.66 (A — D as above).

VV Polarised Spectra of the As-Rich Glasses

VH Polarised Spectra of the As-Rich Glasses

Depolarisation Spectra of the As-Rich Glasses

profile over the $\sim$200 $-$ 250 cm^{-1} region.

As the As content increases, the peak at 315 cm^{-1} in the a-As$_{40}$S$_{60}$ VH spectrum is gradually obscured by the emergence of an intense band at 343 cm^{-1} and is present only as a square shoulder in the As$_{43}$S$_{57}$ spectrum. However, the 315 cm^{-1} vibration is clearly present in all these glasses. Also, with increasing As content the low-frequency peak, which is much stronger than the 300 $-$ 400 cm^{-1} band, shifts towards the origin. The 222 and 233 cm^{-1} bands are considerably weaker in the VH spectra relative to the other bands.

The depolarisation spectra for these compositions are shown, vertically displaced, in Figure 5.68. All the features of the a-As$_{40}$S$_{60}$ depolarisation spectrum are present in the As-rich spectra, which have essentially the same shape as the a-As$_{40}$S$_{60}$ spectrum but have, superimposed on it, numerous sharp dips and peaks at frequencies corresponding to the sharp structure in the As-rich Raman spectra. The peaks, which correspond to depolarised bands, emerge at 135, 146, 166 and 190 cm^{-1} while the dips, which arise from polarised bands, appear at 211, 222, 235, 273 and 361 cm^{-1}. It will be shown in Section 5.6.3 that most of these sharp bands are due to the presence of the β polymorph of c-As$_4$S$_4$ in the glass; these results are particularly interesting because none of the published Raman studies of c-As$_4$S$_4$[1,2,9,10,14] contain polarisation data due to the fact that the samples used in each case were not good single crystals. The polarisation properties of β-As$_4$S$_4$, however, are clearly apparent in Figure 5.68. Polarisation measurements can only be made on powdered or polycrystalline samples by immersing them in a medium of similar refractive index, otherwise they tend to depolarise the incident beam[111,112]. The refractive index of the glassy matrix must be sufficiently well matched to that of the As$_4$S$_4$ crystallites that they do not depolarise the beam.

These polarisation results are in agreement with Solin's polarisation data on As$_2$S$_3$ vapour[45], which is thought to contain some of the monomer

species present in the glasses, in particular the As_4S_4 molecule (see Section 5.6.3).

The $a-As_{40}S_{60}$ features, consisting of the dips at ~106, 338 and 400 cm^{-1}, the hump at 160 cm^{-1} and the shoulder at 315 cm^{-1}, are not only present in the As-rich spectra but also do not shift in frequency as the As content increases. The weak feature at 272 cm^{-1} in the Raman spectra of the compositions $As_{42}S_{58}$ and $As_{43}S_{57}$ is more obvious in the depolarisation spectra.

5.6.3   Discussion

The glass-forming region of the As-S system is known to extend only to ~43 at.% As [108 –110]. For compositions more As-rich than $As_{43}S_{57}$ crystal-glass phase separation occurs [109] and this accounts for the change in transparency, colour and texture of these materials that was mentioned earlier (Section 4.2.2.1). In their study of the thermal properties of As-S glasses, Myers and Felty [110] attribute the inability to quench such glasses with more than 43 at.% As to melting behaviour. They suggest that the corresponding liquids are composed mainly of small molecules, such as As_4S_4, which readily order into a crystal lattice as the melt is cooled. Thus addition of As to the $As_{40}S_{60}$ composition results in a break-down of the continuity of the As-S network and the formation of small molecular species. Ward, who has also recorded the Raman spectra of As-rich compositions in this system [1], compares his data with the Raman spectrum of crystalline As_4S_4 and concludes that the sharp structure which grows with increasing As content arises from the appearance of As_4S_4 molecules in these materials. The spectra of Figure 5.62 are in good agreement with Ward's results but our interpretation of them differs slightly from his, for on closer inspection the sharp structure is seen to bear only a general resemblance to his $c-As_4S_4$ spectrum. In particular, there are some lines in the glass

spectra that have no counterparts in the c-As$_4$S$_4$ spectrum.

The presence of the numerous sharp features makes it difficult to observe any spectral changes caused by structural changes in the As-S network, which is responsible for the continuous background in the spectra. Those lines of the glass spectra that are not associated with the As$_4$S$_4$ molecule cannot be unambiguously attributed to a change in the network structure since they might arise from the presence of other As-S monomers in the glass. Accordingly, the first step in the analysis of the glass spectra was to compare them with the vibrational spectra of the various As-S species in order to distinguish the monomer bands from those due to the network. There are, as was shown in Section 2.2, numerous molecular species in the As-S system, some only recently discovered, and not all of these have had their vibrational spectra recorded. Samples of as many of these molecular forms as possible were obtained in the present study and their Raman spectra measured.

Figures 5.69 to 5.71 compare the spectra of a-As and some As-S compounds with the As$_{45}$S$_{55}$ spectrum, in which the sharp features are clearest. It is obvious from Figure 5.69 that c-As$_2$S$_3$ is not present in significant amounts in the As-rich glasses for many of its strongest bands (e.g. those at 292 and 310 cm^{-1}) are absent from the glass spectrum. The spectrum of α-As$_4$S$_4$ also shown in this figure is identical with the one obtained by Ward[1] with which he compared his glass data. There is a certain resemblance between the α-As$_4$S$_4$ spectrum and the prominent structure in the glass spectrum and one can see that if the very sharp lines in the α-As$_4$S$_4$ spectrum were considerably broadened due to disorder it could account for many of the glass bands. The α-As$_4$S$_4$ doublet centred near 187 cm^{-1} could, for example, coalesce on broadening to form the single broad glass band at this frequency. However, some of the glass bands do not occur exactly at the frequency of their expected α-As$_4$S$_4$ counterparts —

Figure 5.69

Raman spectra: A — c-As$_2$S$_3$

B — As$_{45}$S$_{55}$

C — α-As$_4$S$_4$

Figure 5.70

Raman spectra: A — β-As$_4$S$_3$

B — As$_{45}$S$_{55}$

C — β-As$_4$S$_4$

Figure 5.71

Raman spectra: A — c-As$_4$S$_5$

B — As$_{45}$S$_{55}$

C — a-As

Raman Spectra: c-As$_4$S$_4$, As$_{45}$S$_{55}$ and c-As$_2$S$_3$
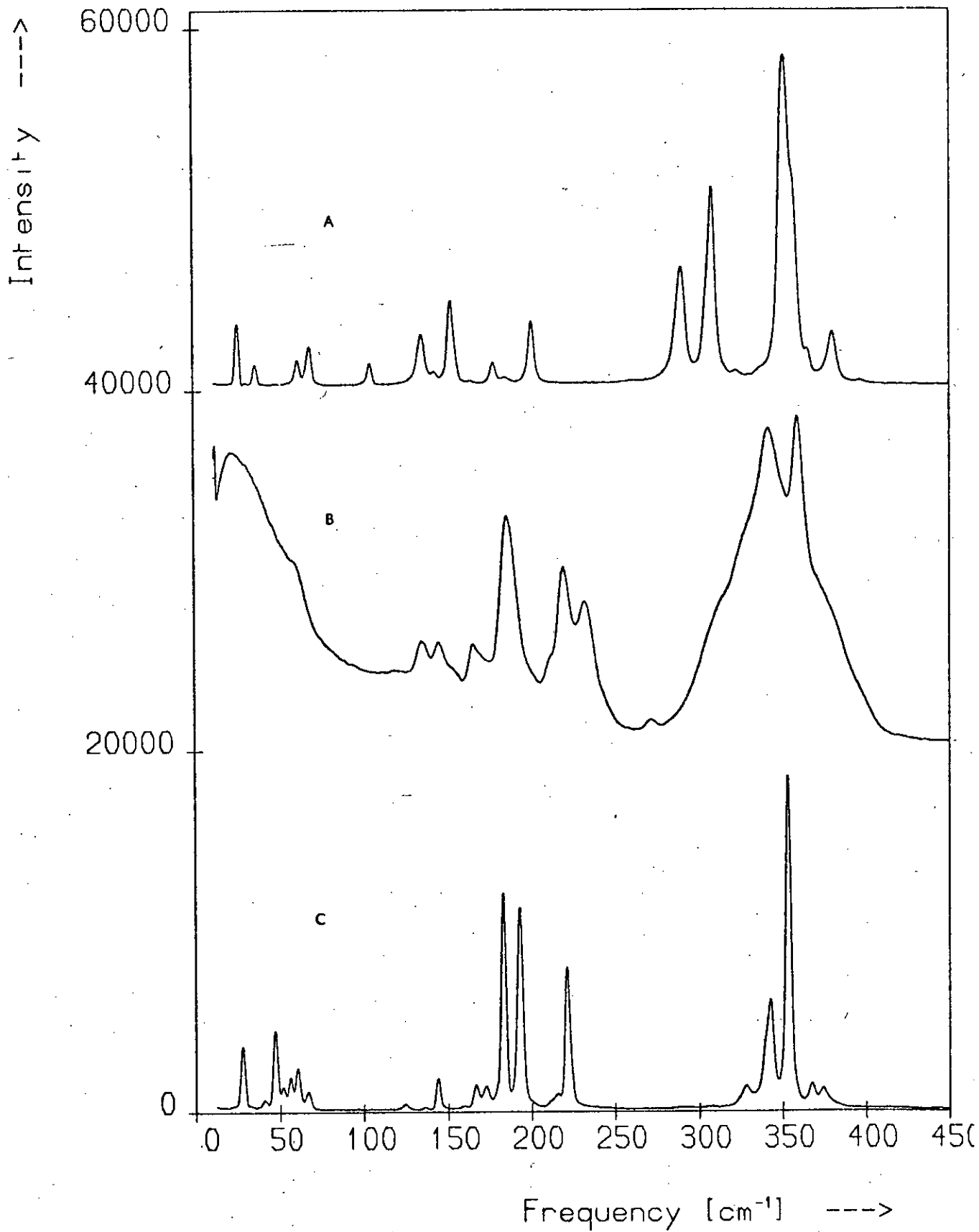
Raman Spectra: c-As$_4$S$_4$, As$_{45}$S$_{55}$ and c-As$_4$S$_3$
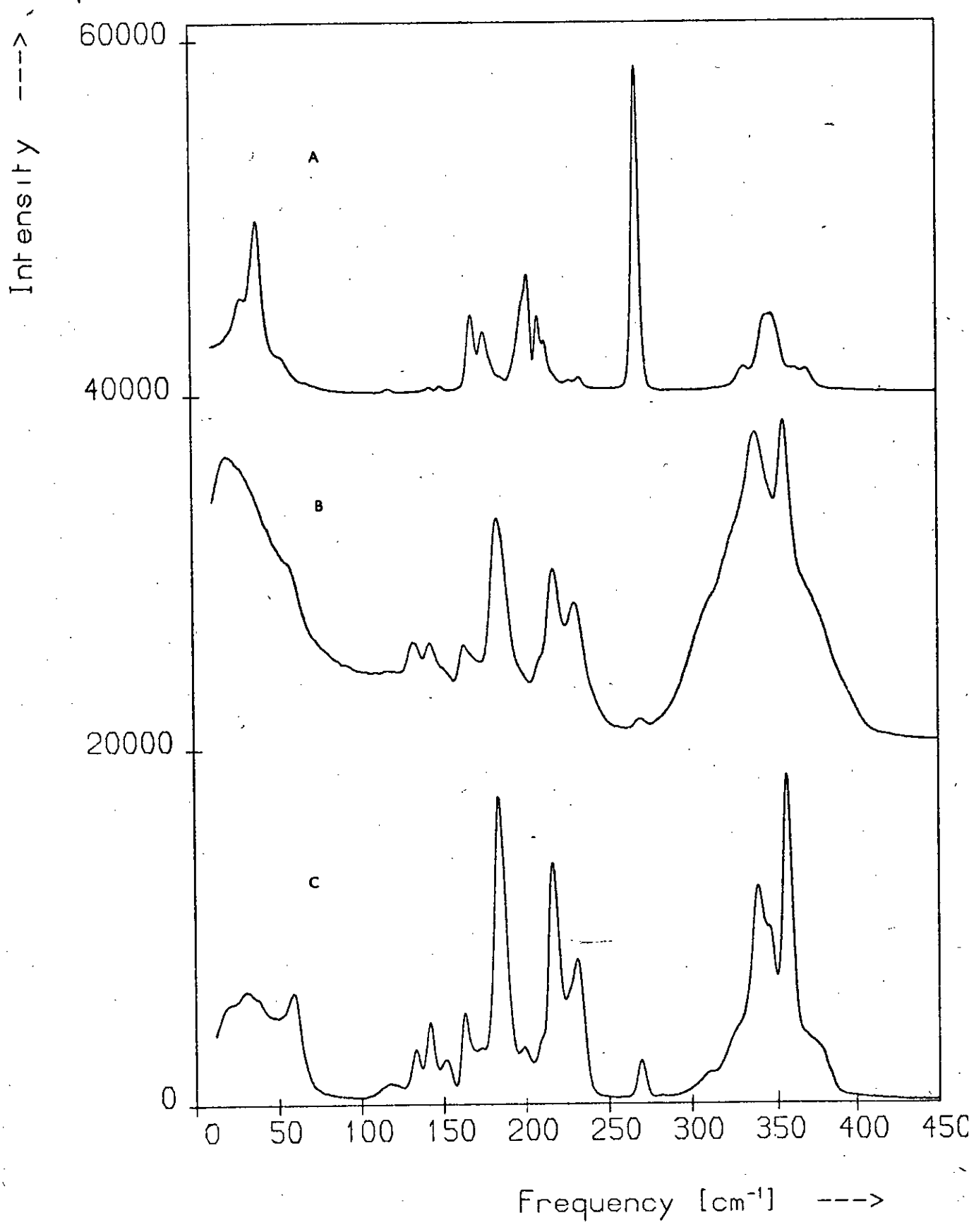
Raman Spectra: a-As, As$_{45}$S$_{55}$ and c-As$_4$S$_5$
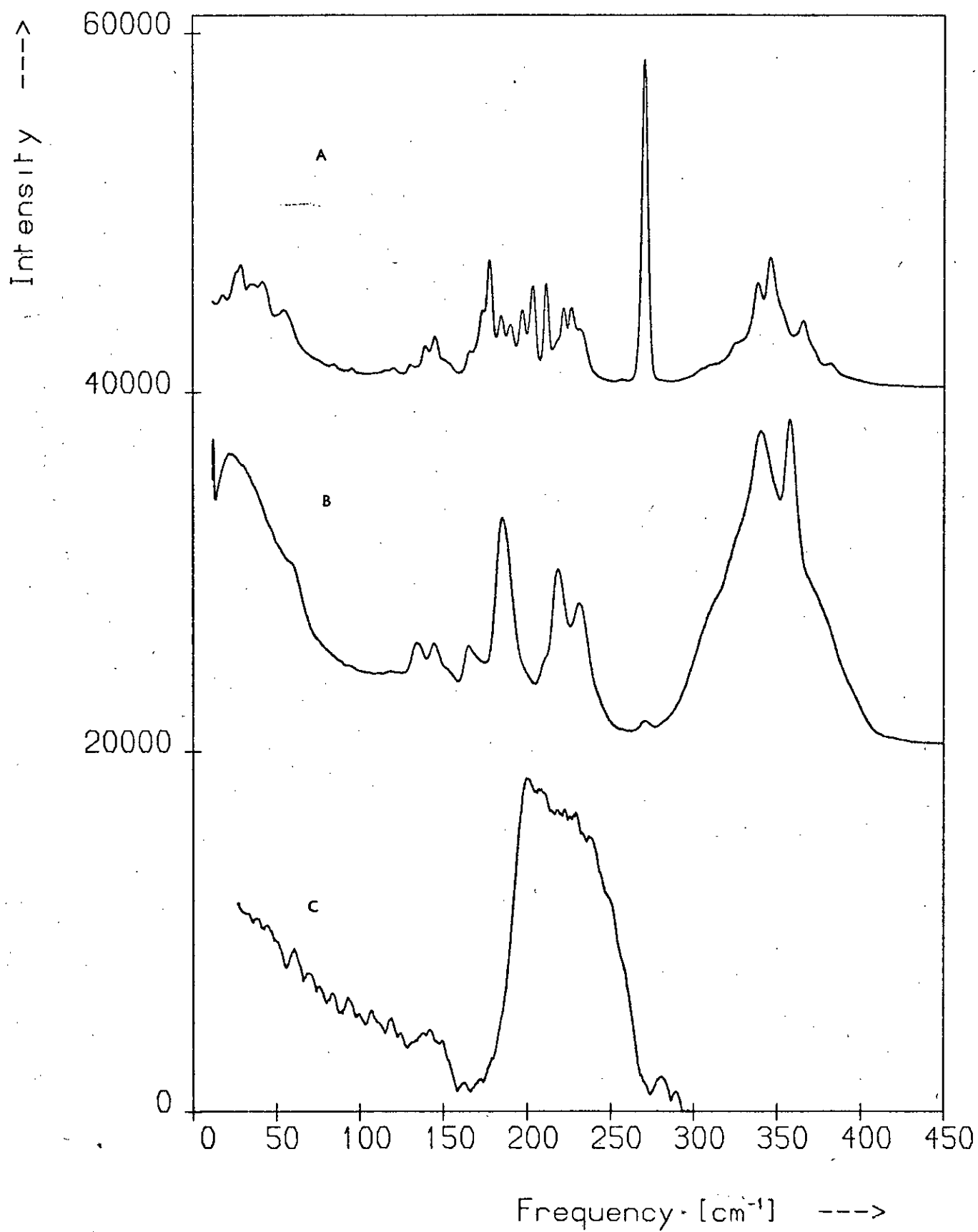
in particular the 360 cm^{-1} $As_{45}S_{55}$ band occurs $\sim$6 cm^{-1} above the main α-As_4S_4 band — and, more important, the structure at 135, 153, 233 and 272 cm^{-1} in the glass spectra do not correspond to any features in the α-As_4S_4 spectrum. Thus Ward's analysis is not entirely satisfactory.

Figure 5.70 shows the spectra of c-As_4S_3, $As_{45}S_{55}$ and a supposedly crystalline sample of As_4S_4 made in the Department by slowly cooling a melt of this composition. The c-As_4S_4 spectrum in this figure is very similar to the $As_{45}S_{55}$ spectrum, the only differences are that in the former some extra structure is resolved, the bands are sharper and more pronounced, and the continuous background is considerably smaller. Because of this similarity of the spectra it was thought at first that the As_4S_4 sample was not crystalline and basically had the same nature as the As-rich glasses but comparison of its spectrum with the published Raman data for β-As_4S_4[14] showed that the sample was indeed predominantly crystalline and consisted mainly of the β polymorph (see Section 5.7). The features near 135, 153, 233 and 272 cm^{-1} in the $As_{45}S_{55}$ and Department-made β-As_4S_4 spectra are absent from the published spectra of both α- and β-As_4S_4 but the remaining sharp structure can be confidently attributed to regions of β-As_4S_4 in the glasses and since it corresponds exactly to the β-As_4S_4 spectrum there are no line shifts to explain and there is no need to postulate disorder-induced line-broadening as there was when accounting for the features in terms of α-As_4S_4. Porter and Sheldrick[14] suggest that β-As_4S_4 is more stable at higher temperature than α-As_4S_4 which would explain why the β rather than the α polymorph is formed in the glasses.

Although attributing most of the sharp structure in the glass spectra to β- instead of α-As_4S_4 is an improvement on Ward's analysis the extra lines remain unaccounted for. From Figure 5.70 it is seen that the most intense line in the spectrum of c-As_4S_3 occurs at 271 cm^{-1} which corresponds to the frequency of one of the non-As_4S_4 bands. Some of the other

unassigned glass bands have no counterparts in the c-As_4S_3 spectrum and so this compound cannot account for all the extra lines. Also, the very weak intensity of the 272 cm^{-1} band in the glass spectra suggests that the other c-As_4S_3 bands would not be detected in them. The unassigned 135 and 233 cm^{-1} bands are both several times larger than the 272 cm^{-1} feature. Comparison of the c-As_4S_3 spectrum of Figure 5.70 with the i.r. spectrum of β-As_4S_3[11] suggests that the sample made in the Department was the β polymorph. The i.r. spectra of the α and β polymorphs are similar and as the α form may thus also have a band at 271 cm^{-1} it is uncertain which of the two polymorphs is responsible for the 272 cm^{-1} glass feature. Although the α form may have bands at 135 and 233 cm^{-1} these are unlikely to be stronger than the 271 cm^{-1} feature so these extra lines are probably not due to α-As_4S_3 either.

Figure 5.71 compares the spectra of $As_{45}S_{55}$, c-As_4S_5 and a-As. The strongest line in the c-As_4S_5 spectrum also occurs at 271 cm^{-1} so it is possible that this material may be responsible for the glass feature at this frequency. As in the case of c-As_4S_3, the other bands of the c-As_4S_5 would not be detectable in the glass spectra and could not in any case account for the other unassigned features. The 272 cm^{-1} feature in the glass spectra may therefore arise from the presence of c-As_4S_3 or c-As_4S_5 or both.

It is clear from Figure 5.71 that a-As itself cannot account for any of the unassigned glass features and is not present in significant quantities in the glasses. However, it will be shown below that the 233 cm^{-1} feature may be due to the vibration of As—As bonds in the As-S network. The vibrational spectra of a- and c-As[33,34] have features near this frequency.

Samples of the other solid compounds in the As-S system were not available and as the vibrational spectra of these materials have not

yet been published no conclusions could be drawn about their presence in the glasses. However, the Raman spectra of some of the monomer species in the vapour phase have been recorded[17,45]. The spectrum of vaporised As_2S_3 glass exhibits at least 18 bands of which 9 or more are strongly polarised[45]. The As_4S_6 molecule should give rise to 8 bands of which 2 are polarised. By analogy with its isomorph As_4O_6 the 2 polarised bands are expected at 395 and 271 cm^{-1}. Polarised bands are observed in the vapour spectrum at 416 and 269 cm^{-1} which suggests that the As_4S_6 molecule is present. (It was shown in Section 5.6.2 that the 272 cm^{-1} glass feature is also polarised.) The other bands in the vapour spectrum are mainly due to the As_4S_4 monomer. Those lines not arising from As_4S_6 or As_4S_4 molecules are attributed to As_4, S_2 and other 'as yet unidentified' species. As the As-rich glass spectra contain no features near 416 cm^{-1} it is unlikely that As_4S_6 molecules are present in these glasses and so the 272 cm^{-1} feature cannot be attributed to this molecule. Of the other unassigned glass bands only the 233 cm^{-1} peak is near to a band in the vapour spectrum. This vapour band occurs at 235 cm^{-1}; it is polarised (as is the 233 cm^{-1} glass band) and must be due to one of the unidentified species present since neither As_4[113] nor S_2[93] has a band at this frequency.

Raman data on As-rich mixtures of arsenic and sulphur vapours suggest that they contain As_4, As_4S_3, As_4S_4 and As_2S_2 molecules[17]. The only band in the spectra of these mixtures which coincides with an unassigned glass band is the 271 cm^{-1} line characteristic of As_4S_3.

The Raman spectrum of rhombohedral c-As has been recorded and exhibits 2 bands, one at 195 cm^{-1} and the other at 257 cm^{-1} [33,34]. Clearly these cannot account for the unassigned glass features.

These unassigned features also behave differently from the β-As_4S_4 bands as a function of laser dosage. This effect, which is discussed in more detail in Section 5.7, consists of a change in the peak intensity

of the unassigned bands relative to the β-As_4S_4 lines as a function of exposure to the incident light. This effect probably accounts for the small differences in the relative intensities of some of the sharp structure in Figures 5.62 and 5.63. For example, Figure 5.63 shows that in the $As_{45}S_{55}$ spectrum the 135 cm^{-1} peak is larger than its neighbour but in all the others it is smaller. These intensity changes in the unassigned bands relative to the β-As_4S_4 component of the spectra cannot be accounted for by the decrease in intensity of the continuous background arising form the As-S network (see Section 5.7) and confirm the fact that these bands are not associated with β-As_4S_4. The intensities of these unassigned bands also change relative to each other as a function of exposure to light, which suggests that they arise from different structural features in the glasses. In Figure 5.76 (after p.193), for example, the 233 cm^{-1} peak is smaller than that at 271 cm^{-1}.

The 272 cm^{-1} peak has been attributed to the presence of either As_4S_3 or As_4S_5 molecules in the glasses. The remaining unassigned bands must be due to other As-S compounds, possibly not yet isolated, or must be associated with features of the As-S network. Photostructural changes in c-As_4S_4 provide some evidence that the 233 cm^{-1} band arises from As—As bonds in the network. It is generally believed[9,114,115] that c-As_4S_4 is transformed by light predominantly into c-As_2S_3, though some workers observe no photodecomposition at all[10,116]. Porter and Sheldrick[14] have monitored the Raman spectra of both α- and β-As_4S_4 as a function of laser dosage and have shown that they change considerably, both degenerating into the same spectrum. In each spectrum the lattice modes disappear completely and a sloping background, similar to that in the glasses, develops over the region 0 — 200 cm^{-1}. The internal bands decrease in intensity and seem to broaden and coalesce in some cases. Numerous weak bands appear in the 100 — 200 cm^{-1} region. The most interesting change, as far as the present study is concerned, is the growth of

a very intense band near 230 cm^{-1}. The complexity of the resulting spectrum together with the disappearance of the lattice modes suggests to these authors that the photodecomposition product is polymeric. The resulting spectrum bears little resemblance to that of c-As$_2$S$_3$. If polymerisation is occurring then As—As bonds will almost certainly be formed in the product. One expects a frequency in the region of 260 cm^{-1} [11] for a stretching vibration of such bonds and the i.r. and Raman spectra of a-As have a relatively strong feature near this frequency.

The 233 cm^{-1} feature appears in some of the published c-As$_4$S$_4$ Raman spectra[9,10,14] but not in others[1,2,14]. It was completely absent from the α-As$_4$S$_4$ spectrum recorded in the present study (see Figure 5.3) and neither were any light-induced changes observed in this spectrum. However, Porter and Sheldrick state that spectral changes are observable after laser irradiation for ~1 hour and their photodecomposition spectra were obtained after 'prolonged' irradiation. In the present case the time taken to record the spectrum was ~20 minutes and any spectral changes occurring over this period might not be noticeable. Schuermann and Ritter[10] observe no change in the Raman spectrum of realgar even after twelve hours' exposure to 60 mW of focussed 6328 Å radiation.

Porter and Sheldrick also state that the β form converts more slowly than the α. If the As$_4$S$_4$ molecules polymerise via the formation of As—As bonds then the difference in photodecomposition rates may arise from the fact that the shortest intermolecular As$\cdots$As contacts in β-As$_4$S$_4$ are appreciably longer than in α-As$_4$S$_4$[14]. Whitfield[11] also attributes the weak ~233 cm^{-1} peak that occurs in the Raman spectrum of c-As$_4$S$_4$ to As—As bonds.

In the spectra of the As-rich glasses we have observed photo-induced changes similar to those occurring in the case of c-As$_4$S$_4$. The photo-decomposition is gradual, as it is for c-As$_4$S$_4$, so that only small changes

are observed over a one-hour period, which is approximately the time taken to record the spectrum. This suggests that the structural features giving rise to the unassigned bands are not formed solely by the incident light but are already present in significant quantities in the glasses before irradiation, since these bands are prominent in all the glass spectra. If the unassigned bands arose only as a result of irradiation then they would have to grow to this extent in the first ~15 minutes of exposure, which seems unlikely.

Another spectral change observed in c-As_4S_4 by Porter and Sheldrick is the growth of a band at ~270 cm^{-1}. It seems that when the As and S atoms combine to form a network rather than As_4S_4 molecules (either as a result of irradiation or during the glass-forming process) As_4S_3 or As_4S_5 molecules are also formed. If network formation requires less of one element than the other then these monomers may be produced to take up the surplus atoms.

At present it cannot be determined whether or not the other unassigned bands are due to network features. It was thought at first that a valence force field calculation for an As_2S_4 'molecule' (i.e. the network unit $_S^S$>As—As$<_S^S$) might account for some of these bands. The calculation for the general X_2Y_4 molecule is fairly lengthy so a preliminary calculation was made using Herzberg's frequency formulae[64] for the simpler case of the planar X_2Y_4 molecule, which has 12 normal modes, 6 being Raman active. However, too many unknowns were involved to fix the frequencies with any certainty. Lucovsky[46] has also used the molecular model approach to interpret his i.r. and Raman data on $As_{43}S_{57}$ glass. He calculates the vibrational frequencies of an isolated $S_2As—AsS_2$ cluster and maintains that such clusters account for the sharp Raman bands, which are attributed in the present study simply to the presence of β-As_4S_4 in the glass. Such an analysis will inevitably yield frequencies near c-As_4S_4 bands since, as Lucovsky observes, 'the network former

$S_2As-AsS_2$ is also a natural precursor to the molecule As_4S_4' and the unknown values of the geometrical parameters in the calculation must be based on the molecular structure of As_4S_4. It is unlikely that the frequencies of an As_2S_4 network unit would coincide exactly with those of $\beta-As_4S_4$ as suggested by Lucovsky's analysis. A molecular calculation may be appropriate at a later stage when the structure of the network is known more exactly. The features at 135 and 153 cm^{-1} must remain unassigned at present.

The 315 and 395 cm^{-1} features of the $a-As_{40}S_{60}$ spectra are also present in the spectra of the As-rich glasses, at least up to the composition $As_{43}S_{57}$, though they become less pronounced due to the emergence of strong $\beta-As_4S_4$ bands near these frequencies (see Figures 5.62, 5.63, 5.66 and 5.67). It follows that AsS_3 pyramids and As—S—As links are still present in the network, which is to be expected. This is more obvious in the depolarisation spectra (Figure 5.68), where the characteristic AsS_3 and As_2S features at 106, 160, 315, 338 and 400 cm^{-1} clearly persist right up to the $As_{43}S_{57}$ composition. Furthermore, the fact that none of these features shift in frequency suggests that no geometrical changes occur in the pyramids and links as the As content is increased.

The extent of the glass-forming region in the As-S system has been determined by Flaschen et al.[108]. These workers show that the region terminates approximately at the composition $As_{43}S_{57}$. As was mentioned in Section 4.2.2.1 all the sulphide glasses examined in the present study were transparent to visible light apart from the compositions $As_{44}S_{56}$ and $As_{45}S_{55}$, which were pink, opaque and granular in appearance. Figures 5.72(a) — (e) show photographs of some of the As-rich glasses taken through a scanning electron microscope. The specimen compositions for the micrographs are: (a) — $As_{43}S_{57}$; (b) and (c) — $As_{44}S_{56}$; (d) and (e) — $As_{45}S_{55}$. The magnifications are given in the figure. The $As_{43}S_{57}$ micrograph shows no features but those of the two opaque compositions show pockets of material
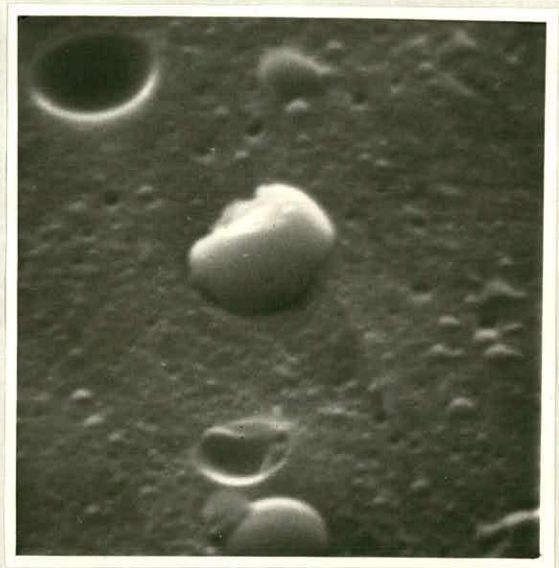
Figure 5.72

Electron micrographs of $As_{43}S_{57}$, $As_{44}S_{56}$ and $As_{45}S_{55}$.
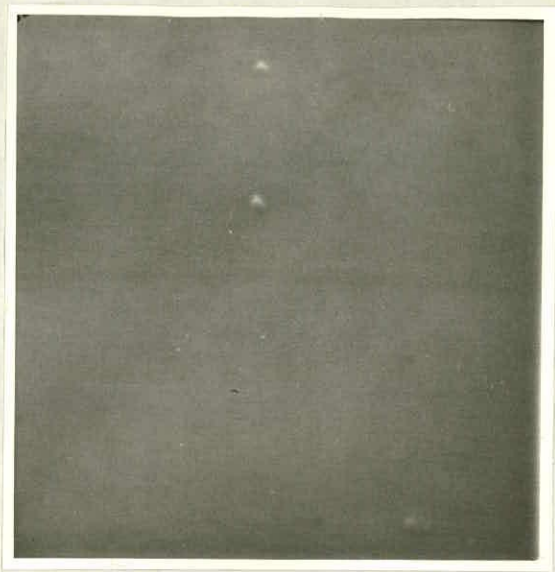
(a) $As_{43}S_{57}$: x 20,000
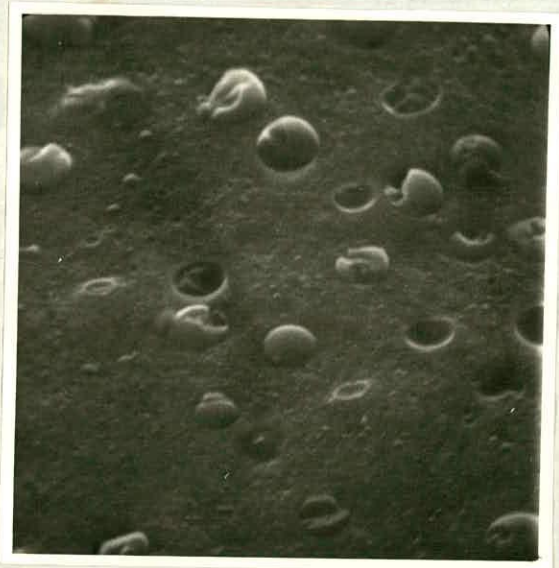
(b) $As_{44}S_{56}$: x 10,000

(c) $As_{44}S_{56}$: x 20,000
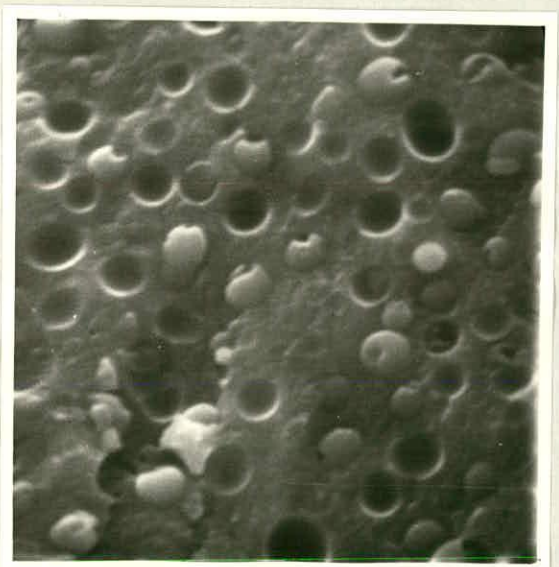
(d) $As_{45}S_{55}$: x 10,000
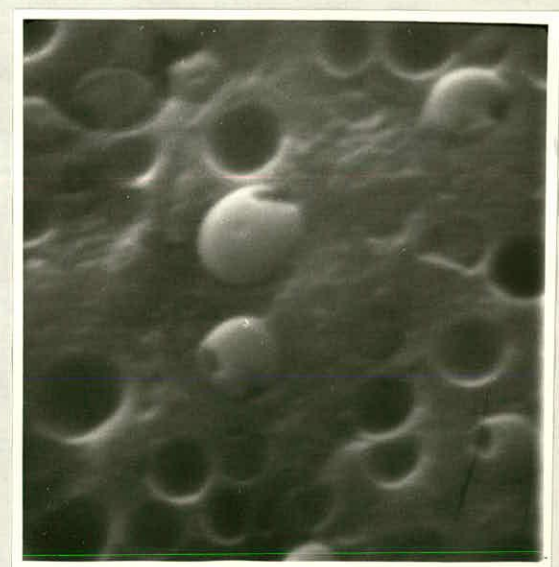

(e) $As_{45}S_{55}$: x 20,000

embeded in a matrix. Crystal-glass phase-separation is occurring in the compositions outwith the glass-forming region and the pockets are presumably mainly crystallites of β-As_4S_4. The matrix in which they are embedded will be glassy in nature and will account for the continuous background in the Raman spectra of these compositions. The crystallites are $\sim 1\mu$ in diameter for both $As_{44}S_{56}$ and $As_{45}S_{55}$ but are more numerous in the latter. The presence of these crystallites accounts for the opacity and granular appearance of these two compositions. Similar micrographs of glasses in the range $As_{40}S_{60}$ to $\sim As_{45}S_{55}$ have been obtained by Maruno and Noda[109], who also record the X-ray diffraction patterns of these materials. They conclude from their X-ray data that the crystallites are realgar and show that its characteristic X-ray pattern is present in the spectra of only those annealed glasses with As content in excess of ~ 43 at.%.

Figure 5.72(a) shows that the materials seemed to be homogeneous glasses up to 43 at.% As. The change from transparent to opaque occurs abruptly at some composition between $As_{43}S_{57}$ and $As_{44}S_{56}$. This abrupt change, however, is not apparent in the Raman spectra, where the 'crystalline' lines grow steadily as the As content is increased beyond 40 at.%. The As_4S_4 molecules in α- and β-As_4S_4 are identical and it is the different packing arrangements of the molecules in the two poly-morphs that is responsible for the differences in the Raman spectra. Consequently, as the As_4S_4 bands of the As-rich glasses correspond exactly to those of the β polymorph, the As_4S_4 molecules are not dispersed randomly through the glasses but must mainly form 'crystallites' of β-As_4S_4. Micrograph (a) suggests that in the glasses containing between 40 and 43 at.% As these regions are less than ~ 300 Å in diameter.

During the course of the present study similar results to those shown in Figure 5.62 have been obtained by Bertoluzza et al.[117]. These authors also attribute the sharp structure in the As-rich spectra to β-As_4S_4.
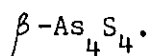
5.7 Photo-induced spectral changes

The main photo-induced change observed in the Raman spectra of these materials was described in Section 4.3.5 and consisted of a gradual decrease in intensity over the whole spectral range studied. This effect occurred in all the glasses examined and the average rate of signal loss was ~3% per hour though it was higher than this in all the As-rich glasses, and was ~10% per hour in the only non-annealed specimen. The count loss was approximately linear with time over the first few hours but eventually tapered off. There was no sign of recovery in the first ~12 hours after irradiation ceased. Apart from absorption effects, there was no change at all in the spectral density in the case of the S-rich glasses and a-As_2S_3, that is no new spectral features appeared and those initially present did not alter. It follows from this last observation that no significant structural changes are taking place in these glasses during irradiation and so if the gradual intensity loss is due to a structural change, it must be associated with one that preserves the basic units making up these materials.

Berkes et al.[118] have studied photo-induced changes in a-As_2S_3 thin films and report that illumination with band-gap radiation leads to dissociation:

$$As_2S_3 \xrightarrow{h\nu} 2As + 3S$$
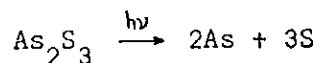
A more recent study of structural changes occurring in such films on exposure to band-gap radiation was carried out by deNeufville et al.[119] using X-ray diffraction. These authors found no evidence of dissociation and attributed the photo-response of this material to polymerisation of As_4S_6 molecules. They suggested that freshly evaporated a-As_2S_3 films were composed of 'hard sphere' As_4S_6 molecules and on illumination these monomers cross-link to form the network structure characteristic of the bulk glass. They also showed that annealing the films produced structural changes that were essentially identical to those induced by illumination

and the X-ray pattern of the annealed or irradiated film was very similar to that of the bulk glass.

Solin[45] has since performed a Raman scattering investigation of these structural transformations in a-As_2S_3 films and basically confirms the model of deNeufville et al. He states, however, that there appears to be more than one molecular species in the freshly evaporated film and As_4S_6 molecules are not necessarily present. Whereas the Raman spectrum of the bulk glass consists of broad features, that of the as-deposited evaporated a-As_2S_3 film contains numerous sharp, intense bands superimposed on a continuous background similar to the bulk spectrum. Much of this structure can be attributed to the As_4S_4 monomer and the remaining lines indicate the presence of other species in the glass, possibly As_4S_6.

Neither dissociation nor polymerisation can account for the spectral changes observed in the present study since the basic shape of the spectra did not change at all during illumination. There is no sign of growing As or S bands and no sharp monomer features are present in the initial spectra, apart from in the case of the As-rich glasses.

Finkman et al.[39,120] have observed a decrease in the reduced Raman intensity of a-As_2S_3 with increasing temperature and attribute it to short range structural changes causing a decrease in vibrational coherence. (These authors state that the intensity decrease cannot be attributed to the disappearance of As—S bonds, as the observed activation energy of the effect is ~0.2 eV and thus much smaller than the bond energy.) They suggest that the local atomic configuration changes as the temperature increases and these configurational changes decrease the size of the 'coherence regions', i.e. the regions in which atoms vibrate with fixed phase relations. The waves scattered by the 'molecules' in such a region are in phase and thus the amplitudes add but the vibrations in different coherence regions have no fixed phase relationships and so the resulting scattered intensity is the sum of the intensities produced by the coherence

regions. The scattered intensity therefore depends on the average number of 'molecules' in a coherence region and on what proportion of the total number of 'molecules' in the scattering volume are in coherence regions. The Raman intensity will decrease if the average population of a coherence region decreases or if the number of 'molecules' outside coherence regions increases. If this process continues the reduced Raman intensity is expected to saturate.

There is evidence that a-As_2S_3 contains remnants of the layers present in c-As_2S_3 and Finkman et al.[39] suggest that the coherence regions may be identical with these layer regions. They describe a configurational change which disrupts the layer structure without changing the nature of the basic structural units. In this change bridging S atoms move as shown in Figure 5.73 so that adjacent pairs of AsS_3 pyramid units no longer share only one S atom as they do in the crystal layer. This change results in the formation of $-As\genfrac{<}{>}{0pt}{}{S}{S}As-S$ units which when connected to one another produce chain-like structures. Finkman et al. assume that in the layer-like regions there are definite phase relationships between the AsS_3 pyramid vibrations and they propose that the above configurational change reduces the extent of these coherence regions so that the scattered intensity decreases.

There is no significant change in the shape of the a-As_2S_3 spectrum with increasing temperature which suggests that this configurational change does not alter the geometry of the AsS_3 and As_2S units involved.

The As-rich glasses seemed to be more susceptible to photo-induced effects than did the S-rich compositions. The rate of signal loss was slightly higher in the As-rich glasses and they were more easily damaged by focussed radiation. As mentioned in Section 4.3.5, when unfocussed radiation was used neither the As- nor the S-rich samples sustained any damage but the spectra of both types exhibited a decrease in intensity with exposure. However, in the case of the As-rich glasses this signal
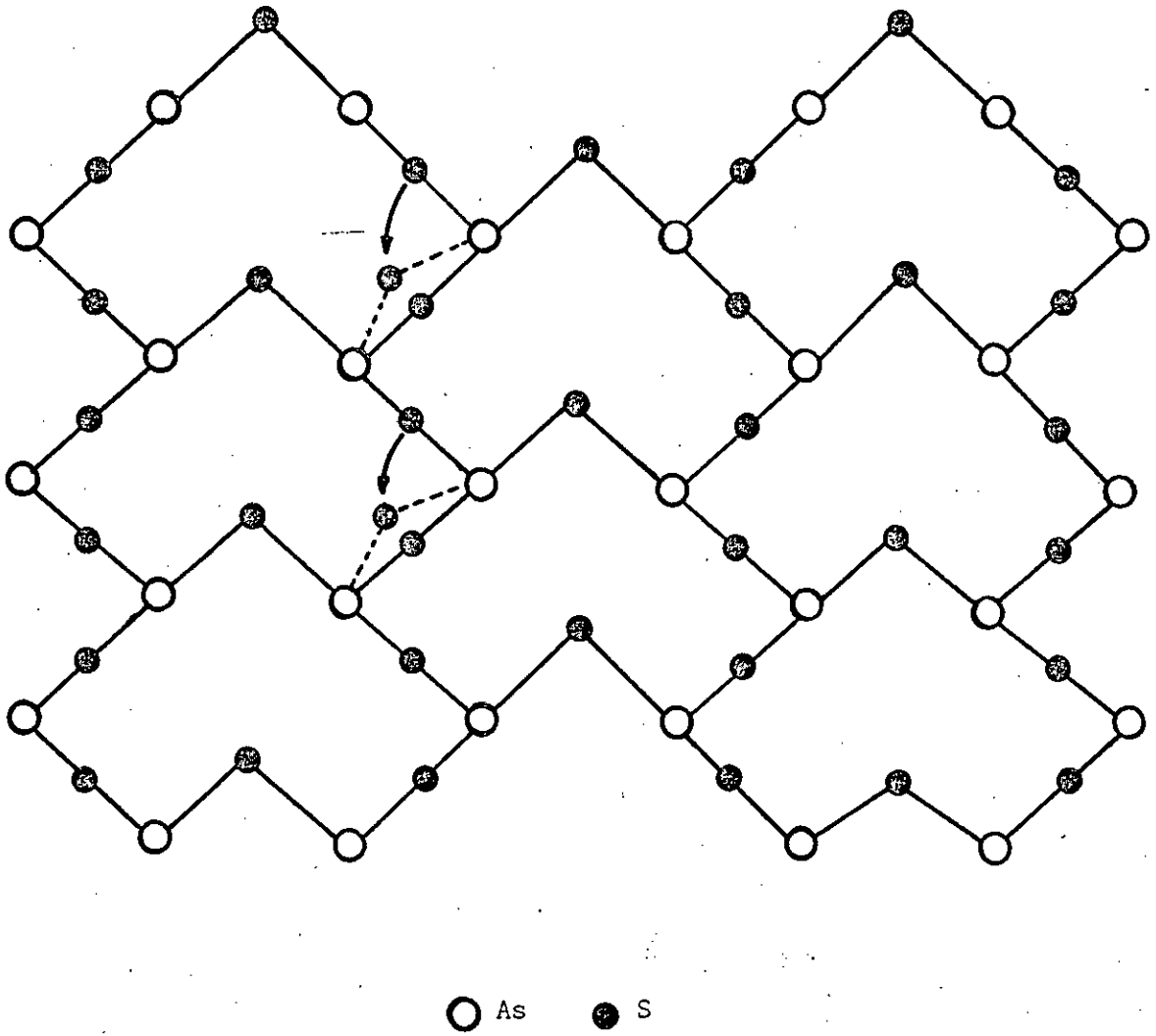
O As   ● S

Figure 5.73

Schematic representation of the configurational change in the $c-As_2S_3$
layer structure proposed by Finkman et al. (Reference 39) to account
for the decrease in the reduced Raman intensity with increasing temperature.

loss _is_ accompanied by a small change in spectral density. This change

consists of a decrease in the peak intensity of some of the sharp bands

relative to others and accounts for the discrepancies in relative peak

heights in the Raman spectra, e.g. in Figures 5.62 and 5.63.

The effect is best seen in the $As_{45}S_{55}$ spectrum since the sharp

structure is most pronounced for this composition. Figure 5.74 shows

six spectra of the composition $As_{45}S_{55}$ recorded in an investigation of

this effect. In this experiment eight spectra were recorded from the

sample, each spectrum being recorded immediately after the previous one

and there being no change in the experimental conditions between runs.

Each spectrum took ~17 minutes to record so the total period of continuous

irradiation was ~$2\frac{1}{4}$ hours. After irradiation was terminated the sample

was left for ~12 hours and then a ninth spectrum was obtained to see

whether any recovery took place over this interval. The photo-response

of the material tends to saturate, making later spectra indistinguishable

from each other, so for clarity only six of the nine spectra are shown.

The spectra are as recorded and have not been normalised in any way or

corrected for the signal loss. The time, t, elapsed between the start

of each run and the commencement of irradiation is marked by the 187 cm^{-1}

peak.

The usual decrease in intensity over the whole spectrum is clearly

present and is particularly obvious over the 40 — 120 cm^{-1} region. The

intensity at 80 cm^{-1} falls by more than 20% during the first 20 minutes

of exposure. The rate of signal loss is much greater for the two opaque

compositions $As_{44}S_{56}$ and $As_{45}S_{55}$ mainly because a focussed beam is used

in obtaining their spectra. However, the rate of signal loss soon tapers

off and the continuous background changes only slightly after the first

20 minutes of irradiation.

Although the decrease in the intensity of the glassy component of

Figure 5.74

Photo-induced changes in the $As_{45}S_{55}$ spectrum.   t is the time elapsed

since the start of irradiation.

Photo-Induced Changes in the As₄₅S₅₅ Spectrum
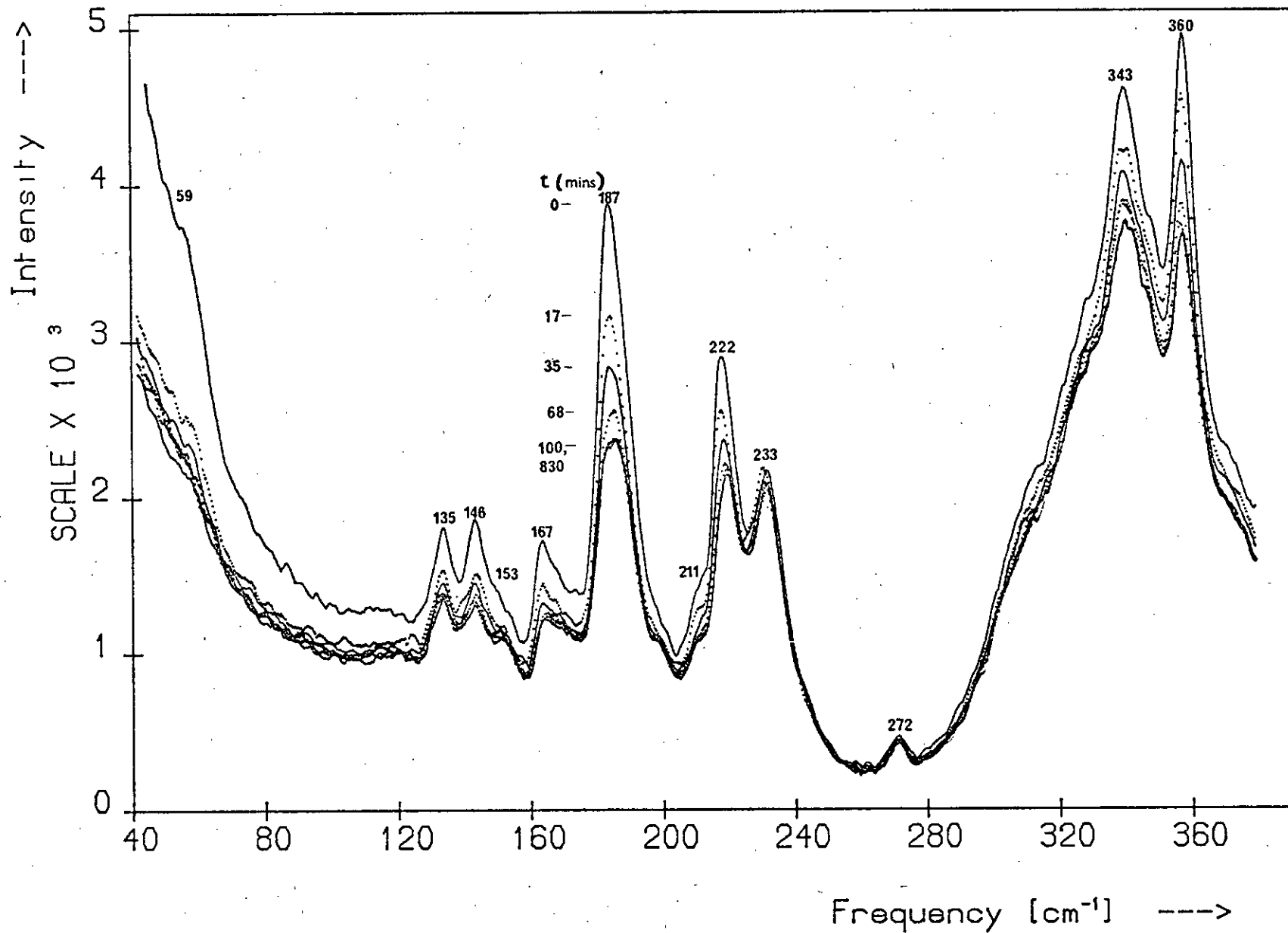
the spectrum must affect the intensity of the sharp structure super-
imposed on it, the changes taking place in the major peaks cannot be
entirely accounted for by this decrease. For example, during the
2 hour exposure the intensity of the 187 cm^{-1} band falls by ~1500 counts
while the background on which it stands decreases by only ~300 counts.
Also, as the contribution of the glassy matrix to the scattered intensity
is greater at 343 cm^{-1} than at 360 cm^{-1} one would expect the band at the
latter frequency to decrease less than that at the former — this is not
the case and in fact the two bands undergo a reversal of intensities.
In addition, the spectra for $t \geqslant 17$ minutes show that most of the sharp
structure continues to decrease in intensity even though the signal loss
in the continuous background has virtually ceased. These results suggest
that some photo-induced change must be taking place in the molecules
associated with these changing bands, as well as in the matrix in which
they are embeded.

The bands at 233 and 272 cm^{-1}, however, change hardly at all. This
is partly because they occur in regions where the glass background is
weak but it also suggests that they may arise from structural features
different from those responsible for the changing bands.

It was shown in Section 5.6.3 that most of the sharp structure is
due to the presence of β-As$_4$S$_4$ in the glass. Porter and Sheldrick[14]
have recorded the Raman spectrum of this crystal and show that it does
indeed change as a function of exposure to red light. They observe
that the internal bands decrease in intensity and the external bands
disappear completely. The three bands at 343, 351 and 360 cm^{-1} are
replaced by a very broad, structured band centred around ~340 cm^{-1} —
this may account for the reversal in the peak intensities of the 343 and
360 cm^{-1} As$_{45}$S$_{55}$ bands noted above. Although there are initially no
features in the β-As$_4$S$_4$ spectrum at 233 and 272 cm^{-1}, bands do grow near
these frequencies during irradiation. These authors show that the

spectrum resulting from the prolonged irradiation of α-As$_4$S$_4$ is very similar to that produced on irradiating β-As$_4$S$_4$. Comparing the α- and β-As$_4$S$_4$ product spectra suggests that the 233 and 272 cm^{-1} bands do not grow at the same rate as the broad band centred at $\sim$340 cm^{-1} and so may not arise from the same structural feature as the latter. Thus although the intensity reversal of the 343 and 360 cm^{-1} bands suggests that the broad 340 cm^{-1} feature is growing, it is not necessarily expected that the 233 and 272 cm^{-1} bands should also be growing. It is thought that the structural features responsible for the 233 and 272 cm^{-1} bands are already present in As$_{45}$S$_{55}$ before irradiation (see Section 5.6.3).

Because the product spectra are complex and the lattice modes disappear, the changes in the c-As$_4$S$_4$ spectra are attributed by Porter and Sheldrick to laser-induced polymerisation of the constituent As$_4$S$_4$ molecules. Although this process continues in c-As$_4$S$_4$ until the crystal spectrum is almost completely obliterated, Figure 5.74 shows that for As$_{45}$S$_{55}$ the decrease in intensity of the β-As$_4$S$_4$ bands comes virtually to a halt while they are still fairly intense. However, the process in the As-rich glasses does go almost to completion when band-gap radiation is used. The Raman spectra A and B of Figure 5.75 were recorded from As$_{43}$S$_{57}$ glass using 5145 Å and 6328 Å radiation respectively. In spectrum A all that remains of the β-As$_4$S$_4$ bands is the weak feature at $\sim$187 cm^{-1}. The disappearance of the β-As$_4$S$_4$ features is accompanied by the growth of the 233 cm^{-1} feature, as observed by Porter and Sheldrick, but its size in this case may be largely due to resonance enhancement since the 5145 Å radiation is close to the band gap of this material[43,44,121] (see Section 5.4.5).

During the course of the present study similar results to those shown in Figure 5.74 were reported by Bertoluzza et al.[117] These authors also attribute the change in intensity of the sharp structure to polymerisation of the As$_4$S$_4$ molecules.

Figure 5.75

Raman spectra of the glass $As_{43}S_{57}$: one spectrum was excited with near band-gap radiation (λ_{exc}= 5145 Å) and the other with 6328 Å radiation, which is weakly absorbed.
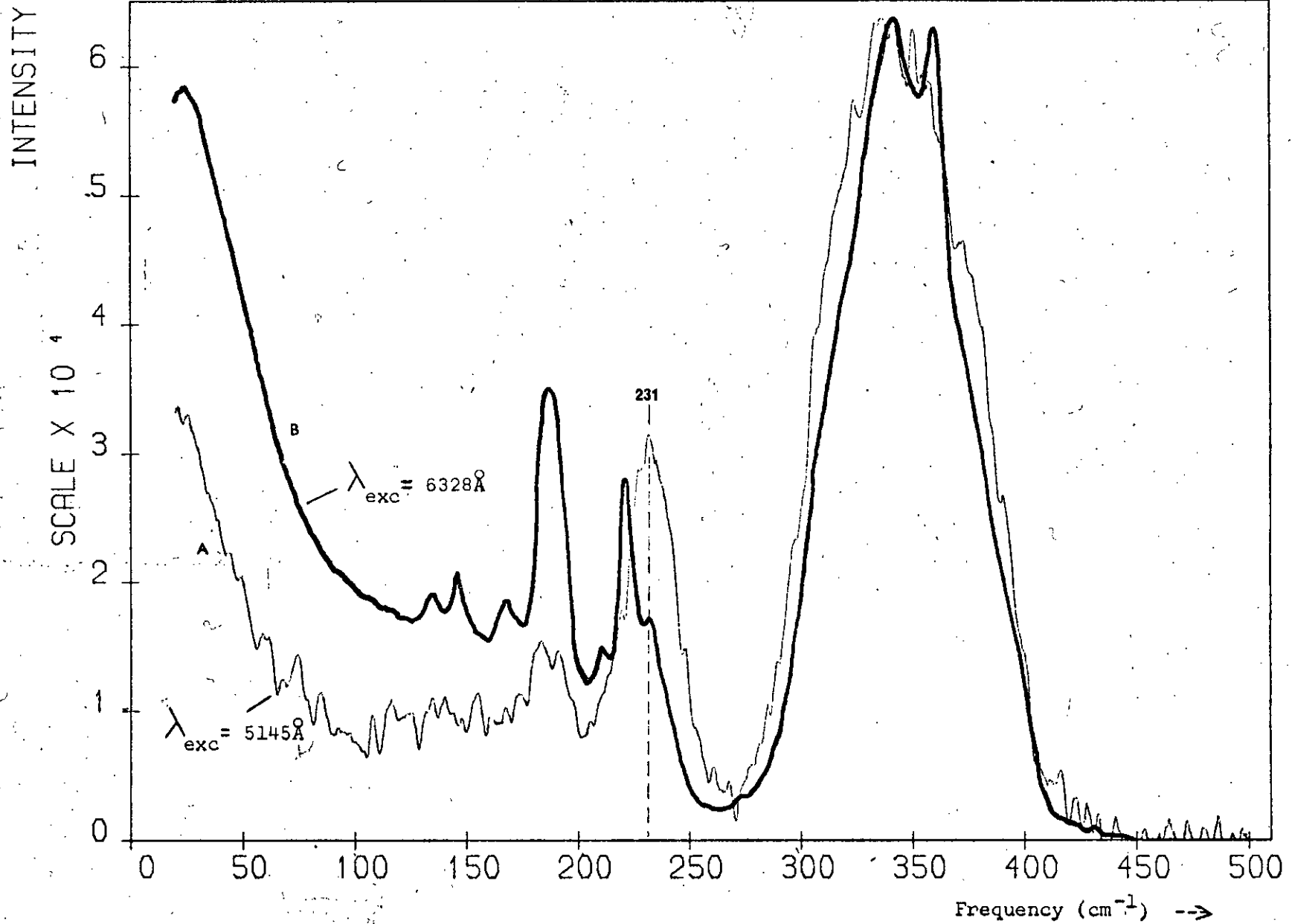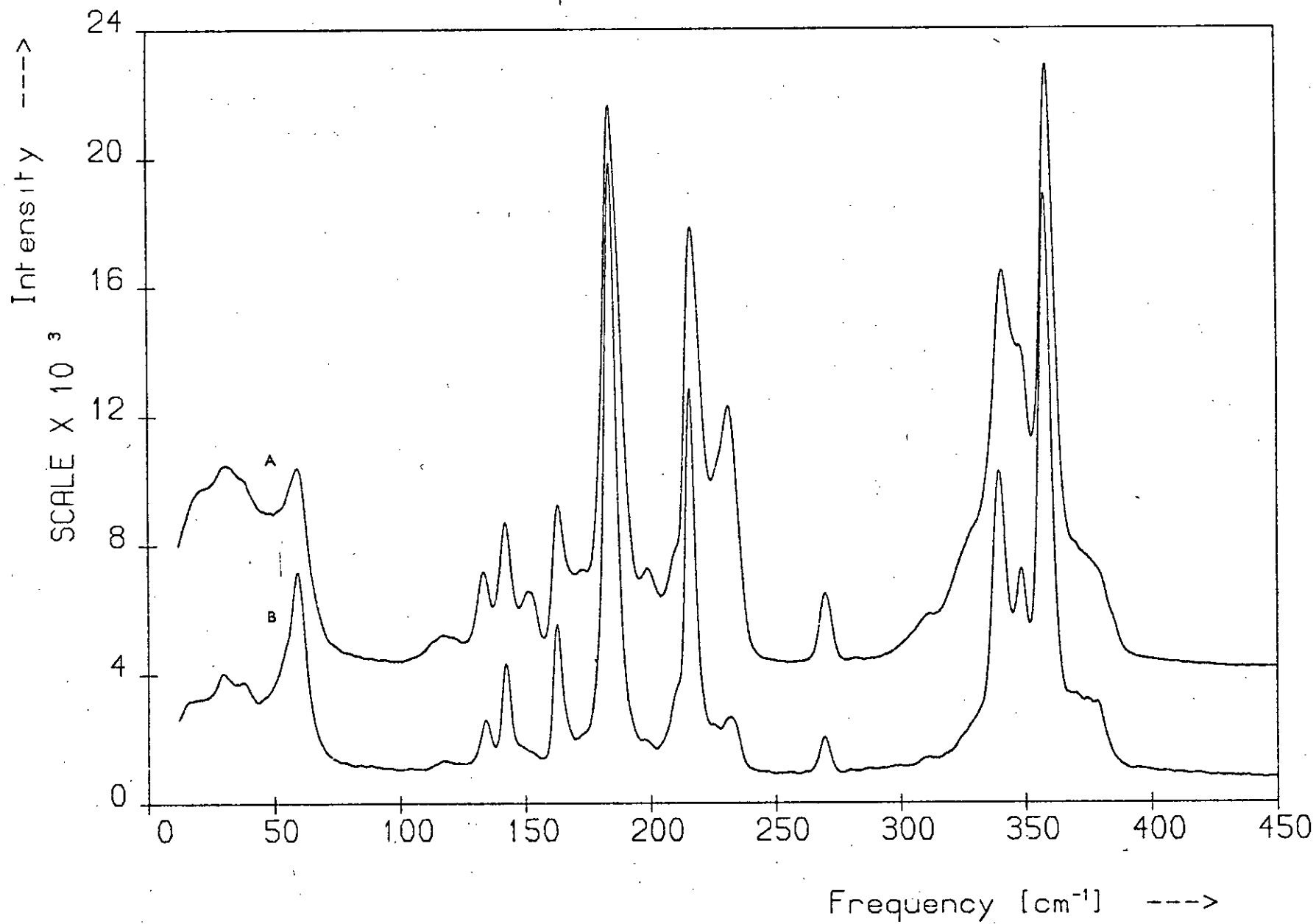

Figure 5.76

Raman spectra of β-As_4S_4:

A — 2 months after sample was produced

B — 4 months after sample was produced

THE RAMAN SPECTRUM OF $As_{43}S_{57}$ GLASS

Raman Spectra: c-As$_4$S$_4$

As the spectrum recorded ~12 hours after the irradiation was terminated is almost indistinguishable from the 'saturated' spectra, the irradiated region recovers little, if at all, over this period. However, in the case of c-As$_4$S$_4$ it is possible that the sample does recover but very gradually. Spectrum A of Figure 5.76 was recorded from the As$_4$S$_4$ specimen made in the Department two months after it was produced. The spectrum is similar to the As-rich glass spectra, the only differences being that for the As$_4$S$_4$ the sharp structure is more pronounced and the continuous background is less noticeable. The As$_4$S$_4$ spectrum also exhibited the same photo-induced changes as the As-rich spectra. Spectrum B was recorded from an unused sample of the same melt four months after it was produced and is clearly more crystalline in nature. The continuous background has almost completely disappeared, with the result that the 351 cm^{-1} band is now well resolved. The ~230 and ~270 cm^{-1} features which appear in the spectra of irradiated c-As$_4$S$_4$ that were obtained by Porter and Sheldrick are much less intense and many of the unassigned bands (see Section 5.6.3) have diminished or disappeared completely. These unassigned bands must correspond to the numerous weak bands observed by Porter and Sheldrick in the irradiated c-As$_4$S$_4$ spectra. The sample from which spectrum B was obtained was stored in a light-proof cabinet at room temperature after production. The conditions under which the sample was produced must affect the material in the same way as irradiation so that the sample is initially partly polymeric and partly crystalline. On being left in a relatively cool and lightless environment the material clearly recovers and crystallises. The polymeric regions must break up to form discrete As$_4$S$_4$ molecules.

It should be emphasised that the material of composition As$_4$S$_4$ was the only one whose spectrum changed significantly over the course of the study. The Raman spectra of the other As-rich compositions examined showed no evidence of transformation with time — for example the As$_{43}$S$_{57}$

spectrum B of Figure 5.75 was recorded 24 months after that displayed in Figure 5.62 but is essentially identical and shows no sign of crystallisation.

5.8   References

1.   Ward, A.T., Adv. in Chemistry 110, 163 (1972).

2.   Ward, A.T., J. Phys. Chem. 72, 4133 (1968).

3.   Kobliska, R.J. and Solin, S.A., Phys. Rev. B 8, 756 (1973).

4.   Kobliska, R.J. and Solin, S.A., J. Non-Cryst. Solids 8, 191 (1972).

5.   Zallen, R., Slade, M.L. and Ward, A.T., Phys. Rev. B 3, 4257 (1971).

6.   Zallen, R. and Slade, M.L., Phys. Rev. B 9, 1627 (1974).

7.   Mathieu, J.P. and Poulet, H., Bull. Soc. Fr. Mineral. Cristallogr. 93, 532 (1970).

8.   Markov, Y.F. and Reshetnyak, N.B., Sov. Phys. Solid State 14, 1063 (1972).

9.   Forneris, R., Am. Miner., 54, 1062 (1969).

10.   Scheuermann, W. and Ritter, G.J., Z. Naturforsch. 24A, 408 (1969).

11.   Whitfield, H.J., Aust. J. Chem. 24, 697 (1971).

12.   Treacy, D. and Taylor, P.C., Phys. Rev. B 11, 2941 (1975).

13.   Zallen, R., Phys. Rev. B 9, 4485 (1974).

14.   Porter, E.J. and Sheldrick, G.M., J.C.S. Dalton, 1347 (1972).

15.   Bastow, T.J. and Whitfield, H.J., J.C.S. Dalton, 1739 (1973).

16.   Siebert, H., 'Schwingunspektroskopie in der anorganischen Chemie', Springer Verlag, Berlin, 1966, p.68.

17.   Rogstad, A., J. Mol. Structure 14, 421 (1972).

18.   Whitfield, H.J., J.C.S. Dalton, 1740 (1973).

19.   Bastow, T.J., Cambell, I.D. and Whitfield, H.J., Aust. J. Chem. 25, 2291 (1972).

20.   Bernstein, H.J. and Powling, J., J. Chem. Phys. 18, 1018 (1950).

21.   Barrow, G.M., J. Chem. Phys. 21, 219 (1953).

22.   Chantry, G.W., Anderson, A. and Gebbie, H.A., Spectrochim. Acta 20, 1223 (1964).

23.   Ward, A.T., J. Phys. Chem. 72, 744 (1968).

24. Ozin, G.A., J. Chem. Soc. (A), 116, (1969).

25. Gautier, G. and Debeau, M., Spectrochim. Acta 30A, 1193 (1974).

26. Ward, A.T. and Myers, M.B., J. Phys. Chem. 73, 1374 (1969).

27. Anderson, A. and Loh, Y.T., Can. J. Chem. 47, 879 (1969).

28. Arthur, J.W. and Mackenzie, G.A., J. Raman Spectrosc. 2, 199 (1974).

29. Scott, D.W., McCullough, J.P. and Kruse, F.H., J. Mol. Spectrosc. 13, 313 (1964).

30. Lannin, J.S., A.I.P. Conf. Proc. 31, 123 (1976).

31. Lannin, J.S., Phys. Rev. B 15, 3863 (1977).

32. Lucovsky, G. and Knights, J.C., Phys. Rev. B 10, 4324 (1974).

33. Renucci, J.B., Richter, W., Cardona, M. and Schönherr, E., Phys. Stat. Sol. (b) 60, 299 (1973).

34. Lannin, J.S., Calleja, J.M. and Cardona, M., Phys. Rev. B 12, 585 (1975).

35. Lucovsky, G., Proc. 5th Int. Conf. on Amorphous and Liquid Semiconductors, Garmisch-Partenkirchen, Germany (Stuke, J. and Brenig, W., editors), Taylor and Francis, London, 1974, p.1099.

36. Greaves, G.N. and Davis, E.A., Phil. Mag. 29, 1201 (1974).

37. Ing, S.W., Jr., Chiang, Y.S. and Ward, A.T., American Ceramic Society Meeting, 1969 (unpublished).

38. Kobliska, R.J. and Solin, S.A., Solid State Commun. 10, 231 (1972).

39. Finkman, E., DeFonzo, A.P. and Tauc, J., Proc. 5th Int. Conf. on Amorphous and Liquid Semiconductors, Garmisch-Partenkirchen, Germany (Stuke, J. and Brenig, W., editors), Taylor and Francis, London, 1974, p.1275.

40. Nemanich, R.J., Solin, S.A. and Lucovsky, G., Proc. 3rd Int. Conf. on Light Scattering in Solids, Campinas, Brazil, Flammarion, Paris, 1976, p.631.

41. Tauc, J., Proc. 3rd Int. Conf. on Light Scattering in Solids, Campinas, Brazil, Flammarion, Paris, 1976, p.621.

42. Lucovsky, G., Nemanich, R.J. and Solin, S.A., Solid State Commun. 17, 1567 (1975).

43. Razzetti, C. and Fontana, M.P., Phys. Stat. Sol. (b) 70, 173 (1975).

44. Howard, R.E., Macedo, P.B. and Moynihan, C.T., Solid State Commun. 17, 1475 (1975).

45. Solin, S.A. and Papatheodorou, G.N., Phys. Rev. B $\underline{15}$, 2084 (1977).

46. Lucovsky, G., Galeener, F.L., Geils, R.H. and Keezer, R.C., in 'The Structure of Non-Crystalline Materials' (Gaskell, P.H., editor), Taylor and Francis, London, 1977, p.127.

47. Zlatkin, L.B. and Markov, Y.F., Phys. Stat. Sol. (a) $\underline{4}$, 391 (1971).

48. Onomichi, M., Arai, T. and Kudo, K., J. Non-Cryst. Solids $\underline{6}$, 362 (1971).

49. Lucovsky, G., Phys. Rev. B $\underline{6}$, 1480 (1972).

50. Taylor, P.C., Bishop, S.G. and Mitchell, D.L., Solid State Commun. $\underline{8}$, 1783 (1970).

51. Taylor, P.C., Bishop, S.G., Mitchell, D.L. and Treacy, D., Proc. 5th Int. Conf. on Amorphous and Liquid Semiconductors, Garmisch-Partenkirchen, Germany (Stuke, J. and Brenig, W., editors), Taylor and Francis, London, 1974, p.1267.

52. Shuker, R. and Gammon, R.W., Phys. Rev. Lett. $\underline{25}$, 222 (1970).

53. Shuker, R. and Gammon, R.W., Proc. 2nd Int. Conf. on Light Scattering in Solids, Paris (Balkanski, M., editor), Flammarion, Paris, 1971, p.334.

54. Bermudez, V., J. Chem. Phys. $\underline{57}$, 2793 (1972).

55. Vaipolin, A.A. and Porai-Koshits, E.A., Sov. Phys. Solid State $\underline{5}$, 178 (1963).

56. Konnert, J.H., Karle, J. and Ferguson, G.A., Science $\underline{179}$, 177 (1973).

57. Bishop, S.G. and Shevchik, N.J., Solid State Commun. $\underline{15}$, 629 (1974).

58. Nabitovich, I.D., Stetsiv, Ya. I. and Andreiko, A.M., Sov. Phys. Crystallogr. $\underline{21}$, 348 (1976).

59. Taylor, P.C., Bishop, S.G. and Mitchell, D.L., Phys. Rev. Lett. $\underline{27}$, 414 (1971).

60. Papatheodorou, G.N. and Solin, S.A., Phys. Rev. B $\underline{13}$, 1741 (1976).

61. Nemilov, S.V., Sov. Phys. Solid State $\underline{6}$, 1075 (1964).

62. Lucovsky, G. and Martin, R.M., J. Non-Cryst. Solids $\underline{8} - \underline{10}$, 185 (1972).

63. Austin, I.G. and Garbett, E.S., Phil. Mag. $\underline{23}$, 17 (1971).

64. Herzberg, G., 'Infrared and Raman Spectra of Polyatomic Molecules', Van Nostrand, New York, 1945.

65. Bell, R.J., Bird, N.F. and Dean, P., J. Phys. C $\underline{1}$, 299 (1968).

66. Rubinstein, M. and Taylor, P.C., Phys. Rev. Lett. $\underline{29}$, 119 (1972); Rubinstein, M. and Taylor, P.C., Phys. Rev. B $\underline{9}$, 4258 (1974).

67. Papatheodorou, G.N. and Solin, S.A., Solid State Commun. **16**, 5 (1975).

68. Nakamoto, K., 'Infrared Spectra of Inorganic and Coordination Compounds', Wiley, New York, 1963.

69. Gordy, W., J. Chem. Phys. **14**, 305 (1946).

70. Mullen, D.J.E. and Nowacki, W., Z. Krist. **136**, 48 (1972).

71. Davies, J.E.D. and Long, D.A., J. Chem. Soc. (A), 1757 (1968).

72. 'American Institute of Physics Handbook', 3rd ed., McGraw-Hill, New York, 1972, 7-193.

73. Renninger, A.L. and Averbach, B.L., Acta Cryst. B**29**, 1583 (1973).

74. Wilson, E.B., Jr., Decius, J.C. and Cross, P.C., 'Molecular Vibrations', McGraw-Hill, New York, 1955.

75. Lucovsky, G., Galeener, F.L., Keezer, R.C., Geils, R.H. and Six, H.A., Phys. Rev. B **10**, 5134 (1974).

76. Klein, P.B., Taylor, P.C. and Treacy, D.J., Phys. Rev. B **16**, 4511, 1977.

77. Maklad, M.S., Mohr, R.K., Howard, R.E., Macedo, P.B. and Moynihan, C.T., Solid State Commun. **15**, 855 (1974).

78. Wilkinson, G.R., in 'The Raman Effect' (Anderson, A., editor), Vol.2, Marcel Dekker, New York, 1973, p.965.

79. Kosek, F. and Tauc, J., Czech. J. Phys. B**20**, 94 (1970).

80. Meyer, B., Chem. Rev. **64**, 429 (1964).

81. Tsuchihashi, S. and Kawamoto, Y., J. Non-Cryst. Solids **5**, 286 (1971).

82. Lucovsky, G., Mooradian, A., Taylor, W., Wright, G.B. and Keezer, R.C., Solid State Commun. **5**, 113 (1967).

83. Brodsky, M.H., Gambino, R.J., Smith, J.C., Jr., and Yacoby, Y., Phys. Stat. Sol. (b) **52**, 609 (1972).

84. Gorman, M. and Solin, S.A., Solid State Commun. **18**, 1401 (1976).

85. Gautier, G. and Debeau, M., Spectrochim. Acta **32A**. 1007 (1976).

86. Berkowitz, J., Chupka, W.A., Bromels, E. and Belford, R.L., J. Chem. Phys. **47**, 4320 (1967).

87. Gardener, M. and Rogstadt, A., J.C.S. Dalton, 599 (1973).

88. Steudel, R. and Rebsch, M., J. Mol. Spectrosc. **51**, 189 (1974).

89. Steudel, R., Spectrochim, Acta **31A**, 1065 (1975).

90. Barletta, R.E. and Brown, C.W., J. Phys. Chem. **75**, 4059 (1971).

91. Meyer, B. and Schumacher, E., Nature 186, 801 (1960).

92. Dultz, W., Hochheimer, H.D. and Müller-Lierheim, W., Proc. 5th Int. Conf. on Amorphous and Liquid Semiconductors, Garmisch-Partenkirchen, Germany (Stuke, J. and Brenig, W., editors), Taylor and Francis, London, 1974, p.1281.

93. Meyer, B., J. Chem. Phys. 37, 1577 (1962).

94. Meyer, B. and Stroyer-Hansen, T., J. Phys. Chem. 76, 3968 (1972).

95. Tobolsky, A.V., and Eisenberg, A., J. Polymer Sci. 46, 19 (1960).

96. Tobolsky, A.V., and Eisenberg, A., J. Colloid Sci. 17, 49 (1962).

97. Apling, A.J., in 'Electronic and Structural Properties of Amorphous Semiconductors' (Proc. Scottish Univ. Summer School in Physics, Aberdeen, Aug. 1972) (Le Comber, P. and Mort, J., editors), Academic Press, London, 1973, p.243.

98. Leadbetter, A.J. and Apling, A.J., J. Non-Cryst. Solids 15, 250 (1974).

99. Gill, E.K. and Laidler, K.J., Proc. Roy. Soc. A251, 66 (1959).

100. Decius, J.C., J. Chem. Phys. 16, 1025 (1948).

101. Gans, P., 'Vibrating Molecules', Chapman and Hall, London, 1971.

102. Elvebredd, I. and Cyvin, S.J., Z. Anorg. Allg. Chem. 370, 310 (1969).

103. Giguère, P.A. and Srinivasan, T.K.K., J. Raman Spectrosc. 2, 125 (1974).

104. Frenzel, C.A. and Blick, K.E., J. Chem. Phys. 55, 2715 (1971).

105. Ramaswamy, K. and Jayaraman, S., Acta Phys. Pol. A40, 883 (1971).

106. Bradley, E.B., Maya, S.M. and Frenzel, C.A., J. Chem. Phys. 47, 4325 (1967).

107. Winnewisser, B.P. and Winnewisser, M., Z. Naturforsch. 23A, 832 (1968).

108. Flaschen, S., Pearson, A. and Northover, W., J. Amer. Ceram. Soc. 42, 450 (1959).

109. Maruno, S. and Noda, M., J. Non-Crystalline Solids 7, 1 (1972).

110. Myers, M.B. and Felty, E.J., Mat. Res. Bull. 2, 535 (1967).

111. Bulkin, B.J., J. Opt. Soc. Amer. 59, 1387 (1969).

112. Shriver, D.F., Appl. Spectrosc. 23, 552 (1969).

113. Brumbach, S.B. and Rosenblatt, G.M., J. Chem. Phys. 56, 3110 (1972).

114. Lagowski, J.J., 'Modern Inorganic Chemistry', Marcel Dekker, New York, 1973, p.424.

115. Ursu, I., Lupei, A. and Lupei, V., Rev. Roum. Phys. **15**, 569 (1970).

116. Street, G.B. and Gill, W.D., Phys. Stat. Sol. **18**, 601 (1966).

117. Bertoluzza, A., Fagnano, C. and Monti, P., Proc. 12th European Congress on Molecular Spectroscopy, Strasbourg, France, Elsevier, Amsterdam, 1976, p.405.

118. Berkes, J.S., Ing, S.W., Jr., and Hillegas, W.J., J. Appl. Phys. **42**, 4908 (1971).

119. deNeufville, J.P., Moss, S.C. and Ovshinsky, S.R., J. Non-Cryst. Solids **13**, 191 (1974).

120. DeFonzo, A.P. and Tauc, J., Proc. 3rd Int. Conf. on Light Scattering in Solids, Campinas, Brazil, Flammarion, Paris, 1976, p.636.

121. Ewen, P.J.S. and Owen, A.E., Report on S.R.C. Grant GR/A/1924.2, March 1977 (unpublished).

CHAPTER 6

RESULTS AND DISCUSSION: THE As-Se SYSTEM

6.1 Introduction

In this chapter the results of the Raman experiments on materials in the As-Se system are presented and discussed, particularly in relation to the corresponding results for the arsenic sulphides. The compositions examined range throughout the As-Se system and are shown in Figure 6.1. The region within ± 5 at.% of the stoichiometric composition As_2Se_3 has been investigated in detail: eleven near-stoichiometric compositions extending from $As_{35}Se_{65}$ to $As_{45}Se_{55}$ in 1 at.% steps have been examined. Figure 6.1 also shows the compositions investigated in other vibrational studies of this system. The Raman and i.r. spectra of a number of glasses with Se content $\geqslant 60$ at.% have been recorded by Ward and co-workers[1,2] and Vasko[3] respectively but only i.r. data has hitherto been reported for the As-rich selenide glasses[3].

In their investigations of Raman scattering in As-Se glasses Ward and co-workers monitored only the high-frequency part of the spectra. In the present study, however, the use of 7993 Å excitation has made it possible to obtain the low-frequency region as well; good quality spectra have been recorded to within 10 cm^{-1} of the exciting line and in every case the boson peak has been resolved from the stray-light background. Also, Ward made no polarisation measurements. In the present study HV- and HH-polarised spectra have been recorded for each composition and used to generate the depolarisation spectra.

The Raman spectra presented in this chapter are substantially in agreement with the corresponding spectra obtained in other studies, though some new features have been observed in the glass spectra. Generally, only the spectral region below 300 cm^{-1} is shown in the figures of this chapter since the structure observed above this frequency arises from overtones and
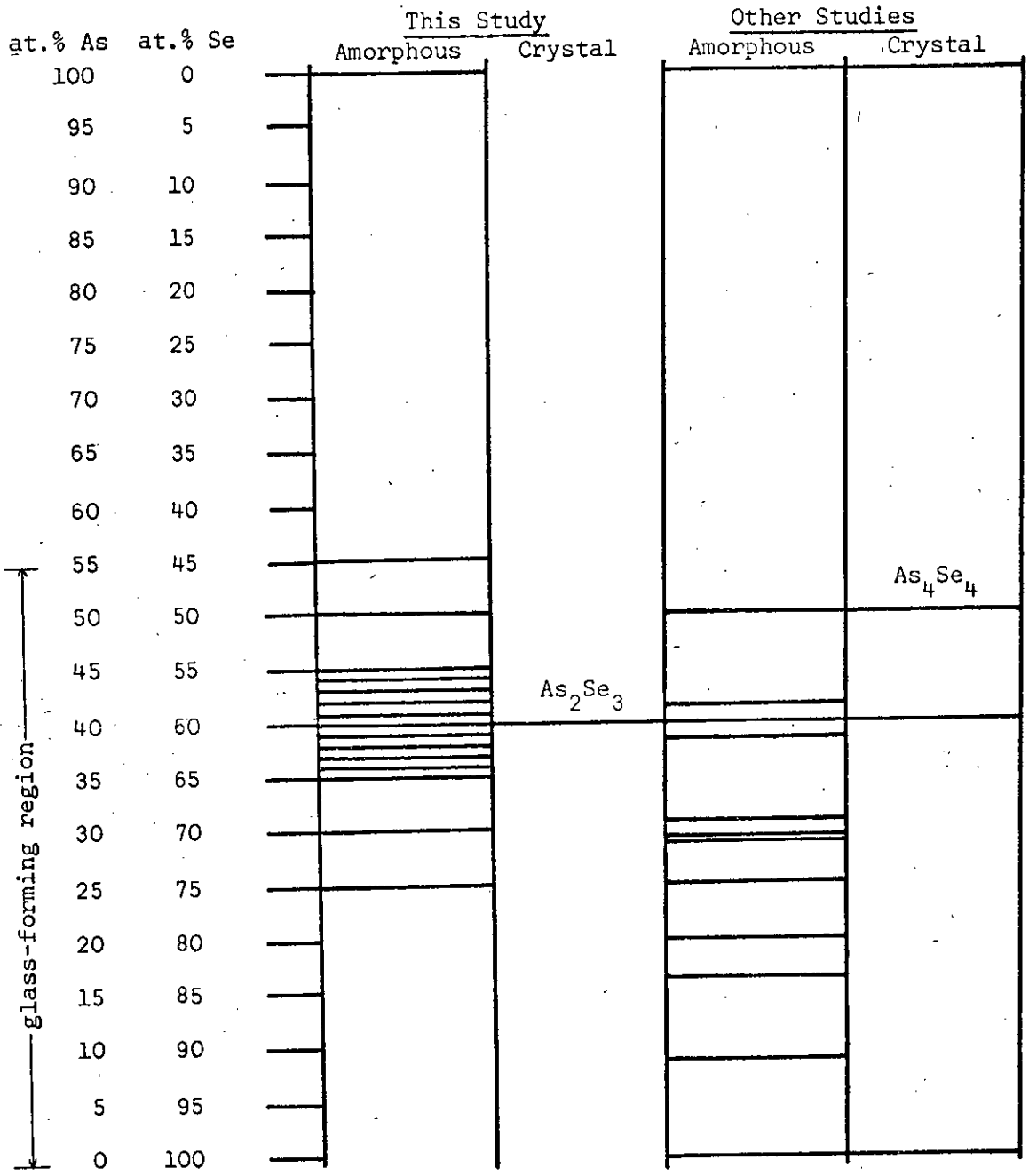
Figure 6.1

The compositions investigated in vibrational studies of materials in the As-Se system.

combinations of the first-order bands. All the spectra are Stokes spectra and were recorded at room temperature.

The polarisation-unanalysed spectra, with the exception of those for the compositions $As_{25}Se_{75}$, $As_{50}Se_{50}$ and $As_{55}Se_{55}$, were recorded by Dr. M.J.Sik. Dr. Sik also carried out the preliminary analysis of his data (Figures 6.14 and 6.34 were prepared by him). All the polarisation measurements were made by the present author using the technique developed by Dr. Sik for recording the selenide spectra.

6.2 Spectra of the crystalline As-Se compounds

6.2.1 $c-As_2Se_3$

The two crystalline phases best known in the As-Se system are $c-As_2Se_3$ and $c-As_4Se_4$. The Raman[4,5] and i.r.[4,6 — 9] spectra of the former have been recorded by a number of workers. Since $c-As_2Se_3$ has the same structure as $c-As_2S_3$ the vibrational analysis presented in Section 5.2.1 for $c-As_2S_3$ is also applicable to $c-As_2Se_3$. This analysis was based on the work of Zallen et al.[4,5] who investigated the vibrational spectra of both isomorphs.

Figure 6.2 shows the Raman spectrum of $c-As_2Se_3$ recorded in the present study. Zallen et al.[4,5] have shown that the vibrational frequencies of $c-As_2Se_3$ scale with those of $c-As_2S_3$, hence the distribution of the lines in Figure 6.2 is similar to that in the $c-As_2S_3$ spectrum (Figure 5.2). The $c-As_2Se_3$ bands occur in three distinct spectral regions: between 275 and 195 cm^{-1}, between 150 and 70 cm^{-1} and below 60 cm^{-1}. The bands in the first and second regions arise from bond-stretching and bond-bending modes respectively, while the three low-frequency lines at 20, 30 and 53 cm^{-1} and the doublet at ~ 50 cm^{-1} are due to the rigid-layer vibrations (see Section 5.2.1). The scaling relation, which is a consequence of the close isomorphicity of $c-As_2Se_3$ and $c-As_2S_3$, is discussed more fully in Section 6.4.5.

Figure 6.2

The Raman spectrum of c-As_2Se_3.

Raman Spectrum of Crystalline As_2Se_3.

Raman Spectrum of Crystalline As_2Se_3. Intensity (SCALE X 10^4) vs Frequency [cm^{-1}].
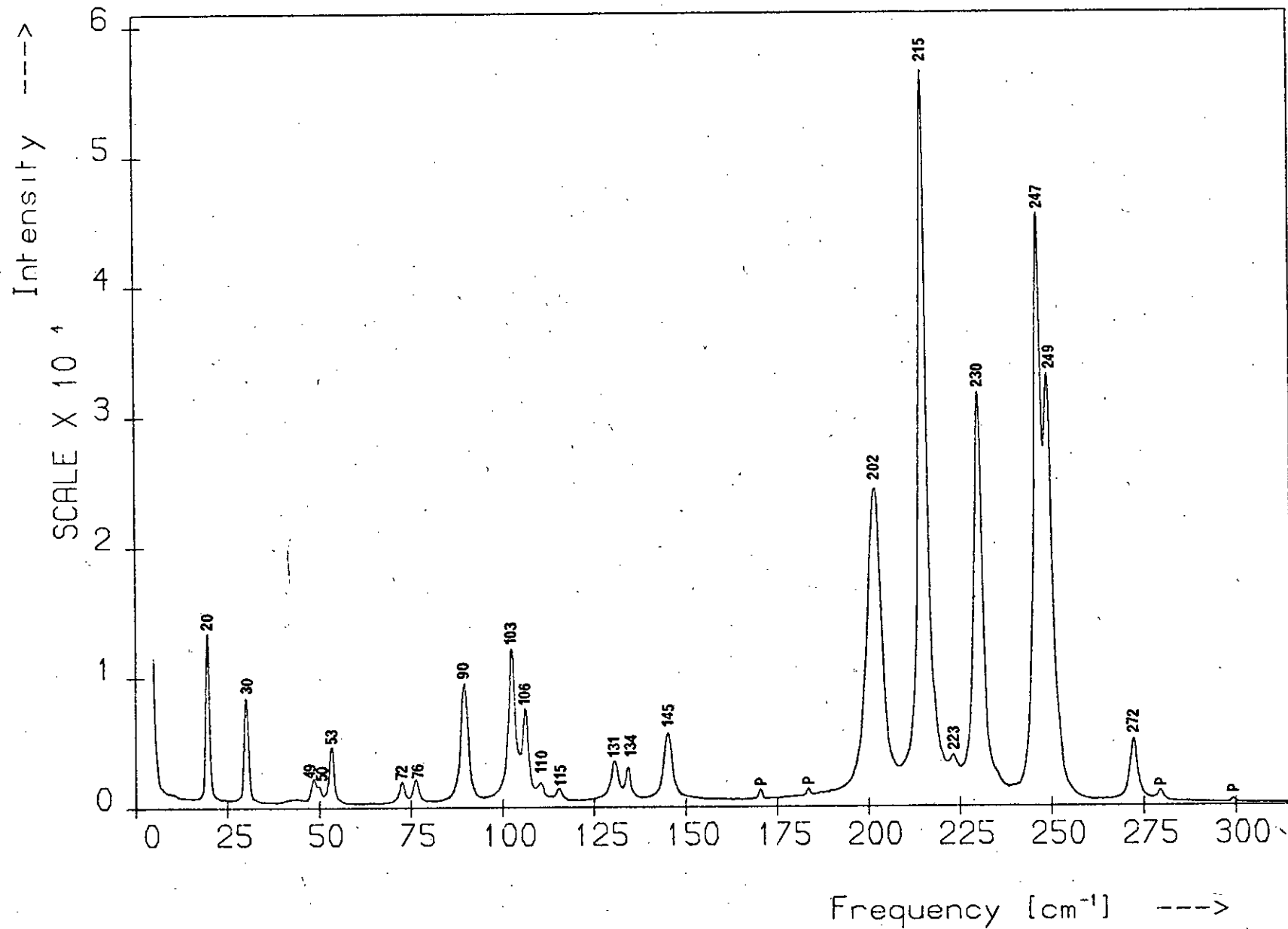
6.2.2 c-As$_4$Se$_4$

In the case of c-As$_4$Se$_4$ only the i.r. spectrum has so far been recorded[10]. The vibrational analysis for c-As$_4$Se$_4$ is identical with that given in Section 5.2.2 for α-As$_4$S$_4$ since both crystals have the same structure. Each line in the c-As$_4$Se$_4$ spectrum corresponds to one in the spectrum of α-As$_4$S$_4$; the corresponding pairs and the scale factor for each pair are given in Reference 10.

6.3 Spectra of the elements

The vibrational spectra of the various forms of elemental As were discussed in Section 5.3.2. The i.r. and Raman spectra of the trigonal[2,11,12,13] and α-monoclinic[2,12,13] crystalline modifications of Se have been recorded by several workers. The vibrational analysis for α-monoclinic Se, which is composed of Se$_8$ rings, is identical with that given in Section 5.3.1 for α-S$_8$. Lucovsky et al.[12] have shown that the vibrational frequencies, ν_{Se} and ν_S, of the Se$_8$ and S$_8$ rings in the corresponding crystals are related by a scale factor: $\nu_S/\nu_{Se} \approx 1.9$. The normal modes of trigonal Se, which is composed of helical chains, have been determined by Caldwell and Fan[14].

Numerous workers have studied the i.r. and Raman spectra of amorphous Se[1,2,12,13,15]; the most recent Raman investigation[15] also includes the depolarisation spectrum of this material. Figure 6.3, which is adapted from Reference 13, shows the Raman spectra of a-Se and the two crystalline forms. Despite the fact that the structure in the vibrational spectra of a-Se coincides with bands in the crystal spectra, there is some controversy over the assignment of the a-Se features to ring and chain modes, although it is agreed the vibrational data suggests that, as expected[16], both rings and chains are present in the amorphous form. The features at 235 and 250 cm^{-1} in the Raman spectrum of a-Se were originally associated with chains and rings respectively since there are

Figure 6.3

The Raman spectra of trigonal, amorphous and monoclinic Se, showing
the frequencies of the principal spectral features.   (After Reference 13.)

TRIGONAL Se

234

142

AMORPHOUS Se

250

50

80

112

138

235

MONOCLINIC Se

114

254

84

SHIFT (cm−1)

0   100   200   300
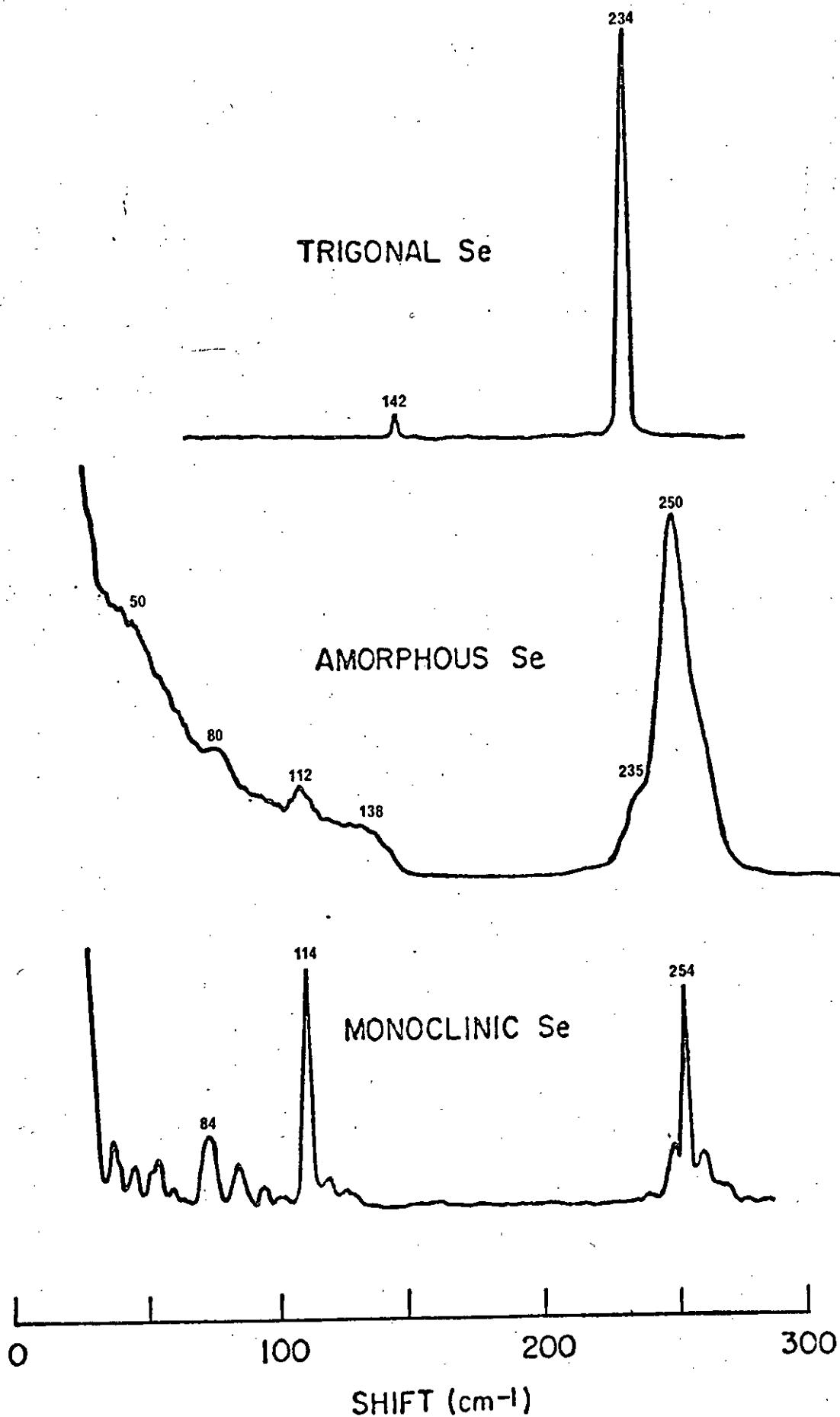
bands near 235 cm^{-1} in the spectrum of trigonal Se and near 250 cm^{-1} in that of α-monoclinic Se. Smith et al.[17] have since shown, however, that the intensity ratio of the a-Se features at 235 and 250 cm^{-1} does not change as this material is heated to above T_g ($T_g \approx 40^\circ$ C for Se) and is also unaffected by preparation parameters such as substrate temperature and quenching rate. These factors are expected to alter the ratio of rings to chains and hence it seems unlikely that the original assignment is correct.

Brodsky et al.[18] have pointed out that the local environment of a ring or chain may alter its normal frequencies, and hence the coincidence of an a-Se band with one in the spectrum of trigonal/ α-monoclinic Se does not necessarily imply that it arises from a chain/ring vibration. Force field calculations[19] show that for free Se_8 rings and free Se_n chains the principal high-frequency vibration occurs at ~255 cm^{-1} but that chain-chain interactions in the trigonal crystal shift the Se_n mode to ~235 cm^{-1}. Intermolecular forces in the monoclinic crystal are presumably small, since its dominant high-frequency mode is actually located at ~255 cm^{-1}. The dominant band in the vibrational spectra of a-Se also occurs near 255 cm^{-1} so that if intermolecular interactions are also negligible in the amorphous form, this band may be due to both rings _and_ chains. The spectral invariance observed by Smith et al.[17] would be accounted for if the rings and chains in a-Se did make indistinguishable contributions to the spectrum.

Gorman and Solin[15] point out that the frequency of an a-Se band together with its state of polarisation may be sufficient to determine whether it arises from a ring or chain mode. These authors consider the a-Se band at 112 cm^{-1} and argue that it must be a ring mode since the nearest Raman-active chain mode of comparable symmetry occurs at 237 cm^{-1} and the local environment should not shift a vibrational frequency by ~100%. Thus it seems that the ring frequencies are the same for both the crystalline and the amorphous environments; this is also found in the

case of the S_8 ring, whose frequencies in the crystal and liquid phases are almost identical[20].

6.4 The stoichiometric glass: $As_{40}Se_{60}$

6.4.1 The polarisation-unanalysed spectrum

The polarisation-unanalysed Raman spectrum of vitreous As_2Se_3 recorded in the present investigation is shown in Figure 6.4. The Raman[1,2,21 − 23] and i.r.[3,6 − 9,24 − 28] spectra of a-As_2Se_3 have been measured by several workers and the spectrum of Figure 6.4 is in agreement with their results. The use in the present study of the 7993 Å i.r. line of a Kr-ion laser has enabled good spectra to be obtained to within 10 cm^{-1} of the exciting line. Figure 6.4 shows that the spectral region below 175 cm^{-1} contains a peak at 24 cm^{-1} and weak structure at 106 and 136 cm^{-1}. During the course of the present investigation similar results for the low-frequency part of the a-As_2Se_3 spectrum were reported by Lucovsky et al.[21,22], who also used the 7993 Å line as excitation.

Table 6.1 (after p.210) compares the published vibrational frequencies of a-As_2Se_3 with those obtained in this study. The intense peak at 24 cm^{-1}, which is well resolved from the exciting line, is due to the thermal population of the lower vibrational levels and corresponds to the 29 cm^{-1} peak of a-As_2S_3.

### 6.4.2 Polarisation measurements

Figure 6.5 shows the HH- and HV-polarised spectra of a-As_2Se_3 recorded in the present study. Since the spectra were obtained by back reflection the incident radiation was horizontally polarised to increase its coupling to the sample. The polarised spectra of this material have not been previously reported, although its depolarisation spectrum was presented in the recent studies by Lucovsky et al.[21,22].

In Figure 6.5 the curves marked HH and HV are the as-measured polarised

The polarisation-unanalysed Stokes Raman spectrum of vitreous As_2Se_3.

Raman Spectrum of a-As$_{40}$Se$_{60}$
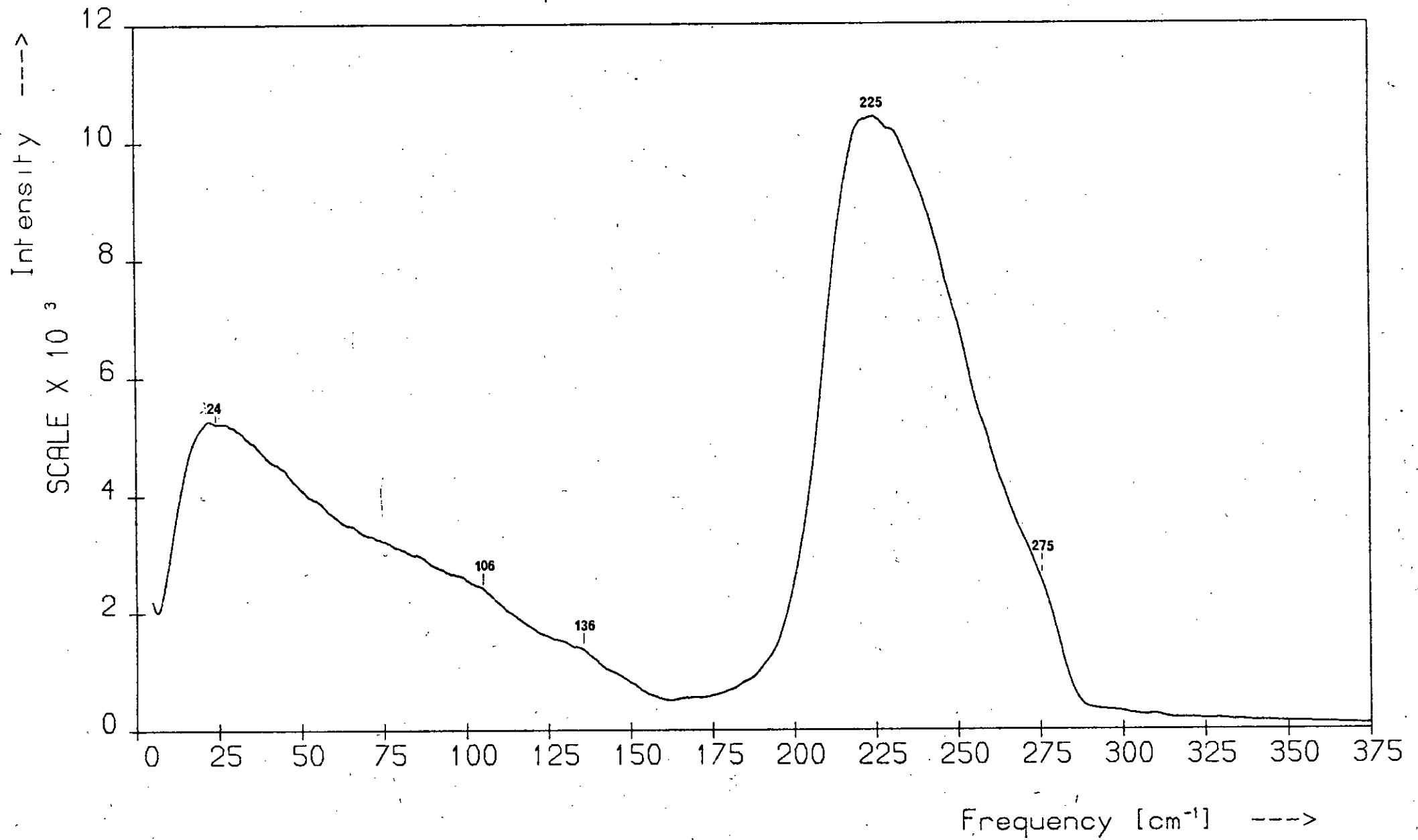
spectra and HVN is the HV spectrum scaled so that its intensity at 223 cm^{-1} equals that of the HH spectrum at 227 cm^{-1}. The two polarised spectra differ considerably in intensity but are similar in shape and closely resemble the polarisation-unanalysed spectrum. The only differences in spectral profile between the two polarised spectra are that in the HV spectrum the main band is sharper, falling away faster on the high-frequency side, it peaks at a slightly lower frequency, and the boson peak is more pronounced.

The depolarisation spectrum of a-As_2Se_3 measured in the present study is shown in Figure 6.6. It is in agreement with the published results[21,22] as far as structure is concerned but differs from them with respect to absolute value for $\rho(w)$. Compared with the data of Lucovsky et al.[21,22], the spectrum of Figure 6.6 is displaced up the $\rho(w)$ axis and occupies a narrower range of $\rho(w)$ values. However, this discrepancy, which is probably due to the poor optical quality of the samples used in the present study, does not affect the interpretation of the spectrum.

The structure in the depolarisation spectrum consists of a peak at 223 cm^{-1}, a broad peak or plateau centred at 136 cm^{-1} and two broad troughs, one at 86 cm^{-1} and one centred at $\sim$250 cm^{-1}; no structure occurs at 106 cm^{-1}. The high-frequency trough contains a well-defined dip at 275 cm^{-1} corresponding to the knee on the main band of the Raman spectra. Comparison of the a-As_2Se_3 depolarisation spectrum with that of a-As_2S_3 (see Figure 6.20 after p.218) suggests that the low-frequency 'corner' of the trough, which occurs at $\sim$240 cm^{-1}, also corresponds to a vibration, although there is nothing in the Raman spectra of a-As_2Se_3 at this frequency. The broad trough at 86 cm^{-1} has no corresponding feature in the Raman spectra either. Thus, as in the case of a-As_2S_3, the depolarisation measurements have revealed vibrations not readily observable in the Raman spectra. This aspect of depolarisation spectroscopy has been

Figure 6.5

The as-measured HH- and HV-polarised Raman spectra of a-As_2Se_3. Spectrum HVN is the HV spectrum normalised so that its intensity at 223 cm^{-1} equals that of the HH spectrum at 227 cm^{-1}.
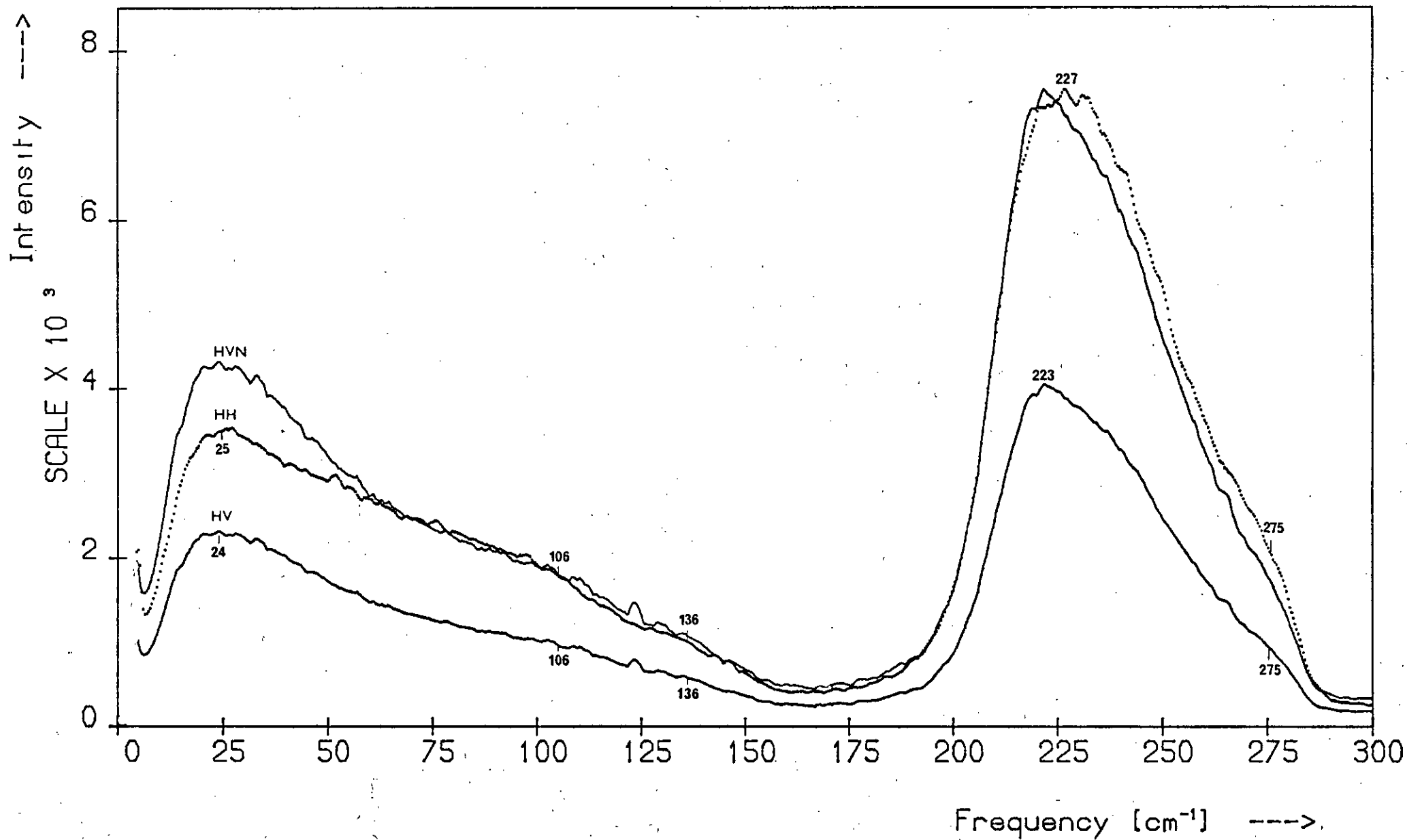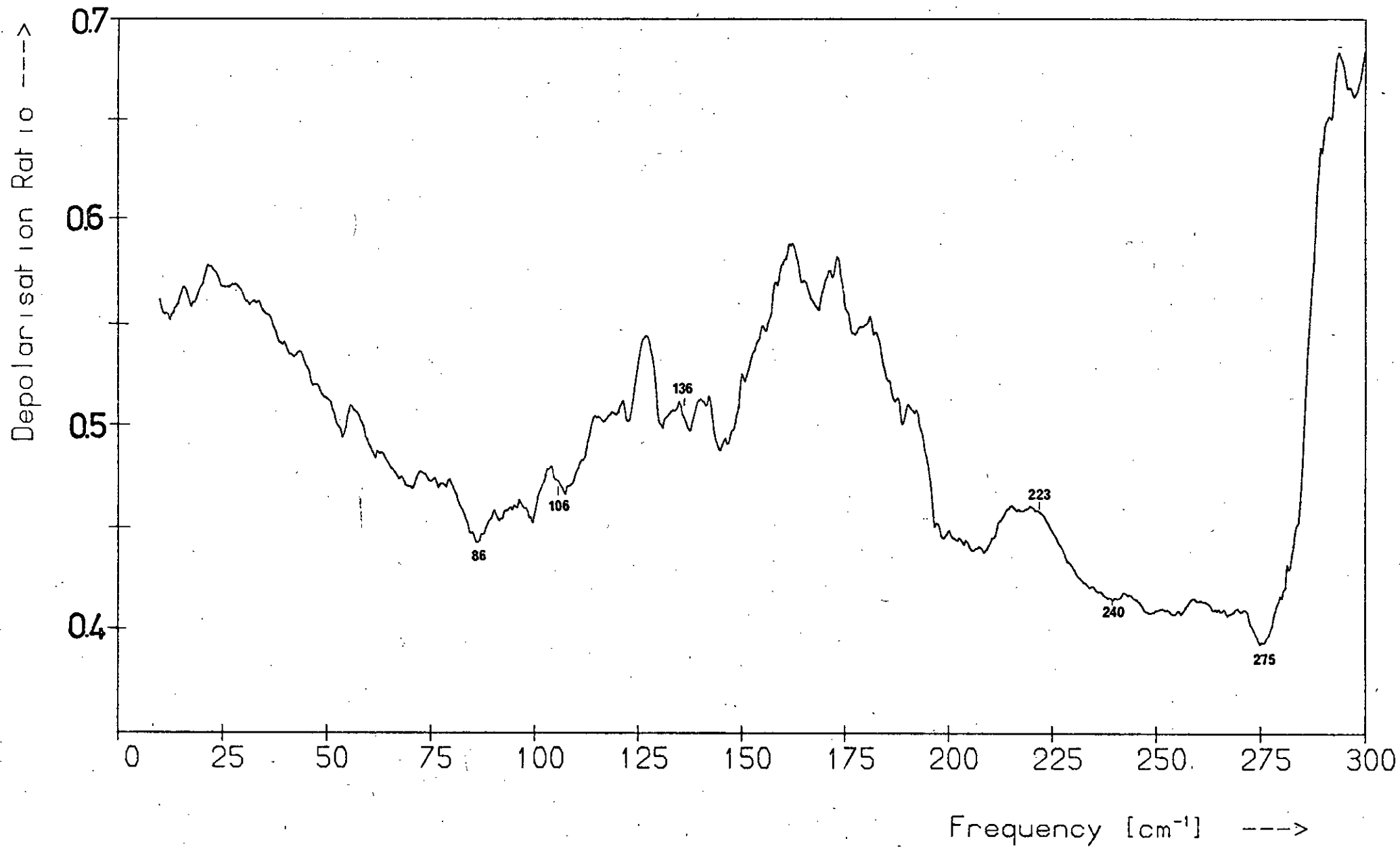

Figure 6.6

The depolarisation spectrum of a-As_2Se_3.

Figure 6.7

The HH, HV, depolarisation (D) and polarisation-unanalysed (PU) spectra of a-As_2Se_3.
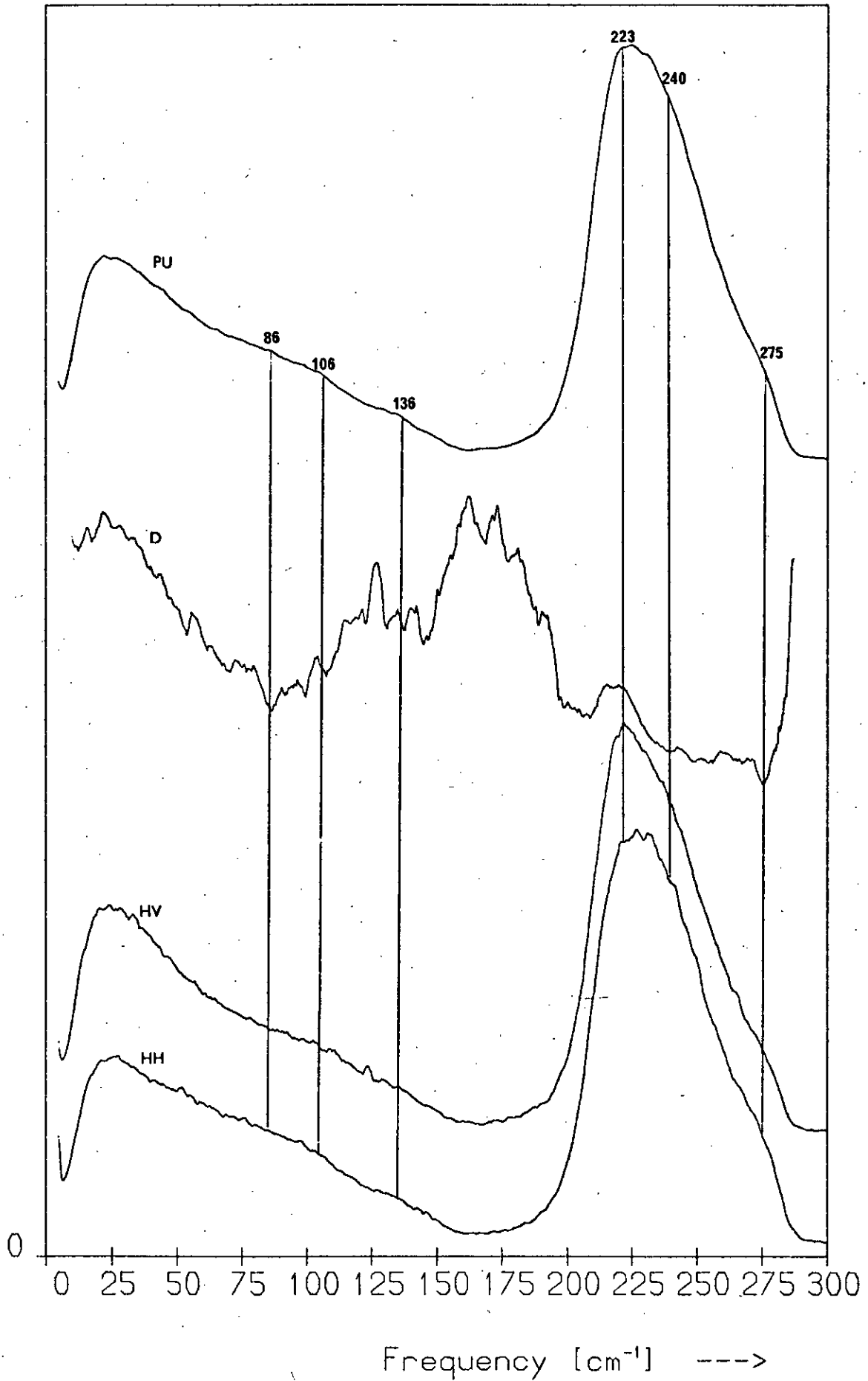
HV and HH Polarised Spectra of a-$As_{40}Se_{60}$

Depolarisation Spectrum of a-As$_{40}$Se$_{60}$

H, HV, Depolarisation and Unanalysed Spectra

emphasised by Solin[29,30] who has uncovered hidden bands in the Raman spectrum of a-As_2O_3 using such measurements.

Despite the fact that the 136 cm^{-1} Raman feature corresponds to a raised region in $\rho(w)$ it is possible that it is a polarised band, for the Raman intensity is fairly weak near 136 cm^{-1} and is decreasing as w increases. Since $\rho(w)$ tends to rise towards the depolarisation ratio of the background radiation as the Raman signal becomes very weak, the dip that should occur near 136 cm^{-1} in $\rho(w)$ if this band is polarised may have been transformed into the plateau that occurs in the increasing section of $\rho(w)$ between ~90 and ~175 cm^{-1}. (The weak 231 cm^{-1} polarised band in the a-As_2S_3 Raman spectrum gives rise to a similar 'step' feature in the depolarisation spectrum of this material — see Figure 5.14.)

Although the polarisation states of the 106 and 136 cm^{-1} Raman bands cannot be deduced with certainty from Figure 6.6, the i.r. spectra of a-As_2Se_3 support the assignment suggested in the present study, viz that the 106 cm^{-1} and 136 cm^{-1} bands are depolarised and polarised respectively. All the i.r. studies of this material show that the dominant low-frequency mode occurs near 106 cm^{-1} but none detect any mode near 136 cm^{-1}; since polarised/depolarised Raman bands are expected to have weak/strong i.r. counterparts[27] the i.r. observations are consistent with the above assignment. The polarisation states of all the observed Raman bands of a-As_2Se_3 are given in Table 6.1 along with the measured frequencies.

The depolarisation spectrum is compared with the unanalysed and polarised spectra of a-As_2Se_3 in Figure 6.7. Since both polarised spectra are similar to the unanalysed spectrum — unlike the case of a-As_2S_3 —, individually they yield no extra information; it is only when they are combined to produce the depolarisation spectrum that additional vibrational information is obtained.

6.4.3   Deconvolution of the main band

According to Taylor et al.[31] the shape of the main i.r. absorption band of a-As_2Se_3 is best fitted by Gaussian lines. In this section it will be seen whether the main band of the Raman spectrum of a-As_2Se_3 can be constructed by summing a set of overlapping Gaussian lines, each line being centred on an observed vibrational frequency of a-As_2Se_3. The analysis parallels that given in Section 5.4.3 for a-As_2S_3.

The main Raman band of a-As_2Se_3, after subtraction of the weak background, is shown in Figure 6.8 (dotted curve); it is highly asymmetric, as is that of a-As_2S_3. The high-frequency side is less steep than the low-frequency side and has a knee at ~275 cm^{-1} similar to that at ~395 cm^{-1} in the a-As_2S_3 spectrum. The 275 cm^{-1} knee and the peak at 225 cm^{-1} are the only features of the main band of a-As_2Se_3; there is nothing on the low-frequency side corresponding to the 315 cm^{-1} shoulder in the a-As_2S_3 spectrum.

It was found, however, that two Gaussian lines centred at or near the knee and peak frequencies of a-As_2Se_3 could not be made to fit its main band, though the low-frequency side could be fitted satisfactorily. The full curve in Figure 6.8 is the sum of two Gaussians centred at 223 and 270 cm^{-1}; it is in good agreement with the measured spectrum over the region 200 to 225 cm^{-1}, but not on the high-frequency side. The inability to fit the main band with these two Gaussians suggests that other lines are present between 223 and 275 cm^{-1}.

It was also found that the generated curve was a good fit to the low-frequency side of the main band only for values of the standard deviation, σ, near 13 cm^{-1} — this was the value used in the deconvolution of the a-As_2S_3 main band. For both Gaussians used in generating the fitted curve of Figure 6.8, $\sigma = 13$ cm^{-1}. As in the case of a-As_2S_3, a smaller value of σ for the high-frequency Gaussian would improve the fit to the

Figure 6.8

The main band (dotted curve) of the a-As_2Se_3 spectrum after subtraction of the background. The full curve has been fitted to the low-frequency side of the main band and is the sum of two Gaussians.

Figure 6.9

The difference curve (dotted line) obtained by subtracting the fitted curve of Figure 6.8 from the main band of the polarisation-unanalysed spectrum. The full line is a single Gaussian fitted to the difference curve.
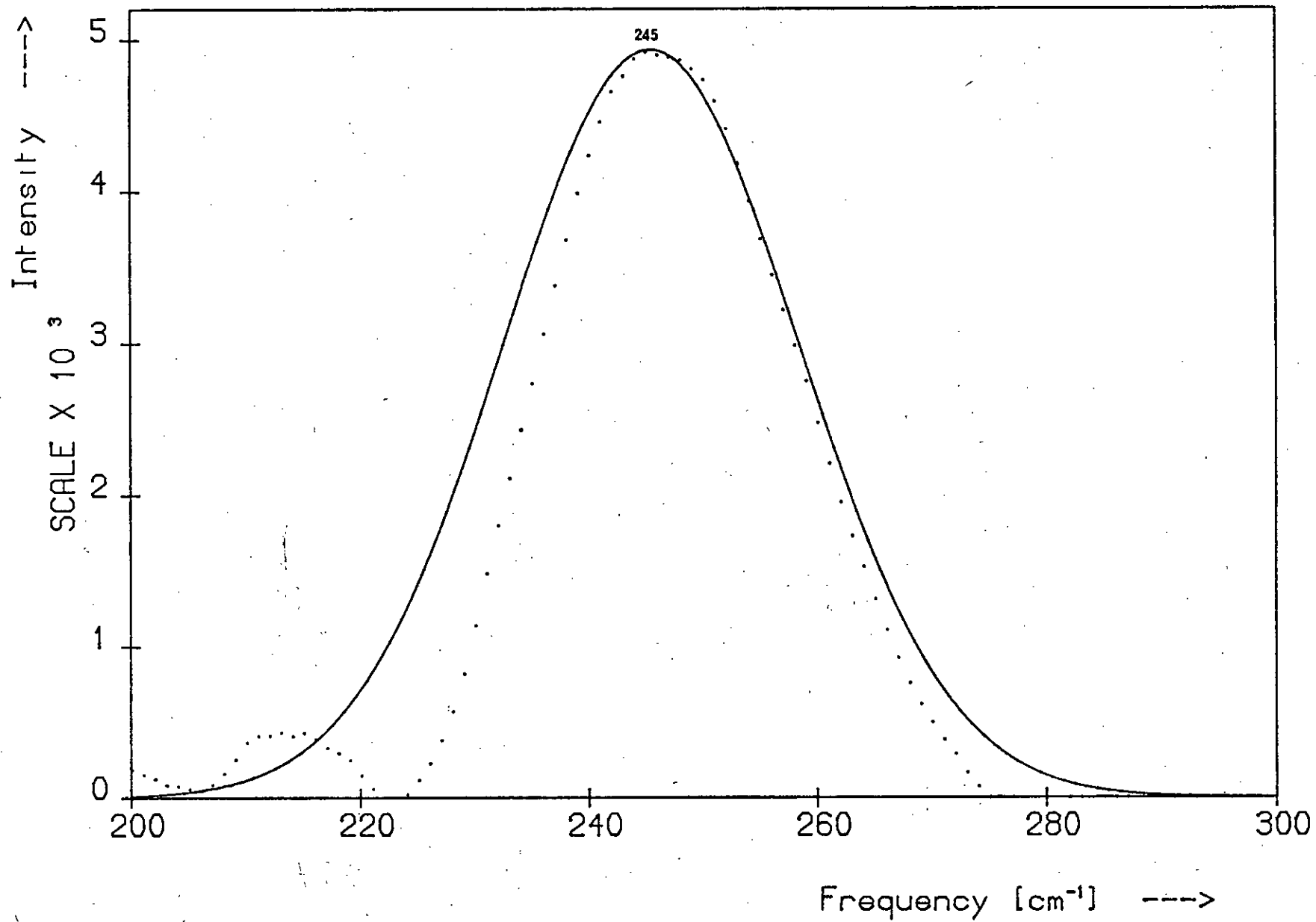
Figure 6.10

The three Gaussians used in the analysis and the curve generated by summing them (A). Curve B is the observed main band of the polarisation-unanalysed spectrum after subtraction of the background.
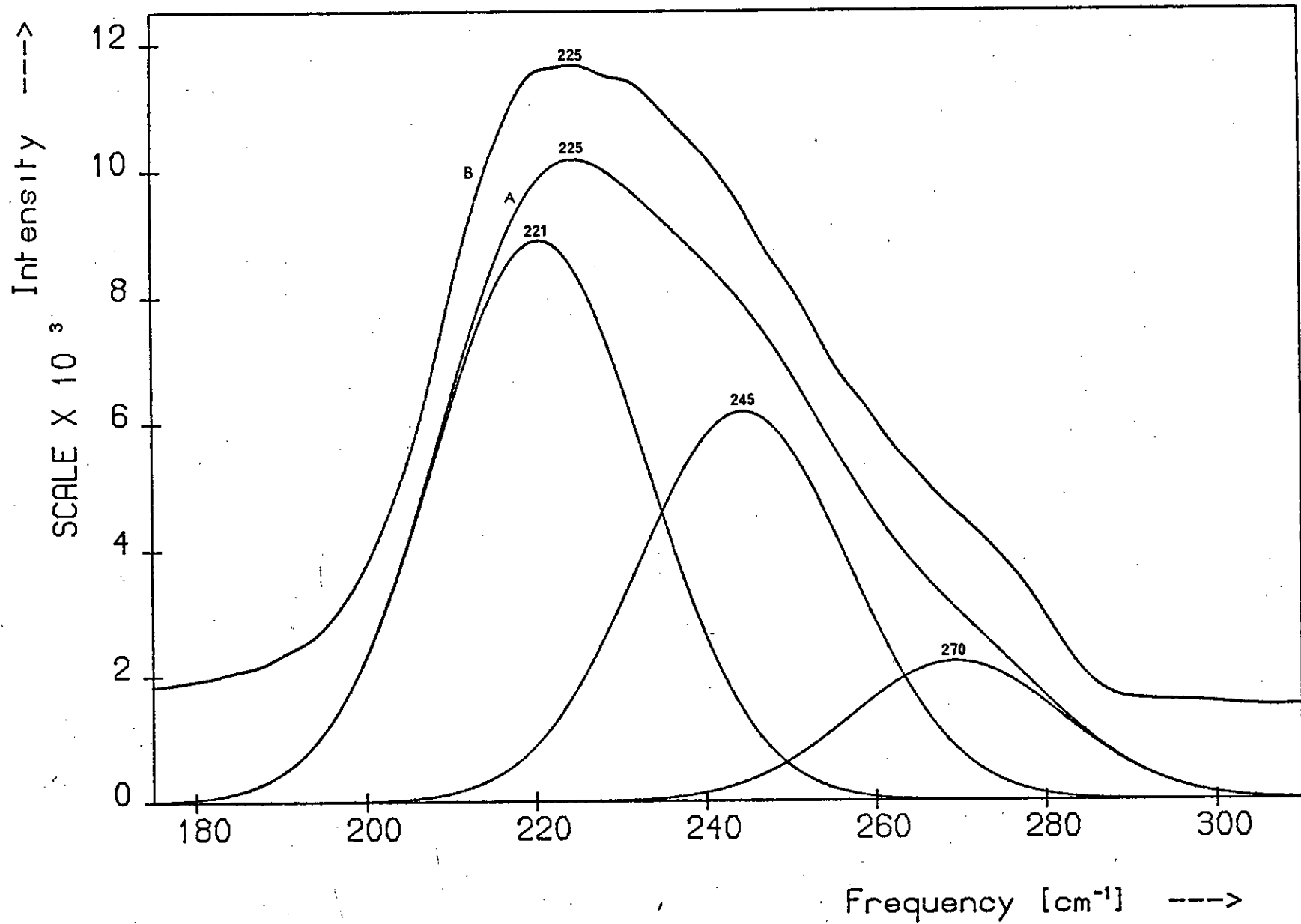
The Main Band of the a-As$_2$Se$_3$ Spectrum
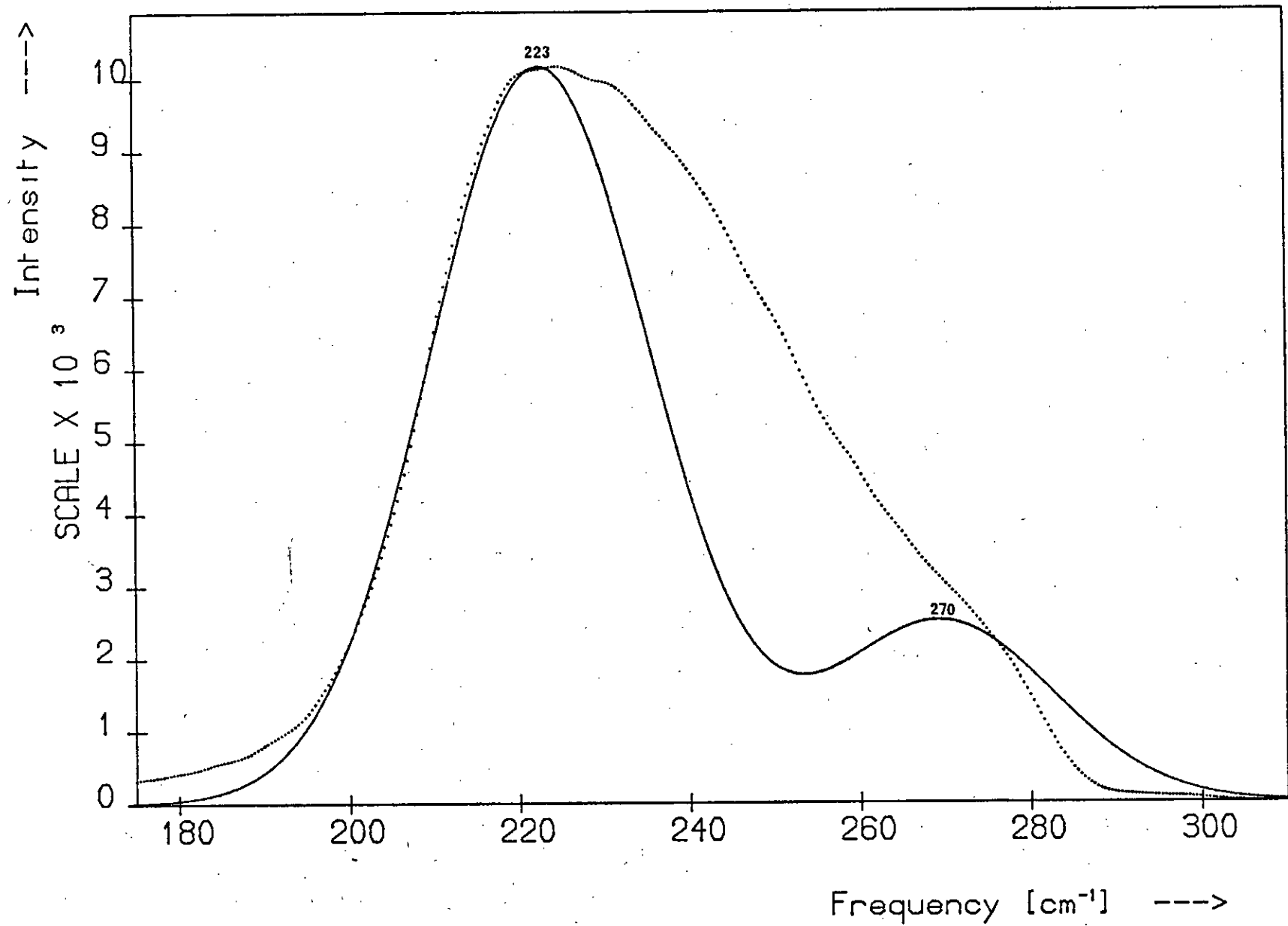
Difference Curve

Deconvolution of the Main Band

knee feature, since above $\sim$275 cm^{-1} the generated curve falls off more slowly than the main band. In Section 6.4.4.4 it will be shown that the 223 and 275 cm^{-1} bands arise from different 'molecular' units, viz an AsSe$_3$ pyramid and an As$_2$Se bridge respectively; the fact that different values of σ are necessary to reproduce exactly the peak and knee of the main band is consistent with these spectral features being associated with different 'molecules'. This was found to be the case for the sulphide also.

Figure 6.9 shows the difference curve (dotted line) obtained by subtracting the fitted curve of Figure 6.8 from the measured spectrum. The principal feature of the difference curve is a peak at 245 cm^{-1} which is slightly asymmetric, tailing off more gradually on the high-frequency side. The structure between $\sim$200 and 225 cm^{-1} probably arises from inaccuracies in the fitting procedure, although As—As bonds in the network may be partly responsible for the peak at $\sim$215 cm^{-1}. (Such bonds are present in the As-rich selenide glasses — see Section 6.6.1.3 — and give rise to a vibration at 220 cm^{-1}; it is possible that these bonds are also present in the As$_2$Se$_3$ glass — see Section 6.4.6 —, just as they are in a-As$_2$S$_3$.)

The full curve in Figure 6.9 is a Gaussian centred at 245 cm^{-1} with σ = 13 cm^{-1}. Above 245 cm^{-1} it is a reasonable fit to the difference curve but agreement is poor below this frequency, probably because over-lapping between the 223 and 245 cm^{-1} bands was neglected when generating the fitted curve of Figure 6.8.

These results suggest that there is a third mode at $\sim$245 cm^{-1} contributing to the main band of a-As$_2$Se$_3$. Further evidence for this is provided by the results of Lucovsky[27] who, in his analysis of the main i.r. band of this material, deduces the presence of a vibration at 246 cm^{-1}.

Curve A of Figure 6.10 was obtained by summing three Gaussians similar to those derived in the above analysis and is clearly a reasonable facsimilie of the main a-As$_2$Se$_3$ band (curve B). In order to take into account overlapping between lines, the heights, central frequencies and standard deviations of the Gaussians used to generate curve A were chosen to give the best overall fit to the main band and so differ slightly from the values given above. The three Gaussians used are shown in the figure; σ = 12.5 cm^{-1} for each.

As in the case of a-As$_2$S$_3$, the deconvolution analysis has revealed a hidden vibration on the high-frequency side of the main Raman band. However, whereas four Gaussians are needed to reproduce the main band of the sulphide, only three are required for generating that of a-As$_2$Se$_3$. This does not necessarily mean that a fourth vibration is not present on the main band of the selenide. It will be shown in Section 6.4.6 that this unobserved band corresponds to the 367 cm^{-1} band of a-As$_2$S$_3$ and is expected to occur at ~261 cm^{-1}. Figure 6.10 shows that it will therefore largely overlap the 245 and 270 cm^{-1} bands and so, if weak, will not be easily detected.

6.4.4   Structural interpretations of the vibrational spectrum

6.4.4.1 The density-of-states description

Figure 6.11 shows the reduced Raman spectrum of a-As$_2$Se$_3$ obtained by the method described in Section 5.4.4.1. The reduction process has removed the boson peak at 24 cm^{-1} but has not affected the genuine vibrational features of the spectrum, apart from changing their relative intensity and shifting them to higher frequencies. For most of the bands this shift is negligible but in the case of the main band it is ~6 cm^{-1}, which is considerably larger than any of the shifts observed for the sulphide. The reason for this large shift is that in the Raman spectrum of a-As$_2$Se$_3$ the intensity is a slowly varying function of

Reduced Raman Spectrum of a-As$_{40}$Se$_{60}$
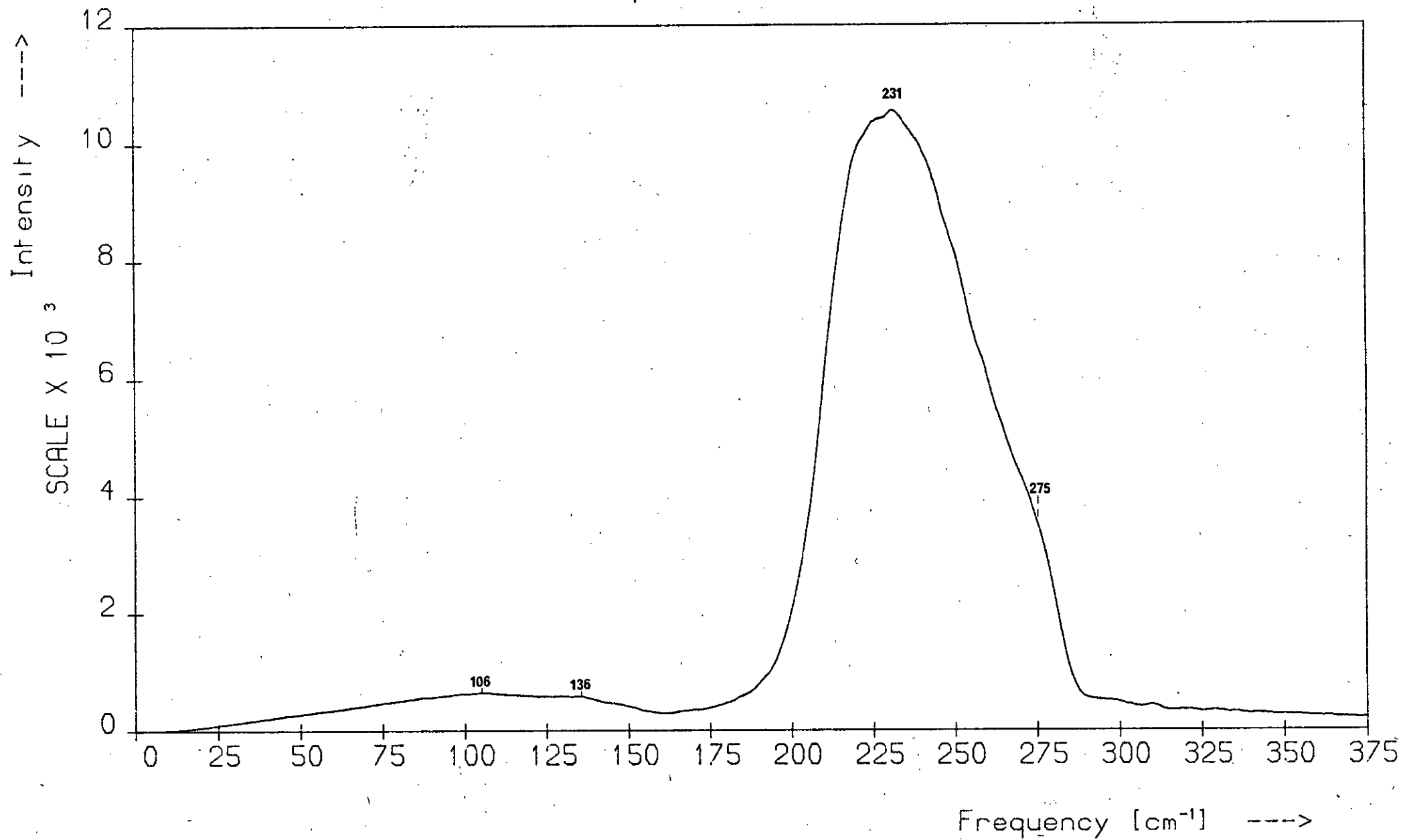
Raman and Reduced Spectra of a-As₄₀Se₆₀
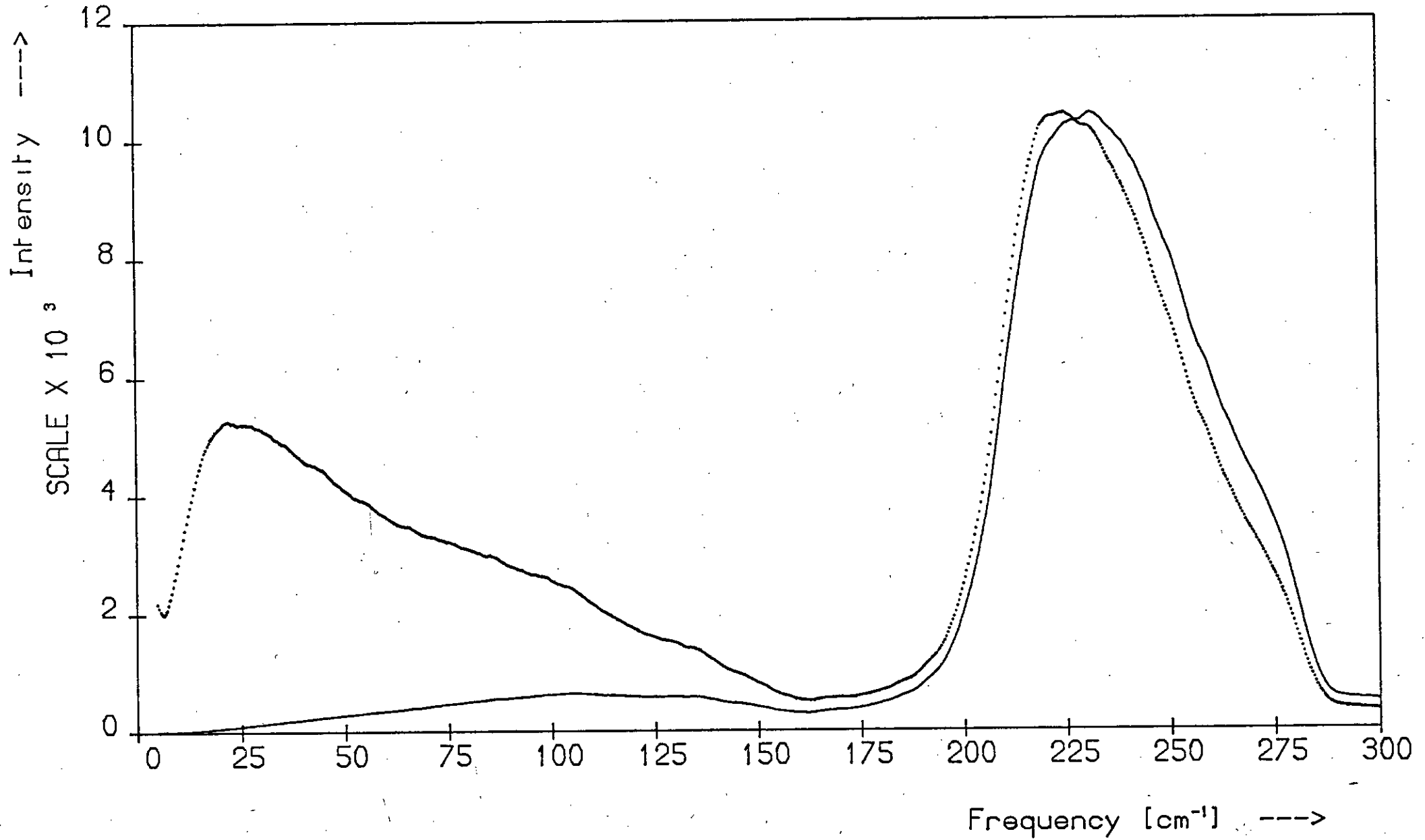
Reduced Spectra of a- and c-$As_{40}Se_{60}$
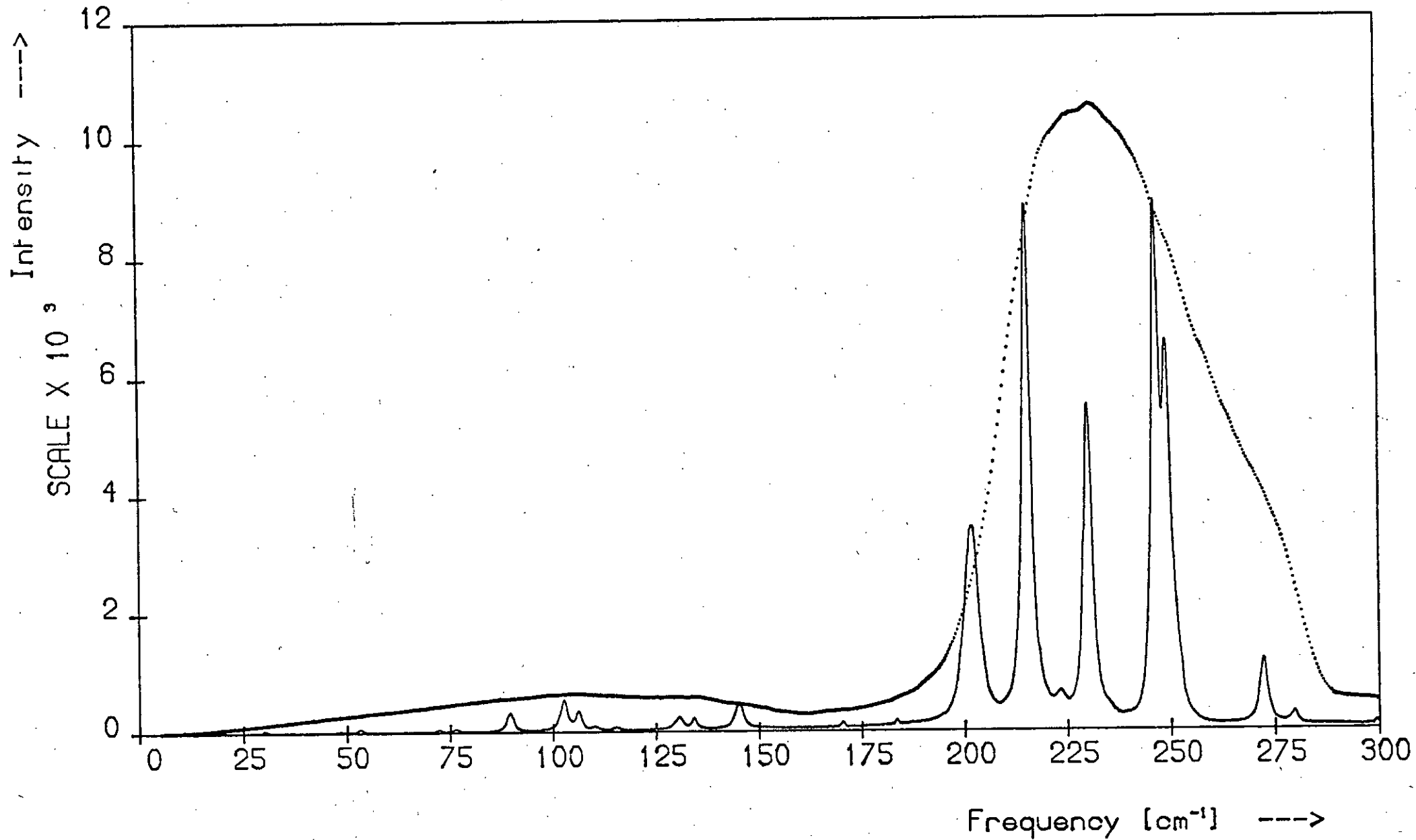
| OTHER STUDIES | | | | | | | | THIS STUDY | | | | | | | | | |
| RAMAN | | | I.R. | | | | | UNREDUCED | | | REDUCED | | | | | | |
Ref. 1/2	Ref. 23	Ref. 22	Ref. 24	Ref. 8	Ref. 25	Ref. 27	Ref. 3	HH	HV	PU	HH	HV	PU	DS	ALL	PS	ASSIGNMENT
			45		38			25	24	24					24	dp	boson peak
														86	86	p	ν_2 As$_2$Se
	90		102	100	113	100	110	106	106	106	106	106	106		106	dp?	ν_4 AsSe$_3$
								136	136	136	136	136	136	136	136	p?	ν_2 AsSe$_3$
227		225	237	221	228	210	218	227	223	225	233	226	231	223	223	dp	ν_3 AsSe$_3$
	237	239				235								240	245*	p	ν_1 AsSe$_3$
						250									261ᵠ	?	ν_3 As$_2$Se
	270					280	270	275	275	275	275	275	275	275	275	p	ν_1 As$_2$Se

PU - polarisation unanalysed; PS - polarisation state; p - polarised; dp - depolarised; DS - depolarisation spectrum; HH and HV refer to the polarised spectra.
All frequencies in cm^{-1}.

*This value is deduced from the deconvolution analysis.
ᵠThis value is obtained by scaling the 367 cm^{-1} frequency of a-As$_2$S$_3$ by 0.71.
⊛Recorded at 1.6° K.
*Recorded at 9° K.

Notes: 1. Many of the other vibrational studies show structure near some of the frequencies observed in the present study but do not quote frequency values.
2. In the present study the uncertainty in the frequencies is not the same for each value shown in the table.
3. Some i.r. studies report very weak structure at 156 and 178 cm^{-1}; the existence of these bands is uncertain but the former may arise from the presence of As—As bonds in the network.

Table 6.1   The observed vibrational frequencies of a-As$_2$Se$_3$.

frequency near the peak of the main band — i.e. the band has a flat top — and slowly varying regions are sensitive to the reduction process. Figure 6.12, which compares the reduced and unreduced spectra, shows clearly the effect of the reduction process on the main band (cf. Figure 5.21). The 6 cm^{-1} difference in the main-band peak positions is obvious.

The complementary nature of the i.r. and Raman spectra of a-As$_2$Se$_3$ together with the pronounced structure in its depolarisation spectrum suggest that, as for a-As$_2$S$_3$, the reduced spectrum is not a good approximation to the density of states, G(w). The reduced spectrum is, however, similar to the density of states derived from the crystal spectrum, as was found in the case of the sulphide. Figure 6.13 compares the reduced spectra of a- and c-As$_2$Se$_3$, the two curves being normalised at 247 cm^{-1}. Clearly, the glass spectrum is approximately the envelope of the crystal lines.

Comparison of Figure 6.13 with Figure 5.22, which shows the corresponding sulphide spectra, reveals an interesting similarity. In both figures one of the high-frequency lines protrudes well through the envelope of the glass spectrum; these are the lines at 292 and 202 cm^{-1} in the c-As$_2$S$_3$ and c-As$_2$Se$_3$ spectra respectively (it is the former line which in the layer model for a-As$_2$S$_3$ is responsible for exaggerating the shoulder on the main band — see Section 5.4.4.3). In Section 6.4.5 it will be shown that these are corresponding lines and arise from the same mode of vibration. The protrusion of the lines through the glass spectra would be accounted for if for both the sulphide and the selenide the disordering of the crystal structure somehow leads to the contribution from this mode being supressed or shifted to higher frequencies. It has been suggested[32] that differences in layer separation between the crystalline and amorphous forms might lead to the displacement of these lines, for in the case of c-As$_2$S$_3$ Zallen[33] has shown that with decreasing pressure (and hence with increasing layer separation) the 292 cm^{-1} band

and the weak 324 cm^{-1} band shift to higher frequencies whereas all the others decrease in frequency. X-ray measurements[34] indicate that the layer separation in a-As$_2$S$_3$ and a-As$_2$Se$_3$ is larger than in the corresponding crystals; the increased layer separation in the glasses is responsible for their density deficit relative to the crystals.

The reduced HV and HH spectra of a-As$_2$Se$_3$ do not differ significantly from the reduced unanalysed spectrum. The low-temperature ($\sim$11° K) HH spectrum was reported in the studies of Lucovsky et al.[21,22] and, as expected, is similar to the reduced HH spectrum; the low-temperature and reduced HH spectra peak at 239 and 233 cm^{-1} respectively.

6.4.4.2 The random network model

The two-dimensional c.r.n. model proposed by Bermudez[35] was described in Section 5.4.4.2. It yields a vibrational density of states for a-As$_2$Se$_3$ that is in reasonable agreement with experiment, although the computed spectrum has no feature corresponding to the 275 cm^{-1} knee which is observed in many of the experimental studies. However, as in the case of the sulphide, the main failing of the model is that it predicts the wrong polarisation properties for the main band. According to the model, the principal low-frequency stretching band is polarised while the principal high-frequency stretching band is depolarised; the experimental evidence shows that the reverse is true, for the 223 cm^{-1} band is depolarised while the $\sim$245 cm^{-1} band is polarised.

6.4.4.3 The layer model

The layer model put forward by Taylor et al.[31] to account for the vibrational spectra of a-As$_2$S$_3$ and a-As$_2$Se$_3$ was discussed at length in Section 5.4.4.3. These authors reported that the general features of the i.r. absorption spectrum of a-As$_2$Se$_3$ were reproduced by the model. Figure 6.14, which was prepared by Dr. M.J.Sik, compares the main band of the reduced Raman spectrum (full curve) with that of a computed

Figure 6.14

The main band of the a-As_2Se_3 spectrum. The full curve is the main
band of the reduced spectrum and the dotted curve is the main band of
a computed spectrum obtained by broadening the reduced Raman spectrum
of c-As_2Se_3 using a Gaussian convolution function. (Courtesy of
Dr. M.J.Sik).
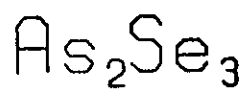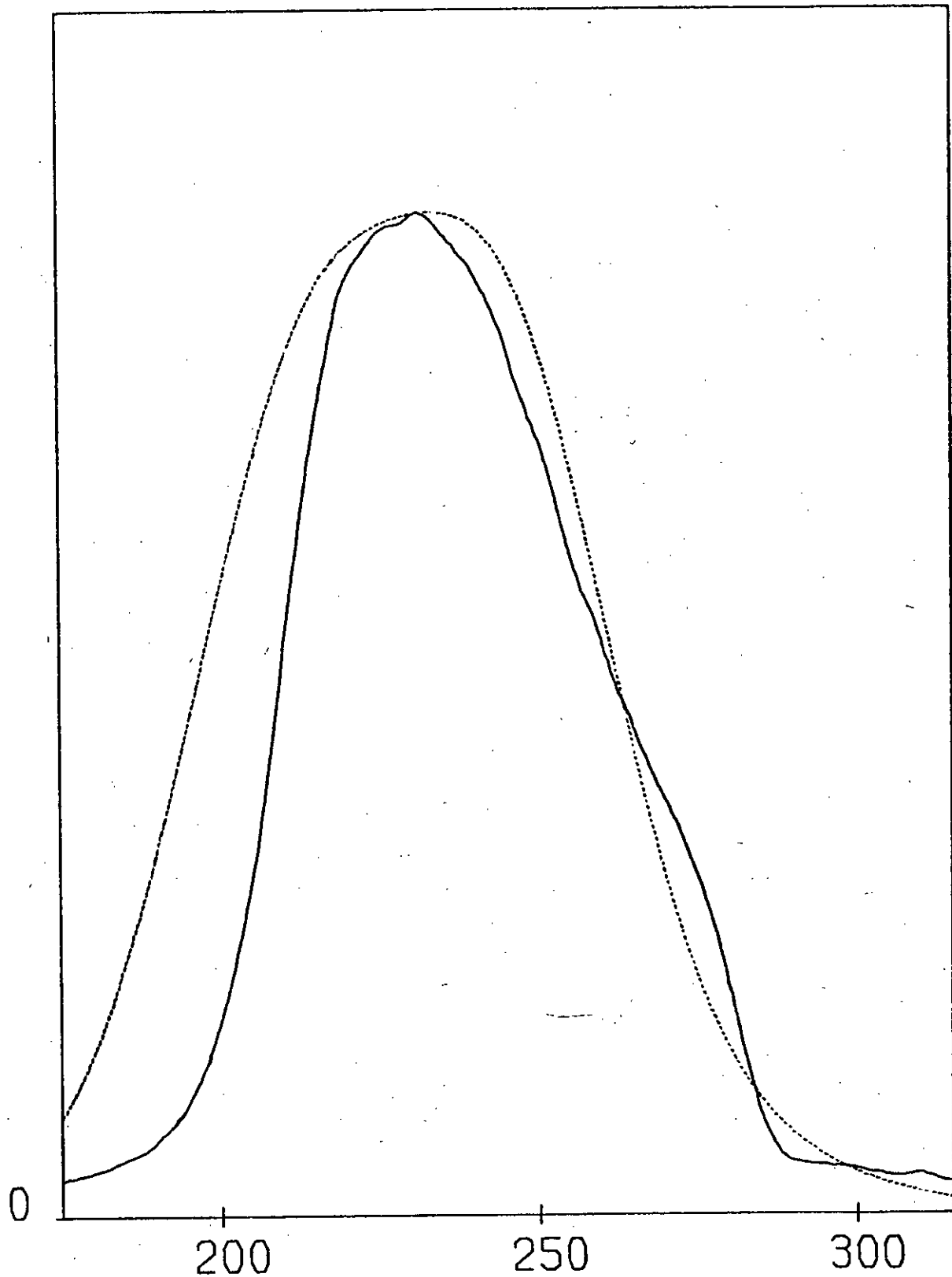
As₂Se₃

spectrum (dotted curve) generated by broadening the bands of the reduced spectrum of crystalline As_2Se_3 using a Gaussian convolution function (cf. Figure 5.24). It is clear from the figure that the model spectrum has similar shortcomings to those found in the case of the sulphide, for the agreement on the low-frequency side of the peak is poor, due to the strong crystal band at 202 cm^{-1}, and there is no feature in the model spectrum corresponding to the observed knee at 275 cm^{-1}.

The stretching modes of any As—As or Se—Se bonds in the glass are expected to occur near 220 and 265 cm^{-1} respectively and thus will fall in the frequency range occupied by the main band. Since these 'wrong'-bond bands, if present, will be superimposed on the main band and weak in comparison to it, they are not observed in the measured spectrum and hence the presence of 'wrong' bonds in a-As_2Se_3 does not significantly affect the agreement between the observed and the computed spectrum, which is in contrast to the case of a-As_2S_3.

As was found for a-As_2S_3, however, the polarisation measurements do not support the layer model, for the depolarisation spectrum of a-As_2Se_3, like that of a-As_2S_3, exhibits pronounced structure at lower frequencies instead of having the constant amplitude of $\sim\frac{1}{2}$ which is expected from the model. Thus the vibrational spectrum of a-As_2Se_3 is no more amenable to this quasi-crystalline approach than was that of a-As_2S_3. The general objections to the layer model were outlined in Section 5.4.4.3.

Nevertheless, the fact that the low-frequency regions of the a-As_2S_3 and a-As_2Se_3 spectra scale by the same factor that relates the interlayer bands of the two crystal spectra (see Section 6.4.5) suggests that if layer-like regions are present in a-As_2S_3 they are also present in a-As_2Se_3.

6.4.4.4 The molecular model

The molecular model and its application to a-As$_2$S$_3$ was discussed at length in Section 5.4.4.4; much of what was stated there is also applicable in the case of a-As$_2$Se$_3$. Lucovsky and Martin[36] and Austin and Garbett[6] have both used a molecular approach in interpreting the i.r. and Raman spectra of a-As$_2$Se$_3$, which, like those of the sulphide, are complementary and contain sharp features.

In the model the 'molecular' unit for a-As$_2$Se$_3$ is taken to be an AsSe$_3$ pyramid — the basic structural unit of c-As$_2$Se$_3$. These pyramids are connected to one another via bent As—Se—As chains and are randomly positioned (see Figure 5.25). The interaction between the pyramid units is accounted for by considering the vibrations of the non-linear As$_2$Se linking 'molecule'. The bond lengths and bond angles are based on those of c-As$_2$Se$_3$ and the force constants for the AsSe$_3$ pyramid are obtained by scaling those of the AsBr$_3$ molecule, which is isostructural with the AsSe$_3$ pyramid and has the same mass ratio. The detais of the application of the model to a-As$_2$Se$_3$ are given in Section 6.4.6.

Lucovsky and Martin obtain for the frequencies of the ν_1, ν_2, ν_3 and ν_4 modes of the AsSe$_3$ 'molecule' the values 227, 102, 220 and 78 cm^{-1} respectively and calculate the frequencies of the ν_1, ν_2 and ν_3 modes of the As$_2$Se 'molecule' to be 178, 39 and 282 cm^{-1} respectively. The calculated frequencies are all close to structure in the observed i.r. and Raman spectra. Lucovsky and co-workers[21,22,27,36,37] have also shown that the model accounts for the complementarity of the i.r. and Raman spectra of a-As$_2$Se$_3$ and for the polarisation properties of the high-frequency bands.

Of the various approaches used in interpreting the vibrational spectra of a-As$_2$Se$_3$ the molecular model is the most successful but in the form used by Lucovsky and co-workers it does not yield complete

agreement with experiment. The shortcomings of the model as it stands are discussed in Section 6.4.6 where it will also be shown how the model can be modified to give better agreement with experiment.

6.4.4.5 The composite model

Although the composite model of Finkman et al. has only been used to interpret the vibrational spectra of a-As_2S_3 [38] and a-As_2O_3 [29,39] it is probably also applicable to a-As_2Se_3 since the crystalline forms of these materials are isomorphous (only the claudetite polymorph of c-As_2O_3 is being considered here). The model, which is discussed in Sections 5.4.4.5 and 5.7, was originally proposed to account for changes in the reduced Raman intensity of a-As_2S_3 as a function of temperature; it may also account for the photo-induced decrease in Raman signal observed for a-As_2S_3. Since similar effects in a-As_2Se_3 have not yet been investigated no comparison is possible with the results for the sulphide. In the present study the absence of a signal loss in the Raman experiments on a-As_2Se_3 may be due to the use of a spinning sample.

6.4.5 The scaling relation

Zallen cnd co-workers [4,5] have shown that the vibrational frequencies of c-As_2Se_3 (ν_i^{As-Se}) are related to those of c-As_2S_3 (ν_i^{As-S}) by a simple scaling relation:

$$\nu_i^{As-Se} = K \nu_i^{As-S}$$

where i indexes the modes and $K = 0.71 \pm 0.01$ for the intralayer modes and $K = 0.81 \pm 0.05$ for the rigid-layer modes. These authors point out that the existence of the scaling relation is a result of the close isomorphicity of c-As_2Se_3 and c-As_2S_3. By considering the AsX_3 (X = S or Se) units that make up the crystals, they derive an expression relating the intralayer scaling factor to the reduced-mass and force-constant ratios for the two crystals and show that its value of 0.71 ± 0.01 arises mainly from the difference in the masses of the S and Se atoms.

Using this expression they further show that the intralayer scaling relation implies that the bond-stretching force constant of c-As_2Se_3 is ∼10% smaller than that of c-As_2S_3. The scaling relation is illustrated in Figure 6.15 which compares the Raman spectrum of c-As_2Se_3 with that of c-As_2S_3, the latter having been compressed along the frequency axis by a factor of 0.71.

In their first report of this scaling relation Zallen et al.[4] obtained a value of 0.70 ± 0.03 for the intralayer scale factor and remarked that the vibrational spectra of vitreous As_2Se_3 and As_2S_3 were also related by this factor. In the case of the Raman spectra, Zallen et al. matched the peak frequency of the main band of a-As_2Se_3 (∼230 cm^{-1}) with that of the a-As_2S_3 main band (340 cm^{-1}), obtaining a value of 0.68 for the frequency scale factor; this value is within the range 0.70 ± 0.03. The frequencies used were taken from Ward's Raman study of the glasses[1,2,20]. At the time, the ∼230 cm^{-1} band of a-As_2Se_3 was the only feature of its Raman spectrum that had been observed so no other values for the frequency scale factor could be obtained.

In a subsequent paper Zallen and Slade[5] investigate the spectra of the two crystals in more detail and obtain a more accurate value for the intralayer scale factor, viz 0.71 ± 0.01. Zallen and Slade do not comment on the glass spectra in this second paper. The value of 0.68 derived for the glasses is now well outside the new range of values for the crystal scale factor. When more recent values for the main band peak frequencies are used instead of Ward's values, the agreement between the crystal and glass scale factors is even poorer: for example, using the values measured in the present study (225 and 338 cm^{-1}) yields a glass scale factor of 0.67.

Since c-As_2Se_3 and c-As_2S_3 are isomorphic it is reasonable to expect that the structure of a-As_2Se_3 will be similar to that of a-As_2S_3. Assuming the two glasses do have essentially the same structure, their

Figure 6.15

The Raman spectra of c-As_2Se_3 and c-As_2S_3. The c-As_2S_3 spectrum has been compressed along the frequency axis by a factor of 0.71.
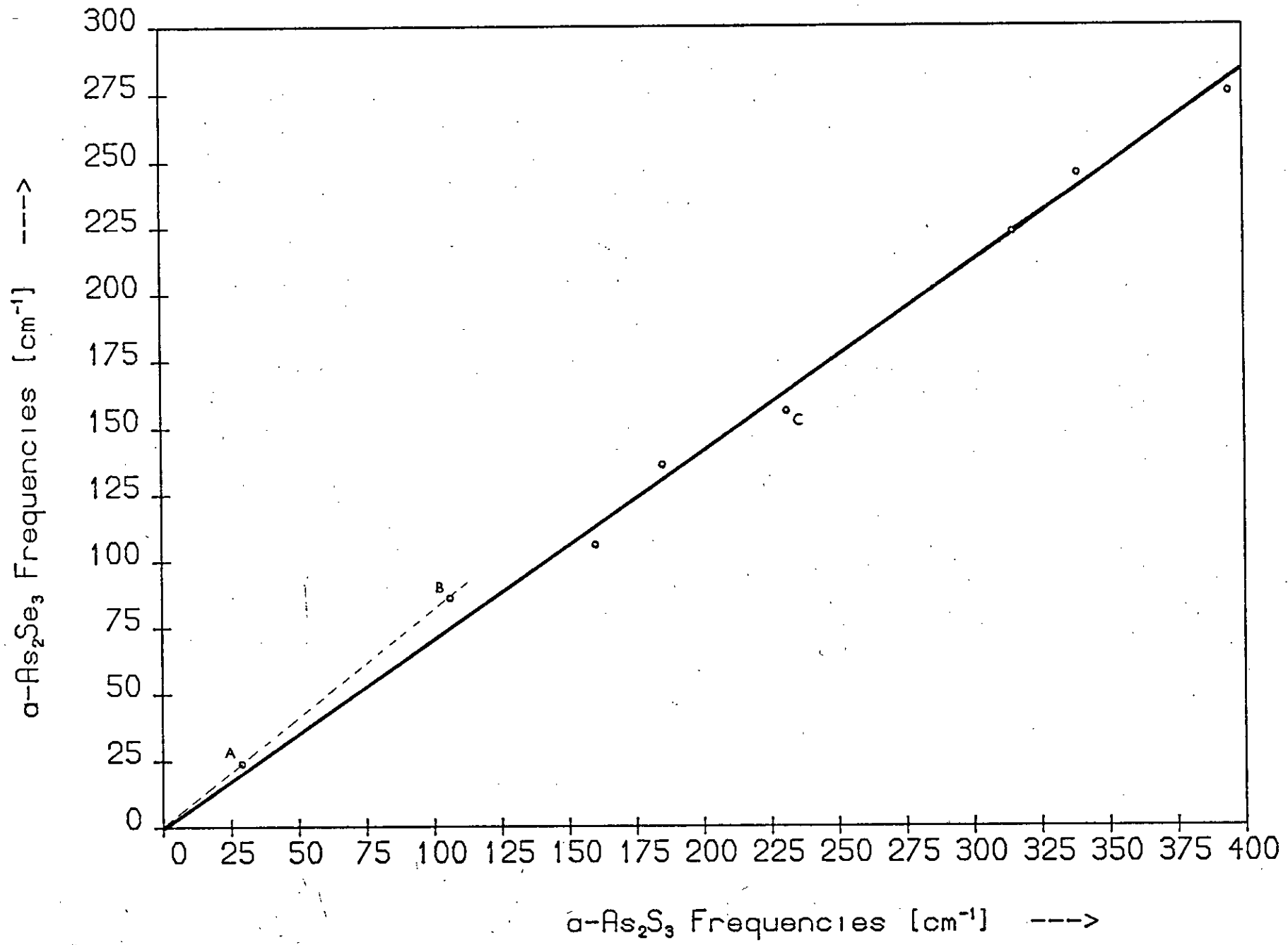
Raman Spectra : c-As₂S₃ and c-As₂Se₃.
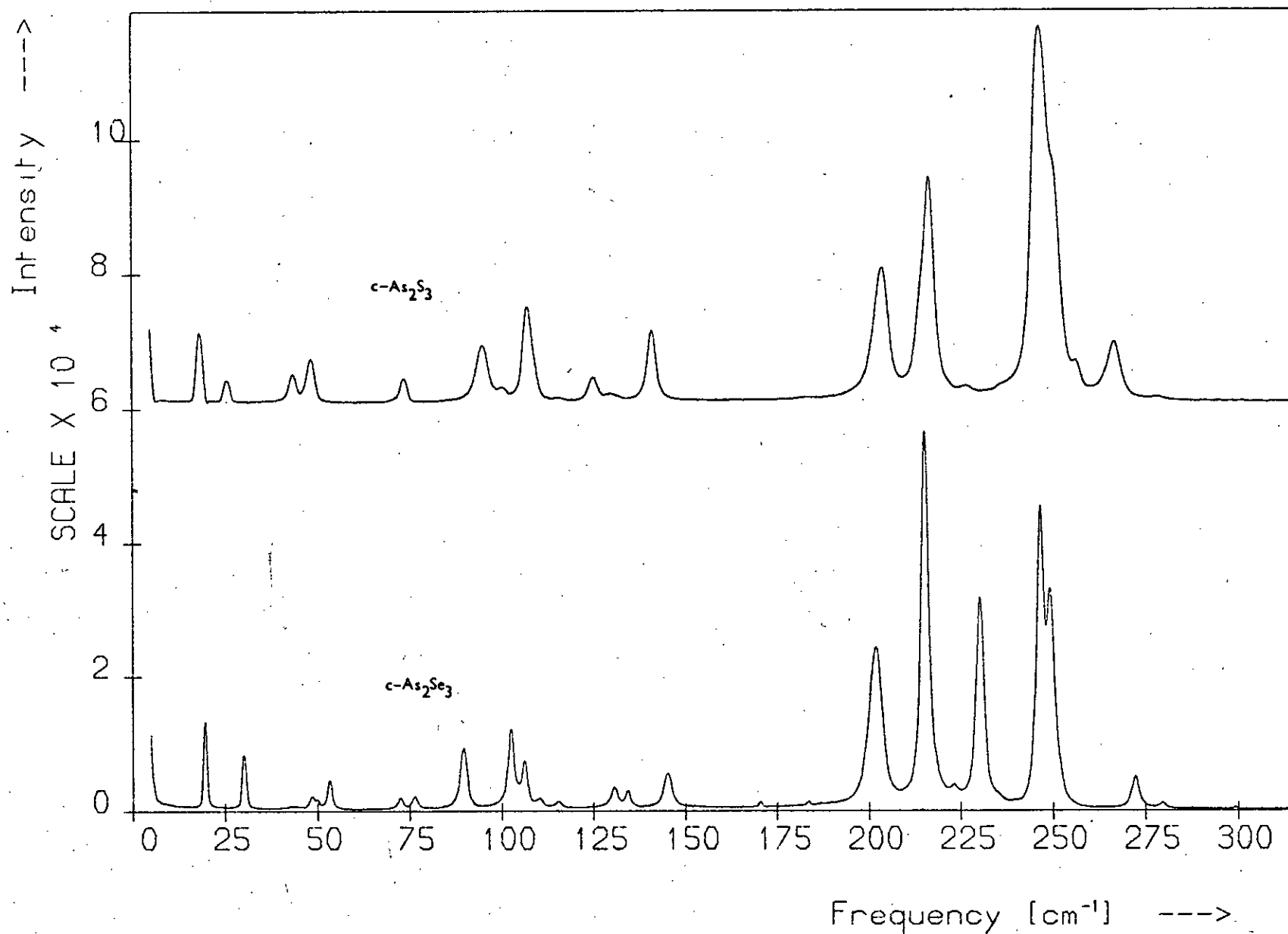
vibrational spectra should scale. If the 225 cm^{-1} band of the a-As$_2$Se$_3$ spectrum does correspond to the 338 cm^{-1} a-As$_2$S$_3$ band, so that the glass scale factor really is ~0.68, then there should be a band at ~214 cm^{-1} in the a-As$_2$Se$_3$ spectrum corresponding to the a-As$_2$S$_3$ band at 315 cm^{-1}. In the present study a thorough search was made for structure down the low-frequency side of the main band of a-As$_2$Se$_3$ but none was discovered. Also, it was found that taking the frequency of the ν_1 mode of the AsSe$_3$ pyramid as ~225 cm^{-1} in the molecular model yields an As—Se bond-stretching force constant that is ~20% smaller than that for the As—S bond, whereas the crystal scaling relation implies that the As—Se bonds are only 10% softer than the As—S bonds. Since the bond-stretching force constant for a-As$_2$Se$_3$(a-As$_2$S$_3$) is expected to be virtually the same as that for c-As$_2$Se$_3$(c-As$_2$S$_3$) this discrepancy in relative bond strengths is surprising.

The above results suggest that the 225 cm^{-1} a-As$_2$Se$_3$ band does not correspond to the 338 cm^{-1} a-As$_2$S$_3$ band. This is confirmed by the depolarisation measurements, which show that the latter band is polarised while the former is depolarised (see Figures 5.14 and 6.6). Thus although the 225 and 338 cm^{-1} bands are the principal bands in their respective spectra they do not arise from the same mode of vibration. In fact, there is no reason to suppose that just because they are the strongest bands in their spectra that they correspond, for the most intense line in the c-As$_2$Se$_3$ spectrum (that at 215 cm^{-1}) does not correspond to the most intense line in the c-As$_2$S$_3$ spectrum (that at 353 cm^{-1}).

Figure 6.16 shows a plot of the Raman frequencies of a-As$_2$Se$_3$ against those of a-As$_2$S$_3$. Polarisation states were taken into account when pairing the bands in the two spectra and the As$_2$S$_3$ bands thought to be due to S—S bonds have been ignored. The frequency pairs are given in Table 6.2, from which it is seen that the 225 cm^{-1} a-As$_2$Se$_3$ band corresponds to the 315 cm^{-1} band of a-As$_2$S$_3$ rather than that at 338 cm^{-1}. The full line is a least squares fit to the underlined points and has a gradient of 0.71 ± 0.03,

Figure 6.16

The Raman frequencies of a-As_2Se_3 plotted against the corresponding frequencies of a-As_2S_3. The frequency pairs are given in Table 6.2. The full line has a gradient of 0.71 and the dashed line a gradient of 0.82.

The Scaling Relation

a-As₂S₃ Frequencies [cm⁻¹] --->

a-As₂Se₃ Frequencies [cm⁻¹] --->

γ_i^{As-Se}	γ_i^{As-S}	$\dfrac{\gamma_i^{As-Se}}{\gamma_i^{As-S}}$
24	29	0.828
86	106	0.811
106	160	0.663
136	185	0.735
156*	231	0.675
223	315	0.708
245	338	0.725
275	395	0.696

All frequencies in cm^{-1}.

*Taken from i.r. studies[24,25].

Table 6.2   Frequency pairs for the scaling relation between the

spectra of the glasses.   In Figure 6.16 A$\equiv$(29,24),

B$\equiv$(106,86) and C$\equiv$(231,156).

which is the same as the crystal value for the intralayer scale factor. The dashed line passes through the origin and the points A and B (see below) and has a gradient of ~0.82.

The points A and B lie in the frequency regions occupied by the rigid-layer modes of the crystals and were not included in the least squares fit since their frequencies should scale by a factor of ~0.81. The low-frequency features of the Raman spectra are discussed below. C is the point (231 cm^{-1}, 156 cm^{-1}); as both these frequencies may arise from As—As bonds in the respective glasses this point was also excluded from the least squares fit.

When the Raman and depolarisation spectra of a-As$_2$S$_3$ are compressed along the frequency axis by a factor of 0.71 they match the corresponding a-As$_2$Se$_3$ spectra reasonably well (ignoring the frequency region below ~120 cm^{-1}), as Figures 6.17 — 6.20 show. Also, when the sulphide and selenide frequencies are paired as in Table 6.2 the molecular model calculations yield a force constant ratio, k_1^{As-Se}/k_1^{As-S}, of ~0.9, which is the same as that for the crystals. Thus it can be concluded that the intralayer regions of both the crystal and the glass spectra scale by the same factor, viz 0.71.

The frequency region below 70 cm^{-1} in the c-As$_2$Se$_3$ spectrum and that below 100 cm^{-1} in the c-As$_2$S$_3$ spectrum are occupied by the rigid-layer bands, which scale by a factor of 0.81. The existence of a scaling relation for these regions of the glass spectra is not immediately obvious. Only two spectral features occur in the low-frequency regions of the glass spectra: the Bose peak and the broad dip in $\rho(w)$. The relative uncertainty in the frequencies of these features is large, which leads to a large uncertainty in the scale factor. However, when these features are considered as a whole it is found that they do scale by a factor closer to 0.81 than to 0.71. This is seen in Figure 6.21 which compares the Bose peak of a-As$_2$Se$_3$ with that of a-As$_2$S$_3$; the peaks are normalised by

Figure 6.17

The polarisation-unanalysed Raman spectra of a-As_2S_3 and a-As_2Se_3.[*]

Figure 6.18

The reduced Raman spectra of a-As_2S_3 and a-As_2Se_3.[*]

Figure 6.19

The VH- and HV-polarised Raman spectra of a-As_2S_3 and a-As_2Se_3 respectively.[*]

Figure 6.20

The depolarisation spectra of a-As_2S_3 and a-As_2Se_3.[*]   The bracketed

frequencies are those actually measured for a-As_2S_3.

[*]
  In each case the a-As_2S_3 spectrum has been compressed along the frequency

  axis by a factor of 0.71.

Raman Spectra : $a\text{-}As_2S_3$ and $a\text{-}As_2Se_3$.
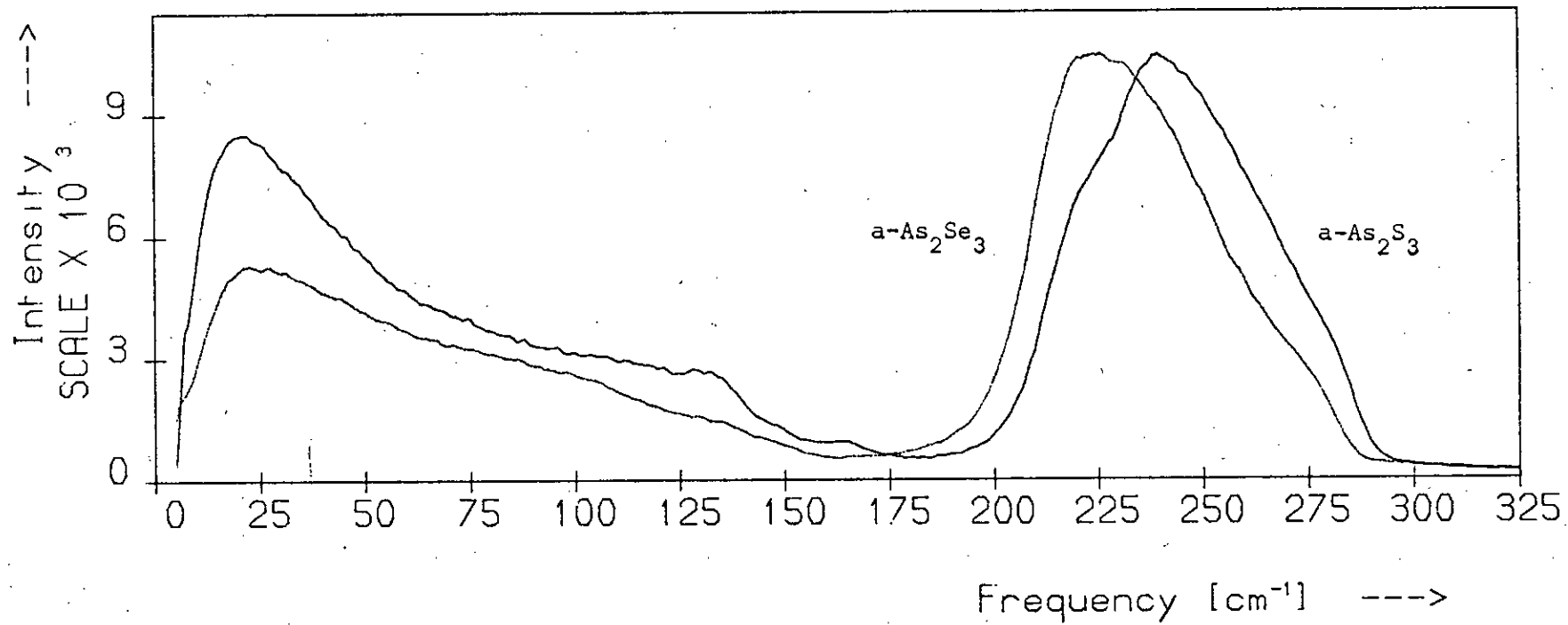
Raman Spectra : a-As$_2$S$_3$ and a-As$_2$Se$_3$.

Intensity ---> SCALE X 10^3

9

6

3

0

a-As$_2$Se$_3$

a-As$_2$S$_3$

0   25   50   75   100   125   150   175   200   225   250   275   300   325

Frequency [cm^{-1}]   --->

Polarised Spectra : a-As$_2$S$_3$ and a-As$_2$Se$_3$

Intensity ---->

SCALE X 10^3
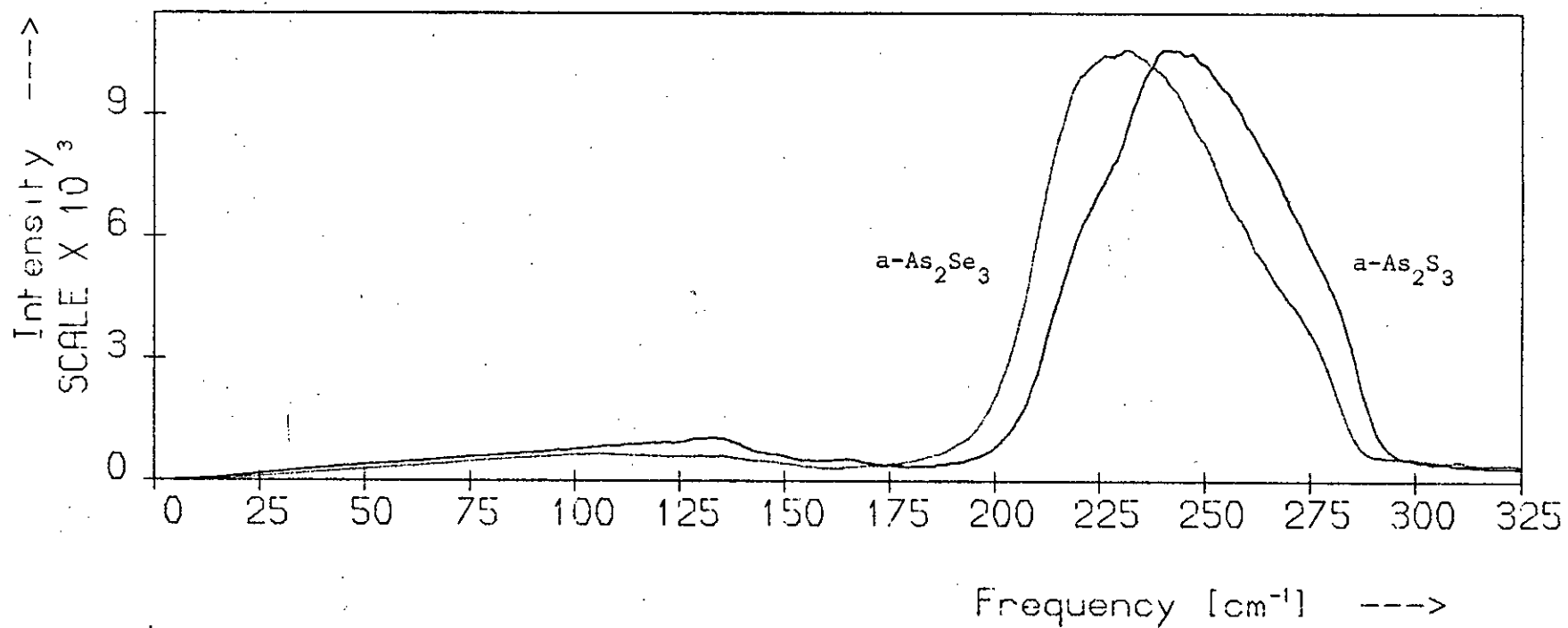
a-As$_2$S$_3$ (VH)

a-As$_2$Se$_3$ (HV)
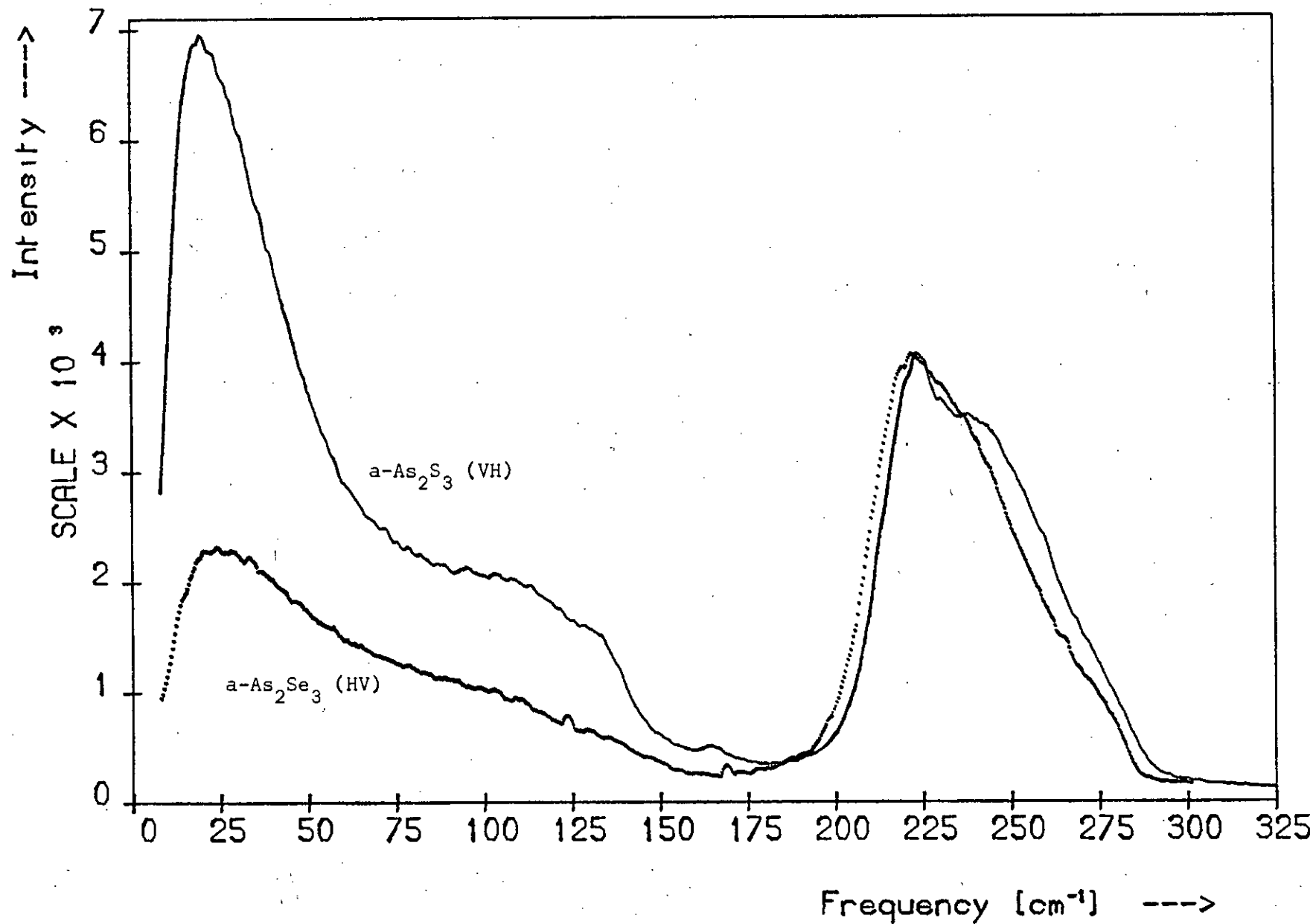
Frequency [cm^{-1}] ---->

Depolarisation Spectra: a-As₂S₃ & a-As₂Se₃
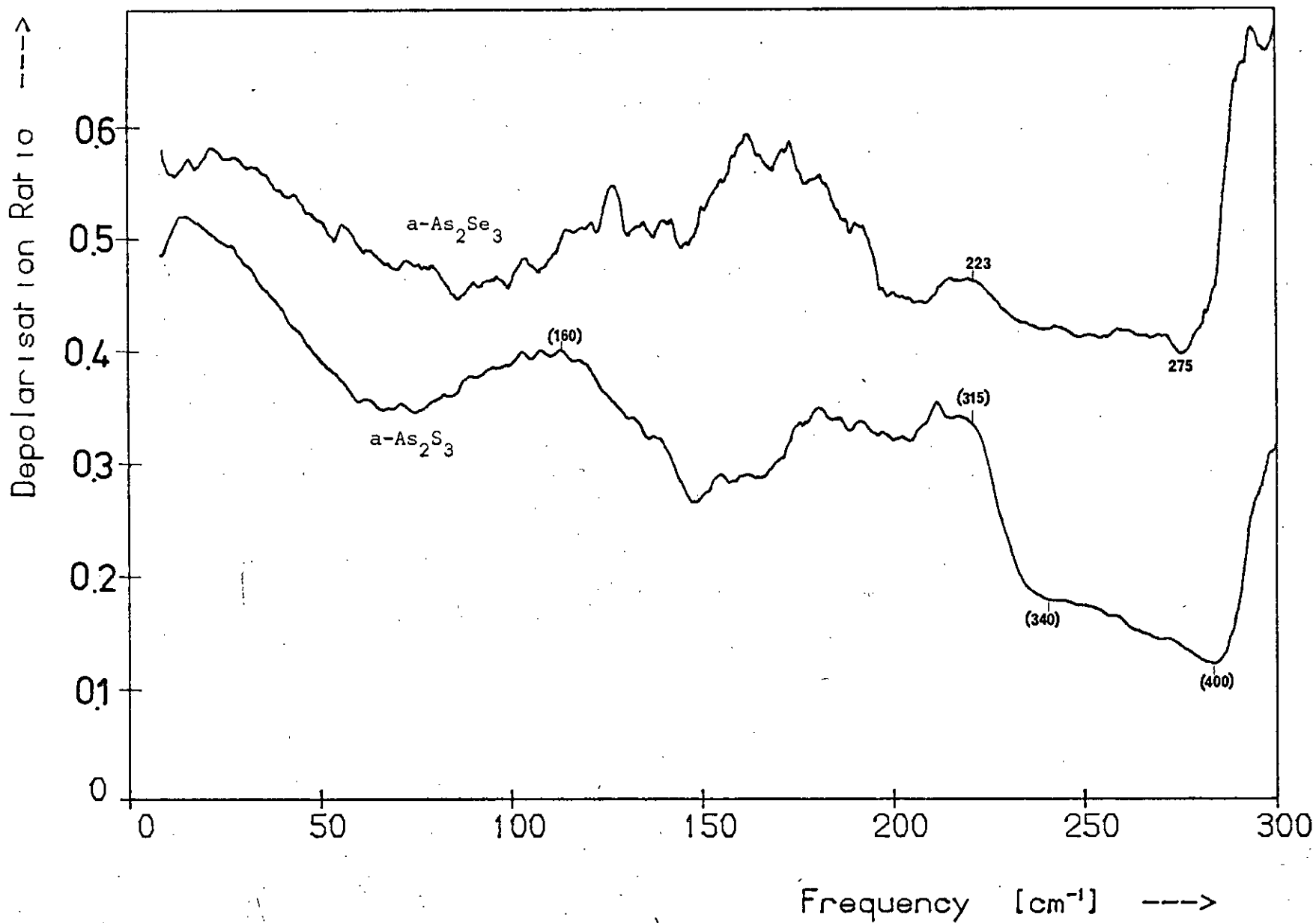
Figure 6.21

The boson peaks of $a-As_2S_3$ and $a-As_2Se_3$.   A, B and C are the boson

peak of $a-As_2S_3$ compressed along the frequency axis by factors of 0.71,

0.76 and 0.81 respectively.   D is the boson peak of $a-As_2Se_3$.

Figure 6.22

The low-frequency section of the depolarisation spectra of $a-As_2S_3$ and

$a-As_2Se_3$.   A, B and C are the $a-As_2S_3$ spectrum compressed along the

frequency axis by factors of 0.71, 0.76 and 0.81 respectively.   D is

the $a-As_2Se_3$ spectrum.

Bose Peaks
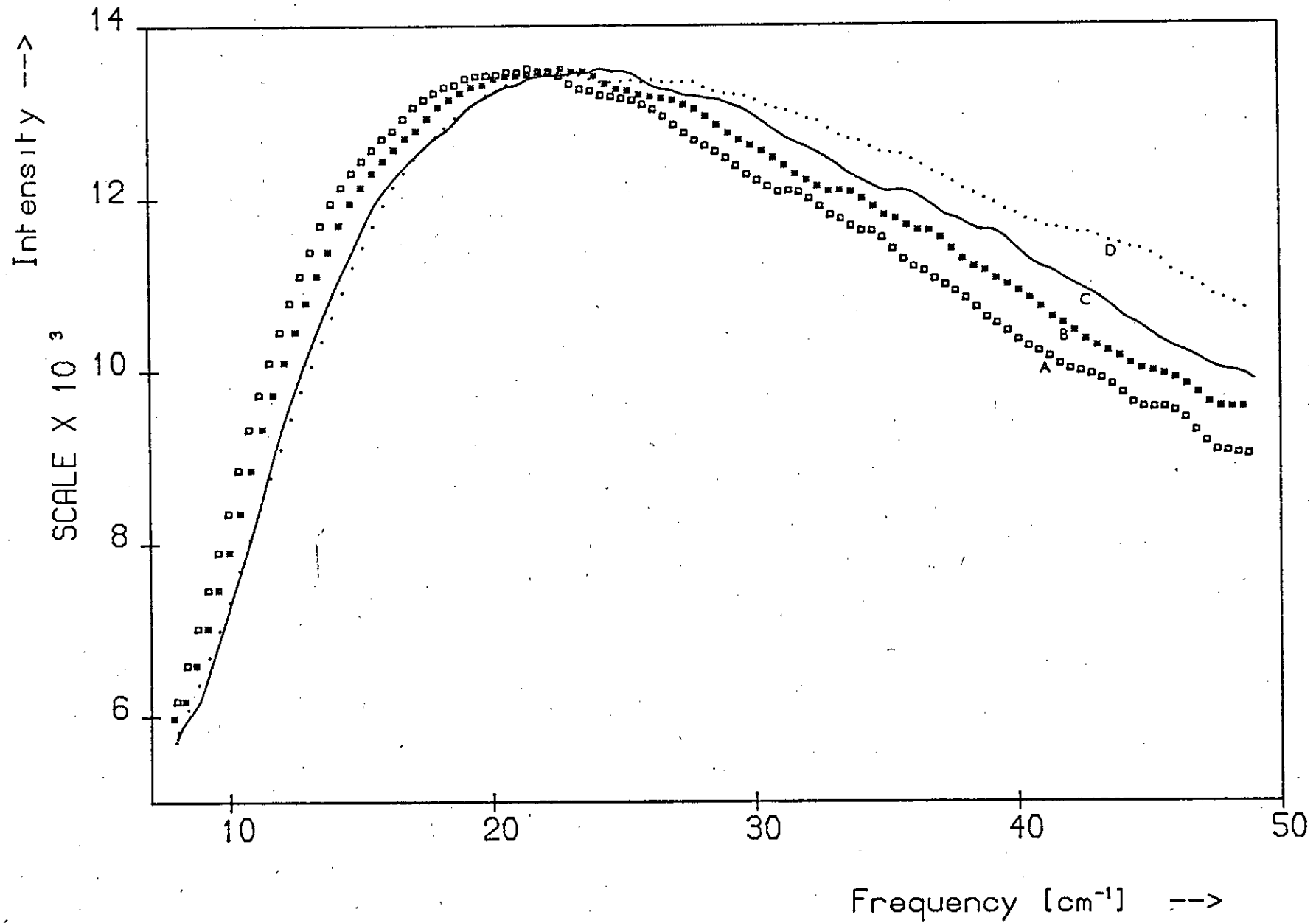
Depolarisation Spectra: $As_{40}S_{60}$ & $As_{40}Se_{60}$
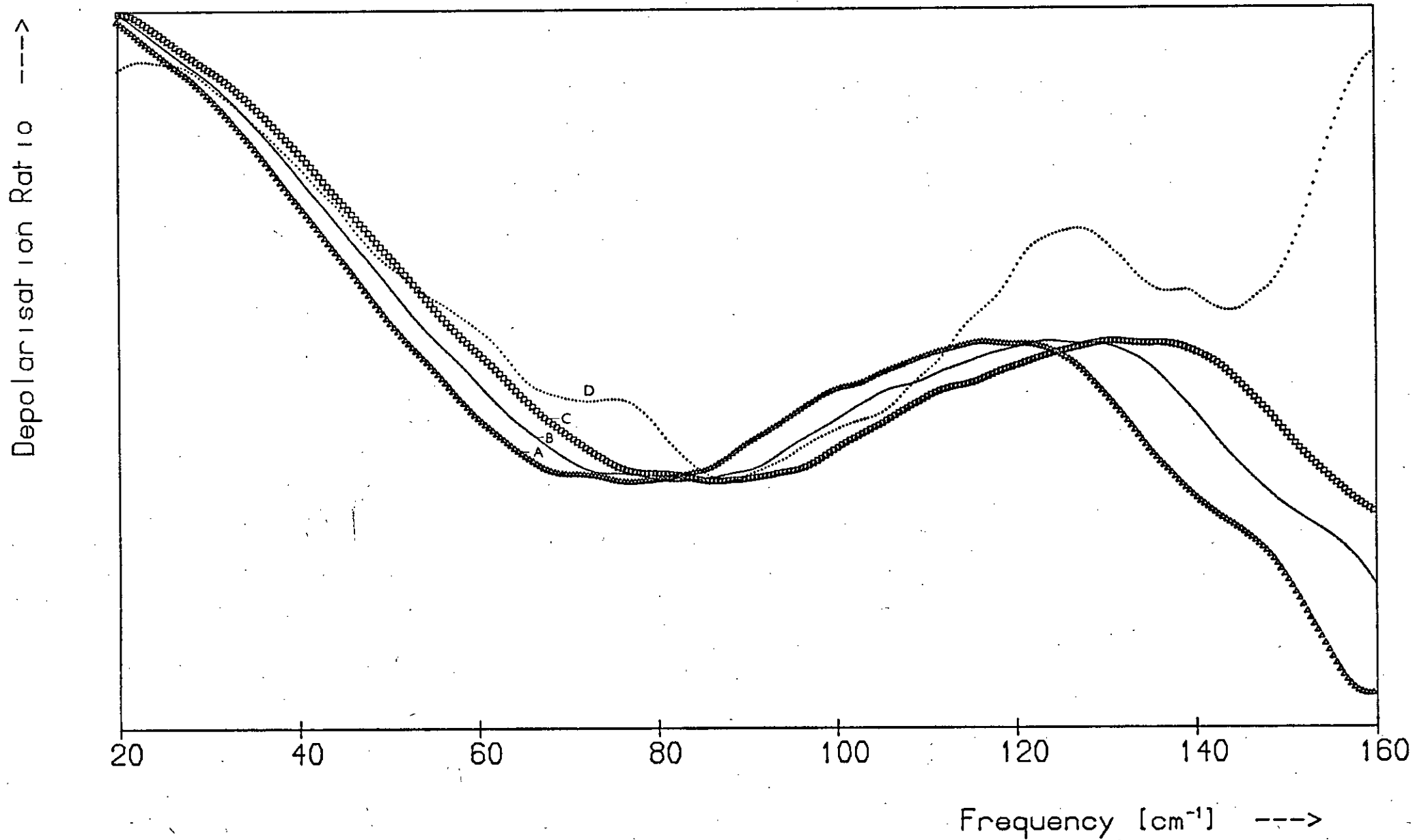
maximum intensity and the peaks A, B and C have been obtained by compressing the a-As_2S_3 spectrum along the frequency axis by factors of 0.71, 0.76 and 0.81 respectively. Curve C is clearly the best fit to the a-As_2Se_3 peak (D). Similar results were obtained for the dips in the depolarisation spectra, as Figure 6.22 shows. The curves are normalised in such a way that the minimum and maximum values of $\rho(w)$ over the range 30 — 110 cm^{-1} are approximately the same for each. Curves A, B and C were obtained by compressing the depolarisation spectrum of a-As_2S_3 along the frequency axis by factors of 0.71, 0.76 and 0.81 respectively. Curve C is in best agreement with the a-As_2Se_3 curve (D).

The fact that the low-frequency regions of the glasses scale by approximately the same factor that relates the rigid-layer modes of the crystals suggests that layer-like regions are still present in the glasses. Other types of experiment[34,40,41] have yielded evidence in support of the existence of layer remnants in these materials.

6.4.6   Discussion

In this section it will be shown that the frequencies, activities and polarisation properties of the vibrations of a-As_2Se_3 can all be accounted for by the molecular model. Originally the vibrational frequencies of a-As_2Se_3 were mainly determined through i.r. measurements: only one vibrational feature — a peak at 227 cm^{-1} — was observed in the first Raman studies. However, by using the weakly absorbed 7993 Å line of a Kr-ion laser as excitation, later investigations, including the present one, have uncovered additional features in the Raman spectrum[21,22].

In the model the frequencies of the AsSe$_3$ pyramid are calculated from Equations A.1 — A.4 (see Appendix I) using the average values of $\mathcal{l}$ and β for crystalline As_2Se_3 and force constants scaled from the AsBr$_3$ molecule (the scaling relation was derived in Section 5.4.5). Lucovsky and

Martin[36] take as ν_1 for the $AsSe_3$ pyramid the frequency of the principal Raman band of $a-As_2Se_3$ and obtain the scale factor, n, by comparing this measured frequency with the observed value of ν_1 for $AsBr_3$. Using the notation of Section 5.4.5 and taking $AsBr_3$ and $AsSe_3$ as molecules I and II respectively, the actual values used are $\nu_1^I = 284$ cm^{-1} [42], $\nu_1^{II} = 227$ cm^{-1} [1,2] and n = 227/284 $\simeq 0.80$. Proceeding as described in Section 5.4.5 one obtains the values 1.05, 0.11, 0.095 and 0:013 md/Å for the force constants k_1^{II}, k_δ^{II}, $k_{1'}^{II}$ and $k_{\delta'}^{II}$ respectively. The $AsSe_3$ pyramid frequencies obtained by solving Equations A.1 — A.4 using the above values for the force constants are given by Lucovsky and Martin and are in reasonable agreement with the observed frequencies.

However, as pointed out in Section 5.4.5, the model frequencies for $a-As_2Se_3$ do not scale with those for $a-As_2S_3$ by the same factor that relates the spectra of the two crystals, and, moreover, the ratio of the calculated bond-stretching force constants differs from the value for k_1^{As-Se}/k_1^{As-S} derived from the crystal scaling relation. It was shown in Section 6.4.5 that the observed spectra of the glasses do obey the crystal scaling relation when their features are paired correctly. The selenide band corresponding to that at 338 cm^{-1} in the $a-As_2S_3$ spectrum occurs at ~245 cm^{-1} rather than 227 cm^{-1}; the 227 cm^{-1} selenide band is the counterpart of the 315 cm^{-1} sulphide band. Hence the most intense peak in each of the unanalysed spectra does not correspond to the same vibration. Taking ν_1 for the $AsSe_3$ pyramid as 245 cm^{-1} instead of 227 cm^{-1} yields n = 245/284 ≈ 0.86 and results in the following values for the frequencies and force constants of the 'molecule':

k_j = 1.25, 0.11, 0.13, 0.015 md/Å for j = 1, 1', δ, δ' respectively

ν_i = 246, 109, 239, 84 cm^{-1} for i = 1, 2, 3, 4 respectively

The geometrical parameters used to derive the above values of the k_j and ν_i were taken from the most recent determination of the structure of

c-As$_2$Se$_3$[43]. The calculations were carried out by computer in exactly the same way as those for the sulphide. The force constants for AsBr$_3$ were taken from the vibrational analysis of Claeys and Van der Kelen[44] and the values of β used were 60.4° [45] and 62° for the AsBr$_3$ and AsSe$_3$ pyramids respectively, the selenide angle being calculated from the average Se—As—Se angle of the crystal.

The new value obtained for k_1^{As-Se} (1.25 md/Å) is ~7$\frac{1}{2}$% smaller than that calculated for k_1^{As-S} from the molecular model (1.35 md/Å); this is in reasonable agreement with the findings of Zallen and Slade[5] who deduce from the crystal scaling relation that the As—Se bond-stretching force constant is 10% softer than that of the As—S bond. Gordy's rule predicts a value of 1.76 md/Å for k_1^{As-Se} but this discrepancy is not significant since the atomic-radius ratio, r_{As}/r_{Se}, is approximately 1.035 for the AsSe$_3$ 'molecule'. (This value of 1.76 md/Å for k_1^{As-Se} is 11% smaller than the value obtained for k_1^{As-S} from Gordy's rule — viz 1.98 md/Å — so although these values are in poor agreement with those calculated from the molecular model, their ratio is consistent with the findings of Zallen and Slade.)

The calculated frequencies, ν_i, are in reasonable agreement with the observed values (see Table 6.3). As in the case of a-As$_2$S$_3$, the two low frequencies are not in such good agreement as the two high frequencies due to the greater solid state interactions they experience[37] (the calculated frequencies 84 cm^{-1} (ν_4) and 109 cm^{-1} (ν_2) are taken to correspond to the observed vibrations at 106 and 136 cm^{-1} respectively since the latter frequencies scale with the observed values of ν_4 and ν_2 for the AsS$_3$ pyramid). Inspection of Figure 6.6 shows that in the case of the two high-frequency modes the model also predicts the correct polarisations, for ν_1 and ν_3 are expected to be polarised and depolarised respectively. The polarisation states of the observed bands at 106 and 136 cm^{-1} are uncertain but they are probably depolarised and polarised

respectively (see Section 6.4.2); if this is correct then the model also accounts for the polarisation properties of these two bands, since ν_4 and ν_2 are expected to be depolarised and polarised respectively.

The frequencies of the As—Se—As bent chain 'molecule' which accounts for the coupled modes are calculated from Equations A.5 — A.7. The bond-stretching force constant, k_1, is identical with that used in the pyramid calculation and Lucovsky and Martin assume that the ratio of k_1 to k_δ, the bond-bending force constant, is 100 : 1 (k_1 and k_δ now refer to Equations A.5 — A.7). The three frequencies obtained by these authors are close to features in the observed spectra.

In the present study the calculation for determining the frequencies, ν_i (i = 1, 2, 3), of the As_2Se 'molecule' was carried out on a computer. Lucovsky and Martin's calculation was repeated, first using their value for k_1 and then the corrected value but in both cases the frequencies reported by them could not be obtained. Varying the interaction constant, k_{12}, did not make it possible to generate the reported frequencies either, but they could be obtained by taking α — which is half the As—Se—As angle — as $104°$ instead of $47.2°$, the value derived from the $c-As_2Se_3$ structure. (Taking $\alpha = 104°$ is equivalent to taking the full value of the As—Se—As angle as $\sim150°$ — see p.137.) The reported frequencies are reproduced exactly when the values 1.26, 0, 0.0126 md/Å and $104°$ are used for k_1, k_{12}, k_δ and α respectively.

Assuming that the ratio of k_1 to k_δ is $\overline{10}$: 1, which is more realistic than the 100 : 1 ratio assumed by Lucovsky and Martin, and taking the corrected value of 1.25 md/Å for k_1, k_δ is 0.125 md/Å. If these force constants are inserted in Equations A.5 — A.7 together with the correct value for α, viz $\sim47°$, the following frequencies result for the simple valence force field case ($k_{12} = 0$): $\nu_1 = 237$, $\nu_2 = 91$ and $\nu_3 = 239$ cm^{-1}. As was found for $a-As_2S_3$, this represents a different arrangement of bands to that obtained by Lucovsky and Martin: their calculation predicts a

very low frequency line (39 cm^{-1}), a line at high frequency (282 cm^{-1}) and one intermediate between these (178 cm^{-1}), whereas the above calculation suggests there is one medium-frequency line (91 cm^{-1}) and two high-frequency lines (238 and 239 cm^{-1}) falling on the main band of the a-As$_2$Se$_3$ spectrum.   In view of the scaling relation that exists between the vibrational frequencies of a-As$_2$Se$_3$ and a-As$_2$S$_3$ the latter arrangement of bands is more acceptable since it matches that for the As$_2$S 'molecule'.   The predicted frequencies fall in the region of the two observed bands that are as yet unaccounted for, viz those at 86 and 275 cm^{-1}.   As will be shown later, several modes due to the stretching of As—As and Se—Se bonds also occur in the main band region and it is possible that the second high-frequency As$_2$Se band is present but unobservable as a result of overlapping — altogether 8 bands are expected to occur between 200 and 285 cm^{-1} (this does not include the bands of elemental Se that occur in this region).   As the existence of the reported i.r. bands at 170 and 45 cm^{-1} is uncertain this distribution of bands is more compatible with the experimental results.

A further objection to the Lucovsky-Martin calculation of the As$_2$Se chain frequencies is that it implies that the 275 cm^{-1} band arises from the antisymmetric mode, ν_3, and is thus depolarised; Figure 6.6 shows, however, that this band corresponds to the minimum in the depolarisation spectrum and is therefore polarised.   The polarised stretching mode, ν_1, occurs at 178 cm^{-1}, according to their calculation, and so is too far away to be associated with the observed band at 275 cm^{-1}.   Because the frequency difference between the observed and predicted value for ν_1 is so large (~100 cm^{-1}), agreement with experiment cannot be obtained by varying the interaction constant, k_{12}, within realistic limits.   In the calculation proposed in the present study, however, ν_1 and ν_3 are virtually degenerate at ~239 cm^{-1} for $k_{12} = 0$.   As k_{12} increases, ν_1 increases while ν_3 decreases and it is found that $\nu_1 > \nu_3$ for all

values of k_{12} greater than ~ 0.01 md/Å.

By applying the 0.71 scale factor to the observed value of ν_3 for the As_2S 'molecule' (367 cm^{-1}) one can deduce that the antisymmetric mode for the selenide chain should occur near 261 cm^{-1} and hence quantitative agreement with experiment cannot be obtained by varying k_{12} since the cross-over frequency, 238 cm^{-1}, is already well below 261 cm^{-1}. As in the case of the sulphide, however, quantitative agreement can be improved by extending the simple valence force field to include a central force between the two non-bonded As atoms. Taking $k_1 = 1.25$ md/Å, $k_\delta = 0.125$ md/Å, $\alpha = 47.2^\circ$ and a_{33}, the central force constant, as 0.07 md/Å the following frequencies were obtained: $\nu_1 = 243$, $\nu_2 = 93$ and $\nu_3 = 239$ cm^{-1}. The value for a_{33} was chosen so that ν_1 scales by a factor of 0.71 with the corresponding calculated frequency (342 cm^{-1}) for the As_2S 'molecule'; it is smaller than that used for the As_2S chain because the As-As separation is larger for the selenide (3.52 Å) than for the sulphide (3.43 Å).

A summary of the preceeding results is given in Tables 6.3 and 6.4.

Including the hidden 245 cm^{-1} band, seven features have been detected in the first-order Raman and depolarisation spectra of a-As_2Se_3 (see Table 6.1). One of these is the boson peak, four arise from vibrations of the $AsSe_3$ pyramid and two are due to the As_2Se links between these pyramids. In contrast to the case for a-As_2S_3 there are no unaccounted-for bands which might be associated with 'wrong' bonds. As will be seen later, As–As and Se–Se bonds are present in the As- and Se-rich glasses respectively; the most intense line due to the former occurs at 220 cm^{-1} and that due to the latter at 265 cm^{-1}. Because these lines fall in the main band region and will be relatively weak for the stoichiometric glass, which is expected to contain only a small number of 'wrong' bonds, they may be unobservable in the a-As_2Se_3 spectrum. Indirect evidence for the presence of 'wrong' bonds in the stoichiometric

Observed values	Parameter	Model value	% Diff. in freqs.
	k_1	1.25	
	$k_{1'}$	0.11	
	k_δ	0.13	
	$k_{\delta'}$	0.015	
62	β	62	
245	ν_1	246	0.4
136	ν_2	109	20
223	ν_3	239	7
106	ν_4	84	21

All frequencies and force constants are in units of cm^{-1} and $md/\mathring{A}$ respectively; β is in degrees.

Table 6.3   The molecular model parameters and frequencies for the $AsSe_3$ 'molecule'.   The last column gives the difference between the observed and calculated frequencies expressed as a percentage of the former.

Observed values	Para-meter	Model value	% Diff. in freqs.	Model value	% Diff. in freqs.	Model value	% Diff. in freqs.	Model value	% Diff. in freqs.
	k_1	1.26		1.25		1.25		1.25	
	k_6	0.0126		0.125		0.125		0.125	
	k_{12}	0		0		0.01		0	
	a_{33}	0		0		0		0.07	
47.2	α	76(104)		47.2		47.2		47.2	
275	ν_1	178	—	238	14	238	14	243	12
86	ν_2	39	—	91	6	91	6	93	8
261*	ν_3	282	—	239	8	238	9	239	8

All frequencies and force constants are in units of cm^{-1} and $md/\overset{o}{A}$ respectively; α is in degrees.

*This value is obtained by multiplying the corresponding a-As_2S_3 frequency (367 cm^- by the scale factor 0.71.

Table 6.4   The molecular model parameters and frequencies for the As_2Se 'molecule'. The differences between the observed and calculated frequencies expressed as a percentage of the former are also given.

glass is provided by the difference spectra obtained for the Se-rich

glasses (see Figure 6.25 after p.226): these spectra suggest that as

the Se content increases, a band at $\sim$205 cm^{-1} disappears and this is

close to the frequency characteristic of the As—As bonds, viz 220 cm^{-1}.

For many chalcogenide glasses it has been shown[46] that bonds between

like atoms do not occur in compositions which are deficient in that

species of atom relative to the stoichiometric composition (this is true

for the As-S glasses). If this is also the case for the As-Se glasses

it is expected that any spectral features arising from As—As bonds would

disappear as the Se content is increased beyond 60 at.%. The presence

of As—As bonds in a-As$_2$Se$_3$ implies the presence of Se—Se bonds also,

assuming that the number of dangling bonds is negligible. Although the

difference spectra for the As-rich glasses do not provide any evidence

for the disappearance of Se—Se bonds this is possibly due to the growth

near 265 cm^{-1} of features associated with c-As$_4$Se$_4$ (see Figure 6.40 after

p.246).

6.5   The selenium-rich glasses

6.5.1   The compositions As$_{40}$Se$_{60}$ — As$_{35}$Se$_{65}$

6.5.1.1 Normalisation

As in the case of the As-S glasses, before the spectral changes

occurring as a function of composition could be interpreted the normal-

isation of the spectra had to be considered. Three methods were

investigated: normalisation by maximum intensity, by area under the

reduced spectra, and by intensity at the peak frequency of the main band

in the spectrum of a-As$_{40}$Se$_{60}$. All three methods lead to spectral changes

that were ordered with respect to composition and the interpretation of

these changes was the same in each case. For the compositions As$_{40}$Se$_{60}$ —

As$_{35}$Se$_{65}$ the first and last methods are virtually equivalent because there

is little shift in the peak frequency of the main band over this composition

range. The first method, however, was found to be unsuitable for the As-rich glasses since an intense line grows near the peak of the main band as the As content is increased beyond 40 at.%. This method was not, therefore, adopted. Of the other two methods, normalisation by intensity at the peak frequency of the main band in the a-$As_{40}Se_{60}$ spectrum is preferable since it shows the spectral changes more clearly. Thus, unless otherwise stated, this is the normalisation procedure used in the present analysis of the As-Se data.

It is clear from Figure 6.24, which shows the reduced spectra of the compositions $As_{40}Se_{60}$ — $As_{35}Se_{65}$ normalised at 231 cm^{-1} and superimposed, that this method is almost equivalent to normalisation by the basewidth of the main band (the procedure used in the case of the As-S data) since the six spectra approximately coincide in the base regions, particularly on the high-frequency side. The figure shows that no spectral changes occur below ~150 cm^{-1} for this composition range and as the spectra are coincident below this frequency the normalisation procedure used is also equivalent to normalisation over the region 0 — 150 cm^{-1}.

6.5.1.2   The polarisation-unanalysed spectra

The polarisation-unanalysed Raman spectra for the six compositions in the range $As_{40}Se_{60}$ — $As_{35}Se_{65}$ are presented in Figure 6.23. The spectra, which have been normalised by intensity at 225 cm^{-1}, are shown displaced above one another. It is seen in the figure that as the Se content increases from 60 at.% a feature grows at 265 cm^{-1} and the peak of the main band shifts slightly. No change occurs below ~150 cm^{-1} in the spectra apart from an increase in the intensity of the boson peak relative to the main band (this increase is not obvious in this figure but is clearly apparent in the difference spectra — see Figure 6.25).

The corresponding reduced spectra, normalised at 231 cm^{-1} and superimposed, are shown in Figure 6.24. The spectra change in an

Figure 6.23

The polarisation-unanalysed Raman spectra of the compositions $As_{40}Se_{60} - As_{35}Se_{65}$.
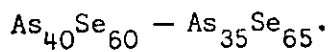
Spectrum		Composition
A	—	$As_{35}Se_{65}$
B	—	$As_{36}Se_{64}$
C	—	$As_{37}Se_{63}$
D	—	$As_{38}Se_{62}$
E	—	$As_{39}Se_{61}$
F	—	$As_{40}Se_{60}$

Figure 6.24

The reduced spectra corresponding to those of Figure 6.23. The spectra are shown superimposed (A — F as above).

Figure 6.25

Difference spectra obtained from the spectra of Figure 6.23 by subtracting the a-$As_{40}Se_{60}$ spectrum from each.

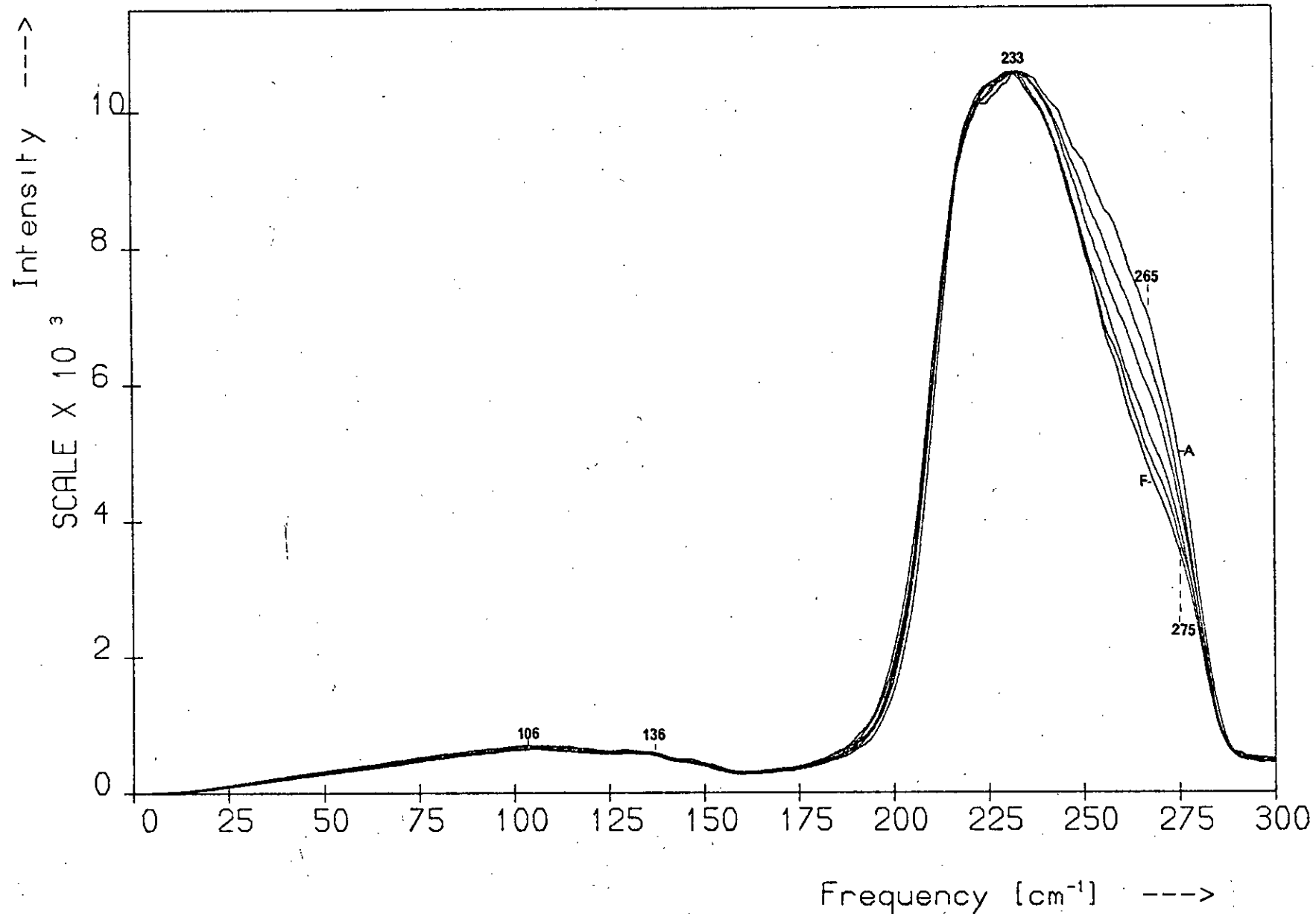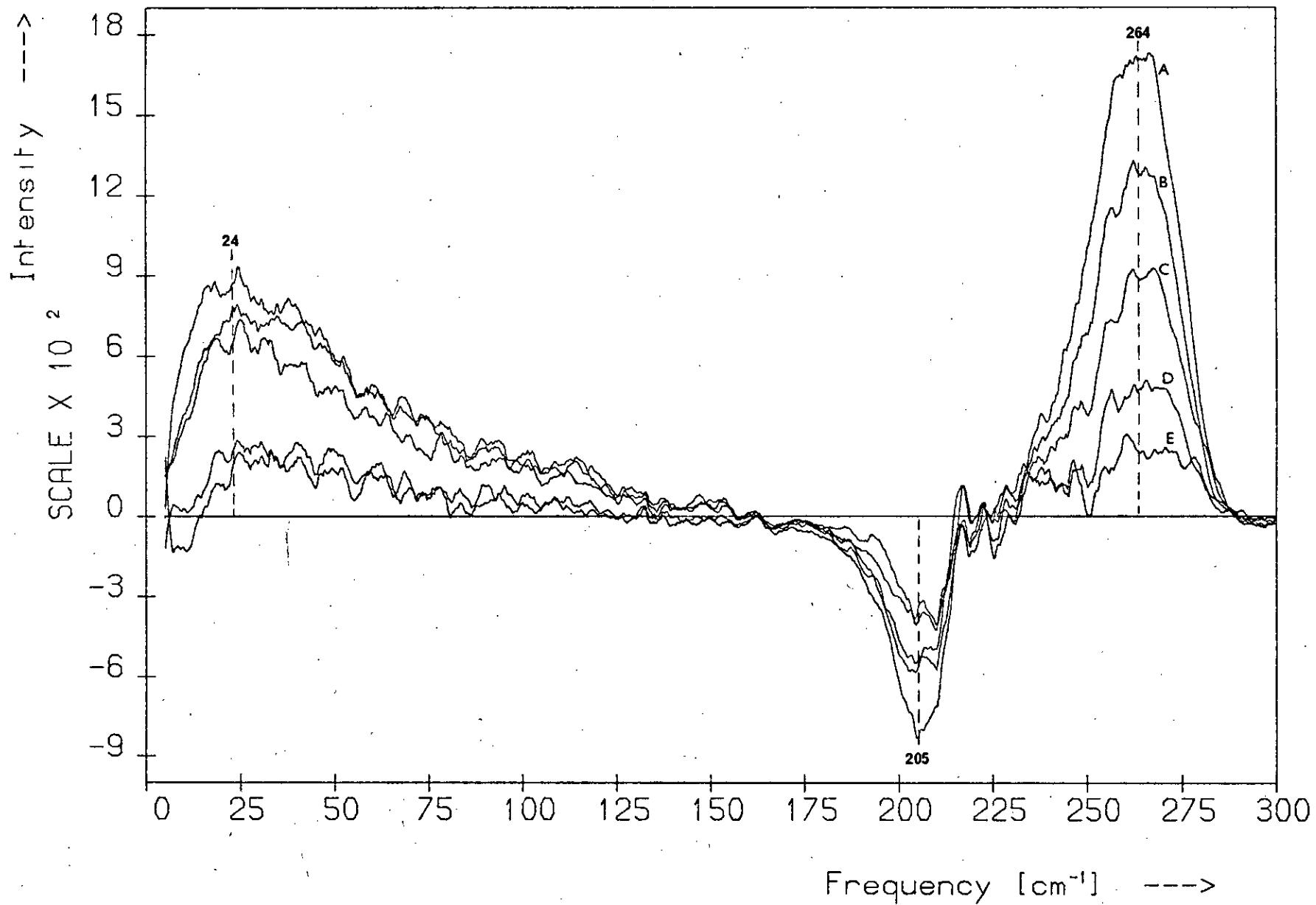| Spectrum		Compositions
A	—	$As_{35}Se_{65} - As_{40}Se_{60}$
B	—	$As_{36}Se_{64} - As_{40}Se_{60}$
C	—	$As_{37}Se_{63} - As_{40}Se_{60}$
D	—	$As_{38}Se_{62} - As_{40}Se_{60}$
E	—	$As_{39}Se_{61} - As_{40}Se_{60}$

Raman Spectra: As$_{35}$Se$_{65}$ — As$_{40}$Se$_{60}$
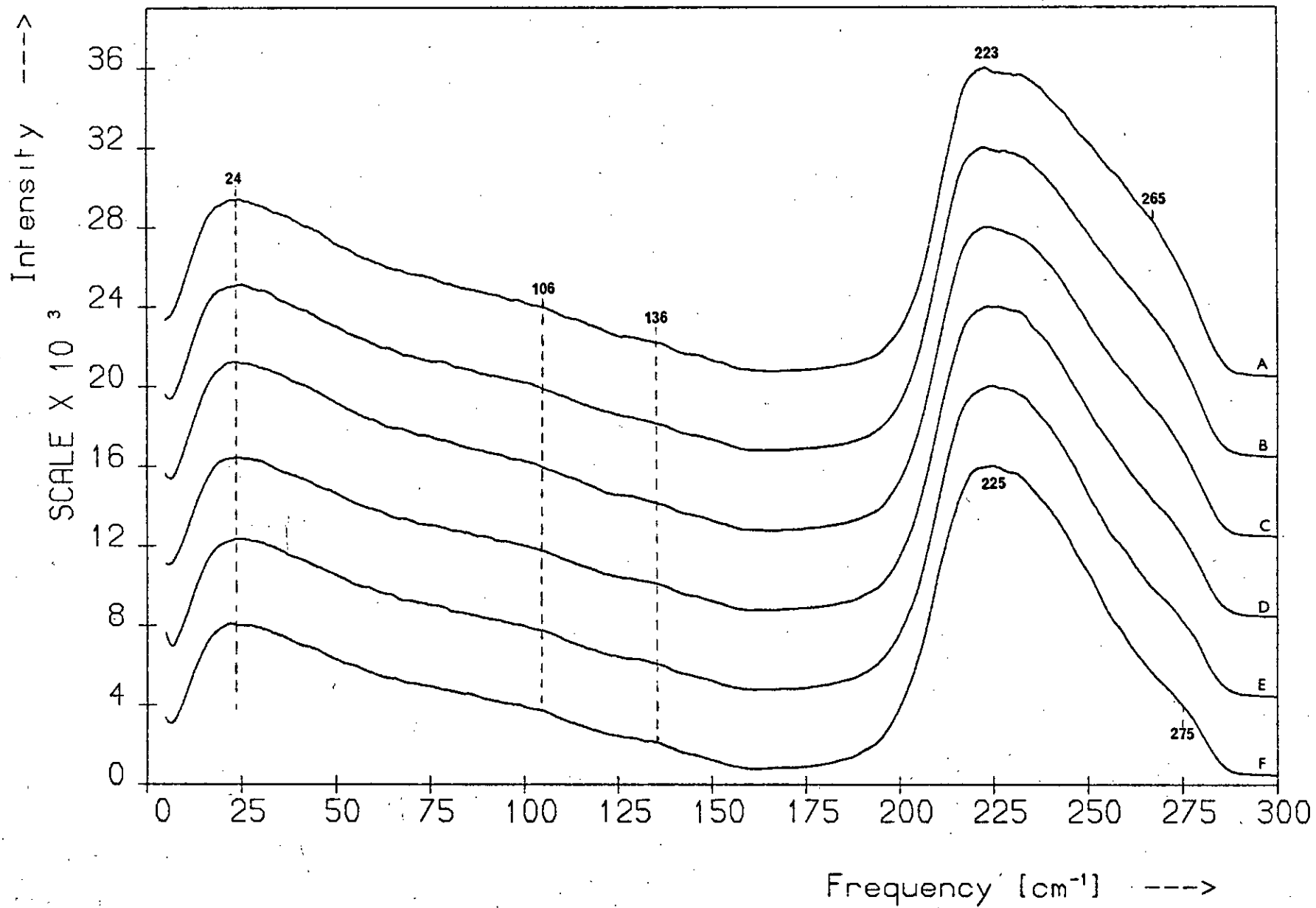
Reduced Raman Spectra: $As_{35}Se_{65}$ – $As_{40}Se_{60}$

Difference Spectra for the Se-Rich Glasses

ordered way as the Se content is increased. Apart from the increasing boson peak, all the spectral changes noted above are exhibited by these spectra. Superimposition of the spectra has made the growth of the 265 cm^{-1} feature obvious and shows clearly the absence of spectral changes in the region below $\sim$150 cm^{-1}.

Figure 6.25 shows the difference spectra derived from the normalised spectra of Figure 6.23 by subtracting the a-$As_{40}Se_{60}$ spectrum from each of the others. Three features develop as the Se content increases: a peak centred at $\sim$264 cm^{-1}, a dip at 205 cm^{-1} and a broad peak at $\sim$24 cm^{-1}. The peak at 264 cm^{-1} corresponds to the growing shoulder in the region of this frequency in the Raman spectra. It is evident from Figure 6.24 that some change occurs down the steep low-frequency side of the main band and it is this change that gives rise to the steadily growing dip at 205 cm^{-1} in the difference spectra. The broad peaks at $\sim$24 cm^{-1} in Figure 6.25 correspond to the boson peak in the Raman spectra and show that it is growing as the Se content increases. No other structure occurs in the difference spectra.

6.5.1.3 Polarisation measurements

The observed HH- and HV-polarised Raman spectra of the compositions $As_{40}Se_{60} - As_{35}Se_{65}$ are shown in Figures 6.26 and 6.27 respectively. In each figure the spectra have been normalised by intensity at the peak frequency of the main band of the appropriate a-$As_{40}Se_{60}$ spectrum and have been displaced above one another. The two sets of spectra do not differ greatly, unlike the corresponding sulphide spectra; the growing shoulder at 265 cm^{-1} is more obvious in the HH spectra, while in the HV spectra the boson peaks are more pronounced and the main bands more sharply peaked. The HH spectra are very similar to the polarisation-unanalysed spectra.

The depolarisation spectra for the above compositions are shown in Figure 6.28; they have been displaced vertically in order of increasing

Figure 6.26

The HH-polarised Raman spectra of the compositions $As_{40}Se_{60} - As_{35}Se_{65}$.

Spectrum		Composition
A	—	$As_{35}Se_{65}$
B	—	$As_{36}Se_{64}$
C	—	$As_{37}Se_{63}$
D	—	$As_{38}Se_{62}$
E	—	$As_{39}Se_{61}$
F	—	$As_{40}Se_{60}$

Figure 6.27

The HV-polarised Raman spectra of the compositions $As_{40}Se_{60} - As_{35}Se_{65}$.
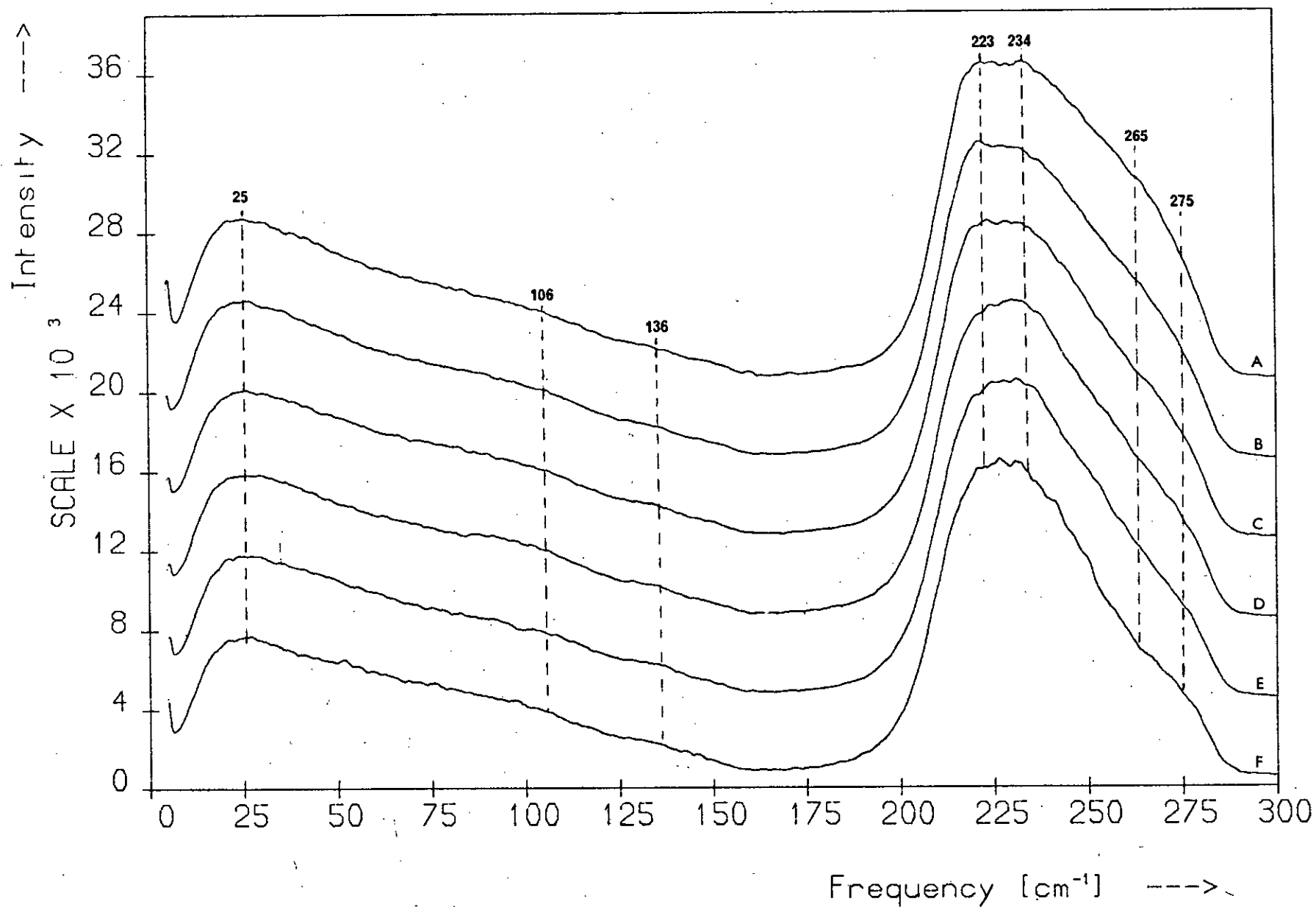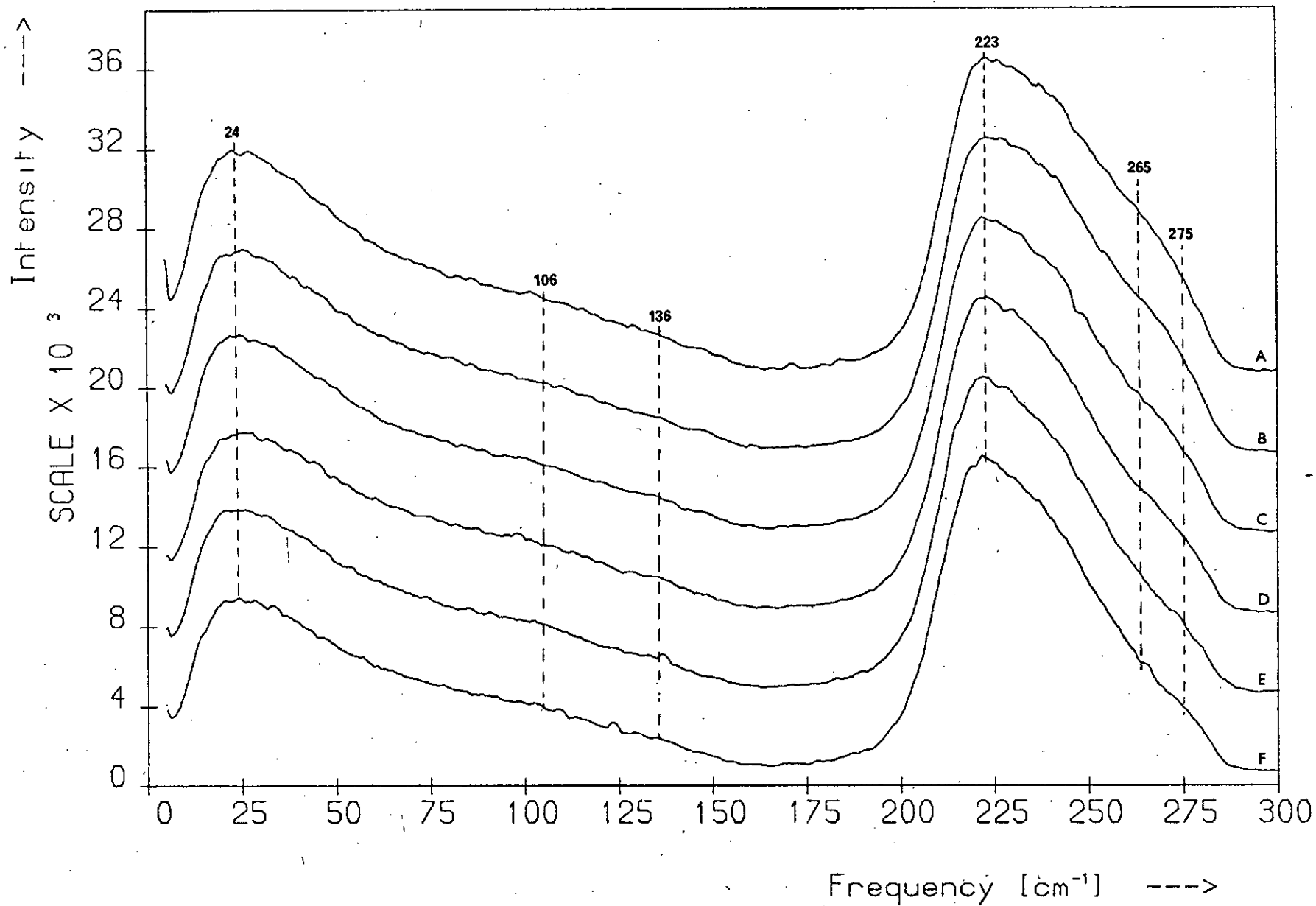A — F as for Figure 6.26.

Figure 6.28

The depolarisation spectra of the compositions $As_{40}Se_{60} - As_{35}Se_{65}$.
A — F as for Figure 6.26.

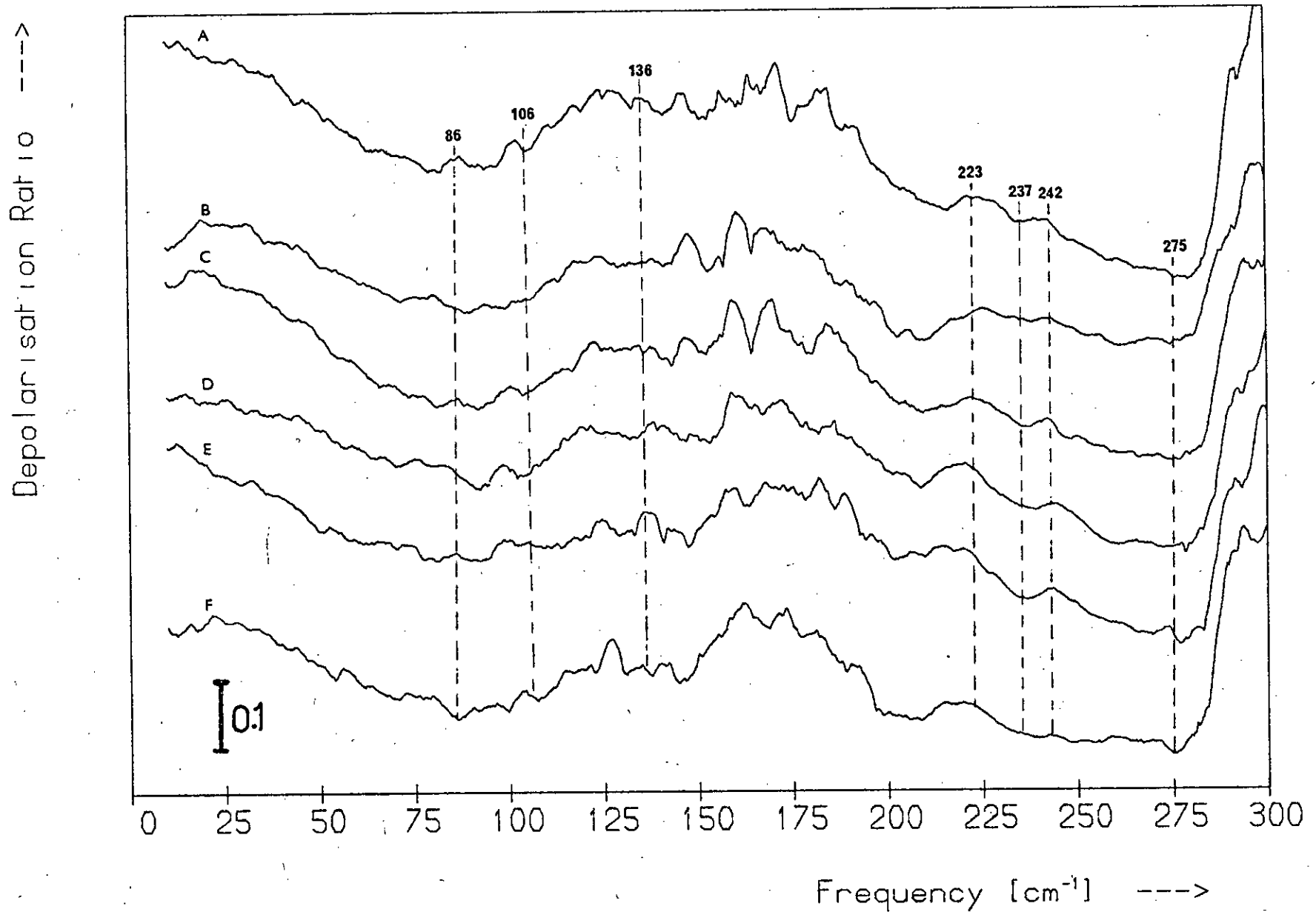HH Polarisation Spectra: $As_{40}Se_{60} - As_{35}Se_{65}$

HV Polarisation Spectra: $As_{40}Se_{60}$ – $As_{35}Se_{65}$

Depolarisation Spectra: $As_{40}Se_{60}$ – $As_{35}Se_{65}$

Se content. All the spectra decrease initially to a minimum around 86 cm^{-1} and have a broad peak or plateau centred at $\sim$136 cm^{-1} and, from $\sim$200 — 290 cm^{-1}, a trough with a sloping bottom (similar features are observed in the depolarisation spectra of the corresponding sulphide compositions — see Figure 5.49). Each trough slopes to a minimum at $\sim$275 cm^{-1} and has two raised regions at $\sim$223 and $\sim$242 cm^{-1} and a dip at $\sim$237 cm^{-1}. Although there is a feature in the Raman spectra at 106 cm^{-1} there is no feature at this frequency in the depolarisation spectra. The raised, noisy section from $\sim$150 — 200 cm^{-1} corresponds to the region of minimum Raman signal.

The depolarisation spectra of the selenides, like those of the As-S glasses, were found to be in poor quantitative agreement with one another. This is probably because the polarised spectra were recorded by back reflection and the samples used were of insufficient optical quality (as the samples were opaque, internal defects were unobservable). However, the depolarisation spectra yield reliable qualitative information.

6.5.1.4 Second-order spectra

For a selection of compositions the spectral region beyond 300 cm^{-1} was examined for any additional features. Weak bands were, indeed, detected above 300 cm^{-1} in these experiments but could all be accounted for as overtones and combinations of first-order bands. It was thus concluded that the one-phonon spectra of these glasses lie entirely below 300 cm^{-1}.

6.5.1.5 Discussion

The four mechanisms that can lead to spectral changes as the Se content is increased beyond 60 at.% are: distortion of the a-$As_{40}Se_{60}$ geometry; the appearance of elemental Se in some form; the disappearance of structural features of a-$As_{40}Se_{60}$; and the formation of new features, such as As—Se—Se—As bridges. These mechanisms were described in more detail for the sulphide glasses (see Section 5.5.1.5).

6.5.1.5.1 <u>Geometrical changes</u>

The results presented in Figures 6.23 — 6.28 show that none of the a-$As_{40}Se_{60}$ vibrations shift significantly in frequency as the Se content is increased from 60 to 65 at.%. Hence it can be concluded that no significant changes in the bond-length and bond-angle distributions of the network occur over this composition range.

6.5.1.5.2 <u>The presence of selenium allotropes</u>

Selenium, like sulphur, exhibits extensive allotropy: the existence of amorphous, trigonal and monoclinic Se is well established[47,48] (two monoclinic forms, α and β, are known to exist) and cubic modifications have been reported[49] but not confirmed. Trigonal Se is composed of infinite unbranched helical chains stacked in parallel, while monoclinic Se is made up of Se_8 ring-molecules, the packing being different in the α and β forms. Amorphous Se is believed to contain both chains and rings[50]. In the cubic modification the Se atoms pack as hard spheres and the bonding is presumably metallic in nature[48]. Only trigonal Se is thermodynamically stable at room temperature and pressure; the other allotropes are meta-stable and eventually revert to the trigonal form.

By comparing the Raman spectra of the various allotropes with the spectra of Figure 6.23 it is possible to determine whether any of them are present in the glasses to any significant extent. Since there is no evidence of phase separation in these materials and their optical properties are those of a homogeneous system[51], any regions of elemental Se that do form as the Se content increases cannot be large in size. The Raman spectra of trigonal, α-monoclinic and amorphous Se have been recorded by several workers (see Section 6.3); the spectrum of β-monoclinic Se should be similar to that of the α form since the Se_8 molecules that make up both allotropes are identical. Cubic Se is not expected to exhibit a first-order Raman spectrum[52].

None of the allotropes have first-order Raman or i.r. bands beyond ~255 cm^{-1} and their Raman spectra all contain an intense band in the region 230 — 255 cm^{-1}. Thus, assuming that the allotrope spectra are not significantly affected by the environment in the As-Se glasses, it can be concluded that the presence of elemental Se in some form cannot account for the emerging band at 265 cm^{-1} in the glass spectra and, moreover, no elemental Se is formed in appreciable quantities as the Se content is increased from 60 to 65 at.%, for there is no evidence in the glass spectra of any band growing in the range 230 — 255 cm^{-1}. It is possible, however, that the elemental Se component of the glass spectra is undetectable due to its comparative weakness and the fact that the principal Se lines fall on the main As-Se band. In the case of the corresponding sulphide glasses the S_8 band detected at 472 cm^{-1} in the Raman spectra occurs in a region where the scattering due to other structural features is weak and even in the $As_{35}S_{65}$ spectrum the intensity of this band is only ~$1/_{20}$th that of the main peak at 338 cm^{-1}. Thus elemental Se may be present in an amount comparable with the level of S_8 present in the sulphide glasses; whether it occurs as rings or chains cannot be determined, though in the glasses with Se content >70 at.% both species may be present (see Section 6.5.2).

6.5.1.5.3 Disappearing features

Much of the discussion in Section 5.5.1.5.3 concerning disappearing features is also applicable in the case of the selenide glasses. The dip developing at 205 cm^{-1} in the difference spectra of Figure 6.25 results from changes occurring on the low-frequency side of the main band and suggests that there are As—As bonds in the network and that these are disappearing as the Se content increases, for, as will be shown in Section 6.6.1.3, such bonds give rise to a vibration near this frequency. The disappearance of As—As bonds was also observed for the corresponding sulphide glasses and is consistent with the chemically ordered network

model, which has been shown to be applicable to many amorphous chalcogenides[46]. As in the case of the sulphide glasses, there is no indication of any increase in the ratio of pyramids to single-chalcogen bridges over this composition range; this is probably due to the fact that two of the bands of the As_2Se 'molecule' fall near the growing 265 cm^{-1} feature while the third (that at 86 cm^{-1}) is weak and diffuse. A small increase in the above ratio is expected since, as will be shown below, some of the As_2Se links are being replaced by As_2Se_2 chains.

6.5.1.5.4 The appearance of new features — the As—Se—Se—As bridge

The spectra of the compositions $As_{40}Se_{60}$ — $As_{35}Se_{65}$ show no indication of the presence of As-Se monomers or regions of elemental As, which is as expected since the increase in Se content is unlikely to lead to a break-up of the a-$As_{40}Se_{60}$ network[53]. Any new structural feature appearing (excluding Se species, which were discussed earlier) must therefore be part of the network, and since, as was shown in the previous section, the number of As—As bonds is decreasing, these new features must be due to the incorporation of the extra Se atoms between the As atoms. Because selenium, like sulphur, is divalent, forming only rings and unbranched chains, the Se atoms between the As atoms must form a chain. Hence the new features are simply As—Se_n—As ($n > 1$) bridges.

Only one new band (that at 265 cm^{-1}) is observed to emerge in the spectra as the Se content is increased from 60 to 65 at.%, which suggests that, as for the sulphide case, one type of bridge 'molecule' preponderates. The value of n for the dominant species is most likely to be 2. Other workers[34,54] have also suggested that some of the additional Se atoms in the Se-rich glasses go into the formation of As—Se—Se—As links in the network.

As n increases, the vibrations of the As_2Se_n chain will be less

influenced by the terminal As atoms and will increasingly approximate to those of Se_n chains. If the equations for determining the vibrational frequencies of the X_2Y and X_2Y_2 chain molecules are solved for the case $X = Y$ using the principal force constants and geometrical parameters of trigonal Se it can be shown that the frequencies of 3- and 4-membered Se chains are essentially those of trigonal Se. Hence the vibrational frequencies of the $As-Se_n-As$ chains for $n > 2$ can be taken to be those of trigonal Se. Although the most intense line of trigonal Se has not been detected in the spectra of these compositions this may be due to the fact that it coincides with the main As-Se band (see Section 6.5.2.3), so As_2Se_n bridges with $n > 2$ may be present, but not in appreciable quantities. The presence of longer chains is perhaps more likely in the selenide case than the sulphide since the stable allotrope of the former is made up of chains while that of the latter is formed from 8-membered rings.

On applying the molecular model analysis described in Section 5.5.1.5.4 to the As-Se-Se-As link it was found that, as for the sulphide case, a linear 'molecule' did not yield a satisfactory value for ν_2, the symmetric-stretch frequency of the chalcogen-chalcogen bond, unless an exceptionally large interaction constant or an exceptionally small value of the Se-Se bond-stretching force constant, k_{Se-Se}, was used. k_{Se-Se} is usually in the range $1.85 - 2.10$ md/Å and the interaction constant is expected to be less than one tenth of k_{Se-Se}. Table 6.5, which gives the computer-calculated value of ν_2 for various sets of potential constants, shows that taking $k_{Se-Se} = 1.9$ md/Å, $k_{As-Se} = 1.25$ md/Å (the value derived from the molecular model analysis of $a-As_{40}Se_{60}$ — see Section 6.4.6) and $k_{int} = 0$ (i.e. only a simple valence force field is being considered) yields a value of 342 cm^{-1} for ν_2. However, the only unassigned spectral feature is the emerging shoulder at 265 cm^{-1} and no first-order bands are observed beyond 290 cm^{-1} so the calculated value is in error by at least 29%. It was found that ν_2 could be made less than 290 cm^{-1} only by

k_{Se-Se}	k_{As-Se}	k_{int}	ν_2
1.90	1.25	0	342
1.90	1.25	0.45	267
0.65	1.25	0	268
1.50	1.25	0.30	265
1.90	0	0	286

All frequencies and force constants are in units of cm^{-1} and $md/\mathring{A}$ respectively.

Table 6.5   The symmetric Se-Se bond-stretching frequency, ν_2, of the linear As_2Se_2 'molecule' for various values of the force constants affecting it.

using an unrealistic value for k_{Se-Se} or k_{int}.

The characteristic range of stretching frequencies for the Se—Se bond is $\sim 230 - 360$ cm^{-1}. Lucovsky et al.[12] have shown that the vibrational frequencies of the S_8 ring scale with those of the Se_8 ring by a factor of ~ 1.9. Applying this factor to the observed symmetric-stretch frequency of the S—S bond in the As_2S_2 'molecule' (viz 492 cm^{-1}) one obtains a value of 259 cm^{-1} for the corresponding vibration of the As_2Se_2 link. This value is close to 265 cm^{-1}, the frequency of the emerging shoulder in the selenide spectra. The force field calculations show that for both linear and non-linear, non-planar As_2Se_2 'molecules' three modes have frequencies in the region of the main As-Se band; two of these modes arise from the symmetric stretching of As—Se and Se—Se bonds and should yield polarised lines, while the third arises from the antisymmetric stretching of As—Se bonds and should give rise to a depolarised line. It is clear from Figure 6.32 (after p.236) that the emerging feature at 265 cm^{-1} is polarised and so must be due to one of the symmetric stretching modes. Since no new bands are observed to emerge above 265 cm^{-1} and since the calculations show that the stretching frequency of the As—Se bond is always less than that of the Se—Se bond for all reasonable values of the geometrical and force-field parameters, the observed band at 265 cm^{-1} can be assigned to the Se—Se bond-stretching mode of the As_2Se_2 link.

The shoulder at 265 cm^{-1} is, in fact, the only feature of the Se-rich spectra that can be attributed to the As_2Se_2 link with any confidence. This is in contrast to the sulphide case since five As_2S_2 frequencies were located. The small dip and peak at 237 and 242 cm^{-1} respectively in the depolarisation spectra of the Se-rich glasses (see Figure 6.28) may correspond to the two other high-frequency As_2Se_2 modes, but this is uncertain since, as will be shown in Section 6.5.2, Se allotropes may also be causing features near these frequencies in the depolarisation

spectra. The results of Section 6.5.2 also indicate the presence of a weak band at ~150 cm^{-1} but this may similarly be due to Se allotropes.

The calculation for determining the six vibrational frequencies of the non-linear, non-planar X_2Y_2 molecule was described in Section 5.5.1.5.4. When this calculation was performed for the As_2Se_2 'molecule' it was found that ν_1, the frequency of the mode involving the symmetric stretching of the Y—Y bond, was in the region of 265 cm^{-1} for all reasonable values of the various parameters (these were specified in Section 5.5.1.5.4). As in the case of the As_2S_2 bent chain, only k_D, $k_{D\alpha}$ and α significantly influence ν_1. k_D is expected to be close to its value in other molecules with Se—Se bonds, i.e. ~1.9 md/$\overset{o}{A}$, and for the simple valence force field approximation $k_{D\alpha} = 0$, so only α can be varied to bring ν_1 closer to 265 cm^{-1}. ν_1 decreases as α is increased from 0° but reaches a minimum at $\alpha \approx 93^\circ$ and then starts to increase with increasing α (this behaviour is similar to that observed for the As_2S_2 'molecule'). For all reasonable values of the various parameters $\nu_1 > 265$ cm^{-1}, so taking $\alpha = 93^\circ$ gives the value of ν_1 closest to 265 cm^{-1}. On setting $\alpha = 93^\circ$ and taking for the other parameters the values given in column 2 of Table 6.7, the minimum value of ν_1 was found to be 294 cm^{-1}, which is ~11% greater than the observed value of 265 cm^{-1}. ν_1 remains within 14% of 265 cm^{-1} for all values of α between 75° and 110°, which covers the range of values for α observed in other compounds with Se—Se bonds (see Table 6.6). Hence the bent As_2Se_2 chain, unlike the linear one, can account for the emerging 265 cm^{-1} band.

The six frequencies were found to be insensitive to the dihedral angle, ϕ. Using the parameter values given in column 1 of Table 6.7 it was found that varying ϕ over the range 90 $\pm$ 25° had no effect on ν_1 and did not alter any other frequency by more than 7% of its value for $\phi = 90^\circ$.

Molecule	Se—Se bond length ($\overset{o}{A}$)	Bond angle (degrees)	Dihedral angle (degrees)
Se_2Cl_2[55]	2.32	106	84
Se_2Br_2[55]	2.32	106	84
Se_8[48]	2.336	105.7	101.0
Se_n[48]	2.373	103.1	103.1

Table 6.6   Geometrical parameters of Se_8, Se_n and two X_2Y_2 molecules

containing Se—Se bonds.

Observed freqs. & polns.	Para-meter	Value 1	% Diff. in freqs.	Value 2	% Diff. in freqs.	Value 3	% Diff. in freqs.	Value 4	% Diff. in freqs.
	k_D	2.0	-----	1.9		1.9		1.9	
	k_d	1.25		1.25		1.25		1.25	
	k_α	0.2		0.2		0.2		0.25	
	k_ϕ	0.1		0.1		0.1		0.14	
	$k_{D\alpha}$	0		0		0.15		0.15	
	α	90		106		106		106	
	ϕ	90		84		84		84	
265 p	ν_1	302	14	299	13	286	8	287	8
237? p	ν_2	240	1	237	0	225	5	231	3
152? p	ν_3	118	22	133	13	136	11	155	2
—	ν_4	73	—	75	—	76	—	87	—
242? dp	ν_5	241	0.4	243	0.4	243	0.4	246	2
148? dp	ν_6	122	18	134	9	134	9	148	0

p - polarised; dp - depolarised.
All frequencies and force constants are in units of cm^{-1} and md/Å respectively; α and ϕ are in degrees.

Table 6.7   Parameter values and frequencies of the As_2Se_2 'molecule' of C_2

symmetry.   The differences between the observed and calculated

frequencies expressed as a percentage of the former are also given.

Because only one of the six X_2Y_2 frequencies has been located with certainty for the selenides the evidence for the presence of such a 'molecule' is less conclusive than in the case of the sulphides and little can be deduced about its force constants and geometry. Excluding the ~150 cm^{-1} band which is observed in the spectra of the very Se-rich glasses, there is no sign at all of the As_2Se_2 bending modes; over the composition range $As_{40}Se_{60}$ — $As_{35}Se_{65}$ there is no obvious change in the spectra between 50 and 175 cm^{-1}, the range in which these modes are expected to occur. It should be noted, however, that the bending modes in a-$As_{40}Se_{60}$ are extremely weak.

Table 6.7 shows the calculated frequencies of the As_2Se_2 'molecule' for various sets of parameter values. In each case the bond-bending force constants are about one tenth of the bond-stretching force constants and all interaction constants, apart from $k_{D\alpha}$, have been taken as zero. The values of $106°$ and $84°$ for α and ϕ respectively are averages of the compound values (see Table 6.6). From columns 3 and 4 of Table 6.7 it is seen that the value of $k_{D\alpha}$ needed to give good agreement with experiment for ν_1 is the same as the value of $k_{D\alpha}$ used for the As_2S_2 'molecule'. For each set of parameters, ν_2, ν_3, ν_5 and ν_6 are close to features in the observed Raman and depolarisation spectra but as remarked earlier these features may be due to Se allotropes.

Although the polarisation of the 265 cm^{-1} feature cannot be deduced from the depolarisation spectra of these compositions the results for the glasses with Se content >65 at.% show that this band is polarised. The absence of structure at 265 cm^{-1} in the depolarisation spectra of the compositions $As_{40}Se_{60}$ — $As_{35}Se_{65}$ is probably due to the overlapping of bands. Table 6.7 shows that the polarisations of the observed bands at 148, 152, 237 and 242 cm^{-1} are consistent with these bands being attributed to the As_2Se_2 chain. However, the polarisations of the bands at 148 and 242 cm^{-1} also match the polarisations of the Se allotrope bands near these

frequencies and the dip at 237 cm^{-1} in the depolarisation spectra of the compositions $As_{40}Se_{60}$ — $As_{35}Se_{65}$ does not necessarily indicate the presence of a vibration at this frequency.

In conclusion, the accommodation of the additional Se atoms in the As-Se network is the only one of the four processes that satisfactorily accounts for the growth of the 265 cm^{-1} band as the Se content is increased. The results indicate that the extra Se atoms go mainly into the formation of As—Se—Se—As bridges and these are non-linear. This behaviour parallels that found in the corresponding sulphide glasses.

6.5.2 The compositions $As_{35}Se_{65}$ — $As_{25}Se_{75}$

6.5.2.1 The polarisation-unanalysed spectra

Figure 6.29 shows the polarisation-unanalysed Raman spectra of the compositions $As_{30}Se_{70}$ and $As_{25}Se_{75}$. For comparison the corresponding spectra of the $As_{40}Se_{60}$ and $As_{35}Se_{65}$ glasses are also shown. The spectra, which have been displaced above one another, are normalised to intensity at 225 cm^{-1}.

Several spectral changes occur as the Se content is increased beyond 65 at.%, the most obvious being the growth of an intense broad peak at 253 cm^{-1}. The boson peak has also grown considerably, as it did in the case of the sulphide glasses with S content > 65 at.%, and a weak feature centred at ~150 cm^{-1} has appeared. Possibly as a result of the growth of the boson peak, the weak feature at 106 cm^{-1} in the a-$As_{40}Se_{60}$ spectrum disappears gradually and is not detectable in the $As_{25}Se_{75}$ spectrum. The boson peak is the only feature of the a-$As_{40}Se_{60}$ spectrum that shifts in frequency as the Se content increases, but the shift is only small. The two weak features between ~160 and 190 cm^{-1} in the $As_{30}Se_{70}$ and $As_{25}Se_{75}$ spectra are plasma lines.

Figure 6.29

The polarisation-unanalysed Raman spectra of the compositions in the

range $As_{40}Se_{60} - As_{25}Se_{75}$.

Spectrum		Composition
A	—	$As_{25}Se_{75}$
B	—	$As_{30}Se_{70}$
C	—	$As_{35}Se_{65}$
D	—	$As_{40}Se_{60}$

Figure 6.30

The HH-polarised Raman spectra of the compositions in the range

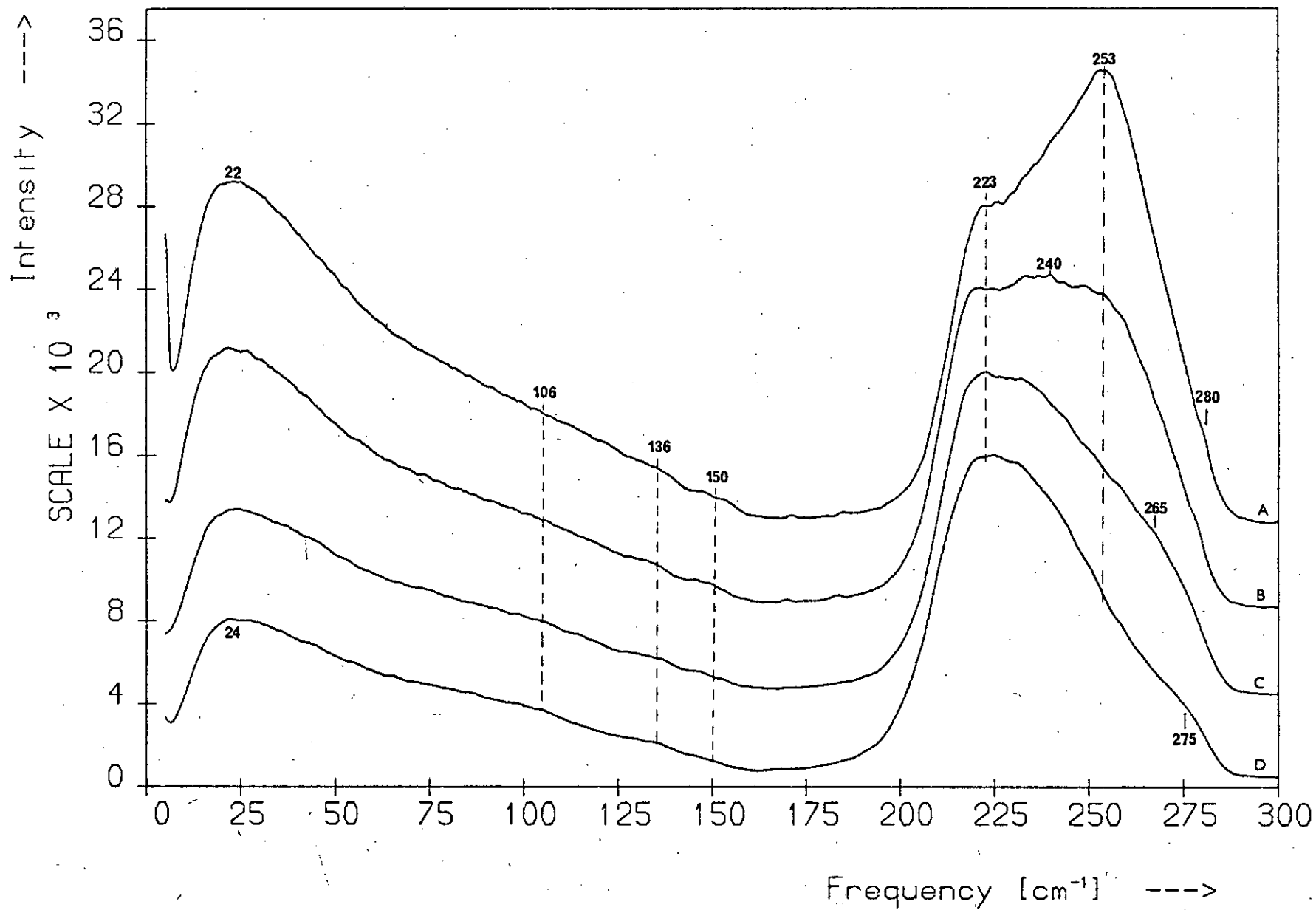$As_{40}Se_{60} - As_{25}Se_{75}$. A — D as for Figure 6.29.

Figure 6.31

The HV-polarised Raman spectra of the compositions in the range
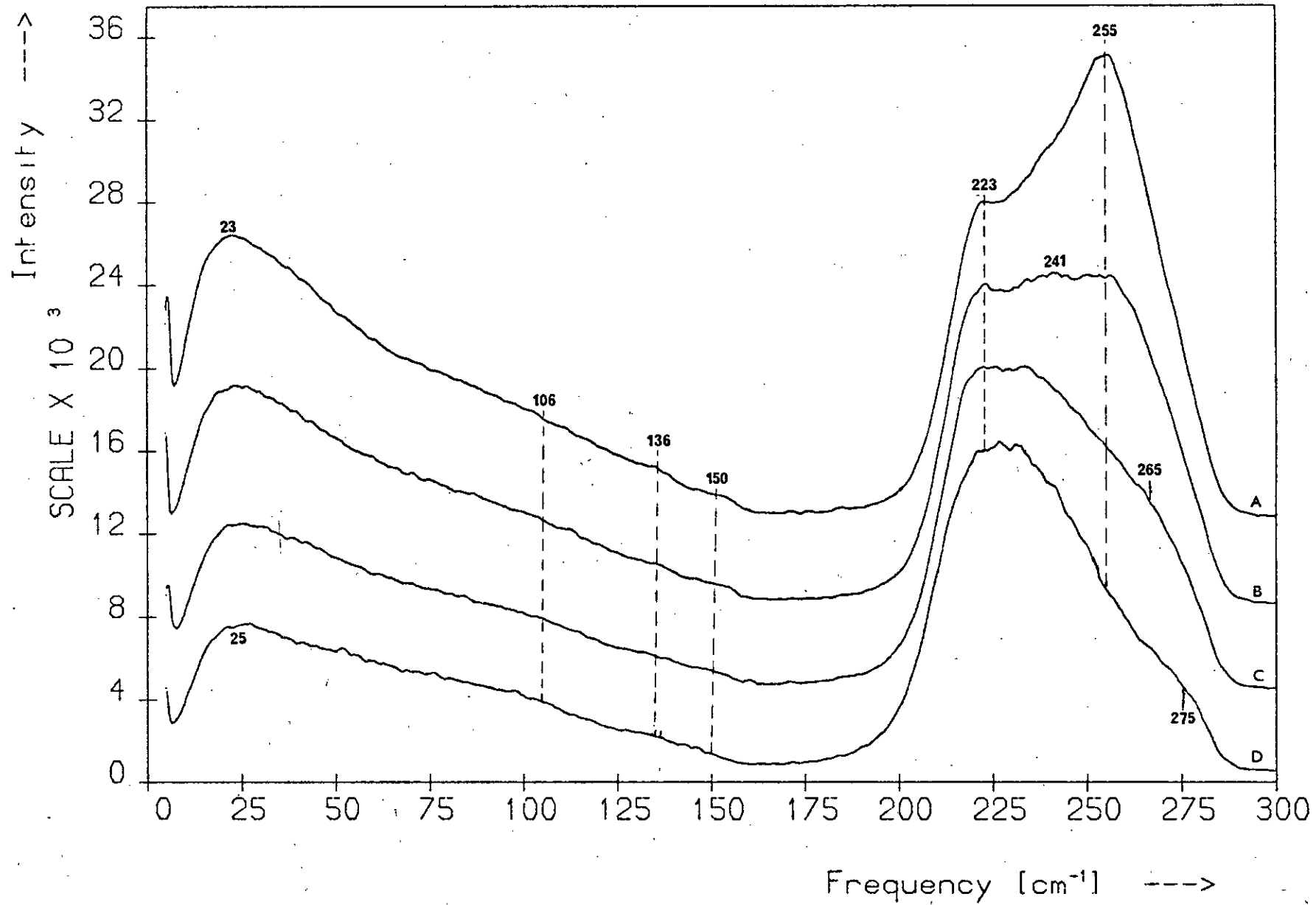
$As_{40}Se_{60} - As_{25}Se_{75}$. A — D as for Figure 6.29.

Figure 6.32

The depolarisation spectra of compositions in the range $As_{40}Se_{60} - As_{25}Se_{75}$.

A — D as for Figure 6.29.

Raman Spectra: As₄₀Se₆₀ – As₂₅Se₇₅
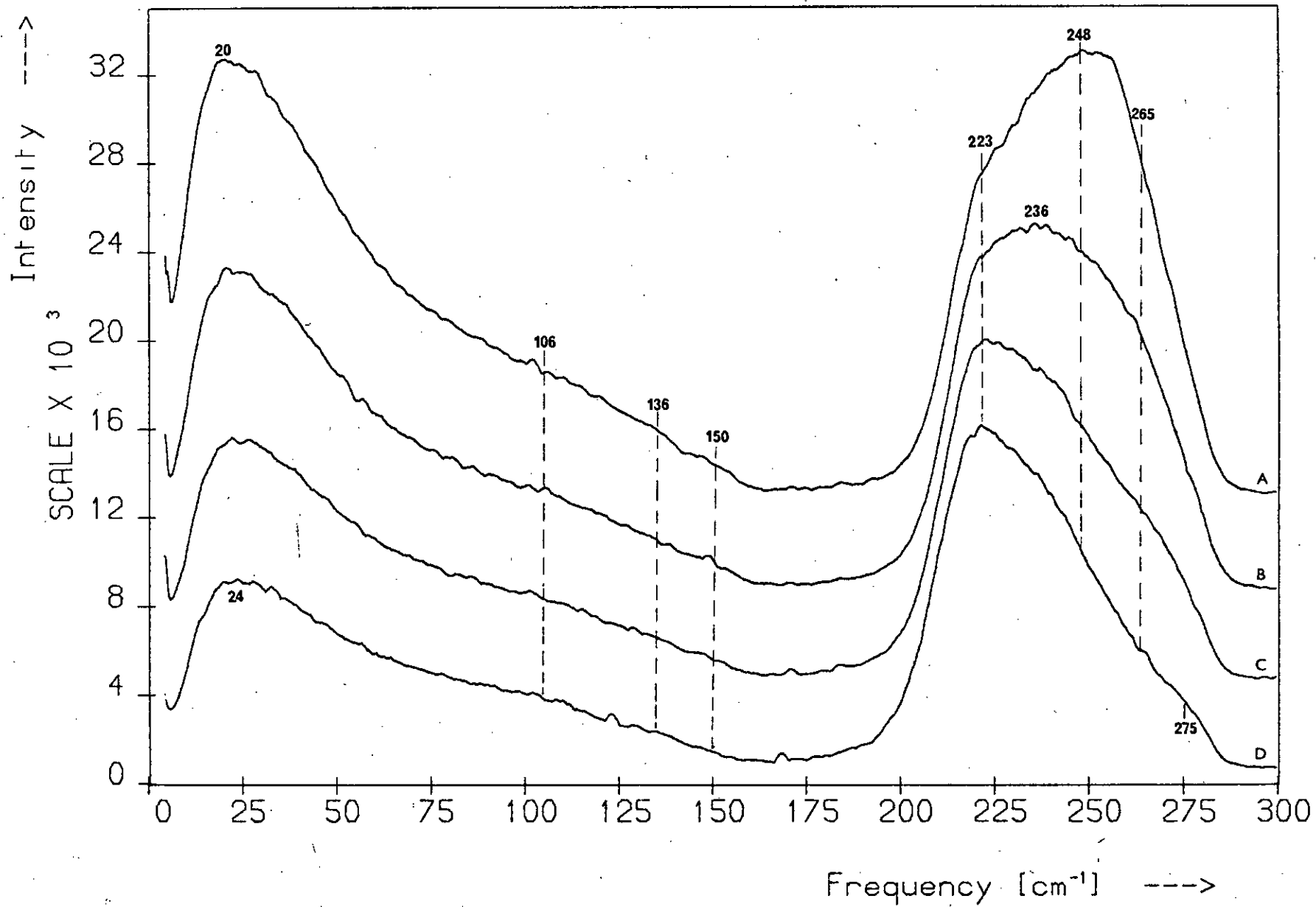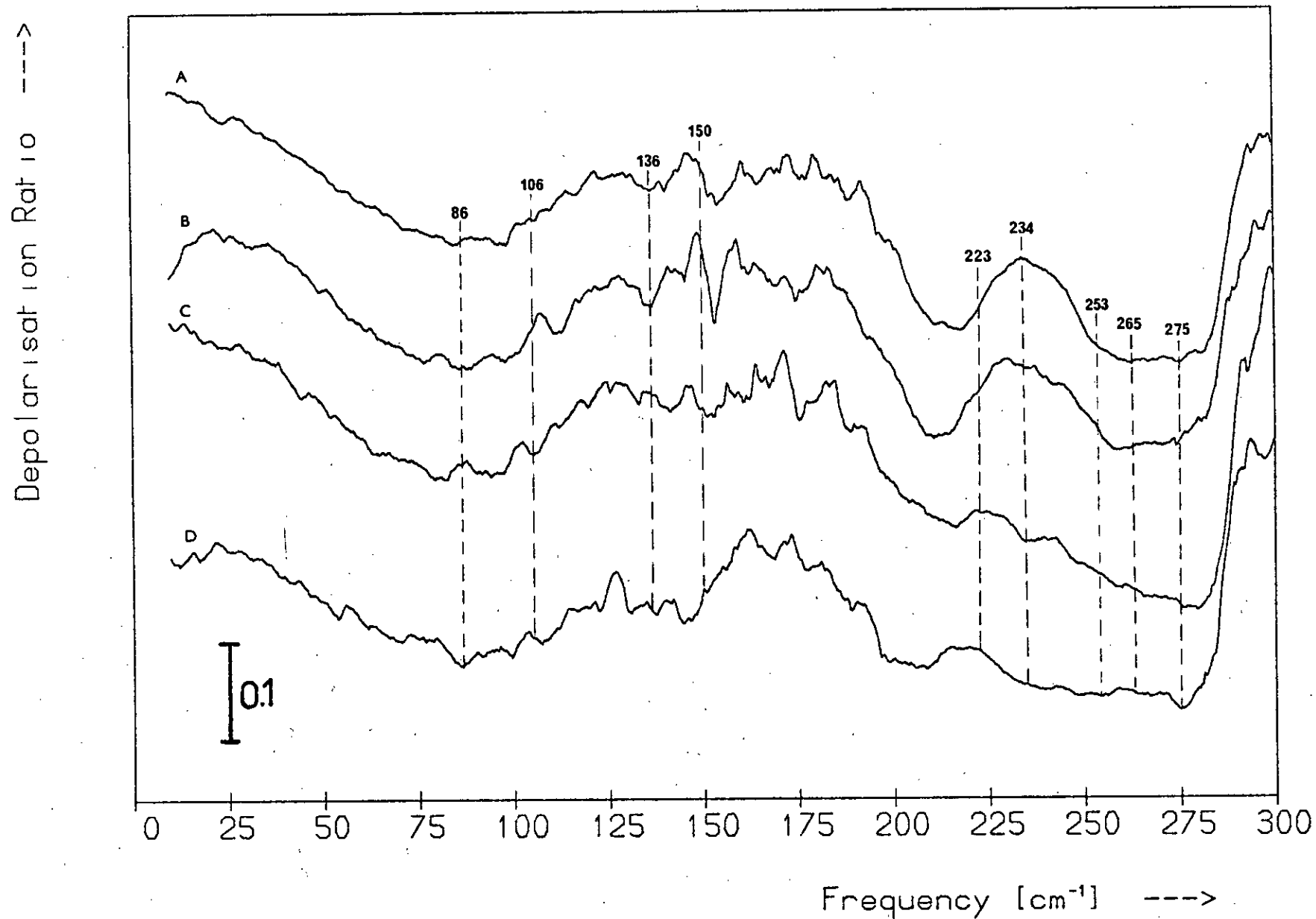
HH Polarised Spectra: $As_{40}Se_{60}$ – $As_{25}Se_{75}$

HV Polarised Spectra: $As_{40}Se_{60}$ – $As_{25}Se_{75}$

Depolarisation Spectra: $As_{40}Se_{60} - As_{25}Se_{75}$

6.5.2.2 Polarisation measurements

The HH- and HV-polarised spectra of the compositions $As_{30}Se_{70}$ and $As_{25}Se_{75}$ are shown along with the corresponding spectra of the $As_{40}Se_{60}$ and $As_{35}Se_{65}$ glasses in Figures 6.30 and 6.31 respectively. The HH and HV spectra are normalised by intensity at 227 and 223 cm^{-1} respectively and are shown vertically displaced. The spectral changes occurring as the Se content increases beyond 65 at.% are similar for both sets of spectra and consist of the growth of the boson peak, an intense band near 250 cm^{-1} and a weak feature centred at ~150 cm^{-1}. The HH spectra of the compositions $As_{30}Se_{70}$ and $As_{25}Se_{75}$ are similar to their polarisation-unanalysed counterparts, although the boson and main band peaks are shifted to slightly higher frequencies in the former. There are, however, several differences between the HH and HV spectra of these glasses. In the HV spectra the main bands are more rounded, having no pronounced feature at 223 cm^{-1}, and peak at slightly lower frequencies; also, the boson peaks are more pronounced and comparable in intensity with the main bands.

The depolarisation spectra for the above four compositions are shown in Figure 6.32. The three Se-rich spectra are basically similar in shape, particularly below ~200 cm^{-1}; the only significant spectral change is the growth of a large, broad peak at ~234 cm^{-1} with a shoulder at ~242 cm^{-1}. In the $As_{30}Se_{70}$ and $As_{25}Se_{75}$ spectra there is no sign of any feature at 106 cm^{-1} nor, surprisingly, of one at 253 cm^{-1}, the frequency of the intense emerging Raman band. None of the features shifts in frequency as the Se content increases.

6.5.2.3 Discussion

The most striking spectral change occuring over the composition range $As_{40}Se_{60}$ — $As_{25}Se_{75}$ is the growth of a broad, intense line centred at ~253 cm^{-1}. This band is not apparent in the spectra of the glasses with less than 65 at.% Se but has overtaken the 265 cm^{-1} band when the Se

content has reached 70 at.%. Similar results were reported by Ward and co-workers[1,2].

The most intense high-frequency band in the first-order Raman spectrum of α-monoclinic Se occurs at 254 cm^{-1} (see Figure 6.3) and is polarised. Figure 6.32 shows that the 253 cm^{-1} band in the spectra of the compositions $As_{30}Se_{70}$ and $As_{25}Se_{75}$ is also polarised so that the presence of Se_8 rings in these glasses could account for this spectral feature. Such behaviour was exhibited by the S-rich sulphide glasses, with the additional S atoms initially being mainly incorporated in the network but at S concentrations greater than $\sim$70 at.%, going predominantly into the formation of S_8 rings. However, Se_n chains in an environment that prevents interchain interactions also have a polarised band near 253 cm^{-1} [19]. There is no evidence for the presence of trigonal Se itself in these compositions (this crystal has an intense band near 234 cm^{-1}) but Se_n chains may be contributing to the intensity of the 253 cm^{-1} band. Nevertheless, the characteristics of the 253 cm^{-1} band are, as will be shown below, similar to those of the S_8 band in the sulphide glasses and so it seems likely that this growing peak mainly arises from the presence of Se_8 rings in the glasses.

The 253 cm^{-1} band in the spectra of Figure 6.29 is too broad to be attributed to α-monoclinic Se itself and were this crystal present one would expect to observe its most intense band (which occurs at 114 cm^{-1}) in the glass spectra. The 253 cm^{-1} band in the As-Se spectra must therefore be due either to the presence of a-Se (which is believed to contain both Se_8 rings and Se_n chains) or randomly arranged Se_8 rings only. Although a-Se does have an intense, broad, polarised band at 250 cm^{-1} there is no sign of its other Raman bands at 80, 112, 138 and 235 cm^{-1}; these should be observable in view of the intensity of the 253 cm^{-1} band in the $As_{30}Se_{70}$ and $As_{25}Se_{75}$ spectra. There is a pronounced peak at $\sim$234 cm^{-1} in the depolarisation spectra of these two

glasses but this cannot be attributed to a-Se since the 235 cm^{-1} band of a-Se is polarised[15] and should give rise to a dip in $\rho(w)$. It seems unlikely, therefore, that a-Se is present in these glasses in significant quantities. The growth of the 253 cm^{-1} band in the As-Se glasses can thus be attributed to the formation of Se_8 rings (ignoring any contribution from Se_n chains); these rings are randomly positioned relative to one another.

The 253 cm^{-1} feature of the As-Se spectra is much broader than the 254 cm^{-1} band of α-monoclinic Se and has a depolarised wing on the low-frequency side extending to ~225 cm^{-1}. The latter band corresponds to the 472 cm^{-1} band of α-S_8, for both arise from the same vibrational mode of the 8-membered ring and their frequencies are related by the scale factor determined by Lucovsky et al.[12] (viz ~1.9). The 472 cm^{-1} band of the As-S glasses arises from the presence of S_8 rings and it, too, is broader than its crystal counterpart and has a wing on the low-frequency side (this wing may be depolarised, though the evidence is inconclusive — see Section 5.5.2.3). The broadness of the 472 cm^{-1} band in the As-S spectra was attributed to the random positioning of the rings in the glasses while the wing was thought to be due to disorder-induced distortion of the rings themselves. It seems that the Se_8 rings in the As-Se glasses are also randomly positioned and distorted. The depolarised wing which gives rise to the peak at ~234 cm^{-1} in $\rho(w)$ will be due to the appearance of depolarised Raman-forbidden Se_8 fundamentals as a result of the distortion of the ring structure. These fundamentals will correspond to the S_8 vibrations at ~471 and 411 cm^{-1} and thus should occur at ~248 and 216 cm^{-1}, applying the frequency scale factor of 1.9.

In Section 5.5.2.1 it was remarked that the 472 cm^{-1} band in the liquid sulphur spectrum and in the spectra of the As-S glasses is much more intense relative to the other S_8 lines than it is in α-S_8. It has been suggested that this enhancement of the 472 cm^{-1} band of liquid sulphur is due to

the contribution of nearby Raman-forbidden bands that appear as a result of thermally-induced distortion of the rings[20]. A similar effect seems to be occurring in a-Se and the As-Se glasses: for the latter the Raman intensity is considerably greater at 253 cm^{-1} than at 114 cm^{-1} — even allowing for the As-Se network contribution — whereas in α-monoclinic Se the 254 and 114 cm^{-1} bands are of comparable intensity (it is assumed that Se_n chain modes are not contributing to the intensity of the 253 cm^{-1} band in the glasses). If the 253 cm^{-1} band of the Se_8 rings in the As-Se glasses _is_ enhanced relative to the other Se_8 bands it might account for the fact that these other Se_8 bands are not observed in the spectra of the As-Se glasses.

The presence of the characteristic a-$As_{40}Se_{60}$ spectral features at 86, 106, 136, 223 and 275 cm^{-1} in the Raman and depolarisation spectra of the Se-rich glasses of Figures 6.29 — 6.32 suggests that the $AsSe_3$ and As_2Se units of the a-$As_{40}Se_{60}$ structure are retained as the Se content is increased from 60 to 75 at.%. Since none of these characteristic spectral features of a-$As_{40}Se_{60}$ shifts in frequency it can also be concluded that there is no change in the geometry of these units. (The 275 cm^{-1} band is probably responsible for the knee at ~280 cm^{-1} in the $As_{30}Se_{70}$ and $As_{25}Se_{75}$ spectra of Figure 6.29 — the depolarisation spectra show that the band does not actually shift in frequency.) Similarly, the AsS_3 and As_2S units of the a-$As_{40}S_{60}$ glass are retained unchanged in the very S-rich sulphide glasses. The low-frequency dip in the depolarisation spectra of the sulphide glasses does, however, shift to higher frequencies as the S content increases (see Figure 5.60); this is thought to be a consequence of the increase in the intensity of the depolarised boson peak. In the case of the Se-rich selenide glasses the change in the boson peak is less marked.

Although there is no sign of structure at 265 cm^{-1} in the Raman spectra of the compositions $As_{30}Se_{70}$ and $As_{25}Se_{75}$, the region of low depolarisation

ratio around this frequency in $\rho(w)$ suggests that As_2Se_2 units are also still present in the network. (The fact that 265 cm^{-1} corresponds to a minimum in $\rho(w)$ indicates that the band at this frequency is polarised.) In the case of the S-rich sulphide glasses, As—S—S—As links were found to be present up to S concentrations of 95 at.%.

In addition to the intense 253 cm^{-1} band, a much weaker feature at ~150 cm^{-1} also emerges in the spectra of the As-Se glasses as the Se content increases beyond 65 at.%. In some of the spectra the feature appears to be a doublet. The depolarisation spectra also suggest a doublet structure, one component being polarised and the other depolarised. The 150 cm^{-1} feature does not grow at the same rate as the 253 cm^{-1} band and thus cannot be associated with Se_8 rings, the structural feature mainly responsible for this band.

No Se_8 bands occur near 150 cm^{-1} but there is a weak band at 142 cm^{-1} in the Raman spectrum of trigonal Se so this structure may be due to the presence of free Se_n chains in the glasses. Alternatively, the 150 cm^{-1} doublet may be associated with Se—Se bonds in the network: 150 cm^{-1} is close to the values calculated for the ν_3 and ν_6 bending modes of the As_2Se_2 'molecule' (see columns 3 and 4 of Table 6.7). The 150 cm^{-1} band also seems to be present in the spectra of the $As_{35}Se_{65}$ glass (in which the As_2Se_2 bridges preponderate over Se molecules) and its slow growth compared to that of the 253 cm^{-1} band would be due to the fact that at Se concentrations above ~65 at.% the additional Se atoms go mainly into the formation of Se_8 rings rather than Se—Se bonds in the network.

In conclusion, although there was no indication of Se_8 rings in the compositions $As_{40}Se_{60}$ — $As_{35}Se_{65}$ they are definitely present in the glasses with Se content above 70 at.%. In these very Se-rich glasses Se_8 ring production predominates over the formation of Se—Se bonds in the network, though such bonds are still present. The rings are randomly positioned and distorted, as were the S_8 rings in the S-rich sulphide glasses. Se_n

chains may also be present, though in small amounts, and the AsSe$_3$ and As$_2$Se units of the stoichiometric glass are retained unchanged.   These findings for the glasses with Se content greater than 65 at.% are essentially identical with those deduced for the corresponding sulphides.

6.6   The arsenic-rich glasses

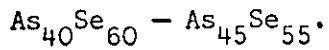### 6.6.1   The compositions As$_{40}$Se$_{60}$ — As$_{45}$Se$_{55}$

6.6.1.1   The polarisation-unanalysed spectra

The polarisation-unanalysed Raman spectra of the compositions As$_{40}$Se$_{60}$ — As$_{45}$Se$_{55}$ are shown in Figure 6.33.   The spectra are normalised to intensity at 225 cm^{-1} and are shown displaced above one another. Several spectral changes occur as the As content is increased above 40 at.%, the most obvious being the growth of an intense peak at 220 cm^{-1}. A very weak band grows at 156 cm^{-1} and the boson peak shifts to lower frequencies, as it did in the case of the corresponding sulphide glasses. Figure 6.34 is an enlargement of the 130 — 180 cm^{-1} sections of the spectra. The sections have been superimposed and the figure shows the emerging 156 cm^{-1} band clearly.   The weak 106 cm^{-1} band of the a-As$_{40}$Se$_{60}$ spectrum also appears to shift slightly as the As content increases.   A knee at 275 cm^{-1} and a weak feature at 136 cm^{-1} are present in all the spectra. Although c-As$_4$Se$_4$ exists there is no sign of sharp structure similar to that observed for the As-rich sulphide glasses.

The corresponding reduced spectra, normalised to intensity at 231 cm^{-1} and superimposed, are shown in Figure 6.35.   The spectra change in an ordered way as the As content is increased.   The emergence of the weak band at 156 cm^{-1} is obvious in this figure, as is the fact that this feature and the emerging high-frequency peak (which is shifted to 221 cm^{-1} by the reduction process) grow in an ordered way with increasing As content. Below 140 cm^{-1} the spectral changes are less obvious: the boson peak is

Figure 6.33

The polarisation-unanalysed Raman spectra of the compositions
$As_{40}Se_{60} - As_{45}Se_{55}$.

Spectrum		Composition
A	—	$As_{45}Se_{55}$
B	—	$As_{44}Se_{56}$
C	—	$As_{43}Se_{57}$
D	—	$As_{42}Se_{58}$
E	—	$As_{41}Se_{59}$
F	—	$As_{40}Se_{60}$

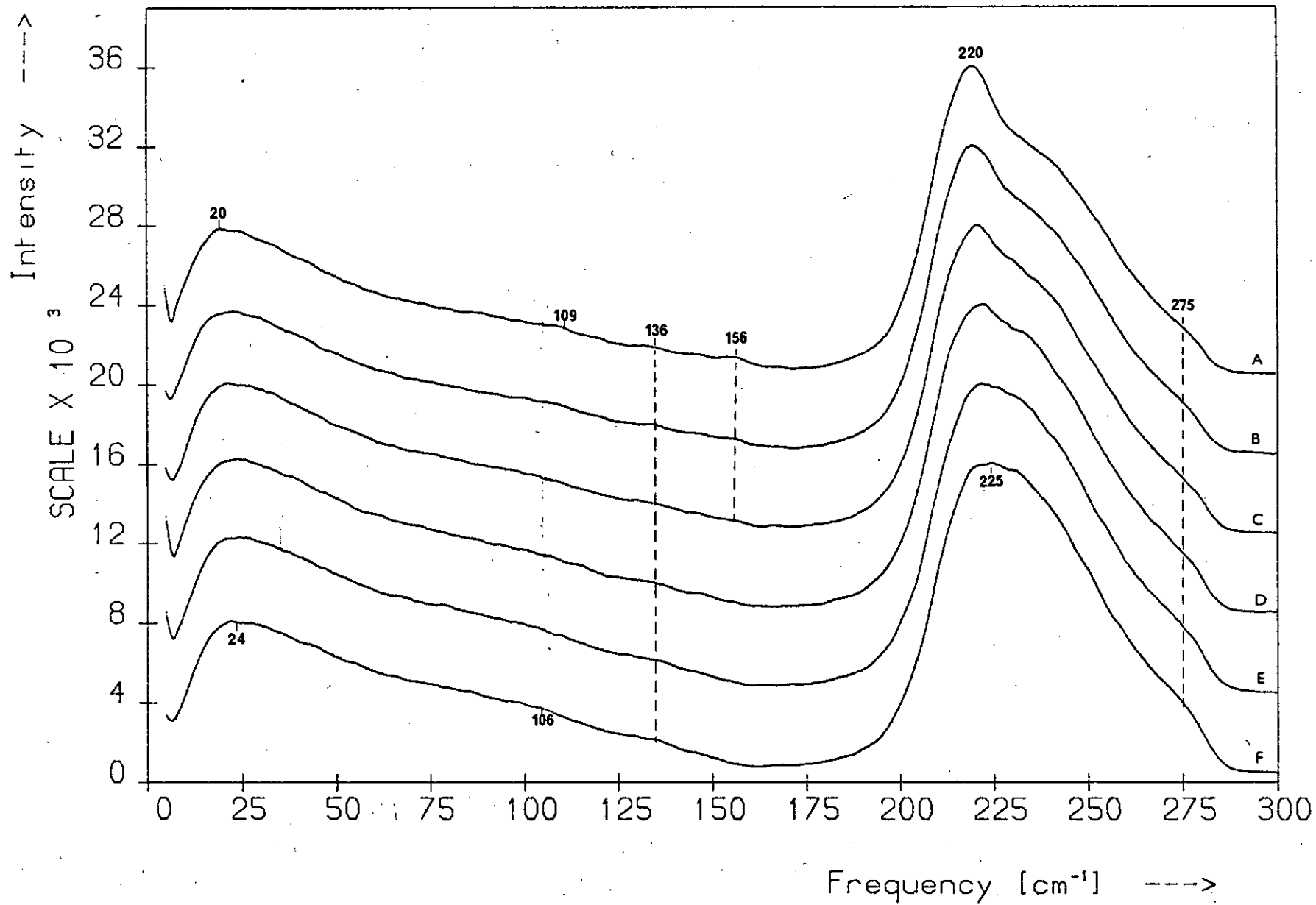## Figure 6.34

An enlargement of the $130 - 180$ cm^{-1} sections of the spectra of the
compositions $As_{40}Se_{60} - As_{45}Se_{55}$. The sections have been superimposed.
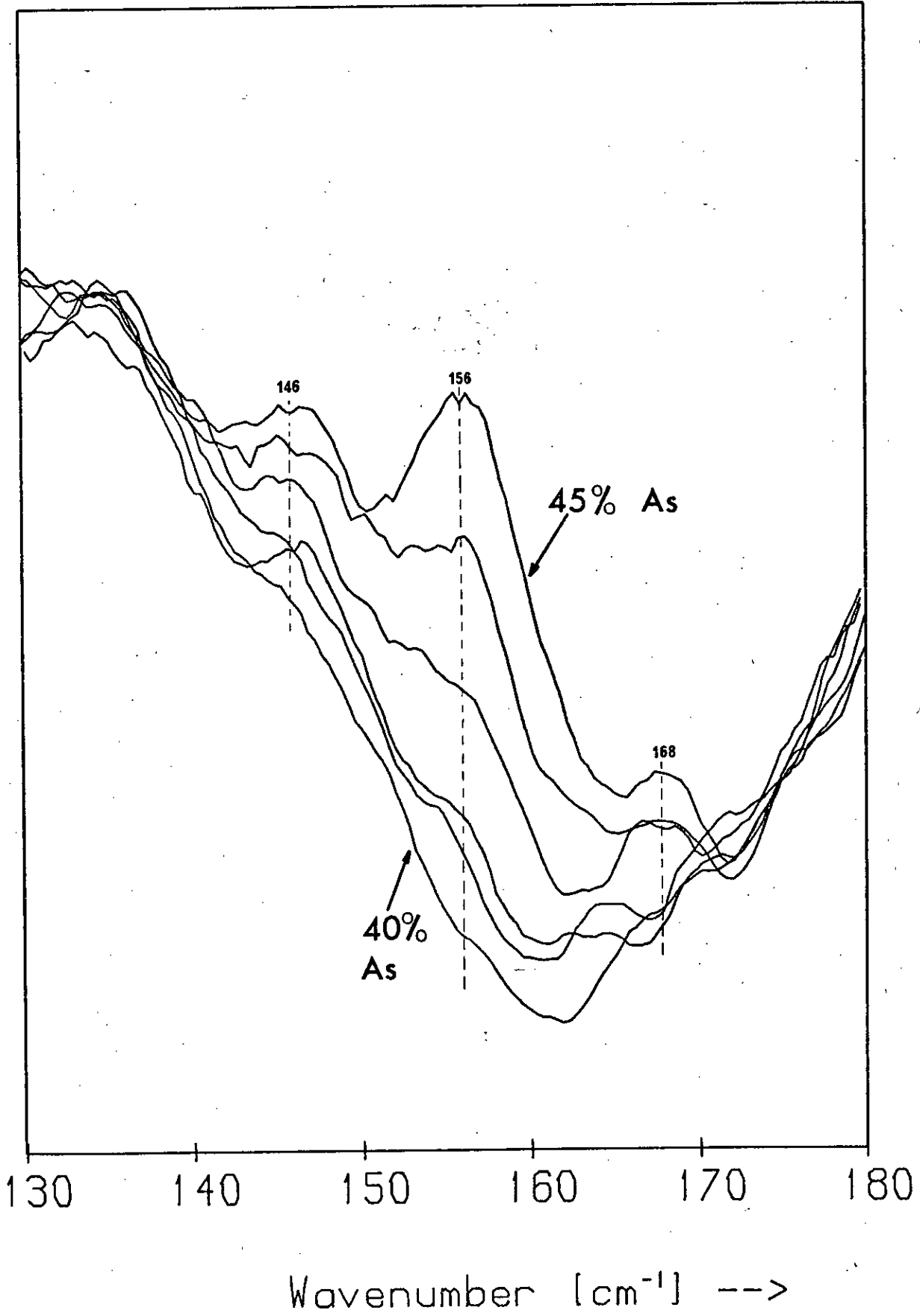(Courtesy of Dr. M.J.Sik.)

Figure 6.35

The reduced spectra corresponding to those of Figure 6.33. The spectra
are shown superimposed.
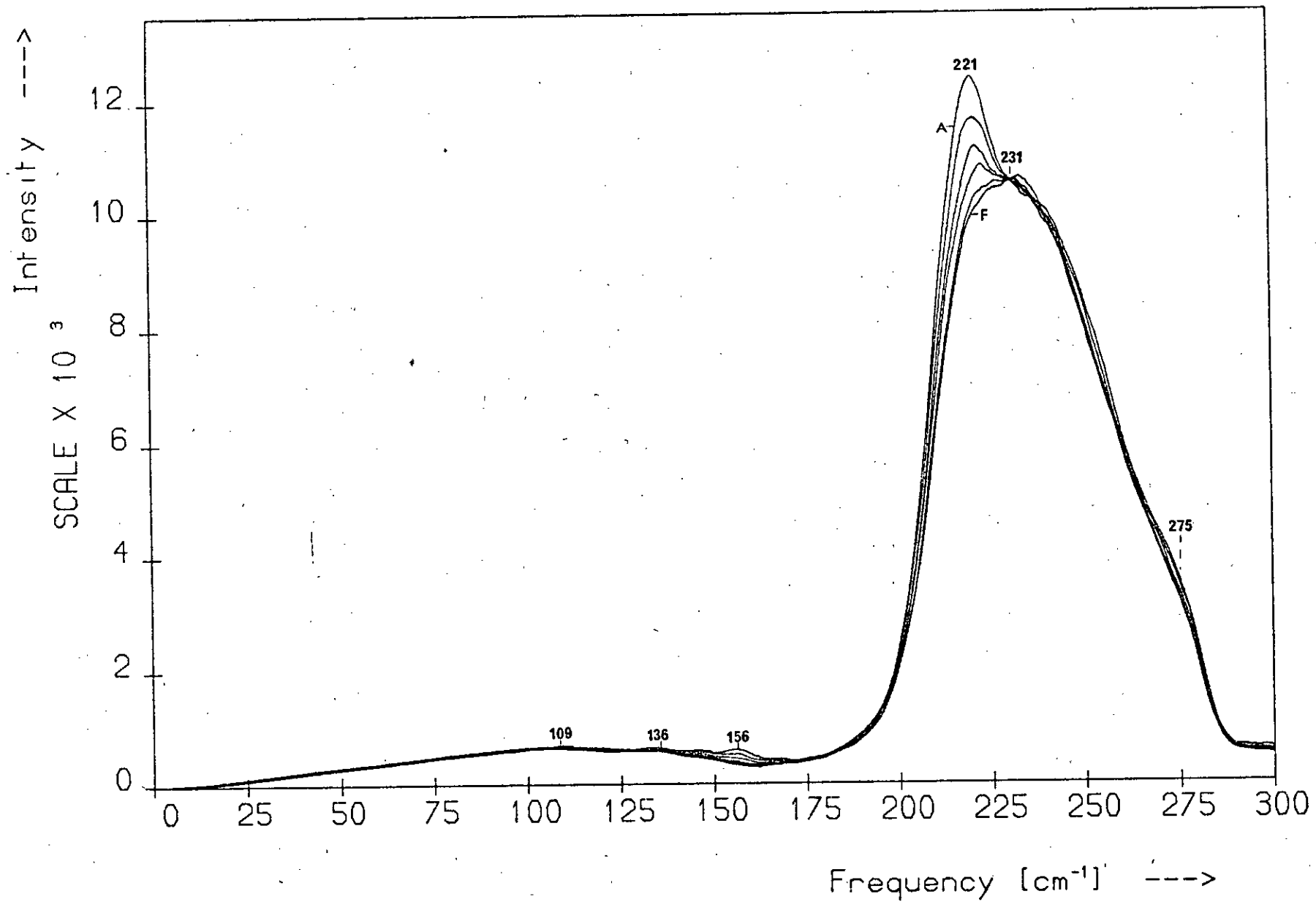
Raman Spectra: $As_{40}Se_{60}$ - $As_{45}Se_{55}$

As-Rich Glasses

Reduced Raman Spectra: $As_{40}Se_{60}$ – $As_{45}Se_{55}$

completely absent and the change occurring in the 106 – 109 cm^{-1} region

is not apparent, although enlargement of the low-frequency sections of

the reduced spectra shows that they peak at 106 and 109 cm^{-1} in the case

of a-$As_{40}Se_{60}$ and $As_{45}Se_{55}$ respectively, and at intermediate frequencies

in the case of the other compositions.

Figure 6.35 also shows that the high-frequency side of the main

band does not change significantly in shape but that almost the entire

low-frequency side is affected by the emerging feature at 221 cm^{-1}.

Since the six spectra are approximately coincident in the two base regions

of the main band, normalisation at 231 cm^{-1} is equivalent to normalisation

by basewidth in this case. Ignoring the small changes near 109 cm^{-1},

these spectra are approximately coincident over the region 0 – 140 cm^{-1}

as well, so the method of normalisation used is also equivalent to

normalisation over the low-frequency part of the spectra.

6.6.1.2 Polarisation measurements

The HH- and HV-polarised spectra of the above six compositions are

shown in Figures 6.36 and 6.37 respectively. The HH/HV spectra are

normalised to intensity at 227 cm^{-1}/223 cm^{-1} and have been vertically

displaced. It is seen in these figures that corresponding HH and HV

spectra are similar in shape, the only noticeable difference between

them being that the boson peak and the emerging 156 cm^{-1} feature are

more pronounced in the latter. Comparison with Figure 6.33 shows that

the polarised spectra resemble their polarisation-unanalysed counterparts

and thus the spectral changes they exhibit are the same as those described

in the previous section. One change which is not apparent in the polarised

spectra is the shift in the frequency of the boson peak: since the Raman

intensity varies slowly with frequency near the maximum, the peak frequency

is sensitive to the signal/noise ratio and this is poorer for the polarised

spectra than it is in the case of the polarisation-unanalysed results.

Figure 6.36

The HH-polarised Raman spectra of the compositions $As_{40}Se_{60} - As_{45}Se_{55}$.

Spectrum		Composition
A	—	$As_{45}Se_{55}$
B	—	$As_{44}Se_{56}$
C	—	$As_{43}Se_{57}$
D	—	$As_{42}Se_{58}$
E	—	$As_{41}Se_{59}$
F	—	$As_{40}Se_{60}$

Figure 6.37

The HV-polarised Raman spectra of the compositions $As_{40}Se_{60} - As_{45}Se_{55}$.
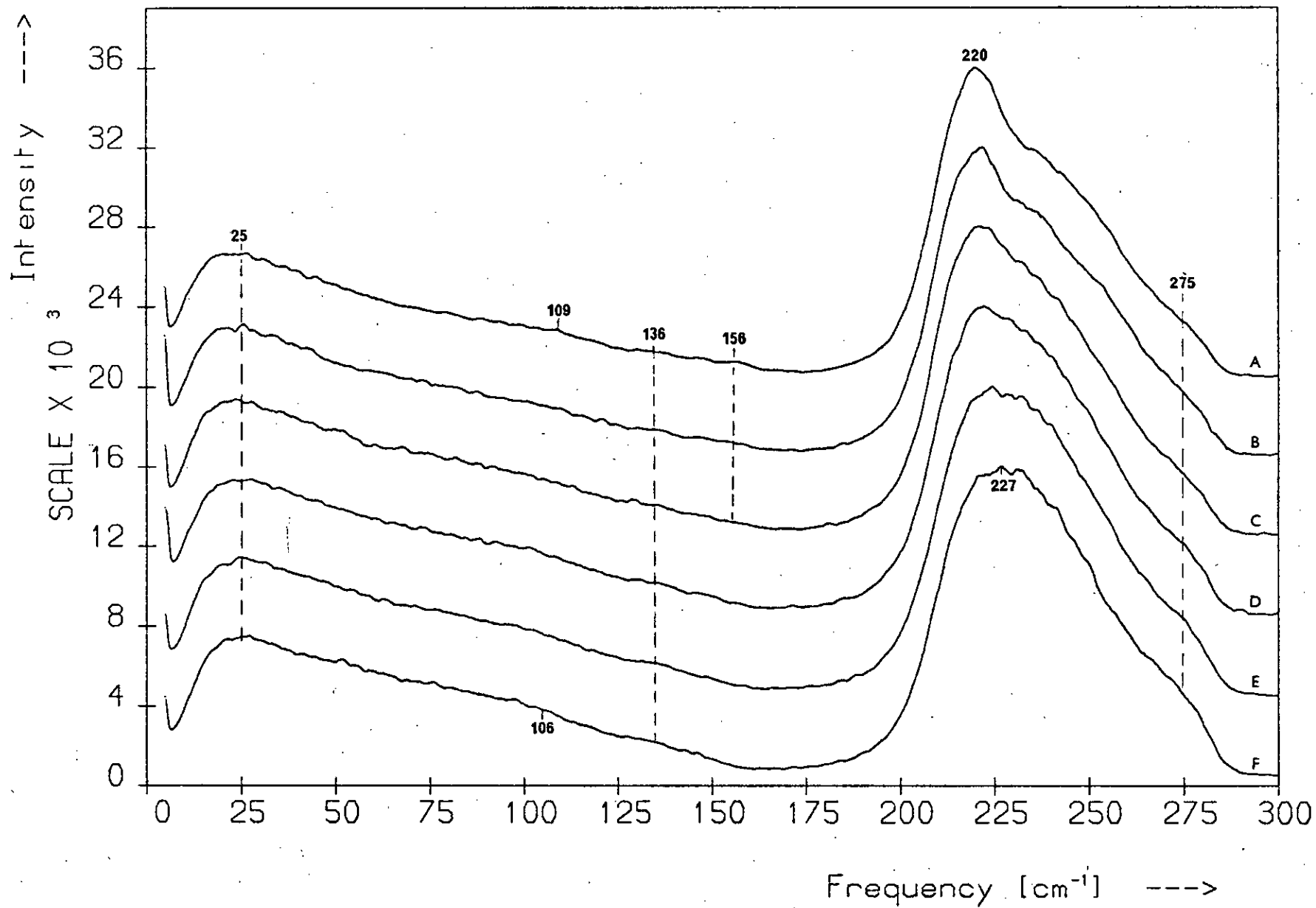A — F as for Figure 6.36.

Figure 6.38
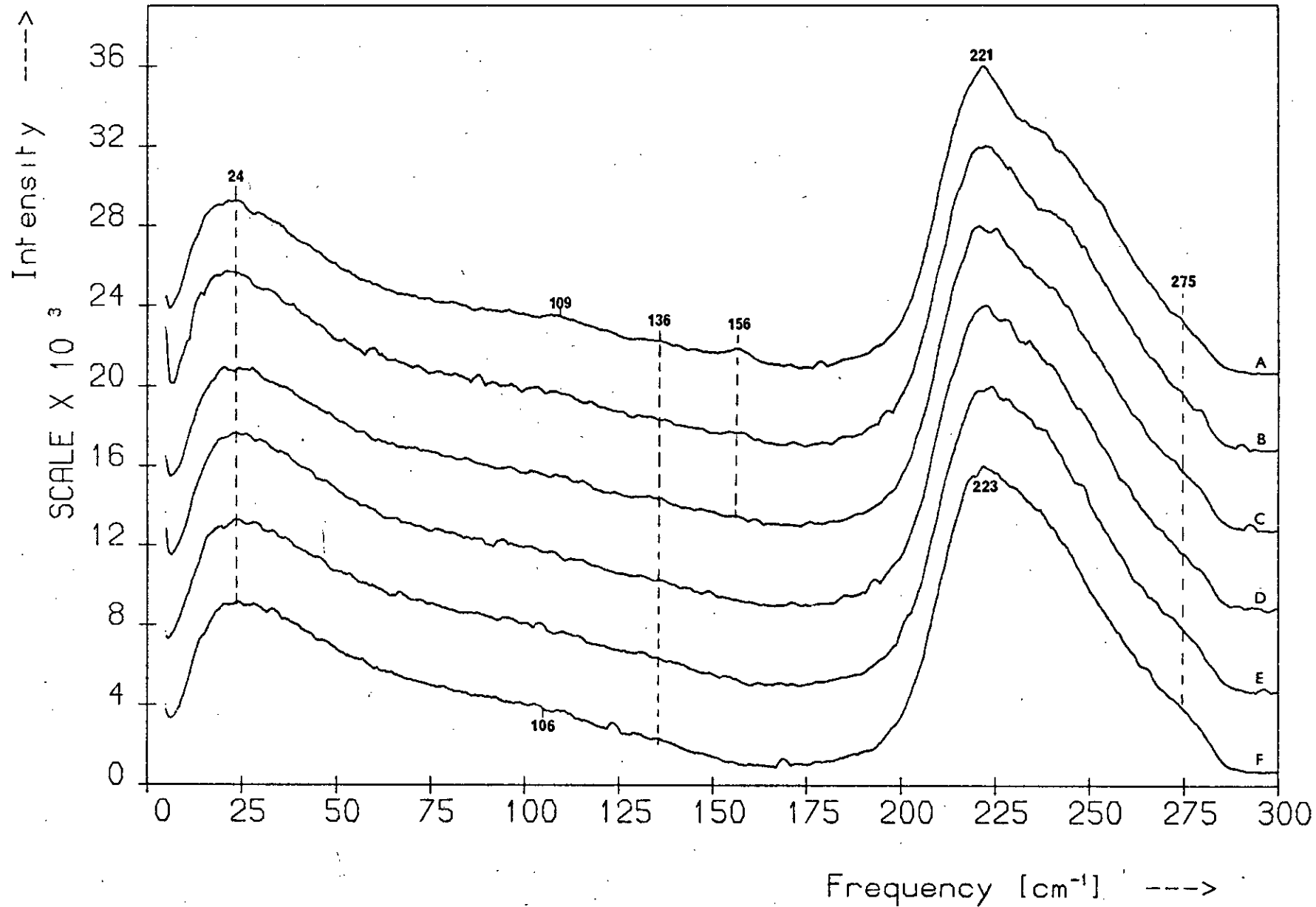
The depolarisation spectra of the compositions $As_{40}Se_{60} - As_{45}Se_{55}$.   A — F
as for Figure 6.36.

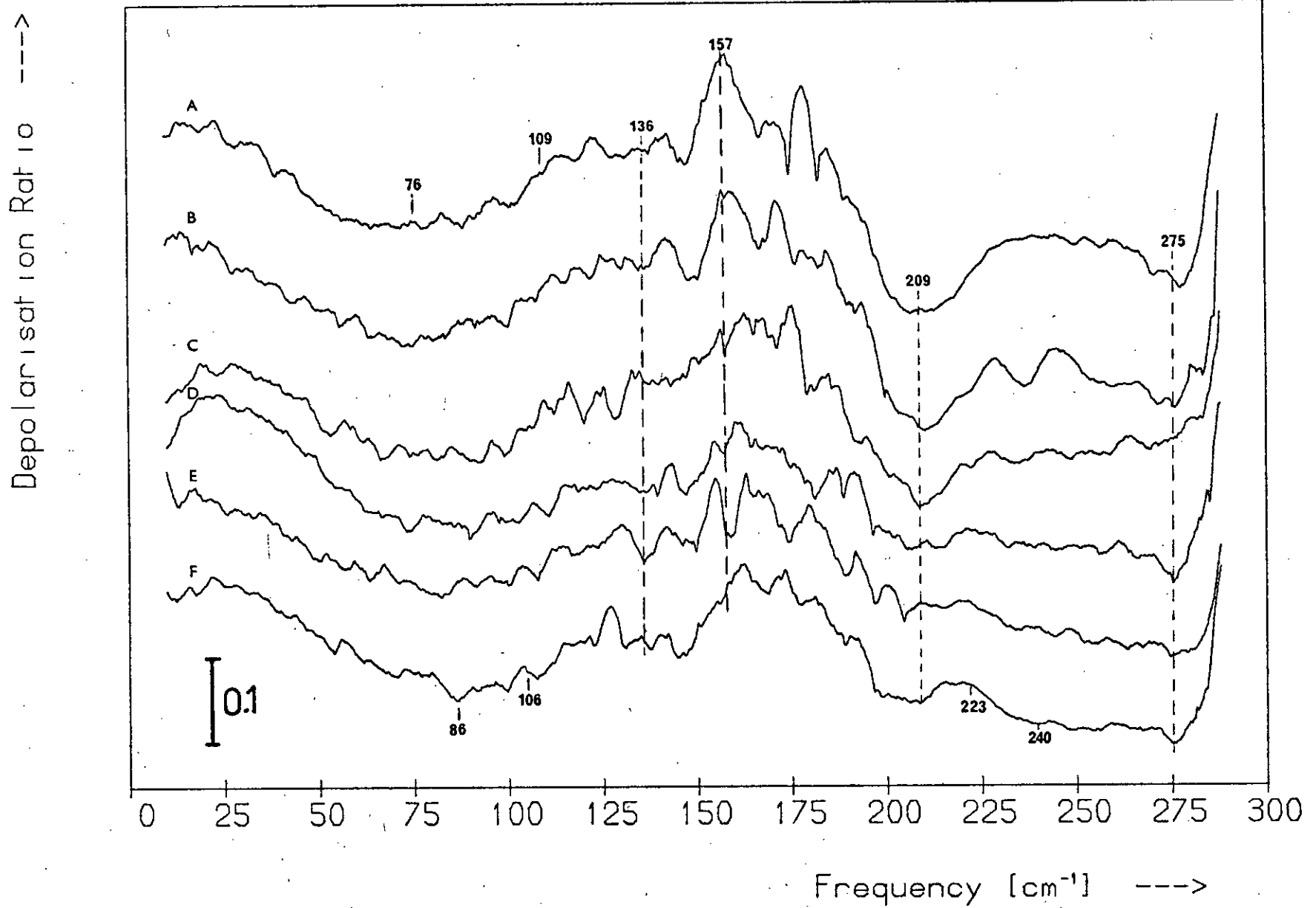HH Polarised Spectra: $As_{40}Se_{60}$ – $As_{45}Se_{55}$

Intensity ---->

SCALE X 10^3

Frequency [cm^{-1}] ---->

HV Polarised Spectra: $As_{40}Se_{60}$ – $As_{45}Se_{55}$

Depolarisation Spectra: $As_{40}Se_{60}$ – $As_{45}Se_{55}$

The depolarisation spectra for these six compositions are shown, vertically displaced, in Figure 6.38. The spectra are basically similar: each has a broad dip centred at ~80 cm^{-1}, a raised region around ~136 cm^{-1} and a trough from 200 to 290 cm^{-1}. As the As content increases beyond 40 at.% a peak grows at ~157 cm^{-1} and a broad, pronounced dip develops at ~209 cm^{-1}; also, the low-frequency dip shifts nearer the origin. The raised region around 136 cm^{-1} and the dip near 275 cm^{-1} do not shift in frequency.

Although features are present in the 106 — 109 cm^{-1} region of the Raman spectra there is no structure in this frequency range of the depolarisation spectra. The noisy sections of the spectra between 150 and 200 cm^{-1} correspond to the regions of minimum Raman signal.

6.6.1.3 Discussion

It is clear from Figure 6.33 that the spectra of the glasses in the composition range $As_{40}Se_{60}$ — $As_{45}Se_{55}$, unlike those of the corresponding sulphide glasses, do not exhibit a series of sharp lines growing rapidly with increasing As content. The principal spectral changes for these selenide glasses consist of the growth of two bands only, one at 220 cm^{-1} and a considerably weaker one at 156 cm^{-1}. The spectra of c-As_2Se_3 and c-As_4Se_4 do not have bands at these frequencies and in any case the band at 220 cm^{-1} is too broad to be of crystalline origin. Also, the glass-forming region of the As-Se system has been shown to extend to 55 at.% As[56] and there is no evidence of significant crystal-glass phase separation over the range 40 — 45 at.% As.

Figure 6.39 compares the spectrum of the composition $As_{45}Se_{55}$ with that of a-As. Although there are bands in the a-As spectrum near 220 and 156 cm^{-1} the $As_{45}Se_{55}$ bands at these frequencies do not match them exactly. Since, also, there is no evidence of any phase separation in these compositions it seems unlikely that the bands at 220 and 156 cm^{-1}

<u>Figure 6.39</u>

The polarisation-unanalysed spectra of a-As and the composition $As_{45}Se_{55}$.

Raman Spectra: a-As & As$_{45}$Se$_{55}$
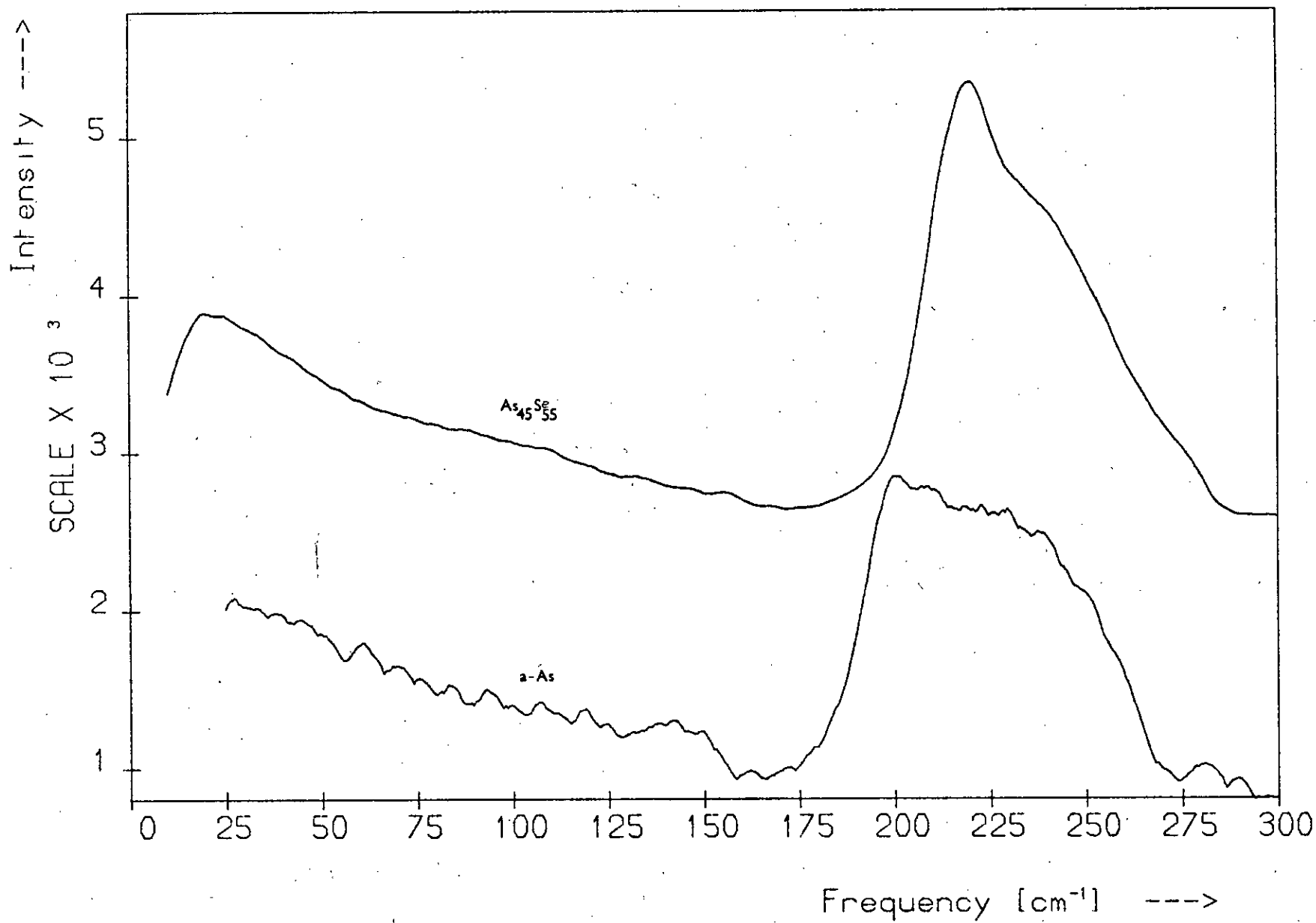
in the As-rich spectra arise from the presence of a-As in the glasses.

If the additional As atoms do not go into the formation of crystalline species or a-As they must be being incorporated in the As-Se network through the formation of As—As bonds. The vibrational frequencies arising from such bonds in the network are difficult to calculate exactly, as Lucovsky et al.[46] have pointed out, since there are many possibilities for the 6-atomic 'molecule' formed, e.g. $\underset{Se}{\overset{Se}{>}}As—As\underset{Se}{\overset{Se}{<}}$, $\underset{Se}{\overset{As}{>}}As—As\underset{As}{\overset{Se}{<}}$ etc. However, since a-As has bands near 220 and 156 cm^{-1} the features at these frequencies in the As-rich spectra can reasonably be associated with As—As bonds in the network: the 220 cm^{-1} band will arise from the stretching of this bond and the 156 cm^{-1} band will probably be due to its bending. The depolarisation spectra of Figure 6.38 show that the 220 cm^{-1} band is polarised while that at 156 cm^{-1} is depolarised and hence the corresponding vibrations are symmetric and antisymmetric respectively. In the As-rich sulphide glasses the band attributed to the stretching of As—As bonds in the network occurs at 231 cm^{-1} and is also polarised (the lower value of 220 cm^{-1} for the selenide case may reflect the greater atomic mass of selenium relative to sulphur).

Although there seems to be no evidence in the spectra of Figure 6.33 for the presence of As_4Se_4 molecules in these glasses, a careful comparison of this data with the results of Section 6.6.2 on the two very As-rich glasses $As_{50}Se_{50}$ and $As_{55}Se_{45}$ indicates that a small number of these molecules are indeed present. Figure 6.41 (after p.247) shows that the spectra of $As_{50}Se_{50}$ and $As_{55}Se_{45}$ exhibit numerous relatively sharp bands and that the region of the $As_{45}Se_{55}$ spectrum below 175 cm^{-1} contains corresponding structure, though it is extremely weak; the frequencies of six of the ten sharp bands (the 156 cm^{-1} band is being ignored) match frequencies in the i.r. spectrum of c-As_4Se_4[7]. The growth of the As_4Se_4 bands below 175 cm^{-1} as the As content is increased from 40 to 45 at.% is barely discernible in the spectra of Figures 6.33, 6.36 and 6.37. The

region below 175 cm^{-1} does not seem to exhibit any change at all over this composition range, apart from an apparent shift of the 106 cm^{-1} a-As$_{40}$Se$_{60}$ band to 109 cm^{-1} and the growth of the 156 cm^{-1} band (note that the As$_4$Se$_4$ structure is even weaker than this feature). It is the growth of the 110 cm^{-1} As$_4$Se$_4$ band that is responsible for the apparent shift of the 106 cm^{-1} a-As$_{40}$Se$_{60}$ feature. The high-frequency As$_4$Se$_4$ bands are not directly observable in the spectra of Figures 6.33, 6.36 and 6.37 because they occur in a region where the Raman signal from the As-Se network is very intense and changing rapidly as a function of frequency.

The difference spectra for the compositions As$_{40}$Se$_{60}$ — As$_{45}$Se$_{55}$ (see Figure 6.40) provide further evidence for the presence of As$_4$Se$_4$ bands in the Raman spectra of these glasses. The spectra exhibit a series of sharp features growing regularly as the As content is increased and many of these features occur near frequencies found in the i.r. spectrum of c-As$_4$Se$_4$. Note that the high-frequency As$_4$Se$_4$ bands as well as the low-frequency ones are detectable in the difference spectra.

The polarisation states of the As$_4$Se$_4$ bands can be deduced from Figure 6.44, which shows the depolarisation spectra of the compositions As$_{50}$Se$_{50}$ and As$_{55}$Se$_{45}$. The intense As$_4$Se$_4$ band at 204 cm^{-1} is polarised and corresponds to the minimum in the depolarisation spectra of these two glasses. The fact that in the depolarisation spectra of the compositions As$_{40}$Se$_{60}$ — As$_{45}$Se$_{55}$ the minimum corresponding to the As–As bond-stretching band at 220 cm^{-1} does not occur at this frequency but at 209 cm^{-1} may be due to the proximity of the polarised 204 cm^{-1} As$_4$Se$_4$ band.

It is clear from Figures 6.33 and 6.40 that as the As content is increased beyond 40 at.% the additional As atoms initially go mainly into the network rather than into the formation of As$_4$Se$_4$ molecules, for the 220 and 156 cm^{-1} bands grow much faster than the As$_4$Se$_4$ bands. This is in contrast to the situation in the corresponding As-S glasses and reflects

Figure 6.40

Difference spectra obtained from the spectra of Figure 6.33 by subtracting the a-$As_{40}Se_{60}$ spectrum from each.

Spectrum		Composition
A	—	$As_{45}Se_{55}$ - $As_{40}Se_{60}$
B	—	$As_{44}Se_{56}$ - $As_{40}Se_{60}$
C	—	$As_{43}Se_{57}$ - $As_{40}Se_{60}$
D	—	$As_{42}Se_{58}$ - $As_{40}Se_{60}$
E	—	$As_{41}Se_{59}$ - $As_{40}Se_{60}$

Difference Spectra for the As-Rich Glasses
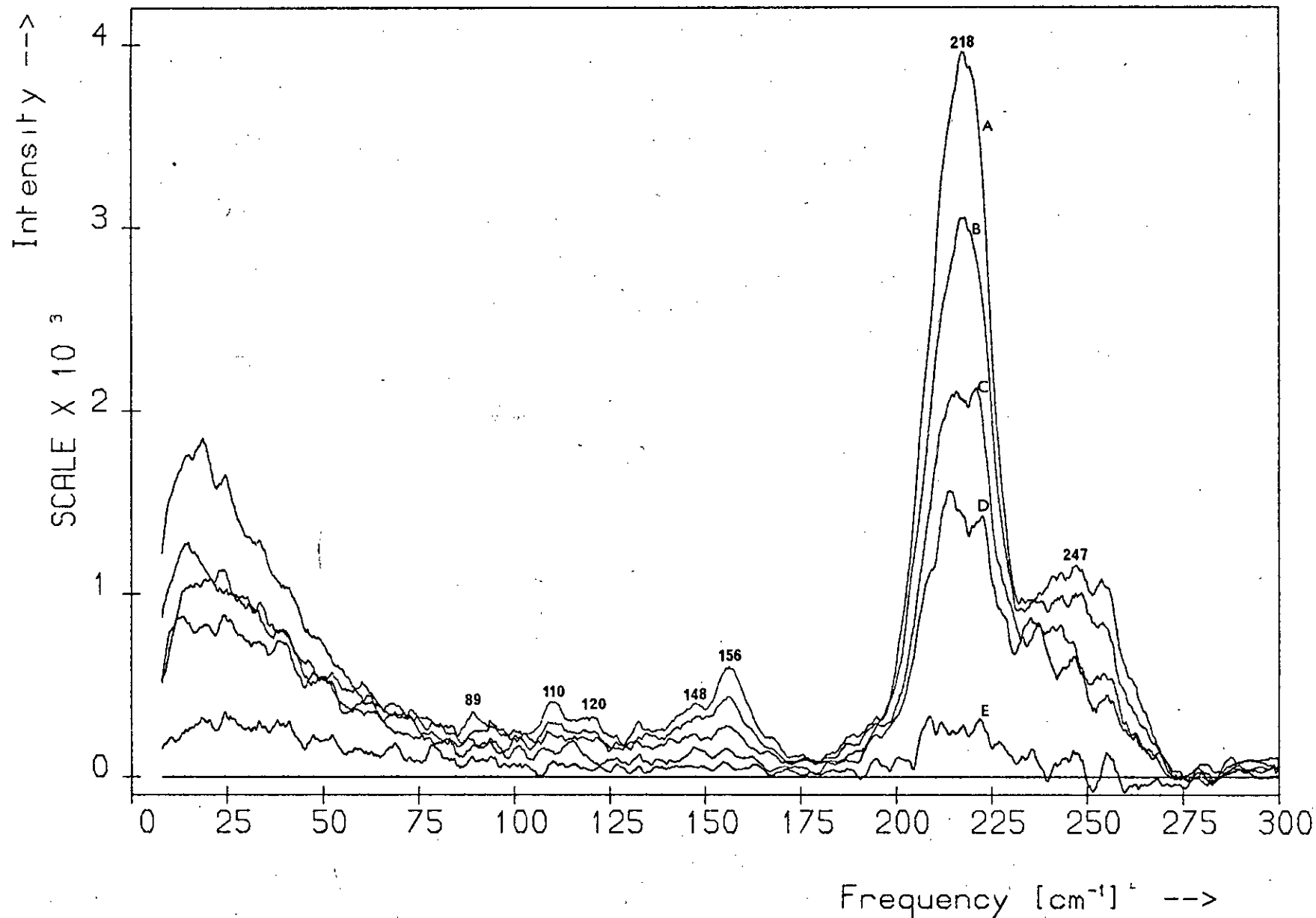
the different melting behaviour of c-As_4S_4 and c-As_4Se_4. c-As_4S_4 melts congruently to a liquid of the same composition and when this liquid is cooled the small As_4S_4 molecules of which it is composed readily order into a crystal lattice. c-As_4Se_4, however, decomposes at 264° C to a liquid and c-As_2Se_3; when liquid As_4Se_4 is cooled the presence of the As_2Se_3 network regions inhibits crystallisation[53].

It will be shown in Section 6.6.2 that at large excess As concentrations the formation of As–As bonds in the network is superceded by the formation of As_4Se_4 molecules and the As_4Se_4 bands overtake the 220 and 156 cm^{-1} bands. The different growth rates of the two sets of features is further evidence that the 220 and 156 cm^{-1} bands are not associated with As_4Se_4 molecules.

The presence of the plateau at 136 cm^{-1} and the dips at 275 and ~ 80 cm^{-1} in all the depolarisation spectra of the compositions $As_{40}Se_{60}$ – $As_{45}Se_{55}$ suggests that the $AsSe_3$ pyramids and As_2Se bridges of a-$As_{40}Se_{60}$ are retained in these glasses. Since the 275 and 136 cm^{-1} a-$As_{40}Se_{60}$ features do not shift in frequency no change in the geometry of these 'molecules' can be occurring as the As content is increased. It is unlikely that the 86 cm^{-1} vibration of the As_2Se bridge shifts to 76 cm^{-1} as suggested by the depolarisation results, for the dip at 275 cm^{-1}, which also arises from this bridge, does not shift at all. The shift in the frequency of the low-frequency dip is probably related with the shift of the boson peak to lower frequencies (see Figure 6.33); these shifts may be due to an increase in the layer separation with increasing As content[34].

6.6.2 The compositions $As_{45}Se_{55}$ – $As_{55}Se_{45}$

6.6.2.1 The polarisation-unanalysed spectra

The polarisation-unanalysed Raman spectra of the compositions $As_{50}Se_{50}$ and $As_{55}Se_{45}$ are shown in Figure 6.41 together with the corresponding spectra of the $As_{40}Se_{60}$ and $As_{45}Se_{55}$ glasses for comparison.

<u>Figure 6.41</u>

The polarisation-unanalysed Raman spectra of the compositions in the

range $As_{40}Se_{60} - As_{55}Se_{45}$.

	Spectrum		Composition
	A	—	$As_{55}Se_{45}$
	B	—	$As_{50}Se_{50}$
	C	—	$As_{45}Se_{55}$
	D	—	$As_{40}Se_{60}$

<u>Figure 6.42</u>

The HH-polarised Raman spectra of the compositions in the range

$As_{40}Se_{60} - As_{55}Se_{45}$.   A — D as for Figure 6.41.

<u>Figure 6.43</u>

The HV-polarised Raman spectra of the compositions in the range

$As_{40}Se_{60} - As_{55}Se_{45}$.   A — D as for Figure 6.41.

<u>Figure 6.44</u>

The depolarisation spectra of the compositions in the range

$As_{40}Se_{60} - As_{55}Se_{45}$.   A — D as for Figure 6.41.

Raman Spectra: $As_{40}Se_{60} - As_{55}Se_{45}$
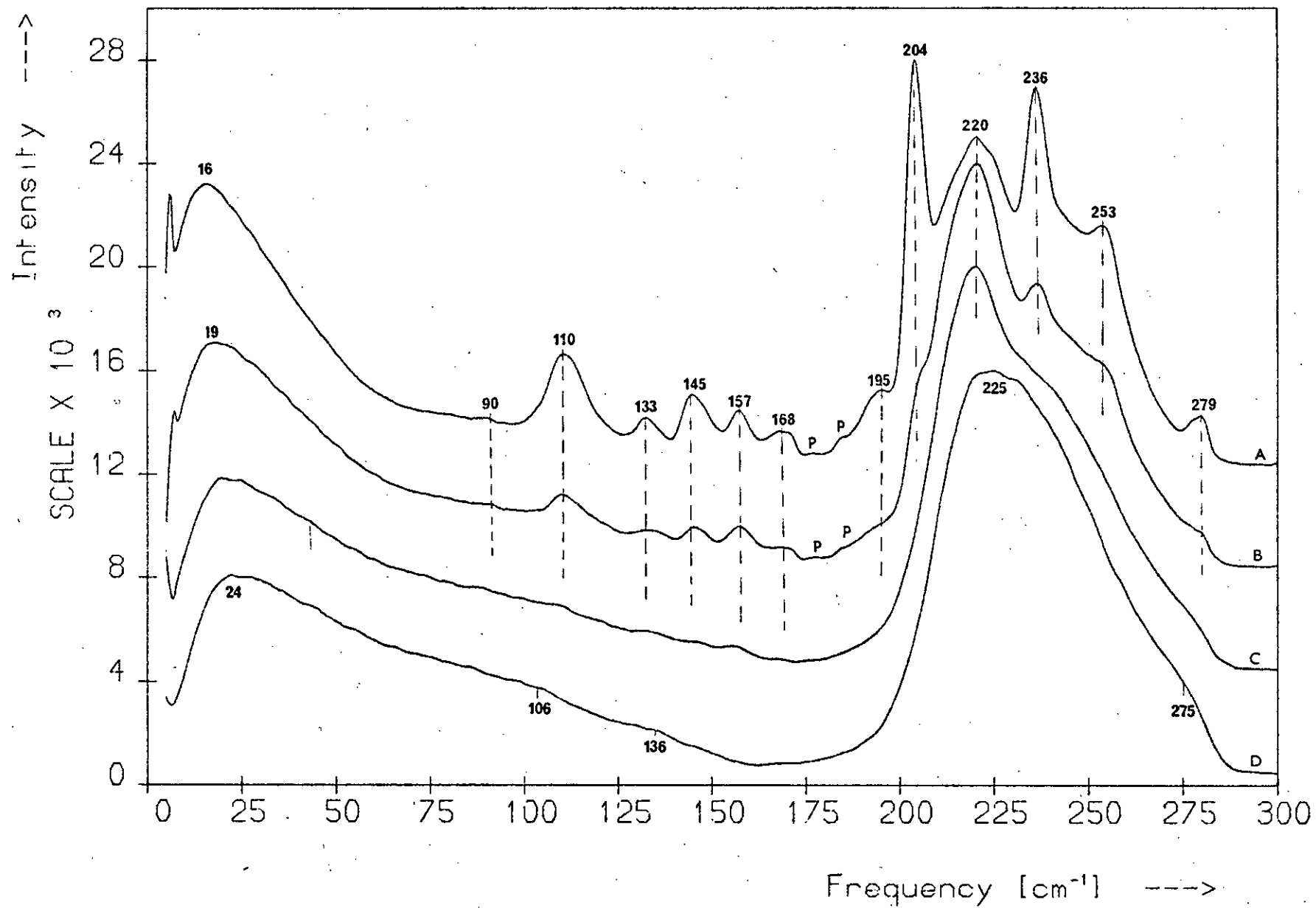
HH Polarised Spectra: $As_{40}Se_{60}$ – $As_{55}Se_{45}$

HV Polarised Spectra: $As_{40}Se_{60} - As_{55}Se_{45}$

Intensity ---->

SCALE X 10^3

Frequency [cm^{-1}] ---->
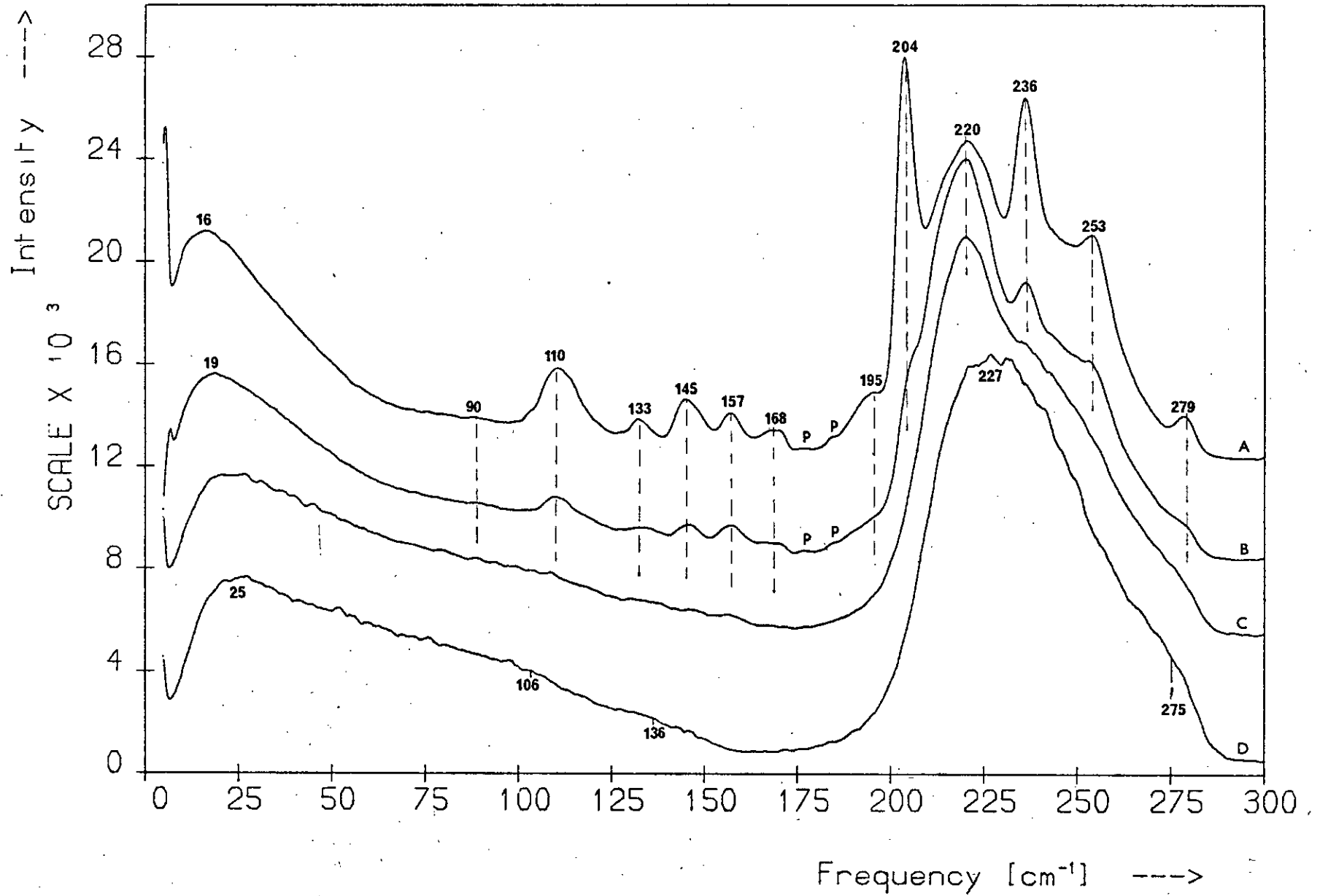
Depolarisation Spectra: $As_{40}Se_{60}$ – $As_{55}Se_{45}$

The spectra are normalised by maximum intensity and are shown displaced above one another.

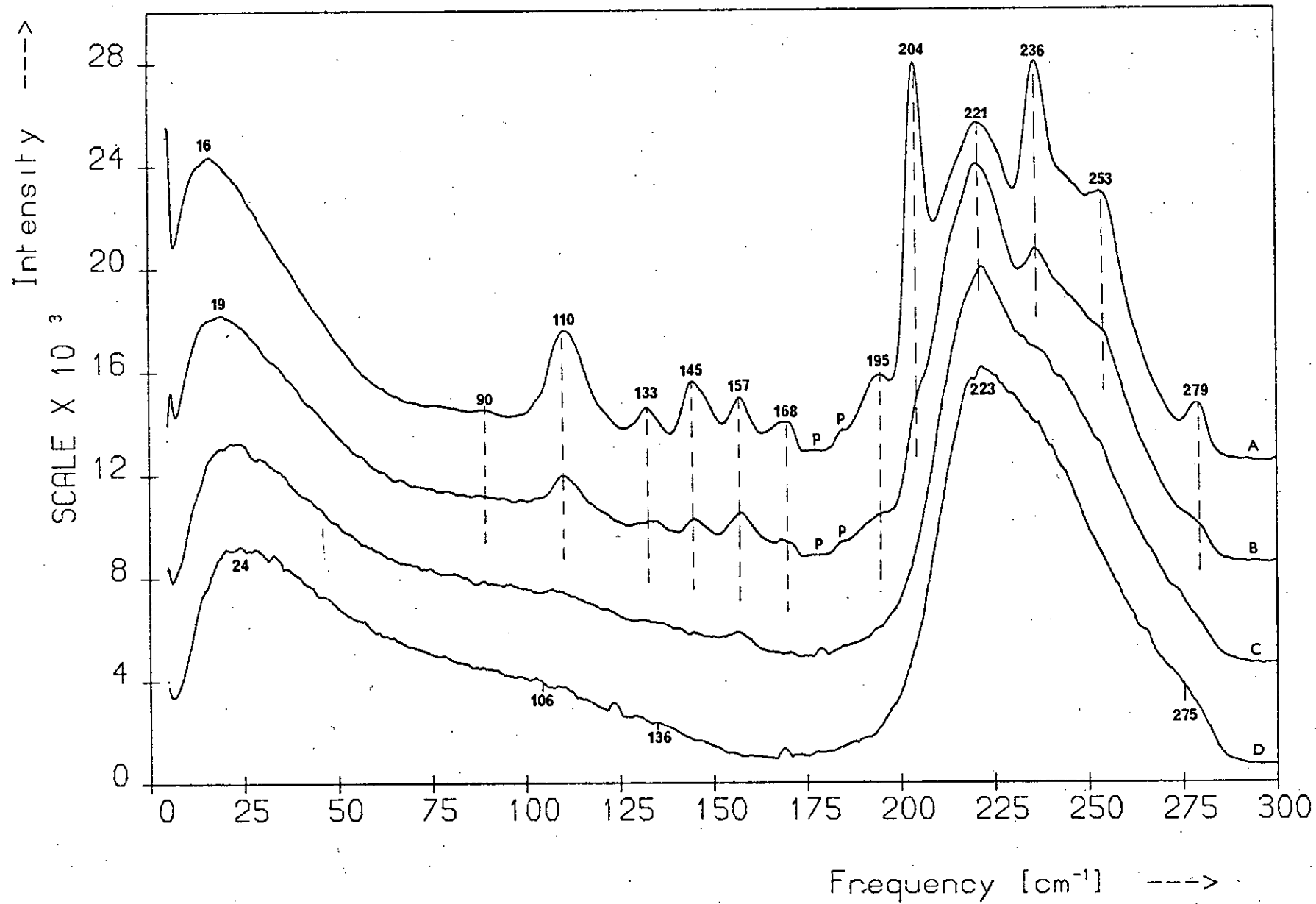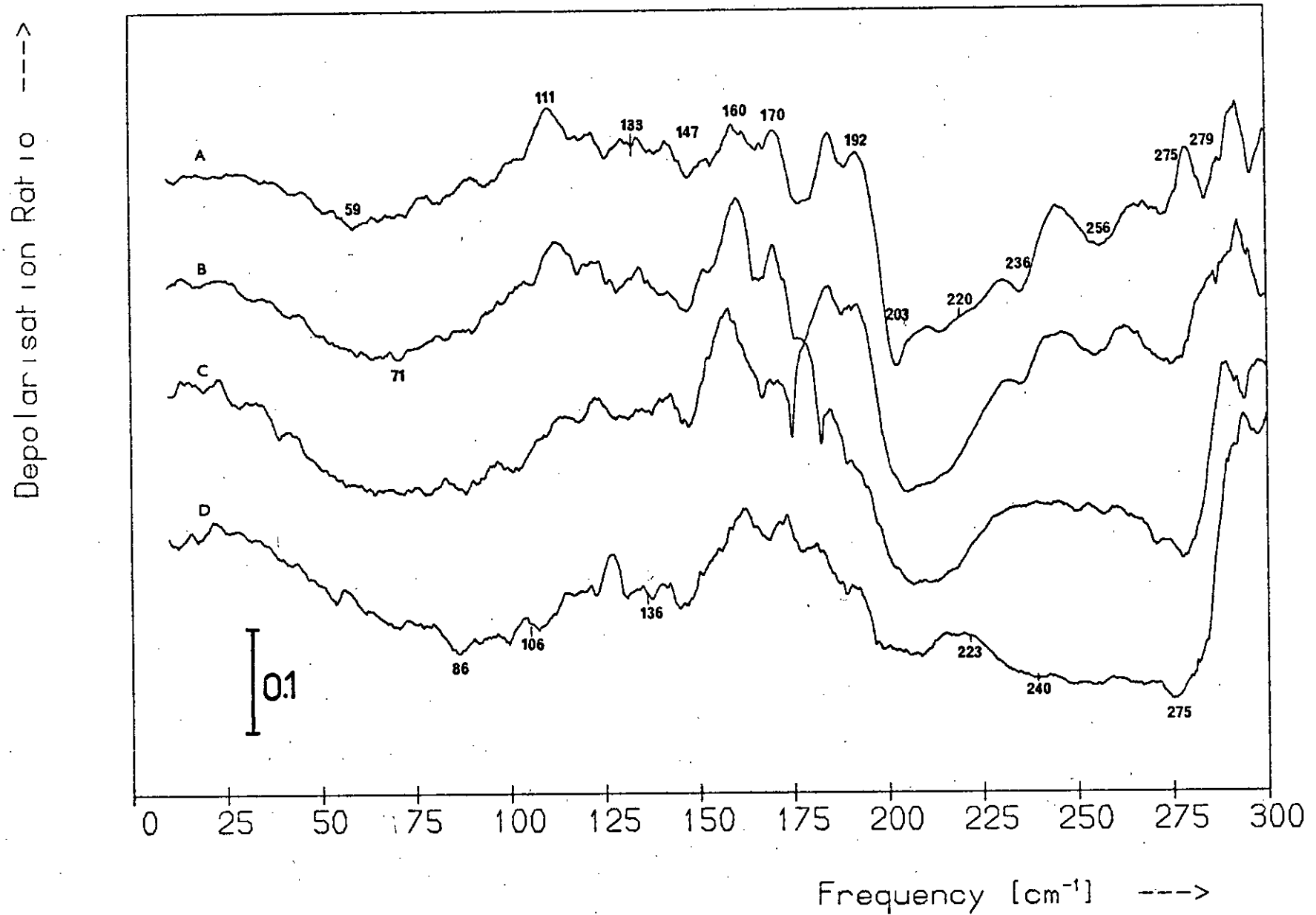The spectral changes occurring as the As content is increased beyond 45 at.% consist of the growth of numerous sharp peaks (this behaviour is similar to that observed in the case of the sulphide glasses containing more than 40 at.% As — see Figure 5.62). Also, the boson peak grows relative to the 220 cm^{-1} band and continues shifting to lower frequencies. It is clear from the spectrum of the $As_{55}Se_{45}$ composition that these sharp features eventually overtake the 220 and 156 cm^{-1} bands, which emerged when the As content was increased above 40 at.%.

6.6.2.2 Polarisation measurements

The HH- and HV-polarised spectra of the compositions $As_{50}Se_{50}$ and $As_{55}Se_{45}$ are shown along with the corresponding spectra of the $As_{40}Se_{60}$ and $As_{45}Se_{55}$ glasses in Figures 6.42 and 6.43 respectively. The spectra are normalised by maximum intensity and are shown vertically displaced.

For the $As_{50}Se_{50}$ and $As_{55}Se_{45}$ glasses the HH spectra are basically similar to the HV spectra, the only differences being in the intensity of the boson peak, which is more pronounced in the HV spectra, and in the intensities of the emerging sharp peaks relative to one another. Since the polarised spectra of these two compositions resemble their polarisation-unanalysed counterparts the spectral changes occurring as the As content increases above 45 at.% are the same as those described in the previous section.

The depolarisation spectra for these four compositions are shown, displaced above one another, in Figure 6.44. Each spectrum has a broad dip in the 25 — 110 cm^{-1} region followed by a raised section centred at $\sim$130 cm^{-1}, and also a trough from $\sim$200 to 290 cm^{-1}, though this differs considerably in shape from spectrum to spectrum. Several spectral changes occur as the As content is increased beyond 45 at.%: the

low-frequency dip becomes shallower and shifts nearer the origin, the $110 - 175$ cm^{-1} section rises relative to the maximum in the spectra at ~ 25 cm^{-1}, and numerous sharp features appear. Dips are present at $203 - 209$ and ~ 275 cm^{-1} in all the As-rich spectra.

The sharp features occurring in the depolarisation spectra of the $As_{50}Se_{50}$ and $As_{55}Se_{45}$ glasses coincide with the emerging structure in the corresponding Raman spectra. These sharp dips and peaks in $\rho(w)$ indicate the polarisation states of the growing bands; the states are given in Table 6.8 along with the frequencies of these bands. Since a number of the sharp features in the depolarisation spectra are not well defined and are comparable with the noise structure the polarisation states of some of the bands are uncertain; this is indicated in the table.

6.6.2.3 Discussion

The emergence of numerous, relatively sharp bands in the spectra of the As-Se glasses as the As content is increased beyond 45 at.% is reminiscent of the spectral changes that occurred in the As-rich sulphide glasses. Figures 6.41 — 6.43 show that when the As content reaches 55 at.% these new bands have overtaken those at 220 and 156 cm^{-1}, which were the first to appear as the As content was increased beyond 40 at.%. This suggests that the new structure and the bands at 220 and 156 cm^{-1} have different origins. It is notable that traces of this structure are observable in the spectra of $As_{45}Se_{55}$.

The frequencies of six of the ten new bands are near frequencies in the i.r. spectrum of c-As_4Se_4. The glass forming region in the As-Se system extends to 55 at.% As and it appears that as the As content approaches this level the excess As atoms go more and more into the formation of As_4Se_4 molecules and less and less into the formation of As-As bonds in the network, though the presence of the bands at 220 and

i.r. frequency (cm^{-1}) (Reference 10)		Raman frequency (cm^{-1}) (this work)		Raman poln. state
93	(s)	90	(vw)	?
104.5	(m)			
114.5	(w)	110	(s)	dp
129	(w)			
134.5	(m)	133	(w)	dp?
		145	(m)	p
		168	(w)	dp
		195	(m)	dp
205	(m)	204	(vs)	p
220	(m)	220*	(s)	p
235	(m)	236	(s)	p
241.5	(vs)			
252.5	(m)	253	(m)	p
		279	(m)	p

p - polarised; dp - depolarised; s - strong;
w - weak; v - very; m - medium.

*This frequency is also associated with vibrations
of As—As bonds in the network.

Table 6.8   The frequencies and polarisation states of the As_4Se_4 bands

observed in the spectra of the As-rich selenide glasses.

The i.r. frequencies are those of c-As_4Se_4 (Reference 10).

157 cm^{-1} in the spectra of the compositions As$_{50}$Se$_{50}$ and As$_{55}$Se$_{45}$ indicate that such bonds are still present in these glasses. The sharp features in the spectra of these glasses cannot be compared directly with the Raman spectrum of c-As$_4$Se$_4$ since it has not yet been recorded but the breadth of the As$_4$Se$_4$ bands in the glass spectra suggests that they do not arise from c-As$_4$Se$_4$ itself.

Figure 6.44 shows that a low-frequency dip, a plateau centred at ~136 cm^{-1} and a dip at 275 cm^{-1} occur in all the depolarisation spectra. These features are characteristic of $\rho(w)$ for a-As$_{40}$Se$_{60}$ and hence indicate that the AsSe$_3$ and As$_2$Se structural units of this glass are retained in these very As-rich compositions. The shift in the frequency of the low-frequency dip from 86 to 59 cm^{-1} is attributable to the shift of the boson peak towards the origin. Since the other dip and the plateau do not shift there is no change in the geometry of these units.

It appears that in the As-Se glasses, as well as in the sulphides, monomer species are produced as the As content approaches the maximum value permitting glass formation. In the case of the As-S glasses As$_4$S$_4$ is produced together with much smaller quantities of As$_4$S$_5$ or As$_4$S$_3$ (or both). In the selenides, however, As$_4$Se$_4$ monomers only are formed.

6.7   Photo-induced spectral changes

In contrast to the case for the As-S glasses, no changes as a function of irradiation were observed in the selenide spectra. This absence of photo-induced spectral changes may, however, be due to the fact that the selenide samples were rapidly rotated during the scans in order to overcome the damaging effect of focussed radiation (see Section 4.3.1). It is possible that the effective incident power density in these experiments was reduced to such an extent by the spinning technique that negligible photo-induced change occurred in the samples.

At incident power densities greater than those used in the present experiments, but below the level at which physical damage is produced, there may occur a Raman signal loss due to photostructural changes within these materials, for, like the sulphides, they also undergo photo-darkening[57,58]. There is evidence that the layer structure of c-As_2Se_3 is retained in a-As_2Se_3[34,40,41] so if a Raman signal loss does occur in the As-Se glasses it may well arise from the mechanism put forward in Section 5.7 to account for this effect in the sulphides, viz the break-up of the layer remnants: the layers would be disrupted by the formation of $-As\overset{Se}{\underset{Se}{<\,>}}As-$ units and this would result in a decrease in vibrational coherence.

Photostructural changes in a-As_2Se_3 have been observed by other workers but under different conditions to those prevailing in the present experiments. DeFonzo and Tauc[59] have shown that at temperatures between T_g and T_m a-As_2Se_3 is transformed into c-As_2Se_3 when illuminated with 5145 Å radiation. (This is a stable glass and it does not crystallise in the dark in this temperature range.) Cernogora et al.[23] report that at low temperatures (1.6° K) illumination of a-As_2Se_3 with red light results in a feature growing near 260 cm^{-1} in the Raman spectrum. For 6764 Å excitation they also observe a decrease in Raman intensity as a function of exposure. These authors attribute the effects to changes in the local atomic configuration but do not specify any particular structural alteration.

6.8 References

1. Schottmiller, J., Tabak, M., Lucovsky, G. and Ward, A., J. Non-Cryst. Solids 4, 80 (1970).

2. Ward, A.T., Adv. in Chemistry 110, 163 (1972).

3. Văsko, A. and Kieslich, K., Proc. 7th Int. Conf. on Amorphous and Liquid Semiconductors, Edinburgh (Spear, W.E., editor), C.I.C.L., Edinburgh, 1977, p.105.

4. Zallen, R., Slade, M.L. and Ward, A.T., Phys. Rev. B 3, 4257 (1971).

5. Zallen, R. and Slade, M.L., Phys. Rev. B 9, 1627 (1974).

6. Austin, I.G. and Garbett, E.S., Phil. Mag. 23, 17 (1971).

7. Whitfield, H.J., Aust. J. Chem. 24, 697 (1971).

8. Zlatkin, L.B. and Markov, Yu.F., Phys. Stat. Sol. (a) $\underline{4}$, 391 (1971).

9. Arai, T., Komiya, S. and Kudo, K., J. Non-Cryst. Solids $\underline{18}$, 289 (1975).

10. Bastow, T.J. and Whitfield, H.J., J.C.S. Dalton, 1739 (1973).

11. Geick, R., Schröder, U. and Stuke, J., Phys. Stat. Sol. $\underline{24}$, 99 (1967).

12. Lucovsky, G., Mooradian, A., Taylor, W., Wright, G.B. and Keezer, R.C., Solid State Commun. $\underline{5}$, 113 (1967).

13. Mooradian, A. and Wright, G.B., in 'Physics of Selenium and Tellurium' (Cooper, W.C., editor), Pergamon Press, Oxford, 1969, p.169.

14. Caldwell, R.S. and Fan, H.Y., Phys. Rev. $\underline{114}$, 664 (1959).

15. Gorman, M. and Solin, S.A., Solid State Commun. $\underline{18}$, 1401 (1976).

16. Eisenberg, A. and Tobalsky, A.V., J. Polym. Sci. $\underline{46}$, 19 (1960).

17. Smith, J.E., Jr., Brodsky, M.H. and Gambino, R.J., Bull. Am. Phys. Soc. II $\underline{17}$, 336 (1972).

18. Brodsky, M.H., Gambino, R.J., Smith, J.C., Jr. and Yacoby, Y., Phys. Stat. Sol (b) $\underline{52}$, 609 (1972).

19. Martin, R.M. and Lucovsky, G., Proc. 12th Int. Conf. on the Physics of Semiconductors, Stuttgart (Pilkuhn, M.H., editor), Teubner, Stuttgart, 1974, p.184.

20. Ward, A.T., J. Phys. Chem. $\underline{72}$, 4133 (1968).

21. Nemanich, R.J., Solin, S.A. and Lucovsky, G., Proc. 3rd Int. Conf. on Light Scattering in Solids, Campinas, Brazil, Flammarion, Paris, 1975, p.631.

22. Lucovsky, G., Nemanich, R.J., Solin, S.A. and Keezer, R.C., Solid State Commun. $\underline{17}$, 1567 (1975).

23. Cernogora, J., Mollot, F. and Benôit à la Guillaune, C., Solid State Commun. $\underline{19}$, 465 (1976).

24. Taylor, P.C., Bishop, S.G. and Mitchell, D.L., Solid State Commun. $\underline{8}$, 1783 (1970).

25. Onomichi, M., Arai, T. and Kudo, K., J. Non-Cryst. Solids $\underline{6}$, 362 (1971).

26. Taylor, P.C., Bishop, S.G. and Mitchell, D.L., Phys. Rev. Lett. $\underline{27}$, 414 (1971).

27. Lucovsky, G., Phys. Rev. B $\underline{6}$, 1480 (1972).

28. Väsko, A. and Vondrich, J., Proc. Int. Conf. on Amorphous Semiconductors, Balatonfured, Hungary, Akad. Kiado, Budapest, 1976, p.265.

29. Papatheodorou, G.N. and Solin, S.A., Solid State Commun. 16, 5 (1975).

30. Solin, S.A., A.I.P. Conf. Proc. 31, 205 (1976).

31. Taylor, P.C., Bishop, S.G., Mitchell, D.L. and Treacy, D., Proc. 5th Int. Conf. on Amorphous and Liquid Semiconductors, Garmisch-Partenkirchen, Germany (Stuke, J. and Brenig, W., editors), Taylor and Francis, London, 1974, p.1267.

32. Sik, M.J., private communication.

33. Zallen, R., Phys, Rev. B 9, 4485 (1974).

34. Leadbetter, A.J. and Apling, A.J., J. Non-Cryst. Solids 15, 250 (1974).

35. Bermudez, V.M., J. Chem. Phys. 57, 2793 (1972).

36. Lucovsky, G. and Martin, R.M., J. Non-Cryst. Solids 8 — 10, 185 (1972).

37. Lucovsky, G., Proc. 5th Int. Conf. on Amorphous and Liquid Semiconductors, Garmisch-Partenkirchen, Germany (Stuke, J. and Brenig, W., editors), Taylor and Francis, London 1974, p.1099.

38. Finkman, E., DeFonzo, A.P. and Tauc, J., Proc. 5th Int. Conf. on Amorphous and Liquid Semiconductors, Garmisch-Partenkirchen, Germany (Stuke, J. and Brenig, W., editors), Taylor and Francis, London, 1974, p.1275.

39. Papatheodorou, G.N. and Solin, S.A., Phys, Rev. B 13, 1741 (1976).

40. Bishop, S.G. and Shevchik, N.J., Solid State Commun. 15, 629 (1974).

41. Rubenstein, M. and Taylor, P.C., Phys. Rev. B 9, 4258 (1974).

42. Nakamoto, K., 'Infrared Spectra of Inorganic and Coordination Compounds', Wiley, New York, 1963.

43. Renninger, A.L. and Averbach, B.L., Acta Cryst. B29, 1583 (1973).

44. Claeys, E.G. and Van der Kelen, G.P., Spectrochim. Acta 22, 2095 (1966).

45. Trotter, J., Z. Krist. 122, 230 (1965).

46. Lucovsky, G., Galeener, F.L., Geils and Keezer, R.C., in 'The Structure of Non-Crystalline Materials' (Gaskell, P.H., editor), Taylor and Francis, London, 1977, p.127.

47. Bagnall, K.W., 'The Chemistry of Selenium, Tellurium and Polonium', Elsevier, Amsterdam, 1966, ff33.

48. Cherin, P. and Unger, P., Acta Cryst. B 28, 313 (1972).

49. Andriovskii, A.I. and Nabitovich, I.D., Kristallografiya 5, 465 (1970).

50. Renninger, A.L., Rechtin, M.D. and Averbach, B.L., J. Non-Cryst. Solids 16, 1 (1974).

51. Pétursson, J., Ph.D. Thesis, University of Edinburgh, 1975.

52. Porto, S.P.S., The Spex Speaker 14, 2 (1969) (Newsletter of Spex Industries Inc.).

53. Myers, M.B. and Felty, E.J., Mat. Res. Bull. 2, 535 (1967).

54. Leadbetter, A.J. and Apling, A.J., J. Non-Cryst. Solids 15, 250 (1974).

55. Ramaswamy, K. and Jayaraman, S., Acta Phys. Pol. A40, 883 (1971).

56. Flaschen, S.S., Pearson, A.D. and Northover, W.R., J. Amer. Ceram. Soc. 42, 450 (1959).

57. Asahara, Y. and Izumitani, T., Phys. Chem. Glasses 16, 29 (1975).

58. deNeufville, J.P., Moss, S.C. and Ovshinsky, S.R., J. Non-Cryst. Solids 13, 191 (1974).

59. Finkman, E., DeFonzo, A.P. and Tauc, J., Proc. 12th Int. Conf. on the Physics of Semiconductors, Stuttgart (Pilkuhn, M.H., editor), Teubner, Stuttgart, 1974, p.1022.

CHAPTER 7

CONCLUSIONS

7.1 $a\text{-}As_2S_3$ and $a\text{-}As_2Se_3$

Of the various models used in interpreting the vibrational spectra of amorphous materials the molecular model was found to be the most appropriate in the case of $a\text{-}As_2S_3$ and $a\text{-}As_2Se_3$. For both materials the model could account for the number of observed bands and their frequencies and polarisation states. The results confirm that the short-range order in the two glasses is similar to that in the corresponding crystals and indicate that they have a network structure composed of AsX_3 pyramid units linked via As_2X bridges (X = S or Se). It was found that the Raman spectra of the two glasses are related by the same two scale factors that relate the spectra of the corresponding crystals; the applicability of the interlayer scale factor to the glass spectra supports the presence of layer regions in the glasses.

In the case of $a\text{-}As_2S_3$ the spectra indicate that As—As and S—S bonds are present in the network, though in very small quantities (about 1% of bonds are 'like-atom'). Possibly due to the overlapping of bands, no features attributable to 'like-atom' bonds were detected in the $a\text{-}As_2Se_3$ spectra but the results for the non-stoichiometric glasses suggest that As—As and Se—Se bonds may be present in $a\text{-}As_2Se_3$. There is no evidence for the presence of any molecular species such as S_8, As_4S_4 and As_4Se_4 in these two glasses.

7.2   The chalcogen-rich glasses

In the case of the S-rich glasses, for compositions with S content between 60 and 65 at.% the extra sulphur is mainly accommodated in the As-S network through the formation of As—S—S—As bridges; these bridges are non-planar. S_8 rings are also formed in the glasses more S-rich

than $As_{37}S_{63}$ though As_2S_2 bridge formation is the dominant process in this composition range. S_8 rings may even be present in the glasses with S content between 61 and 63 at.%. The As—As bonds in the As-S network rapidly disappear as the S content is increased above 60 at.%.

The spectral changes occurring in the composition range $As_{40}S_{60}$ — $As_{35}S_{65}$ can all be accounted for by the appearance of As_2S_2 bridges and S_8 rings, and the disappearance of As—As bonds. There is no indication of any change in the geometry of the AsS_3 pyramids and As_2S links.

As the S content increases beyond 65 at.% the extra S atoms go less and less into the formation of As_2S_2 bridges, and S_8 ring production becomes the favoured process; in compositions containing more than $\sim$70 at.% S S_8 ring formation is the dominant process. The As_2S_2 bridges are, however, present in the glasses up to S concentrations of 95 at.%.

There is no evidence for the presence of S_n chains either in the As-S network or 'free'. Also, there is no indication of the presence of any of the other cyclic sulphur molecules — the S_8 ring is the only sulphur species present in appreciable quantities. The S_8 rings in the glasses are randomly positioned and distorted. No significant changes occur in the geometry of the AsS_3 and As_2S 'molecules' as the S content increases beyond 65 at.%.

The conclusions for the Se-rich glasses are similar to those for the S-rich glasses. In the compositions $As_{40}Se_{60}$ — $As_{35}Se_{65}$ the additional selenium is mainly accommodated in the As-Se network through the formation of non-linear As—Se—Se—As bridges. Although no bands attributable to the Se_8 ring were detected in the spectra of these compositions this is possibly because they are swamped by the intense As-Se network bands they overlap; such rings could be present in small quantities. There is no indication of any change in the geometry of the $AsSe_3$ and As_2Se network units.

Se$_8$ rings are certainly present in the glasses containing more than ~70 at.% Se. In the compositions more Se-rich than As$_{30}$Se$_{70}$ Se$_8$ ring production predominates over the formation of Se—Se bonds in the network, though such bonds are still present. The rings are randomly positioned and distorted. Se$_n$ chains may also be present in these glasses, though in small amounts. No significant change occurs in the geometry of the AsSe$_3$ and As$_2$Se 'molecules' as the Se content is increased beyond 65 at.%.

7.3   The As-rich glasses

The limit of the glass-forming region in the As-S system occurs at ~43 at.% As and the sulphide compositions with As content greater than this are phase separated; they consist of crystallites (predominantly of the β polymorph of c-As$_4$S$_4$) approximately 1μ in diameter embeded in a glassy matrix. The glasses containing between 40 and 43 at.% As have similar Raman spectra to the phase-separated compositions and must also contain crystallites of β-As$_4$S$_4$, although in the scanning electron microscope these glasses appear homogeneous. As$_4$S$_3$ or As$_4$S$_5$ molecules are also present in small quantities.

The results indicate that the glassy matrix in which the crystallites are embeded has essentially the same network structure as a-As$_{40}$S$_{60}$ — the AsS$_3$ and As$_2$S units of the stoichiometric composition are retained unchanged in these As-rich glasses. There are no S—S bonds in the As-S network for these compositions but As—As bonds are present in the network.

In the case of the selenides, for the compositions between As$_{40}$Se$_{60}$ and As$_{45}$Se$_{55}$ the additional As atoms go mainly into the formation of As—As bonds in the network. As$_4$Se$_4$ molecules are also produced though in very small amounts. For compositions containing more than 50 at.% As the production of As$_4$Se$_4$ molecules predominates over the formation of As—As bonds in the network, although these are still present. There is no significant change in the structure of the AsSe$_3$ and As$_2$Se units of the network.

APPENDIX I

FREQUENCY FORMULAE

This appendix gives the frequency formulae for the normal modes of the three simple polyatomic molecules considered in this study. The formulae are for a general valence force field and are taken from Herzberg, G., 'Infrared and Raman Spectra of Polyatomic Molecules', Van Nostrand, New York, 1945.

The pyramidal XY_3 molecule

$$\lambda_1 + \lambda_2 = (1 + 3\frac{m_Y}{m_X}\cos^2\beta)\frac{k_1 + 2k_{1'}}{m_Y} + (1 + 3\frac{m_Y}{m_X}\sin^2\beta)\frac{12\cos^2\beta(k_\delta + 2k_{\delta'})}{m_Y\ell^2(1 + 3\cos^2\beta)} \quad (A.1)$$

$$\lambda_1\lambda_2 = \frac{12\cos^2\beta}{1 + 3\cos^2\beta}(1 + 3\frac{m_Y}{m_X})\frac{(k_1 + 2k_{1'})(k_\delta + 2k_{\delta'})}{m_Y^2\ell^2} \quad (A.2)$$

$$\lambda_3 + \lambda_4 = (1 + \frac{3m_Y}{2m_X}\sin^2\beta)\frac{(k_1 - k_{1'})}{m_Y} + \frac{3(1 + \cos^2\beta + \frac{3m_Y}{2m_X}\sin^4\beta)(k_\delta - k_{\delta'})}{m_Y\ell^2(1 + 3\cos^2\beta)} \quad (A.3)$$

$$\lambda_3\lambda_4 = \frac{3(1 + \cos^2\beta + 3\frac{m_Y}{m_X}\sin^2\beta)(k_1 - k_{1'})(k_\delta - k_{\delta'})}{m_Y^2\ell^2(1 + 3\cos^2\beta)} \quad (A.4)$$

In the above formulae: $\lambda_i = 4\pi^2\nu_i^2$, the ν_i being the normal frequencies;

m_X and m_Y are the atomic masses of the X and Y atoms;

k_1 is the X—Y bond-stretching force constant;

k_δ is the bond-bending force constant;

$k_{1'}$ and $k_{\delta'}$ are interaction constants;

ℓ is the X—Y bond length;

β is the angle between the X—Y bond and the symmetry axis.

The non-linear symmetric X_2Y molecule

$$\lambda_1 + \lambda_2 = (1 + \frac{2m_X}{m_Y}\cos^2\alpha)\frac{k_1 + k_{12}}{m_X} + 2(1 + \frac{2m_X}{m_Y}\sin^2\alpha)\frac{k_\delta}{m_X\ell^2} \qquad (A.5)$$

$$\lambda_1\lambda_2 = 2(1 + \frac{2m_X}{m_Y})\frac{k_\delta(k_1 + k_{12})}{m_X^2\ell^2} \qquad (A.6)$$

$$\lambda_3 = (1 + \frac{2m_X}{m_Y}\sin^2\alpha)\frac{k_1 - k_{12}}{m_X} \qquad (A.7)$$

In the above formulae: k_δ is the bond-bending force constant at the

Y atom;

k_{12} is an interaction constant;

α is half the angle between the X–Y bonds;

the other symbols are as for the XY_3 molecule.

The linear symmetric X_2Y_2 molecule

$$\lambda_1 + \lambda_2 = \frac{2k_1 - 4k_{12}}{m_Y} + (1 + \frac{m_X}{m_Y})\frac{k_2}{m_X} \qquad (A.8)$$

$$\lambda_1\lambda_2 = \frac{2k_1k_2 - 4k_{12}^2}{m_X m_Y} \qquad (A.9)$$

$$\lambda_3 = (1 + \frac{m_X}{m_Y})\frac{k_2}{m_X} \qquad (A.10)$$

$$\lambda_4 = \frac{k_\delta - k_\delta}{\ell_1^2\ell_2^2}\left[\frac{\ell_1^2}{m_X} + \frac{(\ell_1 + 2\ell_2)^2}{m_Y}\right] \qquad (A.11)$$

$$\lambda_5 = (1 + \frac{m_X}{m_Y})\frac{k_\delta + k_\delta'}{m_X\ell_2^2} \qquad (A.12)$$

In the above formulae: k_1 is the Y–Y bond-stretching force constant;[*]

k_2 is the X–Y bond stretching force constant;[*]

k_δ is the bending force constant corresponding

to the change of angle between the Y—Y

and X—Y bonds;

k_{12} is an interaction constant;[*]

ℓ_1 is the Y—Y bond length;

ℓ_2 is the X—Y bond length;

all other symbols are as for the XY_3 molecule.

[*] For clarity, k_1, k_2 and k_{12} are referred to in the text as k_{Z-Z}, k_{As-Z} and k_{int} respectively (Z = S or Se).

APPENDIX II

G-MATRIX ELEMENTS FOR THE NON-PLANAR X_2Y_2 MOLECULE

In this appendix are given the elements G_{ij} of the inverse kinetic energy matrix for the non-planar X_2Y_2 molecule of C_2 symmetry. The elements are for the unsymmetrised G-matrix and are taken from Decius, J.C.; J. Chem. Phys. 16, 1025 (1948).

$$G_{11} = 2m_Y \qquad\qquad G_{33} = G_{22}$$

$$G_{12} = m_Y\cos\alpha \qquad G_{34} = G_{25}$$

$$G_{13} = G_{12} \qquad\qquad G_{35} = G_{24}$$

$$G_{14} = -\frac{m_X}{d}\sin\alpha \qquad G_{36} = G_{26}$$

$$G_{15} = G_{14} \qquad\qquad G_{44} = \frac{1}{d^2}m_X + (\frac{2}{D^2} + \frac{1}{d^2} - \frac{2}{dD}\cos\alpha)m_Y$$

$$G_{16} = 0 \qquad\qquad G_{45} = -\frac{2}{D}m_Y(\frac{1}{D} - \frac{1}{d}\cos\alpha)\cos\phi$$

$$G_{22} = m_X + m_Y \qquad G_{46} = \frac{1}{D}m_Y\left[\frac{2}{D}\cos\alpha - \frac{1}{d}(1 + \cos^2\alpha)\right]\frac{\sin\phi}{\sin\alpha}$$

$$G_{23} = 0 \qquad\qquad G_{55} = G_{44}$$

$$G_{24} = -\frac{m_X}{D}\sin\alpha \qquad G_{56} = G_{46}$$

$$G_{25} = \frac{1}{D}m_X\sin\alpha\cos\phi \qquad G_{66} = \frac{2}{\sin^2\alpha}\left\{\frac{1}{d^2}m_X + \left[\frac{2}{D}(1 + \cos\phi)(\frac{1}{D}\cos\alpha - \frac{1}{d})\cos\alpha + \frac{1}{d^2}\right]m_Y\right\}$$

$$G_{26} = -\frac{1}{D}m_X\cos\alpha\sin\phi \qquad G_{ij} = G_{ji}$$

In the above expressions m_X and m_Y are the masses of the X and Y atoms and D, d, α and ϕ are the geometrical parameters of the molecule (see Figure 5.54).

APPENDIX III

PUBLISHED RESULTS

'The Raman spectra and structure of glasses in the As-S and As-Se systems', Ewen, P.J.S., Sik, M.J. and Owen, A.E., in 'The Structure of Non-Crystalline Materials' (Gaskell, P.H., editor), Taylor and Francis, London, 1977, p.231.

The Raman spectra and structure of glasses in the As–S and As–Se systems

P. J. S. Ewen, M. J. Sik* & A. E. Owen

Department of Electrical Engineering, University of Edinburgh

The room-temperature Raman spectra of bulk glasses in the range $As_{35}S/Se_{65}$ to $As_{55}S/Se_{45}$ have been recorded. The spectra of the glasses on the S/Se-rich side of stoichiometry have been analysed in terms of the Lucovsky-Martin molecular model and indicate the replacement of the As–S/Se–As links between the AsS/Se$_3$ pyramid units by As–S/Se–S/Se–As links as the S/Se content is increased. There is no indication of Se$_8$ rings in the selenides, but the presence of S$_8$ rings is increasingly apparent in the compositions more S-rich than $As_{37}S_{63}$. In the case of the As-rich sulphides sharp spectral features characteristic of c-As$_4$S$_4$ appear near stoichiometry and increase smoothly as the As content is increased. The presence of c-As$_4$S$_3$, c-As$_4$S$_5$ and As–As bonds in the glassy matrix is also indicated. The spectra of the As-rich selenides show no crystalline features and indicate only the increasing presence of As–As bonds with increasing As content.

1. Introduction

This paper is a detailed study of the Raman spectra of glasses within ± 5 atomic % of the stoichiometric composition $As_{40}X_{60}$ (where X = S or Se). Measurements have been made on eleven near-stoichiometric glasses extending in each system from 35 to 45 atomic % As in one atomic % steps, augmenting Ward's[1,2] broader investigation of these systems. Some crystalline and amorphous compositions outside this range have also been examined.

Kobliska & Solin[3] have emphasized the importance of polarization measurements in Raman scattering investigations of amorphous solid structure and have defined a new type of spectrum called the depolarization spectrum. Accordingly, the polarization spectra for each glass have been measured, in addition to the unanalysed spectra, and from these have been derived the depolarization spectra.

2. Experimental

All the amorphous samples were annealed bulk glasses. Chemical analysis showed no significant difference from the expected compositions and no measurable inhomogeneity throughout the samples. The near-stoichiometric sulphide glasses were red and transparent, apart from the two most As-rich compositions which were pink, opaque and granular

in appearance. All the selenides were black and opaque.

The c-As$_4$S$_3$ used was prepared by slowly cooling a melt of this composition and the c-As$_4$S$_5$ was obtained using the method outlined by Whitfield[4]. Crystalline samples of As$_2$Se$_3$, As$_2$S$_3$ and As$_4$S$_4$ were obtained from external sources.

The sulphide spectra were excited with red light of either 6328 Å from a He–Ne laser or 6471 Å from a Kr-ion laser. The sulphides are very strong scatterers at these wavelengths and peak signals of ≈ 5000 counts/sec were typical. Because of the high absorption coefficients of the selenides at red wavelengths, the selenide spectra were obtained using the 7993 Å IR line of the Kr laser.

A Spex 1400 monochromator with a cooled RCA-C31034A photomultiplier operating in the photon-counting mode was used for detection. The spectra were all recorded at room temperature using right angle transmission geometry for the transparent samples and back reflection for the opaque glasses. A spectral slit width of ≈ 3 cm^{-1} was used.

To avoid the damaging effect of focused radiation[3] the selenide samples were spun in the focused beam, while an unfocused 3 mm diameter beam was used for the sulphides. The beam powers used were approximately 50 mW (6328 Å), 60 mW (7993 Å) and 240 mW (6471 Å). Although no gross physical damage occurred in the sulphides when unfocused radiation was used, a gradual loss of signal, $\approx 3\%$ per hour, was observed. A non-annealed sample of As$_{36}$S$_{64}$ gave three times this rate of count loss. The decrease in signal could not be attributed to changes in beam power. When an irradiated sample was examined under a polarizing microscope, the cylindrical path of the laser beam through the sample was clearly visible, indicating that laser-induced changes are taking place inside the glass. All the spectra presented here have been corrected for this intensity decrease, which is approximately linear with time over the first few hours of exposure. The effect is consistent with an increase in the optical absorption coefficient of these materials with exposure.[5,6]

Several experiments were performed to show that this count loss was not accompanied by any spectral changes which might be attributed to structural changes in the glasses. The selenide spectra, recorded from the spinning samples, did not exhibit any signal loss.

*Present address: Department of Clinical Physics and Bio-Engineering, 11 West Graham St, Glasgow G4 9LF.

Some features in Ward's spectrum of a-As_2S_3[1] have been attributed to plasma lines[7] and particular care was taken to exclude such spurious features. Spectra obtained with the He-Ne laser were identical with corresponding spectra excited with the Kr laser so that the spectral features presented in this study cannot be attributed to plasma lines.

3. Results and discussion

A. The Stoichiometric Glasses

With the IR Kr laser line as excitation the low energy region of the a-As_2Se_3 Raman spectrum was recorded, as well as the main band, and the spectra indicate vibrations at 106, 136, 223 and 275 cm^{-1} plus a thermal peak at 23 cm^{-1}. The polarization spectra, the unanalysed spectrum (see Figure 3) and the depolarization spectrum (see Figure 2) were all taken into account in deriving these frequencies. In the case of the sulphide the results indicate vibrations at 160, 185, 208, 231, 315, 338, 395 and 490 cm^{-1} plus the thermal peak at 29 cm^{-1}. The 160 cm^{-1} frequency is obtained from the depolarization spectrum[5,8] (see Figure 2), though there is a broad weak feature around this frequency in the Raman spectra. The vibration at 315 cm^{-1} appears as a shoulder in the unanalysed spectrum (see Figure 1) but is present as a sharp peak in the VH polarization spectrum. The knee at 395 cm^{-1} has not been reported in previous Raman studies and corresponds to the minimum in the depolarization spectrum. A similar knee and minimum are found at 275 cm^{-1} in the corresponding selenide spectra.

In the molecular model[9,10] the glasses are considered to be made up of pyramidal AsX_3 units loosely coupled via bent As–X–As chains. c-As_2S_3 and c-As_2Se_3 are also made up of pyramidal units bridged by S or Se atoms so it is not surprising that the two amorphous vibrational spectra scale by a factor of 0·71, as in the crystal spectra[11,12]. The corresponding pairs of frequencies are 106/160, 136/185, 223/315, 246[13]/338 and 275/395; the three exceptions, the features at 208, 231 and 490 cm^{-1} in a-As_2S_3, are discussed below. As in the crystal spectra the most intense Raman peak in each of the unanalysed glass spectra does not correspond to the same vibration. In Figure 2 the depolarization spectrum of a-As_2S_3 has been compressed along the frequency axis by the scaling factor 0·71.

The sulphide features at 208, 231 and 490 cm^{-1} probably arise from structural features not present in perfect c-As_2S_3, viz., As–As and S–S bonds. 230 cm^{-1} is the dominant frequency in the IR spectrum of a-As[14] while the Raman spectrum of a-As contains a broad, flat-topped band extending from ≈190 to ≈250 cm^{-1}. The feature at 231 cm^{-1} in a-As_2S_3 becomes more pronounced as the As content of the glass is increased (see Section C) and resonance Raman studies of this material[15,16] show that the region around 230 cm^{-1} behaves differently from the rest of the spectrum and resonates about the "optical gap" energy, ≈2·32 eV at 300°K. The
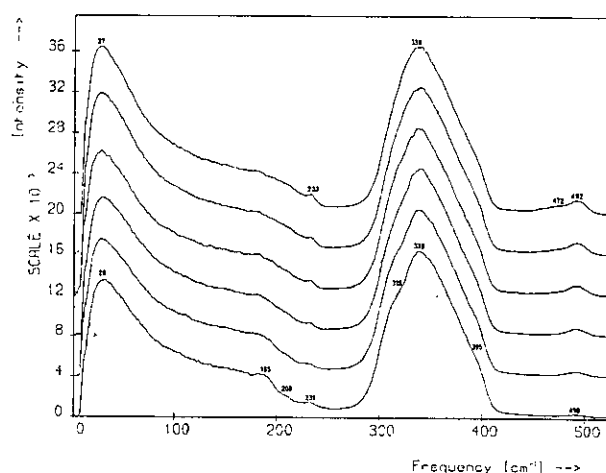
Figure 1. *The unanalyzed Stokes Raman spectra of the compositions* $As_{40}S_{60}$–$As_{35}S_{65}$. *The spectra are normalized to the height of the 338 cm^{-1} band and are displaced above one another, starting with the* a–$As_{40}S_{60}$ *spectrum at the bottom and going up in order of increasing S content to the* $As_{35}S_{65}$ *spectrum at the top.*

features at 208 and 490 cm^{-1} are discussed in Section B. Similar features may be present in the spectrum of a-As_2Se_3 but probably coincide with the main band and are not so easily detected. The other frequencies can all be accounted for by the molecular model.

B. The Chalcogen-rich Glasses: $As_{40}X_{60}$–$As_{35}X_{65}$

The molecular model can be extended to the chalcogen-rich glasses if the extra chalcogen atoms are incorporated in the chains linking the pyramidal molecules. In the case of the S-rich glasses it was found that the changes in the spectra with respect to the a-$As_{40}S_{60}$ spectrum arise from two sources: the appearance of S_8 rings and the above-mentioned replacement of As–S–As links with the As–S–S–As chains. Figure 1 shows the unanalysed S-rich spectra and three regions of change can be seen. As the sulphur content is increased a new band grows steadily at ≈492 cm^{-1}, the shoulder at 315 cm^{-1} disappears gradually and a change in profile occurs around 180–240 cm^{-1}, with a small peak appearing at 233 cm^{-1}. The shoulder on the 492 cm^{-1} band appears at ≈63 atomic % sulphur and is resolved into
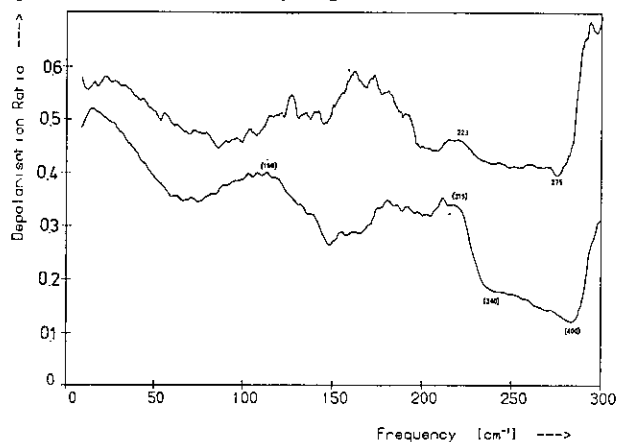

Figure 2. *The depolarization spectra of a–$As_{40}S_{60}$ and a–$As_{40}Se_{60}$. The frequency scale applies only to the a–$As_{40}Se_{60}$ since the a–$As_{40}S_{60}$ spectrum has been compressed by a factor of 0·71 along the frequency axis. The bracketed frequencies are those actually measured for a–$As_{40}S_{60}$.*

a peak at 472 cm^{-1} in the VV spectra. The knee at 395 cm^{-1} and the maximum at 160 cm^{-1} in the depolarization spectrum are present for all five S-rich glasses and there is no shift in the positions of the main peak frequencies. These observations are not surprising as it is expected that the pyramids and As–S–As chains are retained in the structure.

A more exact set of values for the new frequencies is provided by the difference spectra obtained by subtracting the a-$As_{40}S_{60}$ spectrum from each of the others. They are 176, 208, 233, 325, 472 and 492 cm^{-1}, with the possibility of another frequency on the high energy side of the asymmetric main band. Ward's work[1,2] on the very S-rich glasses shows two new features appearing on the main band at 337 and 354 cm^{-1}, which may correspond to the frequencies in this region suggested by the difference spectra.

The features at 233 and 472 cm^{-1}, which first appear at the composition $As_{37}S_{63}$, are associated with the presence of S_8 rings. In the spectra of the glasses more S-rich than $As_{35}S_{65}$, also reported by Ward[1,2], these lines are accompanied by others of the S_8 spectrum and grow very rapidly with increasing S-content, soon overtaking the other emerging features.

Standard valence force field calculations show that the non-S_8 frequencies can be attributed to a bent As–S–S–As chain but not to a linear chain. The A_2B_2 molecule of C_2 symmetry has six normal modes of vibration, all Raman active[17]. It is found that the torsional frequency for the A_2S_2 "molecule" is very low and would be difficult to detect in the glass spectra. The other five frequencies, however, are in reasonable agreement with the five experimental values. The 492 cm^{-1} vibration corresponds to the symmetric stretch of the S–S bond and is responsible for the weak feature at ≈ 490 cm^{-1} in the a-As_2S_3 spectrum.

In the case of the selenides the analysis is complicated by the fact that many of the observed frequencies for the various forms of pure selenium and the predicted frequencies for the pyramid and chains are close to one another. Figure 3 shows the unanalysed, reduced Se-rich spectra normalized by area and superimposed. There are no changes in the low frequency region, the only change in the spectrum being the growth of a feature on the high energy side of the main band. Difference spectra in this region show a peak growing at ≈ 265 cm^{-1}. The most intense line in the Raman spectra of Se_8 and a-Se occurs at 250 cm^{-1}. Although there is nothing in the difference spectra to suggest the presence of these forms in the glasses Ward's work on the Se-rich compositions beyond $As_{35}Se_{65}$ show a feature steadily growing at this frequency.

There is, however, no feature in the pure selenium spectra at 265 cm^{-1}. The valence force field calculation for the As–Se–Se–As chain yields a value of 268 cm^{-1} for the symmetric stretch frequency of the Se–Se bond. The ratio of the frequencies designated symmetric stretch for the sulphur and selenium rich glasses is 1·86, which agrees with the frequency scale
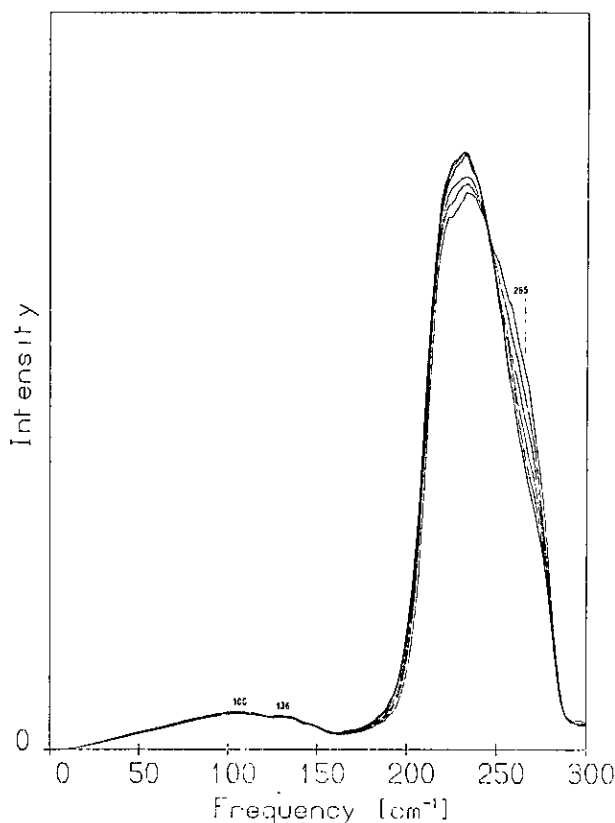

Figure 3. *The unanalyzed Stokes Raman spectra of the compositions $As_{40}Se_{60}$–$As_{35}Se_{65}$. The spectra have been reduced by the Shuker–Gammon method and are normalized by area. The changes occurring at the peak frequency are due to the normalization.*

factor relating S_8 to Se_8 observed by Lucovsky et al.[18]

Although structure has been observed in the difference spectra near other frequencies predicted by the chain calculation, it cannot be definitely attributed to the As–Se–Se–As "molecule" for the reason mentioned earlier. There is no sign of the low frequency bending modes of the As–Se–Se–As chain in the region < 160 cm^{-1}, which does not change at all, but this might be expected since the bending modes of the pyramids and As–Se–As links yield very weak features in the spectrum of a-As_2Se_3.

C. The As-rich Glasses: $As_{40}X_{60}$–$As_{45}X_{55}$

In the As-rich sulphide glasses sharp features start to appear in the spectra for even small amounts of excess arsenic, as also observed by Ward[1,2]. The lines are mostly characteristic of the crystal β-As_4S_4[19], but some frequencies – 133, 231 and 270 cm^{-1} – cannot be ascribed to α- or β-As_4S_4. These results indicate the presence of small amounts of c-As_4S_3 and possibly c-As_4S_5, but no c-As_2S_3, in the glasses, although in the scanning electron microscope the material still appeared to be a homogeneous glass up to 43% As. The feature at 231 cm^{-1} probably arises from As–As bonds in the glassy matrix, which is also responsible for the continuous background in the spectra.

The change from transparent to opaque occurs abruptly at some composition between $As_{43}S_{57}$ and $As_{44}S_{56}$. Electron micrographs of the As-rich sulphides show no features in the transparent glasses but

for the opaque samples reveal pockets of material embedded in a matrix. These abrupt changes are not apparent in the Raman spectra, where the "crystalline" lines grow steadily as the As content is increased beyond 40 atomic %.

In the case of the As-rich selenides phase-separation does not occur, although c-As_4Se_4 also exists. The spectral features (see Figure 4) remain broad and can be associated with the appearance of As–As bonds in
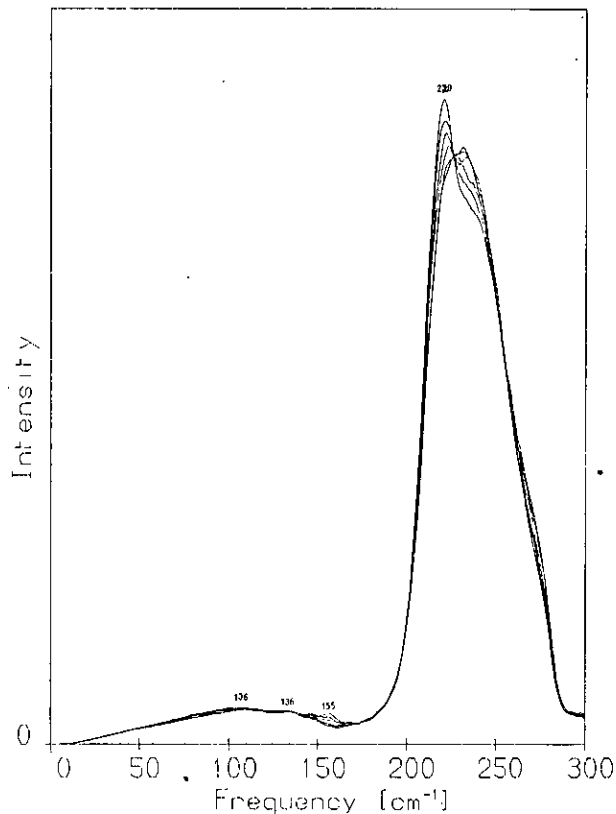

Figure 4. *The unanalyzed Stokes Raman spectra of the compositions $As_{40}Se_{60}$–$As_{45}Se_{55}$. The spectra have been reduced by the Shuker– Gammon method and are normalized by area. The changes occurring on the high energy side of the main peak are due to the normalization.*

the glasses. The new bands growing at 230 and $\approx 155\, cm^{-1}$ both appear in the vibrational spectra of a-As.

Similar conclusions on the structure of the chalcogen- and arsenic-rich glasses have been reached by Lucovsky et al.[20]

Acknowledgements

References

1. Ward, A. T. (1968). *J. Phys. Chem.* **72**, 4143.
2. Ward, A. T. (1972). *Adv. in Chemistry* **110**, 163.
3. Kobliska, R. J. & Solin, S. A. (1973). *Phys. Rev.* **B 8**, 756.
4. Whitfield, H. J. (1973). *JCS Dalton* 1740.
5. Tanaka, K. & Kikuchi, M. (1972). *Solid State Commun.* **11**, 1311.
6. de Neufville, J. P., Moss, S. C. & Ovshinsky, S. R. (1974). *J. Non-Cryst. Solids* **13**, 191.
7. Kobliska, R. J. & Solin, S. A. (1972). *J. Non-Cryst. Solids* **8**, 191.
8. Finkman, E., De Fonzo, A. P. & Tauc, J. (1973). *Proc. 5th Int. Conf. on Amorphous and Liquid Semiconductors*, Garmisch-Partenkirchen, Taylor & Francis Ltd, p. 1275.
9. Austin, I. G. & Garbett, E. S. (1971). *Phil. Mag.* **23**, 17.
10. Lucovsky, G. & Martin, R. M. (1972). *J. Non-Cryst. Solids* **8–10**, 185.
11. Zallen, R., Slade, M. L. & Ward, A. T. (1971). *Phys. Rev.* **B 3**, 4257.
12. Zallen, R. & Slade, M. L. (1974). *Phys. Rev.* **B 9**, 1627.
13. Lucovsky, G. (1972). *Phys. Rev.* **B 6**, 1480.
14. Lucovsky, G. & Knights, J. C. (1974). *Phys. Rev.* **B 10**, 4324.
15. Razzetti, C. & Fontana, M. P. (1975). *Phys. Stat. Sol.* **(B) 70**, 173.
16. Howard, R. E., Macedo, P. B. & Moynihan, C. T. (1975). *Solid State Commun.* **17**, 1475.
17. Herzberg, G. (1945). *Infrared and Raman Spectra of Polyatomic Molecules*, Van Nostrand, New York.
18. Lucovsky, G., Mooradian, A., Taylor, W., Wright, G. B. & Keezer, R. C. (1967). *Solid State Commun.* **5**, 113.
19. Porter, E. J. & Sheldrick, G. M. (1972). *JCS Dalton*, 1347.
20. Lucovsky, G., Galeener, F. L., Geils, R. H. & Keezer, R. C. Paper presented at this symposium.